

Coupled-Cluster Theory

for

Nuclear Structure



Vom Fachbereich Physik
der Technischen Universität Darmstadt

zur Erlangung des Grades
eines Doktors der Naturwissenschaften
(Dr. rer. nat.)

genehmigte Dissertation von
M.Sc. Sven Binder
aus Mannheim

Darmstadt 2014
D17

Referent: Prof. Dr. R. Roth
Korreferent: Prof. Dr. J. Wambach
Tag der Einreichung: 05.02.2014
Tag der Prüfung: 23.04.2014

Abstract

Nuclear Hamiltonians constructed within chiral effective field theory provide an unprecedented opportunity to access nuclear phenomena based on low-energy quantum chromodynamics and, in combination with sophisticated many-body methods, allow for an *ab initio* description of nuclei without resorting to phenomenology.

This work focuses on the inclusion of chiral two-, and in particular three-body Hamiltonians into many-body calculations, with emphasis on the formal and computational aspects related to the three-body interactions.

Through similarity renormalization group evolutions, the chiral Hamiltonians are transformed into a form in which strong short-range correlations are tamed in order to accelerate the convergence in the subsequent many-body calculations.

The many-body method mainly used is an angular-momentum coupled formulation of coupled-cluster theory with an iterative treatment of singly and doubly excited clusters, and two different approaches to non-iteratively include effects of triply excited clusters. Excited nuclear states are accessed via the equation-of-motion coupled-cluster framework.

The extension of coupled-cluster theory to three-body Hamiltonians is considered to verify the approximate treatment of three-nucleon interactions via the normal-ordering two-body approximation as a highly efficient and accurate way to include three-nucleon interactions into the many-body calculations, particularly for heavier nuclei.

Using a single chiral Hamiltonian whose low-energy constants are fitted to three- and four-body systems, a qualitative reproduction of the experimental trend of nuclear binding energies, from ^{16}O up to ^{132}Sn , is achieved, which hints at the predictive power of chiral Hamiltonians, even in the early state of development they are at today.

Zusammenfassung

Nukleare Hamiltonoperatoren die aus chiraler effektiver Feldtheorie abgeleitet werden bieten eine einzigartige Gelegenheit, nukleare Phänomene auf Grundlage niederenergetischer Quantenchromodynamik zu untersuchen. In Verbindung mit fortgeschrittenen Vielteilchenmethoden ermöglicht dies eine *ab initio* Beschreibung von Atomkernen ohne auf Phänomenologie zurückzugreifen.

Die vorliegende Arbeit beschäftigt sich mit der Inklusion chiraler Zwei-, und insbesondere Dreinukleonen-Hamiltonoperatoren in Vielteilchenrechnungen, mit Schwerpunkt auf den formalen und rechnerischen Aspekten der Behandlung der Dreinukleonenwechselwirkungen.

Durch Evolution mittels der Similarity Renormalization Group werden die chiralen Hamiltonoperatoren derart transformiert, dass die starken kurzreichweitigen Korrelationen gemildert werden um die Konvergenz in den anschließenden Vielteilchenrechnungen zu beschleunigen.

Die hauptsächlich eingesetzte Vielteilchenmethode ist eine drehimpulsgekoppelte Formulierung von Coupled-Cluster-Theorie mit einer iterativen Behandlung von ein- und zweifach angeregten Clustern, sowie einer nicht-iterativen Berücksichtigung dreifach angeregter Cluster. Angeregte Kernzustände werden über die Coupled-Cluster Bewegungsgleichungsmethode bestimmt.

Es wird die Erweiterung von Coupled-Cluster-Theorie auf Dreiteilchen-Hamiltonoperatoren betrachtet um die Behandlung von Dreinukleonen-Wechselwirkungen in der Normalordnungsapproximation zu verifizieren als eine hocheffiziente und akkurate Methode diese Wechselwirkungen näherungsweise in Vielteilchenrechnungen einzubeziehen, insbesondere für schwere Kerne.

Ein einzelner Hamiltonoperator dessen Niederenergiekonstanten in Drei- und Vierteilchensystemen bestimmt wurden genügt, um den experimentellen Trend nuklearer Bindungsenergien von ^{16}O bis ^{132}Sn qualitativ zu reproduzieren was, trotz ihres gegenwärtig frühen Entwicklungsstadiums, auf das Potential chiraler Wechselwirkungen hinweist Vorhersagen zu ermöglichen.

Contents

| | | |
|----------|---|-----------|
| 1 | Introduction | 1 |
| 1.1 | <i>Ab Initio</i> Nuclear Structure | 2 |
| 1.2 | Chiral Nuclear Interactions | 8 |
| 1.3 | Similarity Renormalization Group | 14 |
| 1.4 | Hartree-Fock Method | 19 |
| 1.5 | Normal-Ordering Approximation | 21 |
| 1.6 | Configuration Interaction and No-Core Shell Model | 25 |
| 1.6.1 | Full Configuration Interaction | 26 |
| 1.6.2 | Truncated Configuration Interaction | 28 |
| 1.6.3 | No-Core Shell Model | 30 |
| 1.6.4 | Importance-Truncated No-Core Shell Model | 31 |
| 2 | Coupled-Cluster Theory | 33 |
| 2.1 | Introduction | 34 |
| 2.2 | The Exponential Ansatz | 34 |
| 2.3 | Coupled-Cluster Equations | 38 |
| 2.4 | Effective Hamiltonian | 43 |
| 2.5 | The Λ CCSD Equations | 47 |
| 2.6 | Expectation Values | 51 |
| 2.7 | The Λ CCSD(T) Energy Correction | 55 |
| 2.8 | The Completely-Renormalized Coupled-Cluster Method CR-CC(2,3) | 57 |
| 2.9 | Equation-of-Motion Coupled Cluster | 62 |
| 2.9.1 | Reduced Density Matrices | 66 |

| | | |
|----------|--|------------|
| 3 | Coupled-Cluster Theory for Three-Body Hamiltonians | 69 |
| 3.1 | CCSD for Three-Body Hamiltonians | 70 |
| 3.1.1 | Introduction | 70 |
| 3.1.2 | The CCSD Equations for Three-Body Hamiltonians | 71 |
| 3.2 | Effective Hamiltonian | 79 |
| 3.3 | The ACCSD Equations for Three-Body Hamiltonians | 87 |
| 3.4 | The ACCSD(T) Energy Correction for Three-Body Hamiltonians . . . | 91 |
| 4 | Spherical Coupled-Cluster Theory | 95 |
| 4.1 | Introduction | 96 |
| 4.2 | Spherical Tensor Operators | 98 |
| 4.3 | Angular-Momentum Coupling | 100 |
| 4.4 | One-Body Operators | 102 |
| 4.5 | Cross-Coupled Matrix Elements | 104 |
| 4.5.1 | Scalar Case | 104 |
| 4.5.2 | General Case | 105 |
| 4.6 | Diagram Coupling | 111 |
| 4.6.1 | Antisymmetrized Diagram Coupling | 116 |
| 4.6.2 | Cross-Coupled Evaluation | 121 |
| 4.7 | Spherical CCSD | 123 |
| 4.8 | Convergence Acceleration | 125 |
| 4.9 | Spherical CCSD for Three-Body Hamiltonians | 136 |
| 4.9.1 | Three-Body Matrix Elements | 136 |
| 4.9.2 | Conversion to Reduced Format | 141 |
| 4.9.3 | Spherical CCSD Equations for Three-Body Hamiltonians . . . | 144 |
| 4.10 | Spherical ACCSD(T) | 145 |
| 4.11 | Spherical ACCSD(T) for Three-Body Hamiltonians | 147 |
| 4.12 | The CR-CC(2,3) Energy Correction | 148 |
| 4.13 | Spherical EOM-CCSD | 154 |
| 4.14 | Spherical Reduced Density Matrices | 156 |
| 5 | Results | 161 |
| 5.1 | Comparison of the IT-NCSM with the Coupled-Cluster Method . . . | 164 |
| 5.2 | CCSD with SRG-Transformed Chiral Two-Body Hamiltonians | 168 |
| 5.3 | Reduced-Cutoff Chiral Three-Body Interaction | 172 |
| 5.4 | Relevance of the $E_{3\max}$ Cut | 178 |
| 5.5 | The ACCSD(T) Energy Correction | 182 |
| 5.6 | The CR-CC(2,3) Energy Correction | 187 |

| | | |
|----------|--|------------|
| 5.7 | CCSD with Explicit 3N Interactions | 191 |
| 5.8 | Λ CCSD(T) with Explicit 3N Interactions | 195 |
| 5.8.1 | Benchmark of the NO2B Approximation | 195 |
| 5.8.2 | Approximation Schemes for the Amplitudes | 199 |
| 5.9 | <i>Ab Initio</i> Description of Heavy Nuclei | 202 |
| 5.9.1 | Self-Consistent Hartree-Fock Reference Normal- Ordering | 204 |
| 5.9.2 | Role of the SRG Model Space | 206 |
| 5.9.3 | Results for Heavy Nuclei | 213 |
| 6 | Conclusion | 221 |
| A | Excited Nuclear States | 225 |
| B | Trapped Neutrons | 235 |
| C | CCSD Diagrams and Spherical Expressions | 247 |
| C.1 | Diagrams | 248 |
| C.2 | Spherical Equations | 250 |
| C.3 | Diagrams for Three-Body Hamiltonians | 254 |
| C.4 | Spherical Equations for Three-Body Hamiltonians | 257 |
| D | Effective Hamiltonian Diagrams and Spherical Expressions | 269 |
| D.1 | Spherical Equations | 270 |
| D.2 | Diagrams for Three-Body Hamiltonians | 274 |
| D.3 | Spherical Equations for Three-Body Hamiltonians | 279 |
| E | ΛCCSD Diagrams and Spherical Expressions | 291 |
| E.1 | Diagrams | 292 |
| E.2 | Spherical Equations | 293 |
| E.3 | Spherical Equations for Three-Body Hamiltonians | 295 |
| F | Spherical Reduced Density Matrix | 307 |
| G | ΛCCSD(T) Spherical Expressions | 315 |
| G.1 | Spherical Equations | 316 |
| G.2 | Spherical Equations for Three-Body Hamiltonians | 323 |

| | | |
|----------|--|------------|
| H | EOM-CCSD Diagrams and Spherical Expressions | 327 |
| H.1 | Diagrams | 328 |
| H.2 | Spherical Equations | 329 |
| H.3 | Spherical Equations (Scalar) | 335 |
| I | Publications | 339 |
| | Bibliography | 344 |

Chapter 1

Introduction

1.1 *Ab Initio* Nuclear Structure

Nuclear physics is surprisingly complex. Starting around the 1950s, early microscopic models of the atomic nucleus considered it as a compound of elementary building blocks – the *nucleons* – where the large mean free path of these nucleons inside the nucleus suggested that they form some sort of weakly interacting gas. The nuclear interaction itself was quickly identified as being caused by meson exchange which helped the understanding of two-nucleon properties. Therefore, this early picture of nuclear physics gave rise to the hope that the nuclear many-body problem could be solved using meson-exchange interactions – such as the one-boson exchange model [1], or the more recent CD-Bonn potential [2] – in many-nucleon systems, and that, because of the apparent weak interaction among the nucleons, these many-body problems could eventually be solved using perturbation-theory based methods.

The discovery of *Quantum Chromodynamics* (QCD) put the earlier insights into perspective: Nucleons are *not* fundamental but are rather composed of quarks and gluons. However, in retrospect, *color confinement* at low energies justifies an approximate treatment of nucleons as being fundamental. Of course, a fundamental theory of the nuclear interaction necessarily has to be derived from QCD. However, the non-perturbative nature of QCD in the low-energy regime relevant for nuclear physics has defied any attempts of a direct derivation so far. There are attempts to extract nuclear potentials from QCD calculations on the lattice, but these calculations do not yet operate at the physical quark masses. Today, the most promising path towards QCD-based nuclear interactions is via *chiral effective field theory* [3–12], an effective theory in terms of low-energy degrees of freedom constrained by the symmetries of the underlying theory. This leads to a set of *consistent* QCD-based many-nucleon interactions which can be used in *ab initio* nuclear structure calculations. However, the practical treatment of such many-body forces is far from trivial.

Once the Hamiltonian is known, the focus is on the solution of the many-body problem. Here, the early weakly-interacting-gas picture of the nucleus turns out to be too simplistic. Instead, the nuclear many-body problem has a complex structure, particularly due to strong short-range correlations induced by the nuclear interaction (see [13] for a discussion based on the Argonne V18 [14] potential). In practice, in order to obtain realistic solutions for the many-body problem, vast computational resources are required which have simply not been available

in the past. The former sentiment towards the many-body problem is captured in a quote by Igal Talmi from 1993 about the task of solving the non-relativistic Schrödinger equation for a many-body system with strong interactions [15]:

"Such a problem cannot be treated exactly by many-body theory.

Not even useful approximation procedures have been developed."

Nowadays, considering the impressive advances that many-body theory has made, this statement seems too pessimistic. By applying renormalization-group techniques to the initial nuclear Hamiltonian, for instance in the framework of the *Similarity Renormalization Group* (SRG) [16, 17], the troubling short-range correlations can be weakened which then eases the burden on the many-body method. But also nuclear many-body methods themselves have seen much progress in recent years. For instance, using SRG-transformed interactions, the *No-Core Shell Model* (NCSM) [18, 19] and its *Importance-Truncated* extension (IT-NCSM) [20, 21] provide quasi-exact solutions of the Schrödinger equation for nuclei in the *p*-shell and even beyond. For medium-mass and heavy closed-shell nuclei the *Coupled-Cluster* Method [22–27] has been established as one of the most powerful approximate schemes and the recently introduced *In-Medium Similarity Renormalization Group* [28–30] approach has also been successfully applied in this mass region even for open-shell nuclei.

In this work, non-relativistic configuration-space based *ab initio* approaches to the nuclear many-body problem are considered in which all nucleonic degrees of freedom $\{\mathbf{r}_i, m_{s_i}, m_{t_i}, \dots, \mathbf{r}_A, m_{s_A}, m_{t_A}\}$ are taken into account explicitly. All information about the system is therefore contained in the *A*-body state $|\Psi\rangle$ that lives in the Hilbert space \mathcal{V} ,

$$\mathcal{V} = \bigwedge_{i=1}^A L_2(\mathbb{R}^3 \otimes \{\pm \frac{1}{2}\} \otimes \{\pm \frac{1}{2}\}). \quad (1.1)$$

Since the nucleus is a purely Fermionic system, the antisymmetric product \bigwedge enforces the Pauli exclusion principle on the many-body state. According to the postulates of quantum mechanics, the stationary nuclear state $|\Psi\rangle$ is solution of the nonrelativistic stationary Schrödinger equation

$$\hat{H} |\Psi\rangle = E |\Psi\rangle, \quad (1.2)$$

i.e., it is an eigenfunction of the nuclear Hamiltonian operator \hat{H} ,

$$\hat{H} = \frac{1}{A} \sum_{i < j}^A \frac{(\hat{\mathbf{p}}_i - \hat{\mathbf{p}}_j)^2}{2m} + \sum_{i < j}^A \hat{V}_{ij}^{\text{NN}} + \sum_{i < j < k}^A \hat{V}_{ijk}^{\text{3N}} + \lambda_{\text{CM}} \hat{H}_{\text{CM}}. \quad (1.3)$$

In (1.3), for convenience a scalable (via the parameter λ_{CM}) center-of-mass harmonic-oscillator potential

$$\hat{H}_{\text{CM}} = \frac{1}{2A m} \hat{\mathbf{P}}_{\text{CM}}^2 + \frac{1}{2} (A m \Omega_{\text{CM}})^2 \hat{\mathbf{R}}_{\text{CM}} - \frac{3}{2} \hbar \Omega_{\text{CM}} \quad (1.4)$$

is added to suppress center-of-mass motion. Although the nuclear Hamiltonian derived from chiral effective field theory formally contains up to A -nucleon interactions, present-day nuclear applications consider only Hamiltonians of the form (1.3), where only up to three-nucleon interactions are included. One strategy for the numerical solution of the partial differential equation $\hat{H}|\Psi\rangle = E|\Psi\rangle$ is to put it into its weak form [31], in which $|\Psi\rangle$ has to satisfy the equation

$$\langle \Phi | (\hat{H} - E) | \Psi \rangle = 0, \quad \langle \Psi | \Psi \rangle = 1, \quad \forall |\Phi\rangle \in \mathcal{V}. \quad (1.5)$$

The weak formulation is a common starting point for the application of Galerkin methods for discretizing the original continuous operator eigenvalue problem. Once the problem is discretized, approximate solutions (E_S, Ψ_S) may be obtained from finite-dimensional subspaces $\mathcal{V}_S \subset \mathcal{V}$. For instance, the Rayleigh-Ritz procedure for the ground-state energy and wavefunction – the foundation of many nuclear many-body methods such as Hartree-Fock or configuration interaction – may straightforwardly be applied to the finite-dimensional case,

$$E_S = \min_{|\Psi\rangle \in \mathcal{V}_S, |\Psi\rangle \neq 0} \frac{\langle \Psi | \hat{H} | \Psi \rangle}{\langle \Psi | \Psi \rangle}, \quad |\Psi_S\rangle = \operatorname{argmin}_{|\Psi\rangle \in \mathcal{V}_S, |\Psi\rangle \neq 0} \frac{\langle \Psi | \hat{H} | \Psi \rangle}{\langle \Psi | \Psi \rangle}. \quad (1.6)$$

In this work, the finite-dimensional model spaces \mathcal{V}_S are always spanned by a finite set of A -body Slater determinant basis functions $\{|\Phi_\mu\rangle\}$,

$$\mathcal{V}_S = \operatorname{span}\left\{ |\Phi_\mu\rangle : \mu = 1, \dots, \dim \mathcal{V}_S \right\}, \quad (1.7)$$

with

$$|\Phi_\mu\rangle = \hat{\mathcal{A}} |\phi_{\mu_1} \dots \phi_{\mu_A}\rangle \quad (1.8)$$

$$= \frac{1}{\sqrt{A!}} \sum_{\pi \in S(N)} \operatorname{sgn}(\pi) |\phi_{\pi(\mu_1)} \dots \phi_{\pi(\mu_A)}\rangle, \quad (1.9)$$

where $|\phi_{\mu_1} \dots \phi_{\mu_A}\rangle$ denotes the tensor-product state constructed from the single-particle states $|\phi_{\mu_1}\rangle, \dots, |\phi_{\mu_A}\rangle$,

$$|\phi_{\mu_1} \dots \phi_{\mu_A}\rangle = |\phi_{\mu_1}\rangle \otimes \dots \otimes |\phi_{\mu_A}\rangle, \quad (1.10)$$

which is not subjected to antisymmetrization. A common choice for the single-particle wavefunctions in nuclear structure calculations from which the Slater

determinants are build are *ls*-coupled harmonic-oscillator wavefunctions [32], which in coordinate representation read

$$\begin{aligned} \langle \mathbf{r} \boldsymbol{\sigma} \boldsymbol{\tau} | n(l s) j m_j t m_t \rangle \\ = \sum_{m_l m_s} \begin{pmatrix} l & s & j \\ m_l & m_s & m_j \end{pmatrix}_{\text{CG}} R_{nl}(r) Y_{lm_l}(\theta, \varphi) \chi_{m_s}^{(s)}(\boldsymbol{\sigma}) \chi_{m_t}^{(t)}(\boldsymbol{\tau}), \end{aligned} \quad (1.11)$$

where $Y_{lm_l}(\theta, \varphi)$ are the spherical harmonics, $\chi_{m_s}^{(s)}(\boldsymbol{\sigma})$ are the spinor functions and $R_{nl}(r)$ are the radial wavefunctions that satisfy the radial single-particle Schrödinger equation [32, 33]

$$\left[-\frac{\hbar^2}{2m} \frac{\partial}{\partial r} \left(r^2 \frac{\partial}{\partial r} \right) + \frac{\hbar^2 l(l+1)}{2m r^2} + \frac{1}{2} m \Omega^2 r^2 \right] R_{nl}(r) = \epsilon_{nl} R_{nl}(r), \quad (1.12)$$

for a harmonic-oscillator potential of frequency Ω . Working in this framework, what is left in order to solve the nuclear Schrödinger equation for an approximate wavefunction, is to specify an Ansatz for the wavefunction and to choose a convenient Slater-determinant basis set.

Two *ab initio* many-body methods are considered in this work. The first one is the (Importance-Truncated) No-Core Shell Model, employing a linear Ansatz

$$|\Psi\rangle = \left(\hat{\mathbb{I}} + \sum_{n=1}^A \hat{C}_n^{(\text{NCSM})} \right) |\Phi\rangle \quad (1.13)$$

for the many-body state, where $\hat{C}_n^{(\text{NCSM})}$ generates all possible n -particle- n -hole (n pnh) excitations of a single-determinant reference state $|\Phi\rangle$. The second *ab initio* many-body method is Coupled-Cluster theory, corresponding to an exponential form of the wave operator,

$$|\Psi\rangle = e^{\sum_{n=1}^A \hat{T}_n} |\Phi\rangle, \quad (1.14)$$

where the \hat{T}_n also are n pnh excitation operators. The No-Core Shell Model is widely used in nuclear structure calculations [34–54]. It is a universal tool to study the nuclear system in which ground and excited states as well as properties are accessible in the same framework. The numerical solution of the Schrödinger equation is obtained from large-scale diagonalizations of the Hamiltonian projected onto a finite space, which is a standard task in the calculation of quantum systems and benefits greatly from parallel computing architectures available nowadays. The *curse of dimensionality* of the No-Core Shell Model – which limits the

method to p -shell nuclei due to the exponential growth of the Slater-determinant basis dimension – can be overcome by the Importance Truncation [21] which allows to select the many-body basis states according to their importance for the calculation at hand, allowing to incorporate basis states well out of reach of the standard No-Core Shell Model while keeping its variational character and well preserving the original translational invariance.

After the exponential Ansatz was introduced by Coester and Kümmel in the late 1950s [22, 23], Čížek and Paldus laid the foundation for its application in many-body Fermionic theory [24, 55, 56]. Nowadays, the Coupled-Cluster method has emerged as one of the most powerful methods in high-precision quantum chemistry calculations. In the quantum chemistry context, many variants of the Coupled-Cluster method have been developed over the years, starting from *Coupled-Cluster with Singles and Doubles excitations* (CCSD), going to the perturbative inclusion of triples- and even quadruples-excitations contributions [57–59], and many more. Although introduced in nuclear physics, the Coupled-Cluster method has not seen as much attention there as it has in the quantum chemistry community. In the 1990s, Mihaila and Heisenberg [60] brought the method back to the focus of nuclear physicists, and more recently Dean, Hagen, Papenbrock, *et al.* made significant progress in establishing the method particularly in medium-mass and nuclear reaction calculations [27, 61–75]. In this work, the Coupled-Cluster methods considered for ground-state calculations are the CCSD approximation, and the ACCSD(T) as well as the CR-CC(2,3) method for the non-iterative inclusion of triples contributions to the energy. Excited states are accessed with the EOM-CCSD Ansatz [76]. The reason for employing these rather low-order approximations of the full Coupled-Cluster method lies in the rather hard interaction encountered in the case of nuclear physics, which causes strong multi-nucleon correlations. This results in the necessity of large basis sets in order to obtain converged results with respect to the many-body model space size, which renders the application of higher-order Coupled-Cluster approximations practically impossible. Even for the case of CCSD, the standard formulation of the method in m -scheme basis representation proves to be not practical anymore beyond ^{40}Ca . Therefore, the *spherical Coupled-Cluster* scheme for closed-shell nuclei, originally introduced by Hagen, Papenbrock, *et al.* [27] is used throughout this work. This scheme achieves the required reduction of computational complexity which in principle makes the method applicable for closed-shell nuclei across the nuclear chart. Another substantial difference to quantum chemistry applications is the aforementioned need to incorporate three-body forces. This can be achieved by ei-

ther the approximate consideration through the use of effective two-body Hamiltonians, or by extending Coupled-Cluster theory to explicitly treat three-body Hamiltonians. Both approaches have first been considered again by Hagen, Papenbrock, *et al.* in ^4He proof-of-principle calculations [63] and will be extended to the medium-mass regime using the spherical formulation in this work.

This work is organized as follows: Basic aspects of *ab initio* nuclear structure physics are reviewed in Chapter 1, such as the nuclear interaction and some auxiliary methods used in the calculations. Chapter 2 presents the traditional Coupled-Cluster theory which is generalized for three-body Hamiltonians in Chapter 3. The following chapter discusses the spherical formulation of Coupled-Cluster theory and results are presented in Chapter 5. Finally, a conclusion is given in Chapter 6. The Appendix provides results of proof-of-principle calculations, and a compilation of diagrams and spherical equations that entered this work. Diagrams for many standard Coupled-Cluster method can also be found in [25, 26]. For documentary purposes, the spherical equations are presented exactly as they are used in the computer implementation.

1.2 Chiral Nuclear Interactions

The determination of the nuclear interaction is a long-standing problem in theoretical nuclear physics [10]. Although it is well-known that QCD is the underlying theory, a direct derivation of the nuclear interaction from QCD is not possible yet, due to the non-perturbative nature of QCD in the low-energy regime relevant for nuclear physics.

Phenomenological approaches, such as the Argonne V18 potential [14, 77], have been successful in describing two-nucleon (NN) properties. In the NN sector, the nuclear interaction already has a rather complicated form built from all operator structures that can contribute [78], but the corresponding radial functions can be determined from a large base of experimental data. However, the description of finite nuclei beyond the two-nucleon system requires the incorporation of many-nucleon forces, and these are difficult to deal with in such an approach. On the one hand, with the number of nucleons involved the number of operator structures grows dramatically while, on the other hand, the experimental data base shrinks. Furthermore, many-nucleon interactions need to be defined *consistently* to the NN interaction [79].

Therefore, physical insight is needed to proceed. Such physical insight was already inherent in the first attempts of a field-theoretic description of the nuclear interaction based on Yukawa's idea of pion exchange [80], but these were only partly successful as well. While the one-pion exchange could be used to understand NN scattering data, the multi-pion exchange picture failed. The discovery of heavy mesons then led to the one-boson exchange model [81], which could accurately describe the NN interaction. However, not for all of the bosons used in this model experimental evidence exists. Finally, the discovery of QCD and the introduction of the concept of *effective field theories* [3–12] allowed to formulate a theory of nuclear interactions rooted in QCD. In order for an effective theory to work, a separation of scales is required, each scale with its own set of relevant degrees of freedom. In the case of QCD, these scales are identified as the asymptotic free and the hadronic phase, which makes hadrons the more appropriate choice as degrees of freedom for low-energy QCD than quarks and gluons. Furthermore, due to the large mass gap in the hadron spectrum between the pions and the heavier mesons, the most relevant degrees of freedom for low-energy nuclear physics clearly are the nucleons and pions.

According to Weinberg [3], an effective field theory can be obtained by con-

structuring the most general Lagrangian for these degrees of freedom which is consistent with the symmetries of the underlying theory. Since such a Lagrangian usually contains infinitely many terms and accompanying low-energy constants, for practical applications a scheme has to be devised that allows to group and select these terms according to their individual importance. Such characterization is provided by a power counting scheme introduced by Weinberg for the Lagrangian in the chiral expansion, in which it is expanded in a power series in Q/Λ_χ , where the soft scale Q is a momentum typical for the interaction and the hard scale Λ_χ is the limit where the theory is expected to break down. In order to make real progress over the old pion-exchange theories, which already had nucleons and pions as degrees of freedom, chiral symmetry needs to be taken into account as an important constraint on the theory. The resulting *chiral effective field theory* (χ EFT) then represents the solution to the problems mentioned above: It is clearly connected to QCD via the effective field theory framework by retaining all relevant symmetries of QCD. Furthermore, it not only gives rise to consistent two- and many-body interactions, but through power-counting it also allows to identify the most important of the many operator structures. Since nuclear interactions from chiral effective field theory will be employed throughout this work, a more detailed review in the spirit of Refs. [10–12] is given in the following.

Chiral symmetry is closely related to vanishing quark masses, and for the energy scales relevant in the nuclear structure context, the up and down quark masses may be considered approximately zero, which motivates to focus on chiral symmetry in the up and down sector of QCD. The two-flavor QCD Lagrangian has the form

$$\mathcal{L}_{\text{QCD}} = \bar{q}(i\gamma^\mu \mathcal{D}_\mu - \mathcal{M})q - \frac{1}{4} \mathcal{G}_{\mu\nu,a} \mathcal{G}_a^{\mu\nu}, \quad (1.15)$$

where $q = (u, d)^T$ are the quark fields, \mathcal{D}_μ is the gauge-covariant derivative, $\mathcal{M} = \text{diag}(m_u, m_d)$ denotes the quark mass matrix and $\mathcal{G}_{\mu\nu,a}$ is the gluon field strength tensor. Chiral symmetry is revealed when the Lagrangian is written in terms of left- and right-handed quark fields q_L and q_R ,

$$\begin{aligned} \mathcal{L}_{\text{QCD}} = & \bar{q}_L i \gamma^\mu \mathcal{D}_\mu q_L + \bar{q}_R i \gamma^\mu \mathcal{D}_\mu q_R \\ & - \bar{q}_L \mathcal{M} q_R - \bar{q}_R \mathcal{M} q_L - \frac{1}{4} \mathcal{G}_{\mu\nu,a} \mathcal{G}_a^{\mu\nu}. \end{aligned} \quad (1.16)$$

From (1.16) follows that in the limit of vanishing quark masses – also referred to as the *chiral limit* – left- and right-handed quark fields are decoupled and \mathcal{L}_{QCD} becomes invariant under separate flavor rotations among the left- and right-handed

quark fields,

$$q_L \longrightarrow q'_L = e^{-i\boldsymbol{\theta}_L \cdot \boldsymbol{\tau}/2} q_L \quad (1.17)$$

$$q_R \longrightarrow q'_R = e^{-i\boldsymbol{\theta}_R \cdot \boldsymbol{\tau}/2} q_R, \quad (1.18)$$

generated by Pauli matrices $\boldsymbol{\tau}$ in flavor space, resulting in the SU(2) *chiral symmetry group* $SU(2)_L \times SU(2)_R$ ¹. The corresponding conserved currents may also be expressed in terms of axial and vector currents belonging to an axial and vector subgroup of the chiral symmetry group, $SU(2)_A, SU(2)_V \subset SU(2)_L \times SU(2)_R$. In reality, quarks possess non-vanishing masses and, consequently, chiral symmetry is *explicitly* broken. However, the quark masses of the order of a few MeV are much smaller than the typical hadronic mass scale of the order of 1 GeV and, therefore, chiral symmetry is expected to be at least approximately preserved. Chiral symmetry should be manifest in the hadron spectrum in form of multiplets corresponding to $SU(2)_L \times SU(2)_R$. However, only multiplets corresponding to $SU(2)_V$ are observed in nature, hinting at a *spontaneous* breaking of $SU(2)_A$. Since $SU(2)_A$ has 3 generators, its spontaneous breaking gives rise to the existence of 3 Nambu-Goldstone modes or, more precisely, *pseudo*-Nambu-Goldstone modes, due to the small explicit chiral symmetry breaking. Indeed, in this case, the experimentally observed hadron spectrum provides candidates for Nambu-Goldstone bosons in form of the pions $\pi = (\pi^\pm, \pi^0)$. Then, also the remarkable mass gap between these unnaturally light pions and the other hadrons may simply be explained by the Goldstone nature of the pions which are massless in the chiral limit but in reality acquire a small mass from the explicit breaking of chiral symmetry due to the small but non-vanishing quark masses.

The most general effective Lagrangian for pions and nucleons may be written in the form

$$\mathcal{L}_{\chi\text{EFT}} = \mathcal{L}_{\pi\pi} + \mathcal{L}_{\pi N} + \mathcal{L}_{NN} + \dots \quad (1.19)$$

Considering the pion-only part $\mathcal{L}_{\pi\pi}$ for illustration, the Lagrangian is given by

$$\mathcal{L}_{\pi\pi} = \mathcal{L}_{\pi\pi}^{(2)} + \mathcal{L}_{\pi\pi}^{(4)} + \mathcal{O}(\pi^6), \quad (1.20)$$

where the superscript denotes the number of derivatives or pion-mass insertions which has to be even for the pion-only Lagrangian. For example, the lowest-order

¹Additional symmetries of the QCD Lagrangian which are not relevant for the present discussion are $U(1)_V$, corresponding to quark number conservation and $U(1)_A$, broken on the quantum level and therefore also referred to as the $U(1)$ anomaly.

contribution $\mathcal{L}_{\pi\pi}^{(2)}$ reads

$$\mathcal{L}_{\pi\pi}^{(2)} = \frac{1}{2} \partial_\mu \pi \cdot \partial^\mu \pi + \frac{1}{2F_\pi^2} (\partial_\mu \pi \cdot \pi)^2 + \mathcal{O}(\pi^6), \quad (1.21)$$

where F_π is a low-energy constant related to the pion-decay constant which can be determined experimentally to be $F_\pi = 92.4$ MeV [6]. In order to apply a power counting scheme, the effective Lagrangian has to be expanded in powers of a soft scale over a hard scale Q/Λ_χ . Due to the Goldstone nature of the pions the soft scale Q is associated with external momenta or the pion mass. The hard scale Λ_χ is usually chosen around the mass of the ρ meson which is the lightest meson that cannot be identified as a Goldstone boson associated with chiral symmetry breaking. Beyond Λ_χ the theory is expected to break down because the ρ dynamics would have to be taken into account explicitly. This is why Λ_χ is also referred to as *chiral symmetry-breaking scale*. Once the effective Lagrangian has been expanded in Q/Λ_χ , the Weinberg power counting scheme

$$v = -4 + 2N + 2L + \sum_i \Delta_i, \quad \Delta_i = d_i + \frac{n_i}{2} - 2, \quad (1.22)$$

is used to determine the power-counting order v of a given Feynman diagram, where N denotes the number of nucleon lines, L the number of pion loops, and the sum runs over all vertices for which Δ_i is the dimension of vertex i that is calculated in terms of the number of derivatives d_i and the number n_i of nucleon lines at this vertex. This perturbative treatment of the effective Lagrangian in powers of Q/Λ_χ motivated by chiral symmetry is referred to as *chiral perturbation theory* [6,7].

The inclusion of nucleons in the effective Lagrangian poses a problem due to the mass m_N of the nucleon which is not small compared to the hard scale and, therefore, does not allow for a perturbative treatment. This problem can be overcome in the *heavy-baryon formalism* [82, 83] in which heavy baryons are treated non-relativistically by further expanding in terms of $1/m_N$, so the nucleons are regarded as static sources of pions. A more detailed discussion is beyond the scope of this section, however, it should be noted that for the chiral interactions used in this work the power counting that is employed is the Weinberg power counting scheme (1.22), whose validity has been questioned (see Ref. [84] for a discussion).

As a consequence of the chiral expansion approach, consistent nuclear forces emerge as a hierarchy in the power-counting order v , as depicted in Figure 1.1. At *leading order* (LO) corresponding to $v = 0$, for instance, the NN interaction is given by two NN contact terms, represented by the diagram



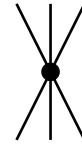
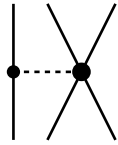
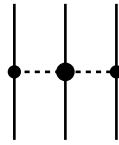
(1.23)

and a one-pion-exchange contribution



(1.24)

which gives rise to a tensor force already at leading order. It should be noted that for $\nu = 1$ all terms vanish due to parity and time-reversal constraints. Therefore, what is referred to as *next-to-leading order* (NLO) actually corresponds to $\nu = 2$ and from there, for any given $\nu > 2$, the next order corresponds to an increase of ν by one. Apparently, according to Figure 1.1, at LO and NLO only two-nucleon forces exist. Three-nucleon forces arise at *next-to-next-to-leading order* (N²LO, etc.),= and four-nucleon forces do not appear before N³LO. This way, chiral perturbation theory reproduces the observed hierarchy of nuclear forces in which the importance of many-nucleon forces decrease with the number of active nucleons involved. The three-nucleon interaction at N²LO is represented by the three diagrams



(1.25)

in which the 5 low-energy constants $c_i, i = 1, 3, 4$ and c_D, c_E enter. The c_i , however, are already determined in the two-nucleon and pion-nucleon sector, which leaves only c_D and c_E , assigned to the two-nucleon-contact with one-pion-exchange and the three-nucleon-contact diagrams respectively, as new low-energy constants that have to be experimentally determined from the three-body system. At present, the part of Figure 1.1 that is currently available for nuclear-structure calculations is given by the NN interaction up to N³LO and the 3N interaction up to N²LO, which constitute the interactions mainly used in this work. When being evaluated, the diagrams have to be regularized by a cutoff momentum. For the NN interaction, a regulator cutoff momentum of $\Lambda_{\text{NN}} = 500$ MeV is used, while for the 3N interaction, the regulator cutoff momenta of $\Lambda_{3\text{N}} = 500$ MeV or 400 MeV will mainly be employed. ²

²The regularization cutoff momenta Λ_{NN} and $\Lambda_{3\text{N}}$ should not be confused with the chiral breakdown scale Λ_χ .

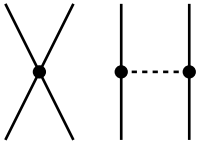
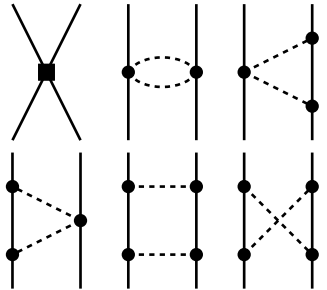
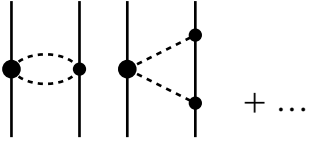
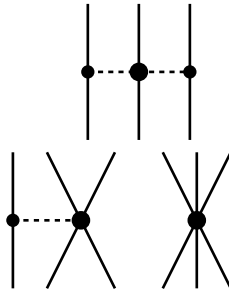
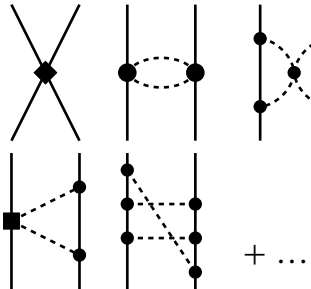
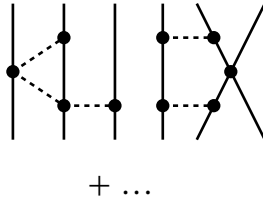
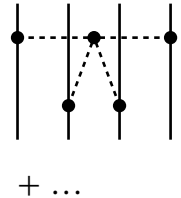
| | NN | 3N | 4N |
|---|---|--|---|
| LO $(Q/\Lambda_\chi)^0$ |  | | |
| NLO $(Q/\Lambda_\chi)^2$ |  | | |
| N ² LO $(Q/\Lambda_\chi)^3$ |  |  | |
| N ³ LO $(Q/\Lambda_\chi)^4$ |  |  |  |

Figure 1.1: Nuclear forces from chiral perturbation theory based on the Weinberg power counting [10]. Solid lines represent nucleon propagators, dashed lines pions. Different symbols (small/large dots, etc.) denote different types of vertices [10].

1.3 Similarity Renormalization Group

Nuclear structure calculations are severely complicated by the existence of the repulsive core in the nucleon-nucleon potential. Nuclear structure theory aims at the low-energy description of nuclei, but the short-range correlations from the repulsive core introduce an energy scale that is not easily resolved by the set of harmonic-oscillator Slater-determinant basis functions used in practical many-body calculations, resulting in a slow convergence of these calculations with respect to model-space size. These correlations manifest themselves in form of the interaction operator coupling low- and high-momentum states. The approach of the *Similarity Renormalization Group* (SRG) [16, 17, 85] is to unitarily transform the initial interaction to a more diagonal form that suppresses the coupling between low- and high-momentum states. Due to the unitary nature of the transformation, in principle, no information is lost and low-energy nuclear structure may then be described by low-energy degrees of freedom.

The initial Hamiltonian \hat{H}_0 is continuously unitarily transformed by the action of a unitary operator \hat{U}_α depending on a continuous real parameter α ,

$$\hat{H}_\alpha = \hat{U}_\alpha^\dagger \hat{H}_0 \hat{U}_\alpha. \quad (1.26)$$

The derivative of the transformed Hamiltonian with respect to α ,

$$\frac{d}{d\alpha} \hat{H}_\alpha = \left[-\hat{U}_\alpha^\dagger \frac{d\hat{U}_\alpha}{d\alpha}, \hat{H}_\alpha \right], \quad (1.27)$$

motivates the definition of $\hat{\eta}_\alpha$,

$$\hat{\eta}_\alpha = -\hat{U}_\alpha^\dagger \frac{d\hat{U}_\alpha}{d\alpha}, \quad (1.28)$$

as the *generator* of the transformation, such that the flow (1.27) of the Hamiltonian along the unitary path reads

$$\frac{d\hat{H}_\alpha}{d\alpha} = [\hat{\eta}_\alpha, \hat{H}_\alpha], \quad \hat{\eta}_\alpha^\dagger = -\hat{\eta}_\alpha. \quad (1.29)$$

This equation is equivalent to the one-step unitary transformation (1.26) and, therefore, the focus may be shifted away from finding the explicit transformation operators \hat{U}_α to finding anti-Hermitean generators $\hat{\eta}_\alpha$ that let the Hamiltonian flow along an appropriate path for the problem at hand. The common choice for $\hat{\eta}_\alpha$ in the context of nuclear structure calculations is given by the commutator of the

intrinsic kinetic energy operator, $\hat{T}_{\text{int}} = \hat{T} - \hat{T}_{\text{CM}}$, with the SRG-evolved Hamiltonian [85],

$$\hat{\eta}_\alpha = \left(\frac{2\mu}{\hbar^2} \right)^2 [\hat{T}_{\text{int}}, \hat{H}_\alpha], \quad (1.30)$$

in terms of the reduced nucleon mass μ . This generator lets the momentum-space representation of the Hamiltonian flow towards band-diagonal form and thus, as desired, leads to a decoupling of low- and high-momentum degrees of freedom. As shown in the example of Figure 1.3, this in turn accelerates the convergence of the many-body calculations with respect to model-space size.

In order to bring the operator flow equation (1.29) using generator (1.30) into matrix-element representation in k -body space, resolutions of the k -body identity of the form

$$\hat{\mathbb{1}}^{(k)} = \sum_p |\phi_p^{(k)}\rangle \langle \phi_p^{(k)}| \quad (1.31)$$

have to be inserted between adjacent operators, leading to

$$\begin{aligned} \frac{d}{d\alpha} \langle \phi_i^{(k)} | \hat{H}_\alpha | \phi_j^{(k)} \rangle = & \left(\frac{2\mu}{\hbar^2} \right)^2 \left\{ \sum_{pq} \langle \phi_i^{(k)} | \hat{T}_{\text{int}} | \phi_p^{(k)} \rangle \langle \phi_p^{(k)} | \hat{H}_\alpha | \phi_q^{(k)} \rangle \langle \phi_q^{(k)} | \hat{H}_\alpha | \phi_j^{(k)} \rangle \right. \\ & - 2 \sum_{pq} \langle \phi_i^{(k)} | \hat{H}_\alpha | \phi_p^{(k)} \rangle \langle \phi_p^{(k)} | \hat{T}_{\text{int}} | \phi_q^{(k)} \rangle \langle \phi_q^{(k)} | \hat{H}_\alpha | \phi_j^{(k)} \rangle \\ & \left. + \sum_{pq} \langle \phi_i^{(k)} | \hat{H}_\alpha | \phi_p^{(k)} \rangle \langle \phi_p^{(k)} | \hat{H}_\alpha | \phi_q^{(k)} \rangle \langle \phi_q^{(k)} | \hat{T}_{\text{int}} | \phi_j^{(k)} \rangle \right\}. \end{aligned} \quad (1.32)$$

Since the resolutions of the identities have to be truncated at some point in practical calculations this introduces errors which have to be monitored (see Section 5.9.3 and [86]).

At this point a crucial difference between the SRG transformation and other renormalization group approaches, such as $V_{\text{low-k}}$ [87] should be mentioned. In the latter, with increasing transformation parameter the UV cutoff of the interaction is lowered and, therefore, removing the high-energy scale from the interaction, as depicted in Figure 1.2. Therefore, for $V_{\text{low-k}}$ the transformation parameter corresponds to a cutoff in the momentum scale. For the SRG on the other hand, as

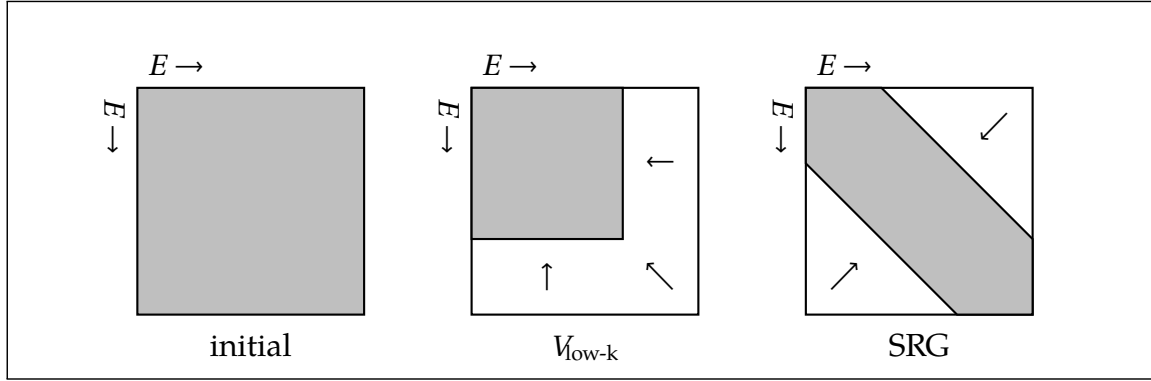


Figure 1.2: Comparison of different renormalization approaches for the initial Hamiltonian (see text and [88]).

the flow parameter α increases, the Hamiltonian is driven to band-diagonal form where α^{-1} is related to the width of the band. High-energy modes are still present in the interaction, only their coupling to low-energy modes is suppressed. Consequently, in the case of the SRG, the flow-parameter does not correspond to a cutoff in the momentum scale – which is also clear from the unitary nature of the SRG transformation.

A major drawback of the SRG transformation (and all other renormalization treatments) is the induction of many-body interactions. From evaluation of the commutators

$$\frac{d\hat{H}_\alpha}{d\alpha} = \left(\frac{2\mu}{\hbar^2}\right)^2 \left[[\hat{T}_{\text{int}}, \hat{H}_\alpha], \hat{H}_\alpha \right] \quad (1.33)$$

it becomes apparent that each infinitesimal evolution step generates operators with particle ranks exceeding the original rank of the interaction. Therefore, at the end of the evolution the transformed Hamiltonian will contain induced many-body interactions up to the number of nucleons in the system,

$$\hat{H}_\alpha = \hat{H}_\alpha^{(1)} + \hat{H}_\alpha^{(2)} + \hat{H}_\alpha^{(3)} + \dots + \hat{H}_\alpha^{(A)}. \quad (1.34)$$

In order to preserve the unitarity of the transformation, if the evolved Hamiltonian is to be used in an A -body calculation, all induced operators up to the A -body level would have to be maintained during and after the SRG flow. For practical reasons, typically only operators up to the three-body level can be kept while the others have to be discarded, resulting in a formal violation of unitarity of the transformation. In many-body calculations this violation of unitarity will emerge as a

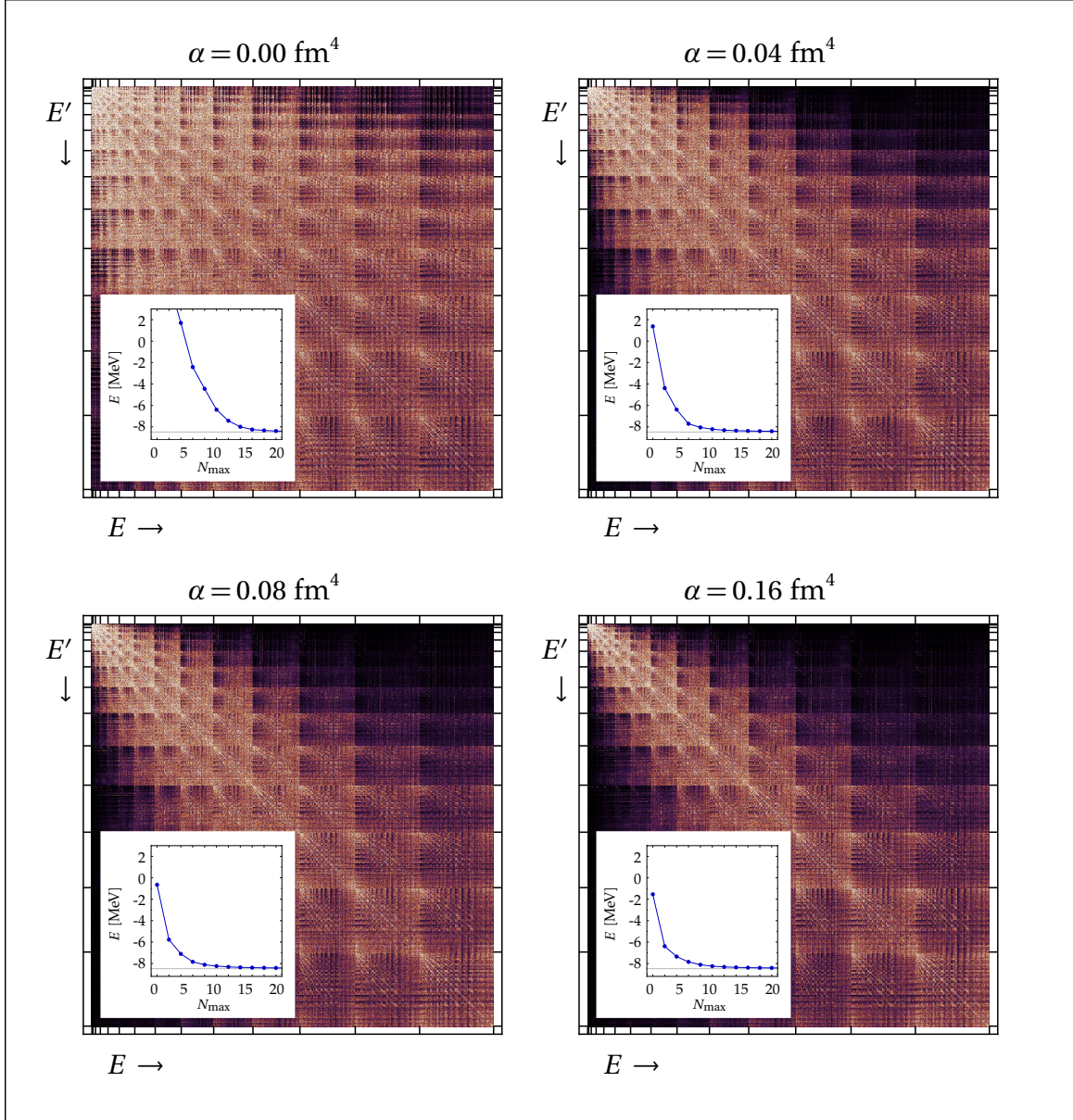


Figure 1.3: *Effect of the SRG evolution on the matrix elements of the NN+3N-full interaction for the triton channel $(J^\pi, T) = (1/2^+, 1/2)$ in an antisymmetrized three-body harmonic-oscillator Jacobi basis with $\hbar\Omega = 28$ MeV. Plotted are the absolute values of the matrix elements, where light colors represent large values, and dark colors represent values near zero (also see [89]). Embedded in the matrix plots are convergence patterns of triton ground-state energies obtained from the NCSM.*

dependence of the observables on the flow parameter α . As long as the observables are independent of the flow parameter it is assumed that unitarity has not been violated and, therefore, conclusions about the initial Hamiltonian may be drawn from the transformed Hamiltonian. However, once unitarity is corrupted so much that flow-parameter dependence sets in, this will no longer be possible. In order to discuss the results obtained from the SRG framework described above, it is convenient to define and investigate the following three Hamiltonians:

- (i) *NN-only* : An initial *two-body* Hamiltonian \hat{H}_0^{NN} is evolved and during the flow only induced operators up to the *two-body level* are kept.
- (ii) *NN+3N-induced* : An initial *two-body* Hamiltonian \hat{H}_0^{NN} is evolved and during the flow only induced operators up to the *three-body level* are kept.
- (iii) *NN+3N-full* : An initial *two- plus three-body* Hamiltonian $\hat{H}_0^{\text{NN}+3\text{N}}$ is evolved and during the flow only induced operators up to the *three-body level* are kept.

In this way contributions of induced three- and higher-body interactions out of the initial Hamiltonian can be quantified. The NN+3N-full Hamiltonian represents the most complete Hamiltonian considered in this work since it contains the full currently available set of chiral interactions. A flow-parameter dependence of the energy eigenvalues hints at significant four- and higher-body interaction contributions stemming from the initial two- or three-body interaction. These considerations are illustrated in Figure 1.4 (also see [17]): For ^4He , the ground-state energies obtained for the NN-only Hamiltonian show a strong flow-parameter dependence, demonstrating the importance of SRG-induced many-body forces that are not considered in this type of calculation. This flow-parameter dependence does not allow to make any prediction of where the result of the untransformed Hamiltonian would come out. However, when induced three-body forces are taken into account using the NN+3N-induced Hamiltonian, this flow-parameter dependence vanishes, indicating that unitarity of the transformation is already restored by the inclusion of induced three-body interactions. This way a prediction for the bare chiral NN Hamiltonian can be made, but the agreement with experiment is rather poor. Including the initial chiral 3N interaction via the NN+3N-full Hamiltonian still produces results that show no dependence on the flow parameter, and at the same time also significantly improve the agreement with experiment. Therefore, chiral Hamiltonians are capable to provide an accurate description of the ^4He system.

For the heavier nucleus ^{12}C , the situation is similar with the exception of an emerging flow-parameter dependence for the NN+3N-full Hamiltonian. Since for ^{12}C no flow-parameter dependence is observed for the NN+3N-induced Hamiltonian, the NN+3N-full results suggest the existence of sizable four- (or higher-) body interactions out of the initial 3N interaction. At this point, this flow-parameter dependence prevents any attempts of making robust predictions, similar to the NN-only case. In order to restore predictive capabilities for the NN+3N-full Hamiltonian in calculations of medium-mass nuclei, a modified initial chiral 3N interaction will be employed that has a reduced regulator cutoff momentum, as discussed in more detail in Section 5.3.

1.4 Hartree-Fock Method

The fact that nucleons show properties of *non-interacting* Fermions, such as the low density or the long mean free path of the nucleons within the nucleus [78], suggests the applicability of *independent-particle* methods such as the *Hartree-Fock* method that is widely used in many-body theory, such as atomic and nuclear physics, or quantum chemistry [78,90].

In the Hartree-Fock method the nuclear interaction is not neglected but replaced by a mean-field potential that is generated by the nucleons and in which they are assumed to move independently. The independent-particle picture allows to approximate the many-body wavefunction by a single Slater determinant, which is then determined by minimizing its energy expectation value according to the variational principle. This is achieved by optimizing the single-particle orbitals from which the Slater determinant is built. These orbitals have to be determined in a self-consistent manner because the orbitals determine the mean-field the nucleons feel, which in turn determines the orbitals in which the nucleons move.

The Hartree-Fock method typically serves two purposes: On the one hand, it is used as an approximate many-body method that provides the best approximation to a many-body wavefunction from the set of single Slater determinants. On the other hand, it provides a set of optimized single-particle orbitals, which can subsequently be used as starting point for a more sophisticated many-body method such as Coupled Cluster. The latter is the main purpose of the Hartree-Fock method in this work. Most of the time, the single-particle orbitals used in the

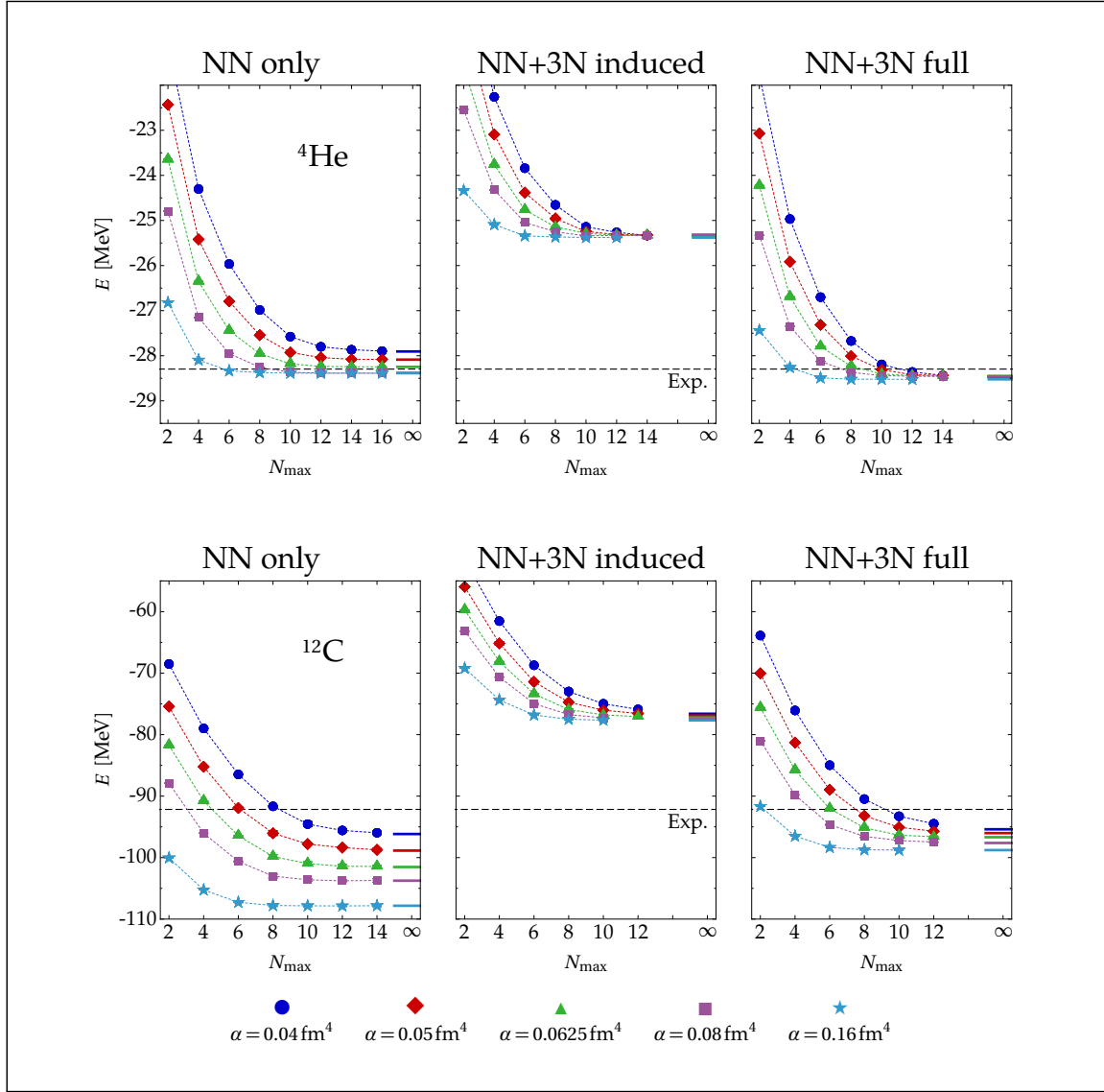


Figure 1.4: IT-NCSM ground-state energies for ${}^4\text{He}$ and ${}^{12}\text{C}$ for the NN-only, NN+3N-induced, and NN+3N-full Hamiltonian for a sequence of SRG flow parameters [17]. Both nuclei the energies show no flow-parameter dependence for the NN+3N induced Hamiltonian, indicating no relevant induced four- or higher-body interactions out of the initial NN interaction. The flow-parameter dependence for the NN+3N-full Hamiltonian in ${}^{12}\text{C}$ suggests the emergence of significant induced higher-body interactions out of the initial 3N interaction.

normal-ordering and Coupled-Cluster calculations have been determined from a preceding Hartree-Fock calculation.

The Hartree-Fock method is well covered in the literature, a standard treatment of this matter can be found in [33, 78, 90], and the extension to incorporate three-body Hamiltonians is discussed in [91].

1.5 Normal-Ordering Approximation

As already discussed in the previous section, for accurate *ab initio* nuclear-structure calculations the inclusion of three-body interactions is mandatory [17, 29, 30, 70, 92, 93]. Along with it comes an array of formal and technical difficulties, such as the increased complexity of the equations to be solved, or the treatment of intractably large Hamiltonian matrix representations. On the other hand, *ab initio* calculations using only two-body Hamiltonians are a standard practice and do not suffer from one of the aforementioned problems. Therefore, the construction of effective lower-rank interactions that approximate the original three-body interaction represents an economic way to include three-body effects in nuclear-structure calculations using the standard two-body Hamiltonian framework.

The effective lower-rank interaction used in this work is obtained from the normal-ordered two-body approximation [63, 92]. The idea behind this approximation is based on the observation that when a three-body operator \hat{h}_3 that is given in normal order with respect to the vacuum ³,

$$\hat{h}_3 = \frac{1}{36} \sum_{pqrstu} \langle pqr | \hat{h}_3 | stu \rangle \hat{a}_p^\dagger \hat{a}_q^\dagger \hat{a}_r^\dagger \hat{a}_u \hat{a}_t \hat{a}_s, \quad (1.35)$$

is represented in normal order with respect to some single-determinant *A*-body reference state $|\Phi\rangle$, the resulting operator has non-vanishing components also at

³The vacuum $|0\rangle$ is understood as the state containing no nucleons such that $\hat{a}_p|0\rangle = 0$.

lower particle ranks,

$$\begin{aligned}
 \hat{h}_3 = & \frac{1}{6} \sum_{ijk} \langle ijk | \hat{h}_3 | ijk \rangle \\
 & + \frac{1}{2} \sum_{pqij} \langle ijp | \hat{h}_3 | ijq \rangle \{ \hat{a}_p^\dagger \hat{a}_q \} \\
 & + \frac{1}{4} \sum_{pqrsi} \langle pqi | \hat{h}_3 | rsi \rangle \{ \hat{a}_p^\dagger \hat{a}_q^\dagger \hat{a}_s \hat{a}_r \} \\
 & + \frac{1}{36} \sum_{pqrstu} \langle pqr | \hat{h}_3 | stu \rangle \{ \hat{a}_p^\dagger \hat{a}_q^\dagger \hat{a}_r^\dagger \hat{a}_u \hat{a}_t \hat{a}_s \} .
 \end{aligned} \tag{1.36}$$

Here, i, j, k denote orbitals occupied in $|\Phi\rangle$ and $\{\dots\}$ indicates normal ordering with respect to $|\Phi\rangle$. Since some contributions of the original three-body operator have been demoted to lower particle ranks, the residual three-body interaction operator

$$\frac{1}{36} \sum_{pqrstu} \langle pqr | \hat{h}_3 | stu \rangle \{ \hat{a}_p^\dagger \hat{a}_q^\dagger \hat{a}_r^\dagger \hat{a}_u \hat{a}_t \hat{a}_s \} \tag{1.37}$$

in (1.36) may be discarded, and yet still allowing to include three-body interaction effects in a computational framework capable of handling at most two-body Hamiltonians. This particular scheme, in which the residual three-body operator is discarded and the remaining zero-, one-, and two-body parts are included in the calculation, is referred to as normal-ordered two-body approximation (NO2B) [63, 92], or normal-ordering approximation for short. Back in the particle-vacuum representation, the three-body operator \hat{h}_3 in NO2B approximation then reads [94]⁴

$$\hat{h}_3^{\text{NO2B}} = \frac{1}{6} w_0 - \frac{1}{2} \sum_{pq} \langle p | \hat{w}_1 | q \rangle \hat{a}_p^\dagger \hat{a}_q + \frac{1}{4} \sum_{pqrs} \langle pq | \hat{w}_2 | rs \rangle \hat{a}_p^\dagger \hat{a}_q^\dagger \hat{a}_s \hat{a}_r , \tag{1.38}$$

with definitions of the matrix elements of the normal-ordered interaction operators

$$w_0 = \sum_{ijk} \langle ijk | \hat{h}_3 | ijk \rangle , \tag{1.39}$$

$$\langle p | \hat{w}_1 | q \rangle = \sum_{ij} \langle ijp | \hat{h}_3 | ijq \rangle , \tag{1.40}$$

⁴The negative sign in front of the one-body part is intended, see [94].

and

$$\langle pq|\hat{w}_2|rs\rangle = \sum_i \langle pqi|\hat{h}_3|rsi\rangle. \quad (1.41)$$

A systematic study of the NO2B approximation using the IT-NCSM was performed in [92] from which Figure 1.5 is taken. Results obtained from the NO2B provide a good approximation to the ones obtained using explicit three-body Hamiltonians, with deviations of about 2% for the case of ^4He and about 1% for ^{16}O . Together with results for ^{40}Ca , the conclusion can be drawn that the NO2B approximation works particularly well for heavier nuclei. This is also confirmed by Coupled-Cluster calculations for medium-mass nuclei [95, 96] in Section 5.7 and 5.8.1.

Coupled-Cluster calculations usually employ a Hartree-Fock basis. The transformation from the spherical harmonic-oscillator single-particle basis into the Hartree-Fock basis reads

$$|p m_{t_p}\rangle^{(\text{HF})} = \sum_{\alpha} C_{p m_{t_p}}^{\alpha} |\alpha m_{t_p}\rangle, \quad (1.42)$$

where $p = \{n_p(l_p s_p)j_p\}$ is a shorthand notation for the set of all quantum numbers except isospin, and the isospin $t_p = 1/2$ will mostly be suppressed. Therefore, the Hartree-Fock reference state $|\Phi\rangle$ is given by a superposition of Slater determinants built from harmonic-oscillator single-particle states,

$$\begin{aligned} |\Phi\rangle &= \hat{\mathcal{A}} |i m_{t_i}\rangle^{(\text{HF})} \otimes \dots \otimes |k m_{t_k}\rangle^{(\text{HF})} \\ &= \sum_{\alpha} \dots \sum_{\gamma} C_{i m_{t_i}}^{\alpha} \dots C_{k m_{t_k}}^{\gamma} |\alpha m_{t_i} \dots \gamma m_{t_k}\rangle. \end{aligned} \quad (1.43)$$

Using angular-momentum coupled three-body matrix elements, the zero-body result of the normal-ordering with respect to the Hartree-Fock reference state is given by

$$\begin{aligned} w_0 &= \sum_{i m_{t_i}} \sum_{j m_{t_j}} \sum_{k m_{t_k}} \sum_{\alpha} \sum_{\beta} \sum_{\gamma} \sum_{\delta} \sum_{\epsilon} \sum_{\kappa} \sum_{J \mathcal{J}} \mathcal{J}^2 \\ &\times C_{i m_{t_i}}^{\alpha} C_{j m_{t_j}}^{\beta} C_{k m_{t_k}}^{\gamma} C_{i m_{t_i}}^{\delta} C_{j m_{t_j}}^{\epsilon} C_{k m_{t_k}}^{\kappa} \\ &\quad \begin{array}{c} \mathcal{J} \mathcal{M} \\ \downarrow \downarrow \\ J \end{array} \quad \begin{array}{c} \mathcal{J} \mathcal{M} \\ \downarrow \downarrow \\ J \end{array} \\ &\times \langle \alpha \beta \gamma, m_{t_i} m_{t_j} m_{t_k} | \hat{h}_3 | \delta \epsilon \kappa, m_{t_i} m_{t_j} m_{t_k} \rangle, \end{aligned} \quad (1.44)$$

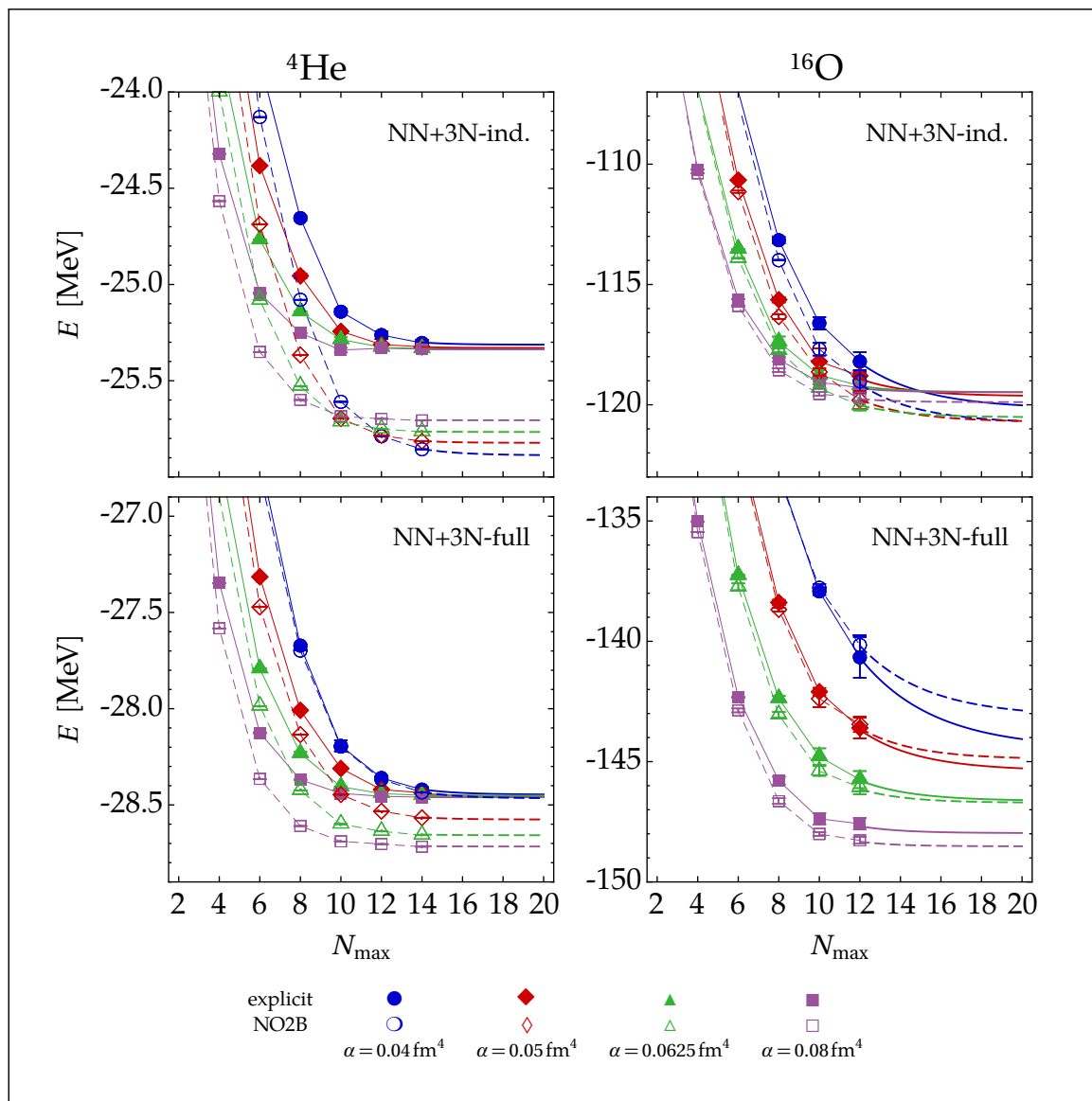


Figure 1.5: Comparison of IT-NCSM ground-state energies of ${}^4\text{He}$ and ${}^{16}\text{O}$ for the SRG-evolved NN+3N induced and NN+3N full Hamiltonians using explicit 3N interactions and the NO2B approximation [92]. The calculations employed a HO basis with oscillator frequency $\hbar\Omega = 20$ MeV.

where here and in the following the summations

$$\sum_{im_{t_i}}, \sum_{jm_{t_j}}, \text{ and } \sum_{km_{t_k}} \quad (1.45)$$

are understood to run only over orbitals $|im_{t_i}\rangle$, $|jm_{t_j}\rangle$, and $|km_{t_k}\rangle$ that are occupied in the reference state $|\Phi\rangle$. The one-body contribution reads

$$\begin{aligned} \langle pm_p m_{t_p} | \hat{w}_1 | qm_q m_{t_q} \rangle &= \hat{p}^{-2} \sum_{im_{t_i}} \sum_{jm_{t_j}} \sum_{\alpha} \sum_{\beta} \sum_{\gamma} \sum_{\delta} \sum_{J\mathcal{J}} \hat{\mathcal{J}}^2 \\ &\times C_{im_{t_i}}^{\alpha} C_{jm_{t_j}}^{\beta} C_{im_{t_i}}^{\gamma} C_{jm_{t_j}}^{\delta} \\ &\times \langle \alpha\beta p, m_{t_i} m_{t_j} m_{t_p} | \hat{h}_3 | \gamma\delta q, m_{t_i} m_{t_j} m_{t_q} \rangle, \end{aligned} \quad (1.46)$$

and the normal-ordered two-body matrix elements are given by

$$\begin{aligned} \langle pq, t_p t_q | \hat{w}_2 | rs, t_r t_s \rangle &= \hat{f}^{-2} \sum_{im_{t_i}} \sum_{\alpha} \sum_{\beta} \sum_{J\mathcal{J}} \hat{\mathcal{J}}^2 \\ &\times C_{im_{t_i}}^{\alpha} C_{im_{t_i}}^{\beta} \langle pq\alpha, t_p t_q m_{t_i} | \hat{h}_3 | rs\beta, t_r t_s m_{t_i} \rangle. \end{aligned} \quad (1.47)$$

The normal-ordered one- and two-body matrix elements – as given above – are still given in the harmonic-oscillator basis and, therefore, need to be transformed to the HF basis after the normal ordering.

1.6 Configuration Interaction and No-Core Shell Model

The *No-Core Shell Model* (NCSM) [21, 51, 54] is an *ab initio* approach to the nuclear many-body problem. All A nucleons are considered active, i.e., no degrees of freedom of the system are combined into effective ones as it is for example done in the traditional single-particle shell model. The nuclear wavefunction is expanded in a set of Slater determinant basis functions, where the expansion coefficients are obtained from a large-scale Hamiltonian matrix diagonalization. The method is

fully variational and yields the *exact* solution for the model space under consideration. Therefore, this method always provides an upper bound for the ground-state energy and, once convergence is reached with respect to model space size, constitutes an ideal tool against which other many-body methods may be benchmarked.

The NCSM belongs to the class of the *Configuration Interaction* (CI) methods. Since the CI methods and its common truncated variants CISD, CISDT etc. (see Section 1.6.2) also share more formal analogies than the NCSM with the Coupled-Cluster method, it is worthwhile to briefly review these methods as well and to introduce basic conventions and notations.

1.6.1 Full Configuration Interaction

In the CI scheme, the continuous Hamiltonian eigenproblem is Galerkin-discretized and converted into a finite-dimensional approximation scheme by introducing a finite set Λ_{SP} of discrete single-particle basis functions $|\phi_k\rangle$ ⁵

$$\Lambda_{\text{SP}} = \left\{ |\phi_k\rangle : k = 1, \dots, \dim \Lambda_{\text{SP}} \right\}. \quad (1.48)$$

As discussed in Section 1.1, a common choice for these single-particle basis functions are the harmonic-oscillator wavefunctions $|n_k(l_k s_k) j_k m_{j_k} t_k m_{t_k}\rangle$ (or linear combinations of these, if canonical orbitals obtained from the Hartree-Fock method are used). For the purpose of deriving appropriate truncation schemes for the many-body basis it is important to note that to each single-particle basis state $|\phi_k\rangle$ a quantum number e_k may be assigned, which characterizes the *energy of the single-particle state* $|\phi_k\rangle$, and is defined by

$$e_k = 2n_k + l_k. \quad (1.49)$$

For the *Full Configuration Interaction* (FCI) method, the constraint in the total number of single-particle states, $\dim \Lambda_{\text{SP}} < \infty$, is the only truncation for the model space that is introduced. Consequently, the FCI many-body basis Λ_{FCI} consists of all Slater determinants constructed from the single-particle basis set Λ_{SP} , which are not equivalent in the sense that they only differ by single-particle index permutations. So the many-body basis may be constructed as

$$\Lambda^{(\text{FCI})} = \left\{ |\Phi_k\rangle = \mathcal{A}|\phi_{k_1} \dots \phi_{k_A}\rangle : k_1 < \dots < k_A = 1, \dots, \dim \Lambda_{\text{SP}} \right\}, \quad (1.50)$$

⁵The single-particle basis is assumed to be orthonormal throughout this work.

with \mathcal{A} being the antisymmetrization operator (1.8), and the FCI model space $\mathcal{V}^{(\text{FCI})}$ is then given by

$$\mathcal{V}^{(\text{FCI})} = \text{span}\{ \Lambda^{(\text{FCI})} \}. \quad (1.51)$$

For this model space the matrix representation (H_{kl}) of the Rayleigh-Ritz projection of the Hamiltonian is calculated,

$$H_{kl} = \langle \Phi_k | \hat{H} | \Phi_l \rangle, \quad (1.52)$$

from which, via diagonalization, the expansion of the Hamiltonian eigenstates in the basis $\Lambda^{(\text{FCI})}$ may be obtained,

$$\sum_l H_{kl} C_l = E C_k \Rightarrow |\Phi^{(\text{FCI})}\rangle = \sum_k C_k |\Phi_k\rangle. \quad (1.53)$$

Since the Hamilton matrix (H_{kl}) is obtained from orthogonal projection techniques it is guaranteed that the FCI wavefunction $|\Psi^{(\text{FCI})}\rangle$ is the best approximation to the exact wavefunction that, in the sense of residual minimization, can be computed from the model space $\mathcal{V}^{(\text{FCI})}$. This is also the reason why the FCI method is fully variational. The main limitation of the method is due to the rapid growth of the many-body basis which goes as

$$\dim \mathcal{V}^{(\text{FCI})} = \frac{(\dim \Lambda_{\text{SP}})!}{A! (\dim \Lambda_{\text{SP}} - A)!}, \quad (1.54)$$

and, thus, is scaling factorially with particle number A and single-particle basis size $\dim \Lambda_{\text{SP}}$.

Regarding truncations of the FCI scheme, it is common practice to introduce a parametrization of the FCI wavefunction using the concept of the reference state and corresponding excitation operators. The reference state

$$|\Phi\rangle = \mathcal{A} |\phi_{i_1} \dots \phi_{i_A}\rangle \quad (1.55)$$

is a single Slater determinant build from the set of single-particle orbitals $\{\phi_{i_1}\}$ that minimize the energy functional

$$E_{\text{ref}} [\{\phi_{i_1}, \dots, \phi_{i_A}\}] = \min_{i_1 < \dots < i_A} \{ e_{i_1} + \dots + e_{i_A} \}, \quad (1.56)$$

with the constraint that the index set $\{i_1, \dots, i_A\}$ has of course the correct number of proton and neutron states for the nucleus under consideration. The reference state may, therefore, serve as zero-order approximation to the wavefunction with

corresponding zero-order energy E_{ref} . Once the reference state is determined, the single-particle basis index set is divided into the orbitals occupied by the reference state (referred to as *hole states*) and the unoccupied (*particle*) states, with the following notational convention :

$$\begin{aligned} \text{hole states} & : i, j, k, \dots \in \text{occupied in } |\Phi\rangle \\ \text{particle states} & : a, b, c, \dots \in \text{unoccupied in } |\Phi\rangle \\ \text{any state} & : p, q, r, \dots \end{aligned} \quad (1.57)$$

The n -particle- n -hole ($npnh$) excitation $|\Phi_{i_1 \dots i_n}^{a_1 \dots a_n}\rangle$ of the reference determinant is defined as the Slater determinant in which, relative to the reference state, n hole states have been replaced by n particle states, i.e.,

$$\begin{aligned} |\Phi_{i_1 \dots i_n}^{a_1 \dots a_n}\rangle & = (\hat{a}_{a_1}^\dagger \hat{a}_{i_1})(\hat{a}_{a_2}^\dagger \hat{a}_{i_2}) \dots (\hat{a}_{a_n}^\dagger \hat{a}_{i_n}) |\Phi\rangle \\ & = \hat{a}_{a_1}^\dagger \dots \hat{a}_{a_n}^\dagger \hat{a}_{i_n} \dots \hat{a}_{i_1} |\Phi\rangle, \end{aligned} \quad (1.58)$$

and the corresponding $npnh$ excitation operator generating all possible $npnh$ excitations reads

$$\hat{C}_n = \frac{1}{(n!)^2} \sum_{\substack{i_1, \dots, i_n \\ a_1, \dots, a_n}} c_{i_1 \dots i_n}^{a_1 \dots a_n} \hat{a}_{a_1}^\dagger \dots \hat{a}_{a_n}^\dagger \hat{a}_{i_n} \dots \hat{a}_{i_1}. \quad (1.59)$$

In terms of excitation operators (1.59), the FCI wavefunction can be parametrized by the linear Ansatz

$$|\Psi^{(\text{FCI})}\rangle = (\hat{\mathbb{1}} + \hat{C}^{(\text{FCI})}) |\Phi\rangle, \quad \hat{C}^{(\text{FCI})} = \sum_{n=1}^A \hat{C}_n^{(\text{FCI})}. \quad (1.60)$$

Since $\hat{C}_m^{(\text{FCI})}|\Phi\rangle$ vanishes for excitation ranks $m > A$, the FCI wave operator \hat{C} naturally terminates at the $A_p A_h$ level.

1.6.2 Truncated Configuration Interaction

A natural way to truncate the full CI Ansatz (1.60) is to truncate the excitation level $X(\hat{C}^{(\text{FCI})})$ of the FCI wave operator at some value M , i.e., $X(\hat{C}^{(\text{CIM})}) = M < A$. The corresponding truncated CI variant is then referred to as CIM, or as *CI with Singles and Doubles excitations* (CISD) for $M = 2$, as *CI with Singles, Doubles and Triples excitations* (CISDT) for $M = 3$, and so on. This truncation is justified by the expectation that in the expansion (1.60) higher excitation ranks are less relevant

than lower ones, provided that the reference state is sufficiently close to $|\Psi^{(\text{FCI})}\rangle$. Therefore, using the CIM Ansatz the Schrödinger equation reads

$$\hat{H} \left(\hat{1} + \sum_{n=1}^M \hat{C}_n^{(\text{CIM})} \right) |\Phi\rangle = E^{(\text{CIM})} \left(\hat{1} + \sum_{n=1}^M \hat{C}_n^{(\text{CIM})} \right) |\Phi\rangle. \quad (1.61)$$

In analogy to the Coupled-Cluster method, a set of coupled equations for the energy $E^{(\text{CIM})}$ and the amplitudes $c_{i_1 \dots i_k}^{a_1 \dots a_k}$ can be obtained by left-projecting the CIM Schrödinger equation (1.61) onto the reference $|\Phi\rangle$ and excited determinants $|\Phi_{i_1 \dots i_k}^{a_1 \dots a_k}\rangle$,

$$\left\{ \begin{array}{l} \langle \Phi | \hat{H} \left(\hat{1} + \sum_{n=1}^M \hat{C}_n^{(\text{CIM})} \right) | \Phi \rangle = E^{(\text{CIM})} \\ \langle \Phi_{i_1}^{a_1} | \hat{H} \left(\hat{1} + \sum_{n=1}^M \hat{C}_n^{(\text{CIM})} \right) | \Phi \rangle = E^{(\text{CIM})} c_{i_1}^{a_1}, \quad \forall a_1, i_1 \\ \vdots \\ \langle \Phi_{i_1 \dots i_M}^{a_1 \dots a_M} | \hat{H} \left(\hat{1} + \sum_{n=1}^M \hat{C}_n^{(\text{CIM})} \right) | \Phi \rangle = E^{(\text{CIM})} c_{i_1 \dots i_M}^{a_1 \dots a_M}, \quad \forall a_1, \dots, i_M. \end{array} \right. \quad (1.62)$$

It is noteworthy that in a specific line of (1.62) not all excitation ranks of $\hat{C}^{(\text{CIM})}$ contribute, because

$$\langle \Phi_{i_1 \dots i_k}^{a_1 \dots a_k} | \hat{H} \left(\hat{1} + \sum_{n=1}^M \hat{C}_n^{(\text{CIM})} \right) | \Phi \rangle = \langle \Phi_{i_1 \dots i_k}^{a_1 \dots a_k} | \hat{H} \left(\hat{1} + \sum_{n=n_{\min}}^{n_{\max}} \hat{C}_n^{(\text{CIM})} \right) | \Phi \rangle, \quad (1.63)$$

with

$$n_{\min} = \max \{ 1, k - X(\hat{H}) \} \quad (1.64)$$

$$n_{\max} = \min \{ M, k + X(\hat{H}) \}. \quad (1.65)$$

Particularly, the energy has an explicit dependence on the $\hat{C}^{(\text{CIM})}$ coefficients of the form

$$E^{(\text{CIM})} = E^{(\text{CIM})} \left(\{ c_{i_1}^{a_1} \}, \dots, \{ c_{i_1 \dots i_{X(\hat{H})}}^{a_1 \dots a_{X(\hat{H})}} \} \right), \quad (1.66)$$

while, due to the coupled nature of (1.62), there is of course an implicit dependence on all coefficients. From a physical point of view, the presence of the CI energy in the *truncated* CI amplitude equations is troubling. This is because, for the truncated CI case, an unequal scaling of both sides of the amplitude equations is introduced as the number of particles in the system is increased. The energy and

the CIM coefficients scale differently, leading to violation of *size extensivity* [25]. In quantum-chemistry applications, this violation of size extensivity of the truncated CI method poses a serious problem which makes the size-extensivity preserving Coupled-Cluster method more favorable there.

1.6.3 No-Core Shell Model

An alternative truncation of the FCI parametrization which aims not at excitation *rank* but rather on excitation *energy* is employed by the *No-Core Shell Model* (NCSM). If the *excitation energy* of a Slater determinant relative to the unperturbed reference state is defined by

$$e_{i_1 \dots i_n}^{a_1 \dots a_n} \equiv \sum_{k=1}^n (e_{a_k} - e_{i_k}) , \quad (1.67)$$

then the NCSM again uses a linear parametrization of the wavefunction similar to the FCI parametrization,

$$|\Psi^{(\text{NCSM})}\rangle = \left(\hat{1} + \sum_{n=1}^A \hat{C}_n^{(\text{NCSM})} \right) |\Phi\rangle , \quad (1.68)$$

with excitation operators $\hat{C}_n^{(\text{NCSM})}$

$$\hat{C}_n^{(\text{NCSM})} = \frac{1}{(n!)^2} \sum'_{\substack{i_1 \dots i_n \\ a_1 \dots a_n}} c_{i_1 \dots i_n}^{a_1 \dots a_n} \hat{a}_{a_1}^\dagger \dots \hat{a}_{a_n}^\dagger \hat{a}_{i_n} \dots \hat{a}_{i_1} \quad (1.69)$$

where the summations

$$\sum'_{\substack{i_1 \dots i_n \\ a_1 \dots a_n}} \quad (1.70)$$

are constrained to maximum excitation energies, generated by the operator string $\hat{a}_{a_1}^\dagger \dots \hat{a}_{a_n}^\dagger \hat{a}_{i_n} \dots \hat{a}_{i_1}$ acting on the reference state, according to

$$e_{i_1 \dots i_n}^{a_1 \dots a_n} \leq N_{\max} . \quad (1.71)$$

This N_{\max} truncation is of particular significance in NCSM calculations using a harmonic-oscillator basis, since despite of the use of single-particle coordinates this truncation allows for any choice of N_{\max} an exact factorization of the NCSM wavefunction into a center-of-mass and a relative part [97],

$$|\Psi^{(\text{NCSM})}\rangle = |\Psi_{\text{int}}\rangle \otimes |\Psi_{\text{CM}}\rangle , \quad (1.72)$$

and, therefore, avoiding mixing center-of-mass and intrinsic excitations. This is the reason why the harmonic-oscillator basis, although exhibiting an undesired asymptotic behavior [98], is commonly preferred over other basis sets.

1.6.4 Importance-Truncated No-Core Shell Model

Despite its heavy use and long history of success in nuclear structure calculations, the NCSM becomes intractable for nuclei beyond ^{16}O , even on massively parallel computational architectures. This is because the NCSM requires unmanageably large N_{max} -parametrized model spaces in order to obtain model-space converged results. A more sophisticated truncation scheme is introduced by the *Importance-Truncated No-Core Shell Model* (IT-NCSM) [20, 21].

The IT-NCSM is motivated by the observation that many of the basis states of a NCSM model space do not significantly contribute to the expansion of a specific wavefunction. Therefore, an *a priori* criterion is introduced that estimates the importance of specific basis states for the expansion of some eigenstate $|\Psi\rangle$. This way only the most relevant basis states can be selectively incorporated in the many-body basis, allowing to go to larger values of N_{max} than would be accessible in the standard NCSM.

In order to do so, a small *reference space* \mathcal{V}_{ref} (typically a full NCSM model space with small N_{max}) is specified from which a first approximation, the *reference state* $|\Psi_{\text{ref}}\rangle$ (not to be confused with the reference state $|\Phi\rangle$, which does not enter the considerations in this section), is calculated,

$$\hat{H}_{|\mathcal{V}_{\text{ref}}}\ |\Psi_{\text{ref}}\rangle = \epsilon_{\text{ref}}\ |\Psi_{\text{ref}}\rangle. \quad (1.73)$$

With this information at hand, the importance κ_{μ} of a basis state $|\Phi_{\mu}\rangle \notin \Lambda_{\text{ref}}$ outside the reference space can be estimated from perturbation theory in first order as

$$\kappa_{\mu} = -\frac{\langle \Phi_{\mu} | \hat{H} | \Psi_{\text{ref}} \rangle}{\epsilon_{\mu} - \epsilon_{\text{ref}}} \quad (1.74)$$

(a detailed review can be found in [21]). Obviously, regarding preserving translational invariance, $|\Phi_{\mu}\rangle$ are taken from full NCSM model spaces of large enough N_{max} to guarantee $\mathcal{V}_{\text{ref}} \subset \mathcal{V}^{(\text{NCSM})}$. The IT-NCSM model space is consequently defined as the reference space and its extension spanned by all determinants which have an importance measure larger than some fixed κ_{min} ,

$$\mathcal{V}^{(\text{IT-NCSM})} = \text{span}\left\{ |\Phi_{\mu}\rangle \in \mathcal{V}^{(\text{NCSM})} : \kappa_{\mu} \geq \kappa_{\text{min}} \right\}. \quad (1.75)$$

The IT-NCSM is clearly a variational approach, converging to the exact result as κ_{min} goes to zero,

$$|\Psi^{(\text{NCSM})}\rangle = \lim_{\kappa_{\text{min}} \rightarrow 0} |\Psi^{(\text{IT-NCSM})}\rangle, \quad (1.76)$$

as well as all observables computed from the wavefunction which typically show a smooth κ_{\min} -dependence and usually can successfully be extrapolated to the $\kappa_{\min} = 0$ limit.

Chapter 2

Coupled-Cluster Theory

2.1 Introduction

Violation of size extensivity and exponential scaling of the model space have proven to be the main limitations of CI-like methods in quantum-chemistry applications. In the nuclear context the importance of size extensivity has not been established yet but the unfortunate scaling behavior has limited *ab initio* methods to the regime of *p*-shell nuclei anyway. By abandoning the variational principle, however, the Coupled-Cluster method [22–27, 99–103] overcomes these obstacles, being size extensive in all truncation orders and exhibiting a polynomial, rather than exponential, scaling of the model space size. In this and the following sections *two-body Hamiltonians* are considered exclusively. The generalization Coupled-Cluster theory to three-body Hamiltonians is postponed to Chapter 3.

2.2 The Exponential Ansatz

Seeking for alternative ways to solve the many-body Schrödinger equation, instead of focusing on truncations of the linear CI-like scheme, more general, and this *nonlinear*, parametrizations may be considered. Among these, the *exponential Ansatz* for the Coupled-Cluster wavefunction is probably the most powerful known to date,

$$|\Psi\rangle = e^{\hat{T}} |\Phi\rangle, \quad \hat{T} = \sum_{n=1}^A \hat{T}_n, \quad (2.1)$$

where the *cluster operator* \hat{T} is defined in close analogy to the CI case, with components

$$\hat{T}_1 = \bigvee = \frac{1}{(1!)^2} \sum_{ai} t_i^a \{\hat{a}_a^\dagger \hat{a}_i\} \quad (2.2)$$

$$\hat{T}_2 = \bigvee\bigvee = \frac{1}{(2!)^2} \sum_{abij} t_{ij}^{ab} \{\hat{a}_a^\dagger \hat{a}_b^\dagger \hat{a}_j \hat{a}_i\} \quad (2.3)$$

$$\begin{aligned} & \vdots \\ \hat{T}_n &= \bigvee \bigvee \bigvee = \frac{1}{(n!)^2} \sum_{\substack{a_1 \dots a_n \\ i_1 \dots i_n}} t_{i_1 \dots i_n}^{a_1 \dots a_n} \{\hat{a}_{a_1}^\dagger \dots \hat{a}_{a_n}^\dagger \hat{a}_{i_n} \dots \hat{a}_{i_1}\}. \end{aligned} \quad (2.4)$$

As in Eqs. (2.2)-(2.4), regarding the diagrammatic treatment of CC equations, it is customary to work with operators that are in normal order relative to the reference

state, indicated by $\{\dots\}$, where it is understood that all particle creation or hole annihilation operators $\hat{a}_a^\dagger, \hat{a}_i$ are to the left of all particle annihilation or hole creation operators $\hat{a}_a, \hat{a}_i^\dagger$. Then, as for the standard normal-ordering prescription, expectation values of normal-ordered operator products in the reference state, which serves as new vacuum, vanish, for example

$$\langle \Phi | \{\hat{a}_a^\dagger \hat{a}_b^\dagger \hat{a}_j \hat{a}_i\} | \Phi \rangle = \langle \Phi | \Phi_{ij}^{ab} \rangle = 0. \quad (2.5)$$

In the case of pure excitation operators, such as \hat{T}_n , or pure de-excitation operators, the operator string is automatically in normal order with respect to the reference state and the brackets $\{\dots\}$ may be dropped. The Hamiltonian operator is put in normal-ordered form as well. A general two-body Hamiltonian in standard form reads

$$\hat{H} = \hat{h}_0 + \hat{h}_1 + \hat{h}_2 \quad (2.6)$$

$$= h_0 + \sum_{pq} \langle p | \hat{h}_1 | q \rangle \hat{a}_p^\dagger \hat{a}_q + \frac{1}{4} \sum_{pqrs} \langle pq | \hat{h}_2 | rs \rangle \hat{a}_p^\dagger \hat{a}_q^\dagger \hat{a}_s \hat{a}_r, \quad (2.7)$$

where *antisymmetrized two-body matrix elements* $\langle pq | \hat{h}_2 | rs \rangle$ are introduced,

$$\langle pq | \hat{h}_2 | rs \rangle = \langle pq | \hat{h}_2 | rs \rangle - \langle pq | \hat{h}_2 | sr \rangle. \quad (2.8)$$

In normal-ordered form, the operator is given by

$$\begin{aligned} \hat{H} = & h_0 + \sum_i \langle i | \hat{h}_1 | i \rangle + \sum_{pq} \langle p | \hat{h}_1 | q \rangle \{\hat{a}_p^\dagger \hat{a}_q\} + \frac{1}{2} \sum_{ij} \langle ij | \hat{h}_2 | ij \rangle \\ & + \sum_{pqi} \langle pi | \hat{h}_2 | qi \rangle \{\hat{a}_p^\dagger \hat{a}_q\} + \frac{1}{4} \sum_{pqrs} \langle pq | \hat{h}_2 | rs \rangle \{\hat{a}_p^\dagger \hat{a}_q^\dagger \hat{a}_s \hat{a}_r\}, \end{aligned} \quad (2.9)$$

where it is conventional to introduce the reference expectation value $\langle \Phi | \hat{H} | \Phi \rangle$, the one-body *Fock operator* \hat{F}_N , and the two-body interaction operator \hat{V}_N , leading to

$$\hat{H} = \langle \Phi | \hat{H} | \Phi \rangle + \sum_{pq} f_q^p \{\hat{a}_p^\dagger \hat{a}_q\} + \frac{1}{4} \sum_{pqrs} v_{rs}^{pq} \{\hat{a}_p^\dagger \hat{a}_q^\dagger \hat{a}_s \hat{a}_r\} \quad (2.10)$$

$$\equiv \langle \Phi | \hat{H} | \Phi \rangle + \hat{F}_N + \hat{V}_N, \quad (2.11)$$

for which the diagrammatic representations used in this work are shown in Figure 2.1, and whose matrix elements are given by

$$\langle \Phi | \hat{H} | \Phi \rangle = h_0 + \sum_i \langle i | \hat{h}_1 | i \rangle + \frac{1}{2} \sum_{ij} \langle ij | \hat{h}_2 | ij \rangle, \quad (2.12)$$

$$f_q^p \equiv \langle p | \hat{f} | q \rangle = \langle p | \hat{h}_1 | q \rangle + \sum_i \langle pi | \hat{h}_2 | qi \rangle, \quad (2.13)$$

$$v_{rs}^{pq} \equiv \langle pq | \hat{v} | rs \rangle = \langle pq | \hat{h}_2 | rs \rangle. \quad (2.14)$$

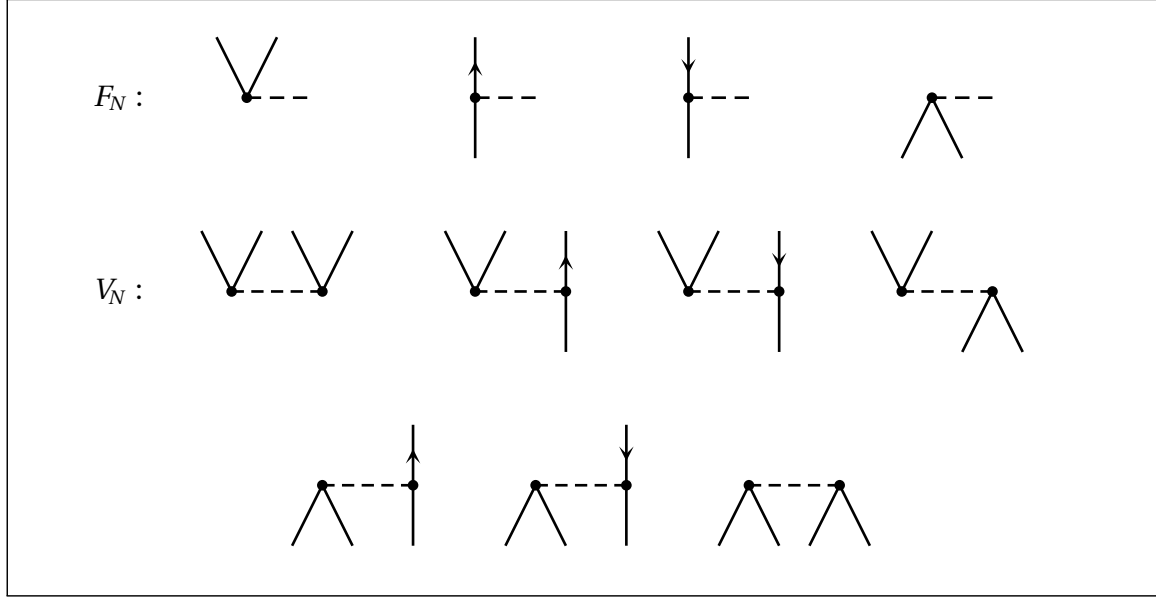


Figure 2.1: Goldstone diagrams representing the Fock operator \hat{F}_N and antisymmetrized Goldstone diagrams for \hat{V}_N that come from distinct corresponding Hugenholtz diagrams.

Anticipating the treatment of three-body Hamiltonians later on, the matrix elements v_{rs}^{pq} are understood as the antisymmetrized matrix elements of the two-body part \hat{V}_N of the *normal-ordered Hamiltonian*, which for two-body Hamiltonians coincide with the ordinary antisymmetrized matrix elements of the two-body Hamiltonian \hat{h}_2 in standard form.

Using the normal-ordered Hamiltonian,

$$\hat{H}_N = \hat{H} - \langle \Phi | \hat{H} | \Phi \rangle, \quad (2.15)$$

and after subtracting the zero-body contribution, the Schrödinger equation can be written in the form

$$\hat{H}_N e^{\hat{T}} |\Phi\rangle = \Delta E e^{\hat{T}} |\Phi\rangle, \quad (2.16)$$

in which the quantity

$$\Delta E \equiv E - \langle \Phi | \hat{H} | \Phi \rangle \quad (2.17)$$

is called the *correlation energy*. Since $\langle \Phi | \hat{H} | \Phi \rangle$ is the expectation value of the Hamiltonian in the reference state, it is also referred to as *reference energy* E_{ref} ,

$$E_{\text{ref}} \equiv \langle \Phi | \hat{H} | \Phi \rangle. \quad (2.18)$$

Clearly, the total energy is then given by the sum of reference and correlation energy. An alternative formulation of (2.16) is obtained by left-multiplication with $e^{-\hat{T}}$, arriving at

$$\mathcal{H} |\Phi\rangle = \Delta E |\Phi\rangle, \quad (2.19)$$

where the (normal-ordered) *Coupled-Cluster effective Hamiltonian* \mathcal{H} is defined as

$$\mathcal{H} \equiv e^{-\hat{T}} \hat{H}_N e^{\hat{T}}. \quad (2.20)$$

The form (2.19) of the Schrödinger equation is of particular importance and will be the starting point for the derivation of the Coupled-Cluster equations. It is convenient since all the complicated exponential structure of the Coupled-Cluster Ansatz is absorbed in \mathcal{H} . By left-multiplication with $e^{-\hat{T}}$ in (2.16), the amplitudes of the cluster operator have been separated from the energy so that the energy will not appear in the amplitude equations. Since it was the presence of the energy in the CI amplitude equations which caused violation of size extensivity there, Coupled-Cluster theory circumvents this problem by introducing the effective Hamiltonian [25].

Since $\hat{T}^\dagger \neq -\hat{T}$, the transformation (2.20) is not unitary, resulting in a non-Hermitean effective Hamiltonian. The transformation is, however, a similarity transformation (which is why (2.19) is also referred to as *similarity transformed Schrödinger equation*) and, therefore, the spectrum of the original Hamiltonian is not altered. But the non-Hermitecity leads to an asymmetric expression for the energy,

$$\langle \Phi | e^{-\hat{T}} \hat{H}_N e^{\hat{T}} | \Phi \rangle = \Delta E, \quad (2.21)$$

which is not subject to variational conditions, causing truncated Coupled-Cluster methods not to give an upper bound for the exact energy, contrary to methods for which the variational principle is fulfilled.

The exponential form (2.1) of the wavefunction is exact in the sense that for the untruncated case it reproduces the Full CI wavefunction. In fact, the CI excitation operators may be expressed by the Coupled-Cluster cluster operators by the one-to-one correspondence

$$\hat{C}_1 = \hat{T}_1 \quad (2.22)$$

$$\hat{C}_2 = \frac{1}{2!} \hat{T}_1^2 + \hat{T}_2 \quad (2.23)$$

$$\hat{C}_3 = \frac{1}{3!} \hat{T}_1^3 + \hat{T}_1 \hat{T}_2 + \hat{T}_3, \quad (2.24)$$

or, for general excitation operators,

$$\hat{C}_n = \sum_{k=1}^n \frac{1}{k!} \sum_{m_1 \dots m_k} \delta_{m_1 + \dots + m_k, n} \prod_{j=1}^k \hat{T}_{m_j}, \quad (2.25)$$

which elucidates the relationship between Coupled Cluster and CI. However, the Coupled-Cluster Ansatz performs differently to CI when the cluster operator is truncated to some excitation rank M ,

$$\hat{T}^{(M)} = \sum_{n=1}^M \hat{T}_n. \quad (2.26)$$

As in the CI case, the corresponding Coupled-Cluster method is called CCM, or for $M = 2$ CCSD, and so on. Due to its nonlinear nature, the Coupled-Cluster Ansatz allows to generate higher-order excitations from products of lower-order excitation operators (Figure 2.2).

The individual importance of the terms in (2.22)-(2.25) may be roughly estimated using simple considerations. For Hartree-Fock bases, the \hat{T}_1 operator is small¹ and, therefore, (2.22) is expected to contribute little. Since \hat{T}_1^2 is even smaller than \hat{T}_1 , the first term in (2.23) will, consequently, also contribute very little, leaving \hat{T}_2 in (2.23) as the dominant term. Analogously, the only term in (2.24) that does not involve \hat{T}_1 is the triples excitations cluster operator \hat{T}_3 , which is expected to be dominant. However, going to higher excitation types $\hat{C}_{4,5,\dots}$, the connected cluster operators $\hat{T}_{4,5,\dots}$ are expected to become less relevant, since they represent a simultaneous correlation of the corresponding number of nucleons. For that reason, \hat{T}_2 is typically already significantly more important than \hat{T}_3 . In summary, for a general excitation operator (2.25), the contributions from \hat{T}_2 and \hat{T}_3 clusters are expected to have most relevance.

2.3 Coupled-Cluster Equations

Analogously to the exact case (2.21), for a given (truncated) CCM methods with

$$\hat{T} \approx \hat{T}^{(M)} = \hat{T}_1 + \hat{T}_2 + \dots + \hat{T}_M, \quad (2.27)$$

the expression for the correlation energy $\Delta E^{(M)} = \Delta E(\mathbf{t}^{(M)})$ as function of the cluster amplitudes

$$\mathbf{t}^{(M)} \equiv \left\{ \left\{ t_i^a \right\}, \left\{ t_{ij}^{ab} \right\}, \dots, \left\{ t_{i_1 \dots i_M}^{a_1 \dots a_M} \right\} \right\}, \quad (2.28)$$

¹Here, an operator is called *small* if its matrix elements have small absolute values.

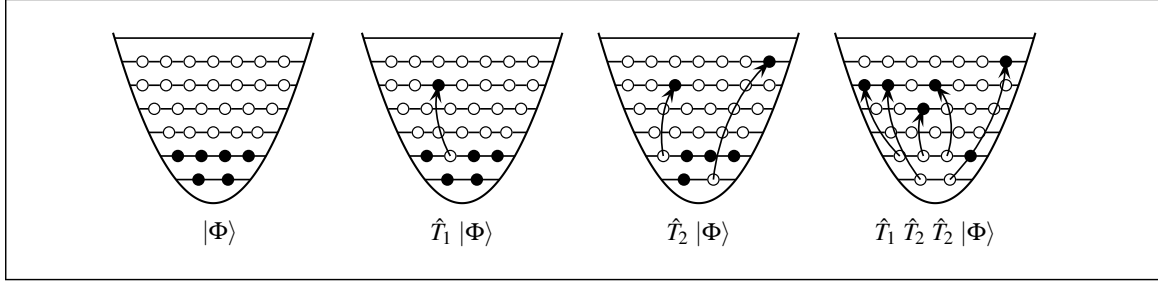


Figure 2.2: Illustration of excitation types in the CC ansatz.

can be derived by left-projecting the similarity-transformed Schrödinger equation

$$\hat{\mathcal{H}}^{(M)} |\Phi\rangle = \Delta E^{(M)} |\Phi\rangle \quad (2.29)$$

with

$$\hat{\mathcal{H}}^{(M)} \equiv e^{-\hat{T}^{(M)}} \hat{H}_N e^{\hat{T}^{(M)}}, \quad (2.30)$$

onto the reference state. In analogy to the CI case, a coupled set of algebraic equations for the determination of the amplitudes $\mathbf{t}^{(M)}$ is obtained by left-projecting the similarity-transformed Schrödinger equation onto the excited determinants $|\Phi_{i_1 \dots i_n}^{a_1 \dots a_n}\rangle$ with $n \leq M$, i.e.,

$$\langle \Phi | \hat{\mathcal{H}}^{(M)} | \Phi \rangle = \Delta E^{(M)} \quad (2.31)$$

$$\langle \Phi_i^a | \hat{\mathcal{H}}^{(M)} | \Phi \rangle = 0, \quad \forall a, i \quad (2.32)$$

$$\langle \Phi_{ij}^{ab} | \hat{\mathcal{H}}^{(M)} | \Phi \rangle = 0, \quad \forall a, b, i, j \quad (2.33)$$

\vdots

$$\langle \Phi_{i_1 \dots i_M}^{a_1 \dots a_M} | \hat{\mathcal{H}}^{(M)} | \Phi \rangle = 0, \quad \forall a_1, \dots, a_M, i_1, \dots, i_M. \quad (2.34)$$

In the case of CCSD, for example, the \hat{T}_1 and \hat{T}_2 amplitudes can be determined by solving the system given by (2.32) and (2.33). Above expressions can be significantly simplified once it is recognized that the expansion of the effective Hamiltonian $\hat{\mathcal{H}}^{(M)}$, containing two exponentials of the cluster operator, actually terminates at finite expansion order. This is due to $\hat{T}^{(M)}$ being an excitation operator, and the

finite expression for $\hat{\mathcal{H}}^{(M)}$ in case of two-body Hamiltonians \hat{H}_N reads ²

$$\begin{aligned}\hat{\mathcal{H}}^{(M)} &= \hat{H}_N + \frac{1}{1!} [\hat{H}_N, \hat{T}^{(M)}] \\ &\quad + \frac{1}{2!} [[\hat{H}_N, \hat{T}^{(M)}], \hat{T}^{(M)}] \\ &\quad + \frac{1}{3!} [[[\hat{H}_N, \hat{T}^{(M)}], \hat{T}^{(M)}], \hat{T}^{(M)}] \\ &\quad + \frac{1}{4!} [[[[\hat{H}_N, \hat{T}^{(M)}], \hat{T}^{(M)}], \hat{T}^{(M)}], \hat{T}^{(M)}] .\end{aligned}\quad (2.35)$$

This commutator expansion of the effective Hamiltonian can be further simplified to the form

$$\hat{\mathcal{H}}^{(M)} = \left(\hat{H}_N e^{\hat{T}^{(M)}} \right)_C , \quad (2.36)$$

where the subscript C restricts the expressions inside the brackets to *connected terms*, where the Hamiltonian has at least one contraction with each cluster operator. Consequently, since a two-body Hamiltonian can be contracted with a maximum number of 4 operators, the expansion of the exponential can be restricted to terms containing not more than 4 cluster operators. Therefore, the most convenient form of the general Coupled-Cluster amplitude equations reads

$$\langle \Phi_{i_1 \dots i_n}^{a_1 \dots a_n} | \left(\hat{H}_N e^{\hat{T}^{(M)}} \right)_C | \Phi \rangle = 0 , \quad n = 1, \dots, M . \quad (2.37)$$

For CCSD [61, 65, 66, 70, 105–114], where the cluster operator is truncated at the singles and doubles excitations,

$$\hat{T}^{(\text{CCSD})} = \hat{T}_1 + \hat{T}_2 , \quad (2.38)$$

the energy and amplitude equations, after expansion of the exponential, are then given by

$$\Delta E^{(\text{CCSD})} = \langle \Phi | \left[\hat{H}_N \left(\hat{T}_1 + \hat{T}_2 + \frac{1}{2!} \hat{T}_1^2 \right) \right]_C | \Phi \rangle \quad (2.39)$$

$$0 = \langle \Phi_i^a | \left[\hat{H}_N \left(1 + \hat{T}_1 + \hat{T}_2 + \frac{1}{2!} \hat{T}_1^2 + \hat{T}_1 \hat{T}_2 + \frac{1}{3!} \hat{T}_1^3 \right) \right]_C | \Phi \rangle \quad (2.40)$$

$$\begin{aligned}0 &= \langle \Phi_{ij}^{ab} | \left[\hat{H}_N \left(1 + \hat{T}_1 + \hat{T}_2 + \frac{1}{2!} \hat{T}_1^2 + \hat{T}_1 \hat{T}_2 \right. \right. \\ &\quad \left. \left. + \frac{1}{2!} \hat{T}_2^2 + \frac{1}{3!} \hat{T}_1^3 + \frac{1}{2!} \hat{T}_1^2 \hat{T}_2 + \frac{1}{4!} \hat{T}_1^4 \right) \right]_C | \Phi \rangle .\end{aligned}\quad (2.41)$$

²Proving the non-terminating form of the commutator expansion is an easy exercise [104]: Setting $\hat{\mathcal{H}}^{(M)} = e^{-\alpha \hat{T}^{(M)}} \hat{H}_N e^{\alpha \hat{T}^{(M)}}$, for the derivate holds $d\hat{\mathcal{H}}^{(M)}/d\alpha = e^{-\alpha \hat{T}^{(M)}} [\hat{H}_N, \hat{T}^{(M)}] e^{\alpha \hat{T}^{(M)}}$ and consequently $d^2 \hat{\mathcal{H}}^{(M)}/d\alpha^2 = e^{-\alpha \hat{T}^{(M)}} [[\hat{H}_N, \hat{T}^{(M)}], \hat{T}^{(M)}] e^{\alpha \hat{T}^{(M)}}$ and so on. Plugging into $\hat{\mathcal{H}}^{(M)} = \sum_n \frac{1}{n!} \alpha^n \left(\frac{d^n \hat{\mathcal{H}}^{(M)}}{d\alpha^n} \right) \Big|_{\alpha=0}$ and setting α to 1 gives the commutator expansion.

$$\begin{aligned}
 & + f_i^{(SA)} + \sum_{ck} f_c^{(SBa)} t_{ik}^{ac} + \frac{1}{2} \sum_{cdk} v_{cd}^{ak} t_{ik}^{cd} - \frac{1}{2} \sum_{ckl} v_{ic}^{kl} t_{kl}^{ac} \\
 & + \sum_c f_c^{(SCa)} t_i^c - \sum_i f_i^{(SCb)} t_k^a + \sum_{ck} v_{ic}^{ak} t_k^c - \frac{1}{2} \sum_{cdkl} v_{cd}^{kl} t_{kl}^{ad} t_i^c \\
 & - \frac{1}{2} \sum_{cdkl} v_{cd}^{kl} t_{il}^{cd} t_k^a + \sum_{cdkl} v_{cd}^{kl} t_{li}^{da} t_k^c - \sum_{ck} f_c^{(SEa)} t_i^c t_k^a \\
 & + \sum_{cdk} v_{cd}^{ak} t_i^c t_k^d - \sum_{ckl} v_{ic}^{kl} t_k^a t_l^c - \sum_{cdkl} v_{cd}^{kl} t_k^a t_i^c t_l^d \\
 & = 0, \forall a, i
 \end{aligned}$$

 Figure 2.3: Algebraic expressions for the CCSD \hat{T}_1 amplitude equations.

Cluster operator products, such as $\frac{1}{4!} \hat{T}_2^4$, have already been left out in (2.39)–(2.41) since their excitation rank is too high for the Hamiltonian to de-excite the resulting determinants to the state the equation is projected on. Therefore, for a Hamiltonian with excitation rank $X(\hat{H})$, in the \hat{T}_n amplitude equation only cluster operator products $\mathcal{P}(\hat{T}^{(M)})$ may appear with excitation ranks $X(\mathcal{P}(\hat{T}^{(M)})) \leq X(\hat{H}_N) + X(\hat{T}_n)$. Evaluating Eqs. (2.39)–(2.41) in terms of matrix elements of the operators involved is a standard task using diagrammatic techniques [25,26]. The diagrams are listed in Appendix C.1, and the corresponding algebraic expressions are given in Figures 2.3 and 2.4. In front of each term the assigned diagram is indicated where the naming convention has been taken from [26]³. This facilitates the identification of the corresponding spherical expression presented later in this work. The expression for the correlation energy reads

$$\Delta E^{(\text{CCSD})} = + \frac{(EA)}{4} \sum_{abij} v_{ab}^{ij} t_{ij}^{ab} + \sum_{ai} f_a^i t_i^a + \frac{(EC)}{2} \sum_{abij} v_{ab}^{ij} t_i^a t_j^b, \quad (2.42)$$

and it is noteworthy that the expression above is also valid for all higher-order Coupled-Cluster methods such as CCSDT, CCSDTQ, etc., provided that two-body Hamiltonians are used. This stems from the obvious fact that it is not possible to form closed diagrams using a two-body interaction and cluster operators beyond \hat{T}_2 . The correlation energy depends on all cluster operator amplitudes, of course, but the $\hat{T}_3, \hat{T}_4, \dots$ amplitudes enter implicitly through the solution of the Coupled-Cluster amplitude equations.

³In Ref. [26], the algebraic expression for (DHa) has an incorrect sign.

$$\begin{aligned}
 & + v_{ij}^{ab} + \hat{P}_{ab} \sum_c f_c^b t_{ij}^{ac} - \hat{P}_{ij} \sum_k f_j^k t_{ik}^{ab} \\
 & + \frac{1}{2} \sum_{cd} v_{cd}^{ab} t_{ij}^{cd} + \frac{1}{2} \sum_k v_{ij}^{kl} t_{kl}^{ab} + \hat{P}_{ab} \hat{P}_{ij} \sum_{ck} v_{cj}^{kb} t_{ik}^{ac} \\
 & + \frac{1}{4} \sum_{cdkl} v_{cd}^{kl} t_{ij}^{cd} t_{kl}^{ab} + \hat{P}_{ij} \sum_{cdkl} v_{cd}^{kl} t_{ik}^{ac} t_{jl}^{bd} \\
 & - \frac{1}{2} \hat{P}_{ij} \sum_{cdkl} v_{cd}^{kl} t_{ik}^{dc} t_{lj}^{ab} - \frac{1}{2} \hat{P}_{ab} \sum_{cdkl} v_{cd}^{kl} t_{lk}^{ac} t_{ij}^{db} \\
 & + \hat{P}_{ij} \sum_c v_{cj}^{ab} t_i^c - \hat{P}_{ab} \sum_k v_{ij}^{kb} t_k^a - \hat{P}_{ij} \sum_{ck} f_c^k t_{kj}^{ab} t_i^c \\
 & - \hat{P}_{ab} \sum_{ck} f_c^k t_{ij}^{cb} t_k^a + \hat{P}_{ab} \hat{P}_{ij} \sum_{cdk} v_{cd}^{ak} t_{kj}^{db} t_i^c \\
 & - \hat{P}_{ab} \hat{P}_{ij} \sum_{ckl} v_{ic}^{kl} t_{lj}^{cb} t_k^a - \frac{1}{2} \hat{P}_{ab} \sum_{cdk} v_{cd}^{kb} t_{ij}^{cd} t_k^a \\
 & + \frac{1}{2} \hat{P}_{ij} \sum_{ckl} v_{cj}^{kl} t_{kl}^{ab} t_i^c + \hat{P}_{ab} \sum_{cdk} v_{cd}^{ka} t_{ij}^{db} t_k^c \\
 & - \hat{P}_{ij} \sum_{ckl} v_{ci}^{kl} t_{lj}^{ab} t_k^c + \sum_{cd} v_{cd}^{ab} t_i^c t_j^d + \sum_{kl} v_{ij}^{kl} t_k^a t_l^b \\
 & - \hat{P}_{ab} \hat{P}_{ij} \sum_{ck} v_{cj}^{kb} t_k^a t_i^c + \frac{1}{2} \sum_{cdkl} v_{cd}^{kl} t_{kl}^{ab} t_i^c t_j^d \\
 & + \frac{1}{2} \sum_{cdkl} v_{cd}^{kl} t_{ij}^{cd} t_k^a t_l^b - \hat{P}_{ab} \hat{P}_{ij} \sum_{cdkl} v_{cd}^{kl} t_{lj}^{db} t_k^a t_i^c \\
 & - \hat{P}_{ij} \sum_{cdkl} v_{cd}^{kl} t_{lj}^{ab} t_k^c t_i^d - \hat{P}_{ab} \sum_{cdkl} v_{cd}^{kl} t_{ij}^{db} t_l^a t_k^c \\
 & - \hat{P}_{ab} \sum_{cdk} v_{cd}^{kb} t_k^a t_i^c t_j^d + \hat{P}_{ij} \sum_{ckl} v_{cj}^{kl} t_k^a t_l^b t_i^c \\
 & + \sum_{cdkl} v_{cd}^{kl} t_k^a t_l^b t_i^c t_j^d = 0, \quad \forall a, b, i, j
 \end{aligned}$$

 Figure 2.4: Algebraic expressions for the CCSD \hat{T}_2 amplitude equations.

The Coupled-Cluster amplitude equations, which are of the form

$$\mathbf{G}(\mathbf{t}) = 0 \quad (2.43)$$

are usually converted into a fixed-point problem

$$\mathbf{I}(\mathbf{t}^{(n)}) = \mathbf{t}^{(n+1)}, \quad \mathbf{I}(\mathbf{t}^*) = \mathbf{t}^*, \quad (2.44)$$

and solved iteratively. A common choice for the iteration scheme is

$$\begin{cases} {}^{(0)}t_{i_1 \dots i_n}^{a_1 \dots a_n} = 0 \\ {}^{(n+1)}t_{i_1 \dots i_n}^{a_1 \dots a_n} = \frac{\langle \Phi_{i_1 \dots i_n}^{a_1 \dots a_n} | (\hat{H}_N e^{\hat{T}})_C(\mathbf{t}^{(n)}) | \Phi \rangle}{f_{i_1}^{i_1} + \dots + f_{i_n}^{i_n} - f_{a_1}^{a_1} - \dots - f_{a_n}^{a_n}}, \quad \hat{F}_N \rightarrow \hat{F}_N^o, \end{cases} \quad (2.45)$$

where in the amplitude equations the Fock operator \hat{F}_N is replaced by its off-diagonal \hat{F}_N^o part [26]. An alternative iteration scheme that leads to more stable iterations is considered in Section 4.8.

2.4 Effective Hamiltonian

Once the CCSD amplitude equations have been solved, the effective Hamiltonian

$$\hat{\mathcal{H}}^{(\text{CCSD})} = e^{-\hat{T}^{(\text{CCSD})}} \hat{H}_N e^{\hat{T}^{(\text{CCSD})}} \quad (2.46)$$

may be constructed explicitly from the cluster amplitudes $\mathbf{t}^{(\text{CCSD})}$. Recalling the commutator expansion of the effective Hamiltonian (2.20), it is apparent that the CCSD effective Hamiltonian $\hat{\mathcal{H}}^{(\text{CCSD})}$ will contain up to six-body operator terms,

$$\hat{\mathcal{H}}^{(\text{CCSD})} = \hat{\mathcal{H}}_0 + \hat{\mathcal{H}}_1 + \hat{\mathcal{H}}_2 + \hat{\mathcal{H}}_3 + \hat{\mathcal{H}}_4 + \hat{\mathcal{H}}_5 + \hat{\mathcal{H}}_6, \quad (2.47)$$

which are generated by the four-fold commutator (2.35). Since each $\hat{\mathcal{H}}_k$ is assumed to be in normal-ordered form, $\hat{\mathcal{H}}^{(\text{CCSD})}$ can directly be written as

$$\begin{aligned} \hat{\mathcal{H}}^{(\text{CCSD})} &= \hat{\mathcal{H}}_0 + \sum_{pq} \hat{\mathcal{H}}_q^p \{ \hat{a}_p^\dagger \hat{a}_q \} + \frac{1}{4} \sum_{pqrs} \hat{\mathcal{H}}_{rs}^{pq} \{ \hat{a}_p^\dagger \hat{a}_q^\dagger \hat{a}_s \hat{a}_r \} \\ &\quad + \frac{1}{36} \sum_{pqrst u} \hat{\mathcal{H}}_{stu}^{pqr} \{ \hat{a}_p^\dagger \hat{a}_q^\dagger \hat{a}_r^\dagger \hat{a}_u \hat{a}_t \hat{a}_s \} + \dots, \\ &\equiv \hat{\mathcal{H}}_0 + \hat{\mathcal{H}}_{\text{open}}, \end{aligned} \quad (2.48)$$

again employing the short-hand notation

$$\hat{\mathcal{H}}_{q_1 \dots q_n}^{p_1 \dots p_n} \equiv \langle p_1 \dots p_n | \hat{\mathcal{H}}_n | q_1 \dots q_n \rangle \quad (2.49)$$

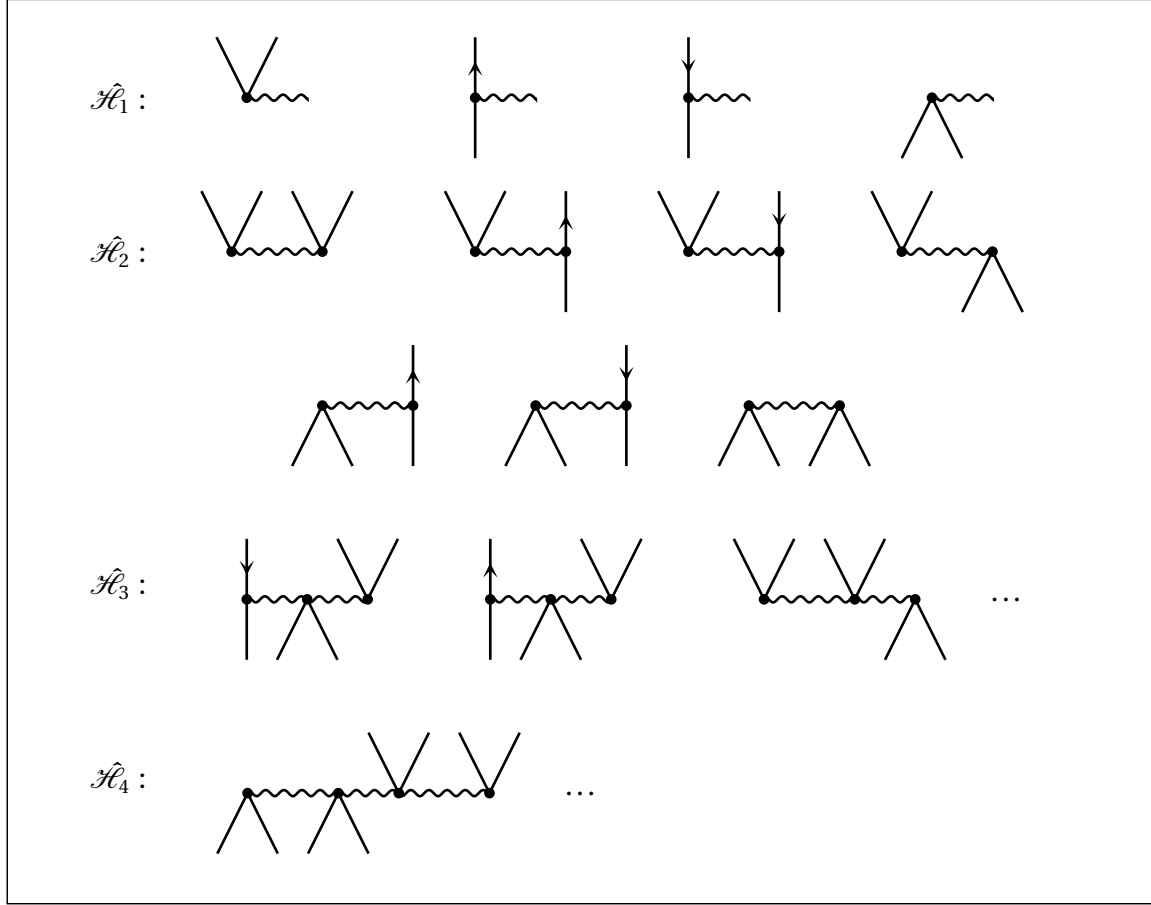


Figure 2.5: Antisymmetrized Goldstone diagrams for $\hat{\mathcal{H}}_1$ and $\hat{\mathcal{H}}_2$ as well as selected $\hat{\mathcal{H}}_3$ and $\hat{\mathcal{H}}_4$ diagrams that arise from distinct corresponding Hugenholtz diagrams.

for antisymmetrized matrix elements, and where $\hat{\mathcal{H}}_{\text{open}}$ denotes the part of the effective Hamiltonian with open Fermion lines, as opposed to the closed effective Hamiltonian diagrams \mathcal{H}_0 . It should be noted that the non-Hermiticity of the effective Hamiltonian implies that

$$\mathcal{H}_{rs\dots}^{pq\dots} \neq \left(\mathcal{H}_{pq\dots}^{rs\dots} \right)^* . \quad (2.50)$$

For the Coupled-Cluster methods considered in this work that only involve two-body Hamiltonians, only the one- and two-body parts of $\hat{\mathcal{H}}^{(\text{CCSD})}$ will be needed. The expressions for the matrix elements depend on the particle-hole character of the orbitals and, therefore, the Hamiltonian is split into different particle-hole

$$\begin{aligned}
\mathcal{H}_0 &= \Delta E^{(\text{CCSD})} \\
\mathcal{H}_a^i &= f_a^i + \sum_{ck} v_{ac}^{ik} t_k^c \\
\mathcal{H}_b^a &= f_b^a + \sum_{ck} v_{bc}^{ak} t_k^c - \sum_k t_k^a \mathcal{H}_b^k - \frac{1}{2} \sum_{ckl} v_{bc}^{kl} t_{kl}^{ac} \\
\mathcal{H}_j^i &= f_j^i + \sum_{ck} v_{jc}^{ik} t_k^c + \sum_c t_j^c \mathcal{H}_c^i + \frac{1}{2} \sum_{cdk} v_{cd}^{ik} t_{jk}^{cd} \\
\mathcal{H}_i^a &= 0 \\
\mathcal{H}_{ab}^{ij} &= v_{ab}^{ij} \\
\mathcal{H}_{ib}^{aj} &= (\chi''')_{ib}^{aj} + \frac{1}{2} \sum_c t_i^c \mathcal{H}_{cb}^{aj} + \sum_{ck} v_{cb}^{kj} t_{ik}^{ac} \\
\mathcal{H}_{bc}^{ai} &= v_{bc}^{ai} - \sum_k v_{bc}^{ki} t_k^a \\
\mathcal{H}_{ja}^{ik} &= v_{ja}^{ik} + \sum_c v_{ca}^{ik} t_j^c \\
\mathcal{H}_{cd}^{ab} &= (\chi')_{cd}^{ab} + \frac{1}{2} \sum_{kl} v_{cd}^{kl} t_{kl}^{ab} \\
\mathcal{H}_{kl}^{ij} &= v_{kl}^{ij} + \hat{P}_{kl} \sum_c t_l^c (\chi')_{kc}^{ij} + \frac{1}{2} \sum_{cd} v_{cd}^{ij} t_{kl}^{cd} \\
\mathcal{H}_{ci}^{ab} &= v_{ci}^{ab} + \sum_d v_{cd}^{ab} t_i^d + \hat{P}_{ab} \sum_k t_k^b (\chi')_{ic}^{ak} - \sum_k t_{ki}^{ab} \mathcal{H}_c^k \\
&\quad + \hat{P}_{ab} \sum_{dk} t_{ki}^{db} \mathcal{H}_{cd}^{ak} + \frac{1}{2} \sum_{kl} t_{kl}^{ab} \mathcal{H}_{ci}^{kl} \\
\mathcal{H}_{jk}^{ia} &= (\chi'')_{jk}^{ia} + \sum_c t_{jk}^{ca} \mathcal{H}_c^i \\
\mathcal{H}_{ij}^{ab} &= 0
\end{aligned}$$

Figure 2.6: Algebraic expressions for the effective Hamiltonian matrix elements. For the definitions of the intermediates χ see Figure 2.7.

$$(\chi')_{bc}^{ai} = v_{bc}^{ai} - \frac{1}{2} \sum_k v_{bc}^{ki} t_k^a$$

$$(\chi')_{ib}^{aj} = v_{ib}^{aj} - \frac{1}{2} \sum_k v_{ib}^{kj} t_k^a + \sum_c t_i^c (\chi')_{cb}^{aj}$$

$$(\chi'')_{ib}^{aj} = v_{ib}^{aj} - \frac{1}{2} \sum_k v_{ib}^{kj} t_k^a + \frac{1}{2} \sum_c t_i^c (\chi')_{cb}^{aj}$$

$$(\chi''')_{ib}^{aj} = v_{ib}^{aj} - \sum_k v_{ib}^{kj} t_k^a + \frac{1}{2} \sum_c t_i^c \mathcal{H}_{cb}^{aj}$$

$$(\chi')_{ja}^{ik} = v_{ja}^{ik} + \frac{1}{2} \sum_c v_{ca}^{ik} t_j^c$$

$$(\chi')_{cd}^{ab} = v_{cd}^{ab} - \hat{P}_{ab} \sum_k t_k^b (\chi')_{cd}^{ak}$$

$$(\chi')_{ci}^{ab} = v_{ci}^{ab} + \frac{1}{2} \sum_d v_{cd}^{ab} t_i^d - \hat{P}_{ab} \sum_k t_k^b (\chi'')_{ci}^{ak}$$

$$(\chi')_{jk}^{ia} = v_{jk}^{ia} - \frac{1}{2} \sum_l v_{jk}^{il} t_l^a$$

$$\begin{aligned} (\chi'')_{jk}^{ia} &= v_{jk}^{ia} - \sum_l v_{jk}^{il} t_l^a - \hat{P}_{jk} \sum_c t_k^c (\chi''')_{jc}^{ai} \\ &\quad + \hat{P}_{jk} \sum_{cl} t_{lk}^{ca} \mathcal{H}_{jc}^{il} + \frac{1}{2} \sum_{cd} t_{jk}^{cd} \mathcal{H}_{cd}^{ia} \end{aligned}$$

Figure 2.7: Intermediates used in Figure 2.6.

topologies, for the one-body part $\hat{\mathcal{H}}_1$

$$\hat{\mathcal{H}}_1 = \sum_{ij} \mathcal{H}_j^i \{\hat{a}_i^\dagger \hat{a}_j\} + \sum_{ia} \mathcal{H}_a^i \{\hat{a}_i^\dagger \hat{a}_a\} + \sum_{ai} \mathcal{H}_i^a \{\hat{a}_a^\dagger \hat{a}_i\} + \sum_{ab} \mathcal{H}_b^a \{\hat{a}_a^\dagger \hat{a}_b\} \quad (2.51)$$

and analogous for $\hat{\mathcal{H}}_2$, where the algebraic expressions of the corresponding matrix elements are listed in Figures 2.6 and 2.7. In effective Hamiltonian terms the CCSD \hat{T}_1 and \hat{T}_2 amplitude equations may be represented as

$$\mathcal{H}_i^a = 0, \quad \forall a, i \quad (2.52)$$

$$\mathcal{H}_{ij}^{ab} = 0, \quad \forall a, b, i, j \quad (2.53)$$

emphasizing that the \mathcal{H}_h^p and \mathcal{H}_{hh}^{pp} matrix elements of $\hat{\mathcal{H}}^{(\text{CCSD})}$ vanish if the CCSD equations are satisfied by the cluster amplitudes.

Having the effective Hamiltonian in explicit form allows to formulate further applications like Λ CCSD(T) or EOM-CCSD – basically being a diagonalization of $\hat{\mathcal{H}}^{(\text{CCSD})}$ – in terms of effective Hamiltonian matrix elements which results in more compact expressions.

2.5 The Λ CCSD Equations

The Coupled-Cluster $\hat{\Lambda}$ operator appears on several occasions in Coupled-Cluster theory, as in the expression for the the energy derivative in the context of response treatment of properties,

$$\frac{d}{d\lambda} \Delta E(\lambda) = \langle \Phi | (\hat{1} + \hat{\Lambda}) \frac{d\hat{\mathcal{H}}(\lambda)}{d\lambda} | \Phi \rangle, \quad (2.54)$$

or in the fundamental energy functional,

$$\mathcal{E}^{(\text{CC})}(\hat{\Lambda}, \hat{T}) = \langle \Phi | (\hat{1} + \hat{\Lambda}) \hat{\mathcal{H}} | \Phi \rangle, \quad (2.55)$$

which, when stationary, gives the Coupled-Cluster correlation energy. From there, it attains importance in the calculation of higher-order contributions to the energy. Furthermore, because the $\hat{\Lambda}$ operator is determined from solving the left-eigenfunction equation for $\hat{\mathcal{H}}$, the $\hat{\Lambda}$ equations are to a large extent equivalent to equations encountered in Equation-of-Motion Coupled-Cluster theory. Since the main motivation for the $\hat{\Lambda}$ operator is from the properties treatment which is of minor interest in this work, only a very brief review is given in the following.

The $\hat{\Lambda}$ operator parametrizes the bra counterpart $\langle\tilde{\Psi}|$ of the Coupled-Cluster ground state $|\Psi\rangle$ according to

$$\langle\tilde{\Psi}| = \langle\Phi| (\hat{1} + \hat{\Lambda}) e^{-\hat{T}}, \quad (2.56)$$

which satisfies the biorthonormality condition

$$\langle\tilde{\Psi}|\Psi\rangle = 1 \quad (2.57)$$

and where

$$\hat{\Lambda} = \sum_{n=1}^A \hat{\Lambda}_n \quad (2.58)$$

is a sum of n ph de-excitation operators $\hat{\Lambda}_n$,

$$\hat{\Lambda}_1 = \overline{\wedge} = \frac{1}{(1!)^2} \sum_{ai} \lambda_a^i \{\hat{a}_i^\dagger \hat{a}_a\} \quad (2.59)$$

$$\hat{\Lambda}_2 = \overline{\wedge\wedge} = \frac{1}{(2!)^2} \sum_{abij} \lambda_{ab}^{ij} \{\hat{a}_i^\dagger \hat{a}_j^\dagger \hat{a}_b \hat{a}_a\} \quad (2.60)$$

$$\begin{aligned} & \vdots \\ \hat{\Lambda}_n &= \overline{\wedge\wedge\wedge} = \frac{1}{(n!)^2} \sum_{\substack{a_1 \dots a_n \\ i_1 \dots i_n}} \lambda_{a_1 \dots a_n}^{i_1 \dots i_n} \{\hat{a}_{i_1}^\dagger \dots \hat{a}_{i_n}^\dagger \hat{a}_{a_n} \dots \hat{a}_{a_1}\}. \end{aligned} \quad (2.61)$$

The corresponding amplitude equations can be obtained by considering the Schrödinger equation

$$\langle\tilde{\Psi}|\hat{H}_N = \Delta E \langle\tilde{\Psi}| \quad (2.62)$$

and using Ansatz (2.56)

$$\langle\Phi| (\hat{1} + \hat{\Lambda}) e^{-\hat{T}} \hat{H}_N = \Delta E \langle\Phi| (\hat{1} + \hat{\Lambda}) e^{-\hat{T}}. \quad (2.63)$$

Right-multiplication with $e^{\hat{T}}$ leads to a formulation in terms of the effective Hamiltonian,

$$\langle\Phi| (\hat{1} + \hat{\Lambda}) \hat{\mathcal{H}} = \Delta E \langle\Phi| (\hat{1} + \hat{\Lambda}), \quad (2.64)$$

which, using

$$\hat{\mathcal{H}} = \mathcal{H}_0 \hat{1} + \hat{\mathcal{H}}_{\text{open}}, \quad (2.65)$$

can be cast in the energy-independent form

$$\langle \Phi | (\hat{1} + \hat{\Lambda}) \hat{\mathcal{H}}_{\text{open}} = 0. \quad (2.66)$$

In the case of Λ CCSD, where the $\hat{\Lambda}$ operator is approximated as

$$\hat{\Lambda} \approx \hat{\Lambda}^{(\text{CCSD})} = \hat{\Lambda}_1 + \hat{\Lambda}_2, \quad (2.67)$$

and the effective Hamiltonian $\hat{\mathcal{H}}_{\text{open}}$ is replaced by $\hat{\mathcal{H}}_{\text{open}}^{(\text{CCSD})}$, the $\hat{\Lambda}_1$ and $\hat{\Lambda}_2$ amplitudes can be obtained from solving the system of *linear* equations [76,115–121]

$$\langle \Phi | (\hat{1} + \hat{\Lambda}_1 + \hat{\Lambda}_2) \hat{\mathcal{H}}_{\text{open}}^{(\text{CCSD})} | \Phi_i^a \rangle = 0 \quad (2.68)$$

$$\langle \Phi | (\hat{1} + \hat{\Lambda}_1 + \hat{\Lambda}_2) \hat{\mathcal{H}}_{\text{open}}^{(\text{CCSD})} | \Phi_{ij}^{ab} \rangle = 0. \quad (2.69)$$

Since these systems of equations are typically very large, they are also solved iteratively, and a similar iteration scheme as for CCSD, Eq. (2.45), can be set up. From excitation rank considerations follows that only one-, two- and three-body components of $\hat{\mathcal{H}}_{\text{open}}^{(\text{CCSD})}$ enter the above system which also can be written as [96]

$$0 = \langle \Phi | \left\{ [(\hat{1} + \hat{\Lambda}_1) \hat{\mathcal{H}}_1]_C + [(\hat{\Lambda}_1 + \hat{\Lambda}_2) \hat{\mathcal{H}}_2]_C + [\hat{\Lambda}_2 \hat{\mathcal{H}}_3]_C \right\} | \Phi_i^a \rangle \quad (2.70)$$

$$0 = \langle \Phi | \left\{ [(\hat{1} + \hat{\Lambda}_1 + \hat{\Lambda}_2) \hat{\mathcal{H}}_2]_C + [\hat{\Lambda}_2 \hat{\mathcal{H}}_1]_C + [\hat{\Lambda}_1 \hat{\mathcal{H}}_1]_{\text{DC}} + [\hat{\Lambda}_2 \hat{\mathcal{H}}_3]_C \right\} | \Phi_{ij}^{ab} \rangle. \quad (2.71)$$

where the label DC represents disconnected operator products. As for the $\hat{T}^{(\text{CCSD})}$ amplitude equations, these expressions can be evaluated using standard diagrammatic techniques (for diagrams see Appendix E.1). The resulting equations for the $\hat{\Lambda}_1$ and $\hat{\Lambda}_2$ amplitudes in terms of effective Hamiltonian matrix elements are listed in Figure 2.8 and the corresponding spherical expressions are appended in Appendix E.2. In Figure 2.8, the matrix elements of the three-body operator $\hat{\mathcal{H}}_3$ have been expressed in terms of matrix elements of lower-rank operators according to [26,96]

$$\mathcal{H}_{kla}^{cdi} = -\hat{P}_{kl} \sum_m \mathcal{H}_{al}^{im} t_{km}^{cd} + \hat{P}_{cd} \sum_e \mathcal{H}_{ae}^{id} t_{kl}^{ce} \quad (2.72)$$

$$\mathcal{H}_{kbl}^{ijc} = -\sum_d t_{kl}^{cd} v_{db}^{ij} \quad (2.73)$$

$$\mathcal{H}_{abk}^{cjd} = -\sum_l t_{kl}^{cd} v_{ab}^{lj} \quad (2.74)$$

$$\begin{aligned}
 & +^{(\Lambda_1 A)} \mathcal{H}_a^i + \sum_c \lambda_c^i \mathcal{H}_a^c - \sum_k \lambda_a^k \mathcal{H}_k^i + \sum_{ck} \lambda_c^k \mathcal{H}_{ka}^{ci} \\
 & +^{(\Lambda_1 E)} \frac{1}{2} \sum_{cdk} \lambda_{cd}^{ik} \mathcal{H}_{ak}^{cd} - \frac{1}{2} \sum_{ckl} \lambda_{ac}^{kl} \mathcal{H}_{kl}^{ic} + \frac{1}{2} \sum_{cdek l} \lambda_{cd}^{kl} \mathcal{H}_{ea}^{di} t_{kl}^{ce} \\
 & - \frac{1}{2} \sum_{cdklm} \lambda_{cd}^{kl} \mathcal{H}_{la}^{mi} t_{km}^{cd} = 0, \quad \forall a, i \\
 \\
 & +^{(\Lambda_2 A)} \mathcal{H}_{ab}^{ij} + \hat{P}_{ab} \hat{P}_{ij} \lambda_b^j \mathcal{H}_a^i + \hat{P}_{ij} \sum_c \lambda_c^i \mathcal{H}_{ab}^{cj} \\
 & - \hat{P}_{ab} \sum_k \lambda_a^k \mathcal{H}_{kb}^{ij} + \hat{P}_{ab} \sum_c \lambda_{ac}^{ij} \mathcal{H}_b^c - \hat{P}_{ij} \sum_k \lambda_{ab}^{ik} \mathcal{H}_k^j \\
 & +^{(\Lambda_2 G)} \hat{P}_{ab} \hat{P}_{ij} \sum_{ck} \lambda_{ac}^{ik} \mathcal{H}_{kb}^{cj} + \frac{1}{2} \sum_{cd} \lambda_{cd}^{ij} \mathcal{H}_{ab}^{cd} \\
 & +^{(\Lambda_2 I)} \frac{1}{2} \sum_{kl} \lambda_{ab}^{kl} \mathcal{H}_{kl}^{ij} - \frac{1}{2} \hat{P}_{ab} \sum_{cdkl} \lambda_{ca}^{kl} t_{kl}^{cd} v_{db}^{ij} \\
 & - \frac{1}{2} \hat{P}_{ij} \sum_{cdkl} \lambda_{cd}^{ki} t_{kl}^{cd} v_{ab}^{lj} = 0, \quad \forall a, b, i, j
 \end{aligned}$$

 Figure 2.8: Algebraic expressions for the Λ CCSD $\hat{\Lambda}_1$ and $\hat{\Lambda}_2$ amplitude equations.

in order to avoid the use of six-index quantities. Therefore, it should be noted that in effective Hamiltonian terms it can be written

$$(\Lambda_1 G) + (\Lambda_1 H) = \text{Diagram} = \frac{1}{4} \sum_{cdkl} \lambda_{cd}^{kl} \mathcal{H}_{kla}^{cdi}, \quad (2.75)$$

$$(\Lambda_2 J) = \text{Diagram} = \frac{1}{4} \hat{P}_{ab} \hat{P}_{ij} \sum_{ckl} \lambda_{ca}^{kl} \mathcal{H}_{kbl}^{ijc}, \quad (2.76)$$

and

$$(\Lambda_2 K) = \text{Diagram} = \frac{1}{4} \hat{P}_{ab} \hat{P}_{ij} \sum_{cdk} \lambda_{cd}^{ki} \mathcal{H}_{abk}^{cjd} . \quad (2.77)$$

2.6 Expectation Values

The evaluation of expectation values

$$\langle \hat{G} \rangle \equiv \frac{\langle \Psi | \hat{G} | \Psi \rangle}{\langle \Psi | \Psi \rangle} = \frac{\langle \Phi | e^{\hat{T}^\dagger} \hat{G} e^{\hat{T}} | \Phi \rangle}{\langle \Phi | e^{\hat{T}^\dagger} e^{\hat{T}} | \Phi \rangle} \quad (2.78)$$

is inherently more complicated in Coupled-Cluster theory than in methods that employ a linear parametrization of the wavefunction. The reason is that the expression $\langle \Phi | e^{\hat{T}^\dagger} \hat{G}_N e^{\hat{T}} | \Phi \rangle$, in which both excitation and de-excitation type operators appear, does not terminate as for instance the expression $\langle \Phi | e^{-\hat{T}} \hat{G}_N e^{\hat{T}} | \Phi \rangle$ does, in which only excitation operators appear.

As for the Coupled-Cluster energy, which in the *untruncated* case must of course be the same as the Hamiltonian expectation value, any expectation value may be separated into its *reference* and *correlation* part,

$$\langle \hat{G} \rangle = \langle \Phi | \hat{G} | \Phi \rangle + \langle \hat{G}_N \rangle , \quad (2.79)$$

with the correlation part being the non-trivial task in the expectation value calculation. However, the denominator cancels against the disconnected parts from the nominator [100],

$$\langle \hat{G}_N \rangle = \frac{\langle \Phi | e^{\hat{T}^\dagger} \hat{G}_N e^{\hat{T}} | \Phi \rangle}{\langle \Phi | e^{\hat{T}^\dagger} e^{\hat{T}} | \Phi \rangle} = \langle \Phi | (e^{\hat{T}^\dagger} \hat{G}_N e^{\hat{T}})_C | \Phi \rangle , \quad (2.80)$$

leaving a connected form for the correlation part. In order to detach the general problem of the expectation value evaluation from the specific operator \hat{G} , the *n-body reduced density operator*

$$\hat{\gamma}_N^{(n)} = \sum_{\substack{p_1 \dots p_n \\ q_1 \dots q_n}} |q_1 \dots q_n\rangle (\gamma_N)_{p_1 \dots p_n}^{q_1 \dots q_n} \langle p_1 \dots p_n| \quad (2.81)$$

with matrix elements

$$(\gamma_N)_{p_1 \dots p_n}^{q_1 \dots q_n} = \langle \Phi | \left[e^{\hat{T}^\dagger} \{ \hat{a}_{p_1}^\dagger \dots \hat{a}_{p_n}^\dagger \hat{a}_{q_n} \dots \hat{a}_{q_1} \} e^{\hat{T}} \right]_C | \Phi \rangle \quad (2.82)$$

$$\begin{aligned}
 (\gamma_N)_a^i &= \begin{pmatrix} \gamma_{\text{h}}^{\text{A}} \\ + \end{pmatrix} \lambda_a^i \\
 (\gamma_N)_i^a &= \begin{pmatrix} \gamma_{\text{h}}^{\text{A}} \\ + \end{pmatrix} t_i^a + \begin{pmatrix} \gamma_{\text{h}}^{\text{B}} \\ + \end{pmatrix} \sum_{ck} \lambda_c^k t_{ik}^{ac} - \begin{pmatrix} \gamma_{\text{h}}^{\text{C}} \\ - \end{pmatrix} \sum_{ck} \lambda_k^c t_k^a t_i^c \\
 &\quad - \frac{1}{2} \sum_{cdkl} \lambda_{cd}^{kl} t_{ki}^{cd} t_l^a - \frac{1}{2} \sum_{cdkl} \lambda_{cd}^{kl} t_{kl}^{ca} t_i^d \\
 (\gamma_N)_a^b &= \begin{pmatrix} \gamma_{\text{h}}^{\text{A}} \\ + \end{pmatrix} \sum_k \lambda_a^k t_k^b + \begin{pmatrix} \gamma_{\text{h}}^{\text{B}} \\ + \end{pmatrix} \frac{1}{2} \sum_{ckl} \lambda_{ca}^{kl} t_{kl}^{cb} \\
 (\gamma_N)_i^j &= \begin{pmatrix} \gamma_{\text{h}}^{\text{A}} \\ - \end{pmatrix} \sum_c \lambda_c^j t_i^c - \begin{pmatrix} \gamma_{\text{h}}^{\text{B}} \\ - \end{pmatrix} \frac{1}{2} \sum_{cdk} \lambda_{cd}^{kj} t_{ki}^{cd}
 \end{aligned}$$

Figure 2.9: Algebraic expressions for the one-body response density matrix elements.

is introduced. It is clearly independent from the operator under consideration, and the expectation value of any n -body operator in normal order may be expressed as the contraction of the operator matrix elements with the density matrix elements,

$$\langle \hat{G}_N \rangle = \sum_{k=1}^n \frac{1}{(k!)^2} \sum_{\substack{p_1 \dots p_k \\ q_1 \dots q_k}} \langle p_1 \dots p_k | \hat{G}_N | q_1 \dots q_k \rangle (\gamma_N)^{q_1 \dots q_k}_{p_1 \dots p_k}. \quad (2.83)$$

For the case of one-body operators \hat{O} , the reference part of the expectation value may directly be incorporated in the contraction by the use of a modified density matrix γ_q^p ,

$$\langle \hat{O} \rangle = \sum_{pq} \langle p | \hat{O} | q \rangle \gamma_p^q, \quad \gamma_p^q \equiv \begin{cases} (\gamma_N)_p^q + \delta_{pq} & : p, q \in \text{holes} \\ (\gamma_N)_p^q & : \text{else} . \end{cases} \quad (2.84)$$

For a two-body operator \hat{V} in vacuum normal order, a formulation of the expectation value involving only the two-body matrix elements $\langle pq | \hat{V} | rs \rangle$ is easily found as [26]

$$\langle \hat{V} \rangle = \frac{1}{4} \sum_{pqrs} \langle pq | \hat{V} | rs \rangle (\gamma_N)_{pq}^{rs} + \sum_{pq} \left[\sum_i \langle pi | \hat{V} | qi \rangle \right] (\gamma_N)_p^q + \frac{1}{2} \sum_{ij} \langle ij | \hat{V} | ij \rangle. \quad (2.85)$$

$$\begin{aligned}
 (\gamma_N)_{ci}^{ab} = & \left(\gamma_{\text{ph}}^{\text{ppA}} + \sum_k t_{ki}^{ab} \lambda_c^k \right) \left(\gamma_{\text{ph}}^{\text{ppB}} + \hat{P}_{ab} \sum_k t_k^a t_i^b \lambda_c^k \right) \\
 & \left(\gamma_{\text{ph}}^{\text{ppC}} + \frac{1}{2} \hat{P}_{ab} \sum_{dkl} t_{kl}^{da} t_i^b \lambda_{dc}^{kl} \right) \left(\gamma_{\text{ph}}^{\text{ppD}} + \hat{P}_{ab} \sum_{dkl} t_{il}^{bd} t_k^a \lambda_{cd}^{kl} \right) \\
 & \left(\gamma_{\text{ph}}^{\text{ppE}} - \frac{1}{2} \sum_{dkl} t_{kl}^{ab} t_i^d \lambda_{cd}^{kl} \right) \left(\gamma_{\text{ph}}^{\text{ppF}} - \hat{P}_{ab} \sum_{dkl} t_k^a t_l^b t_i^d \lambda_{cd}^{kl} \right) \\
 & \left(\gamma_{\text{ph}}^{\text{ppG}} - \hat{P}_{ab} \sum_{dkl} t_{ki}^{ad} t_l^b \lambda_{cd}^{kl} \right) \\
 (\gamma_N)_{ij}^{ab} = & \hat{P}_{ab} \hat{P}_{ij} \left\{ \left(\gamma_{\text{hh}}^{\text{ppA}} + \frac{1}{4} t_{ij}^{ab} \right) \left(\gamma_{\text{hh}}^{\text{ppB}} + t_i^a t_j^b \right) \left(\gamma_{\text{hh}}^{\text{ppC}} + \sum_{ck} t_{ki}^{ca} t_j^b \lambda_c^k \right) \right. \\
 & \left(\gamma_{\text{hh}}^{\text{ppD}} - \frac{1}{2} \sum_{ck} t_{kj}^{ab} t_i^c \lambda_c^k \right) \left(\gamma_{\text{hh}}^{\text{ppE}} - \frac{1}{2} \sum_{ck} t_{ij}^{cb} t_k^a \lambda_c^k \right) \\
 & \left(\gamma_{\text{hh}}^{\text{ppF}} - \sum_{ck} t_k^a t_i^c t_j^b \lambda_c^k \right) \left(\gamma_{\text{hh}}^{\text{ppG}} + \sum_{cdkl} t_{ki}^{ca} t_{jl}^{bd} \lambda_{cd}^{kl} \right) \\
 & \left(\gamma_{\text{hh}}^{\text{ppH}} - \frac{1}{4} \sum_{cdkl} t_{ki}^{cd} t_{lj}^{ab} \lambda_{cd}^{kl} \right) \left(\gamma_{\text{hh}}^{\text{ppI}} - \frac{1}{4} \sum_{cdkl} t_{kl}^{ca} t_{ij}^{db} \lambda_{cd}^{kl} \right) \\
 & \left(\gamma_{\text{hh}}^{\text{ppJ}} + \frac{1}{16} \sum_{cdkl} t_{kl}^{ab} t_{ij}^{cd} \lambda_{cd}^{kl} \right) \left(\gamma_{\text{hh}}^{\text{ppK}} - \frac{1}{2} \sum_{cdkl} t_{ki}^{cd} t_l^a t_j^b \lambda_{cd}^{kl} \right) \\
 & \left(\gamma_{\text{hh}}^{\text{ppL}} - \frac{1}{2} \sum_{cdkl} t_{kl}^{ca} t_i^d t_j^b \lambda_{cd}^{kl} \right) \left(\gamma_{\text{hh}}^{\text{ppM}} - \sum_{cdkl} t_{jl}^{bd} t_k^a t_i^c \lambda_{cd}^{kl} \right) \\
 & \left(\gamma_{\text{hh}}^{\text{ppN}} + \frac{1}{4} \sum_{cdkl} t_{kl}^{ab} t_i^c t_j^d \lambda_{cd}^{kl} \right) \left(\gamma_{\text{hh}}^{\text{ppO}} + \frac{1}{4} \sum_{cdkl} t_{ij}^{cd} t_k^a t_l^b \lambda_{cd}^{kl} \right) \\
 & \left. \left(\gamma_{\text{hh}}^{\text{ppP}} + \sum_{cdkl} t_k^a t_i^c t_l^b t_j^d \lambda_{cd}^{kl} \right) \right\}
 \end{aligned}$$

Figure 2.10: Algebraic expressions for the two-body response density matrix elements.

$$\begin{aligned}
 (\gamma_N)_{bj}^{ia} &= \left(\gamma_{\text{ph}^A}^{\text{hp}} + \gamma_{\text{ph}^B}^{\text{hp}} \right) \sum_{ck} t_{kj}^{ca} \lambda_{cb}^{ki} \left(\gamma_{\text{ph}^C}^{\text{hp}} - \right) \sum_{ck} t_k^a t_j^c \lambda_{bc}^{ik} \\
 (\gamma_N)_{ab}^{ij} &= \left(\gamma_{\text{pp}^A}^{\text{hh}} + \right) \lambda_{ab}^{ij} \\
 (\gamma_N)_{cd}^{ab} &= \left(\gamma_{\text{pp}^A}^{\text{pp}} + \frac{1}{2} \sum_{kl} t_{kl}^{ab} \lambda_{cd}^{kl} \right) \left(\gamma_{\text{pp}^B}^{\text{pp}} + \right) \hat{P}_{ab} \sum_{kl} t_k^a t_l^b \lambda_{cd}^{kl} \\
 (\gamma_N)_{kl}^{ij} &= \left(\gamma_{\text{hh}^A}^{\text{hh}} + \frac{1}{2} \sum_{cd} t_{kl}^{cd} \lambda_{cd}^{ij} \right) \left(\gamma_{\text{hh}^B}^{\text{hh}} + \right) \hat{P}_{kl} \sum_{cd} t_k^c t_l^d \lambda_{cd}^{ij} \\
 (\gamma_N)_{jk}^{ia} &= \left(\gamma_{\text{hh}^A}^{\text{hp}} - \right) \sum_c t_{jk}^{ca} \lambda_c^i \left(\gamma_{\text{hh}^B}^{\text{hp}} - \right) \hat{P}_{jk} \sum_c t_j^c t_k^a \lambda_c^i \\
 &\quad \left(\gamma_{\text{hh}^C}^{\text{hp}} - \right) \frac{1}{2} \hat{P}_{jk} \sum_{cdl} t_{lj}^{cd} t_k^a \lambda_{cd}^{li} \left(\gamma_{\text{hh}^D}^{\text{hp}} - \right) \hat{P}_{jk} \sum_{cdl} t_{kl}^{ad} t_j^c \lambda_{cd}^{il} \\
 &\quad \left(\gamma_{\text{hh}^E}^{\text{hp}} + \right) \frac{1}{2} \sum_{cdl} t_{jk}^{cd} t_l^a \lambda_{cd}^{il} \left(\gamma_{\text{hh}^F}^{\text{hp}} + \right) \hat{P}_{jk} \sum_{cdl} t_j^c t_k^d t_l^a \lambda_{cd}^{il} \\
 &\quad \left(\gamma_{\text{hh}^G}^{\text{hp}} + \right) \hat{P}_{jk} \sum_{cdl} t_{jl}^{ca} t_k^d \lambda_{cd}^{il} \\
 (\gamma_N)_{bc}^{ai} &= \left(\gamma_{\text{pp}^A}^{\text{ph}} + \right) \sum_k t_k^a \lambda_{bc}^{ki} \\
 (\gamma_N)_{ka}^{ij} &= \left(\gamma_{\text{hp}^A}^{\text{hh}} - \right) \sum_c t_k^c \lambda_{ca}^{ij}
 \end{aligned}$$

Figure 2.11: Algebraic expressions for the two-body response density matrix elements, continued.

By solving the $\hat{\Lambda}$ equations an alternative form of the density matrix elements

$$(\gamma_N)_{p_1 \dots p_n}^{q_1 \dots q_n} = \langle \Phi | \left[(\hat{1} + \hat{\Lambda}) \left(\{\hat{a}_{p_1}^\dagger \dots \hat{a}_{p_n}^\dagger \hat{a}_{q_n} \dots \hat{a}_{q_1}\} e^{\hat{T}} \right)_C \right] | \Phi \rangle \quad (2.86)$$

may be used, which, unlike (2.82) leads to terminating expressions. The CCSD one- and two-body matrix elements of the reduced density matrix derived from (2.86) are listed in Figures 2.9-2.11, and the spherical expressions can be found in Appendix F.

2.7 The Λ CCSD(T) Energy Correction

While the CCSD equations are rather easy to solve, the solution of the full CCSDT equations is far out of reach for all but the lightest nuclei. Nonetheless, higher-order excitations may be included in the calculations via a combination of the iterative, infinite-summation techniques obtained from solving the Coupled-Cluster equations for low-rank clusters, with an *a posteriori* non-iterative correction due to higher-rank clusters, typically based on perturbation-theory considerations. There is an abundance of different methods that have emerged in the field of quantum chemistry, such as CCSD[T] [122,123], CCSD(T) [124], CCSD(TQ_f) [125], Λ CCSD(T) [57,126], Λ CCSD(TQ_f) [127], CCSD(2)_T [128–131], CCSD(2) [128–131], CR-CCSD(T) [132–136], CR-CCSD(TQ) [132–136], CR-CC(*m,m'*) [117,119,121,137,138], CR-CC(2,3)+Q [139], LR-CCSD(T) [140], or LR-CCSD(TQ) [140]. In this work, besides the CR-CC(2,3) correction, the main focus will be on the Λ CCSD(T) non-iterative energy correction [57,126] due to its rather simple structure but yet accurate results. However, in this section only a brief overview is given, because the method is discussed in more detail in the context of three-body Hamiltonians, see Section 3.4.

Starting point for the derivation of the Λ CCSD(T) correction is an expansion of the Coupled-Cluster energy functional

$$\mathcal{E}^{(CC)} = \langle \Phi | (\hat{1} + \hat{\Lambda}) \hat{\mathcal{H}} | \Phi \rangle \quad (2.87)$$

for CCSDT up to fourth order perturbative contributions relative to the CCSD ground-state wavefunction, which can be formulated in converged CCSD \hat{T}_1 , \hat{T}_2 and Λ CCSD $\hat{\Lambda}_1$, $\hat{\Lambda}_2$ amplitudes, and by determining the corresponding energy correction from this functional [57,58]. This results in an expression for the energy

$$\begin{aligned}
 \delta E^{(\text{ACCS}(T))} &= \frac{1}{(3!)^2} \sum_{\substack{abc \\ ijk}} \tilde{\lambda}_{abc}^{ijk} \frac{1}{\epsilon_{ijk}^{abc}} \tilde{t}_{ijk}^{abc} \\
 \tilde{\lambda}_{abc}^{ijk} &= \hat{P}_{a/bc} \hat{P}_{k/ij} \sum_d v_{bc}^{dk} \lambda_{ad}^{ij} - \hat{P}_{c/ab} \hat{P}_{i/jk} \sum_l v_{lc}^{jk} \lambda_{ab}^{il} \\
 &\quad + \hat{P}_{i/jk} \hat{P}_{a/bc} \lambda_a^i v_{jk}^{bc} + \hat{P}_{i/jk} \hat{P}_{a/bc} f_a^i \lambda_{bc}^{jk} \\
 \tilde{t}_{ijk}^{abc} &= \hat{P}_{a/bc} \hat{P}_{k/ij} \sum_d v_{dk}^{bc} t_{ij}^{ad} - \hat{P}_{c/ab} \hat{P}_{i/jk} \sum_l v_{jk}^{lc} t_{il}^{ab} \\
 \hat{P}_{p/qr} &= \hat{1} - \hat{T}_{pq} - \hat{T}_{pr}
 \end{aligned}$$

 Figure 2.12: Algebraic expressions for the computation of $\delta E^{(\text{ACCS}(T))}$.

correction of the form

$$\begin{aligned}
 \delta E^{(\text{ACCS}(T))} &= \frac{1}{(3!)^2} \sum_{\substack{abc \\ ijk}} \langle \Phi | \hat{\Lambda} (\hat{F}_N^{\text{od}} + \hat{V}_N) | \Phi_{ijk}^{abc} \rangle \frac{1}{\epsilon_{ijk}^{abc}} \langle \Phi_{ijk}^{abc} | (\hat{V}_N \hat{T}_2)_C | \Phi \rangle, \quad (2.88)
 \end{aligned}$$

where \hat{F}_N^{od} is the off-diagonal part of the normal-ordered Fock operator \hat{F}_N and the energy denominator ϵ_{ijk}^{abc} is defined as

$$\epsilon_{ijk}^{abc} \equiv f_i^a + f_j^b + f_k^c - f_a^a - f_b^b - f_c^c. \quad (2.89)$$

The corrected total energy is therefore given by

$$E^{(\text{ACCS}(T))} = E_{\text{ref}} + \Delta E^{(\text{CCSD})} + \delta E^{(\text{ACCS}(T))}. \quad (2.90)$$

Explicit expressions for the evaluation of (2.88) can be found in Figure 2.12. Because the enormous number ⁴, namely $h^3 p^3$, of six-index amplitudes cannot be stored at once, it is common practice to organize the calculation according to

$$\delta E^{(\text{ACCS}(T))} = \sum_{i < j < k} \left[\frac{1}{3!} \sum_{abc} \tilde{\lambda}_{abc}^{ijk} \frac{1}{\epsilon_{ijk}^{abc}} \tilde{t}_{ijk}^{abc} \right] \quad (2.91)$$

where the bracket is evaluated for each i, j, k index combination separately, requiring only the storage of p^3 tensors. The particle index sum is not restricted to $a < b < c$ in order to use optimized BLAS [141] routines for the calculation of the $\tilde{\lambda}_{abc}^{ijk}$ and \tilde{t}_{ijk}^{abc} tensors.

⁴The number of hole orbitals is denoted by h and p is the number of particle orbitals.

2.8 The Completely-Renormalized Coupled-Cluster Method CR-CC(2,3)

The completely renormalized Coupled-Cluster methods (CR-CC) and particular the CR-CC(2,3) version [114, 117, 119, 120, 137, 138] are promising alternatives to the Λ CCSD(T) approach, since they are more complete, and, therefore, expected to be more accurate. The CR-CC(m, m') methods are based on asymmetric energy expressions and the moment expansion of the full CI energy, defining the method of moments of the Coupled-Cluster equations [132–136, 142, 143]. This framework encompasses all sorts of energy corrections and its comprehensive structure greatly facilitates the theoretical discussion. In this work, for instance, this feature is exploited by using CR-CC(2,3) as the base from which the Λ CCSD(T) method for three-body Hamiltonians is derived in Section 3.4. Apart from the theoretical context, the CR-CC(2,3) method will also be used in practical applications because it is worthwhile to have multiple triples correction methods at hand. This is because as long as full CCSDT calculations remain too expensive, the quality of triples correction approaches has to be estimated from the comparison of different methods. Furthermore, it is encouraging to note that the final CR-CC(2,3) equations are actually not significantly more complex than their Λ CCSD(T) counterparts, resulting in a similar implementational effort.

Using the definitions of the left and right Coupled-Cluster eigenstates,

$$\langle \tilde{\Psi} | = \langle \Phi | (\hat{1} + \hat{\Lambda}) e^{-\hat{T}} \quad \text{and} \quad | \Psi \rangle = e^{\hat{T}} | \Phi \rangle , \quad (2.92)$$

the exact correlation energy

$$\Delta E = \langle \tilde{\Psi} | \hat{H}_N | \Psi \rangle \quad (2.93)$$

may be expressed in terms of the $\hat{\Lambda}$ operator and the effective Hamiltonian,

$$\Delta E = \langle \Phi | (\hat{1} + \hat{\Lambda}) \hat{\mathcal{H}} | \Phi \rangle . \quad (2.94)$$

Of course, in practice neither $\hat{\Lambda}$ nor $\hat{\mathcal{H}}$ are known. However, the exact correlation energy can still be obtained if in (2.94) the CCSD effective Hamiltonian is used, provided that an appropriate redefinition of the operator acting on the left reference state is employed,

$$\Delta E = \langle \Phi | \hat{\mathcal{L}} \hat{\mathcal{H}}^{(\text{CCSD})} | \Phi \rangle , \quad (2.95)$$

with \mathcal{L} being a de-excitation operator of the form

$$\mathcal{L} = \sum_{n=1}^A \mathcal{L}_n, \quad \mathcal{L}_n = \frac{1}{(n!)^2} \sum_{\substack{i_1 \dots i_n \\ a_1 \dots a_n}} l_{a_1 \dots a_n}^{i_1 \dots i_n} \hat{a}_i^\dagger \hat{a}_j^\dagger \hat{a}_k^\dagger \hat{a}_c \hat{a}_b \hat{a}_a. \quad (2.96)$$

Indeed, if \mathcal{L} is determined such that $\langle \Phi | \mathcal{L}$ represents the lowest-energy left eigenstate⁵ of $\hat{\mathcal{H}}^{(\text{CCSD})}$,

$$\langle \Phi | \mathcal{L} \hat{\mathcal{H}}^{(\text{CCSD})} = \Delta E \langle \Phi | \mathcal{L}, \quad (2.97)$$

and assuming the normalization

$$\langle \Phi | \mathcal{L} | \Phi \rangle = 1, \quad (2.98)$$

it is easy to check that (2.95) holds. The ultimate goal is to split (2.95) into the information provided by CCSD and the information for the contributions beyond CCSD, which can be completely absorbed in the operator \mathcal{L} . In order to do so, it is convenient to insert a resolution of the identity of the form

$$\hat{1} = |\Phi\rangle\langle\Phi| + \hat{P} + \hat{Q}, \quad (2.99)$$

with projection operators

$$\hat{P} = \hat{P}_1 + \hat{P}_2 \quad (2.100)$$

$$\hat{Q} = \hat{P}_3 + \dots + \hat{P}_A \quad (2.101)$$

where

$$\hat{P}_n = \sum_{\substack{i_1 < \dots < i_n \\ a_1 < \dots < a_n}} |\Phi_{i_1 \dots i_n}^{a_1 \dots a_n}\rangle \langle \Phi_{i_1 \dots i_n}^{a_1 \dots a_n}|, \quad (2.102)$$

between the \mathcal{L} and $\hat{\mathcal{H}}^{(\text{CCSD})}$ operators in (2.95). This allows to make use of the properties of $\hat{\mathcal{H}}^{(\text{CCSD})}$

$$\langle \Phi | \hat{\mathcal{H}}^{(\text{CCSD})} | \Phi \rangle = \Delta E^{(\text{CCSD})}, \quad (2.103)$$

$$\langle \Phi_i^a | \hat{\mathcal{H}}^{(\text{CCSD})} | \Phi \rangle = 0, \quad (2.104)$$

$$\langle \Phi_{ij}^{ab} | \hat{\mathcal{H}}^{(\text{CCSD})} | \Phi \rangle = 0, \quad (2.105)$$

which immediately allows to write (2.95) in the form

$$\Delta E = \Delta E^{(\text{CCSD})} + \langle \Phi | \mathcal{L} \hat{Q} \hat{\mathcal{H}}^{(\text{CCSD})} | \Phi \rangle \quad (2.106)$$

$$= \Delta E^{(\text{CCSD})} + \delta E. \quad (2.107)$$

⁵Since $\hat{\mathcal{H}}^{(\text{CCSD})}$ is given by a similarity transformation of \hat{H}_N , both operators exhibit the same spectrum and, consequently, the lowest eigenvalue of $\hat{\mathcal{H}}^{(\text{CCSD})}$ is ΔE .

Thus, the exact energy correction δE for the contributions beyond CCSD is given by

$$\delta E = \langle \Phi | \hat{\mathcal{L}} \hat{Q} \hat{\mathcal{H}}^{(\text{CCSD})} | \Phi \rangle \quad (2.108)$$

and the only unknown in this expression is $\hat{\mathcal{L}}$. Consequently, in the following it is $\hat{\mathcal{L}}$ for which approximations are introduced in order to derive manageable expressions.

Since the goal is to derive an energy correction $\delta E^{(\text{T})}$ due to triply excited clusters, the projector \hat{Q} is approximated by the space spanned by the triply excited determinants,

$$\hat{Q} \approx \hat{P}_3, \quad (2.109)$$

which projects the $\hat{\mathcal{L}}_3$ component out of $\hat{\mathcal{L}}$ in the expression ⁶

$$\hat{\mathcal{L}} \hat{Q} = \hat{\mathcal{L}}_3 \hat{P}_3. \quad (2.110)$$

Thus, the triples energy correction $\delta E^{(\text{T})}$ reads

$$\delta E^{(\text{T})} = \langle \Phi | \hat{\mathcal{L}}_3 \hat{P}_3 \hat{\mathcal{H}}^{(\text{CCSD})} | \Phi \rangle. \quad (2.111)$$

Introducing the matrix elements of $\hat{\mathcal{L}}_3$,

$$l_{abc}^{ijk} = \langle \Phi | \hat{\mathcal{L}}_3 | \Phi_{ijk}^{abc} \rangle, \quad (2.112)$$

and using the definition of the so-called *generalized moments* of the CCSD equations [132, 133, 135, 136, 144]

$$\mathfrak{M}_{ijk}^{abc} = \langle \Phi_{ijk}^{abc} | \hat{\mathcal{H}}^{(\text{CCSD})} | \Phi \rangle, \quad (2.113)$$

the triples energy correction can be cast into a form given as contraction of the $\hat{\mathcal{L}}_3$ amplitudes with the moments,

$$\delta E^{(\text{T})} = \frac{1}{(3!)^2} \sum_{\substack{abc \\ ijk}} l_{abc}^{ijk} \mathfrak{M}_{ijk}^{abc}. \quad (2.114)$$

Still, the moments \mathfrak{M}_{ijk}^{abc} only carry CCSD information, while all information beyond CCSD is contained in the yet unknown operator $\hat{\mathcal{L}}_3$. In the CR-CC(2,3)

⁶An alternative point of view is of course to approximate $\hat{\mathcal{L}}_3$ by its three-body part $\hat{\mathcal{L}}_3$.

method [114, 117, 119, 120, 137, 138], the \mathcal{L}_3 operator is determined in a quasi-perturbative manner, using the expression [117, 119]

$$\langle \Phi | \mathcal{L}_3 = \langle \Phi | \left(\hat{1} + \hat{\Lambda}^{(\text{CCSD})} \right) \hat{\mathcal{H}}^{(\text{CCSD})} \hat{\mathcal{R}}_3^{(\text{CCSD})}, \quad (2.115)$$

which exploits the formal similarity between the \mathcal{L} and the $\hat{\Lambda}$ operators [117, 119], and where

$$\hat{\mathcal{R}}_3^{(\text{CCSD})} = \frac{\hat{P}_3}{\Delta E^{(\text{CCSD})} - \hat{\mathcal{H}}^{(\text{CCSD})}} \quad (2.116)$$

is the reduced resolvent of $\hat{\mathcal{H}}^{(\text{CCSD})}$ in the subspace spanned by the triply excited determinants, which has the property

$$\frac{\hat{P}_3}{\Delta E^{(\text{CCSD})} - \hat{\mathcal{H}}^{(\text{CCSD})}} \hat{P}_3 \left(\Delta E^{(\text{CCSD})} - \hat{\mathcal{H}}^{(\text{CCSD})} \right) \hat{P}_3 = \hat{P}_3. \quad (2.117)$$

This allows to write the triples correction in the form

$$\delta E^{(\text{T})} = \langle \Phi | \left(\hat{1} + \hat{\Lambda}^{(\text{CCSD})} \right) \hat{\mathcal{H}}^{(\text{CCSD})} \hat{\mathcal{R}}_3^{(\text{CCSD})} \hat{\mathcal{H}}^{(\text{CCSD})} | \Phi \rangle. \quad (2.118)$$

In order to avoid the explicit construction of the reduced resolvent $\hat{\mathcal{R}}_3^{(\text{CCSD})}$ in the above expression, by right-multiplication with

$$\hat{P}_3 \left(\Delta E^{(\text{CCSD})} - \hat{\mathcal{H}}^{(\text{CCSD})} \right) \hat{P}_3 \quad (2.119)$$

making use of (2.117) and projecting onto $|\Phi_{ijk}^{abc}\rangle$, the CR-CC(2,3) Ansatz (2.115) for \mathcal{L}_3 may be written as

$$\begin{aligned} \sum_{\substack{l < m < n \\ d < e < f}} \langle \Phi_{lmn}^{def} | \left(\Delta E^{(\text{CCSD})} - \hat{\mathcal{H}}^{(\text{CCSD})} \right) | \Phi_{ijk}^{abc} \rangle l_{def}^{lmn} \\ = \langle \Phi | \left(\hat{1} + \hat{\Lambda}^{(\text{CCSD})} \right) \hat{\mathcal{H}}^{(\text{CCSD})} | \Phi_{ijk}^{abc} \rangle, \end{aligned} \quad (2.120)$$

which can be cast into the energy-independent form

$$- \sum_{\substack{l < m < n \\ d < e < f}} \langle \Phi_{lmn}^{def} | \hat{\mathcal{H}}_{\text{open}}^{(\text{CCSD})} | \Phi_{ijk}^{abc} \rangle l_{def}^{lmn} = \langle \Phi | \left(\hat{1} + \hat{\Lambda}^{(\text{CCSD})} \right) \hat{\mathcal{H}}_{\text{open}}^{(\text{CCSD})} | \Phi_{ijk}^{abc} \rangle. \quad (2.121)$$

This formulation of CR-CC(2,3) is invariant under arbitrary rotations of occupied and unoccupied orbitals. This requirement can be lifted due to the fact that the calculations in this work use Hartree-Fock, and thus fixed, orbitals. Then, the system of equations (2.120) or (2.121) can be replaced by a non-iterative expression, such as [117, 119, 137, 138]

$$l_{abc}^{ijk} = \langle \Phi | \left(\hat{1} + \hat{\Lambda}^{(\text{CCSD})} \right) \hat{\mathcal{H}}_{\text{open}}^{(\text{CCSD})} | \Phi_{ijkl}^{abc} \rangle \left(D_{ijk}^{abc} \right)^{-1}, \quad (2.122)$$

$$\begin{aligned}
 \delta E^{(\text{CR-CC}(2,3))} &= \frac{1}{(3!)^2} \sum_{\substack{abc \\ ijk}} l_{abc}^{ijk} \mathfrak{M}_{ijk}^{abc} \\
 \mathfrak{M}_{ijk}^{abc} &= \hat{P}_{abc} \mathfrak{T}_{ijk}^{abc} \\
 \mathfrak{T}_{ijk}^{abc} &= \hat{P}_{ij/k} \left[\frac{1}{2} \sum_e \mathcal{H}_{ke}^{ab} t_{ij}^{ec} - \frac{1}{2} \sum_m J_{ij}^{mc} t_{km}^{ab} \right] \\
 l_{abc}^{ijk} &= N_{abc}^{ijk} / D_{ijk}^{abc} \\
 N_{abc}^{ijk} &= \hat{P}_{abc} \Gamma_{abc}^{ijk} \\
 \Gamma_{abc}^{ijk} &= \hat{P}_{ij/k} \left[\frac{1}{2} \lambda_c^k \mathcal{H}_{ab}^{ij} + \frac{1}{2} \lambda_{ab}^{ij} \mathcal{H}_c^k \right. \\
 &\quad \left. + \frac{1}{2} \sum_e \lambda_{ec}^{ij} \mathcal{H}_{ab}^{ke} - \frac{1}{2} \sum_m \lambda_{ab}^{km} \mathcal{H}_{mc}^{ij} \right] \\
 D_{ijk}^{abc} &= \mathcal{H}_i^i + \mathcal{H}_j^j + \mathcal{H}_k^k - \mathcal{H}_a^a - \mathcal{H}_b^b - \mathcal{H}_c^c \\
 &\quad - \mathcal{H}_{ai}^{ai} - \mathcal{H}_{bi}^{bi} - \mathcal{H}_{ci}^{ci} - \mathcal{H}_{aj}^{aj} - \mathcal{H}_{bj}^{bj} - \mathcal{H}_{cj}^{cj} \\
 &\quad - \mathcal{H}_{ak}^{ak} - \mathcal{H}_{bk}^{bk} - \mathcal{H}_{ck}^{ck} + \mathcal{H}_{ij}^{ij} + \mathcal{H}_{ik}^{ik} + \mathcal{H}_{jk}^{jk} \\
 &\quad + \mathcal{H}_{ab}^{ab} + \mathcal{H}_{ac}^{ac} + \mathcal{H}_{bc}^{bc} \\
 &\quad + \mathcal{H}_{ija}^{ija} + \mathcal{H}_{ika}^{ika} + \mathcal{H}_{jka}^{jka} + \mathcal{H}_{ijb}^{ijb} + \mathcal{H}_{ikb}^{ikb} + \mathcal{H}_{jkb}^{jkb} \\
 &\quad + \mathcal{H}_{ijc}^{ijc} + \mathcal{H}_{ikc}^{ikc} + \mathcal{H}_{jkc}^{jkc} - \mathcal{H}_{abi}^{abi} - \mathcal{H}_{aci}^{aci} - \mathcal{H}_{bci}^{bci} \\
 &\quad - \mathcal{H}_{abj}^{abj} - \mathcal{H}_{acj}^{acj} - \mathcal{H}_{bcj}^{bcj} - \mathcal{H}_{abk}^{abk} - \mathcal{H}_{ack}^{ack} - \mathcal{H}_{bck}^{bck} \\
 \mathcal{H}_{abi}^{abi} &= \sum_m v_{ab}^{im} t_{im}^{ab} \\
 \mathcal{H}_{ija}^{ija} &= - \sum_e v_{ae}^{ij} t_{ij}^{ae} \\
 J_{ij}^{mc} &= \mathcal{H}_{ij}^{mc} - \sum_e \mathcal{H}_e^m t_{ij}^{ec}
 \end{aligned}$$

Figure 2.13: Algebraic expressions for the calculation of the CR-CC(2,3) energy correction for ground states [138].

employing the denominator

$$D_{ijk}^{abc} = \Delta E^{(\text{CCSD})} - \langle \Phi_{ijk}^{abc} | \hat{\mathcal{H}}^{(\text{CCSD})} | \Phi_{ijk}^{abc} \rangle \quad (2.123)$$

$$= - \sum_{n=1}^3 \langle \Phi_{ijk}^{abc} | \hat{\mathcal{H}}_n^{(\text{CCSD})} | \Phi_{ijk}^{abc} \rangle . \quad (2.124)$$

The working equations for the CR-CC(2,3) method can be found in [138], where they are presented in a form that also includes excited-state corrections. In Figure 2.13, the simplified version of these equations is given that only considers the ground-state triples correction. Some minor modifications have already been made for convenience later on regarding the angular-momentum coupled formulation.

2.9 Equation-of-Motion Coupled Cluster

In addition to ground-state wavefunctions and properties, excited states and their properties can be accessed within the Coupled-Cluster framework. In this work, the Equation-of-Motion CCSD (EOM-CCSD) [26,76] approach is employed, where for excited states $|\Psi_\mu^{(\text{CCSD})}\rangle$ a *linear* and thus CI-like excitation operator, truncated at the 2p2h excitation level,

$$\hat{\mathfrak{R}}_\mu^{(\text{CCSD})} = \hat{\mathfrak{R}}_{\mu,0} + \hat{\mathfrak{R}}_{\mu,1} + \hat{\mathfrak{R}}_{\mu,2} \quad (2.125)$$

$$= \hat{\mathfrak{R}}_{\mu,0} + \bigvee + \bigvee\bigvee \quad (2.126)$$

$$= (r_\mu)_0 + \sum_{ai} (r_\mu)_i^a \{ \hat{a}_a^\dagger \hat{a}_i \} + \sum_{abij} (r_\mu)_{ij}^{ab} \{ \hat{a}_a^\dagger \hat{a}_b^\dagger \hat{a}_j \hat{a}_i \} \quad (2.127)$$

is used to generate the excited state from the CCSD ground state,

$$|\Psi_\mu^{(\text{CCSD})}\rangle = \hat{\mathfrak{R}}_\mu^{(\text{CCSD})} e^{\hat{T}^{(\text{CCSD})}} |\Phi\rangle . \quad (2.128)$$

For the excited state $|\Psi_\mu^{(\text{CCSD})}\rangle$ the Schrödinger equation reads

$$\hat{H}_N \hat{\mathfrak{R}}_\mu^{(\text{CCSD})} e^{\hat{T}^{(\text{CCSD})}} |\Phi\rangle = \Delta E_\mu^{(\text{CCSD})} \hat{\mathfrak{R}}_\mu^{(\text{CCSD})} e^{\hat{T}^{(\text{CCSD})}} |\Phi\rangle , \quad (2.129)$$

which, due to the commutation relation $[\hat{\mathfrak{R}}_\mu^{(\text{CCSD})}, \hat{T}^{(\text{CCSD})}] = 0$ can, analogously to the ground-state case, be formulated as an eigenvalue problem of the effective Hamiltonian,

$$\hat{\mathcal{H}}^{(\text{CCSD})} \hat{\mathfrak{R}}_\mu^{(\text{CCSD})} |\Phi\rangle = \Delta E_\mu^{(\text{CCSD})} \hat{\mathfrak{R}}_\mu^{(\text{CCSD})} |\Phi\rangle . \quad (2.130)$$

Disconnected terms can further be removed from this equation by subtracting the ground-state equation $\hat{\mathcal{H}}^{(\text{CCSD})} |\Phi\rangle = \Delta E^{(\text{CCSD})} |\Phi\rangle$,

$$\left[\hat{\mathcal{H}}^{(\text{CCSD})}, \hat{\mathfrak{R}}_\mu^{(\text{CCSD})} \right] |\Phi\rangle = \omega_\mu^{(\text{CCSD})} \hat{\mathfrak{R}}_\mu^{(\text{CCSD})} |\Phi\rangle, \quad (2.131)$$

where

$$\omega_\mu^{(\text{CCSD})} \equiv \Delta E_\mu^{(\text{CCSD})} - \Delta E^{(\text{CCSD})} \quad (2.132)$$

is the excitation energy relative to the ground state. Since the effective Hamiltonian $\hat{\mathcal{H}}^{(\text{CCSD})} = \hat{\mathcal{H}}_0 + \hat{\mathcal{H}}_{\text{open}}^{(\text{CCSD})}$, with $\hat{\mathcal{H}}_0 = \Delta E^{(\text{CCSD})}$, consists of two parts – with and without external lines – and the commutator $[\hat{\mathcal{H}}_0, \hat{\mathfrak{R}}_\mu^{(\text{CCSD})}]$ clearly vanishes, the EOM-CCSD eigenvalue equation can be put into the convenient form

$$\left(\hat{\mathcal{H}}_{\text{open}}^{(\text{CCSD})} \hat{\mathfrak{R}}_\mu^{(\text{CCSD})} \right)_C |\Phi\rangle = \omega_\mu^{(\text{CCSD})} \hat{\mathfrak{R}}_\mu^{(\text{CCSD})} |\Phi\rangle, \quad (2.133)$$

serving as starting point for the derivation of algebraic expressions for the $\hat{\mathfrak{R}}_\mu^{(\text{CCSD})}$ amplitudes. By left-projecting (2.133) onto singly and doubly excited determinants, an eigenvalue problem for the amplitudes $(r_\mu)_i^a$ and $(r_\mu)_{ij}^{ab}$ is obtained

$$\langle \Phi_i^a | \left(\hat{\mathcal{H}}_{\text{open}}^{(\text{CCSD})} \hat{\mathfrak{R}}_\mu^{(\text{CCSD})} \right)_C |\Phi\rangle = \omega_\mu^{(\text{CCSD})} (r_\mu)_i^a \quad (2.134)$$

$$\langle \Phi_{ij}^{ab} | \left(\hat{\mathcal{H}}_{\text{open}}^{(\text{CCSD})} \hat{\mathfrak{R}}_\mu^{(\text{CCSD})} \right)_C |\Phi\rangle = \omega_\mu^{(\text{CCSD})} (r_\mu)_{ij}^{ab}. \quad (2.135)$$

The constant amplitude $(r_\mu)_0$ may afterwards be calculated separately from the solution of (2.134) and (2.135) according to

$$\langle \Phi | \left(\hat{\mathcal{H}}_{\text{open}}^{(\text{CCSD})} \hat{\mathfrak{R}}_\mu^{(\text{CCSD})} \right)_C |\Phi\rangle = \omega_\mu^{(\text{CCSD})} (r_\mu)_0. \quad (2.136)$$

The corresponding diagrams can be found in Appendix H.1, and the algebraic expressions are listed in Figure 2.14. The last 4 terms in the $\hat{\mathfrak{R}}_2$ amplitude equations stem from contributions of the three-body part $\hat{\mathcal{H}}_3$ of the effective Hamiltonian to the $\hat{\mathfrak{R}}_2$ equations which have been explicitly expressed in terms of cluster amplitudes and in order to avoid storing the three-body matrix elements of $\hat{\mathcal{H}}_3$ [76] (for a similar discussion, see Section 3.3).

The excited bra state $\langle \tilde{\Psi}_\mu^{(\text{CCSD})} |$ may be parametrized as [76]

$$\langle \tilde{\Psi}_\mu^{(\text{CCSD})} | = \langle \Phi | \hat{\mathcal{L}}_\mu^{(\text{CCSD})} e^{-\hat{T}^{(\text{CCSD})}}, \quad (2.137)$$

$$\begin{aligned}
 \omega r_0 &= \overset{(\mathfrak{R}_0^A)}{+} \sum_{ai} r_i^a \mathcal{H}_a^i + \frac{1}{4} \overset{(\mathfrak{R}_0^B)}{\sum_{abij} r_{ij}^{ab} \mathcal{H}_{ab}^{ij}} \\
 \langle \Phi_i^a | \left(\mathcal{H}_{\text{open}}^{(\text{CCSD})} \hat{\mathfrak{R}}_{\mu}^{(\text{CCSD})} \right)_C | \Phi \rangle &= \\
 &\overset{(\mathfrak{R}_1^A)}{+} \sum_c r_i^c \mathcal{H}_c^a - \overset{(\mathfrak{R}_1^B)}{\sum_k r_k^a \mathcal{H}_i^k} + \overset{(\mathfrak{R}_1^C)}{\sum_{ck} r_k^c \mathcal{H}_{ic}^{ak}} \\
 &\overset{(\mathfrak{R}_1^D)}{+} \sum_{ck} r_{ik}^{ac} \mathcal{H}_c^k + \frac{1}{2} \overset{(\mathfrak{R}_1^E)}{\sum_{cdk} r_{ik}^{cd} \mathcal{H}_{cd}^{ak}} + \frac{1}{2} \overset{(\mathfrak{R}_1^F)}{\sum_{ckl} r_{kl}^{ac} \mathcal{H}_{ic}^{kl}} \\
 \langle \Phi_{ij}^{ab} | \left(\mathcal{H}_{\text{open}}^{(\text{CCSD})} \hat{\mathfrak{R}}_{\mu}^{(\text{CCSD})} \right)_C | \Phi \rangle &= \\
 &\overset{(\mathfrak{R}_2^A)}{+} \hat{P}_{ij} \sum_c r_i^c \mathcal{H}_{cj}^{ab} - \overset{(\mathfrak{R}_2^B)}{\hat{P}_{ab} \sum_k r_k^a \mathcal{H}_{ij}^{kb}} \\
 &\overset{(\mathfrak{R}_2^C)}{+} \hat{P}_{ab} \sum_c r_{ij}^{ac} \mathcal{H}_c^b - \overset{(\mathfrak{R}_2^D)}{\hat{P}_{ij} \sum_k r_{ik}^{ab} \mathcal{H}_j^k} + \frac{1}{2} \overset{(\mathfrak{R}_2^E)}{\sum_{cd} r_{ij}^{cd} \mathcal{H}_{cd}^{ab}} \\
 &\overset{(\mathfrak{R}_2^F)}{+} \frac{1}{2} \sum_{kl} r_{kl}^{ab} \mathcal{H}_{ij}^{kl} + \overset{(\mathfrak{R}_2^G)}{\hat{P}_{ab} \hat{P}_{ij} \sum_{ck} r_{ik}^{ac} \mathcal{H}_{cj}^{kb}} \\
 &\overset{(\mathfrak{R}_2^H)}{+} \hat{P}_{ab} \sum_{cdk} r_k^d t_{ij}^{ac} \mathcal{H}_{cd}^{bk} + \frac{1}{2} \overset{(\mathfrak{R}_2^I)}{\hat{P}_{ab} \sum_{cdkl} r_{kl}^{da} v_{cd}^{kl} t_{ij}^{cb}} \\
 &\overset{(\mathfrak{R}_2^J)}{-} \hat{P}_{ij} \sum_{ckl} r_l^c t_{ik}^{ab} \mathcal{H}_{jc}^{kl} + \frac{1}{2} \overset{(\mathfrak{R}_2^K)}{\hat{P}_{ij} \sum_{cdkl} r_{il}^{cd} t_{jk}^{ab} v_{cd}^{kl}}
 \end{aligned}$$

Figure 2.14: Algebraic expressions for the $\hat{\mathfrak{R}}^{(\text{CCSD})}$ amplitude equations. The index μ has been dropped.

where $\hat{\mathcal{L}}_\mu^{(\text{CCSD})}$ is a de-excitation operator

$$\hat{\mathcal{L}}_\mu^{(\text{CCSD})} = \hat{\mathcal{L}}_{\mu,0} + \hat{\mathcal{L}}_{\mu,1} + \hat{\mathcal{L}}_{\mu,2} \quad (2.138)$$

$$= \hat{\mathcal{L}}_{\mu,0} + \text{V} + \text{VV} \quad (2.139)$$

$$= (l_\mu)_0 + \sum_{ai} (l_\mu)_a^i \{\hat{a}_i^\dagger \hat{a}_a\} + \sum_{abij} (l_\mu)_{ab}^{ij} \{\hat{a}_i^\dagger \hat{a}_j^\dagger \hat{a}_b \hat{a}_a\}. \quad (2.140)$$

Since $\langle \tilde{\Psi}_\mu^{(\text{CCSD})} |$ satisfies the Schrödinger equation

$$\langle \Phi | \hat{\mathcal{L}}_\mu^{(\text{CCSD})} e^{-\hat{T}^{(\text{CCSD})}} \hat{H}_N = \Delta E_\mu^{(\text{CCSD})} \langle \Phi | \hat{\mathcal{L}}_\mu^{(\text{CCSD})} e^{-\hat{T}^{(\text{CCSD})}} \quad (2.141)$$

it follows that $\langle \Phi | \hat{\mathcal{L}}_\mu^{(\text{CCSD})}$ is also eigenfunction of the effective Hamiltonian,

$$\langle \Phi | \hat{\mathcal{L}}_\mu^{(\text{CCSD})} \hat{\mathcal{H}}^{(\text{CCSD})} = \Delta E_\mu^{(\text{CCSD})} \langle \Phi | \hat{\mathcal{L}}_\mu^{(\text{CCSD})}. \quad (2.142)$$

As for the right eigenproblem, the left one can be formulated in a way that directly provides the excitation energy $\omega_\mu^{(\text{CCSD})}$,

$$\langle \Phi | \hat{\mathcal{L}}_\mu^{(\text{CCSD})} \hat{\mathcal{H}}_{\text{open}}^{(\text{CCSD})} = \left(\Delta E_\mu^{(\text{CCSD})} - \mathcal{H}_0 \right) \langle \Phi | \hat{\mathcal{L}}_\mu^{(\text{CCSD})}, \quad (2.143)$$

and thus, recalling that $\mathcal{H}_0 = \Delta E^{(\text{CCSD})}$,

$$\langle \Phi | \hat{\mathcal{L}}_\mu^{(\text{CCSD})} \hat{\mathcal{H}}_{\text{open}}^{(\text{CCSD})} = \omega_\mu^{(\text{CCSD})} \langle \Phi | \hat{\mathcal{L}}_\mu^{(\text{CCSD})}. \quad (2.144)$$

Unlike the right eigenvalue equation, the left one has no restriction to connected diagrams. Furthermore, it has the same structure as the Λ CCSD equations, and, therefore, the corresponding diagrams are identical. The only difference is in diagrams $(\Lambda_1 A)$ and $(\Lambda_2 A)$, which for the EOM-CCSD case translate into

$$\text{V} = (l_\mu)_0 \chi_a^i, \quad \text{VV} = (l_\mu)_0 v_{ab}^{ij}. \quad (2.145)$$

However, it can be shown that $(l_\mu)_0 = \delta_{\mu 0}$ [26] and, therefore, these diagrams vanish for excited states and are consequently left out in the equations. In conclusion, the effective Hamiltonian matrix, being of non-Hermitian nature, possesses two sets of normalized eigenvectors $\{\mathfrak{L}_\mu^{(\text{CCSD})}\}$ and $\{\mathfrak{R}_\mu^{(\text{CCSD})}\}$,

$$\mathfrak{L}_\mu^{(\text{CCSD})} \equiv \left((l_\mu)_0, \{ (l_\mu)_a^i \}, \{ (l_\mu)_{ab}^{ij} \} \right) \quad (2.146)$$

$$\mathfrak{R}_\mu^{(\text{CCSD})} \equiv \left((r_\mu)_0, \{ (r_\mu)_i^a \}, \{ (r_\mu)_{ij}^{ab} \} \right)^T, \quad (2.147)$$

with

$$\mathfrak{L}_\mu^{(\text{CCSD})} \cdot \mathfrak{L}_\mu^{(\text{CCSD})} = 1 \quad (2.148)$$

$$\mathfrak{R}_\mu^{(\text{CCSD})} \cdot \mathfrak{R}_\mu^{(\text{CCSD})} = 1, \quad (2.149)$$

which share the same eigenvalues but are otherwise distinct. As is well-known from the theory of non-Hermitean eigenvalue problems [145], the eigenvectors $\{\mathfrak{L}_\mu^{(\text{CCSD})}\}$ and $\{\mathfrak{R}_\mu^{(\text{CCSD})}\}$ are not orthogonal among themselves but satisfy a *biorthogonality relation*

$$\mathfrak{L}_\mu^{(\text{CCSD})} \cdot \mathfrak{R}_\nu^{(\text{CCSD})} = \delta_{\mu\nu} \quad (2.150)$$

where the originally normalized left eigenvector $\mathfrak{L}_\mu^{(\text{CCSD})}$ has to be rescaled according to

$$\mathfrak{L}_\mu^{(\text{CCSD})} \rightarrow \frac{1}{\mathfrak{L}_\mu^{(\text{CCSD})} \cdot \mathfrak{R}_\mu^{(\text{CCSD})}} \mathfrak{L}_\mu^{(\text{CCSD})} \quad (2.151)$$

to achieve unit overlap with the corresponding right eigenvector

$$\langle \tilde{\Psi}_\mu^{(\text{CCSD})} | \Psi_\nu^{(\text{CCSD})} \rangle = \langle \Phi | \hat{\mathfrak{L}}_\mu^{(\text{CCSD})} e^{-\hat{T}^{(\text{CCSD})}} e^{\hat{T}^{(\text{CCSD})}} \hat{\mathfrak{R}}_\nu^{(\text{CCSD})} | \Phi \rangle = \delta_{\mu\nu}. \quad (2.152)$$

In order to achieve unit overlap, the choice of $\mathfrak{L}_\mu^{(\text{CCSD})}$ as the vector to be scaled is of course arbitrary. However, to be consistent with the ground-state solution the right vector is normalized to unity and the left vector is rescaled [76].

2.9.1 Reduced Density Matrices

Properties of excited states as well as transition properties can be calculated within the EOM-CCSD approach from the left and right solutions of the effective Hamiltonian eigenproblem by means of a reduced density matrix $(\rho_N^{\mu\nu})_{p_1 \dots p_n}^{q_1 \dots q_n}$ defined similarly to its ground-state counterpart (2.82),

$$(\rho_N^{\mu\nu})_{p_1 \dots p_n}^{q_1 \dots q_n} = \langle \Phi | \left[\hat{\mathfrak{L}}_\mu^{(\text{CCSD})} \left(\hat{a}_{p_1}^\dagger \dots \hat{a}_{p_n}^\dagger \hat{a}_{q_n} \dots \hat{a}_{q_1} e^{\hat{T}^{(\text{CCSD})}} \right)_C \hat{\mathfrak{R}}_\nu^{(\text{CCSD})} \right]_C | \Phi \rangle. \quad (2.153)$$

The quantity of interest is a generalized expectation value of a n -body operator \hat{G} ,

$$\begin{aligned} \langle \hat{G} \rangle_{\mu\nu} &= \langle \tilde{\Psi}_\mu^{(\text{CCSD})} | \hat{G} | \Psi_\nu^{(\text{CCSD})} \rangle \\ &= \langle \tilde{\Psi}_\mu^{(\text{CCSD})} | \Psi_\nu^{(\text{CCSD})} \rangle \langle \Phi | \hat{G} | \Phi \rangle + \langle \hat{G}_N \rangle_{\mu\nu}, \end{aligned} \quad (2.154)$$

which is evaluated analogously to (2.83) in terms of the reduced density matrix as

$$\langle \hat{G}_N \rangle_{\mu\nu} = \sum_{k=1}^n \frac{1}{(k!)^2} \sum_{\substack{p_1 \dots p_k \\ q_1 \dots q_k}} \langle p_1 \dots p_k | \hat{g}_N | q_1 \dots q_k \rangle (\rho_N^{\mu\nu})_{p_1 \dots p_k}^{q_1 \dots q_k}. \quad (2.155)$$

Again, the one-body operator expectation value may be written in the compact form

$$\langle \hat{O} \rangle_{\mu\nu} = \sum_{pq} \langle p | \hat{O} | q \rangle (\rho^{\mu\nu})_p^q, \quad (2.156)$$

$$(\rho^{\mu\nu})_p^q \equiv \begin{cases} (\rho_N^{\mu\nu})_p^q + \delta_{\mu\nu} \delta_{pq} & : p, q \in \text{holes} \\ (\rho_N^{\mu\nu})_p^q & : \text{else,} \end{cases} \quad (2.157)$$

where the orthogonality of the left and right eigenstates of the effective Hamiltonian has been taken into account. This approach works for excited states as well as for ground states, provided that the operators $\hat{\mathcal{L}}_0^{(\text{CCSD})}, \hat{\mathcal{R}}_0^{(\text{CCSD})}$ and vectors $\mathcal{L}_0^{(\text{CCSD})}, \mathfrak{R}_0^{(\text{CCSD})}$, defined as

$$\hat{\mathcal{L}}_0^{(\text{CCSD})} \equiv \hat{1} + \hat{\Lambda}, \quad \mathcal{L}_0^{(\text{CCSD})} = (1, \{\lambda_a^i\}, \{\lambda_{ab}^{ij}\}) \quad (2.158)$$

$$\hat{\mathcal{R}}_0^{(\text{CCSD})} \equiv \hat{1}, \quad \mathfrak{R}_0^{(\text{CCSD})} = (1, \{0\}, \{0\}), \quad (2.159)$$

are assigned to the ground state solutions. As is discussed in Ref. [76], transition moments $\langle \tilde{\Psi}_\mu^{(\text{CCSD})} | \Psi_\nu^{(\text{CCSD})} \rangle$ are not well defined due to the non-Hermiticity of the effective Hamiltonian. Therefore, products of left and right transition moments

$$\langle \hat{O} \rangle_{\mu\nu} \langle \hat{O} \rangle_{\nu\mu} = \langle \tilde{\Psi}_\mu^{(\text{CCSD})} | \hat{O} | \Psi_\nu^{(\text{CCSD})} \rangle \langle \tilde{\Psi}_\nu^{(\text{CCSD})} | \hat{O} | \Psi_\mu^{(\text{CCSD})} \rangle \quad (2.160)$$

are computed instead since these products correspond to the squares of the transition moments which are the only observables in the first place.

Reduced density matrices are not used in actual calculations in this work, consequently no equations are presented, but in later sections useful remarks about the spherical treatment of reduced density matrixes as well as the appropriate normalization (2.152) of the left and right eigenvectors are given.

Chapter 3

Coupled-Cluster Theory for Three-Body Hamiltonians

3.1 CCSD for Three-Body Hamiltonians

3.1.1 Introduction

The normal-ordering approximation discussed in Section 1.5 represents an effective way for the approximate incorporation of three-, or even higher-nucleon interaction effects in many-body calculations that are able to handle effective interactions up to the two-body level. Nevertheless, the desire to include the full three-body interaction still persists, at least for the purpose to benchmark possible approximation schemes.

The inclusion of higher-body interactions into the NCSM framework is – conceptually – relatively simple. A highly efficient implementation of the three-body interaction matrix element handling in the IT-NCSM allows for computations of nuclei even beyond the p shell. The treatment of the full three-body force in the Coupled-Cluster framework comes along with a significant increase of diagrams to be evaluated, resulting in a larger implementational effort. But once implemented, the CCSD method for three-body Hamiltonians benefits greatly from its gentle scaling behaviour as well as from efficient matrix element handling [86] to go beyond the sd shell.

A first derivation of the corresponding CCSD equations in a factorized form was published in 2007 [63]. Here, in this work, the unfactorized derivation is presented, resulting in less compact but structurally simpler expressions. Diagram factorization often comes along with increased memory requirements since intermediates have to be stored. On the other hand, the computational runtime is usually strongly dominated by only a few diagrams that need to be singled out to receive special implementational care.

3.1.2 The CCSD Equations for Three-Body Hamiltonians

The derivation of the three-body CCSD equations requires the same formal steps as for the two-body case. The Hamiltonian in second-quantized standard form reads

$$\hat{H} = \hat{h}_0 + \hat{h}_1 + \hat{h}_2 + \hat{h}_3 \quad (3.1)$$

$$\begin{aligned} &= h_0 + \sum_{pq} \langle p | \hat{h}_1 | q \rangle \hat{a}_p^\dagger \hat{a}_q + \frac{1}{4} \sum_{pqrs} \langle pq | \hat{h}_2 | rs \rangle \hat{a}_p^\dagger \hat{a}_q^\dagger \hat{a}_s \hat{a}_r \\ &+ \frac{1}{36} \sum_{pqrstu} \langle pqr | \hat{h}_3 | stu \rangle \hat{a}_p^\dagger \hat{a}_q^\dagger \hat{a}_r^\dagger \hat{a}_u \hat{a}_t \hat{a}_s . \end{aligned} \quad (3.2)$$

In terms of normal-ordered operator strings the Hamiltonian is represented by

$$\begin{aligned} \hat{H} &= h_0 + \sum_i \langle i | \hat{h}_1 | i \rangle + \sum_{pq} \langle p | \hat{h}_1 | q \rangle \{ \hat{a}_p^\dagger \hat{a}_q \} + \frac{1}{2} \sum_{ij} \langle ij | \hat{h}_2 | ij \rangle \\ &+ \sum_{pqi} \langle pi | \hat{h}_2 | qi \rangle \{ \hat{a}_p^\dagger \hat{a}_q \} + \frac{1}{4} \sum_{pqrs} \langle pq | \hat{h}_2 | rs \rangle \{ \hat{a}_p^\dagger \hat{a}_q^\dagger \hat{a}_s \hat{a}_r \} \\ &+ \frac{1}{6} \sum_{ijk} \langle ijk | \hat{h}_3 | ijk \rangle + \frac{1}{2} \sum_{pqij} \langle ijp | \hat{h}_3 | ijq \rangle \{ \hat{a}_p^\dagger \hat{a}_q \} \\ &+ \frac{1}{4} \sum_{pqrsi} \langle pqi | \hat{h}_3 | rsi \rangle \{ \hat{a}_p^\dagger \hat{a}_q^\dagger \hat{a}_s \hat{a}_r \} \\ &+ \frac{1}{36} \sum_{pqrstu} \langle pqr | \hat{h}_3 | stu \rangle \{ \hat{a}_p^\dagger \hat{a}_q^\dagger \hat{a}_r^\dagger \hat{a}_u \hat{a}_t \hat{a}_s \} , \end{aligned} \quad (3.3)$$

which again can be cast into the compact form

$$\begin{aligned} \hat{H} &= \langle \Phi | \hat{H} | \Phi \rangle + \sum_{pq} f_q^p \{ \hat{a}_p^\dagger \hat{a}_q \} + \frac{1}{4} \sum_{pqrs} v_{rs}^{pq} \{ \hat{a}_p^\dagger \hat{a}_q^\dagger \hat{a}_s \hat{a}_r \} \\ &+ \frac{1}{36} \sum_{pqrstu} w_{stu}^{pqr} \{ \hat{a}_p^\dagger \hat{a}_q^\dagger \hat{a}_r^\dagger \hat{a}_u \hat{a}_t \hat{a}_s \} , \end{aligned} \quad (3.4)$$

or ,

$$\hat{H} = \langle \Phi | \hat{H} | \Phi \rangle + \hat{F}_N + \hat{V}_N + \hat{W}_N . \quad (3.5)$$

In (3.5), $\langle \Phi | \hat{H} | \Phi \rangle$ is the reference state expectation value

$$\langle \Phi | \hat{H} | \Phi \rangle = h_0 + \sum_i \langle i | \hat{h}_1 | i \rangle + \frac{1}{2} \sum_{ij} \langle ij | \hat{h}_2 | ij \rangle + \frac{1}{6} \sum_{ijk} \langle ijk | \hat{h}_3 | ijk \rangle , \quad (3.6)$$

and the following definitions are analogous to the two-body CCSD case,

$$f_q^p \equiv \langle p|\hat{f}|q\rangle = \langle p|\hat{h}_1|q\rangle + \sum_i \langle pi|\hat{h}_2|qi\rangle + \frac{1}{2} \sum_{ij} \langle ij|\hat{h}_3|ij\rangle, \quad (3.7)$$

$$v_{rs}^{pq} \equiv \langle pq|\hat{v}|rs\rangle = \langle pq|\hat{h}_2|rs\rangle + \sum_i \langle pqi|\hat{h}_3|rsi\rangle, \quad (3.8)$$

$$w_{stu}^{pqr} \equiv \langle pqr|\hat{w}|stu\rangle = \langle pqr|\hat{h}_3|stu\rangle. \quad (3.9)$$

Apart from the normal-ordered three-body part \hat{W}_N , the Hamiltonian (3.5)

$$\hat{H} = \langle \Phi|\hat{H}|\Phi\rangle + \hat{H}_N \quad (3.10)$$

has the same topology as for the two-body case, leading to the exact same equations with replaced definitions for the matrix elements of the normal-ordered operators \hat{F}_N , \hat{V}_N and reference expectation value $\langle \Phi|\hat{H}|\Phi\rangle$. Therefore, all new expressions are generated from \hat{W}_N and will consequently always involve the matrix elements $\langle pqr|\hat{w}|stu\rangle$. This observation also allows to write any quantity, such as the correlation energy or amplitude expressions, for instance, in the form

$$\Delta E^{(\text{CCSD})} = \Delta E_{\text{NO2B}}^{(\text{CCSD})} + \Delta E_{\text{3B}}^{(\text{CCSD})} \quad (3.11)$$

$$0 = T_{1,\text{NO2B}}^{(\text{CCSD})} + T_{1,\text{3B}}^{(\text{CCSD})} \quad (3.12)$$

$$0 = T_{2,\text{NO2B}}^{(\text{CCSD})} + T_{2,\text{3B}}^{(\text{CCSD})}, \quad (3.13)$$

where the quantity with label "NO2B" denotes the usual algebraic expressions already known from the Coupled-Cluster theory for two-body Hamiltonians, but with implied usage of the re-definitions of the normal-ordered Hamiltonians matrix elements E_{ref} , f_q^p , and v_{rs}^{pq} , Eqs. (3.6), (3.7) and (3.8), whereas the quantity with label "3B" denotes all the new terms due to the presence of the residual normal-ordered three-body interaction operator \hat{W}_N .

The expansion for the effective Hamiltonian for an arbitrary CC method truncated at the $M_p M_h$ excitation level,

$$\hat{\mathcal{H}}^{(\text{M})} = e^{-\hat{T}^{(\text{M})}} \hat{H}_N e^{\hat{T}^{(\text{M})}}, \quad (3.14)$$

again terminates, this time, due to the six external lines of \hat{W}_N , after the six-fold commutator at the lastest,

$$\hat{\mathcal{H}}^{(\text{M})} = \hat{H}_N + \sum_{n=1}^6 \frac{1}{n!} \underbrace{\left[\dots \left[\hat{H}_N, \hat{T}^{(\text{M})} \right], \dots, \hat{T}^{(\text{M})} \right]}_{n \text{ times}}. \quad (3.15)$$

From this clearly follows that no more than six $\hat{T}^{(M)}$ operators will appear in individual diagrams for the effective Hamiltonian, and consequently in any Coupled-Cluster equations. For CCSD, as can be seen below, the maximum number of $\hat{T}^{(\text{CCSD})}$ operators appearing in the equations is actually only five instead of six.

The Coupled-Cluster equations then follow from left-projection of the similarity transformed Schrödinger equations onto the reference state and corresponding excited determinants,

$$\langle \Phi_{i_1 \dots i_n}^{a_1 \dots a_n} | \hat{\mathcal{H}}^{(M)} | \Phi \rangle = \langle \Phi_{i_1 \dots i_n}^{a_1 \dots a_n} | \left(\hat{H}_N e^{\hat{T}^{(M)}} \right)_C | \Phi \rangle, \quad n = 0, \dots, M. \quad (3.16)$$

As mentioned before, the operator parts \hat{F}_N and \hat{V}_N produce the exact same expressions as for the two-body case, which contributions to the CCSD energy and amplitude equations are abbreviated as $\Delta E_{\text{NO2B}}^{(\text{CCSD})}$ resp. $T_{1,\text{NO2B}}^{(\text{CCSD})}$ and $T_{2,\text{NO2B}}^{(\text{CCSD})}$ and are not written explicitly. Excitation rank considerations¹

$$X(\langle \Phi_{i_1 \dots i_n}^{a_1 \dots a_n} |) + X(\hat{W}_N) + X(e^{\hat{T}^{(\text{CCSD})}}) \stackrel{!}{=} 0 \quad (3.17)$$

yield the following operator expression for the CCSD energy equation

$$\Delta E^{(\text{CCSD})} = \Delta E_{\text{NO2B}}^{(\text{CCSD})} + \langle \Phi | \left[\hat{W}_N \left(\hat{T}_1 + \hat{T}_2 + \frac{1}{2!} \hat{T}_1^2 + \hat{T}_1 \hat{T}_2 + \frac{1}{3!} \hat{T}_1^3 \right) \right]_C | \Phi \rangle \quad (3.18)$$

and for the \hat{T}_1 and \hat{T}_2 amplitude equations

$$\begin{aligned} 0 &= T_{1,\text{NO2B}}^{(\text{CCSD})} \\ &+ \langle \Phi_i^a | \left[\hat{W}_N \left(1 + \hat{T}_1 + \hat{T}_2 + \frac{1}{2!} \hat{T}_1^2 + \hat{T}_1 \hat{T}_2 \right. \right. \\ &\quad \left. \left. + \frac{1}{2!} \hat{T}_2^2 + \frac{1}{3!} \hat{T}_1^3 + \frac{1}{2!} \hat{T}_1^2 \hat{T}_2 + \frac{1}{4!} \hat{T}_1^4 \right) \right]_C | \Phi \rangle \end{aligned} \quad (3.19)$$

$$\begin{aligned} 0 &= T_{2,\text{NO2B}}^{(\text{CCSD})} \\ &+ \langle \Phi_{ij}^{ab} | \left[\hat{W}_N \left(1 + \hat{T}_1 + \hat{T}_2 + \frac{1}{2!} \hat{T}_1^2 + \hat{T}_1 \hat{T}_2 + \frac{1}{2!} \hat{T}_2^2 + \frac{1}{3!} \hat{T}_1^3 + \frac{1}{2!} \hat{T}_1^2 \hat{T}_2 \right. \right. \\ &\quad \left. \left. + \frac{1}{3!} \hat{T}_1^3 \hat{T}_2 + \frac{1}{2!} \hat{T}_1 \hat{T}_2^2 + \frac{1}{4!} \hat{T}_1^4 + \frac{1}{5!} \hat{T}_1^5 \right) \right]_C | \Phi \rangle \end{aligned} \quad (3.20)$$

The energy equation may be simplified right away due to the requirement of producing closed diagrams which is clearly only possible for the cluster operator products² $\hat{T}_1 \hat{T}_2$ and \hat{T}_1^3 , so that

$$\Delta E^{(\text{CCSD})} = \Delta E_{\text{NO2B}}^{(\text{CCSD})} + \langle \Phi | \left[\hat{W}_N \left(\hat{T}_1 \hat{T}_2 + \frac{1}{3!} \hat{T}_1^3 \right) \right]_C | \Phi \rangle. \quad (3.21)$$

¹The excitation ranks of $|\Phi_{i_1 \dots i_n}^{a_1 \dots a_n}\rangle$ and $\langle \Phi_{i_1 \dots i_n}^{a_1 \dots a_n}|$ are understood to be n and $-n$, respectively.

²This is because their number of external lines match the number of external lines of the residual normal-ordered three-body interaction operator \hat{W}_N .

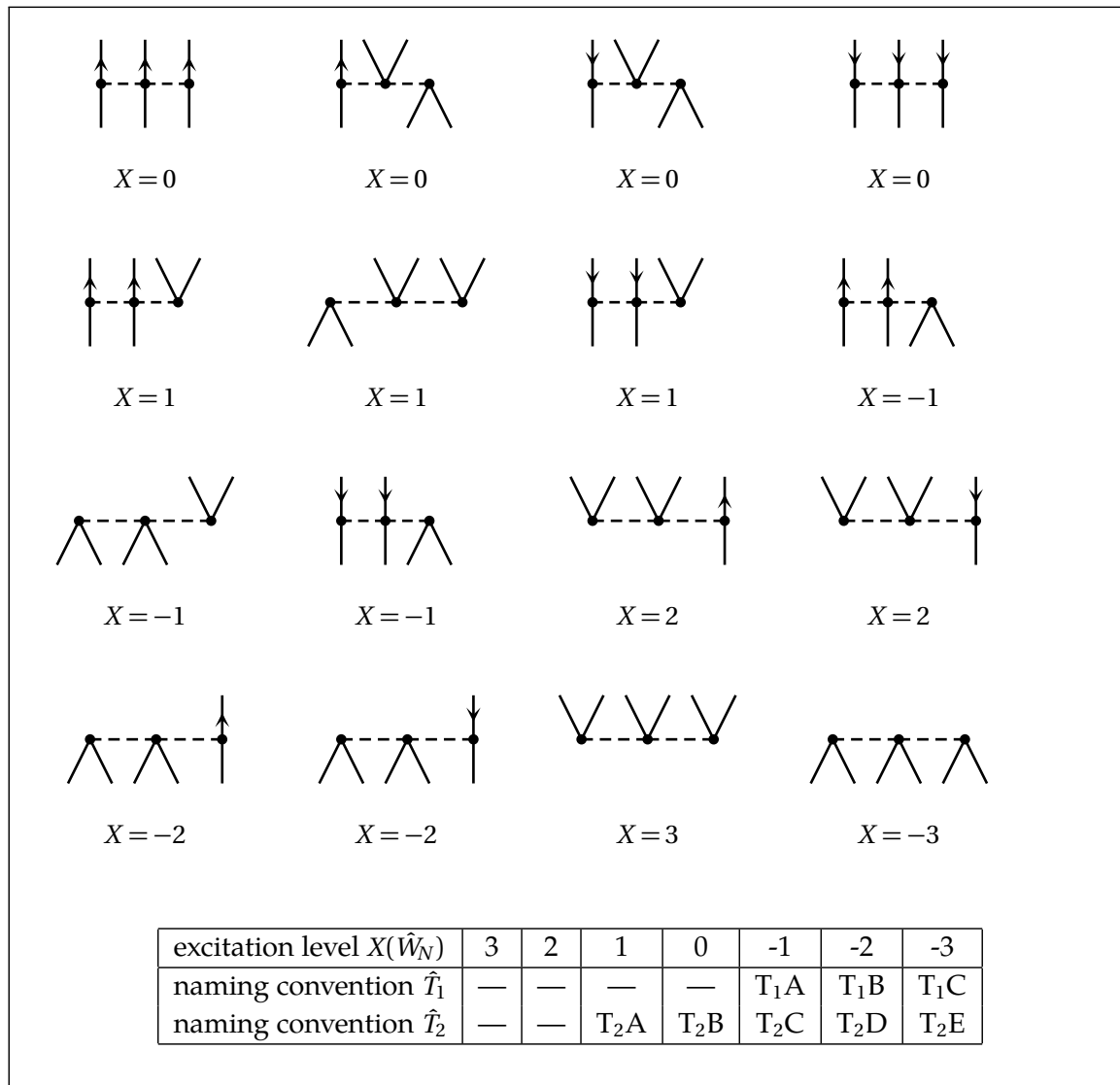


Figure 3.1: Topology and excitation level of the three-body part \hat{W}_N of the normal-ordered Hamiltonian. The table introduces the diagram naming convention that characterizes diagrams by the excitation level of the \hat{W}_N operator part involved. There are no $X(\hat{W}_N) \geq 2$ contributions to the CCSD \hat{T}_1 and \hat{T}_2 equations since this would require at least 5 external lines from the bra determinant.

Analogous considerations lead to minor simplifications of the \hat{T}_1 and \hat{T}_2 amplitude equations,

$$0 = T_{1,\text{NO2B}}^{(\text{CCSD})} + \langle \Phi_i^a | \left[\hat{W}_N \left(\hat{T}_2 + \frac{1}{2!} \hat{T}_1^2 + \hat{T}_1 \hat{T}_2 + \frac{1}{2!} \hat{T}_2^2 + \frac{1}{3!} \hat{T}_1^3 + \frac{1}{2!} \hat{T}_1^2 \hat{T}_2 + \frac{1}{4!} \hat{T}_1^4 \right) \right]_C | \Phi \rangle \quad (3.22)$$

and

$$0 = T_{2,\text{NO2B}}^{(\text{CCSD})} + \langle \Phi_{ij}^{ab} | \left[\hat{W}_N \left(\hat{T}_1 + \hat{T}_2 + \frac{1}{2!} \hat{T}_1^2 + \hat{T}_1 \hat{T}_2 + \frac{1}{2!} \hat{T}_2^2 + \frac{1}{3!} \hat{T}_1^3 + \frac{1}{2!} \hat{T}_1^2 \hat{T}_2 + \frac{1}{3!} \hat{T}_1^3 \hat{T}_2 + \frac{1}{2!} \hat{T}_1 \hat{T}_2^2 + \frac{1}{4!} \hat{T}_1^4 + \frac{1}{5!} \hat{T}_1^5 \right) \right]_C | \Phi \rangle . \quad (3.23)$$

The evaluation of (3.21)-(3.23) in terms of matrix elements is straightforward using standard diagrammatic techniques. In order to catch all topologically distinct diagrams it is recommended to do a Hugenholtz analysis first before translating each Hugenholtz diagram in one equivalent antisymmetrized Goldstone diagram [26]. These diagrams are listed in Section C.3 and the corresponding algebraic expressions are listed in Figures 3.2-3.4. The naming convention has been chosen according to the excitation level of the \hat{W}_N operator part involved in the diagram. The topology of \hat{W}_N along with the corresponding excitation level is given in Figure 3.1. Unlike for two-body Hamiltonians, where the algebraic expression for $\Delta E^{(\text{CCSD})}$ is also valid for all higher-order Coupled-Cluster method, in the case of three-body Hamiltonians this expression only holds for the CCSD approximation. This is because a three-body interaction also allows to form a closed diagram via contraction with a \hat{T}_3 operator,

$$\langle \Phi | (\hat{W}_N \hat{T}_3)_C | \Phi \rangle = \text{Diagram} = \frac{1}{(3!)^2} \sum_{\substack{abc \\ ijk}} w_{abc}^{ijk} t_{ijk}^{abc} . \quad (3.24)$$

Also, it should be noted that the total CCSD ground-state energy reads

$$E^{(\text{CCSD})} = E_{\text{ref}} + \Delta E_{\text{NO2B}}^{(\text{CCSD})} + \Delta E_{\text{3B}}^{(\text{CCSD})} , \quad (3.25)$$

where from the definition of E_{ref} as a reference-state expectation value it is clear that it is not affected, compared to the NO2B treatment, by including the residual normal-ordered three-body interaction in the calculations.

$$\begin{aligned}
 \Delta E^{(\text{CCSD})} &= \Delta E_{\text{NO2B}}^{(\text{CCSD})} + \frac{1}{4} \sum_{cdeklm} w_{cde}^{klm} t_k^c t_l^d t_m^e \\
 &\quad + \frac{1}{6} \sum_{cdeklm}^{(\text{EE})} w_{cde}^{klm} t_k^c t_l^d t_m^e \\
 &\quad + \frac{1}{2} \sum_{cdkl}^{(\text{T}_1\text{Aa})} w_{cdi}^{kla} t_k^c t_l^d + \frac{1}{4} \sum_{cdkl}^{(\text{T}_1\text{Ab})} w_{cdi}^{kla} t_{kl}^{cd} \\
 &\quad + \frac{1}{2} \sum_{cdekl}^{(\text{T}_1\text{Ba})} w_{cde}^{kla} t_k^c t_l^d t_i^e + \frac{1}{4} \sum_{cdekl}^{(\text{T}_1\text{Bb})} w_{cde}^{kla} t_{kl}^{cd} t_i^e \\
 &\quad + \frac{1}{2} \sum_{cdekl}^{(\text{T}_1\text{Bc})} w_{cde}^{kla} t_k^c t_l^d t_i^e - \frac{1}{2} \sum_{cdklm}^{(\text{T}_1\text{Bd})} w_{cdi}^{klm} t_k^c t_l^d t_m^a \\
 &\quad - \frac{1}{4} \sum_{cdklm}^{(\text{T}_1\text{Be})} w_{cdi}^{klm} t_{kl}^{cd} t_m^a - \frac{1}{2} \sum_{cdklm}^{(\text{T}_1\text{Bf})} w_{cdi}^{klm} t_k^c t_l^d t_m^a \\
 &\quad - \frac{1}{2} \sum_{cdeklm}^{(\text{T}_1\text{Ca})} w_{cde}^{klm} t_k^c t_l^d t_m^a t_i^e - \frac{1}{4} \sum_{cdeklm}^{(\text{T}_1\text{Cb})} w_{cde}^{klm} t_{kl}^{cd} t_m^a t_i^e \\
 &\quad - \frac{1}{2} \sum_{cdeklm}^{(\text{T}_1\text{Cc})} w_{cde}^{klm} t_k^c t_l^d t_m^a - \frac{1}{2} \sum_{cdeklm}^{(\text{T}_1\text{Cd})} w_{cde}^{klm} t_k^c t_{lm}^{da} t_i^e \\
 &\quad + \frac{1}{2} \sum_{cdeklm}^{(\text{T}_1\text{Ce})} w_{cde}^{klm} t_k^c t_l^d t_{mi}^{ea} + \frac{1}{4} \sum_{cdeklm}^{(\text{T}_1\text{Cf})} w_{cde}^{klm} t_{kl}^{cd} t_{mi}^{ea} \\
 &\quad - \frac{1}{4} \sum_{cdeklm}^{(\text{T}_1\text{Cg})} w_{cde}^{klm} t_{kl}^{ca} t_{im}^{de} + t_i^a(\text{NO2B}) = 0, \forall a, i
 \end{aligned}$$

Figure 3.2: Algebraic expressions for $\Delta E^{(\text{CCSD})}$ and the CCSD \hat{T}_1 amplitude equations for three-body Hamiltonians.

$$\begin{aligned}
 & \hat{P}_{ab} \hat{P}_{ij} \left\{ \right. \\
 & \quad \stackrel{(T_2Aa)}{+} \frac{1}{4} \sum_{ck} w_{cij}^{kab} t_k^c \stackrel{(T_2Ba)}{+} \frac{1}{2} \sum_{cdk} w_{cjd}^{abk} t_i^c t_k^d \\
 & \quad \stackrel{(T_2Bb)}{-} \frac{1}{2} \sum_{ckl} w_{ijc}^{kbl} t_k^a t_l^c \stackrel{(T_2Bc)}{+} \frac{1}{4} \sum_{cdk} w_{cjd}^{abk} t_{ik}^{cd} \stackrel{(T_2Bd)}{-} \frac{1}{4} \sum_{ckl} w_{ijc}^{kbl} t_{kl}^{ac} \\
 & \quad \stackrel{(T_2Ca)}{+} \frac{1}{4} \sum_{cdek} w_{cde}^{akb} t_i^c t_k^d t_j^e \stackrel{(T_2Cb)}{-} \sum_{cdkl} w_{icd}^{klb} t_k^a t_l^c t_j^d \\
 & \quad \stackrel{(T_2Cc)}{+} \frac{1}{4} \sum_{cklm} w_{icj}^{klm} t_k^a t_l^c t_m^b \stackrel{(T_2Cd)}{+} \frac{1}{8} \sum_{cdek} w_{cde}^{kab} t_k^c t_{ij}^{de} \\
 & \quad \stackrel{(T_2Ce)}{+} \frac{1}{4} \sum_{cdek} w_{cde}^{akb} t_i^c t_{kj}^{de} \stackrel{(T_2Cf)}{-} \frac{1}{2} \sum_{cdkl} w_{cdj}^{akl} t_i^c t_{kl}^{db} \\
 & \quad \stackrel{(T_2Cg)}{-} \frac{1}{2} \sum_{cdkl} w_{icd}^{klb} t_k^a t_{lj}^{cd} \stackrel{(T_2Ch)}{+} \sum_{cdkl} w_{cdj}^{klb} t_l^d t_{ik}^{ac} \\
 & \quad \stackrel{(T_2Ci)}{+} \frac{1}{8} \sum_{cklm} w_{cij}^{klm} t_k^c t_{lm}^{ab} \stackrel{(T_2Cj)}{+} \frac{1}{4} \sum_{cklm} w_{icj}^{klm} t_k^a t_{lm}^{cb} \\
 & \quad \stackrel{(T_2Da)}{-} \frac{1}{2} \sum_{cdekl} w_{cde}^{klb} t_k^c t_l^a t_i^d t_j^e \stackrel{(T_2Db)}{+} \frac{1}{2} \sum_{cdklm} w_{cdj}^{klm} t_k^c t_i^d t_l^a t_m^b \\
 & \quad \stackrel{(T_2Dc)}{-} \frac{1}{4} \sum_{cdekl} w_{cde}^{akl} t_i^c t_j^d t_{kl}^{be} \stackrel{(T_2Dd)}{-} \frac{1}{2} \sum_{cdekl} w_{cde}^{akl} t_i^c t_k^b t_{jl}^{de} \\
 & \quad \stackrel{(T_2De)}{+} \sum_{cdekl} w_{cde}^{akl} t_i^c t_k^d t_{lj}^{eb} \stackrel{(T_2Df)}{-} \frac{1}{4} \sum_{cdekl} w_{cde}^{klb} t_k^c t_l^a t_{ij}^{de} \\
 & \quad \stackrel{(T_2Dg)}{+} \frac{1}{4} \sum_{cdekl} w_{cde}^{kla} t_k^c t_l^d t_{ij}^{eb} \stackrel{(T_2Dh)}{+} \frac{1}{4} \sum_{cdklm} w_{icd}^{klm} t_k^a t_l^b t_{jm}^{cd} \\
 & \quad \stackrel{(T_2Di)}{+} \frac{1}{2} \sum_{cdklm} w_{icd}^{klm} t_k^a t_j^c t_{lm}^{bd} \stackrel{(T_2Dj)}{-} \sum_{cdklm} w_{icd}^{klm} t_k^a t_l^c t_{mj}^{db} \\
 & \quad \stackrel{(T_2Dk)}{+} \frac{1}{4} \sum_{cdklm} w_{cid}^{klm} t_k^c t_j^d t_{lm}^{ab} \stackrel{(T_2Dl)}{+} \frac{1}{8} \sum_{cdekl} w_{cde}^{bkl} t_{ij}^{ac} t_{kl}^{de} \\
 & \quad \stackrel{(T_2Dm)}{-} \frac{1}{8} \sum_{cdekl} w_{cde}^{akl} t_{ij}^{cd} t_{kl}^{be} \stackrel{(T_2Dn)}{+} \frac{1}{2} \sum_{cdekl} w_{cde}^{klb} t_{ik}^{ac} t_{lj}^{de} \left. \right\} + \dots
 \end{aligned}$$

Figure 3.3: Algebraic expressions for the CCSD \hat{T}_2 amplitude equations for three-body Hamiltonians.

$$\begin{aligned}
 & + \hat{P}_{ab} \hat{P}_{ij} \{ \\
 & - \frac{(T_2Do)}{8} \sum_{cdklm} w_{jcd}^{klm} t_{ik}^{ab} t_{lm}^{cd} + \frac{(T_2Dp)}{8} \sum_{cdklm} w_{icd}^{klm} t_{kl}^{ab} t_{jm}^{cd} \\
 & - \frac{(T_2Dq)}{2} \sum_{cdklm} w_{cdj}^{klm} t_{ik}^{ac} t_{lm}^{db} - \frac{(T_2Dr)}{4} \sum_{cdklm} w_{cdi}^{klm} t_k^c t_l^d t_{mj}^{ab} \\
 & + \frac{(T_2Ea)}{4} \sum_{cdeklm} w_{cde}^{klm} t_k^c t_l^a t_i^d t_m^b t_j^e - \frac{(T_2Eb)}{4} \sum_{cdeklm} w_{cde}^{klm} t_k^c t_l^d t_m^a t_{ij}^{eb} \\
 & - \frac{(T_2Ec)}{4} \sum_{cdeklm} w_{cde}^{klm} t_k^c t_l^d t_i^e t_{mj}^{ab} + \frac{(T_2Ed)}{8} \sum_{cdeklm} w_{cde}^{klm} t_k^c t_l^a t_m^b t_{ij}^{de} \\
 & - \sum_{cdeklm} w_{cde}^{klm} t_k^c t_i^d t_l^a t_{mj}^{eb} + \frac{(T_2Ef)}{8} \sum_{cdeklm} w_{cde}^{klm} t_k^c t_i^d t_j^e t_{lm}^{ab} \\
 & + \frac{(T_2Eg)}{4} \sum_{cdeklm} w_{cde}^{klm} t_k^a t_i^c t_j^d t_{lm}^{be} + \frac{(T_2Eh)}{4} \sum_{cdeklm} w_{cde}^{klm} t_k^a t_i^c t_l^b t_{jm}^{de} \\
 & - \frac{(T_2Ei)}{2} \sum_{cdeklm} w_{cde}^{klm} t_j^e t_{ik}^{ac} t_{lm}^{db} + \frac{(T_2Ej)}{8} \sum_{cdeklm} w_{cde}^{klm} t_j^e t_{ki}^{cd} t_{lm}^{ab} \\
 & - \frac{(T_2Ek)}{8} \sum_{cdeklm} w_{cde}^{klm} t_j^c t_{ik}^{ab} t_{lm}^{de} - \frac{(T_2El)}{8} \sum_{cdeklm} w_{cde}^{klm} t_k^b t_{lm}^{de} t_{ij}^{ac} \\
 & + \frac{(T_2Em)}{8} \sum_{cdeklm} w_{cde}^{klm} t_m^b t_{kl}^{ca} t_{ij}^{de} - \frac{(T_2En)}{2} \sum_{cdeklm} w_{cde}^{klm} t_m^b t_{ik}^{ac} t_{lj}^{de} \\
 & - \frac{(T_2Eo)}{4} \sum_{cdeklm} w_{cde}^{klm} t_m^e t_{ij}^{ac} t_{kl}^{bd} + \frac{(T_2Ep)}{16} \sum_{cdeklm} w_{cde}^{klm} t_m^e t_{ij}^{cd} t_{kl}^{ab} \\
 & + \frac{(T_2Eq)}{2} \sum_{cdeklm} w_{cde}^{klm} t_l^d t_{ik}^{ac} t_{mj}^{eb} - \frac{(T_2Er)}{4} \sum_{cdeklm} w_{cde}^{klm} t_m^e t_{ik}^{ab} t_{jl}^{cd} \} \\
 & + t_{ij}^{ab}(\text{NO2B}) = 0, \forall a, b, i, j
 \end{aligned}$$

 Figure 3.4: Algebraic expressions for the CCSD \hat{T}_2 amplitude equations for three-body Hamiltonians, continued.

3.2 Effective Hamiltonian

As already stated in Section 3.1.2, the expression for the effective Hamiltonian for an arbitrary CC method truncated at the $MpMh$ excitation level,

$$\hat{\mathcal{H}}^{(M)} = e^{-\hat{T}^{(M)}} \hat{H}_N e^{\hat{T}^{(M)}} , \quad (3.26)$$

terminates after the six-fold commutator with the cluster operator

$$\begin{aligned} \hat{\mathcal{H}}^{(M)} = & \hat{F}_N + \sum_{n=1}^2 \frac{1}{n!} [\hat{F}_N, \hat{T}^{(M)}]^{(n)} \\ & + \hat{V}_N + \sum_{n=1}^4 \frac{1}{n!} [\hat{V}_N, \hat{T}^{(M)}]^{(n)} \\ & + \hat{W}_N + \sum_{n=1}^6 \frac{1}{n!} [\hat{W}_N, \hat{T}^{(M)}]^{(n)} , \end{aligned} \quad (3.27)$$

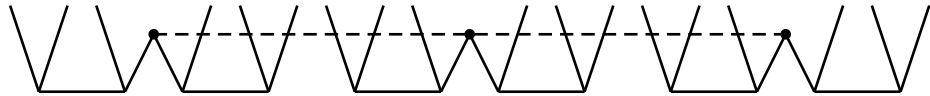
where $[\cdot, \cdot]^{(n)}$ denotes the n -fold commutator. From (3.27) it is evident that all new contributions are given by the last line of (3.27),

$$\hat{W}_N + \sum_{n=1}^6 \frac{1}{n!} [\hat{W}_N, \hat{T}^{(M)}]^{(n)} = (\hat{W}_N e^{\hat{T}^{(M)}})_C , \quad (3.28)$$

again stemming from \hat{W}_N alone, which may be emphasized by the expression

$$\hat{\mathcal{H}}^{(M)} = \hat{\mathcal{H}}_{\text{NO2B}}^{(M)} + (\hat{W}_N e^{\hat{T}^{(M)}})_C . \quad (3.29)$$

In the case of CCSD, $\hat{\mathcal{H}}^{(\text{CCSD})}$ now contains up to nine-body operators, as is apparent from the example



$$. \quad (3.30)$$

If the cluster operator amplitudes have been determined from the CCSD equations including the residual normal-ordered three-body interaction \hat{W}_N , then the zero-body matrix element \mathcal{H}_0 of $\hat{\mathcal{H}}^{(\text{CCSD})}$ is again given by the corresponding CCSD correlation energy (3.21),

$$\mathcal{H}_0 = \Delta E^{(\text{CCSD})} , \quad (3.31)$$

and the \mathcal{H}_h^{P} and $\mathcal{H}_{hh}^{\text{PP}}$ matrix elements vanish because they correspond to the CCSD \hat{T}_1 and \hat{T}_2 equations. Expressions for the complete one- and two-body part

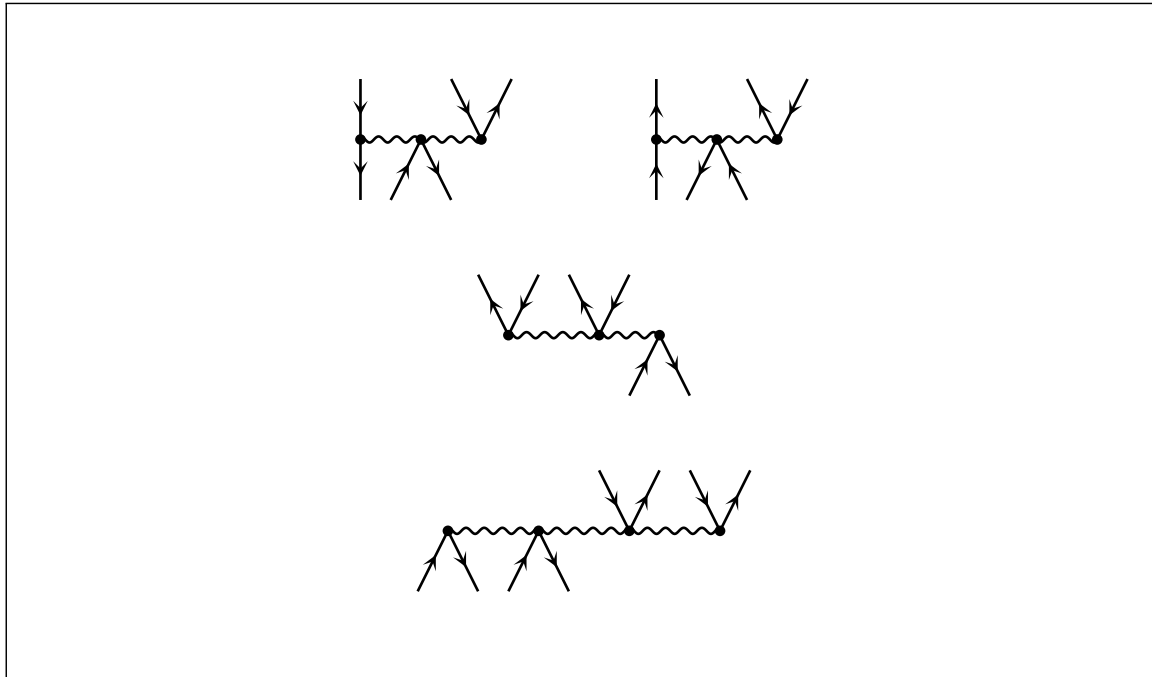


Figure 3.5: Selected topologies of $\hat{\mathcal{H}}_3$ and $\hat{\mathcal{H}}_4$, generated by the residual normal-ordered three-body interaction \hat{W}_N , that enter the ACCSD equations.

of $\hat{\mathcal{H}}^{(\text{CCSD})}$ are listed in Figures 3.6-3.9, and the corresponding diagrams and spherical expressions can be found in Appendices D.2 and D.3. For the three- and four-body part of $\hat{\mathcal{H}}^{(\text{CCSD})}$, expressions have been evaluated only for the selected topologies shown in Figure 3.5, which are the only diagrams required for ACCSD using three-body Hamiltonians, as can be seen in Figures 3.10-3.12.

$$\begin{aligned}
\mathcal{H}_a^i &= \mathcal{H}_a^i(\text{NO2B}) \overset{(\mathcal{H}_{\text{pA}}^{\text{h}})}{+} \frac{1}{4} \sum_{cdkl} w_{acd}^{ikl} t_{kl}^{cd} \overset{(\mathcal{H}_{\text{pB}}^{\text{h}})}{+} \frac{1}{2} \sum_{cdkl} w_{acd}^{ikl} t_k^c t_l^d \\
\mathcal{H}_b^a &= \mathcal{H}_b^a(\text{NO2B}) \overset{(\mathcal{H}_{\text{pA}}^{\text{p}})}{+} \frac{1}{4} \sum_{cdkl} w_{bcd}^{akl} t_{kl}^{cd} \overset{(\mathcal{H}_{\text{pB}}^{\text{p}})}{-} \frac{1}{4} \sum_{cdklm} w_{bcd}^{klm} t_{kl}^{cd} t_m^a \\
&\quad \overset{(\mathcal{H}_{\text{pC}}^{\text{p}})}{+} \frac{1}{2} \sum_{cdklm} w_{bcd}^{klm} t_k^c t_{lm}^{ad} \overset{(\mathcal{H}_{\text{pD}}^{\text{p}})}{+} \frac{1}{2} \sum_{cdkl} w_{bcd}^{akl} t_k^c t_l^d \\
&\quad \overset{(\mathcal{H}_{\text{pE}}^{\text{p}})}{-} \frac{1}{2} \sum_{cdklm} w_{bcd}^{klm} t_k^c t_l^d t_m^a \\
\mathcal{H}_j^i &= \mathcal{H}_j^i(\text{NO2B}) \overset{(\mathcal{H}_{\text{hA}}^{\text{h}})}{+} \frac{1}{4} \sum_{cdkl} w_{cdj}^{ikl} t_{kl}^{cd} \overset{(\mathcal{H}_{\text{hB}}^{\text{h}})}{+} \frac{1}{4} \sum_{cdekl} w_{cde}^{ikl} t_{kl}^{cd} t_j^e \\
&\quad \overset{(\mathcal{H}_{\text{hC}}^{\text{h}})}{-} \frac{1}{2} \sum_{cdekl} w_{cde}^{ikl} t_{kj}^{cd} t_l^e \overset{(\mathcal{H}_{\text{hD}}^{\text{h}})}{+} \frac{1}{2} \sum_{cdkl} w_{cdj}^{ikl} t_k^c t_l^d \\
&\quad \overset{(\mathcal{H}_{\text{hE}}^{\text{h}})}{+} \frac{1}{2} \sum_{cdekl} w_{cde}^{ikl} t_k^c t_l^d t_j^e \\
\mathcal{H}_{ab}^{ij} &= \mathcal{H}_{ab}^{ij}(\text{NO2B}) \overset{(\mathcal{H}_{\text{ppA}}^{\text{hh}})}{+} \sum_{ck} w_{abc}^{ijk} t_k^c \\
\mathcal{H}_{bc}^{ai} &= \mathcal{H}_{bc}^{ai}(\text{NO2B}) \overset{(\mathcal{H}_{\text{ppA}}^{\text{ph}})}{+} \frac{1}{2} \sum_{dkl} w_{bcd}^{ikl} t_{kl}^{ad} \overset{(\mathcal{H}_{\text{ppB}}^{\text{ph}})}{+} \sum_{dl} w_{bcd}^{ail} t_l^d \\
&\quad \overset{(\mathcal{H}_{\text{ppC}}^{\text{ph}})}{+} \sum_{dkl} w_{bcd}^{ikl} t_k^a t_l^d \\
\mathcal{H}_{ja}^{ik} &= \mathcal{H}_{ja}^{ik}(\text{NO2B}) \overset{(\mathcal{H}_{\text{hpA}}^{\text{hh}})}{-} \frac{1}{2} \sum_{cdl} w_{acd}^{ikl} t_{jl}^{cd} \overset{(\mathcal{H}_{\text{hpB}}^{\text{hh}})}{+} \sum_{cl} w_{jac}^{ikl} t_l^c \\
&\quad \overset{(\mathcal{H}_{\text{hpC}}^{\text{hh}})}{-} \sum_{cdl} w_{acd}^{ikl} t_j^c t_l^d
\end{aligned}$$

Figure 3.6: Algebraic expressions for the effective Hamiltonian one- and two-body matrix elements for three-body Hamiltonians.

$$\begin{aligned}
 \mathcal{H}_{cd}^{ab} &= \mathcal{H}_{cd}^{ab}(\text{NO2B}) \overset{(\mathcal{H}_{\text{pp}}^{\text{ppA}})}{-} \frac{1}{2} \hat{P}_{ab} \sum_{ekl} w_{cde}^{akl} t_{kl}^{be} \overset{(\mathcal{H}_{\text{pp}}^{\text{ppB}})}{+} \sum_{ek} w_{cde}^{abk} t_k^e \\
 &\quad \overset{(\mathcal{H}_{\text{pp}}^{\text{ppC}})}{+} \frac{1}{2} \sum_{eklm} w_{cde}^{klm} t_{lm}^{ab} t_k^e \overset{(\mathcal{H}_{\text{pp}}^{\text{ppD}})}{+} \frac{1}{2} \hat{P}_{ab} \sum_{eklm} w_{cde}^{klm} t_k^a t_{lm}^{be} \\
 &\quad \overset{(\mathcal{H}_{\text{pp}}^{\text{ppE}})}{-} \sum_{eklm} w_{cde}^{bkl} t_k^a t_l^e \overset{(\mathcal{H}_{\text{pp}}^{\text{ppF}})}{+} \frac{1}{2} \hat{P}_{ab} \sum_{eklm} w_{cde}^{klm} t_l^a t_m^b t_k^e \\
 \\
 \mathcal{H}_{kl}^{ij} &= \mathcal{H}_{kl}^{ij}(\text{NO2B}) \overset{(\mathcal{H}_{\text{hh}}^{\text{hhA}})}{-} \frac{1}{2} \hat{P}_{kl} \sum_{cdm} w_{kcd}^{ijm} t_{ml}^{cd} \overset{(\mathcal{H}_{\text{hh}}^{\text{hhB}})}{+} \sum_{cm} w_{klc}^{ijm} t_m^c \\
 &\quad \overset{(\mathcal{H}_{\text{hh}}^{\text{hhC}})}{+} \frac{1}{2} \sum_{cdem} w_{cde}^{ijm} t_{kl}^{de} t_m^c \overset{(\mathcal{H}_{\text{hh}}^{\text{hhD}})}{+} \frac{1}{2} \hat{P}_{kl} \sum_{cdem} w_{cde}^{ijm} t_{lm}^{cd} t_k^e \\
 &\quad \overset{(\mathcal{H}_{\text{hh}}^{\text{hhE}})}{+} \sum_{cdm} w_{cdl}^{ijm} t_k^c t_m^d \overset{(\mathcal{H}_{\text{hh}}^{\text{hhF}})}{+} \frac{1}{2} \hat{P}_{kl} \sum_{cdem} w_{cde}^{ijm} t_k^d t_l^e t_m^c \\
 \\
 \mathcal{H}_{ib}^{aj} &= \mathcal{H}_{ib}^{aj}(\text{NO2B}) \overset{(\mathcal{H}_{\text{ph}}^{\text{phA}})}{-} \frac{1}{2} \sum_{cdk} w_{bcd}^{ajk} t_{ik}^{cd} \overset{(\mathcal{H}_{\text{ph}}^{\text{phB}})}{+} \frac{1}{2} \sum_{ckl} w_{bci}^{jkl} t_{kl}^{ac} \\
 &\quad \overset{(\mathcal{H}_{\text{ph}}^{\text{phC}})}{+} \sum_{ck} w_{bci}^{ajk} t_k^c \overset{(\mathcal{H}_{\text{ph}}^{\text{phD}})}{-} \frac{1}{2} \sum_{cdkl} w_{bcd}^{jkl} t_{il}^{cd} t_k^a \\
 &\quad \overset{(\mathcal{H}_{\text{ph}}^{\text{phE}})}{-} \frac{1}{2} \sum_{cdkl} w_{bcd}^{jkl} t_{kl}^{ad} t_i^c \overset{(\mathcal{H}_{\text{ph}}^{\text{phF}})}{+} \sum_{cdkl} w_{bcd}^{jkl} t_{ik}^{ac} t_l^d \\
 &\quad \overset{(\mathcal{H}_{\text{ph}}^{\text{phG}})}{+} \sum_{cdk} w_{bcd}^{ajk} t_k^c t_i^d \overset{(\mathcal{H}_{\text{ph}}^{\text{phH}})}{-} \sum_{ckl} w_{bci}^{jkl} t_k^c t_l^a \\
 &\quad \overset{(\mathcal{H}_{\text{ph}}^{\text{phI}})}{-} \sum_{cdkl} w_{bcd}^{jkl} t_l^a t_k^c t_i^d
 \end{aligned}$$

Figure 3.7: Algebraic expressions for the effective Hamiltonian two-body matrix elements for three-body Hamiltonians, continued.

$$\begin{aligned}
\mathcal{H}_{ci}^{ab} = & \mathcal{H}_{ci}^{ab}(\text{NO2B}) \left(\mathcal{H}_{\text{ph}}^{\text{ppA}} - \right) \sum_{dk} w_{cdi}^{abk} t_k^d \left(\mathcal{H}_{\text{ph}}^{\text{ppB}} + \right) \frac{1}{2} \hat{P}_{ab} \sum_{dekl} w_{cde}^{akl} t_{ik}^{de} t_l^b \\
& \left(\mathcal{H}_{\text{ph}}^{\text{ppC}} + \right) \frac{1}{2} \hat{P}_{ab} \sum_{dekl} w_{cde}^{akl} t_{kl}^{bd} t_i^e \left(\mathcal{H}_{\text{ph}}^{\text{ppD}} + \right) \hat{P}_{ab} \sum_{dekl} w_{cde}^{akl} t_{il}^{be} t_k^d \\
& \left(\mathcal{H}_{\text{ph}}^{\text{ppE}} - \right) \frac{1}{2} \sum_{dklm} w_{cdi}^{klm} t_{lm}^{ab} t_k^d \left(\mathcal{H}_{\text{ph}}^{\text{ppF}} - \right) \frac{1}{2} \hat{P}_{ab} \sum_{deklm} w_{cdi}^{klm} t_{kl}^{bd} t_m^a \\
& \left(\mathcal{H}_{\text{ph}}^{\text{ppG}} - \right) \sum_{dek} w_{cde}^{abk} t_k^d t_i^e \left(\mathcal{H}_{\text{ph}}^{\text{ppH}} + \right) \hat{P}_{ab} \sum_{dkl} w_{cdi}^{bkl} t_k^d t_l^a \\
& \left(\mathcal{H}_{\text{ph}}^{\text{ppI}} + \right) \frac{1}{2} \sum_{deklm} w_{cde}^{klm} t_{im}^{ab} t_k^d t_l^e \left(\mathcal{H}_{\text{ph}}^{\text{ppJ}} - \right) \hat{P}_{ab} \sum_{deklm} w_{cde}^{klm} t_{il}^{be} t_k^d t_m^a \\
& \left(\mathcal{H}_{\text{ph}}^{\text{ppK}} + \right) \frac{1}{4} \hat{P}_{ab} \sum_{deklm} w_{cde}^{klm} t_{il}^{de} t_k^b t_m^a \left(\mathcal{H}_{\text{ph}}^{\text{ppL}} - \right) \frac{1}{2} \hat{P}_{ab} \sum_{deklm} w_{cde}^{klm} t_{lm}^{ae} t_k^b t_i^d \\
& \left(\mathcal{H}_{\text{ph}}^{\text{ppM}} - \right) \frac{1}{2} \sum_{deklm} w_{cde}^{klm} t_{lm}^{ab} t_k^d t_i^e \left(\mathcal{H}_{\text{ph}}^{\text{ppN}} - \right) \hat{P}_{ab} \sum_{deklm} w_{cde}^{akl} t_k^d t_l^b t_i^e \\
& \left(\mathcal{H}_{\text{ph}}^{\text{ppO}} + \right) \frac{1}{2} \hat{P}_{ab} \sum_{dklm} w_{cdi}^{klm} t_m^a t_l^b t_k^d \left(\mathcal{H}_{\text{ph}}^{\text{ppP}} + \right) \frac{1}{2} \hat{P}_{ab} \sum_{cdeklm} w_{cde}^{klm} t_m^a t_l^b t_k^d t_i^e \\
& \left(\mathcal{H}_{\text{ph}}^{\text{ppQ}} - \right) \frac{1}{4} \sum_{deklm} w_{cde}^{klm} t_{ki}^{ab} t_{lm}^{de} \left(\mathcal{H}_{\text{ph}}^{\text{ppR}} + \right) \frac{1}{4} \sum_{deklm} w_{cde}^{klm} t_{kl}^{ab} t_{im}^{de} \\
& \left(\mathcal{H}_{\text{ph}}^{\text{ppS}} - \right) \frac{1}{2} \hat{P}_{ab} \sum_{deklm} w_{cde}^{klm} t_{kl}^{ad} t_{mi}^{eb}
\end{aligned}$$

Figure 3.8: Algebraic expressions for the effective Hamiltonian two-body matrix elements for three-body Hamiltonians, continued.

$$\begin{aligned}
 \mathcal{H}_{jk}^{ia} = & \mathcal{H}_{jk}^{ia}(\text{NO2B}) + \sum_{cl} w_{jkc}^{ial} t_l^c + \frac{1}{2} \hat{P}_{jk} \sum_{cdlm} w_{jcd}^{ilm} t_{lm}^{ac} t_k^d \\
 & + \frac{1}{2} \hat{P}_{jk} \sum_{cdlm} w_{jcd}^{ilm} t_{kl}^{cd} t_m^a + \frac{1}{2} \hat{P}_{jk} \sum_{cdlm} w_{jcd}^{ilm} t_{km}^{ad} t_l^c \\
 & - \frac{1}{2} \sum_{cde} w_{cde}^{ail} t_{jk}^{de} t_l^c + \frac{1}{2} \hat{P}_{jk} \sum_{cde} w_{cde}^{ail} t_{lk}^{cd} t_j^e \\
 & - \sum_{clm} w_{jck}^{ilm} t_l^c t_m^a - \hat{P}_{jk} \sum_{cdl} w_{cdk}^{ail} t_l^c t_j^d \\
 & + \frac{1}{2} \sum_{cdelm} w_{cde}^{ilm} t_{kj}^{ae} t_l^c t_m^d + \hat{P}_{jk} \sum_{cdelm} w_{cde}^{ilm} t_{km}^{ad} t_l^c t_j^e \\
 & - \frac{1}{2} \hat{P}_{jk} \sum_{cdelm} w_{cde}^{ilm} t_{lm}^{ad} t_k^c t_j^e - \frac{1}{2} \hat{P}_{jk} \sum_{cdelm} w_{cde}^{ilm} t_{mj}^{de} t_k^c t_l^a \\
 & + \hat{P}_{jk} \sum_{cdelm} w_{cde}^{ilm} t_{jm}^{ae} t_l^c t_k^d \\
 & - \hat{P}_{jk} \sum_{cdlm} w_{jcd}^{ilm} t_m^a t_l^c t_k^d + \frac{1}{2} \hat{P}_{jk} \sum_{cdel} w_{cde}^{ail} t_l^c t_k^d t_j^e \\
 & - \frac{1}{2} \hat{P}_{jk} \sum_{cdelm} w_{cde}^{ilm} t_m^a t_l^c t_k^d t_j^e + \frac{1}{4} \sum_{cdelm} w_{cde}^{ilm} t_{jk}^{ca} t_{lm}^{de} \\
 & - \frac{1}{4} \sum_{cdelm} w_{cde}^{ilm} t_{jk}^{cd} t_{lm}^{ae} + \frac{1}{2} \hat{P}_{jk} \sum_{cdelm} w_{cde}^{ilm} t_{jl}^{cd} t_{mk}^{ea}
 \end{aligned}$$

Figure 3.9: Algebraic expressions for the effective Hamiltonian two-body matrix elements for three-body Hamiltonians, continued.

$$\begin{aligned}
\mathcal{H}_{kbl}^{ija} &= \mathcal{H}_{kbl}^{ija}(\text{NO2B}) \overset{(\mathcal{H}_{\text{hph}}^{\text{hphA}})}{+} w_{kbl}^{ija} \overset{(\mathcal{H}_{\text{hph}}^{\text{hphB}})}{+} \hat{P}_{kl} \sum_{cm} w_{kbc}^{ijm} t_{lm}^{ac} \\
&\quad \overset{(\mathcal{H}_{\text{hph}}^{\text{hphC}})}{+} \frac{1}{2} \sum_{cd} w_{cbd}^{ija} t_{kl}^{cd} \overset{(\mathcal{H}_{\text{hph}}^{\text{hphD}})}{-} \hat{P}_{kl} \sum_c w_{bcl}^{ija} t_k^c \\
&\quad \overset{(\mathcal{H}_{\text{hph}}^{\text{hphE}})}{+} \sum_m w_{bkl}^{ijm} t_m^a \overset{(\mathcal{H}_{\text{hph}}^{\text{hphF}})}{-} \sum_{cdm} w_{bcd}^{ijm} t_{kl}^{ad} t_m^c \\
&\quad \overset{(\mathcal{H}_{\text{hph}}^{\text{hphG}})}{-} \hat{P}_{kl} \sum_{cdm} w_{bcd}^{ijm} t_{lm}^{ad} t_k^c \overset{(\mathcal{H}_{\text{hph}}^{\text{hphH}})}{+} \frac{1}{2} \sum_{cdm} w_{bcd}^{ijm} t_{kl}^{cd} t_m^a \\
&\quad \overset{(\mathcal{H}_{\text{hph}}^{\text{hphI}})}{+} \hat{P}_{kl} \sum_{cm} w_{bcl}^{ijm} t_k^c t_m^a \overset{(\mathcal{H}_{\text{hph}}^{\text{hphJ}})}{+} \sum_{cd} w_{cbd}^{ija} t_k^c t_l^d \\
&\quad \overset{(\mathcal{H}_{\text{hph}}^{\text{hphK}})}{+} \sum_{cdm} w_{bcd}^{ijm} t_k^c t_l^d t_m^a \\
\\
\mathcal{H}_{cdi}^{ajb} &= \mathcal{H}_{cdi}^{ajb}(\text{NO2B}) \overset{(\mathcal{H}_{\text{pph}}^{\text{pphA}})}{+} w_{cdi}^{ajb} \overset{(\mathcal{H}_{\text{pph}}^{\text{pphB}})}{+} \hat{P}_{ab} \sum_{ek} w_{cde}^{ajk} t_{ik}^{be} \\
&\quad \overset{(\mathcal{H}_{\text{pph}}^{\text{pphC}})}{+} \frac{1}{2} \sum_{kl} w_{cdi}^{kjl} t_{kl}^{ab} \overset{(\mathcal{H}_{\text{pph}}^{\text{pphD}})}{-} \hat{P}_{ab} \sum_k w_{cdi}^{bkj} t_k^a \\
&\quad \overset{(\mathcal{H}_{\text{pph}}^{\text{pphE}})}{-} \sum_e w_{cde}^{abj} t_i^e \overset{(\mathcal{H}_{\text{pph}}^{\text{pphF}})}{+} \sum_{ekl} w_{cde}^{jkl} t_{il}^{ab} t_k^e \\
&\quad \overset{(\mathcal{H}_{\text{pph}}^{\text{pphG}})}{+} \hat{P}_{ab} \sum_{ekl} w_{cde}^{jkl} t_{il}^{be} t_k^a \overset{(\mathcal{H}_{\text{pph}}^{\text{pphH}})}{-} \frac{1}{2} \sum_{ekl} w_{cde}^{jkl} t_{kl}^{ab} t_i^e \\
&\quad \overset{(\mathcal{H}_{\text{pph}}^{\text{pphI}})}{-} \hat{P}_{ab} \sum_{ek} w_{cde}^{ajk} t_k^b t_i^e \overset{(\mathcal{H}_{\text{pph}}^{\text{pphJ}})}{+} \sum_{kl} w_{cdi}^{kjl} t_k^a t_l^b \\
&\quad \overset{(\mathcal{H}_{\text{pph}}^{\text{pphK}})}{-} \sum_{ekl} w_{cde}^{jkl} t_k^a t_l^b t_i^e
\end{aligned}$$

Figure 3.10: Algebraic expressions for selected three-body effective Hamiltonian matrix elements for three-body Hamiltonians.

$$\begin{aligned}
 \mathcal{H}_{ijc}^{abk} = & \mathcal{H}_{ijc}^{abk}(\text{NO2B}) \overset{(\mathcal{H}_{\text{hhp}}^{\text{pphA}})}{+} w_{ijc}^{abk} \overset{(\mathcal{H}_{\text{hhp}}^{\text{pphB}})}{+} \frac{1}{2} \sum_{de} w_{cde}^{abk} t_{ij}^{de} \\
 & \overset{(\mathcal{H}_{\text{hhp}}^{\text{pphC}})}{+} \hat{P}_{ab} \hat{P}_{ij} \sum_{dl} w_{jcd}^{bkl} t_{il}^{ad} \overset{(\mathcal{H}_{\text{hhp}}^{\text{pphD}})}{+} \frac{1}{2} \sum_{lm} w_{ijc}^{klm} t_{lm}^{ab} \\
 & \overset{(\mathcal{H}_{\text{hhp}}^{\text{pphE}})}{-} \frac{1}{2} \hat{P}_{ab} \sum_{delm} w_{cde}^{klm} t_{ij}^{ad} t_{lm}^{be} \overset{(\mathcal{H}_{\text{hhp}}^{\text{pphF}})}{+} \frac{1}{2} \hat{P}_{ab} \hat{P}_{ij} \sum_{delm} w_{cde}^{klm} t_{il}^{ad} t_{jm}^{be} \\
 & \overset{(\mathcal{H}_{\text{hhp}}^{\text{pphG}})}{+} \frac{1}{4} \sum_{delm} w_{cde}^{klm} t_{lm}^{ab} t_{ij}^{de} \overset{(\mathcal{H}_{\text{hhp}}^{\text{pphH}})}{-} \frac{1}{2} \hat{P}_{ij} \sum_{delm} w_{cde}^{klm} t_{il}^{ab} t_{jm}^{de} \\
 & \overset{(\mathcal{H}_{\text{hhp}}^{\text{pphI}})}{+} \hat{P}_{ij} \sum_d w_{cdj}^{abk} t_i^d \overset{(\mathcal{H}_{\text{hhp}}^{\text{pphJ}})}{-} \hat{P}_{ab} \sum_l w_{ijc}^{klb} t_l^a \\
 & \overset{(\mathcal{H}_{\text{hhp}}^{\text{pphK}})}{-} \frac{1}{2} \hat{P}_{ab} \sum_{del} w_{cde}^{klb} t_{ij}^{de} t_l^a \overset{(\mathcal{H}_{\text{hhp}}^{\text{pphL}})}{-} \hat{P}_{ab} \hat{P}_{ij} \sum_{del} w_{cde}^{akl} t_{jl}^{be} t_i^d \\
 & \overset{(\mathcal{H}_{\text{hhp}}^{\text{pphM}})}{+} \frac{1}{2} \hat{P}_{ij} \sum_{dlm} w_{cdj}^{klm} t_{lm}^{ab} t_i^d \overset{(\mathcal{H}_{\text{hhp}}^{\text{pphN}})}{+} \hat{P}_{ab} \hat{P}_{ij} \sum_{dlm} w_{cdi}^{klm} t_{jm}^{bd} t_l^a \\
 & \overset{(\mathcal{H}_{\text{hhp}}^{\text{pphO}})}{-} \hat{P}_{ab} \sum_{del} w_{cde}^{akl} t_{ij}^{be} t_l^d \overset{(\mathcal{H}_{\text{hhp}}^{\text{pphP}})}{+} \hat{P}_{ij} \sum_{dlm} w_{cdi}^{klm} t_{jm}^{ab} t_l^d \\
 & \overset{(\mathcal{H}_{\text{hhp}}^{\text{pphQ}})}{+} \sum_{de} w_{dec}^{abk} t_i^d t_j^e \overset{(\mathcal{H}_{\text{hhp}}^{\text{pphR}})}{-} \hat{P}_{ab} \hat{P}_{ij} \sum_{dl} w_{dj c}^{lbk} t_l^a t_i^d \\
 & \overset{(\mathcal{H}_{\text{hhp}}^{\text{pphS}})}{+} \sum_{lm} w_{ijc}^{lmk} t_l^a t_m^b \overset{(\mathcal{H}_{\text{hhp}}^{\text{pphT}})}{+} \frac{1}{2} \sum_{delm} w_{cde}^{klm} t_{ij}^{de} t_l^a t_m^b \\
 & \overset{(\mathcal{H}_{\text{hhp}}^{\text{pphU}})}{-} \hat{P}_{ab} \hat{P}_{ij} \sum_{delm} w_{cde}^{klm} t_{jm}^{be} t_l^a t_i^d \overset{(\mathcal{H}_{\text{hhp}}^{\text{pphV}})}{+} \frac{1}{2} \sum_{delm} w_{cde}^{klm} t_{lm}^{ab} t_i^d t_j^e \\
 & \overset{(\mathcal{H}_{\text{hhp}}^{\text{pphW}})}{-} \hat{P}_{ab} \sum_{delm} w_{cde}^{klm} t_{ij}^{eb} t_m^a t_l^d \overset{(\mathcal{H}_{\text{hhp}}^{\text{pphX}})}{-} \hat{P}_{ij} \sum_{delm} w_{cde}^{klm} t_{mj}^{ab} t_i^e t_l^d \\
 & \overset{(\mathcal{H}_{\text{hhp}}^{\text{pphY}})}{-} \hat{P}_{ab} \sum_{del} w_{cde}^{klb} t_l^a t_i^d t_j^e \overset{(\mathcal{H}_{\text{hhp}}^{\text{pphZ}})}{+} \hat{P}_{ij} \sum_{dlm} w_{cdj}^{klm} t_l^a t_m^b t_i^d \\
 & \overset{(\mathcal{H}_{\text{hhp}}^{\text{pphAA}})}{+} \sum_{delm} w_{cde}^{klm} t_l^a t_m^b t_i^d t_j^e
 \end{aligned}$$

Figure 3.11: Algebraic expressions for selected three-body effective Hamiltonian matrix elements for three-body Hamiltonians, continued.

$$\begin{aligned} \mathcal{H}_{abcd}^{ijkl} = & \left(\mathcal{H}_{\text{pppp}}^{\text{hhhhA}} + \right) \hat{P}_{cd} \sum_e w_{abe}^{ijc} t_{kl}^{ed} \left(\mathcal{H}_{\text{pppp}}^{\text{hhhhB}} - \right) \hat{P}_{kl} \sum_m w_{abk}^{ijm} t_{ml}^{cd} \\ & \left(\mathcal{H}_{\text{pppp}}^{\text{hhhhC}} - \right) \hat{P}_{cd} \sum_{em} w_{abe}^{ijm} t_{kl}^{ed} t_m^c \left(\mathcal{H}_{\text{pppp}}^{\text{hhhhD}} - \right) \hat{P}_{kl} \sum_{em} w_{abe}^{ijm} t_{ml}^{cd} t_k^e \end{aligned}$$

Figure 3.12: Algebraic expressions for selected four-body effective Hamiltonian matrix elements for three-body Hamiltonians, continued.

3.3 The Λ CCSD Equations for Three-Body Hamiltonians

The Λ CCSD equations for three-body Hamiltonians can straightforwardly be derived in analogy to the two-body case. In terms of the $\hat{\Lambda}^{(\text{CCSD})}$ and $\mathcal{H}^{(\text{CCSD})}$ operators, the Λ CCSD equations may again be cast in the form

$$\langle \Phi | (\hat{1} + \hat{\Lambda}_1 + \hat{\Lambda}_2) \mathcal{H}_{\text{open}}^{(\text{CCSD})} | \Phi_i^a \rangle = 0 \quad (3.32)$$

$$\langle \Phi | (\hat{1} + \hat{\Lambda}_1 + \hat{\Lambda}_2) \mathcal{H}_{\text{open}}^{(\text{CCSD})} | \Phi_{ij}^{ab} \rangle = 0, \quad (3.33)$$

now using Eq. (3.27) as the underlying definition for the effective Hamiltonian. When evaluated in terms of the $\hat{\Lambda}_n$ and \mathcal{H}_n operators, such as in Eq. (2.70)-(2.71), the projection onto the singly excited determinants is identical to (3.34), but the projection onto the doubly excited determinants obtains two new terms, resulting in [96]

$$0 = \langle \Phi | \left\{ [(\hat{1} + \hat{\Lambda}_1) \mathcal{H}_1]_C + [(\hat{\Lambda}_1 + \hat{\Lambda}_2) \mathcal{H}_2]_C + [\hat{\Lambda}_2 \mathcal{H}_3]_C \right\} | \Phi_i^a \rangle \quad (3.34)$$

$$\begin{aligned} 0 = \langle \Phi | \left\{ [(\hat{1} + \hat{\Lambda}_1 + \hat{\Lambda}_2) \mathcal{H}_2]_C + [\hat{\Lambda}_2 \mathcal{H}_1]_C \right. \\ \left. + [\hat{\Lambda}_1 \mathcal{H}_1]_{\text{DC}} + [(\hat{\Lambda}_1 + \hat{\Lambda}_2) \mathcal{H}_3]_C + [\hat{\Lambda}_2 \mathcal{H}_4]_C \right\} | \Phi_{ij}^{ab} \rangle. \end{aligned} \quad (3.35)$$

The two new terms are

$$\langle \Phi | [\hat{\Lambda}_1 \mathcal{H}_3]_C | \Phi_{ij}^{ab} \rangle = \text{diagram} \quad (3.36)$$

and

$$\langle \Phi | [\hat{\Lambda}_2 \hat{\mathcal{H}}_4]_C | \Phi_{ij}^{ab} \rangle = \text{diagram} \quad (3.37)$$

which require a three-body interaction vertex in order to comply with the connectedness condition, for instance

$$\begin{aligned} \langle \Phi | [\hat{\Lambda}_2 \hat{\mathcal{H}}_4]_C | \Phi_{ij}^{ab} \rangle = & \text{diagram 1} + \text{diagram 2} \\ & + \text{diagram 3} + \text{diagram 4} . \end{aligned} \quad (3.38)$$

It is important to realize that only the \hat{W}_N -contributions to $\hat{\mathcal{H}}_3$ and $\hat{\mathcal{H}}_4$ enter (3.36) and (3.37), i.e.,

$$\langle \Phi | [\hat{\Lambda}_1 (\hat{\mathcal{H}}_{3,\text{NO2B}} + \hat{\mathcal{H}}_{3,\text{3B}})]_C | \Phi_{ij}^{ab} \rangle = \langle \Phi | [\hat{\Lambda}_1 \hat{\mathcal{H}}_{3,\text{3B}}]_C | \Phi_{ij}^{ab} \rangle \quad (3.39)$$

$$\langle \Phi | [\hat{\Lambda}_2 (\hat{\mathcal{H}}_{4,\text{NO2B}} + \hat{\mathcal{H}}_{4,\text{3B}})]_C | \Phi_{ij}^{ab} \rangle = \langle \Phi | [\hat{\Lambda}_2 \hat{\mathcal{H}}_{4,\text{3B}}]_C | \Phi_{ij}^{ab} \rangle . \quad (3.40)$$

As before, in order to circumvent storage of the three- and four-body effective Hamiltonian matrix elements, the \hat{W}_N contributions to $\mathcal{H}_{\text{hhp}}^{\text{pph}}$, $\mathcal{H}_{\text{hph}}^{\text{hhp}}$, $\mathcal{H}_{\text{pph}}^{\text{phh}}$ and $\mathcal{H}_{\text{pppp}}^{\text{pppp}}$ in terms of interaction matrix elements and cluster amplitudes are directly inserted into the ΛCCSD equations. The resulting ΛCCSD equations for three-body Hamiltonians are listed in Figures 3.13-3.14 and the spherical expressions can be found in Appendix E.3. It should be noted that once the expressions for the effective Hamiltonian are inserted into the contractions, the permutation operators \hat{P}_{kl} and \hat{P}_{cd} may each be replaced by a factor of 2 because, for example, orbitals k and l are always summed over and additionally always appear as an index pair in antisymmetrized matrix elements.

$$\begin{aligned}
 & (\Lambda_1^{3B_A}) + \frac{1}{4} \sum_{cdkl} \lambda_{cd}^{kl} w_{kla}^{cdi} + \frac{(\Lambda_1^{3B_B})}{8} \sum_{cdefkl} \lambda_{cd}^{kl} w_{aef}^{cdi} t_{kl}^{ef} \\
 & (\Lambda_1^{3B_C}) + \sum_{cdeklm} \lambda_{cd}^{kl} w_{lae}^{dim} t_{km}^{ce} + \frac{(\Lambda_1^{3B_D})}{8} \sum_{cdklmn} \lambda_{cd}^{kl} w_{kla}^{imn} t_{mn}^{cd} \\
 & (\Lambda_1^{3B_E}) - \frac{1}{4} \sum_{cdefklmn} \lambda_{cd}^{kl} w_{aef}^{imn} t_{kl}^{ce} t_{mn}^{df} + \frac{(\Lambda_1^{3B_F})}{2} \sum_{cdefklmn} \lambda_{cd}^{kl} w_{aef}^{imn} t_{km}^{ce} t_{ln}^{df} \\
 & (\Lambda_1^{3B_G}) + \frac{1}{16} \sum_{cdefklmn} \lambda_{cd}^{kl} w_{aef}^{imn} t_{mn}^{cd} t_{kl}^{ef} - \frac{(\Lambda_1^{3B_H})}{4} \sum_{cdefklmn} \lambda_{cd}^{kl} w_{aef}^{imn} t_{km}^{cd} t_{ln}^{ef} \\
 & (\Lambda_1^{3B_I}) + \frac{1}{2} \sum_{cdekl} \lambda_{cd}^{kl} w_{ael}^{cdi} t_k^e - \frac{(\Lambda_1^{3B_J})}{2} \sum_{cdklm} \lambda_{cd}^{kl} w_{kla}^{imd} t_m^c \\
 & (\Lambda_1^{3B_K}) - \frac{1}{4} \sum_{cdefklm} \lambda_{cd}^{kl} w_{aef}^{imd} t_{kl}^{ef} t_m^c + \frac{(\Lambda_1^{3B_L})}{2} \sum_{cdefklm} \lambda_{cd}^{kl} w_{aef}^{cim} t_{lm}^{df} t_k^e \\
 & (\Lambda_1^{3B_M}) + \frac{1}{4} \sum_{cdeklmn} \lambda_{cd}^{kl} w_{ael}^{imn} t_{mn}^{cd} t_k^e + \frac{(\Lambda_1^{3B_N})}{2} \sum_{cdeklmn} \lambda_{cd}^{kl} w_{aek}^{imn} t_{ln}^{de} t_m^c \\
 & (\Lambda_1^{3B_O}) - \frac{1}{4} \sum_{cdefklmn} \lambda_{cd}^{kl} w_{aef}^{cim} t_{kl}^{df} t_m^e + \frac{(\Lambda_1^{3B_P})}{2} \sum_{cdeklmn} \lambda_{cd}^{kl} w_{aek}^{imn} t_{ln}^{cd} t_m^e \\
 & (\Lambda_1^{3B_Q}) + \frac{1}{4} \sum_{cdefkl} \lambda_{cd}^{kl} w_{efa}^{cdi} t_k^e t_l^f - \frac{(\Lambda_1^{3B_R})}{2} \sum_{cdeklm} \lambda_{cd}^{kl} w_{ela}^{mdi} t_m^c t_k^e \\
 & (\Lambda_1^{3B_S}) + \frac{1}{4} \sum_{cdklmn} \lambda_{cd}^{kl} w_{kla}^{mni} t_m^c t_n^d + \frac{(\Lambda_1^{3B_T})}{8} \sum_{cdefklmn} \lambda_{cd}^{kl} w_{efa}^{mni} t_{kl}^{ef} t_m^c t_n^d \\
 & (\Lambda_1^{3B_U}) - \sum_{cdefklmn} \lambda_{cd}^{kl} w_{wfa}^{mni} t_{ln}^{df} t_m^c t_k^e + \frac{(\Lambda_1^{3B_V})}{8} \sum_{cdefklmn} \lambda_{cd}^{kl} w_{efa}^{mni} t_{mn}^{cd} t_k^e t_l^f \\
 & (\Lambda_1^{3B_W}) - \frac{1}{2} \sum_{cdefklmn} \lambda_{cd}^{kl} w_{efa}^{mni} t_{kl}^{fd} t_n^c t_n^e - \frac{(\Lambda_1^{3B_X})}{2} \sum_{cdefklmn} \lambda_{cd}^{kl} w_{efa}^{mni} t_{nl}^{cd} t_k^f t_m^e \\
 & (\Lambda_1^{3B_Y}) - \frac{1}{2} \sum_{cdefklmn} \lambda_{cd}^{kl} w_{efa}^{mdi} t_m^c t_k^e t_l^f + \frac{(\Lambda_1^{3B_Z})}{2} \sum_{cdeklmn} \lambda_{cd}^{kl} w_{ela}^{mni} t_m^c t_k^e t_n^d \\
 & (\Lambda_1^{3B_{AA}}) + \frac{1}{4} \sum_{cdefklmn} \lambda_{cd}^{kl} w_{efa}^{mni} t_m^c t_k^e t_n^d t_l^f + \lambda_a^i [\text{NO2B}] = 0, \quad \forall a, i
 \end{aligned}$$

Figure 3.13: Algebraic expressions for the ACCSD $\hat{\Lambda}_1$ amplitude equations for three-body Hamiltonians.

$$\begin{aligned}
 & \hat{P}_{ab} \hat{P}_{ij} \left(\overset{(\Lambda_{2,J}^{3B,A})}{+} \frac{1}{4} \sum_{ckl} \lambda_{ca}^{kl} w_{kbl}^{ijc} \overset{(\Lambda_{2,J}^{3B,B})}{+} \frac{1}{4} \sum_{cdklm} \lambda_{ca}^{kl} \hat{P}_{kl} w_{kbd}^{ijm} t_{ml}^{dc} \right. \\
 & \overset{(\Lambda_{2,J}^{3B,C})}{+} \frac{1}{8} \sum_{cdekl} \lambda_{ca}^{kl} w_{dbe}^{ijc} t_{kl}^{de} \overset{(\Lambda_{2,J}^{3B,D})}{+} \frac{1}{4} \sum_{cdkl} \lambda_{ca}^{kl} \hat{P}_{kl} w_{dbl}^{ijc} t_k^d \\
 & \overset{(\Lambda_{2,J}^{3B,E})}{-} \frac{1}{4} \sum_{cklm} \lambda_{ca}^{kl} w_{kbl}^{ijm} t_m^c \overset{(\Lambda_{2,J}^{3B,F})}{+} \frac{1}{4} \sum_{cdeklm} \lambda_{ca}^{kl} w_{deb}^{ijm} t_{kl}^{ec} t_m^d \\
 & \overset{(\Lambda_{2,J}^{3B,G})}{+} \frac{1}{4} \sum_{cdeklm} \lambda_{ca}^{kl} \hat{P}_{kl} w_{dbe}^{ijm} t_{ml}^{ec} t_k^d \overset{(\Lambda_{2,J}^{3B,H})}{-} \frac{1}{8} \sum_{cdeklm} \lambda_{ca}^{kl} w_{dbe}^{ijm} t_{kl}^{de} t_m^c \\
 & \overset{(\Lambda_{2,J}^{3B,I})}{-} \frac{1}{4} \sum_{cdklm} \lambda_{ca}^{kl} \hat{P}_{kl} w_{dbl}^{ijm} t_k^d t_m^c \overset{(\Lambda_{2,J}^{3B,J})}{+} \frac{1}{4} \sum_{cdekl} \lambda_{ca}^{kl} w_{dbe}^{ijc} t_k^d t_l^e \\
 & \overset{(\Lambda_{2,J}^{3B,K})}{-} \frac{1}{4} \sum_{cdeklm} \lambda_{ca}^{kl} w_{bed}^{ijm} t_k^d t_l^e t_m^c \overset{(\Lambda_{2,K}^{3B,A})}{+} \frac{1}{4} \sum_{cdk} \lambda_{cd}^{ki} w_{abk}^{cjd} \\
 & \overset{(\Lambda_{2,K}^{3B,B})}{+} \frac{1}{4} \sum_{cdekl} \lambda_{cd}^{ki} \hat{P}_{cd} w_{abe}^{cjl} t_{lk}^{ed} \overset{(\Lambda_{2,K}^{3B,C})}{+} \frac{1}{8} \sum_{cdeklm} \lambda_{cd}^{ki} w_{abk}^{ljm} t_{lm}^{cd} \\
 & \overset{(\Lambda_{2,K}^{3B,D})}{-} \frac{1}{4} \sum_{cdkl} \lambda_{cd}^{ki} \hat{P}_{cd} w_{abk}^{ljd} t_l^c \overset{(\Lambda_{2,K}^{3B,E})}{+} \frac{1}{4} \sum_{cdek} \lambda_{cd}^{ki} w_{abe}^{cjd} t_k^e \\
 & \overset{(\Lambda_{2,K}^{3B,F})}{-} \frac{1}{4} \sum_{cdeklm} \lambda_{cd}^{ki} w_{eab}^{lmj} t_{mk}^{cd} t_l^e \overset{(\Lambda_{2,K}^{3B,G})}{-} \frac{1}{4} \sum_{cdeklm} \lambda_{cd}^{ki} \hat{P}_{cd} w_{abe}^{ljm} t_{mk}^{ed} t_l^c \\
 & \overset{(\Lambda_{2,K}^{3B,H})}{+} \frac{1}{8} \sum_{cdeklm} \lambda_{cd}^{ki} w_{abe}^{ljm} t_{lm}^{cd} t_k^e \overset{(\Lambda_{2,K}^{3B,I})}{-} \frac{1}{4} \sum_{cdekl} \lambda_{cd}^{ki} \hat{P}_{cd} w_{abe}^{cjl} t_l^d t_k^e \\
 & \overset{(\Lambda_{2,K}^{3B,J})}{+} \frac{1}{4} \sum_{cdklm} \lambda_{cd}^{ki} w_{abk}^{ljm} t_l^c t_m^d \overset{(\Lambda_{2,K}^{3B,K})}{+} \frac{1}{4} \sum_{cdeklm} \lambda_{cd}^{ki} w_{abe}^{ljm} t_l^c t_m^d t_k^e \\
 & \overset{(\Lambda_{2,L}^{3B,A})}{+} \sum_{ck} \lambda_c^k w_{abk}^{ijc} \overset{(\Lambda_{2,L}^{3B,B})}{+} \sum_{cdk} \lambda_c^k w_{abd}^{ijc} t_k^d \overset{(\Lambda_{2,L}^{3B,C})}{-} \sum_{ckl} \lambda_c^k w_{abk}^{ijl} t_l^c \\
 & \overset{(\Lambda_{2,L}^{3B,D})}{-} \sum_{cdkl} \lambda_c^k w_{abd}^{ijl} t_{kl}^{cd} \overset{(\Lambda_{2,L}^{3B,E})}{+} \sum_{cdkl} \lambda_c^k w_{abd}^{ijl} t_{kl}^{cd} \overset{(\Lambda_{2,M}^{3B,A})}{+} \frac{1}{2} \sum_{cdekl} \lambda_{cd}^{kl} w_{abe}^{ijc} t_{kl}^{ed} \\
 & \overset{(\Lambda_{2,M}^{3B,B})}{-} \frac{1}{2} \sum_{cdklm} \lambda_{cd}^{kl} w_{abk}^{ijm} t_{ml}^{cd} \overset{(\Lambda_{2,M}^{3B,C})}{+} \frac{1}{2} \sum_{cdeklm} \lambda_{cd}^{kl} w_{abe}^{ijm} t_{kl}^{de} t_m^c \\
 & \overset{(\Lambda_{2,M}^{3B,D})}{-} \frac{1}{2} \sum_{cdeklm} \lambda_{cd}^{kl} w_{abe}^{ijm} t_{ml}^{cd} t_k^e + \lambda_{ab}^{ij} [\text{NO2B}] = 0, \quad \forall a, b, i, j
 \end{aligned}$$

 Figure 3.14: Algebraic expressions for the $\Lambda\text{CCSD } \hat{\Lambda}_2$ amplitude equations for three-body Hamiltonians.

3.4 The Λ CCSD(T) Energy Correction for Three-Body Hamiltonians

The derivation of the Λ CCSD(T) method given in [57] is not quite transparent, making it difficult to extend it to three-body Hamiltonians in an analogous way as it is derived for two-body Hamiltonians. Furthermore, the way the method is presented in [57] also makes it difficult to realize the types of approximations that lead to the final result. Therefore, in this section the Λ CCSD(T) method is rederived as an approximation to the superior CR-CC(2,3) method [114, 117, 119, 120, 137, 138], this way facilitating the identification of new terms corresponding to the inclusion of three-body interactions, and helping to understand the approximate nature of Λ CCSD(T).

Starting from the CR-CC(2,3) method, Λ CCSD(T) is easily derived as a series of approximations to CR-CC(2,3). The generalized moments of the CCSD equations

$$\mathfrak{M}_{ijk}^{abc} = \langle \Phi_{ijk}^{abc} | [\hat{H}_N e^{\hat{T}^{(\text{CCSD})}}]_C | \Phi \rangle \quad (3.41)$$

are approximated by restricting to terms at most linear in the cluster operator,

$$\mathfrak{M}_{ijk}^{abc} \approx \langle \Phi_{ijk}^{abc} | [\hat{H}_N (\hat{1} + \hat{T}_1 + \hat{T}_2)]_C | \Phi \rangle. \quad (3.42)$$

Since the main focus of this section is the extension of Λ CCSD(T) to three-body Hamiltonians and to identify new terms arising from the presence of the residual normal-ordered three-body interaction operator \hat{W}_N in the normal-ordered Hamiltonian \hat{H}_N , the moments are split into the contributions from the normal-ordered two-body approximation, in the following denoted as $\mathfrak{M}_{ijk}^{abc}(\text{NO2B})$, and the contributions due to \hat{W}_N , denoted as $\mathfrak{M}_{ijk}^{abc}(\text{3B})$,

$$\mathfrak{M}_{ijk}^{abc} = \mathfrak{M}_{ijk}^{abc}(\text{NO2B}) + \mathfrak{M}_{ijk}^{abc}(\text{3B}). \quad (3.43)$$

The expressions for $\mathfrak{M}_{ijk}^{abc}(\text{NO2B})$ and $\mathfrak{M}_{ijk}^{abc}(\text{3B})$ in terms of interaction and cluster operators are given by

$$\mathfrak{M}_{ijk}^{abc}(\text{NO2B}) = \langle \Phi_{ijk}^{abc} | [(\hat{F}_N + \hat{V}_N) (\hat{1} + \hat{T}_1 + \hat{T}_2)]_C | \Phi \rangle \quad (3.44)$$

$$= \langle \Phi_{ijk}^{abc} | [\hat{V}_N (\hat{1} + \hat{T}_1 + \hat{T}_2)]_C | \Phi \rangle \quad (3.45)$$

and

$$\mathfrak{M}_{ijk}^{abc}(\text{3B}) = \langle \Phi_{ijk}^{abc} | [\hat{W}_N (\hat{1} + \hat{T}_1 + \hat{T}_2)]_C | \Phi \rangle, \quad (3.46)$$

and programmable expressions in terms of matrix elements of the operators involved can be found in Figure 3.15.

In order to simplify the CR-CC(2,3) expression for \mathcal{L}_3 to the form used in $\Lambda\text{CCSD(T)}$, the reduced resolvent $\hat{\mathcal{R}}_3$ is replaced by its simplified Møller-Plesset form [57,58],

$$\mathcal{R}_3^{(\text{CCSD})} = -\frac{\hat{P}_3}{\hat{\mathcal{H}}_{\text{open}}^{(\text{CCSD})}} \approx -\frac{\hat{P}_3}{\hat{F}_N} \quad (3.47)$$

$$= \sum_{\substack{i < j < k \\ a < b < c}} \left(\epsilon_{ijk}^{abc} \right)^{-1} |\Phi_{ijk}^{abc}\rangle \langle \Phi_{ijk}^{abc}| \quad (3.48)$$

where ϵ_{ijk}^{abc} is defined for the two-body Hamiltonian case,

$$\epsilon_{ijk}^{abc} = f_i^a + f_j^b + f_k^c - f_a^i - f_b^j - f_c^k. \quad (3.49)$$

The latter approximation is equivalent to replacing the $\hat{\mathcal{H}}_{\text{open}}^{(\text{CCSD})}$ on the left-hand side of system (2.121) corresponding to CR-CC(2,3), by the \hat{F}_N operator. Furthermore, in order to arrive at $\Lambda\text{CCSD(T)}$, the effective Hamiltonian $\hat{\mathcal{H}}_{\text{open}}^{(\text{CCSD})}$ on the right-hand side of system (2.121) is approximated by its leading contribution, which is \hat{H}_N . These approximations allow to replace system (2.121) by the simplified form

$$-\sum_{\substack{l < m < n \\ d < e < f}} \langle \Phi_{lmn}^{def} | \hat{F}_N | \Phi_{ijk}^{abc} \rangle = \langle \Phi | \left(\hat{1} + \hat{\Lambda}^{(\text{CCSD})} \right) \hat{H}_N | \Phi_{ijk}^{abc} \rangle, \quad (3.50)$$

which immediately leads to a convenient expression for the \mathcal{L}_3 amplitudes,

$$l_{abc}^{ijk} = \left(\epsilon_{ijk}^{abc} \right)^{-1} \langle \Phi | \left(\hat{1} + \hat{\Lambda}^{(\text{CCSD})} \right) \hat{H}_N | \Phi_{ijk}^{abc} \rangle. \quad (3.51)$$

Again, in order to identify new terms arising from the presence of \hat{W}_N in the normal-ordered Hamiltonian, the \mathcal{L}_3 amplitudes are split into their NO2B part and their part due to \hat{W}_N ,

$$l_{abc}^{ijk} = l_{abc}^{ijk}(\text{NO2B}) + l_{abc}^{ijk}(\text{3B}), \quad (3.52)$$

which are given by

$$\begin{aligned} l_{abc}^{ijk}(\text{NO2B}) = & \left[\langle \Phi | \left(\hat{\Lambda}_1 \hat{V}_N \right)_{\text{DC}} | \Phi_{ijk}^{abc} \rangle + \langle \Phi | \left(\hat{\Lambda}_2 \hat{F}_N \right)_{\text{DC}} | \Phi_{ijk}^{abc} \rangle \right. \\ & \left. + \langle \Phi | \left(\hat{\Lambda}_2 \hat{V}_N \right)_{\text{C}} | \Phi_{ijk}^{abc} \rangle \right] \left(\epsilon_{ijk}^{abc} \right)^{-1} \end{aligned} \quad (3.53)$$

and

$$l_{abc}^{ijk}(3B) = \left[\langle \Phi | \hat{W}_N | \Phi_{ijk}^{abc} \rangle + \langle \Phi | (\hat{\Lambda}_1 \hat{W}_N)_C | \Phi_{ijk}^{abc} \rangle \right. \quad (3.54)$$

$$\left. + \langle \Phi | (\hat{\Lambda}_2 \hat{W}_N)_C | \Phi_{ijk}^{abc} \rangle \right] \left(\epsilon_{ijk}^{abc} \right)^{-1}, \quad (3.55)$$

and a similar splitting, analogously to (3.25), is done for the energy correction $\delta E^{(\Lambda\text{CCSD(T)})}$,

$$\delta E^{(\Lambda\text{CCSD(T)})} = \delta E_{\text{NO2B}}^{(\Lambda\text{CCSD(T)})} + \delta E_{3B}^{(\Lambda\text{CCSD(T)})}, \quad (3.56)$$

where the individual parts are given by

$$\delta E_{\text{NO2B}}^{(\Lambda\text{CCSD(T)})} = \frac{1}{(3!)^2} \sum_{\substack{abc \\ ijk}} l_{abc}^{ijk}(\text{NO2B}) \mathfrak{M}_{ijk}^{abc}(\text{NO2B}) \quad (3.57)$$

and

$$\begin{aligned} \delta E_{3B}^{(\Lambda\text{CCSD(T)})} = \frac{1}{(3!)^2} \sum_{\substack{abc \\ ijk}} & \left[l_{abc}^{ijk}(\text{NO2B}) \mathfrak{M}_{ijk}^{abc}(3B) \right. \\ & \left. + l_{abc}^{ijk}(3B) \mathfrak{M}_{ijk}^{abc}(\text{NO2B}) + l_{abc}^{ijk}(3B) \mathfrak{M}_{ijk}^{abc}(3B) \right]. \end{aligned} \quad (3.58)$$

The final programmable expressions for the \mathcal{L}_3 amplitudes and the energy correction are listed in Figure 3.15 and the corresponding spherical expression can be found in Appendix G.2. In summary, the total Λ CCSD(T) ground-state energy consists of several parts

$$\begin{aligned} E^{(\Lambda\text{CCSD(T)})} = & E_{\text{ref}} + \Delta E_{\text{NO2B}}^{(\text{CCSD})} + \delta E_{\text{NO2B}}^{(\Lambda\text{CCSD(T)})} \\ & + \Delta E_{3B}^{(\text{CCSD})} + \delta E_{3B}^{(\Lambda\text{CCSD(T)})}, \end{aligned} \quad (3.59)$$

where the 3B contributions are only present if the residual normal-ordered three-body interaction is included in the calculations. Furthermore, as it is discussed in [96], it is interesting to note that from the many-body perturbation (MBPT) point of view, the significance of the contributions due to the \hat{T}_3 clusters changes by including the three-body interaction \hat{W}_N . In the NO2B approximation, \hat{T}_3 contributions show up at second MBPT order for the wavefunction and at fourth order in the energy $\delta E^{(\Lambda\text{CCSD(T)})}$, but the inclusion of \hat{W}_N moves these contributions to first order for the wavefunction and second order for the energy.

One appealing aspect of the Λ CCSD(T) correction is the simple structure that makes the method efficient and easy to implement. However, the degree of approximations that enter the method makes it necessary to examine the performance of the method compared to more accurate approaches such as CR-CC(2,3).

$$\begin{aligned}
 \delta E^{(\Lambda\text{CCSD(T)})} &= \frac{1}{(3!)^2} \sum_{\substack{abc \\ ijk}} l_{abc}^{ijk} \mathfrak{M}_{ijk}^{abc} \\
 l_{abc}^{ijk} &= \left\{ l_{abc}^{ijk}(\text{NO2B}) - \hat{P}_{ab/c} \sum_l w_{abl}^{ijk} \lambda_c^l + \hat{P}_{ij/k} \sum_d w_{abc}^{ijd} \lambda_d^k \right. \\
 &\quad + \frac{1}{2} \hat{P}_{ij/k} \sum_{de} w_{abc}^{dek} \lambda_{de}^{ij} + \frac{1}{2} \hat{P}_{ab/c} \sum_{lm} w_{lmc}^{ijk} \lambda_{ab}^{lm} \\
 &\quad \left. + \hat{P}_{ab/c} \hat{P}_{ij/k} \sum_{dl} w_{abl}^{ijd} \lambda_{cd}^{kl} + w_{abc}^{ijk} \right\} (\epsilon_{ijk}^{abc})^{-1} \\
 l_{abc}^{ijk}(\text{NO2B}) &= \tilde{\lambda}_{abc}^{ijk} \\
 \mathfrak{M}_{ijk}^{abc} &= \mathfrak{M}_{ijk}^{abc}(\text{NO2B}) - \hat{P}_{ab/c} \sum_l w_{ijk}^{abl} t_l^c + \hat{P}_{ij/k} \sum_d w_{ijd}^{abc} t_k^d \\
 &\quad + \frac{1}{2} \hat{P}_{ij/k} \sum_{de} w_{dek}^{abc} t_{ij}^{de} + \frac{1}{2} \hat{P}_{ab/c} \sum_{lm} w_{ijk}^{lmc} t_{lm}^{ab} \\
 &\quad + \hat{P}_{ab/c} \hat{P}_{ij/k} \sum_{dl} w_{ijd}^{abl} t_{kl}^{cd} + w_{ijk}^{abc} \\
 \mathfrak{M}_{ijk}^{abc}(\text{NO2B}) &= \tilde{t}_{ijk}^{abc}
 \end{aligned}$$

Figure 3.15: Algebraic expressions for the calculation of the Λ CCSD(T) energy correction for three-body Hamiltonians. See Figure 2.12 for the expressions for \tilde{t}_{ijk}^{abc} and $\tilde{\lambda}_{abc}^{ijk}$.

Chapter 4

Spherical Coupled-Cluster Theory

4.1 Introduction

The m -scheme formulation of Coupled-Cluster theory used in previous chapters allows for CCSD computations for ^{40}Ca up to about 8 oscillator shells using moderate computational resources, whereas the $\Lambda\text{CCSD(T)}$ correction is already out of reach even for smaller numbers of oscillator shells. Manageable three-body calculations in the m -scheme framework are restricted to ^4He and even there to small model spaces [63].

Of course, the best way to reduce the computational expense is by exploitation of symmetries. In this work, only closed-shell nuclei are considered for which the nucleons fill complete (sub-) shells shown in Figure 4.1. For such nuclei the cluster operator is a rank-zero spherical tensor operator and *spherical symmetry* may be exploited using angular-momentum algebra. Spherical Coupled-Cluster theory was first discussed in 2010 [27]. For two-body Hamiltonians, the spherical formulation significantly extends the region of the nuclear chart accessible with Coupled-Cluster theory up to the heavy nuclei regime. Calculations involving three-body Hamiltonians can be performed up to medium-mass nuclei, where they benefit particularly from the efficient matrix element handling using a $\mathcal{J}\mathcal{T}$ -coupled scheme [86]. The price to be paid for this decrease of computational demand by exploiting symmetries is an increased complexity of the initially rather simple Coupled-Cluster equations and the corresponding computer implementation.

For the following discussion of the spherical formulation, a convenient change in notation is introduced: Single-particle m -scheme states are denoted with a bar or with separated angular-momentum projection quantum number as

$$|\bar{p}\rangle \equiv |p\ m_p\rangle \equiv |n_p\ (l_p\ s_p)\ j_p\ m_p\ t_p\ m_{t_p}\rangle \quad (4.1)$$

while a complete angular-momentum shell is represented by

$$|p\rangle \equiv |n_p\ (l_p\ s_p)\ j_p\ t_p\ m_{t_p}\rangle. \quad (4.2)$$

The approach followed in this work to obtain spherical Coupled-Cluster equations is by angular momentum coupling of the corresponding m -scheme diagrams. Therefore, a brief summary of the relevant aspects of angular-momentum algebra and definitions used in this work is given in the following sections.

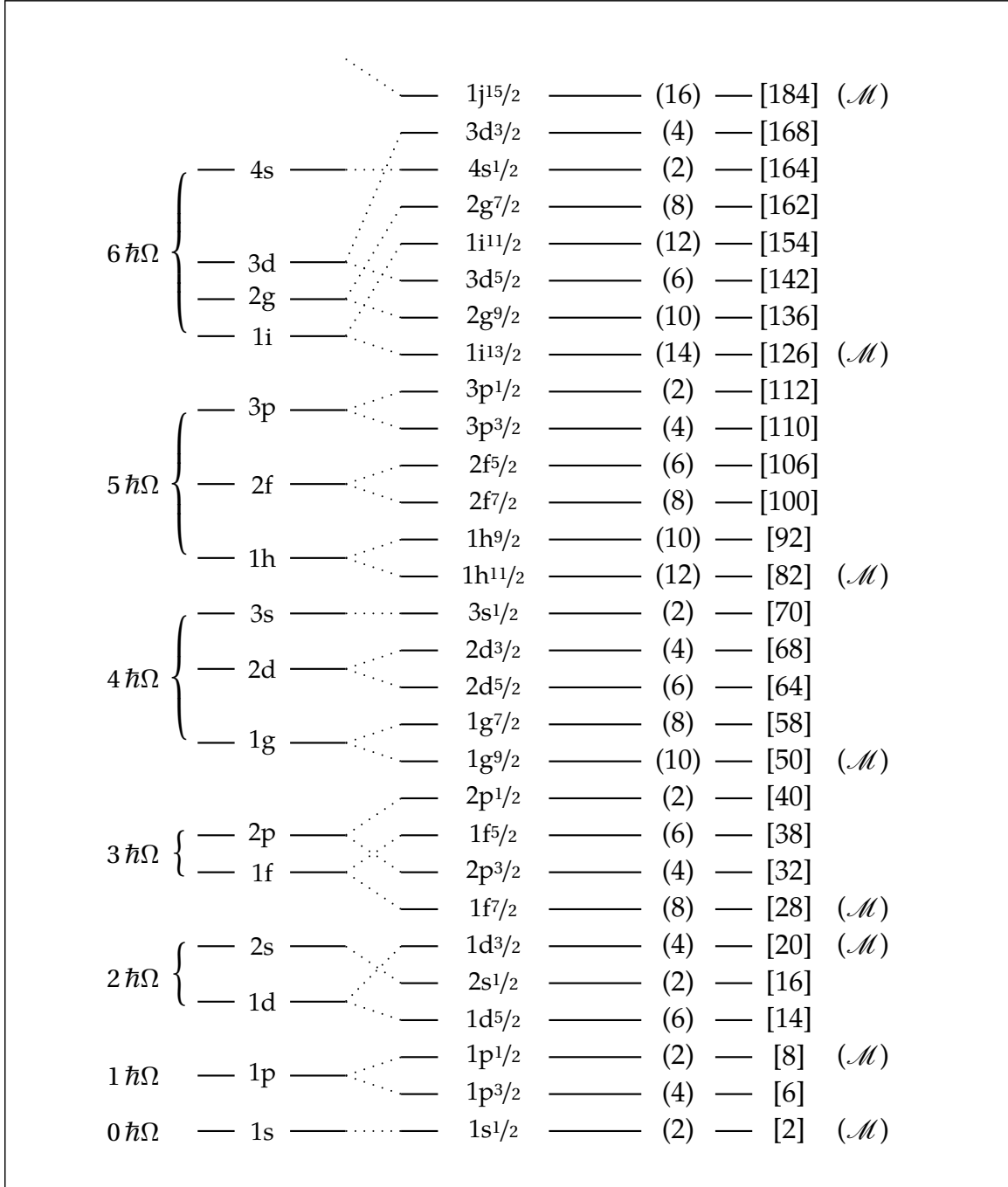


Figure 4.1: Schematic ordering of single-particle states [146] used to generate the spherical reference state. Magic nucleon numbers are marked as (M).

4.2 Spherical Tensor Operators

An *irreducible spherical tensor operator* $\hat{\mathfrak{M}}^{(J)}$ of rank J is defined as the set of $2J+1$ operators $\{\hat{\mathfrak{M}}_{M=-J,\dots,J}^{(J)}\}$ that transform under rotations R the same way as the spherical harmonics do, i.e.,

$$\hat{D}(R) \hat{\mathfrak{M}}_M^{(J)} \hat{D}^\dagger(R) = \sum_{M'=-J}^J D_{M'M}^{(J)} \hat{\mathfrak{M}}_{M'}^{(J)}, \quad (4.3)$$

where $\hat{D}(R)$ is the rotation operator corresponding to the rotation R acting on the Hilbert space and $D_{M'M}^{(J)}$ are the Wigner D functions. However, the Hermitean adjoint operator $(\hat{\mathfrak{M}}^{(J)})^\dagger$ does not transform as an irreducible tensor operator according to (4.3), its components rather transform as

$$(\hat{\mathfrak{M}}_M^{(J)})^\dagger \sim (-1)^{J-M} \hat{\mathfrak{M}}_{-M}^{(J)}. \quad (4.4)$$

It is, therefore, customary to define the *generalized Hermitean adjoint* of an irreducible spherical tensor operator according to,

$$(\hat{\mathfrak{M}}^\dagger)^{(J)} = \{(\hat{\mathfrak{M}}^\dagger)_{M=-J,\dots,J}^{(J)}\} \quad (4.5)$$

with

$$(\hat{\mathfrak{M}}^\dagger)_M^{(J)} \equiv (-1)^{J+M} (\hat{\mathfrak{M}}_{-M}^{(J)})^\dagger, \quad (4.6)$$

which transforms the same way as the original spherical tensor operator does,

$$(\hat{\mathfrak{M}}^\dagger)_M^{(J)} \sim \hat{\mathfrak{M}}_M^{(J)}. \quad (4.7)$$

This difference in transformation property of spherical tensor operators and its Hermitean adjoints has to be taken into account when they are subjected to angular-momentum coupling. When coupling angular momenta, the M component $\hat{\mathfrak{K}}_M^{(J)}$ of an irreducible tensor operator $\hat{\mathfrak{K}}^{(J)}$ may be constructed from the direct product of two irreducible tensor operators $\hat{\mathfrak{M}}^{(J_{\mathfrak{M}})}$ and $\hat{\mathfrak{N}}^{(J_{\mathfrak{N}})}$ using Clebsch-Gordan coefficients,

$$\hat{\mathfrak{K}}_M^{(J)} = \sum_{M_{\mathfrak{M}} M_{\mathfrak{N}}} \begin{pmatrix} J_{\mathfrak{M}} & J_{\mathfrak{N}} & J \\ M_{\mathfrak{M}} & M_{\mathfrak{N}} & M \end{pmatrix}_{\text{CG}} \hat{\mathfrak{M}}_{M_{\mathfrak{M}}}^{(J_{\mathfrak{M}})} \hat{\mathfrak{N}}_{M_{\mathfrak{N}}}^{(J_{\mathfrak{N}})}, \quad (4.8)$$

which may be written in a short-hand tensor product notation as

$$\hat{\mathfrak{K}}_M^{(J)} = \{\hat{\mathfrak{M}}^{(J_{\mathfrak{M}})} \otimes \hat{\mathfrak{N}}^{(J_{\mathfrak{N}})}\}_M^{(J)}. \quad (4.9)$$

Since generalized Hermitean adjoint operators also transform as irreducible spherical tensor operators, *mixed couplings* between these and standard spherical tensor operators are allowed. Coupling Hermitean adjoint operators by the prescription (4.8) is also meaningful because the operators involved have the same transformation properties. It yields an operator that transforms as the Hermitean adjoint of an irreducible spherical tensor operator of rank J ,

$$\sum_{M_{\mathfrak{M}} M_{\mathfrak{N}}} \begin{pmatrix} J_{\mathfrak{M}} & J_{\mathfrak{N}} & J \\ M_{\mathfrak{M}} & M_{\mathfrak{N}} & M \end{pmatrix}_{CG} \left(\hat{\mathfrak{M}}_{M_{\mathfrak{M}}}^{(J_{\mathfrak{M}})} \right)^{\dagger} \left(\hat{\mathfrak{N}}_{M_{\mathfrak{N}}}^{(J_{\mathfrak{N}})} \right)^{\dagger} \quad (4.10)$$

$$= (-1)^{J-M} \sum_{M_{\mathfrak{M}} M_{\mathfrak{N}}} \begin{pmatrix} J_{\mathfrak{M}} & J_{\mathfrak{N}} & J \\ M_{\mathfrak{M}} & M_{\mathfrak{N}} & -M \end{pmatrix}_{CG} \left(\hat{\mathfrak{M}}^{\dagger} \right)_{M_{\mathfrak{M}}}^{(J_{\mathfrak{M}})} \left(\hat{\mathfrak{N}}^{\dagger} \right)_{M_{\mathfrak{N}}}^{(J_{\mathfrak{N}})} \quad (4.11)$$

$$= (-1)^{J-M} \left\{ \left(\hat{\mathfrak{M}}^{\dagger} \right)^{(J_{\mathfrak{M}})} \otimes \left(\hat{\mathfrak{N}}^{\dagger} \right)^{(J_{\mathfrak{N}})} \right\}_{-M}^{(J)}. \quad (4.12)$$

When working with matrix representations of spherical tensor operators the *Wigner-Eckart theorem* is particularly valuable. It allows for a factorization of matrix elements of spherical tensor operators into a *geometric part* that depends on the projection quantum numbers but does not depend on the actual operator under consideration, and a *reduced matrix element* that is operator-specific and independent of the projections. Therefore, if $\hat{\mathfrak{K}}^{(J)}$ is an irreducible spherical two-body tensor operator of rank J , for matrix elements of its components $\hat{\mathfrak{K}}_M^{(J)}$ holds ¹

$$\begin{matrix} J_{pq} M_{pq} & J_{rs} M_{rs} \\ \downarrow & \downarrow \\ \langle pq | \hat{\mathfrak{K}}_M^{(J)} | rs \rangle \end{matrix} = (-1)^{J_{pq}-M_{pq}} \begin{pmatrix} J_{pq} & J & J_{rs} \\ -M_{pq} & M & M_{rs} \end{pmatrix}_{3j} \begin{matrix} J_{pq} & J_{rs} \\ \downarrow & \downarrow \\ \langle pq || \hat{\mathfrak{K}}^{(J)} || rs \rangle \end{matrix}, \quad (4.14)$$

where

$$\begin{matrix} J_{pq} & J_{rs} \\ \downarrow & \downarrow \\ \langle pq || \hat{\mathfrak{K}}^{(J)} || rs \rangle \end{matrix} \quad (4.15)$$

is the reduced matrix element of $\hat{\mathfrak{K}}^{(J)}$. Since the geometric part is already known for all operators, all operator-specific information is encoded in the reduced matrix elements. Furthermore, many problems may be formulated in reduced matrix elements exclusively, thus avoiding the geometric part completely. Two important

¹For one-body operators the Wigner-Eckart theorem analogously reads

$$\langle p m_p | \hat{\mathfrak{K}}^{(J)} | q m_q \rangle = (-1)^{j_p-m_p} \begin{pmatrix} j_p & J & j_q \\ -m_p & M & m_q \end{pmatrix}_{3j} \langle p || \hat{\mathfrak{K}}^{(J)} || q \rangle. \quad (4.13)$$

properties of spherical tensor operators immediately follows from (4.14) due to the presence of the Wigner 3j symbol: The angular momenta involved have to satisfy the triangular condition

$$|J_{pq} - J_{rs}| \leq J \leq J_{pq} + J_{rs} , \quad (4.16)$$

and the projections have to fulfill the condition

$$-M_{pq} + M_{rs} + M = 0 . \quad (4.17)$$

4.3 Angular-Momentum Coupling

The concept of irreducible spherical tensor operators may be applied to the creation and annihilation operators of second quantization. The $2j_p + 1$ operators

$$\hat{a}_p^\dagger \equiv \left\{ \hat{a}_{p, m_p = -j_p, \dots, j_p}^\dagger \right\} \quad (4.18)$$

transform as components of an irreducible spherical tensor operator of rank j_p . They may, therefore, be subjected to angular-momentum coupling, e.g.,

$$\left\{ \hat{a}_p^\dagger \otimes \hat{a}_q^\dagger \right\}_M^{(J)} = \sum_{m_p m_q} \begin{pmatrix} j_p & j_q & J \\ m_p & m_q & M \end{pmatrix}_{\text{CG}} \hat{a}_{p, m_p}^\dagger \hat{a}_{q, m_q}^\dagger . \quad (4.19)$$

When (4.19) is applied to the vacuum, it gives an antisymmetrized two-particle state coupled to good angular momentum J and projection M ,

$$\sum_{m_p m_q} \begin{pmatrix} j_p & j_q & J \\ m_p & m_q & M \end{pmatrix}_{\text{CG}} |p \ m_p \ q \ m_q\rangle \equiv |p \ q\rangle_{JM}^{\downarrow} . \quad (4.20)$$

The coupled bra state is defined as the Hermitean adjoint of the coupled ket state², i.e.,

$$\langle p \ q|_{JM}^{\uparrow} = \sum_{m_p m_q} \begin{pmatrix} j_p & j_q & J \\ m_p & m_q & M \end{pmatrix}_{\text{CG}} \langle p \ m_p \ q \ m_q| = \left(|p \ q\rangle_{JM}^{\downarrow} \right)^\dagger . \quad (4.21)$$

It is important to note that the coupling line always denotes the coupling of the *states* and not the coupling of the *operators* that create them, which makes a difference because of the inverted order of the positions of the operators and the Slater determinant entries for bra determinants, as can be seen from

$$\langle p \ m_p \ q \ m_q| = \langle 0| \hat{a}_{q, m_q} \hat{a}_{p, m_p} . \quad (4.22)$$

²If the Clebsch-Gordan coefficients are chosen to be real.

The generalized Hermitean adjoint of \hat{a}_{p,m_p}^\dagger is given by

$$\hat{\tilde{a}}_{p,m_p} \equiv (-1)^{j_p-m_p} \left(\hat{a}_{p,-m_p}^\dagger \right)^\dagger \quad (4.23)$$

$$= (-1)^{j_p-m_p} \hat{a}_{p,-m_p} \quad (4.24)$$

and states created by the action of this operator will be denoted as

$$\langle \tilde{p} \tilde{m}_p | \equiv \langle 0 | \hat{\tilde{a}}_{p,m_p} = (-1)^{j_p-m_p} \langle p - m_p | . \quad (4.25)$$

These bra states may be coupled among themselves or also to ket states, e.g.,

$$\langle \tilde{p} | \dots | q \rangle \overset{JM}{\overbrace{\quad}} = \sum_{m_p m_q} \begin{pmatrix} j_p & j_q & J \\ m_p & m_q & M \end{pmatrix}_{\text{CG}} \langle \tilde{p} \tilde{m}_p | \dots | q m_q \rangle \quad (4.26)$$

$$= \sum_{m_p m_q} (-1)^{j_p-m_p} \begin{pmatrix} j_p & j_q & J \\ -m_p & m_q & M \end{pmatrix}_{\text{CG}} \langle p m_p | \dots | q m_q \rangle \quad (4.27)$$

where the rules of angular-momentum algebra hold and no distinction between bra and ket states has to be made any more. Equation (4.27) may also be reversed, i.e.,

$$\langle p m_p | \dots | q m_q \rangle = \sum_{JM} (-1)^{j_p-m_p} \begin{pmatrix} j_p & j_q & J \\ -m_p & m_q & M \end{pmatrix}_{\text{CG}} \langle \tilde{p} | \dots | q \rangle \overset{JM}{\overbrace{\quad}} . \quad (4.28)$$

A coupled standard bra state can easily be expressed in terms of states generated by the generalized Hermitian adjoints by

$$\langle \tilde{p} q | \overset{JM}{\overbrace{\quad}} = (-1)^{J-M} \langle \tilde{p} \tilde{q} | \overset{J-M}{\overbrace{\quad}} . \quad (4.29)$$

Angular-momentum algebra is well-known and exhaustively documented [147], so no details such as orthogonality relations for coupling coefficients and recoupling transformations etc. are given here. However, one particularly useful relation that is easily confirmed is listed for future reference

$$\begin{aligned} \sum_{m_p m_q} \begin{pmatrix} j_p & j_q & J \\ -m_p & m_q & M \end{pmatrix}_{\text{CG}} \begin{pmatrix} j_p & J' & j_q \\ -m_p & M' & m_q \end{pmatrix}_{3j} \\ = (-1)^{2j_p} (-1)^{J+M} \hat{J}^{-1} \delta_{JJ'} \delta_{M-M'} , \end{aligned} \quad (4.30)$$

where hat factors \hat{J} are defined by

$$\hat{J} = \sqrt{2J+1} . \quad (4.31)$$

It should be noted that in the definition of coupled antisymmetric states (4.20) no normalization factor has been introduced, as it often is in the literature [33, 78]. Therefore, these states are unnormalized, and the normalized states would be given by

$$\overrightarrow{|p\ q\rangle}_{\text{norm}} \equiv \mathcal{N}_{pq} \overrightarrow{|p\ q\rangle}, \quad (4.32)$$

with normalization factor

$$\mathcal{N}_{pq} \equiv \frac{\sqrt{1 + (-1)^J \delta_{n_p n_q} \delta_{l_p l_q} \delta_{j_p j_q} \delta_{m_{l_p} m_{l_q}}}}{1 + \delta_{n_p n_q} \delta_{l_p l_q} \delta_{j_p j_q} \delta_{m_{l_p} m_{l_q}}}. \quad (4.33)$$

Consequently, if p and q represent two like nucleons in the same shell, this factor prevents coupling to odd angular momenta which is a feature also shared by the unnormalized states.

In most parts of this work the X coefficients [148]

$$\left\{ \begin{matrix} j_p & j_q & J_{pq} \\ j_r & j_s & J_{rs} \\ J_{pr} & J_{qs} & J \end{matrix} \right\}_X = \hat{J}_{pq} \hat{J}_{rs} \hat{J}_{pr} \hat{J}_{qs} \left\{ \begin{matrix} j_p & j_q & J_{pq} \\ j_r & j_s & J_{rs} \\ J_{pr} & J_{qs} & J \end{matrix} \right\}_{9j} \quad (4.34)$$

are used in favor of Wigner 9j symbols for angular momentum recouplings of four angular momenta in order to keep the expressions short. It is convenient to introduce a similar definition also for Wigner 6j symbols,

$$\left\{ \begin{matrix} j_p & j_q & j_r \\ j_s & j_t & j_u \end{matrix} \right\}_X = \hat{j}_p \hat{j}_q \hat{j}_r \left\{ \begin{matrix} j_p & j_q & j_r \\ j_s & j_t & j_u \end{matrix} \right\}_{6j}, \quad (4.35)$$

in order to shorten the equations encountered in the spherical formulation of $\Lambda\text{CCSD(T)}$ (see. Appendix G.1).

4.4 One-Body Operators

The purpose of this section is to define *coupled one-body matrix elements* which are inevitably encountered when Coupled-Cluster diagrams are evaluated in the spherical scheme. For a one-body spherical tensor operator component $\mathfrak{K}_M^{(J)}$ the definition of coupled matrix elements used in this work is

$$\overrightarrow{\langle \tilde{p} | \mathfrak{K}_M^{(J)} | q \rangle} = \sum_{m_p m_q} (-1)^{p-m_p} \left(\begin{matrix} j_p & j_q & J' \\ -m_p & m_q & M' \end{matrix} \right)_{\text{CG}} \langle p\ m_p | \mathfrak{K}_M^{(J)} | q\ m_q \rangle. \quad (4.36)$$

The decoupling employs the same phase factor, i.e.,

$$\langle p \ m_p | \mathfrak{K}_M^{(J)} | q \ m_q \rangle = \sum_{J'M'} (-1)^{p-m_p} \begin{pmatrix} j_p & j_q & J' \\ -m_p & m_q & M' \end{pmatrix}_{\text{CG}} \overbrace{\langle \tilde{p} | \mathfrak{K}_M^{(J)} | q \rangle}^{J'M'}. \quad (4.37)$$

The coupled one-body matrix elements may be expressed in terms of reduced one-body matrix elements as

$$\overbrace{\langle \tilde{p} | \mathfrak{K}_M^{(J)} | q \rangle}^{J-M} = (-1)^{2j_p} (-1)^{J-M} \hat{J}^{-1} \langle p || \mathfrak{K}^{(J)} || q \rangle, \quad (4.38)$$

and, furthermore,

$$\overbrace{\langle \tilde{p} | \mathfrak{K}_M^{(J)} | q \rangle}^{J'M'} = \delta_{JJ'} \delta_{M-M'} \overbrace{\langle \tilde{p} | \mathfrak{K}_M^{(J)} | q \rangle}^{J-M}. \quad (4.39)$$

So the only non-vanishing coupling corresponds to the rank J and the negative projection $-M$ of the spherical tensor operator. This can be seen as follows. Replacing the m -scheme matrix elements in

$$\overbrace{\langle \tilde{p} | \mathfrak{K}_M^{(J)} | q \rangle}^{J'M'} = \sum_{m_p m_q} (-1)^{p-m_p} \begin{pmatrix} j_p & j_q & J' \\ -m_p & m_q & M' \end{pmatrix}_{\text{CG}} \langle p \ m_p | \mathfrak{K}_M^{(J)} | q \ m_q \rangle \quad (4.40)$$

by their reduced matrix elements according to the Wigner-Eckart theorem leads to

$$\begin{aligned} \overbrace{\langle \tilde{p} | \mathfrak{K}_M^{(J)} | q \rangle}^{J'M'} &= \sum_{m_p m_q} (-1)^{p-m_p} \begin{pmatrix} j_p & j_q & J' \\ -m_p & m_q & M' \end{pmatrix}_{\text{CG}} \\ &\quad \times (-1)^{p-m_p} \begin{pmatrix} j_p & J & j_q \\ -m_p & M & m_q \end{pmatrix}_{3j} \langle p || \mathfrak{K}^{(J)} || q \rangle, \end{aligned} \quad (4.41)$$

where the phases cancel and the useful relation (4.30) can be applied to give

$$\overbrace{\langle \tilde{p} | \mathfrak{K}_M^{(J)} | q \rangle}^{J'M'} = (-1)^{2j_p} (-1)^{J'+M'} (\hat{J}')^{-1} \delta_{JJ'} \delta_{M-M'} \langle p || \mathfrak{K}^{(J)} || q \rangle. \quad (4.42)$$

This is equivalent to (4.39) and (4.38) follows immediately.

4.5 Cross-Coupled Matrix Elements

4.5.1 Scalar Case

Matrix elements of scalar two-body spherical tensor operators $\mathfrak{K}_0^{(0)}$ such as the two-body Hamiltonian are routinely used in the J -coupled representation

$$\begin{aligned} \langle \overset{JM}{\downarrow} \tilde{p} \tilde{q} | \mathfrak{K}_0^{(0)} | \overset{JM}{\uparrow} r s \rangle &= \sum_{\substack{m_p m_q \\ m_r m_s}} \begin{pmatrix} j_p & j_q & J \\ m_p & m_q & M \end{pmatrix}_{\text{CG}} \begin{pmatrix} j_r & j_s & J \\ m_r & m_s & M \end{pmatrix}_{\text{CG}} \\ &\times \langle p m_p q m_q | \mathfrak{K}_0^{(0)} | r m_r s m_s \rangle \end{aligned} \quad (4.43)$$

which will be referred to as *standard coupling*. For the Hamiltonian, being a rank-zero spherical tensor operator, the matrix elements are diagonal in J and M .

An alternative coupling scheme that appears naturally in the derivation of spherical Coupled-Cluster equations is the *cross-coupled* scheme. Following [148]³, two types of cross-coupled matrix elements may be defined, referred to as *cross-coupled scheme A* (CCA)

$$\langle \overset{JM}{\downarrow} \tilde{p} \tilde{q} | \mathfrak{K}_0^{(0)} | \overset{JM}{\uparrow} r s \rangle \equiv (-1)^{J-M} \langle \tilde{p} \tilde{q} | \mathfrak{K}_0^{(0)} | r s \rangle \quad (4.44)$$

$$\begin{aligned} &= (-1)^{J-M} \sum_{\substack{m_p m_q \\ m_r m_s}} (-1)^{j_p-m_p} \begin{pmatrix} j_p & j_r & J \\ -m_p & m_r & -M \end{pmatrix}_{\text{CG}} \\ &\times (-1)^{j_q-m_q} \begin{pmatrix} j_q & j_s & J \\ -m_q & m_s & M \end{pmatrix}_{\text{CG}} \langle p m_p q m_q | \mathfrak{K}_0^{(0)} | r m_r s m_s \rangle \end{aligned} \quad (4.45)$$

and *cross-coupled scheme B* (CCB)

$$\langle \overset{JM}{\downarrow} \tilde{p} \tilde{q} | \mathfrak{K}_0^{(0)} | \overset{JM}{\uparrow} r s \rangle \equiv (-1)^{J-M} \langle \tilde{p} \tilde{q} | \mathfrak{K}_0^{(0)} | r s \rangle \quad (4.46)$$

$$\begin{aligned} &= (-1)^{J-M} \sum_{\substack{m_p m_q \\ m_r m_s}} (-1)^{j_p-m_p} \begin{pmatrix} j_p & j_s & J \\ -m_p & m_s & -M \end{pmatrix}_{\text{CG}} \\ &\times (-1)^{j_q-m_q} \begin{pmatrix} j_q & j_r & J \\ -m_q & m_r & M \end{pmatrix}_{\text{CG}} \langle p m_p q m_q | \mathfrak{K}_0^{(0)} | r m_r s m_s \rangle \end{aligned} \quad (4.47)$$

³However, a different style for the cross-coupling lines is used in order to avoid confusion with standard coupling lines.

where the coupling line runs across the operator. According to the original definition in [148], in both cases the phase $(-1)^{J-M}$ and the negative projection are associated with the coupling involving the state \tilde{p} , although the choice is arbitrary for the scalar case. However, this assignment is convenient for the general case as well, which is why the original choice from [148] is kept in this work. As the standard coupled matrix elements, cross-coupled matrix elements are diagonal in the angular momenta and projections, i.e.,

$$\langle \tilde{p} \tilde{q} | \hat{\mathcal{R}}_0^{(0)} | rs \rangle = \delta_{JJ'} \delta_{MM'} \langle \tilde{p} \tilde{q} | \hat{\mathcal{R}}_0^{(0)} | rs \rangle \quad (4.48)$$

$$\langle \tilde{p} \tilde{q} | \hat{\mathcal{R}}_0^{(0)} | rs \rangle = \delta_{JJ'} \delta_{MM'} \langle \tilde{p} \tilde{q} | \hat{\mathcal{R}}_0^{(0)} | rs \rangle, \quad (4.49)$$

as is proven for the general case in the next section. The transformation equations between the standard coupling and the cross-coupled schemes are listed in Figure 4.2. The transformations for the reduced matrix elements follow directly from the simple relation between reduced and standard matrix elements for the case of scalar spherical tensor operators,

$$\langle \tilde{p} \tilde{q} | \hat{\mathcal{R}}_0^{(0)} | rs \rangle = \hat{J}^{-1} \langle p q | \hat{\mathcal{R}}_0^{(0)} | rs \rangle \quad (4.50)$$

and analogously for the cross-coupled matrix elements. Of course, these transformations are only a special case of the more general transformations in Figure 4.3, but they are more efficient because for the Wigner 9j symbols appearing in the general transformations may be replaced by 6j symbols as in Figure 4.2.

4.5.2 General Case

For applications involving spherical tensor operators of rank different from zero the previous definition of cross-coupled matrix elements has to be generalized. Cross-coupled matrix elements of general spherical tensor operators are straightforwardly defined in analogy to the scalar case by

$$\langle \tilde{p} \tilde{q} | \hat{\mathcal{R}}_M^{(J)} | rs \rangle \equiv (-1)^{J_{pr}-M_{pr}} \langle \tilde{p} \tilde{q} | \hat{\mathcal{R}}_M^{(J)} | rs \rangle \quad (4.51)$$

$$\begin{aligned}
 \langle \tilde{p} \tilde{q} | \mathfrak{K}_0^{(0)} | r s \rangle &= \sum_{J'} (\hat{J}')^2 (-1)^{j_q+j_r+J+J'} \begin{Bmatrix} j_p & j_r & J \\ j_s & j_q & J' \end{Bmatrix}_{6j} \langle \tilde{p} \tilde{q} | \mathfrak{K}_0^{(0)} | r s \rangle^{J'M'} \\
 \langle \tilde{p} \tilde{q} | \mathfrak{K}_0^{(0)} | r s \rangle &= - \sum_{J'} (\hat{J}')^2 (-1)^{j_q+j_r-J} \begin{Bmatrix} j_p & j_s & J \\ j_r & j_q & J' \end{Bmatrix}_{6j} \langle \tilde{p} \tilde{q} | \mathfrak{K}_0^{(0)} | r s \rangle^{J'M'} \\
 \langle p q | \mathfrak{K}_0^{(0)} | r s \rangle &= \sum_{J'} (\hat{J}')^2 (-1)^{j_q+j_r+J+J'} \begin{Bmatrix} j_p & j_r & J' \\ j_s & j_q & J \end{Bmatrix}_{6j} \langle \tilde{p} \tilde{q} | \mathfrak{K}_0^{(0)} | r s \rangle^{J'M'} \\
 &\equiv \text{CCAtoStd} \left[\begin{matrix} p q \\ r s \end{matrix} ; J, J' \right] \langle \tilde{p} \tilde{q} | \mathfrak{K}_0^{(0)} | r s \rangle^{J'M'} \\
 \langle p q | \mathfrak{K}_0^{(0)} | r s \rangle &= - \sum_{J'} (\hat{J}')^2 (-1)^{j_q+j_r-J'} \begin{Bmatrix} j_p & j_s & J' \\ j_r & j_q & J \end{Bmatrix}_{6j} \langle \tilde{p} \tilde{q} | \mathfrak{K}_0^{(0)} | r s \rangle^{J'M'} \\
 &\equiv \text{CCBtoStd} \left[\begin{matrix} p q \\ r s \end{matrix} ; J, J' \right] \langle \tilde{p} \tilde{q} | \mathfrak{K}_0^{(0)} | r s \rangle^{J'M'}
 \end{aligned}$$

Figure 4.2: Transformations between the standard and cross-coupled schemes for scalar spherical tensor operators.

and

$$\langle \tilde{p}\tilde{q} | \hat{\mathcal{R}}_M^{(J)} | rs \rangle \equiv (-1)^{J_{ps}-M_{ps}} \langle \tilde{p}\tilde{q} | \hat{\mathcal{R}}_M^{(J)} | rs \rangle. \quad (4.52)$$

The cross-coupled matrix elements as defined in (4.51) and (4.52) also allow a factorization into a geometric part and a reduced matrix element in the usual sense

$$\langle \tilde{p}\tilde{q} | \hat{\mathcal{R}}_M^{(J)} | rs \rangle = (-1)^{J_{pr}-M_{pr}} \begin{pmatrix} J_{pr} & J & J_{qs} \\ -M_{pr} & M & M_{qs} \end{pmatrix}_{3j} \langle \tilde{p}\tilde{q} || \hat{\mathcal{R}}_M^{(J)} || rs \rangle \quad (4.53)$$

and

$$\langle \tilde{p}\tilde{q} | \hat{\mathcal{R}}_M^{(J)} | rs \rangle = (-1)^{J_{ps}-M_{ps}} \begin{pmatrix} J_{ps} & J & J_{qr} \\ -M_{ps} & M & M_{qr} \end{pmatrix}_{3j} \langle \tilde{p}\tilde{q} || \hat{\mathcal{R}}_M^{(J)} || rs \rangle. \quad (4.54)$$

Only the cross-coupled A case (4.53) is derived in the following. By means of angular-momentum recouplings the cross-coupled matrix element may be written in terms of standard coupled matrix elements as

$$\begin{aligned} \langle \tilde{p}\tilde{q} | \hat{\mathcal{R}}_M^{(J)} | rs \rangle &= (-1)^{J_{pr}-M_{pr}} \sum_{\mathcal{J} \mathcal{M}} \begin{pmatrix} J_{pr} & J_{qs} & \mathcal{J} \\ -M_{pr} & M_{qs} & \mathcal{M} \end{pmatrix}_{\text{CG}} \\ &\times \sum_{J_{pq} J_{rs}} \begin{Bmatrix} j_p & j_r & J_{pr} \\ j_q & j_s & J_{qs} \\ J_{pq} & J_{rs} & \mathcal{J} \end{Bmatrix}_X \sum_{M_{pq} M_{rs}} (-1)^{J_{pq}-M_{pq}} \begin{pmatrix} J_{pq} & J_{rs} & \mathcal{J} \\ M_{pq} & M_{rs} & \mathcal{M} \end{pmatrix}_{\text{CG}} \\ &\times \langle \tilde{p}\tilde{q} | \hat{\mathcal{R}}_M^{(J)} | rs \rangle \quad (4.55) \end{aligned}$$

Replacing the standard coupled matrix element by its reduced matrix element,

$$\begin{aligned}
 \langle \tilde{p}\tilde{q} | \hat{\mathcal{K}}_M^{(J)} | rs \rangle &= (-1)^{J_{pr}-M_{pr}} \sum_{\mathcal{J}\mathcal{M}} \begin{pmatrix} J_{pr} & J_{qs} & \mathcal{J} \\ -M_{pr} & M_{qs} & \mathcal{M} \end{pmatrix}_{\text{CG}} \\
 &\times \sum_{J_{pq}J_{rs}} \begin{Bmatrix} j_p & j_r & J_{pr} \\ j_q & j_s & J_{qs} \\ J_{pq} & J_{rs} & \mathcal{J} \end{Bmatrix}_X \sum_{M_{pq}M_{rs}} \begin{pmatrix} J_{pq} & J_{rs} & \mathcal{J} \\ M_{pq} & M_{rs} & \mathcal{M} \end{pmatrix}_{\text{CG}} \begin{pmatrix} J_{pq} & J & J_{rs} \\ M_{pq} & M & M_{rs} \end{pmatrix}_{3j} \\
 &\times \langle \tilde{p}\tilde{q} | \hat{\mathcal{K}}^{(J)} | rs \rangle, \tag{4.56}
 \end{aligned}$$

allows application of the useful relation (4.30) to give

$$\sum_{M_{pq}M_{rs}} \begin{pmatrix} J_{pq} & J_{rs} & \mathcal{J} \\ M_{pq} & M_{rs} & \mathcal{M} \end{pmatrix}_{\text{CG}} \begin{pmatrix} J_{pq} & J & J_{rs} \\ M_{pq} & M & M_{rs} \end{pmatrix}_{3j} = (-1)^{J+M} \hat{J}^{-1} \delta_{\mathcal{J}J} \delta_{\mathcal{M}-M} \tag{4.57}$$

which in turn eliminates the $\mathcal{J}\mathcal{M}$ summations, leading to

$$\begin{aligned}
 \langle \tilde{p}\tilde{q} | \hat{\mathcal{K}}_M^{(J)} | rs \rangle &= (-1)^{J_{pr}-M_{pr}} (-1)^{J+M} \hat{J}^{-1} \begin{pmatrix} J_{pr} & J_{qs} & J \\ -M_{pr} & M_{qs} & -M \end{pmatrix}_{\text{CG}} \\
 &\times \sum_{J_{pq}J_{rs}} \begin{Bmatrix} j_p & j_r & J_{pr} \\ j_q & j_s & J_{qs} \\ J_{pq} & J_{rs} & J \end{Bmatrix}_X \langle \tilde{p}\tilde{q} | \hat{\mathcal{K}}^{(J)} | rs \rangle. \tag{4.58}
 \end{aligned}$$

By introducing a Wigner 3j symbol and introducing the short-hand notation for the reduced cross-coupled matrix element,

$$\langle \tilde{p}\tilde{q} | \hat{\mathcal{K}}^{(J)} | rs \rangle \equiv \sum_{J_{pq}J_{rs}} \begin{Bmatrix} j_p & j_r & J_{pr} \\ j_q & j_s & J_{qs} \\ J_{pq} & J_{rs} & J \end{Bmatrix}_X \langle \tilde{p}\tilde{q} | \hat{\mathcal{K}}^{(J)} | rs \rangle \tag{4.59}$$

Eq. (4.58) can be written as

$$\langle \tilde{p}\tilde{q} | \hat{\mathcal{K}}_M^{(J)} | rs \rangle = (-1)^{J_{pr}-M_{pr}} \begin{pmatrix} J_{pr} & J & J_{qs} \\ -M_{pr} & M & M_{qs} \end{pmatrix}_{3j} \langle \tilde{p}\tilde{q} | \hat{\mathcal{K}}^{(J)} | rs \rangle, \tag{4.60}$$

arriving at (4.53).

The non-vanishing cross-coupled A matrix elements

$$\langle \tilde{p} \tilde{q} | \hat{\mathcal{K}}_M^{(J)} | r s \rangle \quad (4.61)$$

of a spherical tensor operator component $\hat{\mathcal{K}}_M^{(J)}$ fulfill the triangular and projection conditions

$$|J_{pr} - J_{qs}| \leq J \leq J_{pr} + J_{qs}, \quad -M_{pr} + M_{qs} + M = 0, \quad (4.62)$$

and an analogous statement holds for the cross-coupled scheme B. This follows immediately from the presence of the Wigner 3j symbol in (4.60).

Figure 4.3 summarizes the transformation formulas from standard to cross coupling and vice versa for the case of reduced matrix elements, which are more compact than for the standard matrix elements because the trivial geometrical factor does not appear any more.

$$\begin{aligned}
 \langle \tilde{p}\tilde{q} || \hat{\mathcal{K}}^{(J)} || rs \rangle &= \sum_{J_{pr} J_{qs}} \left\{ \begin{matrix} j_p & j_r & J_{pr} \\ j_q & j_s & J_{qs} \\ J_{pq} & J_{rs} & J \end{matrix} \right\}_\chi \langle \tilde{p}\tilde{q} || \hat{\mathcal{K}}^{(J)} || rs \rangle \\
 \langle \tilde{p}\tilde{q} || \hat{\mathcal{K}}^{(J)} || rs \rangle &= (-1)^{j_r+j_s-J_{rs}} \sum_{J_{ps} J_{qr}} \left\{ \begin{matrix} j_p & j_s & J_{ps} \\ j_q & j_r & J_{qr} \\ J_{pq} & J_{rs} & J \end{matrix} \right\}_\chi \langle \tilde{p}\tilde{q} || \hat{\mathcal{K}}^{(J)} || rs \rangle \\
 \langle \tilde{p}\tilde{q} || \hat{\mathcal{K}}^{(J)} || rs \rangle &= \sum_{J_{pr} J_{qs}} \left\{ \begin{matrix} j_p & j_q & J_{pq} \\ j_r & j_s & J_{rs} \\ J_{pr} & J_{qs} & J \end{matrix} \right\}_\chi \langle \tilde{p}\tilde{q} || \hat{\mathcal{K}}^{(J)} || rs \rangle \\
 &\equiv \text{CCAtoStd} \left[\begin{matrix} pq J_{pq}; J_{pr} \\ rs J_{rs}; J_{qs} \end{matrix} \right] \langle \tilde{p}\tilde{q} || \hat{\mathcal{K}}^{(J)} || rs \rangle \\
 \langle \tilde{p}\tilde{q} || \hat{\mathcal{K}}^{(J)} || rs \rangle &= (-1)^{j_r+j_s-J_{rs}} \sum_{J_{ps} J_{qr}} \left\{ \begin{matrix} j_p & j_q & J_{pq} \\ j_s & j_r & J_{rs} \\ J_{ps} & J_{qr} & J \end{matrix} \right\}_\chi \langle \tilde{p}\tilde{q} || \hat{\mathcal{K}}^{(J)} || rs \rangle \\
 &\equiv \text{CCBtoStd} \left[\begin{matrix} pq J_{pq}; J_{ps} \\ rs J_{rs}; J_{qr} \end{matrix} \right] \langle \tilde{p}\tilde{q} || \hat{\mathcal{K}}^{(J)} || rs \rangle
 \end{aligned}$$

Figure 4.3: Transformations between the standard and cross-coupled schemes for reduced matrix elements of general spherical tensor operators $\hat{\mathcal{K}}^{(J)}$.

4.6 Diagram Coupling

The aim of this section is the evaluation of *angular-momentum coupled diagrams*. An outstanding review of this matter is given in [148] and thus only a brief review is given here. A coupled diagram is obtained by coupling the external lines of the corresponding *m*-scheme diagrams to good angular momentum, i.e., as schematically indicated below,

$$\sum_{m_a m_b} \begin{pmatrix} j_a & j_b & J \\ m_a & m_b & M \end{pmatrix}_{\text{CG}} \begin{array}{c} \bar{a} \quad \bar{b} \\ \diagdown \quad \diagup \\ \bigcirc \end{array} \equiv \begin{array}{c} JM \\ \overbrace{\quad \quad} \\ \diagdown \quad \diagup \\ \bigcirc \end{array} \quad (4.63)$$

If these *m*-scheme diagrams represent matrix elements of some operator, the coupled diagrams clearly represent *coupled matrix elements* of this operator. For example, the (DBc) contribution (see Figure 2.4) to the coupled \hat{T}_2 matrix elements may be written as

$$\begin{array}{c} JM \\ \overbrace{\quad \quad} \\ \diagdown \quad \diagup \\ \bigcirc \end{array} \begin{array}{c} JM \\ \overbrace{\quad \quad} \\ \diagdown \quad \diagup \\ \bigcirc \end{array} = \langle \overbrace{a \ b}^{JM} | \hat{t}_2 | \overbrace{i \ j}^{JM} \rangle$$

$$\stackrel{(DBc)}{\longleftarrow} \sum_{m_a m_b} \sum_{m_i m_j} \begin{pmatrix} j_a & j_b & J \\ m_a & m_b & M \end{pmatrix}_{\text{CG}} \begin{pmatrix} j_i & j_j & J \\ m_i & m_j & M \end{pmatrix}_{\text{CG}} \times \frac{1}{2} \sum_{\bar{c} \bar{d}} \langle \bar{a} \bar{b} | \hat{v} | \bar{c} \bar{d} \rangle \langle \bar{c} \bar{d} | \hat{t}_2 | \bar{i} \bar{j} \rangle. \quad (4.64)$$

This expression is not quite satisfactory yet since for its evaluation still *m*-scheme matrix elements of the operators involved are required. The purpose of the coupling techniques to be presented below is to replace *m*-scheme matrix elements and the corresponding summations over angular momentum projection quantum numbers by products of coupled matrix elements. For instance, the above contribution may in the end be written in a fully angular-momentum-coupled formulation as

$$\langle \overbrace{a \ b}^{JM} | \hat{t}_2 | \overbrace{i \ j}^{JM} \rangle \stackrel{(DBc)}{\longleftarrow} \frac{1}{2} \sum_{cd} \sum_{JM} \langle \overbrace{a \ b}^{JM} | \hat{v} | \overbrace{c \ d}^{JM} \rangle \langle \overbrace{c \ d}^{JM} | \hat{t}_2 | \overbrace{i \ j}^{JM} \rangle. \quad (4.65)$$

Since the external lines are already explicitly coupled, the focus is on coupling of the internal lines. An internal line consists of a bra and a ket part which are summed over, i.e.,

$$\sum_{p m_p} \langle p m_p | \dots | p m_p \rangle \quad \text{or} \quad \sum_{p m_p} | p m_p \rangle \langle p m_p | . \quad (4.66)$$

It is the projection quantum number summation that is of main interest in the following, so the angular momentum summation will be ignored. Since an internal line typically corresponds to the outgoing part of some operator and the ingoing part of another operator, the bra and ket states will belong to different matrix elements. Internal lines may be coupled right away to zero angular momentum using

$$\sum_{m_p} \langle p m_p | \dots | p m_p \rangle = (-1)^{2j_p} \hat{j}_p \overbrace{\langle \tilde{p} | \dots | p \rangle}^{00} , \quad (4.67)$$

$$\sum_{m_p} | p m_p \rangle \langle p m_p | = \hat{j}_p \overbrace{| p \rangle \langle \tilde{p} |}^{00} . \quad (4.68)$$

The simple proof is given in [148] but it is instructive to repeat it here. Using the identity

$$(-1)^{j_p-m_p} \hat{j}_p \begin{pmatrix} j_p & j_p & 0 \\ m_p & -m_p & 0 \end{pmatrix}_{\text{CG}} = 1 , \quad (4.69)$$

(4.67) is easily verified

$$\begin{aligned} & \sum_{m_p} \langle p m_p | \dots | p m_p \rangle \\ &= \hat{j}_p \sum_{m_p} (-1)^{j_p-m_p} \begin{pmatrix} j_p & j_p & 0 \\ m_p & -m_p & 0 \end{pmatrix}_{\text{CG}} \langle p m_p | \dots | p m_p \rangle \end{aligned} \quad (4.70)$$

$$= (-1)^{2j_p} \hat{j}_p \sum_{m_p} (-1)^{j_p-m_p} \begin{pmatrix} j_p & j_p & 0 \\ -m_p & m_p & 0 \end{pmatrix}_{\text{CG}} \langle p m_p | \dots | p m_p \rangle \quad (4.71)$$

$$= (-1)^{2j_p} \hat{j}_p \overbrace{\langle \tilde{p} | \dots | p \rangle}^{00} \quad (4.72)$$

and (4.68) follows similarly.

By coupling the internal lines, example (4.64) becomes

$$\langle \overset{JM}{\downarrow} a \overset{JM}{\downarrow} b \mid \hat{t}_2 \mid \overset{JM}{\downarrow} i \overset{JM}{\downarrow} j \rangle \xleftarrow{(DBc)} \frac{1}{2} \sum_{cd} \hat{j}_c \hat{j}_d \langle \overset{JM}{\downarrow} a \overset{JM}{\downarrow} b \mid \hat{v} \mid \overset{00}{\downarrow} c \overset{00}{\downarrow} d \rangle \langle \overset{JM}{\downarrow} \tilde{c} \overset{JM}{\downarrow} \tilde{d} \mid \hat{t}_2 \mid \overset{JM}{\downarrow} i \overset{JM}{\downarrow} j \rangle. \quad (4.73)$$

The projection summation has been eliminated in favor of coupling lines, but the above form still has the disadvantageous property of coupling lines connecting different matrix elements. However, these matrix elements can be disentangled by recoupling transformations of the internal lines for which an example is given in the below:

Matrix elements connected by scalar coupled internal lines of the form

$$\overset{00}{\downarrow} |pq\rangle \langle \tilde{p}\tilde{q}| \quad (4.74)$$

may be disentangled by the transformation

$$\hat{j}_p \hat{j}_p \overset{00}{\downarrow} |pq\rangle \langle \tilde{p}\tilde{q}| = \sum_{JM} \overset{JM}{\downarrow} |pq\rangle \langle \tilde{p}\tilde{q}|. \quad (4.75)$$

In order to prove this, the idea is to couple the two internal lines to good total angular momentum. Since both angular momenta involved are zero the result is trivial,

$$\hat{j}_p \hat{j}_q \overset{00}{\downarrow} |pq\rangle \langle \tilde{p}\tilde{q}| = \hat{j}_p \hat{j}_q \left\{ \overset{0}{\downarrow} |pq\rangle \langle \tilde{p}\tilde{q}| \right\}_0^{(0)}. \quad (4.76)$$

Having arrived at a fully coupled expression, the disentanglement of the matrix element is only a matter of one standard recoupling transformation of the angular momenta,

$$\hat{j}_p \hat{j}_q \left\{ \overset{0}{\downarrow} |pq\rangle \langle \tilde{p}\tilde{q}| \right\}_0^{(0)} = \hat{j}_p \hat{j}_q \sum_{JJ'} \underbrace{\begin{Bmatrix} j_p & j_p & 0 \\ j_q & j_q & 0 \\ J & J' & 0 \end{Bmatrix}}_{\hat{j}_p^{-1} \hat{j}_q^{-1} \hat{J} \delta_{JJ'}} \left\{ \overset{J}{\downarrow} |pq\rangle \langle \tilde{p}\tilde{q}| \right\}_0^{(0)} \quad (4.77)$$

$$= \sum_J \hat{J} \left\{ \overset{J}{\downarrow} |pq\rangle \langle \tilde{p}\tilde{q}| \right\}_0^{(0)}. \quad (4.78)$$

$$\begin{aligned}
 \hat{J}_p \hat{J}_q \begin{array}{c} \xrightarrow{00} \\ |pq\rangle \langle \tilde{p}\tilde{q}| \\ \xleftarrow{00} \end{array} &= \sum_{JM} \begin{array}{c} JM \\ \nwarrow \nearrow \\ |pq\rangle \langle \tilde{p}\tilde{q}| \end{array} \\
 \hat{J}_p \hat{J}_q \begin{array}{c} \xrightarrow{00} \\ \langle \tilde{p}\tilde{q} | \dots | pq \rangle \\ \xleftarrow{00} \end{array} &= \sum_{JM} \begin{array}{c} JM \\ \nwarrow \nearrow \\ \langle \tilde{p}\tilde{q} | \dots | pq \rangle \end{array} \\
 \hat{J}_p \hat{J}_q \begin{array}{c} \xrightarrow{00} \\ \langle \tilde{p} | \dots | q \rangle \langle \tilde{q} | \dots | p \rangle \\ \xleftarrow{00} \end{array} &= \sum_{JM} (-1)^{J-M} (-1)^{j_p+j_q-J} \begin{array}{c} JM \\ \nwarrow \nearrow \\ \langle \tilde{p} | \dots | q \rangle \langle \tilde{q} | \dots | p \rangle \end{array} \\
 \hat{J}_p \hat{J}_q \begin{array}{c} \xrightarrow{00} \\ \langle \tilde{p} | \dots | q \rangle \dots | p \rangle \dots \langle \tilde{q} | \\ \xleftarrow{00} \end{array} &= (-1)^{2j_q} \sum_{JM} (-1)^{J-M} (-1)^{j_r+j_s-J} \begin{array}{c} JM \\ \nwarrow \nearrow \\ \langle \tilde{p} | \dots | q \rangle \dots | p \rangle \dots \langle \tilde{q} | \end{array}
 \end{aligned}$$

Figure 4.4: Internal line recoupling transformations involving two scalar coupled lines.

Breaking up the scalar coupling leads to

$$\sum_J \hat{J} \left\{ \begin{array}{c} J \\ \nwarrow \nearrow \\ |pq\rangle \langle \tilde{p}\tilde{q}| \end{array} \right\}_0^{(0)} = \sum_J \hat{J} \sum_{MM'} \begin{pmatrix} J & J & 0 \\ M & M' & 0 \end{pmatrix}_{\text{CG}} \begin{array}{c} JM \\ \nwarrow \nearrow \\ |pq\rangle \langle \tilde{p}\tilde{q}| \end{array} \quad (4.79)$$

$$= \sum_{JM} (-1)^{J-M} \begin{array}{c} JM \\ \nwarrow \nearrow \\ |pq\rangle \langle \tilde{p}\tilde{q}| \end{array} \quad (4.80)$$

since $\begin{pmatrix} J & J & 0 \\ M & M' & 0 \end{pmatrix}_{\text{CG}} = (-1)^{J-M} \hat{J}^{-1} \delta_{M-M'}$. By means of (4.29) the final result is obtained,

$$\sum_{JM} (-1)^{J-M} \begin{array}{c} JM \\ \nwarrow \nearrow \\ |pq\rangle \langle \tilde{p}\tilde{q}| \end{array} = \sum_{JM} \begin{array}{c} JM \\ \nwarrow \nearrow \\ |pq\rangle \langle \tilde{p}\tilde{q}| \end{array}. \quad (4.81)$$

Internal line recouplings for other situations may be derived analogously. The most frequent cases are summarized in Figure 4.4. The example (4.64) can still be further simplified since the matrix elements involved do not depend on the

total projection quantum numbers and thus the corresponding summation may be replaced by a factor,

$$\langle \overbrace{a \ b}^{JM} | \hat{t}_2 | \overbrace{i \ j}^{JM} \rangle \xleftarrow{(DBc)} \frac{1}{2} \sum_{cd} \sum_J \hat{J}^2 \langle \overbrace{a \ b}^{JM_0} | \hat{v} | \overbrace{c \ d}^{JM_0} \rangle \langle \overbrace{c \ d}^{JM_0} | \hat{t}_2 | \overbrace{i \ j}^{JM_0} \rangle, \quad (4.82)$$

where M_0 is an arbitrary, physically allowed value for the projection. More complicated diagrams than example (4.64) require other transformations to disentangle individual matrix elements because non-scalar coupled internal lines may appear or the external lines need to be recoupled. The most convenient way to evaluate such diagrams is to choose recouplings of lines that involve at least one scalar coupled line since the transformations clearly become more simple with the number of scalar lines.

For a simple demonstration of such transformations, let $[p]$ denote either $|p\rangle$ or $\langle \tilde{p}|$. Matrix elements connected by one scalar and one non-scalar coupled internal lines may be disentangled by the transformation

$$\begin{aligned} \langle \overbrace{[p][q][r][s]}^{00} | \overbrace{\quad}^{JM} \rangle &= (-1)^{j_p+j_s} \hat{j}_p^{-1} \sum_{J'M'} \sum_{J''M''} (-1)^{J+J'} \hat{J}' \hat{J}'' \\ &\times \left\{ \begin{matrix} J & J' & J'' \\ j_r & j_s & j_q \end{matrix} \right\}_{6j} \left(\begin{matrix} J' & J'' & J \\ M' & M'' & M \end{matrix} \right)_{\text{CG}} \langle \overbrace{[p][q][r][s]}^{J'M' \ J''M''} \rangle \end{aligned} \quad (4.83)$$

To see this, coupling the expression to total angular momentum $\mathcal{J} \mathcal{M}$ is again trivial due to the zero angular momentum involved,

$$\langle \overbrace{[p][q][r][s]}^{00} | \overbrace{\quad}^{JM} \rangle = \sum_{\mathcal{J} \mathcal{M}} \left(\begin{matrix} 0 & J & \mathcal{J} \\ 0 & M & \mathcal{M} \end{matrix} \right)_{\text{CG}} \left\{ \overbrace{[p][q][r][s]}^0 \right\}_{\mathcal{M}}^{(\mathcal{J})} \quad (4.84)$$

$$= \left\{ \overbrace{[p][q][r][s]}^0 \right\}_M^{(J)}. \quad (4.85)$$

This can then be recoupled using X coefficients and the total coupling may again

be broken up, arriving at

$$\begin{array}{c} \xrightarrow{00} \\ [p][q][r][s] \\ \xleftarrow{JM} \end{array} = \sum_{J'J''} \begin{Bmatrix} j_p & j_q & J' \\ j_r & j_s & J'' \\ 0 & J & J \end{Bmatrix}_X \left\{ [p][q][r][s] \right\}_M^{(J)} \quad (4.86)$$

$$= \sum_{J'M'} \sum_{J''M''} \begin{pmatrix} J' & J'' & J \\ M' & M'' & M \end{pmatrix}_{\text{CG}} \begin{Bmatrix} j_p & j_q & J' \\ j_r & j_s & J'' \\ 0 & J & J \end{Bmatrix}_X \left\{ [p][q][r][s] \right\}^{J'M' J''M''}. \quad (4.87)$$

Finally, from the simplification of X coefficients involving one zero angular momentum,

$$\begin{Bmatrix} j_p & j_q & J' \\ j_r & j_s & J'' \\ 0 & J & J \end{Bmatrix}_X = (-1)^{j_p+j_s} \hat{j}_p^{-1} (-1)^{J+J'} \hat{J}' \hat{J}'' \begin{Bmatrix} J & J' & J'' \\ j_r & j_s & j_q \end{Bmatrix}_{6j}, \quad (4.88)$$

Eq. (4.83) follows immediately.

Again, other transformations of this kind are equally easy to derive and the most commonly encountered ones are summarized in Figure 4.5 for reference. These rules simplify significantly if for the final coupling of two states only the scalar coupling is allowed, for instance if these states belong to the bra and ket states of a scalar one-body operator, as discussed in Section 4.4. The transformation rules for the case in which states $[r]$ and $[s]$ are allowed to scalar coupling only is given in the bracketed expressions in Figure 4.5.

4.6.1 Antisymmetrized Diagram Coupling

As for the CCSD \hat{T}_2 m -scheme equations, some expressions are antisymmetrized by the action of permutation operators, such as

$$\begin{aligned} \langle \bar{p}\bar{q}|\hat{g}|\bar{r}\bar{s} \rangle &= \hat{P}_{\bar{p}\bar{q}} \hat{P}_{\bar{r}\bar{s}} (\bar{p}\bar{q}|\hat{g}|\bar{r}\bar{s}) \\ &= (\hat{1} - \hat{T}_{\bar{p}\bar{q}}) (\hat{1} - \hat{T}_{\bar{r}\bar{s}}) (\bar{p}\bar{q}|\hat{g}|\bar{r}\bar{s}), \end{aligned} \quad (4.89)$$

where $\langle \bar{p}\bar{q}|\hat{g}|\bar{r}\bar{s} \rangle$ denotes the antisymmetrized expression obtained from the action of the permutation operators on some non-antisymmetric expression $(\bar{p}\bar{q}|\hat{g}|\bar{r}\bar{s})$. For instance, for the (DBe) contribution to the CCSD \hat{T}_2 amplitudes,

$$\langle \bar{a}\bar{b}|\hat{t}_2|\bar{i}\bar{j} \rangle \stackrel{(DBe)}{\leftarrow} \hat{P}_{\bar{a}\bar{b}} \hat{P}_{\bar{i}\bar{j}} \sum_{\bar{c}\bar{k}} \langle \bar{k}\bar{b}|\hat{v}|\bar{c}\bar{j} \rangle t_{\bar{i}\bar{k}}^{\bar{a}\bar{c}}, \quad (4.90)$$

$$\begin{aligned}
\begin{array}{c} \xrightarrow{00} \\ [p][q][r][s] \\ \xleftarrow{JM} \end{array} &= (-1)^{j_p+j_s} \hat{j}_p^{-1} \sum_{J'M'} \sum_{J''M''} (-1)^{J+J'} \hat{j}' \hat{j}'' \\
&\quad \times \left\{ \begin{array}{ccc} J & J' & J'' \\ j_r & j_s & j_q \end{array} \right\}_{6j} \left(\begin{array}{ccc} J' & J'' & J \\ M' & M'' & M \end{array} \right)_{\text{CG}} \begin{array}{c} \xrightarrow{J'M'} \quad \xrightarrow{J''M''} \\ [p][q][r][s] \end{array} \\
&\quad \left(= -\hat{j}_p^{-1} \hat{j}_s^{-1} (-1)^{j_p+j_q-J} \begin{array}{c} \xrightarrow{JM} \quad \xrightarrow{00} \\ [p][q][r][s] \end{array} \right) \\
\begin{array}{c} \xrightarrow{00} \\ [p][q][r][s] \\ \xleftarrow{JM} \end{array} &= \hat{j}_p^{-1} \sum_{J'M'} \sum_{J''M''} (-1)^{J+J'+J''} \hat{j}' \hat{j}'' \\
&\quad \times \left\{ \begin{array}{ccc} J & J' & J'' \\ j_s & j_r & j_q \end{array} \right\}_{6j} \left(\begin{array}{ccc} J' & J'' & J \\ M' & M'' & M \end{array} \right)_{\text{CG}} \begin{array}{c} \xrightarrow{J'M'} \quad \xrightarrow{J''M''} \\ [p][q][r][s] \end{array} \\
&\quad \left(= \hat{j}_p^{-1} \hat{j}_r^{-1} (-1)^{j_q+j_r-J} \begin{array}{c} \xrightarrow{JM} \quad \xrightarrow{00} \\ [p][q][r][s] \end{array} \right) \\
\begin{array}{c} \xrightarrow{00} \\ [p][q][r][s] \\ \xleftarrow{JM} \end{array} &= \hat{j}_q^{-1} (-1)^{j_p+j_q+j_r+j_s} \sum_{J'M'} \sum_{J''M''} (-1)^J \hat{j}' \hat{j}'' \\
&\quad \times \left\{ \begin{array}{ccc} J & J' & J'' \\ j_r & j_s & j_p \end{array} \right\}_{6j} \left(\begin{array}{ccc} J' & J'' & J \\ M' & M'' & M \end{array} \right)_{\text{CG}} \begin{array}{c} \xrightarrow{J'M'} \quad \xrightarrow{J''M''} \\ [p][q][r][s] \end{array} \\
&\quad \left(= -\hat{j}_q^{-1} \hat{j}_s^{-1} \begin{array}{c} \xrightarrow{JM} \quad \xrightarrow{00} \\ [p][q][r][s] \end{array} \right) \\
\begin{array}{c} \xrightarrow{00} \\ [p][q][r][s] \\ \xleftarrow{JM} \end{array} &= \hat{j}_q^{-1} (-1)^{j_p+j_q} \sum_{J'M'} \sum_{J''M''} (-1)^{J+J''} \hat{j}' \hat{j}'' \\
&\quad \times \left\{ \begin{array}{ccc} J & J' & J'' \\ j_s & j_r & j_p \end{array} \right\}_{6j} \left(\begin{array}{ccc} J' & J'' & J \\ M' & M'' & M \end{array} \right)_{\text{CG}} \begin{array}{c} \xrightarrow{J'M'} \quad \xrightarrow{J''M''} \\ [p][q][r][s] \end{array} \\
&\quad \left(= \hat{j}_q^{-1} \hat{j}_r^{-1} \begin{array}{c} \xrightarrow{JM} \quad \xrightarrow{00} \\ [p][q][r][s] \end{array} \right)
\end{aligned}$$

Figure 4.5: Internal line recoupling transformations for one scalar and one non-scalar coupling lines. The expressions in brackets correspond to the case in which only a scalar coupling of $[r]$ and $[s]$ is allowed.

the non-antisymmetric part would be

$$(\bar{a}\bar{b}|\hat{t}_2|\bar{i}\bar{j}) = \sum_{\bar{c}\bar{k}} \langle \bar{k}\bar{b}|\hat{v}|\bar{c}\bar{j} \rangle t_{\bar{i}\bar{k}}^{\bar{a}\bar{c}}. \quad (4.91)$$

In practice, the expression $(\bar{p}\bar{q}|\hat{g}|\bar{r}\bar{s})$ is calculated for the whole index range, which allows to access elements with swapped indices, $(\bar{q}\bar{p}|\hat{g}|\bar{r}\bar{s})$, for instance. The antisymmetrized expression is then simply obtained by

$$(\bar{p}\bar{q}|\hat{g}|\bar{r}\bar{s}) = (\bar{p}\bar{q}|\hat{g}|\bar{r}\bar{s}) - (\bar{q}\bar{p}|\hat{g}|\bar{r}\bar{s}) - (\bar{p}\bar{q}|\hat{g}|\bar{s}\bar{r}) + (\bar{q}\bar{p}|\hat{g}|\bar{s}\bar{r}). \quad (4.92)$$

For the spherical case, an antisymmetrized coupled diagram is obtained by coupling the antisymmetrized m -scheme expressions,

$$\begin{aligned} & \overset{J_{pq}M_{pq}}{\overbrace{\langle p\ q | \hat{g} | r\ s \rangle}} \overset{J_{rs}M_{rs}}{\overbrace{\langle r\ s | \hat{g} | p\ q \rangle}} \\ &= \sum_{\substack{m_p m_q \\ m_r m_s}} \begin{pmatrix} j_p & j_q & J_{pq} \\ m_p & m_q & M_{pq} \end{pmatrix}_{\text{CG}} \begin{pmatrix} j_r & j_s & J_{rs} \\ m_r & m_s & M_{rs} \end{pmatrix}_{\text{CG}} \langle \bar{p}\bar{q}|\hat{g}|\bar{r}\bar{s} \rangle \end{aligned} \quad (4.93)$$

Formally, the evaluation requires the coupling of each individual index permutation of the m -scheme expression,

$$\begin{aligned} & \overset{J_{pq}M_{pq}}{\overbrace{\langle p\ q | \hat{g} | r\ s \rangle}} \overset{J_{rs}M_{rs}}{\overbrace{\langle r\ s | \hat{g} | p\ q \rangle}} \\ &= \sum_{\substack{m_p m_q \\ m_r m_s}} \begin{pmatrix} j_p & j_q & J_{pq} \\ m_p & m_q & M_{pq} \end{pmatrix}_{\text{CG}} \begin{pmatrix} j_r & j_s & J_{rs} \\ m_r & m_s & M_{rs} \end{pmatrix}_{\text{CG}} \\ & \quad \times \left((\bar{p}\bar{q}|\hat{g}|\bar{r}\bar{s}) - (\bar{q}\bar{p}|\hat{g}|\bar{r}\bar{s}) - (\bar{p}\bar{q}|\hat{g}|\bar{s}\bar{r}) + (\bar{q}\bar{p}|\hat{g}|\bar{s}\bar{r}) \right) \end{aligned} \quad (4.94)$$

$$\begin{aligned} &= \overset{J_{pq}M_{pq}}{\overbrace{\langle p\ q | \hat{g} | r\ s \rangle}} \overset{J_{rs}M_{rs}}{\overbrace{\langle r\ s | \hat{g} | p\ q \rangle}} - \overset{J_{pq}M_{pq}}{\overbrace{\langle q\ p | \hat{g} | r\ s \rangle}} \overset{J_{rs}M_{rs}}{\overbrace{\langle r\ s | \hat{g} | p\ q \rangle}} - \overset{J_{pq}M_{pq}}{\overbrace{\langle p\ q | \hat{g} | s\ r \rangle}} \overset{J_{rs}M_{rs}}{\overbrace{\langle r\ s | \hat{g} | p\ q \rangle}} \\ & \quad - \overset{J_{pq}M_{pq}}{\overbrace{\langle q\ p | \hat{g} | s\ r \rangle}} \overset{J_{rs}M_{rs}}{\overbrace{\langle r\ s | \hat{g} | p\ q \rangle}}. \end{aligned} \quad (4.95)$$

Reversing the couplings that go from the right to the left introduces phases,

$$\begin{aligned}
& \langle \overset{J_{pq}M_{pq}}{\downarrow} \overset{J_{rs}M_{rs}}{\downarrow} \bar{p} \bar{q} | \hat{g} | r s \rangle \\
&= \langle \overset{J_{pq}M_{pq}}{\downarrow} \overset{J_{rs}M_{rs}}{\downarrow} \bar{p} \bar{q} | \hat{g} | r s \rangle - (-1)^{j_p+j_q-J_{pq}} \langle \overset{J_{pq}M_{pq}}{\downarrow} \overset{J_{rs}M_{rs}}{\downarrow} \bar{q} \bar{p} | \hat{g} | r s \rangle \\
&\quad - (-1)^{j_r+j_s-J_{rs}} \langle \overset{J_{pq}M_{pq}}{\downarrow} \overset{J_{rs}M_{rs}}{\downarrow} \bar{p} \bar{q} | \hat{g} | s r \rangle \\
&\quad + (-1)^{j_p+j_q-J_{pq}} (-1)^{j_r+j_s-J_{rs}} \langle \overset{J_{pq}M_{pq}}{\downarrow} \overset{J_{rs}M_{rs}}{\downarrow} \bar{q} \bar{p} | \hat{g} | s r \rangle.
\end{aligned} \tag{4.96}$$

This result suggests the definition of a permutation operator

$$\hat{P}_{pq}(J_{pq}) \equiv \hat{1} - (-1)^{j_p+j_q-J_{pq}} \hat{T}_{pq} \tag{4.97}$$

so that the antisymmetrized coupled expression can be written as

$$\langle \overset{J_{pq}M_{pq}}{\downarrow} \overset{J_{rs}M_{rs}}{\downarrow} \bar{p} \bar{q} | \hat{g} | r s \rangle = \hat{P}_{pq}(J_{pq}) \hat{P}_{rs}(J_{rs}) \langle \overset{J_{pq}M_{pq}}{\downarrow} \overset{J_{rs}M_{rs}}{\downarrow} \bar{p} \bar{q} | \hat{g} | r s \rangle. \tag{4.98}$$

In the m -scheme, if an expression $\langle \bar{p}\bar{q} | \hat{g} | \bar{r}\bar{s} \rangle$ is already antisymmetric in the orbital pair $\bar{p}\bar{q}$, an additional antisymmetrizer $\hat{P}_{\bar{p}\bar{q}}$ corresponds to a factor of 2, e.g.,

$$\langle \bar{p}\bar{q} | \hat{g} | \bar{r}\bar{s} \rangle = \frac{1}{2} \hat{P}_{\bar{p}\bar{q}} \langle \bar{p}\bar{q} | \hat{g} | \bar{r}\bar{s} \rangle, \tag{4.99}$$

which is sometimes used to write the equations in a more symmetric form. The same holds for the spherical case for the operators $\hat{P}_{pq}(J_{pq})$, i.e., for an expression that is already antisymmetric in the sense that

$$\hat{T}_{pq} \langle \overset{J_{pq}M_{pq}}{\downarrow} \overset{J_{rs}M_{rs}}{\downarrow} \bar{p} \bar{q} | \hat{g} | r s \rangle = - (-1)^{j_p+j_q-J_{pq}} \langle \overset{J_{pq}M_{pq}}{\downarrow} \overset{J_{rs}M_{rs}}{\downarrow} \bar{p} \bar{q} | \hat{g} | r s \rangle, \tag{4.100}$$

an additional antisymmetrization operator may introduced by

$$\langle \overset{J_{pq}M_{pq}}{\downarrow} \overset{J_{rs}M_{rs}}{\downarrow} \bar{p} \bar{q} | \hat{g} | r s \rangle = \frac{1}{2} \hat{P}_{pq}(J_{pq}) \langle \overset{J_{pq}M_{pq}}{\downarrow} \overset{J_{rs}M_{rs}}{\downarrow} \bar{p} \bar{q} | \hat{g} | r s \rangle. \tag{4.101}$$

The above results, that for the spherical case an original m -scheme permutation operator $\hat{P}_{\bar{p}\bar{q}}$ can simply be replaced by the operator $\hat{P}_{pq}(J_{pq})$, only holds if the states that are permuted also are the states that are coupled together to angular momentum J_{pq} . This is typically the case for diagrams that are evaluated in

the standard coupling scheme, but not if a diagram is first evaluated in the cross-coupled scheme and then transformed to standard coupling. In the latter case, for a component $\hat{\mathcal{K}}_M^{(J)}$ of a spherical tensor operator, the transformation that generates an *antisymmetrized standard coupled reduced matrix element* from a *non-antisymmetric cross-coupled A expression* is given by

$$\begin{aligned}
 & \overset{J_{pq}}{\downarrow} \langle \tilde{p} \tilde{q} | | \hat{\mathcal{K}}^{(J)} | | r s \rangle \overset{J_{rs}}{\downarrow} \\
 &= \sum_{J_{pr} J_{qs}} \left\{ \begin{Bmatrix} j_p & j_q & J_{pq} \\ j_r & j_s & J_{rs} \\ J_{pr} & J_{qs} & J \end{Bmatrix}_X - (-1)^{j_r+j_s-J_{rs}} \begin{Bmatrix} j_p & j_q & J_{pq} \\ j_s & j_r & J_{rs} \\ J_{ps} & J_{qr} & J \end{Bmatrix}_X \right\} \hat{T}_{rs} \\
 &+ (-1)^{j_p+j_q-J_{pq}} (-1)^{j_r+j_s-J_{rs}} \begin{Bmatrix} j_q & j_p & J_{pq} \\ j_s & j_r & J_{rs} \\ J_{qs} & J_{pr} & J \end{Bmatrix}_X \hat{T}_{pq} \hat{T}_{rs} \\
 &- (-1)^{j_p+j_q-J_{pq}} \begin{Bmatrix} j_q & j_p & J_{pq} \\ j_r & j_s & J_{rs} \\ J_{qr} & J_{ps} & J \end{Bmatrix}_X \hat{T}_{pq} \left\{ (\tilde{p} \tilde{q} | | \hat{\mathcal{K}}^{(J)} | | r s) \right\} \\
 &\equiv \text{CCAtStd}^{(A)} \left[\begin{matrix} p q J_{pq}; J_{pr} \\ r s J_{rs}; J_{qs} \end{matrix} \right] \left(\tilde{p} \tilde{q} | | \hat{\mathcal{K}}^{(J)} | | r s \right). \quad (4.102)
 \end{aligned}$$

Since this transformation depends on the rank of the spherical tensor operator, simplifications are possible for the case of scalar tensor operators. For these, the transformation for the standard matrix elements reads ⁴

$$\begin{aligned}
 & \overset{JM}{\downarrow} \langle \tilde{p} \tilde{q} | | \hat{\mathcal{K}}_0^{(0)} | | r s \rangle \overset{JM}{\downarrow} \\
 &= \left\{ \sum_{J'} (\hat{J}')^2 (-1)^{j_q+j_r+J+J'} \begin{Bmatrix} j_p & j_r & J' \\ j_s & j_q & J \end{Bmatrix}_{6j} \left(\hat{1} + \hat{T}_{pq} \hat{T}_{rs} \right) \right. \\
 &+ \left. \sum_{J'} (\hat{J}')^2 (-1)^{j_q+j_r+J'} \begin{Bmatrix} j_p & j_s & J' \\ j_r & j_q & J \end{Bmatrix}_{6j} \left(\hat{T}_{pq} + \hat{T}_{rs} \right) \right\} (\tilde{p} \tilde{q} | | \hat{\mathcal{K}}_0^{(0)} | | r s) \quad (4.103)
 \end{aligned}$$

⁴For half-integer values of j_p, j_q, j_r, j_s .

for which the shorthand notation

$$\langle \overset{JM}{\downarrow} p q | \hat{\mathfrak{K}}_0^{(0)} | \overset{JM}{\downarrow} r s \rangle = \text{CCAtoStd}^{(A)} \left[\begin{matrix} p q \\ r s \end{matrix} ; J; J' \right] \langle \overset{J'M'_0}{\downarrow} \tilde{p} \tilde{q} | \hat{\mathfrak{K}}_0^{(0)} | \overset{J'M'_0}{\uparrow} r s \rangle \quad (4.104)$$

is used. For the scalar case, this transformation may easily be written in terms of the non-antisymmetric cross-coupling transformations as

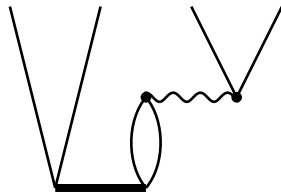
$$\begin{aligned} \text{CCAtoStd}^{(A)} \left[\begin{matrix} p q \\ r s \end{matrix} ; J; J' \right] &= \text{CCAtoStd} \left[\begin{matrix} p q \\ r s \end{matrix} ; J; J' \right] \left(\hat{1} + \hat{T}_{pq} \hat{T}_{rs} \right) \\ &\quad - \text{CCBtoStd} \left[\begin{matrix} p q \\ r s \end{matrix} ; J; J' \right] \left(\hat{T}_{pq} + \hat{T}_{rs} \right). \end{aligned} \quad (4.105)$$

For partial antisymmetrizations in which, e.g., only orbitals p and q are to be antisymmetrized, the corresponding transformation may be obtained from (4.102) or (4.103) simply by setting the other permutation operator \hat{T}_{rs} to 0.

4.6.2 Cross-Coupled Evaluation

As mentioned in the previous chapter, it is sometimes advantageous to evaluate a diagram in the cross-coupled scheme first, before transforming it to the standard coupling. This is because in order to obtain a cross-coupled matrix element less internal and external recouplings may be required than for the standard coupling and, thus, less summations over intermediate angular momenta and coupling coefficients may be required.

For instance, the $(\mathfrak{R}_2\text{G})$ contribution


(4.106)

to the EOM-CCSD $\hat{\mathfrak{R}}_2$ amplitudes, when directly evaluated in standard coupled evaluation, is given by

$$\begin{aligned}
 & \langle \overset{J_{ab}}{\downarrow} ab || \overset{J_{ij}}{\downarrow} \hat{\mathfrak{R}}_2^{(J)} || ij \rangle \xleftarrow{(\mathfrak{R}_2\mathbb{G})} (-1)^{J_{ab}-M_{ab}} \left(\begin{array}{ccc} J_{ab} & J & J_{ij} \\ -M_{ab} & M & M_{ij} \end{array} \right)_{3j}^{-1} \hat{P}_{ab}(J_{ab}) \hat{P}_{ij}(J_{ij}) \\
 & \times (-1)^{j_i+j_j-J_{ij}} \sum_{ck} \sum_{JJ'J''} \left\{ \begin{array}{ccc} J' & J'' & J_{ab} \\ j_b & j_a & j_c \end{array} \right\}_{6j} \left\{ \begin{array}{ccc} J'' & J''' & J_{ij} \\ j_i & j_j & j_k \end{array} \right\}_{6j} \hat{J}' (\hat{J}'')^2 \hat{J}''' \\
 & \times \sum_{M'M''} (-1)^{J'+M'} \left(\begin{array}{ccc} J' & J'' & J_{ab} \\ M' & -M'' & -M_{ab} \end{array} \right)_{CG} \left(\begin{array}{ccc} J''' & J'' & J_{ij} \\ -M' & M'' & M_{ab} \end{array} \right)_{CG} \\
 & \times \left(\begin{array}{ccc} J' & J & J''' \\ M' & M & -M' \end{array} \right)_{3j} \langle \overset{J'}{\downarrow} ca || \overset{J}{\downarrow} \hat{\mathfrak{R}}_2^{(J)} || ik \rangle \langle \overset{J''}{\downarrow} \tilde{b} \tilde{k} | \overset{J''M''}{\downarrow} \hat{\mathcal{H}}_2 | cj \rangle, \quad (4.107)
 \end{aligned}$$

where the triple sum over angular momenta and the product of two coupling coefficients cannot be factorized in any way. This is the result of the many recouplings that are required in order to disentangle the two matrix elements.

On the other hand, if the m -scheme expression is first transferred into cross-coupled form A, that requires the couplings

$$\begin{array}{c} \begin{array}{ccc} J_{ai} & & J_{bj} \\ \downarrow & & \downarrow \\ \tilde{a} & i & \tilde{b} \\ & \downarrow & \downarrow \\ & j & \end{array} \end{array} = \langle \tilde{a} \tilde{b} || \overset{J}{\downarrow} \hat{\mathfrak{R}}_2^{(J)} || ij \rangle,$$

then it becomes apparent that in this case the $(\tilde{a}i)$ and $(\tilde{b}j)$ coupling lines already belong to distinct matrix elements, requiring recoupling transformations for the c and k internal lines only. Therefore, the resulting expression for the standard coupled reduced matrix element is *much simpler*,

$$\begin{aligned}
 & \langle \overset{J_{ab}}{\downarrow} ab || \overset{J_{ij}}{\downarrow} \hat{\mathfrak{R}}_2^{(J)} || ij \rangle \xleftarrow{(\mathfrak{R}_2\mathbb{G})} \text{CCAtoStd}^{(A)} \left[\begin{array}{c} ab J_{ab}; J_{ai} \\ ij J_{ij}; J_{bj} \end{array} \right] \\
 & \times \sum_{ck} (-1)^{j_c+j_k-J_{bj}} \langle \overset{J_{ai}}{\downarrow} \tilde{a} \tilde{c} || \overset{J}{\downarrow} \hat{\mathfrak{R}}_2^{(J)} || ik \rangle \langle \overset{J_{bj}M_{bj}}{\downarrow} \tilde{b} \tilde{k} | \overset{J_{bj}M_{bj}}{\downarrow} \hat{\mathcal{H}}_2 | cj \rangle, \quad (4.108)
 \end{aligned}$$

and it is more efficient because the only sums over total angular momenta are the ones in the transformation from the cross-coupled to the standard coupling scheme. Furthermore, the problem factorizes into first evaluating the expression in cross-coupled form, which cost is basically determined by \sum_{ck} and the transformation to standard coupling *afterwards*. Another inconvenience of the form (4.107) is that it can not longer solely be evaluated using optimized matrix multiplication routines, which is due to the appearance of orbital indices in both matrix elements and coupling coefficients.

4.7 Spherical CCSD

Using the techniques described in previous sections, the spherical Coupled-Cluster equations are easily obtained. For CCSD, the m -scheme amplitude equations are of the form

$$0 = \bar{a} \begin{array}{c} \diagup \diagdown \\ \diagdown \diagup \\ \text{---} \end{array} \bar{i} + \dots, \quad \forall \bar{a}, \bar{i} \quad (4.109)$$

$$0 = \bar{a} \begin{array}{c} \diagup \diagdown \\ \diagdown \diagup \\ \text{---} \end{array} \bar{i} \bar{b} \begin{array}{c} \diagup \diagdown \\ \diagdown \diagup \\ \text{---} \end{array} \bar{j} + \dots, \quad \forall \bar{a}, \bar{b}, \bar{i}, \bar{j}. \quad (4.110)$$

Therefore, coupling both sides of these equations by taking linear combinations of m -scheme expressions, the coupled formulation follows immediately,

$$0 = a \begin{array}{c} \overbrace{\diagup \diagdown}^{00} \\ \diagdown \diagup \\ \text{---} \end{array} i + \dots, \quad \forall a, i \quad (4.111)$$

$$0 = a \begin{array}{c} \overbrace{\diagup \diagdown}^{JM} \\ \diagdown \diagup \\ \text{---} \end{array} i b \begin{array}{c} \overbrace{\diagup \diagdown}^{JM} \\ \diagdown \diagup \\ \text{---} \end{array} j + \dots, \quad \forall a, b, i, j, J, M, \quad (4.112)$$

where the right hand side diagrams have to be evaluated according to diagram coupling techniques. In (4.111) and (4.112), the scalar character of the cluster operator \hat{T} has already been taken into account by constraining the coupling of external lines to total angular momenta and projection to 00 for the \hat{T}_1 matrix elements and JM for bra and ket coupling in the \hat{T}_2 matrix elements. The energy expression

$$E = \begin{array}{c} \diagup \diagdown \\ \diagdown \diagup \\ \text{---} \end{array} + \begin{array}{c} \diagup \diagdown \\ \diagdown \diagup \\ \text{---} \end{array} + \begin{array}{c} \diagup \diagdown \\ \diagdown \diagup \\ \text{---} \end{array}$$

consists of closed diagrams only, and is, therefore, not subjected to external line coupling, but the internal lines will have to be coupled in order to get an expression in terms of coupled matrix elements only. The result for the spherical energy expression is

$$\begin{aligned}
 \Delta E^{(\text{CCSD})} = & \stackrel{(EA)}{+} \frac{1}{4} \sum_{cdkl} \sum_J \hat{J}^2 \overset{JM}{\overleftarrow{\downarrow}} \langle cd|\hat{t}_2|kl\rangle \overset{JM}{\overleftarrow{\downarrow}} \langle kl|\hat{v}|cd\rangle \\
 & + \sum_{ck} \overset{00}{\overleftarrow{\downarrow}} \langle \tilde{c}|\hat{t}_1|k\rangle \overset{00}{\overleftarrow{\downarrow}} \langle \tilde{k}|\hat{f}|c\rangle \\
 & + \stackrel{(EC)}{\frac{1}{2}} \sum_{cdkl} \hat{J}_c^{-1} \hat{J}_d^{-1} \sum_J \hat{J}^2 \overset{00}{\overleftarrow{\downarrow}} \langle \tilde{c}|\hat{t}_1|k\rangle \overset{00}{\overleftarrow{\downarrow}} \langle \tilde{d}|\hat{t}_1|l\rangle \overset{JM}{\overleftarrow{\downarrow}} \langle kl|\hat{v}|cd\rangle, \quad (4.113)
 \end{aligned}$$

and the spherical CCSD \hat{T}_1 and \hat{T}_2 amplitude equations are listed in Appendix C.2.

The matrix elements of the normal-ordered Hamiltonian (2.10) should also be expressed in terms of coupled matrix elements. Using the identity

$$\hat{J}_p \hat{J}_q \overset{00}{\overleftarrow{\downarrow}} \langle \tilde{p}\tilde{q}|\hat{v}|pq\rangle = \hat{J}_p \hat{J}_q \overset{00}{\overleftarrow{\downarrow}} \langle \tilde{p}\tilde{q}|\hat{v}|pq\rangle = \sum_J \hat{J}^2 \overset{JM}{\overleftarrow{\downarrow}} \langle \tilde{p}\tilde{q}|\hat{v}|pq\rangle, \quad (4.114)$$

the corresponding expressions are straightforwardly found to be

$$\langle \Phi|\hat{H}|\Phi\rangle = h_0 - \sum_i \hat{J}_i \overset{00}{\overleftarrow{\downarrow}} \langle \tilde{i}|\hat{h}_1|i\rangle + \frac{1}{2} \sum_{ij} \sum_J \hat{J}^2 \overset{JM}{\overleftarrow{\downarrow}} \langle \tilde{i}\tilde{j}|\hat{v}|ij\rangle \quad (4.115)$$

$$\overset{00}{\overleftarrow{\downarrow}} \langle \tilde{p}|\hat{f}|q\rangle = \overset{00}{\overleftarrow{\downarrow}} \langle \tilde{p}|\hat{h}_1|q\rangle - \hat{J}_p^{-1} \sum_i \sum_J \hat{J}^2 \overset{JM}{\overleftarrow{\downarrow}} \langle \tilde{p}\tilde{i}|\hat{v}|qi\rangle. \quad (4.116)$$

The spherical CCSD equations be written as

$$\langle \Phi|\hat{\mathcal{H}}^{(\text{CCSD})}|\Phi\rangle = \Delta E^{(\text{CCSD})} \quad (4.117)$$

$$\overset{00}{\overleftarrow{\downarrow}} \langle \tilde{a}|\hat{\mathcal{H}}^{(\text{CCSD})}|i\rangle = 0, \quad \forall a, i \quad (4.118)$$

$$\overset{JM}{\overleftarrow{\downarrow}} \langle \tilde{a}\tilde{b}|\hat{\mathcal{H}}^{(\text{CCSD})}|ij\rangle = 0, \quad \forall a, b, i, J, M. \quad (4.119)$$

Using this notation, the spherical analogue to the standard iterative scheme (2.45) for the self-consistent solution of the CCSD equations reads

$$\left\{ \begin{array}{l} \begin{array}{c} \overbrace{\langle \tilde{a} | \hat{t}_1 | i \rangle}^{00} \\ \downarrow \\ {}^{(0)}\langle \tilde{a} | \hat{t}_1 | i \rangle \end{array} = \begin{array}{c} \begin{array}{cc} \overbrace{\langle ab | \hat{t}_2 | ij \rangle}^{JM} & \overbrace{\langle ab | \hat{t}_2 | ij \rangle}^{JM} \\ \downarrow & \downarrow \end{array} \\ {}^{(0)}\langle ab | \hat{t}_2 | ij \rangle = 0 \end{array} \\ \\ \begin{array}{c} \overbrace{\langle \tilde{a} | \hat{t}_1 | i \rangle}^{00} \\ \downarrow \\ {}^{(n+1)}\langle \tilde{a} | \hat{t}_1 | i \rangle \end{array} = \begin{array}{c} \overbrace{\langle \tilde{a} | \hat{\mathcal{H}}^{(\text{CCSD})}(\mathbf{t}^{(n)}) | i \rangle}^{00} \\ \downarrow \\ \langle \tilde{a} | \hat{\mathcal{H}}^{(\text{CCSD})}(\mathbf{t}^{(n)}) | i \rangle \end{array} \left(\begin{array}{c} \overbrace{\langle \tilde{a} | \hat{f} | a \rangle}^{00} \\ \downarrow \\ \langle \tilde{a} | \hat{f} | a \rangle \end{array} - \begin{array}{c} \overbrace{\langle \tilde{i} | \hat{f} | i \rangle}^{00} \\ \downarrow \\ \langle \tilde{i} | \hat{f} | i \rangle \end{array} \right)^{-1} \\ \\ \begin{array}{c} \begin{array}{cc} \overbrace{\langle ab | \hat{t}_2 | ij \rangle}^{JM} & \overbrace{\langle ab | \hat{t}_2 | ij \rangle}^{JM} \\ \downarrow & \downarrow \end{array} \\ {}^{(n+1)}\langle ab | \hat{t}_2 | ij \rangle \end{array} = \begin{array}{c} \begin{array}{cc} \overbrace{\langle ab | \hat{\mathcal{H}}^{(\text{CCSD})}(\mathbf{t}^{(n)}) | ij \rangle}^{JM} & \overbrace{\langle ab | \hat{\mathcal{H}}^{(\text{CCSD})}(\mathbf{t}^{(n)}) | ij \rangle}^{JM} \\ \downarrow & \downarrow \end{array} \\ \langle ab | \hat{\mathcal{H}}^{(\text{CCSD})}(\mathbf{t}^{(n)}) | ij \rangle \end{array} \\ \\ \times \left(\begin{array}{c} \overbrace{\langle \tilde{a} | \hat{f} | a \rangle}^{00} \\ \downarrow \\ \langle \tilde{a} | \hat{f} | a \rangle \end{array} + \begin{array}{c} \overbrace{\langle \tilde{b} | \hat{f} | b \rangle}^{00} \\ \downarrow \\ \langle \tilde{b} | \hat{f} | b \rangle \end{array} - \begin{array}{c} \overbrace{\langle \tilde{i} | \hat{f} | i \rangle}^{00} \\ \downarrow \\ \langle \tilde{i} | \hat{f} | i \rangle \end{array} - \begin{array}{c} \overbrace{\langle \tilde{j} | \hat{f} | j \rangle}^{00} \\ \downarrow \\ \langle \tilde{j} | \hat{f} | j \rangle \end{array} \right)^{-1} \end{array} \right. \quad (4.120)$$

where, as in the m -scheme case, $\hat{F}_N \rightarrow \hat{F}_N^o$ is set in the amplitude equations. The $n = 1$ amplitudes are then easily obtained from the relations

$$\begin{array}{c} \overbrace{\langle \tilde{a} | \hat{\mathcal{H}}^{(\text{CCSD})}(\mathbf{t}^{(0)}) | i \rangle}^{00} \\ \downarrow \\ \langle \tilde{a} | \hat{\mathcal{H}}^{(\text{CCSD})}(\mathbf{t}^{(0)}) | i \rangle \end{array} = \begin{array}{c} \overbrace{\langle \tilde{a} | \hat{f} | i \rangle}^{00} \\ \downarrow \\ \langle \tilde{a} | \hat{f} | i \rangle \end{array} \quad (4.121)$$

$$\begin{array}{c} \begin{array}{cc} \overbrace{\langle ab | \hat{\mathcal{H}}^{(\text{CCSD})}(\mathbf{t}^{(0)}) | ij \rangle}^{JM} & \overbrace{\langle ab | \hat{\mathcal{H}}^{(\text{CCSD})}(\mathbf{t}^{(0)}) | ij \rangle}^{JM} \\ \downarrow & \downarrow \end{array} \\ \langle ab | \hat{\mathcal{H}}^{(\text{CCSD})}(\mathbf{t}^{(0)}) | ij \rangle \end{array} = \begin{array}{c} \begin{array}{cc} \overbrace{\langle ab | \hat{v} | ij \rangle}^{JM} & \overbrace{\langle ab | \hat{v} | ij \rangle}^{JM} \\ \downarrow & \downarrow \end{array} \\ \langle ab | \hat{v} | ij \rangle \end{array}. \quad (4.122)$$

4.8 Convergence Acceleration

In practical applications the iteration schemes (2.45) or (4.120) for solving the CCSD amplitude equations or the analogous scheme for solving the Λ CCSD amplitude equations is not sufficient due to slow convergence, or even divergence, of the iterations. Consequently, the iterations have to be accelerated and stabilized. There are mainly two possibilities to improve the situation. On the one hand, the iteration scheme (2.45) may be used and the resulting sequence of vectors $\{\mathbf{t}^{(k)}\}$ may be used to construct an improved, faster converging vector sequence. Methods like the *simple mixing* [149], the *Anderson mixing* [150], or the *Broyden mixing* [149] achieve such a stabilized and accelerated convergence. On the other hand, the standard iteration scheme (2.45) itself may be modified, which may then again be combined with convergence accelerators such as the Broyden mixing. Both approaches are considered in the following.

According to (2.44), the Coupled-Cluster amplitude equations are converted into a fixed-point problem

$$\mathbf{t}^{(n+1)} = \mathbf{I}(\mathbf{t}^{(n)}), \quad \mathbf{t}^* = \mathbf{I}(\mathbf{t}^*). \quad (4.123)$$

If the iterations are divergent, the simple mixing method, in which the new vector is given by

$$\mathbf{t}^{(n+1)} = \alpha \mathbf{I}(\mathbf{t}^{(n)}) + (1 - \alpha) \mathbf{t}^{(n)}, \quad (4.124)$$

may help to bring the sequence to convergence. By mixing the new vector $\mathbf{I}(\mathbf{t}^{(n)})$ with the old one, regulated by the mixing parameter α , this mixing guarantees that the iteration scheme does not depart too far from the initial guess, which slows the overall convergence down but at the same time makes it more robust against poor choices of the start vector.

The Anderson and Broyden mixing presented Figures 4.6 and 4.7 are more sophisticated convergence acceleration methods based on the multidimensional Newton method and they are widely used in the quantum chemistry context. Detailed reviews can be found in [149–151] and only the practical application is discussed in the following. As for the simple mixing, the Anderson and Broyden mixings also have a mixing parameter α but both methods have an additional backward range parameter M which determines the number of previous vectors $\mathbf{t}^{(n)}$ that should be taken into consideration for constructing the new vector $\mathbf{t}^{(n+1)}$. It can be easily verified that the simple mixing is contained in the Anderson mixing if for the latter $M = 0$ is chosen.

Figure 4.8 shows an illustration of the convergence rates of the Anderson, Broyden and simple mixing and for the case of no mixing at all. Convergence is monitored in terms of the norm of the residual vector, i.e.,

$$\text{residual}^{(k)} = \|\mathbf{I}(\mathbf{t}^{(k)}) - \mathbf{t}^{(k)}\|_2. \quad (4.125)$$

The no-mixing case exhibits a slow divergence, making the use of convergence-enhancing methods mandatory. The simple mixing, with an for all methods universally chosen mixing parameter $\alpha = 0.6$ leads to convergence, however, at a very slow rate. Therefore, as mentioned above, mixing methods do not only improve the convergence, they may also be vital for the iterations to converge at all. The Anderson and Broyden show a very similar performance which is far superior to the previous scenarios, leading to residuals below 10^{-7} within 20–30 iterations. Of course, the convergence is improved as the backward range parameter M is increased, i.e., more information about previous iterations is used in order to determine the new vector.

Figure 4.9 shows the influence of the mixing parameter α for the Anderson and Broyden mixing for fixed range M . In the cases presented in Figure 4.9, where the

$$\mathbf{t}^{(1)} = \mathbf{I}(\mathbf{t}^{(0)})$$

For $k = 1, 2, \dots$

$$m_k = \min\{k, M\}$$

$$\mathbf{F}^{(k)} = \mathbf{I}(\mathbf{t}^{(k)}) - \mathbf{t}^{(k)}$$

Determine $\boldsymbol{\beta}^{(k)} = (\beta_0^{(k)}, \dots, \beta_{m_k}^{(k)})^T$ that solves

$$\min_{\boldsymbol{\beta}=(\beta_0, \dots, \beta_{m_k})^T} \left\| \left(\mathbf{F}^{(k-m_k)}, \dots, \mathbf{F}^{(k)} \right) \boldsymbol{\beta} \right\|_2, \quad \sum_{i=0}^{m_k} \beta_i = 1$$

$$\mathbf{t}^{(k+1)} = (1 - \alpha) \sum_{i=0}^{m_k} \beta_i^{(k)} \mathbf{t}^{(k-m_k+i)} + \alpha \sum_{i=0}^{m_k} \beta_i^{(k)} \mathbf{I}(\mathbf{t}^{(k-m_k+i)})$$

Figure 4.6: The Anderson convergence acceleration method [150].

vector series is nicely converging, α may be chosen large since there is no need to slow the convergence down. As can be seen in in Figure 4.9, fastest convergence is achieved at $\alpha = 0.6$. Therefore, the combination of parameters $M \approx 8$ and $\alpha \approx 0.6$ typically is a good choice for obtaining fast and robust convergence.

As already mentioned above, another possibility – which does not seem to have been paid much attention in the past – to enhance the convergence of the Coupled-Cluster amplitude equations is by introducing a new iteration scheme, alternative to (2.45), which is used to generate the vector sequence used in the mixing methods. In the following, an improved iteration scheme is proposed. In order to do so, it is instructive to review how the standard iteration scheme (2.45) is constructed. Using the \hat{T}_1 amplitude equations

$$0 = \dots + \sum_c^{(SCa)} f_c^a t_i^c - \sum_k^{(SCb)} f_i^k t_k^a + \sum_{ck}^{(SCc)} v_{ic}^{ak} t_k^c + \dots \quad (4.126)$$

as an example, the amplitude t_i^a may be introduced on the left-hand side by adding $t_i^a D_i^a$ on both sides and dividing by D_i^a , arriving at

$$t_i^a = \frac{1}{D_i^a} \left\{ \dots + \sum_c^{(SCa)} f_c^a t_i^c - \sum_k^{(SCb)} f_i^k t_k^a + \sum_{ck}^{(SCc)} v_{ic}^{ak} t_k^c + \dots + t_i^a D_i^a \right\}. \quad (4.127)$$

$$\mathbf{t}^{(1)} = \mathbf{I}(\mathbf{t}^{(0)})$$

For $m = 1, 2, \dots$

$$\mathbf{t}^{(m+1)} = \mathbf{t}^{(m)} + \alpha \mathbf{F}^{(m)} - \sum_{n=\tilde{m}}^{m-1} w_n \gamma_{mn} \mathbf{u}^{(n)}$$

where

$$\tilde{m} = \max\{1, m - M\}$$

$$\gamma_{mn} = \sum_{k=\tilde{m}}^{m-1} c_k^m \beta_{kn}$$

$$\beta_{kn} = (w_0^2 \mathbb{1} + \mathbf{a})_{kn}^{-1}$$

$$c_k^m = w_k (\Delta \mathbf{F}^{(k)})^\dagger \mathbf{F}^{(m)}$$

$$a_{kn} = w_k w_n (\Delta \mathbf{F}^{(n)})^\dagger \Delta \mathbf{F}^{(k)}$$

$$\mathbf{u}^{(n)} = \alpha \Delta \mathbf{F}^{(n)} + \Delta \mathbf{t}^{(n)}$$

$$\Delta \mathbf{t}^{(n)} = (\mathbf{t}^{(n+1)} - \mathbf{t}^{(n)}) / \|\mathbf{F}^{(n+1)} - \mathbf{F}^{(n)}\|_2$$

$$\Delta \mathbf{F}^{(n)} = (\mathbf{F}^{(n+1)} - \mathbf{F}^{(n)}) / \|\mathbf{F}^{(n+1)} - \mathbf{F}^{(n)}\|_2$$

$$\mathbf{F}^{(k)} = \mathbf{I}(\mathbf{t}^{(k)}) - \mathbf{t}^{(k)}$$

Figure 4.7: The (modified) Broyden algorithm [149].

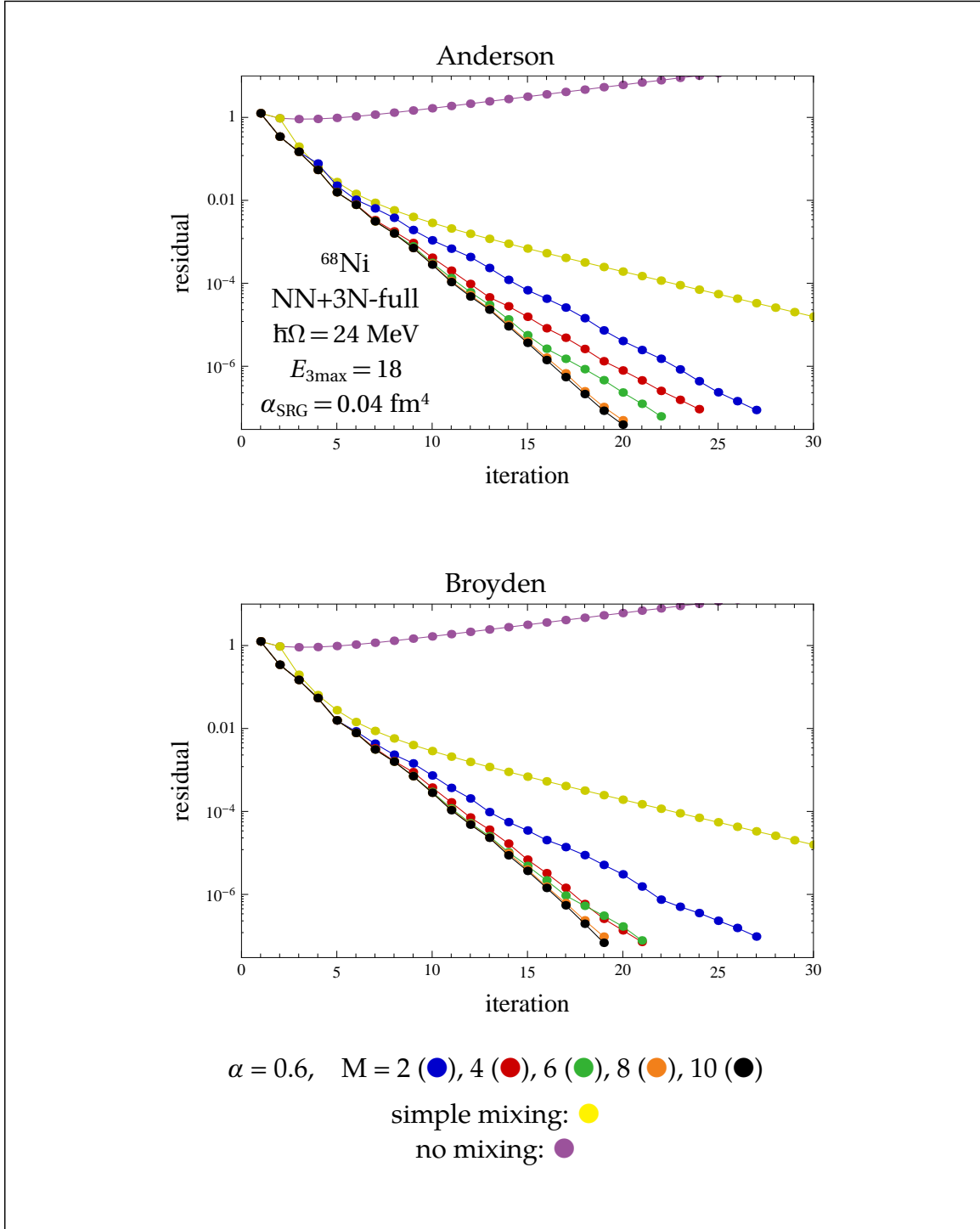


Figure 4.8: Comparison of the Anderson and Broyden method to the simple mixing or with no mixing at all, for fixed mixing parameter α and varying backward range M , for the CCSD amplitude equations.

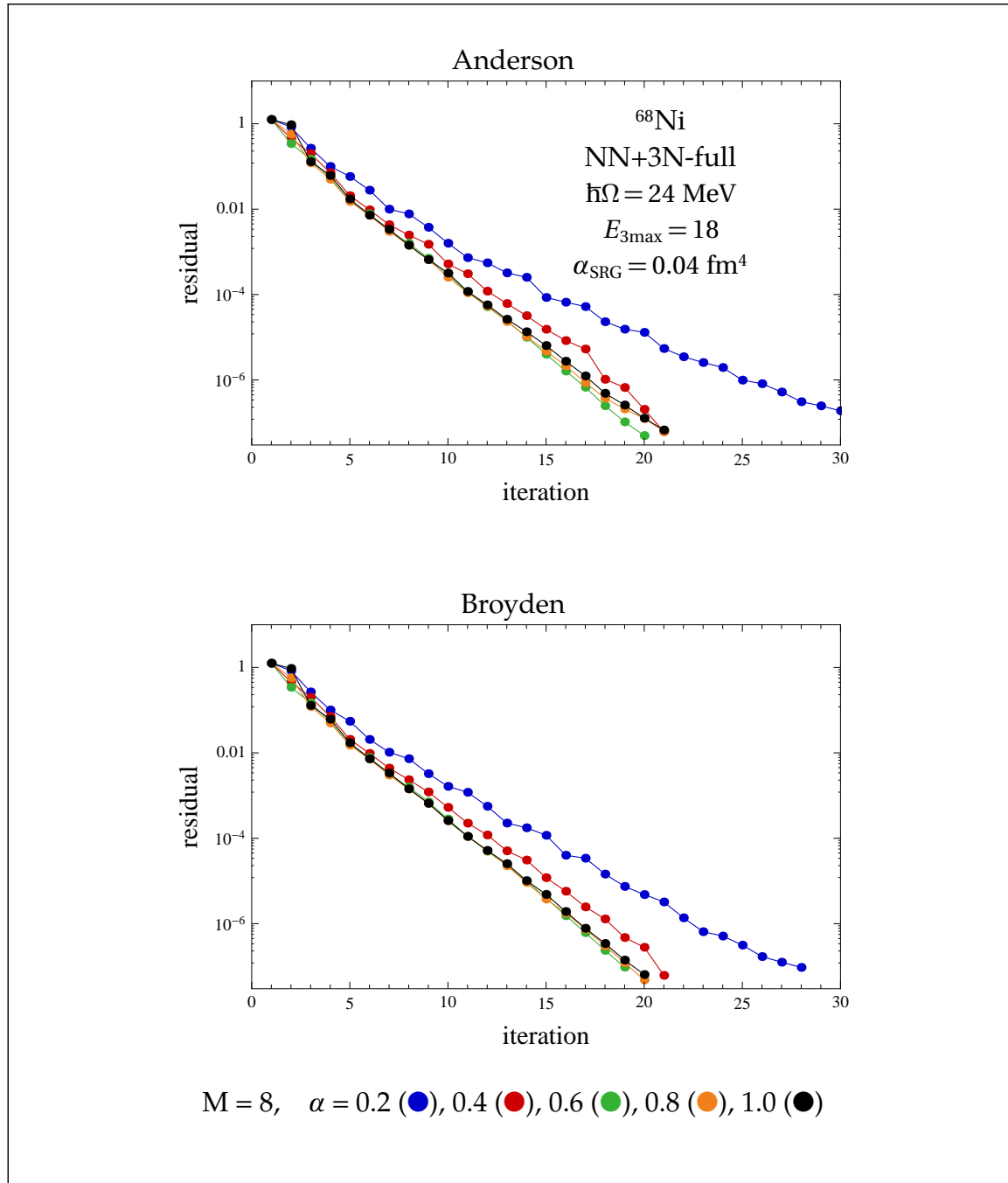


Figure 4.9: Comparison of the Anderson and Broyden mixing for fixed backward range M and varying mixing parameter α , for the CCSD amplitude equations.

The denominator D_i^a is chosen to be

$$D_i^a = f_i^i - f_a^a. \quad (4.128)$$

As a result of this choice of D_i^a , the t_i^a amplitudes are removed from the expression involving the contractions with the Fock operator,

$$+ \sum_c^{(SCa)} f_c^a t_i^c - \sum_k^{(SCb)} f_i^k t_k^a + t_i^a D_i^a = \sum_{c \neq a} f_c^a t_i^c - \sum_{k \neq i} f_i^k t_k^a. \quad (4.129)$$

Thus, another way to describe this procedure is to move the terms involving a single t_i^a and a single Fock matrix element to the left side and to divide by the prefactor D_i^a in order to isolate t_i^a . For the \hat{T}_2 equations, there is an analogous procedure. Equation (4.127) is then used as starting point to set up the standard iterative scheme,

$$\begin{aligned} {}^{(n+1)}t_i^a = \frac{1}{D_i^a} \bigg\{ & \dots + \sum_c^{(SCa)} f_c^a {}^{(n)}t_i^c - \sum_k^{(SCb)} f_i^k {}^{(n)}t_k^a \\ & + \sum_{ck}^{(SCc)} v_{ic}^{ak} {}^{(n)}t_k^c + \dots + t_i^a D_i^a \bigg\}. \end{aligned} \quad (4.130)$$

The definition of the denominator D_i^a eliminates the specific amplitude t_i^a on the right-hand side from the terms (SCa) and (SCb), which involve a contraction of the \hat{T}_1 operator with the Fock operator, but in other terms such as (SCc) the t_i^a remain. It would be more natural, as it is done in the Jacobi scheme for linear systems, to eliminate t_i^a *completely* from the right-hand side. For the example contributions considered in (4.127), this is achieved simply by using the modified denominator

$$D_i^a = f_i^i - f_a^a - v_{ia}^{ai}. \quad (4.131)$$

Unlike this example, it is not possible to remove all occurrences of t_i^a from the right-hand side, as can be seen, for instance, for the diagram

$$+ \sum_{cdk}^{(SEb)} v_{cd}^{ak} t_i^c t_k^d. \quad (4.132)$$

In such cases, the strategy followed here is to simply pick one of these t_i^a and move it to the left-hand side. One possible realization of the improved iteration scheme, in terms of spherical denominators D_i^a and $D_{ij}^{ab}(J)$, is given in Figures 4.10 and 4.11. Diagrams of the \hat{T}_2 amplitude equations that are evaluated in cross-coupled form are not easy to deal with and have been excluded from the considerations⁵. Since this iteration scheme is analogous to the Jacobi scheme for linear systems, it will be referred to as *Jacobi iteration scheme* in the following.

$$\begin{aligned}
 D_i^a = & \quad (SCa) \quad - \hat{j}_a^{-1} \overbrace{\langle \tilde{a} | \hat{f} | a \rangle}^{00} \\
 & \quad (SCb) \quad + \hat{j}_a^{-1} \overbrace{\langle \tilde{i} | \hat{f} | i \rangle}^{00} \\
 & \quad (SCc) \quad + \hat{j}_a^{-2} \sum_J \hat{j}^2 \overbrace{\langle a i | \hat{v} | i a \rangle}^{JM \quad JM} \\
 & \quad (SDa) \quad - \frac{1}{2} \hat{j}_a^{-2} \sum_{d k l} \sum_J \hat{j}^2 \overbrace{\langle a d | \hat{t}_2 | k l \rangle}^{JM \quad JM} \overbrace{\langle k l | \hat{v} | a d \rangle}^{JM \quad JM} \\
 & \quad (SDB) \quad - \frac{1}{2} \hat{j}_a^{-2} \sum_{c k l} \sum_J \hat{j}^2 \overbrace{\langle i l | \hat{v} | c d \rangle}^{JM \quad JM} \overbrace{\langle c d | \hat{t}_2 | i l \rangle}^{JM \quad JM} \\
 & \quad (SDc) \quad + \hat{j}_a^{-2} \sum_{d l} \hat{j}_d^{-2} \sum_{J J'} \hat{j}^2 (\hat{j}')^2 \overbrace{\langle i l | \hat{v} | a d \rangle}^{JM \quad JM} \overbrace{\langle d a | \hat{t}_2 | l i \rangle}^{J' M' \quad J' M'} \\
 & \quad (SEa) \quad - \hat{j}_a^{-2} \overbrace{\langle \tilde{i} | \hat{f} | a \rangle}^{00} \overbrace{\langle \tilde{a} | \hat{t}_1 | i \rangle}^{00} \\
 & \quad (SEb) \quad - \hat{j}_a^{-2} \sum_{d k} \hat{j}_k^{-1} \sum_J \hat{j}^2 \overbrace{\langle a k | \hat{v} | a d \rangle}^{JM \quad JM} \overbrace{\langle \tilde{d} | \hat{t}_1 | k \rangle}^{00} \\
 & \quad (SEc) \quad + \hat{j}_a^{-2} \sum_{c l} \hat{j}_c^{-1} \sum_J \hat{j}^2 \overbrace{\langle i l | \hat{v} | i c \rangle}^{JM \quad JM} \overbrace{\langle \tilde{c} | \hat{t}_1 | l \rangle}^{00} \\
 & \quad (SF) \quad - \hat{j}_a^{-3} \sum_{d k l} \hat{j}_d^{-1} \sum_J \hat{j}^2 \overbrace{\langle k l | \hat{v} | a d \rangle}^{JM \quad JM} \overbrace{\langle \tilde{a} | \hat{t}_1 | k \rangle}^{00} \overbrace{\langle \tilde{d} | \hat{t}_1 | l \rangle}^{00}
 \end{aligned}$$

 Figure 4.10: Denominator for the Jacobi iteration for the CCSD \hat{T}_1 amplitude equations.

$$\begin{aligned}
D_{ij}^{ab}(J) = & (1 + \hat{T}_{ab})(1 + \hat{T}_{ij}) \left\{ \overset{00}{\overbrace{-\frac{1}{2} \hat{J}_b^{-1} \langle \tilde{b} | \hat{f} | b \rangle}}^{(DBa)} + \overset{00}{\overbrace{\frac{1}{2} \hat{J}_j^{-1} \langle \tilde{j} | \hat{f} | j \rangle}}^{(DBb)} \right. \\
& + \overset{JM}{\overbrace{\frac{1}{8} \langle ab | \hat{v} | ab \rangle}}^{(DBc)} + \overset{JM}{\overbrace{\frac{1}{8} \langle ij | \hat{v} | ij \rangle}}^{(DBd)} + \overset{JM}{\overbrace{\frac{1}{16} \sum_{cd} \langle ij | \hat{v} | cd \rangle \langle cd | \hat{t}_2 | ij \rangle}}^{(DCa)} \\
& - \overset{J'M'}{\overbrace{\frac{1}{4} \hat{J}_i^{-2} \sum_{cdk} \sum_{J'} (\hat{J}')^2 \langle ki | \hat{v} | cd \rangle \langle cd | \hat{t}_2 | ki \rangle \delta_{ji j_l}}^{(DCC)}} \\
& - \overset{J'M'}{\overbrace{\frac{1}{4} \hat{J}_a^{-2} \sum_{ckl} \sum_{J'} (\hat{J}')^2 \langle ca | \hat{t}_2 | kl \rangle \langle kl | \hat{v} | ca \rangle \delta_{ja j_d}}^{(DCd)}} \\
& - \overset{00}{\overbrace{\frac{1}{2} \hat{J}_i^{-2} \sum_c \langle \tilde{c} | \hat{t}_1 | i \rangle \langle \tilde{i} | \hat{f} | c \rangle}}^{(DEa)}} - \overset{00}{\overbrace{\frac{1}{2} \hat{J}_a^{-2} \sum_k \langle \tilde{a} | \hat{t}_1 | k \rangle \langle \tilde{k} | \hat{f} | a \rangle}}^{(DEb)}} \\
& + \overset{JM}{\overbrace{\frac{1}{4} \hat{J}_a^{-1} \sum_k \langle \tilde{a} | \hat{t}_1 | k \rangle \langle kb | \hat{v} | ab \rangle}}^{(DEe)}} - \overset{JM}{\overbrace{\frac{1}{4} \hat{J}_i^{-1} \sum_c \langle \tilde{c} | \hat{t}_1 | i \rangle \langle ij | \hat{v} | cj \rangle}}^{(DEf)}} \\
& - \overset{J'M'}{\overbrace{\frac{1}{2} \hat{J}_a^{-2} \sum_{ck} \hat{J}_c^{-1} \sum_{J'} (\hat{J}')^2 \langle \tilde{c} | \hat{t}_1 | k \rangle \langle ka | \hat{v} | ca \rangle}}^{(DEg)}} \\
& + \overset{J'M'}{\overbrace{\frac{1}{2} \hat{J}_i^{-2} \sum_{ck} \hat{J}_c^{-1} \sum_{J'} (\hat{J}')^2 \langle \tilde{c} | \hat{t}_1 | k \rangle \langle ki | \hat{v} | ci \rangle}}^{(DEh)}} \\
& + \overset{JM}{\overbrace{\frac{1}{8} \hat{J}_b^{-1} \hat{J}_c^{-1} \sum_{kl} \langle \tilde{a} | \hat{t}_1 | k \rangle \langle \tilde{b} | \hat{t}_1 | l \rangle \langle kl | \hat{v} | ab \rangle}}^{(DGa)}} \\
& + \overset{JM}{\overbrace{\frac{1}{8} \hat{J}_i^{-1} \hat{J}_j^{-1} \sum_{cdkl} \langle \tilde{c} | \hat{t}_1 | i \rangle \langle \tilde{d} | \hat{t}_1 | j \rangle \langle ij | \hat{v} | cd \rangle}}^{(DGb)}} \\
& \left. - \overset{J'M'}{\overbrace{\frac{1}{2} \hat{J}_a^{-3} \sum_{ckl} \hat{J}_c^{-1} \sum_{J'} (\hat{J}')^2 \langle \tilde{a} | \hat{t}_1 | l \rangle \langle \tilde{c} | \hat{t}_1 | k \rangle \langle kl | \hat{v} | ca \rangle}}^{(DGe)}} \right\}
\end{aligned}$$

Figure 4.11: Denominator for the Jacobi iteration for the CCSD \hat{T}_2 amplitude equations.

Figure 4.12 shows a comparison of the standard and Jacobi iteration scheme combined with the Broyden mixing for ^{68}Ni CCSD calculations at the HO frequencies $\hbar\Omega = 24$ MeV and 40 MeV, where the former frequency corresponds to the optimal frequency at which the convergence of the CCSD equations is typically also the best. At the optimal frequency (Figure 4.12 top), both iteration schemes perform similarly, where the Jacobi scheme converges a little faster. The real use of the Jacobi scheme, however, is when the equations do not converge quickly or do even diverge. This is illustrated in Figure 4.12 at the bottom, where for the not optimal frequency the standard iteration scheme converges slower, but the convergence rate of the Jacobi scheme remains unchanged. Even in cases where the equations are highly divergent in the standard iteration scheme, a combination of the Jacobi scheme with a low- α Broyden mixing often leads to convergence. Of course, evaluating the denominators in Figures 4.10 and 4.11 is significantly more expensive than for the standard scheme. However, particularly in CCSD calculations for three-body Hamiltonians where the iteration steps become quite costly, using these improved denominators saves a significant amount of computing time.

⁵These are the diagrams (DBe), (DCb), (DEc), (DEd), (DGc), and (DGd).

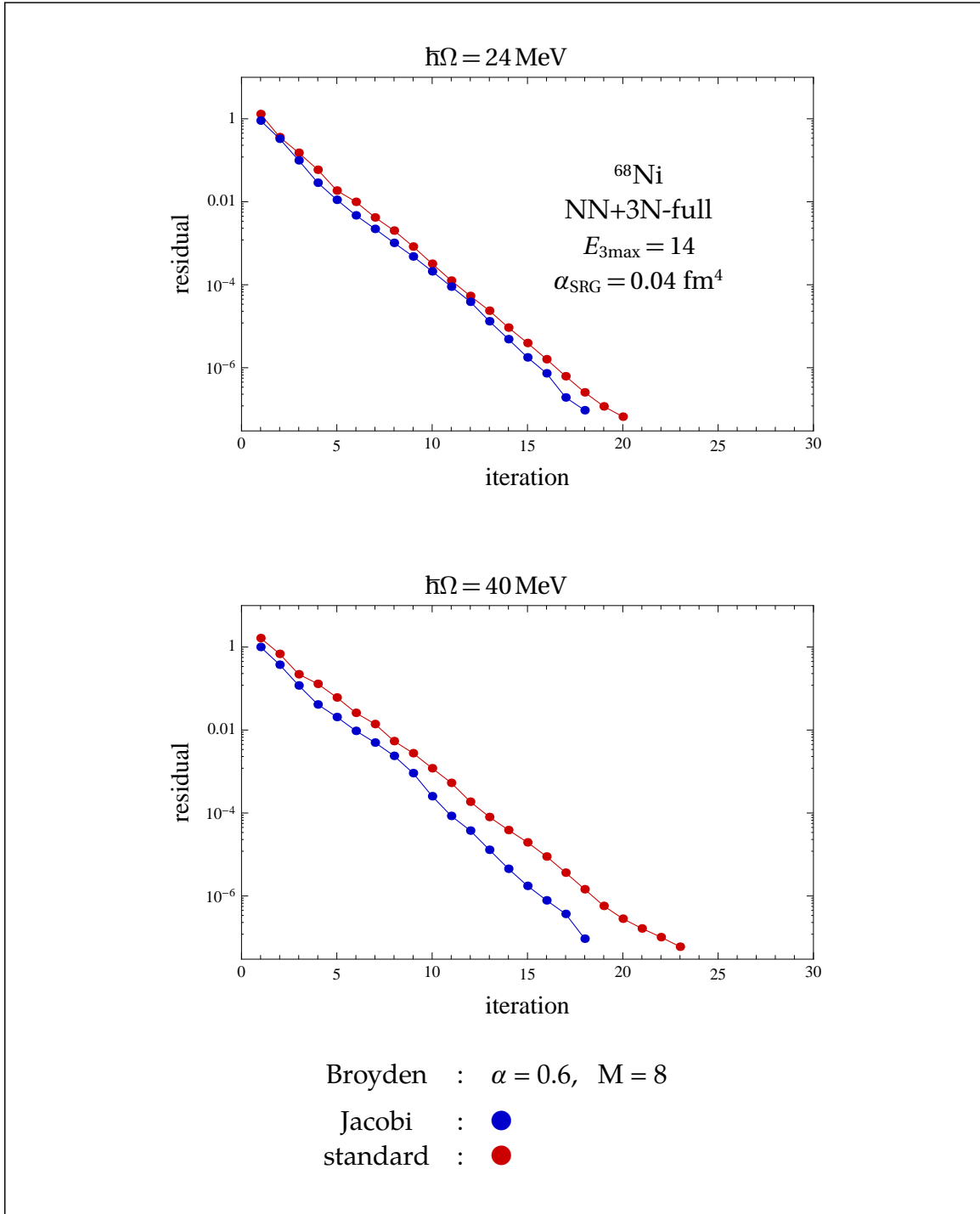


Figure 4.12: Comparison of the standard and the Jacobi iteration scheme for the CCSD amplitude equations.

4.9 Spherical CCSD for Three-Body Hamiltonians

4.9.1 Three-Body Matrix Elements

The $\mathcal{J}\mathcal{T}$ -coupled matrix element scheme [86] provides fast access to matrix elements of the form ⁶

$$\begin{array}{c} \mathcal{J} \mathcal{M} \mathcal{T} \mathcal{M}_{\mathcal{T}} \quad \mathcal{J} \mathcal{M} \mathcal{T} \mathcal{M}_{\mathcal{T}} \\ \begin{array}{c} \downarrow J_{ab} T_{ab} \\ \downarrow J_{de} T_{de} \end{array} \\ \langle a \ b \ c \mid \hat{w} \mid d \ e \ f \rangle, \end{array} \quad (4.133)$$

whereas for Coupled-Cluster applications matrix elements of the form

$$\begin{array}{c} J_{ab} M_{ab} \quad J_{de} M_{de} \\ \downarrow \quad \downarrow \\ \langle a \ m_{t_a} \ b \ m_{t_b} \ \tilde{c} \ m_{t_c} \mid \hat{w} \mid d \ m_{t_d} \ e \ m_{t_e} \ f \ m_{t_f} \rangle \\ \uparrow J_{cf} M_{cf} \end{array} \quad (4.134)$$

are required ⁷. In (4.134), the isospin projections are written explicitly in order to stress that the isospin is not coupled there. However, the matrix elements that are stored will be reduced matrix elements that correspond to the more compact isospin-coupled form,

$$\begin{array}{c} J_{ab} M_{ab} \quad J_{de} M_{de} \\ T_{ab} M_{T_{ab}} \quad T_{de} M_{T_{de}} \\ \downarrow \quad \downarrow \\ \langle a \ b \ \tilde{c} \mid \hat{w} \mid d \ e \ f \rangle. \\ \uparrow J_{cf} M_{cf} \\ T_{cf} M_{T_{cf}} \end{array} \quad (4.135)$$

Ignoring isospin for the moment, the matrix elements (4.135) can be expressed

⁶Total angular momentum and isospin projections \mathcal{M} and $\mathcal{M}_{\mathcal{T}}$ have a fixed value of $1/2$ because the interaction is independent of \mathcal{M} due to rotational invariance, and through the an isospin averaging the interaction also becomes independent of $\mathcal{M}_{\mathcal{T}}$.

⁷It is actually the *reduced* matrix elements that are required.

in terms of the standard coupled matrix elements (4.134) as

$$\begin{aligned}
 \langle \overset{J_{ab}M_{ab}}{\overbrace{a\ b\ \tilde{c}}} | \hat{w} | \overset{J_{de}M_{de}}{\overbrace{d\ e\ f}} \rangle &= (-1)^{J_{ab}-M_{ab}} \begin{pmatrix} J_{ab} & J_{de} & J_{cf} \\ -M_{ab} & M_{de} & M_{cf} \end{pmatrix}_{3j} \\
 &\times \sum_{\mathcal{J}} (-1)^{\mathcal{J}-j_c-J_{ab}} \hat{J}_{cf} \hat{\mathcal{J}}^2 \begin{Bmatrix} J_{ab} & J_{de} & J_{cf} \\ j_f & j_c & \mathcal{J} \end{Bmatrix}_{6j} \langle \overset{\mathcal{J}\mathcal{M}}{\overbrace{a\ b\ c}} | \hat{w} | \overset{\mathcal{J}\mathcal{M}}{\overbrace{d\ e\ f}} \rangle.
 \end{aligned} \tag{4.136}$$

To proof this, straightforward recouplings lead to

$$\begin{aligned}
 \langle \overset{J_{ab}M_{ab}}{\overbrace{a\ b\ \tilde{c}}} | \hat{w} | \overset{J_{de}M_{de}}{\overbrace{d\ e\ f}} \rangle &= \sum_{m_c m_f} (-1)^{j_c-m_c} \begin{pmatrix} j_c & j_f & J_{cf} \\ -m_c & m_f & M_{cf} \end{pmatrix}_{CG} \\
 &\times \sum_{\mathcal{J}\mathcal{M}} \begin{pmatrix} J_{ab} & j_c & \mathcal{J} \\ M_{ab} & m_c & \mathcal{M} \end{pmatrix}_{CG} \sum_{\mathcal{J}'\mathcal{M}'} \begin{pmatrix} J_{de} & j_f & \mathcal{J}' \\ M_{de} & m_f & \mathcal{M}' \end{pmatrix}_{CG} \langle \overset{\mathcal{J}\mathcal{M}}{\overbrace{a\ b\ c}} | \hat{w} | \overset{\mathcal{J}'\mathcal{M}'}{\overbrace{d\ e\ f}} \rangle,
 \end{aligned} \tag{4.137}$$

where the diagonality of the three-body matrix elements in \mathcal{J} and \mathcal{M} can be exploited to arrive at

$$\begin{aligned}
 \langle \overset{J_{ab}M_{ab}}{\overbrace{a\ b\ \tilde{c}}} | \hat{w} | \overset{J_{de}M_{de}}{\overbrace{d\ e\ f}} \rangle &= \sum_{\mathcal{J}} \langle \overset{\mathcal{J}\mathcal{M}}{\overbrace{a\ b\ c}} | \hat{w} | \overset{\mathcal{J}\mathcal{M}}{\overbrace{d\ e\ f}} \rangle \\
 &\times \underbrace{\sum_{m_c m_f \mathcal{M}} (-1)^{j_c-m_c} \begin{pmatrix} j_c & j_f & J_{cf} \\ -m_c & m_f & M_{cf} \end{pmatrix}_{CG} \begin{pmatrix} J_{ab} & j_c & \mathcal{J} \\ M_{ab} & m_c & \mathcal{M} \end{pmatrix}_{CG} \begin{pmatrix} J_{de} & j_f & \mathcal{J} \\ M_{de} & m_f & \mathcal{M} \end{pmatrix}_{CG}}_{\equiv \Omega}.
 \end{aligned} \tag{4.138}$$

Then, the relation [147]

$$\begin{aligned}
 \sum_{\alpha\beta\delta} (-1)^{b+\beta} \begin{pmatrix} a & b & c \\ \alpha & \beta & \gamma \end{pmatrix}_{CG} \begin{pmatrix} b & e & d \\ -\beta & \epsilon & \delta \end{pmatrix}_{CG} \begin{pmatrix} a & f & d \\ \alpha & \phi & \delta \end{pmatrix}_{CG} \\
 = (-1)^{b+c+d+f} \hat{c} \hat{d}^2 \hat{e}^{-1} \begin{pmatrix} c & f & e \\ \gamma & \phi & \epsilon \end{pmatrix}_{CG} \begin{Bmatrix} a & b & c \\ e & f & d \end{Bmatrix}_{6j}
 \end{aligned} \tag{4.139}$$

can be written in the form

$$\begin{aligned}
 & \sum_{\alpha\beta\delta} (-1)^{b-\beta} \begin{pmatrix} b & a & c \\ -\beta & \alpha & \gamma \end{pmatrix}_{\text{CG}} \begin{pmatrix} e & b & d \\ \epsilon & \beta & \delta \end{pmatrix}_{\text{CG}} \begin{pmatrix} f & a & d \\ \phi & \alpha & \delta \end{pmatrix}_{\text{CG}} \\
 &= (-1)^{-2a-b+2c+3d-e} \hat{c} \hat{d}^2 \hat{e}^{-1} \begin{pmatrix} c & f & e \\ \gamma & \phi & \epsilon \end{pmatrix}_{\text{CG}} \left\{ \begin{matrix} a & b & c \\ e & f & d \end{matrix} \right\}_{6j}
 \end{aligned} \quad (4.140)$$

which allows to simplify Ω to give

$$\begin{aligned}
 \Omega &= (-1)^{\mathcal{J}-j_c+J_{ab}} \hat{J}_{ab}^{-1} \hat{J}_{cf} \mathcal{J}^2 \\
 &\quad \times \begin{pmatrix} J_{cf} & J_{de} & J_{ab} \\ M_{cf} & M_{de} & M_{ab} \end{pmatrix}_{\text{CG}} \left\{ \begin{matrix} J_{ab} & J_{de} & J_{cf} \\ j_f & j_c & \mathcal{J} \end{matrix} \right\}_{6j}
 \end{aligned} \quad (4.141)$$

$$\begin{aligned}
 &= (-1)^{J_{ab}-M_{ab}} \begin{pmatrix} J_{ab} & J_{de} & J_{cf} \\ -M_{ab} & M_{de} & M_{cf} \end{pmatrix}_{3j} \\
 &\quad \times (-1)^{\mathcal{J}-j_c-J_{ab}} \hat{J}_{cf} \mathcal{J}^2 \left\{ \begin{matrix} J_{ab} & J_{de} & J_{cf} \\ j_f & j_c & \mathcal{J} \end{matrix} \right\}_{6j}.
 \end{aligned} \quad (4.142)$$

Plugging this into (4.138),

$$\begin{aligned}
 & \langle \overset{J_{ab}M_{ab}}{\overbrace{a \ b}^{\downarrow}} \tilde{c} \mid \hat{w} \mid \overset{J_{de}M_{de}}{\overbrace{d \ e}^{\downarrow}} f \rangle = (-1)^{J_{ab}-M_{ab}} \begin{pmatrix} J_{ab} & J_{de} & J_{cf} \\ -M_{ab} & M_{de} & M_{cf} \end{pmatrix}_{3j} \mathcal{J} \mathcal{M} \\
 & \quad \underbrace{\hspace{1.5cm}}_{J_{cf}M_{cf}} \times \sum_{\mathcal{J}} (-1)^{\mathcal{J}-j_c-J_{ab}} \hat{J}_{cf} \mathcal{J}^2 \left\{ \begin{matrix} J_{ab} & J_{de} & J_{cf} \\ j_f & j_c & \mathcal{J} \end{matrix} \right\}_{6j} \langle \overset{J_{ab}}{\overbrace{a \ b}^{\downarrow}} c \mid \hat{w} \mid \overset{J_{de}}{\overbrace{d \ e}^{\downarrow}} f \rangle,
 \end{aligned} \quad (4.143)$$

gives the desired expression (4.136).

It is clear that the above result holds for the isospin as well. Furthermore, since all projection-quantum-number dependence is in the prefactor

$$(-1)^{J_{ab}-M_{ab}} \begin{pmatrix} J_{ab} & J_{de} & J_{cf} \\ -M_{ab} & M_{de} & M_{cf} \end{pmatrix}_{3j}, \quad (4.144)$$

the corresponding reduced matrix elements may immediately be defined as

$$\langle ab\tilde{c} || \hat{w} || def \rangle \equiv \sum_{\mathcal{J}} (-1)^{\mathcal{J}-j_c-J_{ab}} \hat{J}_{cf} \hat{\mathcal{J}}^2 \left\{ \begin{matrix} J_{ab} & J_{de} & J_{cf} \\ j_f & j_c & \mathcal{J} \end{matrix} \right\}_{6j} \langle \overset{\mathcal{J} \mathcal{M}}{\overbrace{a \ b \ c}} | \hat{w} | \overset{\mathcal{J} \mathcal{M}}{\overbrace{d \ e \ f}} \rangle, \quad (4.145)$$

or, including isospin,

$$\begin{aligned} \langle ab\tilde{c} || \hat{w} || def \rangle &\equiv \sum_{\mathcal{J}} (-1)^{\mathcal{J}-j_c-J_{ab}} \hat{J}_{cf} \hat{\mathcal{J}}^2 \left\{ \begin{matrix} J_{ab} & J_{de} & J_{cf} \\ j_f & j_c & \mathcal{J} \end{matrix} \right\}_{6j} \times \sum_{\mathcal{T}} (-1)^{\mathcal{T}-t_c-T_{ab}} \hat{T}_{cf} \hat{\mathcal{T}}^2 \left\{ \begin{matrix} T_{ab} & T_{de} & T_{cf} \\ t_f & t_c & \mathcal{T} \end{matrix} \right\}_{6j} \\ &\quad \langle \overset{\mathcal{J} \mathcal{M} \mathcal{T} \mathcal{M} \mathcal{T}}{\overbrace{a \ b \ c}} | \hat{w} | \overset{\mathcal{J} \mathcal{M} \mathcal{T} \mathcal{M} \mathcal{T}}{\overbrace{d \ e \ f}} \rangle. \end{aligned} \quad (4.146)$$

The prefactor (4.144) looks similar to the geometric part of the traditional definition of reduced matrix elements (4.14), however, the rank of the tensor, which is zero in this case, does not appear in the Wigner 3j symbol any more. Instead, the third total angular momentum appears in the 3j symbol, resulting in the requirements

$$|J_{ab} - J_{de}| \leq J_{cf} \leq J_{ab} + J_{de}, \quad (4.147)$$

and

$$|T_{ab} - T_{de}| \leq T_{cf} \leq T_{ab} + T_{de} \quad (4.148)$$

for non-vanishing matrix elements.

When needed, the isospin m -scheme matrix elements are calculated from the

isospin-coupled ones by straightforward decoupling,

$$\begin{aligned}
 & \langle \overset{J_{ab}M_{ab}}{\downarrow} a \ m_{t_a} \ b \ m_{t_b} \ \tilde{c} \ m_{t_c} \ | \ \hat{w} \ | \ \overset{J_{de}M_{de}}{\downarrow} d \ m_{t_d} \ e \ m_{t_e} \ f \ m_{t_f} \rangle \\
 & \quad \quad \quad \underbrace{\hspace{10em}}_{J_{cf}M_{cf}} \\
 &= \sum_{T_{ab}M_{T_{ab}}} \sum_{T_{de}M_{T_{de}}} \sum_{T_{cf}M_{T_{cf}}} (-1)^{T_{ab}-M_{T_{ab}}} \begin{pmatrix} T_{ab} & T_{de} & T_{cf} \\ -M_{T_{ab}} & M_{T_{de}} & M_{T_{cf}} \end{pmatrix}_{3j} \\
 & \quad \times \begin{pmatrix} t_a & t_b & T_{ab} \\ m_{t_a} & m_{t_b} & M_{T_{ab}} \end{pmatrix}_{CG} \begin{pmatrix} t_d & t_e & T_{de} \\ m_{t_d} & m_{t_e} & M_{T_{de}} \end{pmatrix}_{CG} \\
 & \quad \times (-1)^{t_c-m_{t_c}} \begin{pmatrix} t_c & t_f & T_{cf} \\ m_{t_c} & m_{t_f} & M_{T_{cf}} \end{pmatrix}_{CG} \underbrace{\overset{J_{ab}T_{ab}}{\downarrow} \langle ab\tilde{c} || \hat{w} || \overset{J_{de}T_{de}}{\downarrow} def \rangle}_{J_{cf}T_{cf}}. \tag{4.149}
 \end{aligned}$$

Since the total projections $M_{T_{ab}}$, $M_{T_{de}}$, $M_{T_{cf}}$ are fixed by the m -scheme isospin projections, the corresponding summations may be removed. The 2^9 transformation coefficients $T[\dots]$ may easily be precomputed and stored, so that the transformation simply reads

$$\begin{aligned}
 & \langle \overset{J_{ab}M_{ab}}{\downarrow} a \ m_{t_a} \ b \ m_{t_b} \ \tilde{c} \ m_{t_c} \ | \ \hat{w} \ | \ \overset{J_{de}M_{de}}{\downarrow} d \ m_{t_d} \ e \ m_{t_e} \ f \ m_{t_f} \rangle \\
 & \quad \quad \quad \underbrace{\hspace{10em}}_{J_{cf}M_{cf}} \\
 &= \sum_{T_{ab}} \sum_{T_{de}} \sum_{T_{cf}} T \begin{bmatrix} m_{t_a} & m_{t_b} & m_{t_c} \\ m_{t_d} & m_{t_e} & m_{t_f} \\ T_{ab} & T_{de} & T_{cf} \end{bmatrix} \underbrace{\overset{J_{ab}T_{ab}}{\downarrow} \langle ab\tilde{c} || \hat{w} || \overset{J_{de}T_{de}}{\downarrow} def \rangle}_{J_{cf}T_{cf}}. \tag{4.150}
 \end{aligned}$$

Due to the coupling running across the operator, these matrix elements are not Hermitean. Nevertheless, they fulfill the symmetry relation

$$\begin{aligned}
 & \underbrace{\overset{J_{de}T_{de}}{\downarrow} \langle def || \hat{w} || \overset{J_{ab}T_{ab}}{\downarrow} abc \rangle}_{J_{cf}T_{cf}} = (-1)(-1)^{J_{ab}+J_{de}+J_{cf}} (-1)^{j_c+j_f-J_{cf}} \\
 & \quad \times (-1)(-1)^{T_{ab}+T_{de}+T_{cf}} (-1)^{t_c+t_f-T_{cf}} \underbrace{\overset{J_{ab}T_{ab}}{\downarrow} \langle ab\tilde{c} || \hat{w} || \overset{J_{de}T_{de}}{\downarrow} def \rangle}_{J_{cf}T_{cf}} \tag{4.151}
 \end{aligned}$$

that still allows to exploit the original Hermitecity of the Hamiltonian in standard coupling.

4.9.2 Conversion to Reduced Format

In the $\mathcal{J}\mathcal{T}$ -coupled scheme, the matrix elements (4.133) are stored for orbital index combinations of the form

$$a \geq b \geq c, \quad d \leq a, e \leq \begin{cases} b & : \text{for } a = d \\ d & : \text{else} \end{cases}, f \leq \begin{cases} c & : \text{for } a = d \wedge b = d \\ e & : \text{else} \end{cases}. \quad (4.152)$$

This does not permit to directly access matrix elements with arbitrary orbital indices. Since the purpose of the $\mathcal{J}\mathcal{T}$ -coupled scheme is the calculation of m -scheme matrix elements which have simple index permutation relations, this is not a drawback there. On the other hand, for the reduced matrix elements (4.146) that enter the spherical Coupled-Cluster equations, it is important to have fast access to all possible index combinations. Therefore, only the trivial index swaps in the first two orbitals in bra and ket as well as Hermiticity are exploited in the storage scheme for the reduced matrix elements, i.e.,

$$a \geq b, d \leq a, e \leq \begin{cases} b & : \text{for } a = d \\ d & : \text{else} \end{cases}. \quad (4.153)$$

In order to calculate reduced matrix elements of arbitrary orbital index combinations, standard $\mathcal{J}\mathcal{T}$ -coupled matrix elements with the same orbital indices are required. As mentioned before, these are not directly accessible in the $\mathcal{J}\mathcal{T}$ -coupled scheme, so they have to be expressed in terms of index combinations that are available. Two examples are given by

$$| \overset{\mathcal{J}\mathcal{M}}{\overbrace{p \ q \ r}^{J_{pq}}} \rangle = - \sum_{J_{pr}} (-1)^{j_q + j_r + J_{pq} + J_{pr}} \hat{J}_{pq} \hat{J}_{pr} \left\{ \begin{matrix} j_q & j_p & J_{pq} \\ j_r & \mathcal{J} & J_{pr} \end{matrix} \right\}_{6j} | \overset{\mathcal{J}\mathcal{M}}{\overbrace{p \ r \ q}^{J_{pr}}} \rangle \quad (4.154)$$

and

$$| \overset{\mathcal{J}\mathcal{M}}{\overbrace{p \ q \ r}^{J_{pq}}} \rangle = - \sum_{J_{qr}} (-1)^{j_q + j_r - J_{qr}} \hat{J}_{pq} \hat{J}_{qr} \left\{ \begin{matrix} j_p & j_q & J_{pq} \\ j_r & \mathcal{J} & J_{qr} \end{matrix} \right\}_{6j} | \overset{\mathcal{J}\mathcal{M}}{\overbrace{q \ r \ p}^{J_{qr}}} \rangle \quad (4.155)$$

which can be shown as follows: For (4.154), straightforward angular-momentum recoupling leads to

$$\begin{array}{c} \mathcal{J} \mathcal{M} \\ \downarrow J_{pq} \\ | \begin{array}{ccc} p & q & r \end{array} \rangle \end{array} = \sum_{J_{pr}} (-1)^{j_q+j_r+J_{pq}+J_{pr}} \hat{J}_{pq} \hat{J}_{pr} \left\{ \begin{array}{ccc} j_q & j_p & J_{pq} \\ j_r & \mathcal{J} & J_{pr} \end{array} \right\}_{6j} \left\{ \begin{array}{c} J_{pq} \\ | \begin{array}{ccc} p & r & q \end{array} \rangle \end{array} \right\}^{(J_{pq}r)\mathcal{J}}. \quad (4.156)$$

Exchanging the positions of q and r results in a sign from antisymmetry. There are no further phases because by exchanging q and r no angular momentum couplings are affected. Therefore, (4.154) follows immediately.

For (4.155), again, straightforward angular-momentum recoupling leads to

$$\begin{array}{c} \mathcal{J} \mathcal{M} \\ \downarrow J_{pq} \\ | \begin{array}{ccc} p & q & r \end{array} \rangle \end{array} = \sum_{J_{qr}} (-1)^{j_p+j_q+j_r+\mathcal{J}} \hat{J}_{pq} \hat{J}_{qr} \left\{ \begin{array}{ccc} j_p & j_q & J_{pq} \\ j_r & \mathcal{J} & J_{qr} \end{array} \right\}_{6j} \begin{array}{c} \mathcal{J} \mathcal{M} \\ \downarrow J_{qr} \\ | \begin{array}{ccc} p & q & r \end{array} \rangle \end{array}. \quad (4.157)$$

Using the relation

$$\begin{array}{c} \mathcal{J} \mathcal{M} \\ \downarrow J_{qr} \\ | \begin{array}{ccc} p & q & r \end{array} \rangle \end{array} = (-1)^2 (-1)^{j_p+J_{qr}-\mathcal{J}} \begin{array}{c} \mathcal{J} \mathcal{M} \\ \downarrow J_{qr} \\ | \begin{array}{ccc} q & r & p \end{array} \rangle \end{array}, \quad (4.158)$$

Eq. (4.155) is reproduced.

From each of these two relations another trivial relation can be derived regarding permutations of the first two orbitals on the right-hand side, giving a phase from antisymmetry and reversion of the coupling direction.

It should be noted that the sign in (4.154) stems from antisymmetry when orbitals q and r have been exchanged. It does *not* stem from angular-momentum considerations. Therefore, this sign arises only *once*, even if isospin is considered as well. On the other hand, the sign in (4.155) *does* origin from angular-momentum considerations and will, therefore, cancel with the one from arising in the isospin transformation. The complete set of relevant transformation expressions, including isospin, is given in Figure 4.13.

$$\begin{aligned}
 & \begin{array}{c} \mathcal{J} \mathcal{M} \mathcal{T} \mathcal{M} \mathcal{T} \\ J_{pq} \overline{T_{pq}} \\ | p \ q \ r \rangle \end{array} = -(-1)^{j_p+j_q-J_{pq}} (-1)^{1-T_{pq}} \begin{array}{c} \mathcal{J} \mathcal{M} \mathcal{T} \mathcal{M} \mathcal{T} \\ J_{pq} \overline{T_{pq}} \\ | q \ p \ r \rangle \end{array} \\
 \\
 & \begin{array}{c} \mathcal{J} \mathcal{M} \mathcal{T} \mathcal{M} \mathcal{T} \\ J_{pq} \overline{T_{pq}} \\ | p \ q \ r \rangle \end{array} = - \sum_{J_{pr}} (-1)^{j_q+j_r+J_{pq}+J_{pr}} \hat{J}_{pq} \hat{J}_{pr} \left\{ \begin{array}{ccc} j_q & j_p & J_{pq} \\ j_r & \mathcal{J} & J_{pr} \end{array} \right\}_{6j} \begin{array}{c} \mathcal{J} \mathcal{M} \mathcal{T} \mathcal{M} \mathcal{T} \\ J_{pr} \overline{T_{pr}} \\ | p \ r \ q \rangle \end{array} \\
 & \quad \times \sum_{T_{pr}} (-1)^{1+T_{pq}+T_{pr}} \hat{T}_{pq} \hat{T}_{pr} \left\{ \begin{array}{ccc} 1/2 & 1/2 & T_{pq} \\ 1/2 & \mathcal{T} & T_{pr} \end{array} \right\}_{6j} \\
 \\
 & \begin{array}{c} \mathcal{J} \mathcal{M} \mathcal{T} \mathcal{M} \mathcal{T} \\ J_{pq} \overline{T_{pq}} \\ | p \ q \ r \rangle \end{array} = \sum_{J_{pr}} (-1)^{j_p+j_q+J_{pq}} \hat{J}_{pq} \hat{J}_{pr} \left\{ \begin{array}{ccc} j_q & j_p & J_{pq} \\ j_r & \mathcal{J} & J_{pr} \end{array} \right\}_{6j} \begin{array}{c} \mathcal{J} \mathcal{M} \mathcal{T} \mathcal{M} \mathcal{T} \\ J_{pr} \overline{T_{pr}} \\ | r \ p \ q \rangle \end{array} \\
 & \quad \times \sum_{T_{pr}} (-1)^{1+T_{pq}} \hat{T}_{pq} \hat{T}_{pr} \left\{ \begin{array}{ccc} 1/2 & 1/2 & T_{pq} \\ 1/2 & \mathcal{T} & T_{pr} \end{array} \right\}_{6j} \\
 \\
 & \begin{array}{c} \mathcal{J} \mathcal{M} \mathcal{T} \mathcal{M} \mathcal{T} \\ J_{pq} \overline{T_{pq}} \\ | p \ q \ r \rangle \end{array} = \sum_{J_{qr}} (-1)^{j_q+j_r-J_{qr}} \hat{J}_{pq} \hat{J}_{qr} \left\{ \begin{array}{ccc} j_p & j_q & J_{pq} \\ j_r & \mathcal{J} & J_{qr} \end{array} \right\}_{6j} \begin{array}{c} \mathcal{J} \mathcal{M} \mathcal{T} \mathcal{M} \mathcal{T} \\ J_{qr} \overline{T_{qr}} \\ | q \ r \ p \rangle \end{array} \\
 & \quad \times \sum_{T_{qr}} (-1)^{1-T_{qr}} \hat{T}_{pq} \hat{T}_{qr} \left\{ \begin{array}{ccc} 1/2 & 1/2 & T_{pq} \\ 1/2 & \mathcal{T} & T_{qr} \end{array} \right\}_{6j} \\
 \\
 & \begin{array}{c} \mathcal{J} \mathcal{M} \mathcal{T} \mathcal{M} \mathcal{T} \\ J_{pq} \overline{T_{pq}} \\ | p \ q \ r \rangle \end{array} = - \sum_{J_{qr}} \hat{J}_{pq} \hat{J}_{qr} \left\{ \begin{array}{ccc} j_p & j_q & J_{pq} \\ j_r & \mathcal{J} & J_{qr} \end{array} \right\}_{6j} \begin{array}{c} \mathcal{J} \mathcal{M} \mathcal{T} \mathcal{M} \mathcal{T} \\ J_{qr} \overline{T_{qr}} \\ | q \ r \ p \rangle \end{array} \\
 & \quad \times \sum_{T_{qr}} \hat{T}_{pq} \hat{T}_{qr} \left\{ \begin{array}{ccc} 1/2 & 1/2 & T_{pq} \\ 1/2 & \mathcal{T} & T_{qr} \end{array} \right\}_{6j}
 \end{aligned}$$

Figure 4.13: Transformations between different index permutations for the angular momentum coupling used in the $\mathcal{J} \mathcal{T}$ -coupled scheme.

4.9.3 Spherical CCSD Equations for Three-Body Hamiltonians

Apart from the three-body matrix element handling, the spherical formulation of CCSD for three-body Hamiltonians does not require any new techniques. The three-body contributions to the normal-ordered Hamiltonian in terms of angular-momentum-coupled matrix elements read

$$\langle \Phi | \hat{H} | \Phi \rangle = \langle \Phi | \hat{H} | \Phi \rangle_{2B} - \frac{1}{6} \sum_{ijk} \hat{j}_k \sum_J \hat{J} \langle ij \tilde{k} || \hat{w} || ij k \rangle, \quad (4.159)$$

$$\langle \tilde{p} | \hat{f} | q \rangle = \langle \tilde{p} | \hat{f} | q \rangle_{2B} + \frac{1}{2} \sum_{ij} \sum_J \hat{J} \langle ij \tilde{p} || \hat{w} || ij q \rangle, \quad (4.160)$$

and

$$\langle \tilde{p} q | \hat{v} | rs \rangle = \langle \tilde{p} q | \hat{v} | rs \rangle_{2B} - \hat{J}^{-1} \sum_i \hat{j}_i \langle \tilde{p} q \tilde{i} || \hat{w} || rs i \rangle, \quad (4.161)$$

where $\langle \dots \rangle_{2B}$ denote the already known contributions from the two-body Hamiltonian. The algebraic expressions for the spherical ΔE^{CCSD} , \hat{T}_1 and \hat{T}_2 amplitude equations are listed in Appendix C.4. The computational runtime is dominated by the two diagrams

$$\begin{aligned} & - \frac{1}{4} \hat{P}_{ab}(J) \hat{P}_{ij}(J) \hat{J}^{-1} \hat{j}_i^{-1} \hat{j}_j^{-1} (-1)^{j_a+j_b-J} \sum_{cdek} \sum_{J'J''} (-1)^{J+J'+J''} \hat{J}' \hat{J}'' \\ & \times \left\{ \begin{matrix} J' & J'' & J \\ j_a & j_b & j_e \end{matrix} \right\}_{6j} \langle kl \tilde{a} || \hat{w} || cde \rangle \langle \tilde{c} | \hat{t}_1 | i \rangle \langle \tilde{d} | \hat{t}_1 | j \rangle \langle eb | \hat{t}_2 | kl \rangle \end{aligned} \quad (4.162)$$

and

$$\begin{aligned} & - \frac{1}{4} \hat{P}_{ab}(J) \hat{P}_{ij}(J) \sum_{cdek} \sum_{J'J''} \hat{J}' (\hat{J}'')^2 \left\{ \begin{matrix} J' & J'' & J \\ j_a & j_b & j_d \end{matrix} \right\}_{6j} \left\{ \begin{matrix} J' & J'' & J \\ j_a & j_c & j_d \end{matrix} \right\}_{6j} \\ & \times \langle kl \tilde{m} || \hat{w} || cde \rangle \langle ac | \hat{t}_2 | ij \rangle \langle bd | \hat{t}_2 | kl \rangle \langle \tilde{e} | \hat{t}_1 | m \rangle, \end{aligned} \quad (4.163)$$

which, therefore, require special attention in the implementation.

4.10 Spherical $\Lambda\text{CCSD(T)}$

When attempting to derive the spherical expression for $\delta E^{(\Lambda\text{CCSD(T)})}$ from the m -scheme expression

$$\delta E^{(\Lambda\text{CCSD(T)})} = \frac{1}{(3!)^2} \sum_{\substack{\bar{a}\bar{b}\bar{c} \\ ijk}} \tilde{\lambda}_{\bar{a}\bar{b}\bar{c}}^{\bar{i}\bar{j}\bar{k}} \frac{1}{\epsilon_{ijk}^{\bar{a}\bar{b}\bar{c}}} \tilde{t}_{ijk}^{\bar{a}\bar{b}\bar{c}}, \quad (4.164)$$

the presence of the denominator $\epsilon_{ijk}^{\bar{a}\bar{b}\bar{c}}$ is troubling at first glance. Each angular-momentum projection appears in *three* instead of two matrix elements, and one of them even appears in a *denominator*. It is clear that in general such an expression cannot be disentangled into separate spherical matrix elements. However, $\epsilon_{ijk}^{\bar{a}\bar{b}\bar{c}}$ is given by a sum of matrix elements of the Fock operator, which is a scalar one-body spherical tensor operator. Since its matrix elements are independent of the projection

$$\langle p m_p | \hat{f} | q m_q \rangle = \langle p 0 | \hat{f} | q 0 \rangle = -\hat{j}_p^{-1} \overbrace{\langle \bar{p} | \hat{f} | q \rangle}^{00}, \quad (4.165)$$

the denominator may be drawn in front of the projection summations, thus allowing the angular-momentum coupling techniques from the previous sections to obtain the corresponding spherical expression⁸. Setting

$$\begin{aligned} \epsilon_{ijk}^{\bar{a}\bar{b}\bar{c}} = \epsilon_{ijk}^{abc} = & -\hat{j}_i^{-1} \overbrace{\langle \bar{i} | \hat{f} | i \rangle}^{00} - \hat{j}_j^{-1} \overbrace{\langle \bar{j} | \hat{f} | j \rangle}^{00} - \hat{j}_k^{-1} \overbrace{\langle \bar{k} | \hat{f} | k \rangle}^{00} \\ & + \hat{j}_a^{-1} \overbrace{\langle \bar{a} | \hat{f} | a \rangle}^{00} + \hat{j}_b^{-1} \overbrace{\langle \bar{b} | \hat{f} | b \rangle}^{00} + \hat{j}_c^{-1} \overbrace{\langle \bar{c} | \hat{f} | c \rangle}^{00} \end{aligned} \quad (4.166)$$

the $\delta E^{(\Lambda\text{CCSD(T)})}$ correction reads

$$\begin{aligned} \delta E^{(\Lambda\text{CCSD(T)})} = & -\frac{1}{(3!)^2} \sum_{\substack{abc \\ ijk}} \frac{1}{\epsilon_{ijk}^{abc}} \sum_{JJ'J''} (-1)^{j_c+j_k-J''} \\ & \times (-1)^{J+J'+J''} \underbrace{\langle ij\bar{k} || \hat{\lambda} || abc \rangle}_{J''} \underbrace{\langle ab\bar{c} || \hat{t} || ijk \rangle}_{J''}. \end{aligned} \quad (4.167)$$

⁸Other non-iterative energy corrections such as CR-CC(2,3) [138] also have a denominator which, however, is not as simple as the one encountered for $\Lambda\text{CCSD(T)}$ which then cannot be treated exactly in a spherical formulation, see Sections 2.8 and 5.6.

When evaluating the coupled expressions for the $\hat{\tilde{\lambda}}, \hat{\tilde{t}}$ amplitudes, the permutation operators pose a problem, as, e.g., for the contribution

$$\tilde{\lambda}_{abc}^{ijk} \leftarrow \hat{P}_{a/bc} \hat{P}_{k/ij} \sum_d v_{bc}^{dk} \lambda_{ad}^{ij} \quad (4.168)$$

to the $\tilde{\lambda}$ amplitudes. Similar to Section 4.9.2, it is possible to couple the m -scheme expression for a specific index combination and to work out the transformation that leads to the antisymmetrized coupled expression. However, this transformation is quite memory-consuming in practical applications. The most straightforward approach for dealing with the permutations is to apply them before the angular-momentum coupling, and simply couple each resulting term, i.e.,

$$\tilde{\lambda}_{abc}^{ijk} \leftarrow \left(\hat{1} - \hat{T}_{ab} - \hat{T}_{ac} \right) \left(\hat{1} - \hat{T}_{ik} - \hat{T}_{jk} \right) \sum_d v_{bc}^{dk} \lambda_{ad}^{ij} \quad (4.169)$$

$$\begin{aligned} &= \left(\hat{1} - \hat{T}_{ab} - \hat{T}_{ac} - \hat{T}_{ik} - \hat{T}_{jk} + \hat{T}_{ab} \hat{T}_{ik} + \hat{T}_{ab} \hat{T}_{jk} \right. \\ &\quad \left. + \hat{T}_{ac} \hat{T}_{ik} + \hat{T}_{ac} \hat{T}_{jk} \right) \sum_d v_{bc}^{dk} \lambda_{ad}^{ij} \\ &= \sum_d v_{bc}^{dk} \lambda_{ad}^{ij} \left(\tilde{\lambda}_{A_1} \right) - \sum_d v_{ac}^{dk} \lambda_{bd}^{ij} \left(\tilde{\lambda}_{A_{T_{ab}}} \right) \dots \end{aligned} \quad (4.170)$$

The corresponding spherical expressions are listed in Appendix G.1⁹. These expression make heavy use of X coefficients. Since there are too many of them to pre-store, only X coefficients for fixed values of J, J', J'' are calculated and cached at a time¹⁰. In order to accelerate the computation of these X coefficients, the relation for Wigner 9j symbols

$$\left\{ \begin{matrix} a & b & c \\ d & e & f \\ g & h & j \end{matrix} \right\}_{9j} = \sum_x (-1)^{2x} (2x+1) \left\{ \begin{matrix} a & b & c \\ f & j & x \end{matrix} \right\}_{6j} \left\{ \begin{matrix} d & e & f \\ b & x & h \end{matrix} \right\}_{6j} \left\{ \begin{matrix} g & h & j \\ x & a & d \end{matrix} \right\}_{6j} \quad (4.171)$$

is used in order to compute the X coefficients from pre-cached Wigner 6j symbols. Because of the presence of the coupling coefficients it is no longer possible

⁹The naming convention is such that, for example, $(\tilde{\lambda}_{A_{T_{ab}}})$ is the first term contributing to $\tilde{\lambda}$ after the permutation operator \hat{T}_{ab} has been applied.

¹⁰This is of course because the energy correction contributions for fixed i, j, k, J, J', J'' are calculated at a time.

to use optimized matrix-multiplication routines to compute the \hat{t} , $\hat{\lambda}$ amplitudes for given hole orbitals i, j, k . Therefore, there exists no longer a reason not to constrain the particle index summation in the energy formula. A spherical expression for the energy correction with partially exploited antisymmetry that is used in the implementation, is given by

$$\delta E^{(\Lambda\text{CCSD(T)})} = -\frac{1}{(3!)^2} \sum_{\substack{a \geq b, c \\ i \geq j, k}} (2 - \delta_{ab}) (2 - \delta_{ij}) \frac{1}{\epsilon_{ijk}^{abc}} \\ \times \sum_{JJ'J''} (-1)^{j_c + j_k - J''} (-1)^{J+J'+J''} \underbrace{\langle ij\tilde{k} || \hat{\lambda} || abc \rangle}_{J''} \underbrace{\langle ab\tilde{c} || \hat{t} || ijk \rangle}_{J''}, \quad (4.172)$$

which may be confirmed by recognizing that ϵ_{ijk}^{abc} is invariant under permutations of orbitals and, for instance,

$$\sum_{ab} \overset{J_{ab}}{\downarrow} |ab\rangle \langle ab| = \left(\sum_{a < b} + \sum_{a=b} + \sum_{a > b} \right) \overset{J_{ab}}{\downarrow} |ab\rangle \langle ab| \quad (4.173)$$

$$= \left(\sum_{a < b} + \sum_{a=b} + \sum_{a < b} \left((-1) (-1)^{j_a + j_b - J_{ab}} \right)^2 \right) \overset{J_{ab}}{\downarrow} |ab\rangle \langle ab| \quad (4.174)$$

$$= \sum_{a \leq b} (2 - \delta_{ab}) \overset{J_{ab}}{\downarrow} |ab\rangle \langle ab|. \quad (4.175)$$

4.11 Spherical Λ CCSD(T) for Three-Body Hamiltonians

The Λ CCSD(T) expressions for three-body Hamiltonians are translated into the spherical formulation analogous to the two-body Hamiltonian case. As before, the treatment of permutation operators $\hat{P}_{ab/c}$ etc. is not trivial. For the three-body Λ CCSD(T) a more economic implementation has been chosen than straightforwardly expanding the permutation operator $\hat{P}_{ab/c}$ in terms of transpositions, $\hat{P}_{ab/c} = \hat{1} - \hat{T}_{ac} - \hat{T}_{bc}$. As an illustrative example, the expression

$$- \overset{(\mathcal{A})}{\hat{P}_{ab/c}} \sum_l w_{abl}^{ijk} \lambda_c^l = -(\hat{1} - \hat{T}_{ac} - \hat{T}_{bc}) \sum_l w_{abl}^{ijk} \lambda_c^l \quad (4.176)$$

may also be written as

$$\overset{(\mathcal{A}_1)}{-} \sum_l w_{abl}^{ijk} \lambda_c^l \overset{\left(\overset{(\mathcal{A})}{\hat{P}_{ab/c}} \right)}{-} \hat{P}_{ab} \sum_l w_{bcl}^{ijk} \lambda_a^l. \quad (4.177)$$

The permutation operator \hat{P}_{ab} is easy to deal with because in the spherical scheme it may simply be replaced by $\hat{P}_{ab}(J)$. As a second example, $(\mathcal{L}E)$ may be rewritten as

$$\begin{aligned}
 & + \hat{P}_{ab/c} \hat{P}_{ij/k} \sum_{dl} w_{abl}^{ijd} \lambda_{cd}^{kl} \\
 & = \sum_{dl} w_{abl}^{ijd} \lambda_{cd}^{kl} \left(\mathcal{L}E_{T_{bc}}^{T_{ac}} \right) + \hat{P}_{ab} \sum_{dl} w_{bcl}^{ijd} \lambda_{ad}^{kl} \\
 & \quad + \left(\mathcal{L}E_{T_{jk}}^{T_{ik}} \right) \hat{P}_{ij} \sum_{dl} w_{abl}^{jkd} \lambda_{cd}^{il} \left(\mathcal{L}E_{T_{ac}, T_{bc}}^{T_{ik}, T_{jk}} \right) + \hat{P}_{ab} \hat{P}_{ij} \sum_{dl} w_{bcl}^{jkd} \lambda_{ad}^{il},
 \end{aligned} \tag{4.178}$$

again involving permutation operators that are most convenient for the translation into the spherical scheme. The spherical expressions corresponding to these representations of l_{abc}^{ijk} and \mathfrak{M}_{ijk}^{abc} can be found in Appendix G.2.

4.12 The CR-CC(2,3) Energy Correction

As reviewed in more detail in Section 2.8, the CR-CC(2,3) energy correction is of the form

$$\delta E^{(\text{CR-CC}(2,3))} = \frac{1}{(3!)^2} \sum_{\substack{abc \\ ijk}} l_{abc}^{ijk} \mathfrak{M}_{ijk}^{\bar{a}\bar{b}\bar{c}}, \tag{4.179}$$

where l_{abc}^{ijk} are the amplitudes of the approximated left-eigenstate operator and $\mathfrak{M}_{ijk}^{\bar{a}\bar{b}\bar{c}}$ are the generalized moments of the CCSD equations. As can be seen from (2.122), the denominator

$$D_{ijk}^{\bar{a}\bar{b}\bar{c}} \equiv D_{ijk}^{\bar{a}\bar{b}\bar{c}}(3), \tag{4.180}$$

where

$$D_{ijk}^{\bar{a}\bar{b}\bar{c}}(k) = - \sum_{n=1}^k \langle \Phi_{ijk}^{\bar{a}\bar{b}\bar{c}} | \hat{\mathcal{H}}_n^{(\text{CCSD})} | \Phi_{ijk}^{\bar{a}\bar{b}\bar{c}} \rangle, \tag{4.181}$$

(or $D(k)$ for short) involving one-, two-, and three-body effective Hamiltonian matrix elements, enters the definition of the l_{abc}^{ijk} amplitudes, such that the energy expression can be stated as

$$\delta E^{(\text{CR-CC}(2,3))} = \frac{1}{(3!)^2} \sum_{\substack{abc \\ ijk}} \sum_{\substack{m_a m_b m_c \\ m_i m_j m_k}} N_{abc}^{ijk} \frac{1}{D_{ijk}^{\bar{a}\bar{b}\bar{c}}} \mathfrak{M}_{ijk}^{\bar{a}\bar{b}\bar{c}}. \tag{4.182}$$

Such a denominator containing higher-than-one-body matrix elements is troubling when the energy expression (4.179) is translated into the spherical formulation, because the three-fold appearance of individual orbitals prevents the use of traditional angular-momentum-coupling techniques. A projection-independent denominator, on the other hand, may be pulled in front of the projection sum in (4.182), and the contraction of the $N_{\bar{a}\bar{b}\bar{c}}^{i\bar{j}\bar{k}}$ and $\mathfrak{M}_{i\bar{j}\bar{k}}^{\bar{a}\bar{b}\bar{c}}$ elements can be formulated in angular-momentum-coupled form. One possibility is to truncate the denominator at the $k = 1$ level,

$$D_{i\bar{j}\bar{k}}^{\bar{a}\bar{b}\bar{c}} \approx D_{i\bar{j}\bar{k}}^{\bar{a}\bar{b}\bar{c}}(1) = - \langle \Phi_{i\bar{j}\bar{k}}^{\bar{a}\bar{b}\bar{c}} | \hat{\mathcal{H}}_1^{(\text{CCSD})} | \Phi_{i\bar{j}\bar{k}}^{\bar{a}\bar{b}\bar{c}} \rangle, \quad (4.183)$$

which has the same structure as the denominator encountered in $\Lambda\text{CCSD(T)}$, with the one-body effective Hamiltonian being replaced by the Fock operator, and is independent from the projections. However, while $D_{i\bar{j}\bar{k}}^{\bar{a}\bar{b}\bar{c}}(1)$ is the only denominator that can be treated exactly in spherical Coupled-Cluster theory, it should also be attempted to include the higher-order denominators $D_{i\bar{j}\bar{k}}^{\bar{a}\bar{b}\bar{c}}(2)$ and $D_{i\bar{j}\bar{k}}^{\bar{a}\bar{b}\bar{c}}(3)$ into the calculations, at least in an approximate form. The approach pursued in this work to incorporate denominators beyond $D_{i\bar{j}\bar{k}}^{\bar{a}\bar{b}\bar{c}}(1)$ is to replace the matrix elements $\mathcal{H}_{\bar{p}\bar{q}}^{\bar{p}\bar{q}}$ and $\mathcal{H}_{\bar{p}\bar{q}\bar{r}}^{\bar{p}\bar{q}\bar{r}}$ entering the definition of $D_{i\bar{j}\bar{k}}^{\bar{a}\bar{b}\bar{c}}(2)$ and $D_{i\bar{j}\bar{k}}^{\bar{a}\bar{b}\bar{c}}(3)$ by their projection-averaged counterparts $\overline{\mathcal{H}}_{pq}^{pq}$ and $\overline{\mathcal{H}}_{pqr}^{pqr}$, according to

$$\overline{\mathcal{H}}_{pq}^{pq} = \hat{j}_p^{-2} \hat{j}_q^{-2} \sum_{m_p m_q} \langle \bar{p}\bar{q} | \hat{\mathcal{H}}_2 | \bar{p}\bar{q} \rangle = \sum_J \hat{j}^2 \langle \overset{JM}{\downarrow} \bar{p}\bar{q} | \hat{\mathcal{H}}_2 | \overset{JM}{\downarrow} \bar{p}\bar{q} \rangle \quad (4.184)$$

$$\overline{\mathcal{H}}_{pqr}^{pqr} = \hat{j}_p^{-2} \hat{j}_q^{-2} \hat{j}_r^{-2} \sum_{\substack{m_p m_q \\ m_r}} \langle \bar{p}\bar{q}\bar{r} | \hat{\mathcal{H}}_3 | \bar{p}\bar{q}\bar{r} \rangle \quad (4.185)$$

$$= \sum_{J_{pq}} \sum_J \hat{j}^2 \langle \overset{JM}{\downarrow} \bar{p}\bar{q} \overset{JM}{\downarrow} \bar{r} | \hat{\mathcal{H}}_3 | \overset{JM}{\downarrow} \bar{p}\bar{q} \overset{JM}{\downarrow} \bar{r} \rangle. \quad (4.186)$$

The resulting denominators will correspondingly be referred to as $\overline{D}_{i\bar{j}\bar{k}}^{abc}(2)$ and $\overline{D}_{i\bar{j}\bar{k}}^{abc}(3)$, or $\overline{D}(2)$ and $\overline{D}(3)$ for short. The coupled matrix elements entering (4.186) can be obtained from

$$\langle \overset{JM}{\downarrow} \bar{a}\bar{b}\bar{i} | \hat{\mathcal{H}}_3 | \overset{JM}{\downarrow} \bar{a}\bar{b}\bar{i} \rangle = - \hat{j}_{ab}^2 \sum_m \left\{ \begin{matrix} j_m & j_i & J_{ab} \\ J & j_i & J_{ab} \end{matrix} \right\}_{6j} \langle \overset{J_{ab}M_{ab}}{\downarrow} \bar{a}\bar{b} | \hat{t}_2 | \overset{J_{ab}M_{ab}}{\downarrow} \bar{i}\bar{m} \rangle \langle \overset{J_{ab}M_{ab}}{\downarrow} \bar{i}\bar{m} | \hat{v} | \overset{J_{ab}M_{ab}}{\downarrow} \bar{a}\bar{b} \rangle \quad (4.187)$$

and

$$\langle ija | \hat{\mathcal{H}}_3 | ija \rangle = \tilde{f}_{ij}^2 \sum_e \left\{ \begin{matrix} j_e & j_a & J_{ij} \\ J & j_a & J_{ij} \end{matrix} \right\}_{6j} \langle ij | \hat{v} | ae \rangle \langle ae | \hat{t}_2 | ij \rangle. \quad (4.188)$$

This approximative treatment of the higher-order denominators will be justified by practical calculations in Section 5.6, where it is compared to results corresponding to an exact treatment of the denominators obtained from an m -scheme implementation.

For the spherical derivation of the CR-CC(2,3) working equations, the coupling strategy used for the Λ CCSD(T) method in Section 4.10 is too cumbersome because of the expansion of the permutation operators involved, resulting in many and rather complex terms to consider in the final expressions. The advantage of this approach is little memory consumption in actual calculations. For CR-CC(2,3), an alternative route is followed, where the multi-index permutation operators are applied to the coupled expressions. In order to do so, a different coupled form of the energy-correction expression is more convenient,¹¹

$$\begin{aligned} \delta E^{(\text{CR-CC}(2,3))} &= \frac{1}{(3!)^2} \sum_{\substack{a \geq b; c \\ i \geq j; k}} \sum_{\substack{J_{ab} J_{ij} \\ J}} (2 - \delta_{ab}) (2 - \delta_{ij}) \langle ijk | \hat{l} | abc \rangle \langle abc | \hat{\mathfrak{M}} | ijk \rangle, \end{aligned} \quad (4.189)$$

in which the orbitals connected via angular-momentum coupling that are also the ones that are subject to permutation among each other. The application of angular-momentum coupling and the permutation operators

$$\hat{P}_{abc} = \hat{1} - \hat{T}_{ab} - \hat{T}_{ac} - \hat{T}_{bc} + \hat{T}_{ab} \hat{T}_{ac} + \hat{T}_{ac} \hat{T}_{ab} \quad (4.190)$$

and

$$\hat{P}_{ij/k} = \hat{1} - \hat{T}_{ik} - \hat{T}_{jk} \quad (4.191)$$

at orbitals as they occur in (4.189) may then be evaluated using the transformations $\hat{P}_{abc}(J_{ab}, J_{abc})$ and $\hat{P}_{ij/k}(J_{ij}, J_{ijk})$ listed in Figure 4.14. These transformations

¹¹It should be noted that in (4.189) reduced matrix elements are used while the expressions presented in the following result in the non-reduced matrix elements.

are quite simple, requiring only 6j coupling coefficients and orbital permutations. However, all intermediate angular momenta and orbitals that are permuted have to be held in memory in order to avoid to compute quantities more than once, making this approach more memory consuming, as mentioned earlier, but on the other hand more efficient.

Using the transformations from Figure 4.14 the generalized moments may then be calculated as

$$\begin{array}{c} JM \\ \downarrow J_{ab} \\ \langle abc | \hat{\mathcal{M}} | ijk \rangle \end{array} \quad \begin{array}{c} JM \\ \downarrow J_{ij} \\ \langle abc | \hat{\mathcal{M}} | ijk \rangle \end{array} = \hat{P}_{abc}(J_{ab}, J) \begin{array}{c} JM \\ \downarrow J_{ab} \\ \langle abc | \hat{\mathcal{Z}} | ijk \rangle \end{array} \quad \begin{array}{c} JM \\ \downarrow J_{ij} \\ \langle abc | \hat{\mathcal{Z}} | ijk \rangle \end{array}, \quad (4.192)$$

with

$$\begin{array}{c} JM \\ \downarrow J_{ab} \\ \langle abc | \hat{\mathcal{Z}} | ijk \rangle \end{array} \quad \begin{array}{c} JM \\ \downarrow J_{ij} \\ \langle abc | \hat{\mathcal{Z}} | ijk \rangle \end{array} = \hat{P}_{ij/k}(J_{ij}, J) \left\{ \begin{array}{l} \frac{1}{2} \hat{J}_{ij} \hat{J}_{ab} \sum_m (-1)^{j_c+j_m+J_{ij}} \left\{ \begin{array}{ccc} j_c & j_m & J_{ij} \\ j_k & J & J_{ab} \end{array} \right\}_{6j} \begin{array}{c} J_{ij}M_{ij} \quad J_{ij}M_{ij} \quad J_{ab}M_{ab} \quad J_{ab}M_{ab} \\ \downarrow \quad \downarrow \quad \downarrow \quad \downarrow \\ \langle mc | \hat{J} | ij \rangle \quad \langle ab | \hat{t}_2 | km \rangle \end{array} \\ - \frac{1}{2} \hat{J}_{ij} \hat{J}_{ab} \sum_e (-1)^{j_e+j_c+J_{ij}} \left\{ \begin{array}{ccc} j_c & j_e & J_{ij} \\ j_k & J & J_{ab} \end{array} \right\}_{6j} \begin{array}{c} J_{ab}M_{ab} \quad J_{ab}M_{ab} \quad J_{ij}M_{ij} \quad J_{ij}M_{ij} \\ \downarrow \quad \downarrow \quad \downarrow \quad \downarrow \\ \langle ab | \hat{\mathcal{H}}_2 | ke \rangle \quad \langle ec | \hat{t}_2 | ij \rangle \end{array} \end{array} \right\} \quad (4.193)$$

and where the angular-momentum-coupled form of the J intermediate reads

$$\begin{array}{c} JM \\ \downarrow J_{ab} \\ \langle mc | \hat{J} | ij \rangle \end{array} \quad \begin{array}{c} JM \\ \downarrow J_{ij} \\ \langle mc | \hat{J} | ij \rangle \end{array} = \begin{array}{c} JM \\ \downarrow J_{ab} \\ \langle mc | \hat{\mathcal{H}}_2 | ij \rangle \end{array} + \hat{J}_m^{-1} \sum_e \begin{array}{c} JM \\ \downarrow J_{ab} \\ \langle ec | \hat{t}_2 | ij \rangle \end{array} \quad \begin{array}{c} JM \\ \downarrow J_{ij} \\ \langle \tilde{m} | \hat{\mathcal{H}}_1 | e \rangle \end{array}. \quad (4.194)$$

For the derivation of (4.193), the non-trivial identity

$$\begin{aligned} & \sum_{m_c m_k} \sum_M \begin{pmatrix} J_{ab} & j_c & J \\ M_{ab} & m_c & M \end{pmatrix}_{\text{CG}} \begin{pmatrix} J_{ij} & j_k & J \\ M_{ij} & m_k & M \end{pmatrix}_{\text{CG}} \\ & \quad \times \begin{pmatrix} j_m & j_c & J_{ij} \\ m_m & m_c & M_{ij} \end{pmatrix}_{\text{CG}} \begin{pmatrix} j_k & j_m & J_{ab} \\ m_k & m_m & M_{ab} \end{pmatrix}_{\text{CG}} \\ & = -(-1)^{j_c+j_m+J_{ij}} \hat{J}^2 \hat{J}_{ij} \hat{J}_{ab} \left\{ \begin{array}{ccc} j_c & j_m & J_{ij} \\ j_k & J & J_{ab} \end{array} \right\}_{6j} \end{aligned} \quad (4.195)$$

$$\begin{aligned}
 & \sum_{m_a m_b} \begin{pmatrix} j_a & j_b & J_{ab} \\ m_a & m_b & M_{ab} \end{pmatrix}_{\text{CG}} \sum_{M_{ab} m_c} \begin{pmatrix} J_{ab} & j_c & J_{abc} \\ M_{ab} & m_c & M_{abc} \end{pmatrix}_{\text{CG}} \\
 & \quad \times \hat{P}_{abc} |a m_a b m_b c m_c\rangle \\
 &= \left\{ \hat{1} - (-1)^{j_a+j_b-J_{ab}} \hat{T}_{ab} + \sum_{\mathcal{J}} \hat{\mathcal{J}} \hat{J}_{ab} \begin{Bmatrix} j_c & j_b & \mathcal{J} \\ j_a & J_{abc} & J_{ab} \end{Bmatrix}_{6j} \hat{T}_{ac} \hat{T}_{J_{ab}\mathcal{J}} \right. \\
 & \quad - \sum_{\mathcal{J}} (-1)^{j_b+j_c+\mathcal{J}+J_{ab}} \hat{\mathcal{J}} \hat{J}_{ab} \begin{Bmatrix} j_c & j_a & \mathcal{J} \\ j_b & J_{abc} & J_{ab} \end{Bmatrix}_{6j} \hat{T}_{bc} \hat{T}_{J_{ab}\mathcal{J}} \\
 & \quad - (-1)^{j_a+j_b+J_{ab}} \sum_{\mathcal{J}} \hat{\mathcal{J}} \hat{J}_{ab} \begin{Bmatrix} j_c & j_a & \mathcal{J} \\ j_b & J_{abc} & J_{ab} \end{Bmatrix}_{6j} \hat{T}_{ab} \hat{T}_{ac} \hat{T}_{J_{ab}\mathcal{J}} \\
 & \quad \left. - \sum_{\mathcal{J}} (-1)^{j_b+j_c+\mathcal{J}} \hat{\mathcal{J}} \hat{J}_{ab} \begin{Bmatrix} j_c & j_b & \mathcal{J} \\ j_a & J_{abc} & J_{ab} \end{Bmatrix}_{6j} \hat{T}_{ac} \hat{T}_{ab} \hat{T}_{J_{ab}\mathcal{J}} \right\} | \overset{J_{abc}M_{abc}}{\underset{\substack{\downarrow J_{ab} \\ \downarrow}}{a \ b \ c}} \rangle \\
 &\equiv \hat{P}_{abc}(J_{ab}, J_{abc}) | \overset{J_{abc}M_{abc}}{\underset{\substack{\downarrow J_{ab} \\ \downarrow}}{a \ b \ c}} \rangle \\
 \\
 & \sum_{m_i m_j} \begin{pmatrix} j_i & j_j & J_{ij} \\ m_i & m_j & M_{ij} \end{pmatrix}_{\text{CG}} \sum_{M_{ij} m_k} \begin{pmatrix} J_{ij} & j_k & J_{ijk} \\ M_{ij} & m_k & M_{ijk} \end{pmatrix}_{\text{CG}} \\
 & \quad \times \hat{P}_{i/jk} |i m_i j m_j k m_k\rangle \\
 &= \left\{ \hat{1} + \sum_{\mathcal{J}} \hat{\mathcal{J}} \hat{J}_{ij} \begin{Bmatrix} j_k & j_j & \mathcal{J} \\ j_i & J_{ijk} & J_{ij} \end{Bmatrix}_{6j} \hat{T}_{ik} \hat{T}_{J_{ij}\mathcal{J}} \right. \\
 & \quad \left. - \sum_{\mathcal{J}} (-1)^{j_k+j_j+\mathcal{J}+J_{ij}} \hat{\mathcal{J}} \hat{J}_{ij} \begin{Bmatrix} j_k & j_i & \mathcal{J} \\ j_j & J_{ijk} & J_{ij} \end{Bmatrix}_{6j} \hat{T}_{jk} \hat{T}_{J_{ij}\mathcal{J}} \right\} | \overset{J_{ijk}M_{ijk}}{\underset{\substack{\downarrow J_{ij} \\ \downarrow}}{i \ j \ k}} \rangle \\
 &\equiv \hat{P}_{i/jk}(J_{ij}, J_{ijk}) | \overset{J_{ijk}M_{ijk}}{\underset{\substack{\downarrow J_{ij} \\ \downarrow}}{i \ j \ k}} \rangle
 \end{aligned}$$

Figure 4.14: Transformations required in to obtain angular-momentum coupled and antisymmetrized expressions for $\hat{P}_{abc} |\bar{a}\bar{b}\bar{c}\rangle$ and $\hat{P}_{i/jk} |\bar{i}\bar{j}\bar{k}\rangle$, as needed in the CR-CC(2,3) implementation. The action of, e.g., $\hat{T}_{J_{ab}\mathcal{J}}$ is understood as replacing all occurrences of J_{ab} on the right by \mathcal{J} .

is helpful. Similarly, the \hat{N} amplitudes may be calculated according to

$$\begin{array}{c} JM \\ \downarrow \\ J_{ij} \\ \downarrow \\ \langle ijk|\hat{N}|abc\rangle \end{array} = \begin{array}{c} JM \\ \downarrow \\ J_{ab} \\ \downarrow \\ \hat{P}_{abc}(J_{ab}, J) \end{array} \begin{array}{c} JM \\ \downarrow \\ J_{ij} \\ \downarrow \\ \langle ijk|\hat{\Gamma}|abc\rangle \end{array} \quad (4.196)$$

where

$$\begin{aligned} \begin{array}{c} JM \\ \downarrow \\ J_{ij} \\ \downarrow \\ \langle ijk|\hat{\Gamma}|abc\rangle \end{array} &= \hat{P}_{ij/k}(J_{ij}, J) \left\{ \frac{1}{2} \delta_{J_{ab}J_{ij}} \hat{J}_k^{-1} (-1)^{j_c+j_k+J_{ab}+J_{ij}} \right. \\ &\times \left(\begin{array}{c} J_{ab}M_{ab} \\ \downarrow \\ \langle ij|\hat{\mathcal{H}}_2|ab\rangle \end{array} \begin{array}{c} J_{ab}M_{ab} \\ \downarrow \\ \langle \tilde{k}|\hat{\lambda}_1|c\rangle \end{array} \begin{array}{c} 00 \\ \downarrow \end{array} + \begin{array}{c} J_{ab}M_{ab} \\ \downarrow \\ \langle ij|\hat{\lambda}_2|ab\rangle \end{array} \begin{array}{c} J_{ab}M_{ab} \\ \downarrow \\ \langle \tilde{k}|\hat{\mathcal{H}}_1|c\rangle \end{array} \begin{array}{c} 00 \\ \downarrow \end{array} \right) \\ &- \frac{1}{2} (-1)^{j_c+j_e+J_{ij}} \sum_e \hat{J}_{ab} \hat{J}_{ij} \left\{ \begin{array}{ccc} j_c & j_e & J_{ij} \\ j_k & J & J_{ab} \end{array} \right\}_{6j} \begin{array}{c} J_{ij}M_{ij} \\ \downarrow \\ \langle ij|\hat{\lambda}_2|ec\rangle \end{array} \begin{array}{c} J_{ij}M_{ij} \\ \downarrow \\ \langle ke|\hat{\mathcal{H}}_2|ab\rangle \end{array} \\ &+ \frac{1}{2} (-1)^{j_c+j_m+J_{ij}} \sum_m \hat{J}_{ab} \hat{J}_{ij} \left\{ \begin{array}{ccc} j_c & j_m & J_{ij} \\ j_k & J & J_{ab} \end{array} \right\}_{6j} \begin{array}{c} J_{ij}M_{ij} \\ \downarrow \\ \langle ij|\hat{\mathcal{H}}_2|mc\rangle \end{array} \begin{array}{c} J_{ab}M_{ab} \\ \downarrow \\ \langle km|\hat{\lambda}_2|ab\rangle \end{array} \left. \right\}. \end{aligned} \quad (4.197)$$

4.13 Spherical EOM-CCSD

Excited eigenstates of the Hamiltonian have good angular momentum and projection, so these quantum numbers may be used to label right eigenstates as

$$|\Psi_{\mu,J,M}^{(\text{CCSD})}\rangle \quad (4.198)$$

and the corresponding left eigenstates as

$$\langle \bar{\Psi}_{\mu,J,M}^{(\text{CCSD})} | . \quad (4.199)$$

As in the m -scheme case, these eigenstates will be generated by the action of corresponding excitation operators on the CCSD ground state. If $\hat{\mathfrak{T}}^{(J)}$ is a spherical tensor operator, then the right eigenstate transforms as

$$|\Psi_{\mu,J,M}^{(\text{CCSD})}\rangle \sim \hat{\mathfrak{T}}_M^{(J)} , \quad (4.200)$$

but the left eigenstate transforms differently, according to

$$\langle \bar{\Psi}_{\mu,J,M}^{(\text{CCSD})} | \sim (-1)^{J-M} \hat{\mathfrak{T}}_{-M}^{(J)} . \quad (4.201)$$

Therefore, by introducing excitation operators $\hat{\mathfrak{R}}_{\mu,J,M}^{(\text{CCSD})}$ and de-excitation operators $\hat{\mathfrak{L}}_{\mu,J,M}^{(\text{CCSD})}$ that transform as spherical tensor operators,

$$\hat{\mathfrak{R}}_{\mu,J,M}^{(\text{CCSD})} , \hat{\mathfrak{L}}_{\mu,J,M}^{(\text{CCSD})} \sim \hat{\mathfrak{T}}_M^{(J)} , \quad (4.202)$$

the spherical EOM-CCSD ansatz for the excited states then reads

$$|\Psi_{\mu,J,M}^{(\text{CCSD})}\rangle = \hat{\mathfrak{R}}_{\mu,J,M}^{(\text{CCSD})} e^{\hat{T}^{(\text{CCSD})}} |\Phi\rangle \quad (4.203)$$

$$\langle \bar{\Psi}_{\mu,J,M}^{(\text{CCSD})} | = \langle \Phi | (-1)^{J-M} \hat{\mathfrak{L}}_{\mu,J,-M}^{(\text{CCSD})} e^{-\hat{T}^{(\text{CCSD})}} , \quad (4.204)$$

where the excitation index μ will be dropped in this and the following sections. As before, for EOM-CCSD, the excitation operator $\hat{\mathfrak{R}}_{J,M}^{(\text{CCSD})}$ consists of a zero-, one-, and two-body part,

$$\hat{\mathfrak{R}}_{J,M}^{(\text{CCSD})} = \hat{\mathfrak{R}}_{0,M}^{(J)} + \hat{\mathfrak{R}}_{1,M}^{(J)} + \hat{\mathfrak{R}}_{2,M}^{(J)} . \quad (4.205)$$

It is clear that the zero-body part cannot generate any angular momentum and is therefore of the form

$$\hat{\mathfrak{R}}_{0,M}^{(J)} = \delta_{J0} \delta_{M0} \mathfrak{R}_0 \hat{\mathbb{1}} \quad (4.206)$$

with \mathfrak{R}_0 being a number. This is consistent with the statement that the zero-body part of the excitation operator is only non-zero for excited states that have the same symmetries as the ground state which is always a 0^+ state in our case. Again, the excitation operator satisfies an eigenvalue equation for the effective Hamiltonian of the form

$$\left(\hat{\mathcal{H}}_{\text{open}}^{(\text{CCSD})} \hat{\mathfrak{R}}_{J,M}^{(\text{CCSD})} \right)_C |\Phi\rangle = \omega \hat{\mathfrak{R}}_M^{(J)} |\Phi\rangle. \quad (4.207)$$

Projecting this equation onto the singly and doubly excited m -scheme Slater determinants and coupling the resulting equations leads to the coupled form

$$\overbrace{\langle \tilde{a} | \left(\hat{\mathcal{H}}_{\text{open}}^{(\text{CCSD})} \hat{\mathfrak{R}}_{J,M}^{(\text{CCSD})} \right)_C | i \rangle}^{J-M} = \omega \langle \tilde{a} | \hat{\mathfrak{R}}_{J,M}^{(\text{CCSD})} | i \rangle \quad (4.208)$$

$$\overbrace{\langle ab | \left(\hat{\mathcal{H}}_{\text{open}}^{(\text{CCSD})} \hat{\mathfrak{R}}_M^{(J)} \right)_C | ij \rangle}^{J_{ab}M_{ab} \quad J_{ij}M_{ij}} = \omega \langle ab | \hat{\mathfrak{R}}_{J,M}^{(\text{CCSD})} | ij \rangle \quad (4.209)$$

which more conveniently can be formulated in terms of reduced matrix elements as ¹²

$$\langle a || \left(\hat{\mathcal{H}}_{\text{open}}^{(\text{CCSD})} \hat{\mathfrak{R}}_J^{(\text{CCSD})} \right)_C || i \rangle = \omega \langle a || \hat{\mathfrak{R}}_1^{(J)} || i \rangle \quad (4.210)$$

$$\overbrace{\langle ab || \left(\hat{\mathcal{H}}_{\text{open}}^{(\text{CCSD})} \hat{\mathfrak{R}}_J^{(\text{CCSD})} \right)_C || ij \rangle}^{J_{ab} \quad J_{ij}} = \omega \langle ab || \hat{\mathfrak{R}}_2^{(J)} || ij \rangle. \quad (4.211)$$

The corresponding equations are listed in Appendix H.2.

Analogous considerations for the left eigenvalue problem

$$\langle \Phi | (-1)^{J-M} \hat{\mathfrak{L}}_{J,-M}^{(\text{CCSD})} \hat{\mathcal{H}}_{\text{open}}^{(\text{CCSD})} = \langle \Phi | (-1)^{J-M} \hat{\mathfrak{L}}_{J,-M}^{(\text{CCSD})}$$

lead to the spherical form

$$\langle i || \hat{\mathfrak{L}}_J^{(\text{CCSD})} \hat{\mathcal{H}}_{\text{open}}^{(\text{CCSD})} || a \rangle = \omega \langle i || \hat{\mathfrak{L}}_1^{(J)} || a \rangle \quad (4.212)$$

$$\overbrace{\langle ij || \hat{\mathfrak{L}}_J^{(\text{CCSD})} \hat{\mathcal{H}}_{\text{open}}^{(\text{CCSD})} || ab \rangle}^{J_{ij} \quad J_{ab}} = \omega \langle ij || \hat{\mathfrak{L}}_2^{(J)} || ab \rangle, \quad (4.213)$$

for which the corresponding equations can be found in Appendix H.2.

¹²Since $\hat{\mathcal{H}}_{\text{open}}^{(\text{CCSD})}$ is a scalar under rotation, $\left(\hat{\mathcal{H}}_{\text{open}}^{(\text{CCSD})} \hat{\mathfrak{R}}_J^{(\text{CCSD})} \right)_C$ is a spherical tensor operator of rank J .

The eigenstates of $\hat{\mathcal{H}}^{(\text{CCSD})}$ are also parity eigenstates. In order to target a specific parity, the constraints

$$(-1)^{l_a} \stackrel{!}{=} (-1)^{l_i}, \text{ for matrix elements of } \hat{\mathcal{L}}_1^{(J)}, \hat{\mathcal{R}}_1^{(J)} \quad (4.214)$$

$$(-1)^{l_a+l_b} \stackrel{!}{=} (-1)^{l_i+l_j}, \text{ for matrix elements of } \hat{\mathcal{L}}_2^{(J)}, \hat{\mathcal{R}}_2^{(J)}, \quad (4.215)$$

may be enforced to obtain positive parity states¹³, or

$$(-1)^{l_a} \neq (-1)^{l_i}, \text{ for matrix elements of } \hat{\mathcal{L}}_1^{(J)}, \hat{\mathcal{R}}_1^{(J)} \quad (4.216)$$

$$(-1)^{l_a+l_b} \neq (-1)^{l_i+l_j}, \text{ for matrix elements of } \hat{\mathcal{L}}_2^{(J)}, \hat{\mathcal{R}}_2^{(J)}, \quad (4.217)$$

in order to obtain access the negative parity spectrum.

If one is interested in the $J = 0$ spectrum only, $\hat{\mathcal{R}}_0^{(\text{CCSD})}$ and $\hat{\mathcal{L}}_0^{(\text{CCSD})}$ are scalar tensor operators and the spherical EOM-CCSD equations may significantly be simplified. As for CCSD, these equations may be formulated without the use of coupling coefficients except for cross-coupling transformations. Therefore, simpler code structures and optimized matrix-multiplication routines may again be employed in order to accelerate the calculations. The scalar EOM-CCSD equations have also been worked out and can be found in Appendix H.3.

4.14 Spherical Reduced Density Matrices

The m -scheme expression for the EOM-CCSD reduced density matrices in terms of the spherical tensor operators $\hat{\mathcal{R}}_{\nu, J_R}^{(\text{CCSD})}$ and $\hat{\mathcal{L}}_{\mu, J_L}^{(\text{CCSD})}$ reads

$$\begin{aligned} (\rho_N^{\mu\nu})_{\bar{p}_1 \dots \bar{p}_n}^{\bar{q}_1 \dots \bar{q}_n} &= \langle \bar{\Psi}_{\mu, J_L, M_L}^{(\text{CCSD})} | \{ \hat{a}_{\bar{p}_1}^\dagger \dots \hat{a}_{\bar{p}_n}^\dagger \hat{a}_{\bar{q}_n} \dots \hat{a}_{\bar{q}_1} \} | \Psi_{\nu, J_R, M_R}^{(\text{CCSD})} \rangle \\ &= \langle \Phi | (-1)^{J_L - M_L} \hat{\mathcal{L}}_{\mu, J_L, -M_L}^{(\text{CCSD})} e^{-\hat{T}^{(\text{CCSD})}} \\ &\quad \{ \hat{a}_{\bar{p}_1}^\dagger \dots \hat{a}_{\bar{p}_n}^\dagger \hat{a}_{\bar{q}_n} \dots \hat{a}_{\bar{q}_1} \} e^{\hat{T}^{(\text{CCSD})}} \hat{\mathcal{R}}_{\nu, J_R, M_R}^{(\text{CCSD})} | \Phi \rangle \\ &= \langle \Phi | (-1)^{J_L - M_L} \hat{\mathcal{L}}_{\mu, J_L, -M_L}^{(\text{CCSD})} \\ &\quad \left(\{ \hat{a}_{\bar{p}_1}^\dagger \dots \hat{a}_{\bar{p}_n}^\dagger \hat{a}_{\bar{q}_n} \dots \hat{a}_{\bar{q}_1} \} e^{\hat{T}^{(\text{CCSD})}} \right)_C \hat{\mathcal{R}}_{\nu, J_R, M_R}^{(\text{CCSD})} | \Phi \rangle. \end{aligned} \quad (4.218)$$

¹³This is because the CCSD ground state is a 0^+ state.

This translates into the usual m -scheme expressions in terms of amplitudes $r_{\bar{i}_1 \dots \bar{i}_n}^{\bar{a}_1 \dots \bar{a}_n}$ and $l_{\bar{a}_1 \dots \bar{a}_n}^{\bar{i}_1 \dots \bar{i}_n}$ provided that the following identifications

$$r_{\bar{i}_1 \dots \bar{i}_n}^{\bar{a}_1 \dots \bar{a}_n} = \langle \bar{a}_1 \dots \bar{a}_n | \hat{\mathfrak{R}}_{\mu, J_R, M_R}^{(\text{CCSD})} | \bar{i}_1 \dots \bar{i}_n \rangle \quad (4.219)$$

and

$$l_{\bar{a}_1 \dots \bar{a}_n}^{\bar{i}_1 \dots \bar{i}_n} = \langle \bar{i}_1 \dots \bar{i}_n | (-1)^{J_L - M_L} \hat{\mathfrak{L}}_{\mu, J_L, -M_L}^{(\text{CCSD})} | \bar{a}_1 \dots \bar{a}_n \rangle \quad (4.220)$$

are implied.

The eigenvectors of the effective Hamiltonian need proper normalization in order to compute the density. All vectors belong to the same excitation index so this index will be dropped again. The vectors $\mathfrak{R}_{J_R}^{(\text{CCSD})}$ and $\mathfrak{L}_{J_L}^{(\text{CCSD})}$ are normalized such they lead to the correct normalizations in the corresponding m -scheme expressions for the operators $\hat{\mathfrak{R}}_{J_R, M_R}^{(\text{CCSD})}$ and $(-1)^{J_L - M_L} \hat{\mathfrak{L}}_{J_L, -M_L}^{(\text{CCSD})}$. Therefore, the right eigenvector is rescaled according to

$$\mathfrak{R}_{J_R}^{(\text{CCSD})} \rightarrow \frac{1}{\sqrt{\mathcal{N}_{\mathfrak{R}\mathfrak{R}}}} \mathfrak{R}_{J_R}^{(\text{CCSD})} \quad (4.221)$$

with

$$\begin{aligned} \mathcal{N}_{\mathfrak{R}\mathfrak{R}} &= (\mathfrak{R}_0)^2 + \sum_{\bar{a}\bar{i}} \langle \bar{a} | \hat{\mathfrak{R}}_{1, M_R}^{(J_R)} | \bar{i} \rangle \langle \bar{a} | \hat{\mathfrak{R}}_{1, M_R}^{(J_R)} | \bar{i} \rangle \\ &\quad + \frac{1}{4} \sum_{\bar{a}\bar{b}\bar{i}\bar{j}} \langle \bar{a}\bar{b} | \hat{\mathfrak{R}}_{2, M_R}^{(J_R)} | \bar{i}\bar{j} \rangle \langle \bar{a}\bar{b} | \hat{\mathfrak{R}}_{2, M_R}^{(J_R)} | \bar{i}\bar{j} \rangle \\ &= (\mathfrak{R}_0)^2 + \sum_{ai} [\langle a || \hat{\mathfrak{R}}_1^{(J_R)} || i \rangle]^2 + \frac{1}{4} \hat{J}_R^{-2} \sum_{abij} \sum_{J_{ab} J_{ij}} \left[\langle a \bar{b} || \hat{\mathfrak{R}}_2^{(J_R)} || i \bar{j} \rangle \right]^2 \end{aligned} \quad (4.222)$$

which follows from

$$\sum_{\bar{a}\bar{i}} \langle \bar{a} | \hat{\mathfrak{R}}_{1, M_R}^{(J_R)} | \bar{i} \rangle \langle \bar{a} | \hat{\mathfrak{R}}_{1, M_R}^{(J_R)} | \bar{i} \rangle \quad (4.223)$$

$$= \sum_{ai} \left[(-1)^{j_a - m_a} \begin{pmatrix} j_a & J & i \\ -m_a & M & m_i \end{pmatrix}_{3j} \right]^2 [\langle a || \hat{\mathfrak{R}}_1^{(J_R)} || i \rangle]^2 \quad (4.224)$$

$$= \sum_{ai} [\langle a || \hat{\mathfrak{R}}_1^{(J_R)} || i \rangle]^2 \quad (4.225)$$

and

$$\frac{1}{4} \sum_{\bar{a}\bar{b}\bar{i}\bar{j}} \langle \bar{a}\bar{b} | \hat{\mathfrak{R}}_{2,M_R}^{(J_R)} | \bar{i}\bar{j} \rangle \langle \bar{a}\bar{b} | \hat{\mathfrak{R}}_{2,M_R}^{(J_R)} | \bar{i}\bar{j} \rangle \quad (4.226)$$

$$\begin{aligned} &= \frac{1}{4} \sum_{abij} \sum_{J_{ab} M_{ab}} \sum_{J'_{ab} M'_{ab}} \begin{pmatrix} j_a & j_b & J_{ab} \\ m_a & m_b & M_{ab} \end{pmatrix}_{\text{CG}} \begin{pmatrix} j_i & j_j & J_{ij} \\ m_i & m_j & M_{ij} \end{pmatrix}_{\text{CG}} \\ &\quad \times \begin{pmatrix} j_a & j_b & J'_{ab} \\ m_a & m_b & M'_{ab} \end{pmatrix}_{\text{CG}} \begin{pmatrix} j_i & j_j & J'_{ij} \\ m_i & m_j & M'_{ij} \end{pmatrix}_{\text{CG}} \\ &\quad \times (-1)^{J_{ab}-M_{ab}} \begin{pmatrix} J_{ab} & J_R & J_{ij} \\ -M_{ab} & M & M_{ij} \end{pmatrix}_{3j} (-1)^{J'_{ab}-M'_{ab}} \begin{pmatrix} J'_{ab} & J_R & J'_{ij} \\ -M'_{ab} & M & M'_{ij} \end{pmatrix}_{3j} \\ &\quad \times \langle ab || \hat{\mathfrak{R}}_2^{(J_R)} || ij \rangle \langle ab || \hat{\mathfrak{R}}_2^{(J_R)} || ij \rangle \quad (4.227) \end{aligned}$$

$$= \frac{1}{4} \hat{J}_R^{-2} \sum_{abij} \sum_{J_{ab} J_{ij}} \left[\langle ab || \hat{\mathfrak{R}}_2^{(J_R)} || ij \rangle \right]^2. \quad (4.228)$$

In a next step, $\mathfrak{L}_{J_L}^{(\text{CCSD})}$ is rescaled in order to ensure unity of the state overlap

$$1 = \mathcal{N}_{\mathfrak{L}} = \langle \bar{\Psi}_M^{(J)} | \Psi_M^{(J)} \rangle, \quad (4.229)$$

implying $J_L = J_R \equiv J$ for the moment, which m -scheme expression is given in terms of reduced matrix elements as

$$\mathcal{N}_{\mathfrak{L}} = (-1)^{J-M} \mathfrak{L}_0 \mathfrak{R}_0 + (-1)^{J-M} \sum_{\bar{a}\bar{i}\bar{j}} \langle \bar{i} | \hat{\mathfrak{L}}_{1,-M}^{(J)} | \bar{a} \rangle \langle \bar{a} | \hat{\mathfrak{R}}_{1,M}^{(J)} | \bar{i} \rangle \quad (4.230)$$

$$+ \frac{1}{4} (-1)^{J-M} \sum_{\bar{a}\bar{b}\bar{i}\bar{j}} \langle \bar{i}\bar{j} | \hat{\mathfrak{L}}_{1,-M}^{(J)} | \bar{a}\bar{b} \rangle \langle \bar{a}\bar{b} | \hat{\mathfrak{R}}_{1,M}^{(J)} | \bar{i}\bar{j} \rangle, \quad (4.231)$$

$$\begin{aligned} \mathcal{N}_{\mathfrak{L}} &= -\hat{J}^{-2} \sum_{ai} (-1)^{j_a+j_i-J} \langle i || \hat{\mathfrak{L}}^{(J)} || a \rangle \langle a || \hat{\mathfrak{R}}^{(J)} || i \rangle \\ &\quad + \frac{1}{4} \hat{J}^{-2} \sum_{abij} \sum_{J_{ij} J_{ab}} (-1)^{J+J_{ij}+J_{ab}} \langle ij || \hat{\mathfrak{L}}_2^{(J)} || ab \rangle \langle ab || \hat{\mathfrak{R}}_2^{(J)} || ij \rangle. \quad (4.232) \end{aligned}$$

Since excited states are considered, $\mathfrak{L}_0 = 0$ is implied, so the product $\mathfrak{L}_0 \mathfrak{R}_0$ vanishes. Eq. (4.232) may also be used to check biorthonormality of the left and right eigenvectors. A further check of the implementation, at least for $J_R = 0$ states,

may be done by computing the overlap $\mathcal{N}_{\Lambda\mathfrak{R}}$ of the Λ state with the right eigenvectors [76],

$$\begin{aligned} \mathcal{N}_{\Lambda\mathfrak{R}} = & \mathfrak{R}_0 + \delta_{JR0} \sum_{ai} \langle i || \hat{\Lambda}_1 || a \rangle \langle a || \hat{\mathfrak{R}}_1^{(JR)} || i \rangle \\ & + \frac{1}{4} \delta_{JR0} \sum_{abij} \sum_J \langle ij || \hat{\Lambda}_2 || ab \rangle \langle ab || \hat{\mathfrak{R}}_2^{(JR)} || ij \rangle, \end{aligned} \quad (4.233)$$

which should vanish ¹⁴.

Using the spherical expression of the reduced density matrix, the expectation value of a one-body spherical tensor operator $\hat{O}_M^{(J)}$ may be expressed as

$$\langle \hat{O}_M^{(J)} \rangle_{\mu\nu} = -(-1)^{J-M} \hat{f}^{-2} \sum_{pq} (-1)^{j_p+j_q-J} \langle p || \hat{o}^{(J)} || q \rangle \langle q || \hat{\rho}_N^{\mu\nu(J)} || p \rangle. \quad (4.234)$$

Since it depends on the projection simply by the phase, the calculations can be simplified by setting

$$M_L = M_R = M = 0. \quad (4.235)$$

¹⁴It is of course always possible to compute the corresponding m -scheme vector from the spherical solution and then check overlaps etc., which is a recommended way to verify things anyway.

Chapter 5

Results

The overarching goal of this work is to extend the range of *ab initio* nuclear structure calculations to medium-mass and heavy nuclei. However, the computational framework considered in this work has arrived at a level of complexity at which the interpretation of results is not entirely straightforward. The initial Hamiltonian undergoes a renormalization treatment before it enters the many-body calculation, which itself is a multi-step procedure. Truncations are involved in each of these steps and it is important to understand in which ways they affect the results and to carefully monitor their impact in order to be able to estimate the overall accuracy of the calculations.

Although the accuracy of the Coupled-Cluster method can be estimated from an analysis of the contributions at different orders of the cluster expansion, a more direct approach through a comparison of Coupled-Cluster results with exact solutions is favorable, where possible. In Section 5.1, the quasi-exact results for ^{16}O from the IT-NCSM are compared to the various Coupled-Cluster ground-state methods considered in this work, and it is concluded that CCSD approach in combination with triples corrections can compete with the quasi-exact diagonalizations for this nucleus.

Using NN-only Hamiltonians eliminates all problems and difficulties related to the treatment of 3N interactions and allows to demonstrate the capabilities of the many-body methods detached from technical limitations imposed by the 3N interactions. In Section 5.2 it is shown that at the two-body level Coupled-Cluster calculations can be performed across the nuclear chart, and that the input interaction is the more limiting factor in such calculations.

In ground-state calculations beyond light nuclei, the standard chiral NN+3N-full Hamiltonian exhibits strong contributions from SRG-induced beyond-3N interactions which prevent any attempt to estimate the ground-state energies of the bare NN+3N-full Hamiltonian. In Section 5.3 a reduced cutoff-momentum variant of the chiral 3N interaction is considered that exhibits a much reduced flow-parameter dependence and which will then be used for all of the following calculations beyond light nuclei.

One of the most important truncations related to the inclusion of 3N interactions is an energy-truncation $E_{3\text{max}}$ in the 3N matrix elements, which is considered in Section 5.4.

Triples corrections are indispensable in the Coupled-Cluster framework by providing crucial contributions beyond CCSD, in particular for harder interactions. But even for soft interactions, where the contributions are rather small, triples corrections give important information about the convergence of the cluster expansion. General aspects of triples corrections in nuclear structure calculations are discussed in Section 5.5 in the context of Λ CCSD(T), and the results for the CR-CC(2,3) method, including a comparison to Λ CCSD(T), are presented in Section 5.6.

In practical calculations, the normal-ordered two-body approximation is critical since, in particular for calculations involving heavy nuclei or triples corrections, the NO2B approximation reduces the computing time by orders of magnitude. Since the calculations rely so heavily on this approximation it is worthwhile to verify its validity for medium-mass nuclei using CCSD and Λ CCSD(T) calculations for three-body Hamiltonians in Sections 5.7 and 5.8.1.

Heavy nuclei are considered in Section 5.9. Advancing to larger mass numbers requires to revisit truncations of the SRG model space, and the generation of large- E_{\max} matrix element sets. Nevertheless, despite all technical difficulties, it is shown that reliable *ab initio* calculations can be performed even for nuclei as heavy as ^{132}Sn .

Proof-of-principle calculations of excited states using the spherical EOM-CCSD formalism are attached in Appendix A. In these calculations the EOM-CCSD framework proves to be capable of describing selected low-lying states, making it a more favorable approach to such states than the Random Phase Approximation approach, for instance.

Finally, to extend the calculations beyond common nuclei, in Appendix B neutrons trapped in an external potential are considered. These neutron systems allow to study the extreme-isospin component of the nuclear interactions and serve as simple models for neutron-rich nuclei.

5.1 Comparison of the IT-NCSM with the Coupled-Cluster Method

Comparing CCSD ground-state energies with ones obtained from the IT-NCSM allows to estimate the quality of the CCSD approximation to the exact wavefunction, because converged IT-NCSM results may for present purposes be regarded as the *quasi-exact* solutions of the Schrödinger equation. This is *not* the case for CCSD, since, even in the limit $e_{\max} \rightarrow \infty$, contributions from triple and higher-rank excitations are missing in the wavefunction.

A direct comparison of the N_{\max} and e_{\max} model spaces for the IT-NCSM and CCSD is not immediately possible. For CCSD, a *rough estimate* of the maximum unperturbed excitation energy of the basis Slater determinants that is generated by a operator product $(\hat{T}_1)^n(\hat{T}_2)^m$ is given by $(n+2m)e_{\max}\hbar\Omega$, while for the IT-NCSM the maximum excitation energy is $N_{\max}\hbar\Omega$. Therefore, for $e_{\max} = N_{\max}$, the maximum excitation energy of CCSD exceeds the one of the IT-NCSM. This is why in Figure 5.1 the CCSD results seem to converge more quickly. On the other hand, only *some* determinants (those that are generated by certain products of excitation operators) with such high energies are included in the CCSD model space while the IT-NCSM includes *all* determinants ¹ up to the maximum excitation energy $N_{\max}\hbar\Omega$.

Unlike the IT-NCSM, CCSD is not strictly variational but in practice non-variational behavior is practically never encountered. Therefore, the CCSD results converge from above and the converged results are expected to lie somewhat above the converged IT-NCSM because of the missing beyond-single-and-double excitations in CCSD. These expectations are confirmed in Figure 5.1, where the three types of Hamiltonians NN-only, NN+3N-induced, and NN+3N-full with regular cutoff momentum $\Lambda_{3N} = 500$ MeV are considered in a harmonic-oscillator basis for a sequence of SRG flow parameters. For calculations involving three-body Hamiltonians, the normal-ordered two-body approximation is used. The nucleus ^{16}O has been chosen because it is at the upper end of IT-NCSM capabilities and at the same time marks the beginning of the medium-mass regime, which is the primary interest of this work. Postponing the detailed discussion of Coupled-Cluster results to later sections, good agreement of CCSD and the IT-NCSM is apparent. In the model spaces that are considered, CCSD is converged

¹More strictly speaking, all *relevant* determinants.

beyond any doubt and for the IT-NCSM the extrapolations are trustworthy. For the IT-NCSM, the largest sources of uncertainties come from the importance truncation for non-vanishing κ_{\min} and the extrapolation to infinite model space sizes N_{\max} , which are both of the order of 1 MeV. For the Coupled-Cluster calculations, the truncation of the cluster operator at the \hat{T}_2 excitation level represents the major source of uncertainty of the order of a few MeV, and, consequently, the observed deviations from CCSD to the IT-NCSM are to a large extent attributable to this approximative nature of CCSD. While the NCSM is translational invariant from the outset and the IT-NCSM practically preserves this translational invariance, spurious center-of-mass contaminations may occur in truncated Coupled-Cluster calculations. However, these center-of-mass effects are expected to be small [152].

Conclusions about the bare Hamiltonians at SRG flow-parameter $\alpha = 0.0 \text{ fm}^4$ can often be drawn by analyzing the flow-parameter dependence of ground-state energies of SRG-evolved Hamiltonians. Here, the different quality of the IT-NCSM and Coupled-Cluster results have to be considered. Since the IT-NCSM is a *quasi-exact* method, the flow-parameter dependence may completely be attributed to omitted SRG-induced many-body interactions. On the other hand, the truncations inherent in the CCSD or $\Lambda\text{CCSD(T)}$ approach may cause flow-parameter dependence on their own. A simple example is given by truncation of the cluster operator: Since softer interactions are expected to induce less correlations, it is expected that an approximate method such as CCSD performs better for softer interactions than for harder ones. A second source of flow-parameter dependence is identified as the $E_{3\max}$ cut for three-body matrix elements, as discussed in later sections. In principle, an $E_{3\max}$ truncation should also cause a flow-parameter dependence in the IT-NCSM, however, for all IT-NCSM model spaces $N_{\max} \leq 14$ used in this work, the full set of required matrix elements was included.

A more detailed comparison of IT-NCSM and Coupled-Cluster ground-state energies for ^{16}O – now also including triples corrections to the energy – can be found in Figure 5.2. In all cases the IT-NCSM energies lie halfway between the CCSD and $\Lambda\text{CCSD(T)}$ results. For the NN+3N-induced Hamiltonian at $\alpha = 0.04 \text{ fm}^4$, for instance, CCSD yields -120.2 MeV, the IT-NCSM gives -121.8 MeV and $\Lambda\text{CCSD(T)}$ gives -123.6 MeV. From this follows that CCSD is even a little closer to the IT-NCSM than is $\Lambda\text{CCSD(T)}$. Thus, a naive look at Figure 5.2 suggests CCSD to be the more accurate approximation than is $\Lambda\text{CCSD(T)}$. However, due to its variational character, the *true* exact result is expected to lie below the IT-NCSM and in quantum-chemistry applications $\Lambda\text{CCSD(T)}$ tends to overshoot the exact result a little [153], so the exact result is actually expected to lie in between the IT-NCSM

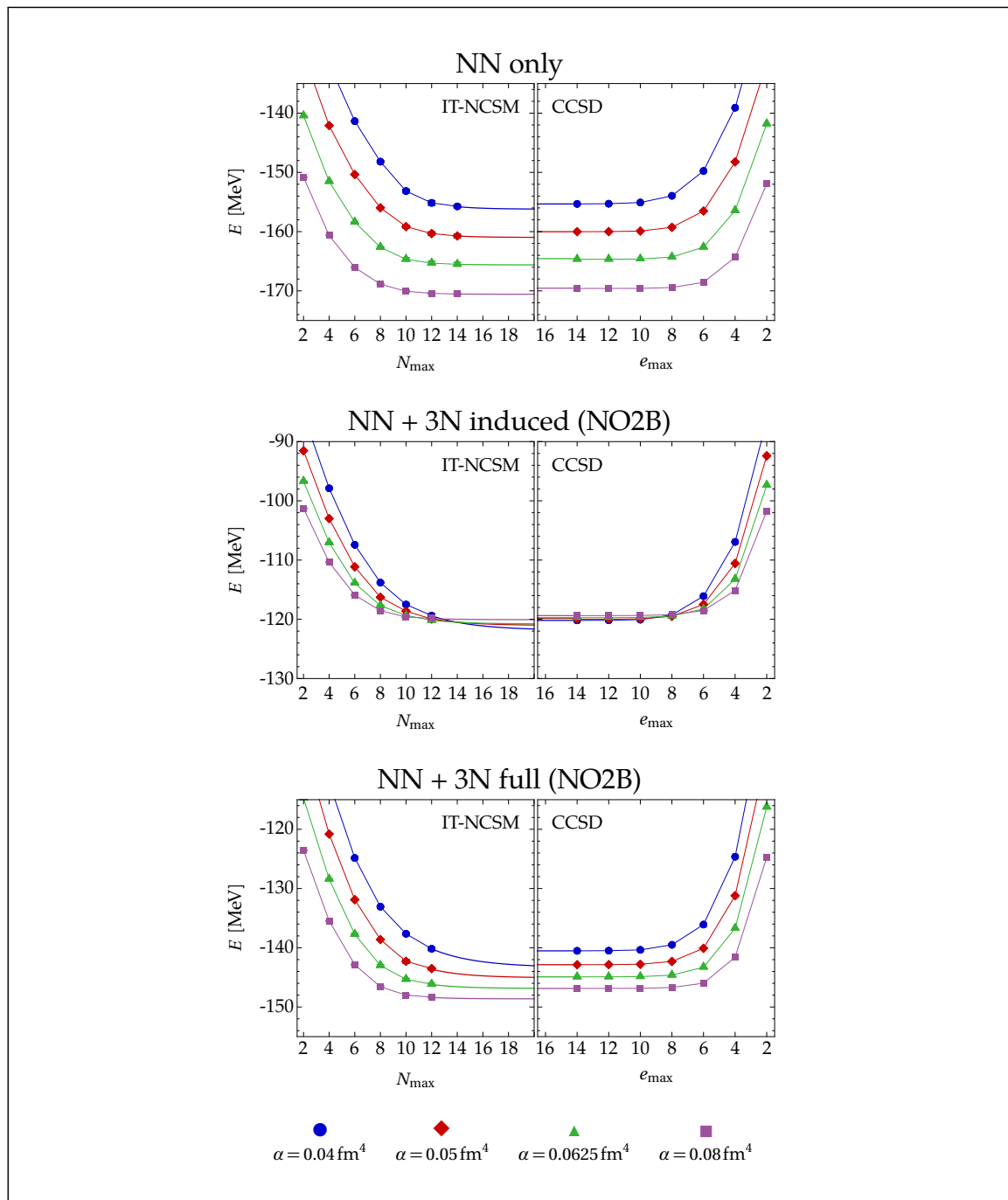


Figure 5.1: Comparison of IT-NCSM and CCSD results for ^{16}O and the three Hamiltonians NN-only, NN+3N-induced, and NN+3N-full for a sequence of SRG flow parameters. The single-particle basis is the harmonic-oscillator basis with oscillator frequency $\hbar\Omega = 20 \text{ MeV}$. For the NN+3N Hamiltonians the NO2B approximation to the 3N interaction was used with $E_{3\max} = 12$.

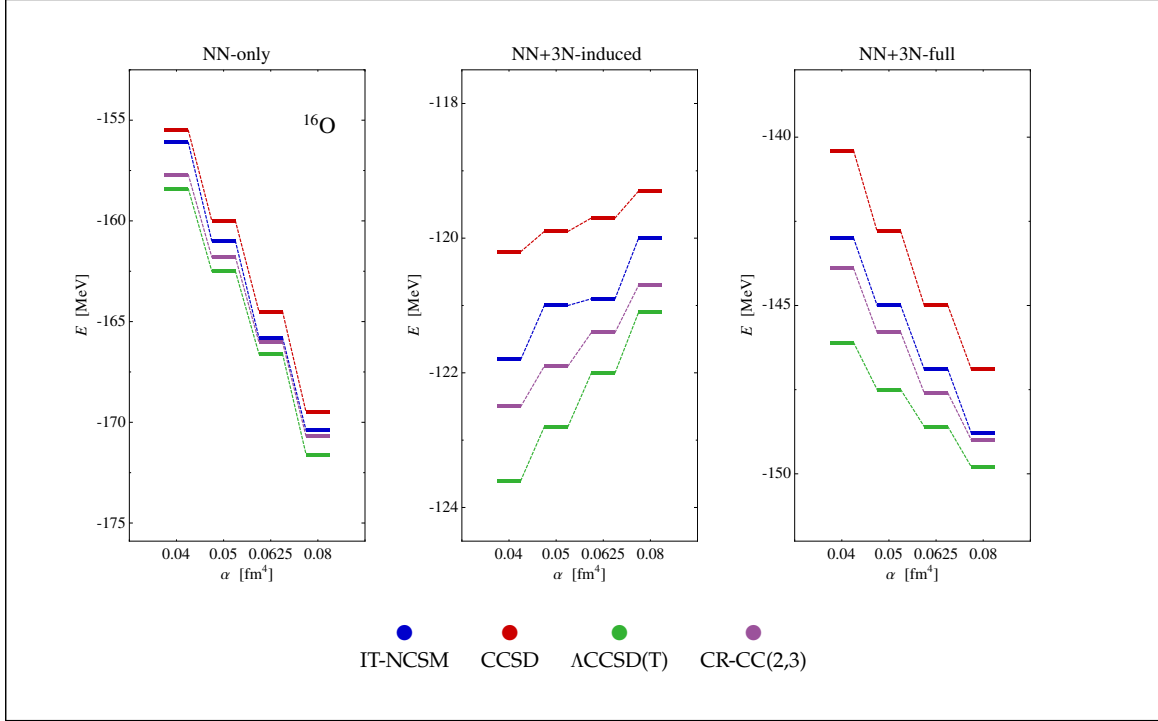


Figure 5.2: Comparison of extrapolated IT-NCSM ground-state energies with converged CCSD, ACCSD(T), and CR-CC(2,3) results for ^{16}O . Parameters of the calculations as in Figure 5.1.

and ACCSD(T) results. This expectation is further confirmed by the CR-CC(2,3) results, which are the more accurate approximation to the exact triples correction, and which lie halfway between the IT-NCSM and ACCSD(T) results, such that in many cases the IT-NCSM and CR-CC(2,3) ground-state energies agree within the remaining uncertainties. Furthermore, the spread between the results for the different many-body methods for individual flow parameters becomes smaller with increasing flow parameter. This is also expected, because, as already mentioned above, for softer interactions approximate many-body methods should perform better. In conclusion, for ^{16}O , Coupled-Cluster theory with singles and doubles excitations combined with a corrective treatment of triples is able to provide ground-state energies that can compete with the quasi-exact diagonalizations that can be performed within the IT-NCSM.

5.2 CCSD with SRG-Transformed Chiral Two-Body Hamiltonians

Calculations using SRG-transformed NN-only Hamiltonians do not provide much useful physical information due to the strong violation of the unitarity of the SRG transformation caused by the omission of SRG-induced three- and higher-body interactions in the NN-only approach. However, by ignoring three-body interactions for the moment, all additional complications related to the handling of 3N interactions are avoided, which for example will later restrict the calculations using 3N interactions to the medium-mass regime. Furthermore, without 3N interactions, CCSD calculations become inexpensive and, therefore, the NN-only framework may be used to demonstrate basic capabilities and limitations of the CCSD implementation itself, without being constrained by limitations of the input Hamiltonian.

Figures 5.3 and 5.4 summarize NN-only results for the reference- and CCSD energy for medium-mass and heavy nuclei ranging from ^{16}O to ^{208}Pb , using both, the harmonic-oscillator (HO) and Hartree-Fock (HF) basis. Considering the reference energies in panel (a), it is apparent that for the HO basis it increases rapidly as one departs from the optimal oscillator frequency, while for the HF case the reference energy is absolutely stable for the whole frequency range considered. It is, therefore, striking to find in panel (b) only small deviations in the final CCSD results in the HO and HF case, for frequencies up to $\hbar\Omega = 32\text{MeV}$. An extreme example for ^{208}Pb is given in Table 5.1: The CCSD energies are all very similar for the HO and HF basis and for both oscillator frequencies $\hbar\Omega = 20$ and 36 MeV . The reference energy, however, differs by up to more than 7 GeV (!). So, at frequency $\hbar\Omega = 36\text{ MeV}$, CCSD contributes about 8 GeV to the energy for the HO basis, while for the HF basis it is only less than 900 MeV, both arriving at the same result within about 200 MeV. This may be regarded as a demonstration of Thouless' theorem [154].

The plots in panel (c) of Figures 5.3 and 5.4 show the convergence of CCSD energies in HF basis with respect to the model space size e_{max} at the optimal oscillator frequency for the individual nuclei. All nuclei show a similar convergence pattern, where at least in $e_{\text{max}} = 14$ model spaces the results are finally fully converged. Therefore, in the NN-only framework, it is possible to obtain converged CCSD results all over the nuclear chart. This is made possible by the spherical formulation of CCSD. For the ^{208}Pb calculations at $e_{\text{max}} = 14$, for example, the m -

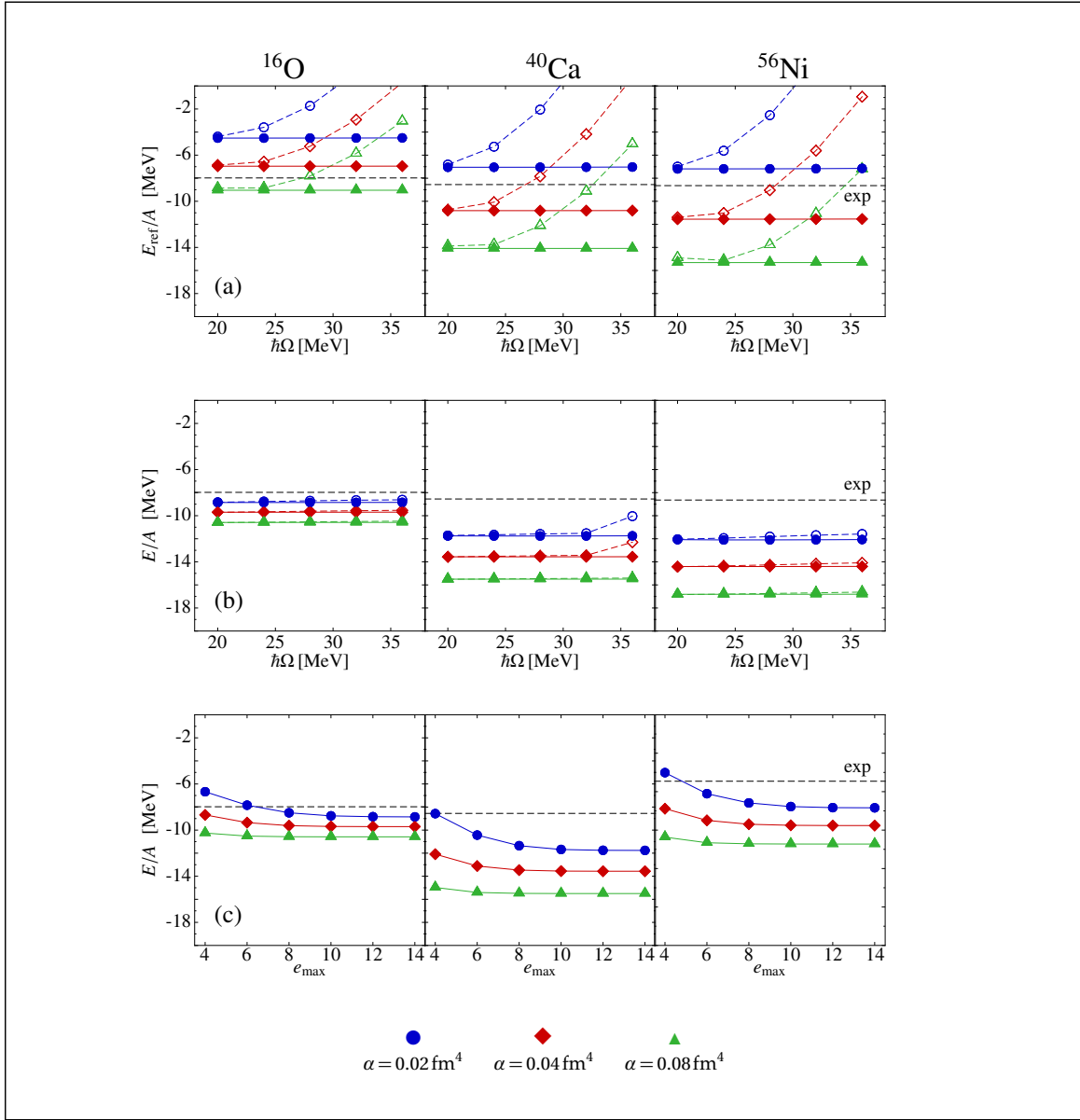


Figure 5.3: Reference energy and CCSD ground-state energy per nucleon for the nuclei ^{16}O , ^{40}Ca and ^{56}Ni , using SRG-transformed chiral $N^3\text{LO}$ two-nucleon interactions for a range of flow parameters. Plots (a) and (b) are obtained from an $e_{\text{max}} = 14$ model space, while for (c) the optimal HO frequencies $\hbar\Omega = 20$ MeV (for ^{16}O) and $\hbar\Omega = 24$ MeV (for ^{40}Ca , ^{56}Ni) are used, which correspond to minima in both, the HO and the HF basis. Open symbols represent the results harmonic-oscillator basis, full symbols the Hartree-Fock basis.

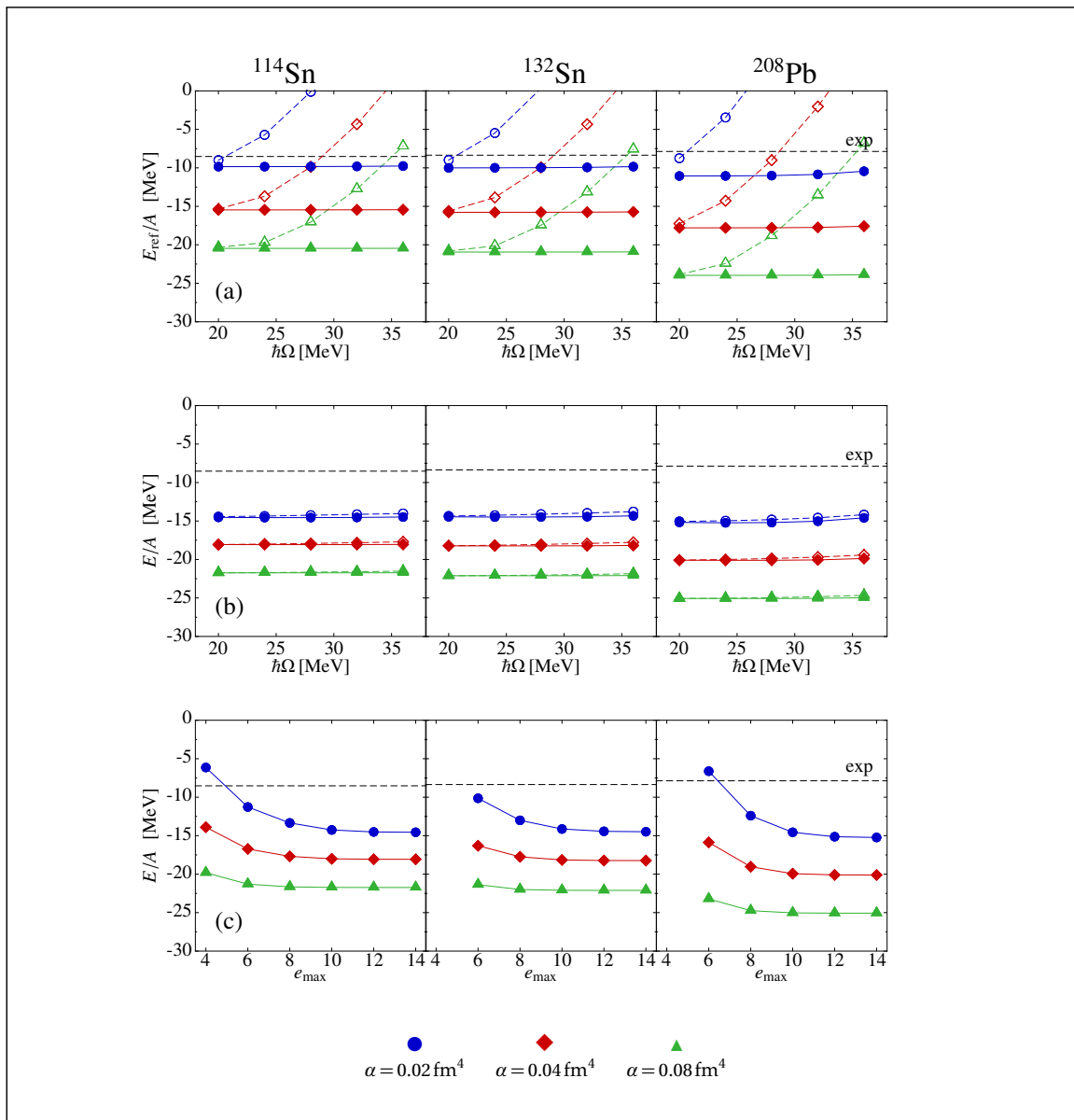


Figure 5.4: As in Figure 5.3 for nuclei ^{114}Sn , ^{132}Sn and ^{208}Pb . In each case the optimal oscillator frequency is $\hbar\Omega = 24 \text{ MeV}$.

| ^{208}Pb : | | |
|--------------------------------|------------------------|---------------------------|
| $\hbar\Omega(\text{HO})$ [MeV] | E_{ref} [MeV] | $E^{(\text{CCSD})}$ [MeV] |
| 20 | -1819 | -3130 |
| 36 | +5025 | -2950 |
| $\hbar\Omega(\text{HF})$ [MeV] | E_{ref} [MeV] | $E^{(\text{CCSD})}$ [MeV] |
| 20 | -2300 | -3157 |
| 36 | -2171 | -3035 |

Table 5.1: Reference energies and CCSD ground-state energies for ^{208}Pb for oscillator frequencies $\hbar\Omega = 20$ MeV and 36 MeV, highlighting Thouless' theorem.

scheme formulation would require to solve the CCSD equations for about 300 billion \hat{T} amplitudes – which is way beyond present capabilities. For the spherical scheme, on the other hand, the number of amplitudes totals to about 600 million, which can be dealt with using modern computers. As mentioned above, comparison with the experimental values at this stage is pointless because of the massive flow-parameter dependence of the energies that does not allow to draw any conclusion about the bare Hamiltonian.

In summary, spherical CCSD with SRG-transformed NN-only Hamiltonians has been demonstrated to be practically applicable to nuclei over a large mass range. This is due to the fact that the interactions considered here are quite soft and well-behaved from a computational point of view. Obviously, (at least) SRG-induced 3N interactions have to be included in the calculation in order to possibly get rid of the flow-parameter dependence and it is expected that at least the chiral 3N interaction needs to be included in any quantitative calculation. However, once 3N interactions are included, the resulting interactions get more difficult to deal with compared to the NN-only case. For example, the CCSD equations usually do not converge for the HO basis if the oscillator frequency does not coincide with the optimal frequency, making using the HF basis mandatory.

5.3 Reduced-Cutoff Chiral Three-Body Interaction

The chiral 3N interaction [155] with regulator cutoff-momentum $\Lambda_{3N} = 500$ MeV can successfully be employed to describe light nuclei [17]. For example, IT-NCSM results for ^4He ground-state energies are presented in Figure 5.5 (top). For the *NN-only* Hamiltonian, the converged energies show a strong dependence on the flow parameter. Therefore, it can be concluded that the unitarity of the SRG transformation is strongly violated by omitting all induced three- and higher-body interactions during the SRG flow. The systematics of the flow-parameter dependence is such that the energy moves downwards for increasing flow parameter. So, from the NN-only plot in Figure 5.5, the bare (untransformed) result for the chiral NN interaction is expected to lie well above the experimental value but the strong flow-parameter dependence prohibits any more detailed prediction. Once the SRG-induced 3N interactions are included in the calculations by using the *NN+3N-induced* Hamiltonian, the flow-parameter dependence of the converged energies practically vanishes. This implies that – for the range of flow parameters considered here – induced four-body interactions are not relevant for the description of the ^4He ground state. Consequently, the NN+3N-induced calculations can be seen as unitarily equivalent to calculations with the chiral NN interaction, which, however, misses the experimental value considerably. The chiral $N^3\text{LO}$ two-nucleon interaction is, therefore, not sufficient for reproducing the ^4He ground-state energy. This is not too surprising since chiral 3N interactions already appear at $N^2\text{LO}$ in the Weinberg power counting, which have not yet been taken into account. Once these chiral 3N interactions are included via the *NN+3N-full* Hamiltonian, the ground-state energies still show no flow-parameter dependence which allows to make a prediction for the bare NN+3N-full Hamiltonian and which also shows good agreement with the experimental value. The flow-parameter independence of the NN+3N-full results provide the important information that SRG-induced four-body interactions out of the initial 3N interaction are not relevant in this case.

For the heavier nucleus ^{12}C shown in Figure 5.5 (middle), the situation is similar. The results for the NN-only Hamiltonian show a strong flow-parameter dependence and thus do not allow for any predictions for the bare chiral NN interaction. Inclusion of the induced 3N interaction eliminates the flow-parameter dependence but as in the case of ^4He , the prediction for the chiral NN interaction is clearly underbound with respect to experiment. The effect of the initial chiral 3N interaction moves the results towards the experimental value, with a

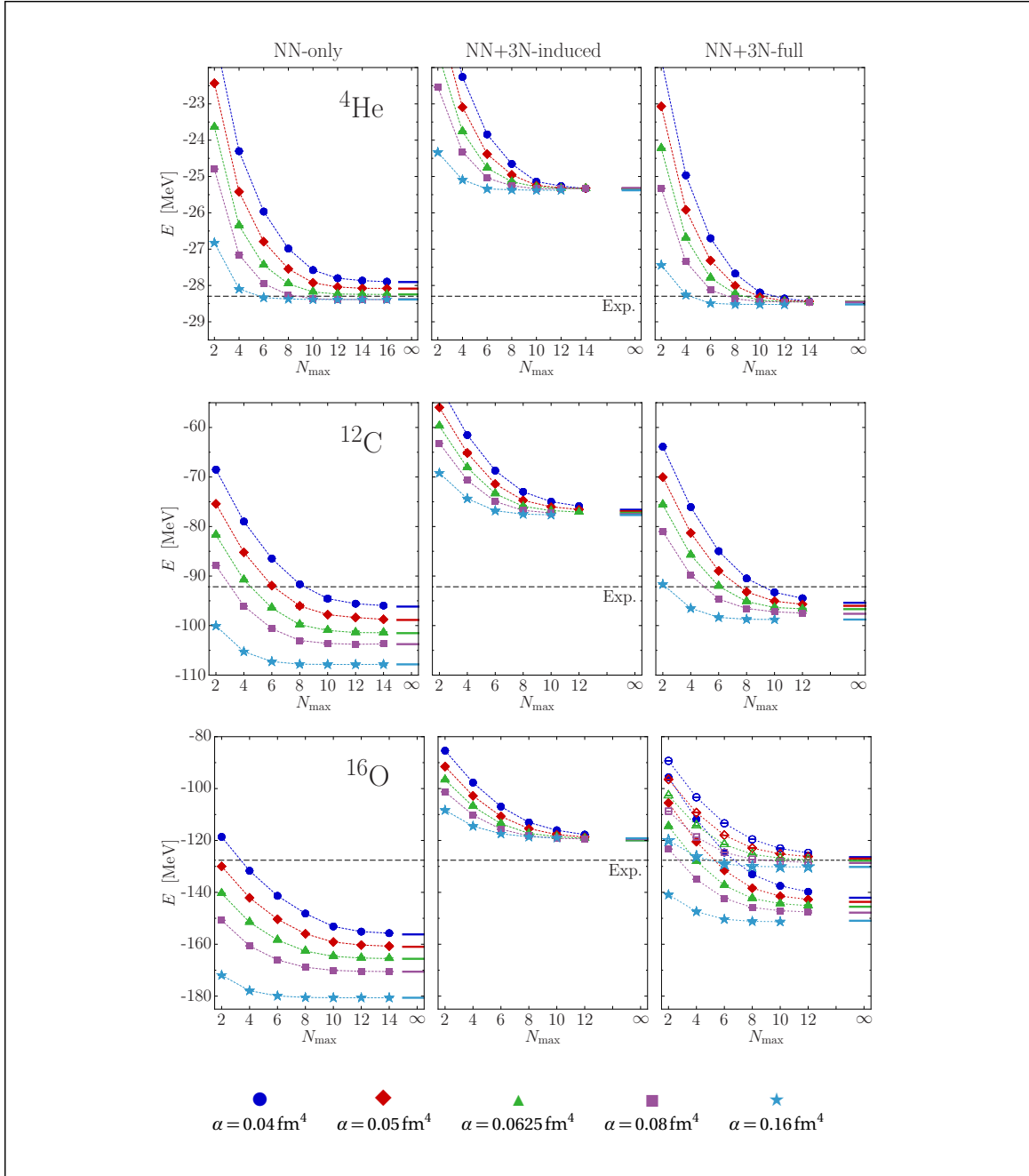


Figure 5.5: IT-NCSM ground-state energies for the nuclei ${}^4\text{He}$, ${}^{12}\text{C}$ and ${}^{16}\text{O}$ for the three Hamiltonians NN-only, NN+3N-induced, and NN+3N-full. For ${}^{16}\text{O}$, also the results for the 400 MeV cutoff-momentum NN+3N-full Hamiltonian are shown (open symbols), which exhibit a much reduced flow-parameter dependence. The calculations were performed using a HO basis with $\hbar\Omega = 20$ MeV and with full inclusion of 3N interactions.

slight overbinding for the flow-parameter values considered here. But since for ^{12}C there is an emerging flow-parameter dependence for the NN+3N-full results, no safe statement can be made for the bare NN+3N-full Hamiltonian. It is clear that the violation of unitarity of the SRG transformation is caused by the omission of induced 4N interactions out of the *initial* 3N – the initial NN interaction can be ruled out as a source of sizeable induced 4N because of the absent flow-parameter dependence of the energies for the NN+3N-induced Hamiltonian.

This flow-parameter dependence of the NN+3N-full results is enhanced for increasing mass number. Considering ^{16}O , in Figure 5.5 (bottom), the results for the *standard NN+3N-full Hamiltonian* (full symbols in the NN+3N-full plot), with the $\Lambda_{3\text{N}} = 500$ MeV cutoff momentum in the regularization function [155], shows a flow-parameter dependence of about 10 MeV for the particular range of flow parameters considered here. As for ^{12}C , the flow-parameter dependence is easily found to be caused by at least 4N interactions induced out of the initial 3N. At this point all predictive capabilities for the NN+3N-full Hamiltonian are lost within the framework used so far. The inclusion of induced 4N interactions in order to reduce the flow-parameter dependence is computationally too demanding and, therefore, a *modified interaction* is used in the following: The NN+3N-full plot for ^{16}O also shows results for a *reduced-cutoff interaction* (open symbols), in which the regulator cutoff-momentum of the chiral 3N has been lowered from its standard value $\Lambda_{3\text{N}} = 500\text{MeV}$ to $\Lambda_{3\text{N}} = 400\text{MeV}$ and the low-energy constant c_E has been refitted to reproduce the ^4He binding energy, while the other LEC that is exclusively related to chiral 3N interactions at N^2LO , c_D , which is fitted to the triton half-life, remains unchanged. The reason why c_D has not to be adapted to the new parameters of the interaction is that altering the 3N cutoff or c_E does not affect the results for the triton half-life. The values of the LECs for various choices of $\Lambda_{3\text{N}}$ can be found in Table 5.2. The main motivation for lowering the cutoff momentum is the observation that this way off-diagonal matrix elements in the 3N interaction, which are a major source of induced many-body interactions, get suppressed (a detailed discussion can be found in [156,157]). Using this 400 MeV cutoff interaction, the ^{16}O ground-state energies show a much reduced flow-parameter dependence, which is the purpose of reducing the 3N cutoff in the first place, as discussed below. Furthermore, the ground-state energies now lie on top of the experimental value. Later on, for calculations of heavy nuclei in Section 5.9.3, also the $\Lambda_{3\text{N}} = 350\text{MeV}$ interaction will be used to study SRG-induced many-body interactions.

| Λ_{3N} [MeV] | c_1 [GeV ⁻¹] | c_3 [GeV ⁻¹] | c_4 [GeV ⁻¹] | c_D | c_E |
|-------------------------|-------------------------------|-------------------------------|-------------------------------|-------|--------|
| 500 | -0.81 | -3.2 | 5.4 | -0.2 | -0.205 |
| 450 | -0.81 | -3.2 | 5.4 | -0.2 | -0.016 |
| 400 | -0.81 | -3.2 | 5.4 | -0.2 | 0.098 |
| 350 | -0.81 | -3.2 | 5.4 | -0.2 | 0.205 |

Table 5.2: Low-energy constants that parametrize the chiral 3N interaction, for various choices of the 3N regular momentum cutoff Λ_{3N} [86]. The constants c_1 , c_3 , and c_4 are fixed through the chiral NN interaction where they enter as well, and c_D also remains unchanged because it is fitted to the triton halflife which is not affected by altering Λ_{3N} . The final LEC c_E is fitted to reproduce the ${}^4\text{He}$ ground-state energy.

Since for the nucleus ${}^{16}\text{O}$ and beyond only the reduced-cutoff interaction allows to obtain more or less flow-parameter independent ground-state energies, it will be the customary choice for medium-mass nuclei. In Figures 5.6 and 5.7 still both, the standard and reduced-cutoff interaction are used for comparison, but in the following sections only the reduced-cutoff interaction will be considered. Figures 5.6 and 5.7 show CCSD ground-state energies for the medium-mass closed-shell nuclei ${}^{16,24}\text{O}$ and ${}^{40,48}\text{Ca}$, using a harmonic-oscillator basis at fixed oscillator frequency $\hbar\Omega = 20\text{ MeV}$. The 3N interactions are included via NO2B, but the large model spaces considered here require an additional cutoff parameter $E_{3\text{max}}$ in the three-body matrix elements, as discussed in more detail in Section 5.4. For the present results $E_{3\text{max}} = 14$ was used. Although this cut is in principle expected to affect the results – particularly for the heavier nuclei ${}^{40,48}\text{Ca}$ – on the large scales used for the plots such $E_{3\text{max}}$ -effects do not play a significant role. Figures 5.6 and 5.7 show essentially the same qualitative behavior as the IT-NCSM results for ${}^{16}\text{O}$, only on a larger scale. In all cases, the NN+3N-induced Hamiltonian provides results that are practically flow-parameter invariant and tend to underbind. The NN+3N-full Hamiltonian with standard 500 MeV regularization of the chiral 3N interaction (full symbols in the NN+3N-full plot) shows a very strong flow-parameter dependence and for the flow parameters considered here, the evolved NN+3N-full Hamiltonians show massive overbinding compared to experiment, which is even comparable to the NN-only case. On the other hand, the NN+3N-full Hamiltonian with the reduced-cutoff 3N interaction (open symbols in the NN+3N-full plot) provides results with a much reduced flow-parameter dependence at the level of the NN+3N-induced results, even for the heaviest nucleus

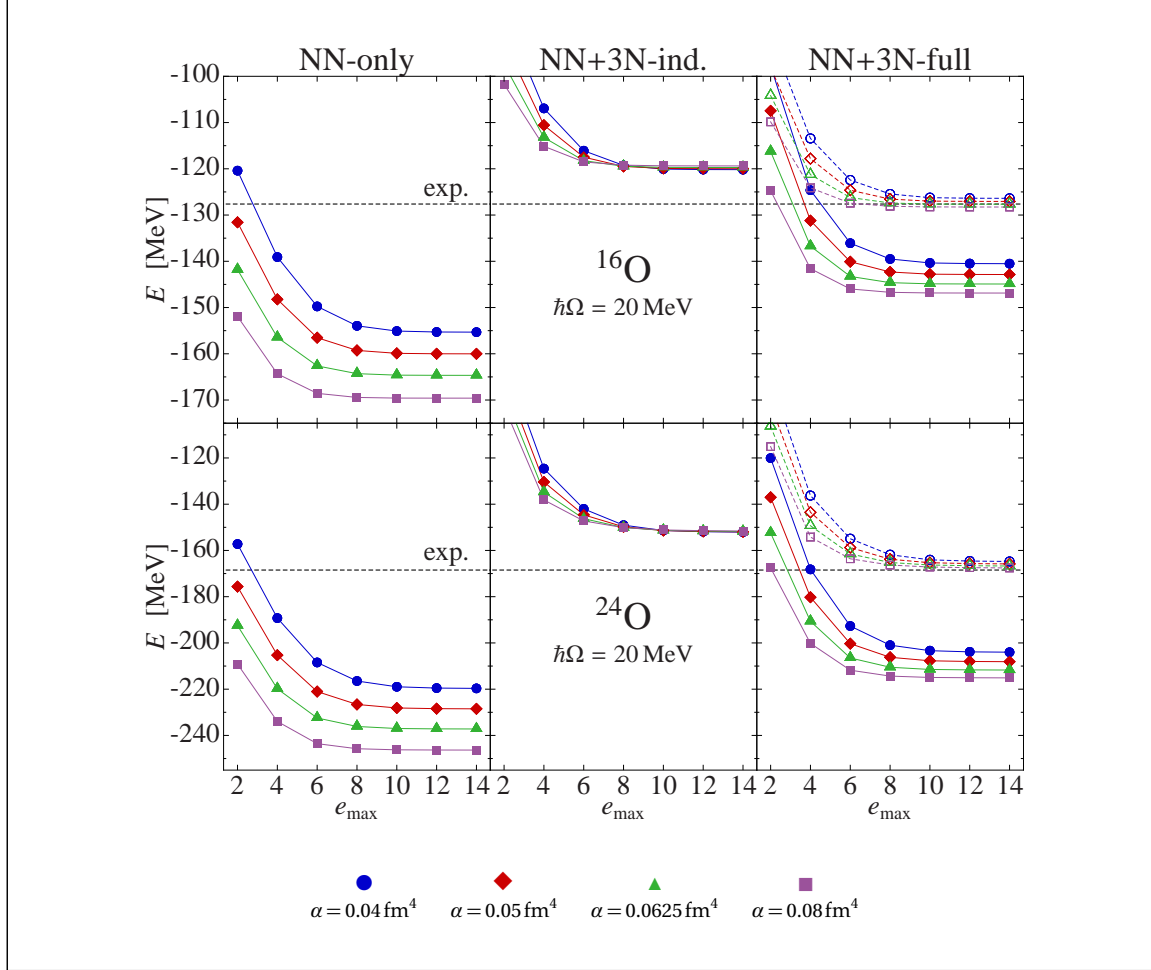
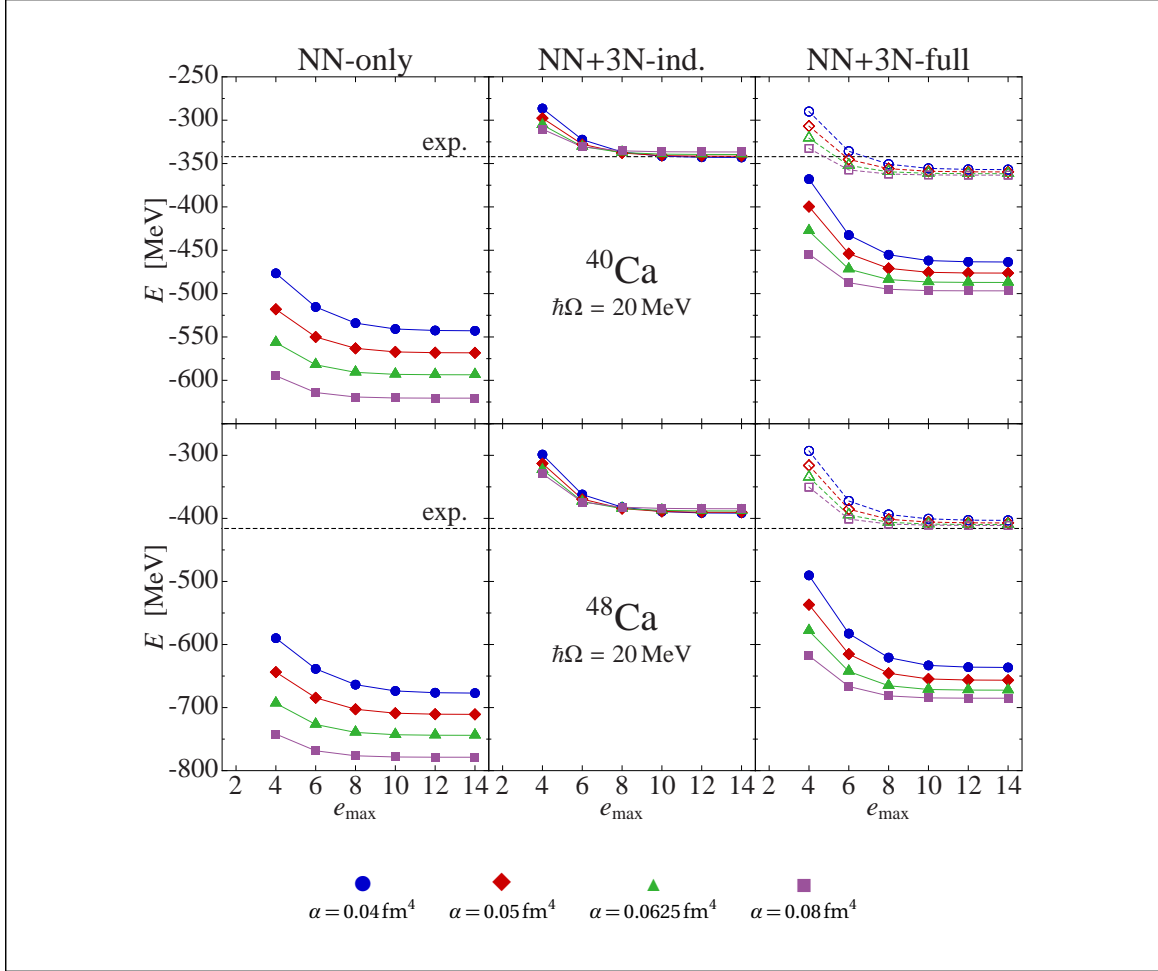


Figure 5.6: Ground-state energies from CCSD for ^{16}O and ^{24}O for the NN-only, NN+3N-induced, and NN+3N-full Hamiltonians. For the NN+3N-full Hamiltonian, the standard regularization ($\Lambda_{3\text{N}} = 500$ MeV) and the low-cutoff variant ($\Lambda_{3\text{N}} = 400$ MeV, open symbols) are shown. The underlying single-particle basis is the harmonic-oscillator basis and for all 3N Hamiltonians the NO2B approximation with $E_{3\text{max}} = 14$ is used. Figure taken from [92].


 Figure 5.7: As in Figure 5.6 for the nuclei ^{40}Ca and ^{48}Ca .

under consideration. Therefore, it is possible to use these results to make predictions for the reduced-cutoff NN+3N-full Hamiltonian. Furthermore, the agreement with the experimental values is impressive: Except for ^{40}Ca , for which the NN+3N-induced energies already lie on top of experiment, all theoretical values are very close to the experimental ones, highlighting the predictive power of chiral Hamiltonians, even in the medium-mass regime. The good performance of the reduced-cutoff interaction is remarkable, considering the fact that no information beyond ^4He went into its construction. In the following sections various aspects of this interaction are investigated, also using more advanced many-body techniques.

5.4 Relevance of the $E_{3\text{max}}$ Cut

Calculations using three-body Hamiltonians are challenging because of the enormous number of matrix elements involved. In most cases, a full representation of the three-body Hamiltonian in an e_{max} -truncated single-particle basis can neither be handled in the many-body calculation nor can it be generated in the first place. Therefore, an additional truncation parameter is required in order to reduce the representation of the Hamiltonian to a manageable size. As already mentioned in Section 5.3, the representation of the three-body Hamiltonian is constrained to matrix elements $\langle pqr|\hat{w}|stu\rangle$ satisfying an energy truncation of the form

$$\max(e_p + e_q + e_r, e_s + e_t + e_r) \leq E_{3\text{max}} \quad (5.1)$$

where $E_{3\text{max}}$ is the truncation parameter and $e_i = 2n_i + l_i$ denotes the single-particle harmonic-oscillator energy quantum number. Current typical values of $E_{3\text{max}}$ are at the order of 14. Since for an $e_{\text{max}} = 12$ calculation the maximum allowed value of $e_p + e_q + e_r$ would be 36, $E_{3\text{max}} = 14$ represents a potentially serious cut whose impact on the results of many-body calculations requires careful inspection.

It should be noted that the following discussion is based on 3N matrix elements evolved in the SRG model space corresponding to the so-called 40C parametrization (see Section 5.9.2) used for most of the medium-mass calculations presented in this work or in calculations of other research groups [17, 29, 30, 86, 92, 96, 158], which makes it worthwhile to investigate the properties of these matrix elements. However, as discussed in Section 5.9.2, the 40C model space is not sufficient any more for heavier nuclei. As a consequence, for the 40C SRG model space parametrization, the $E_{3\text{max}}$ effect is artificially enhanced for the heavier nuclei considered

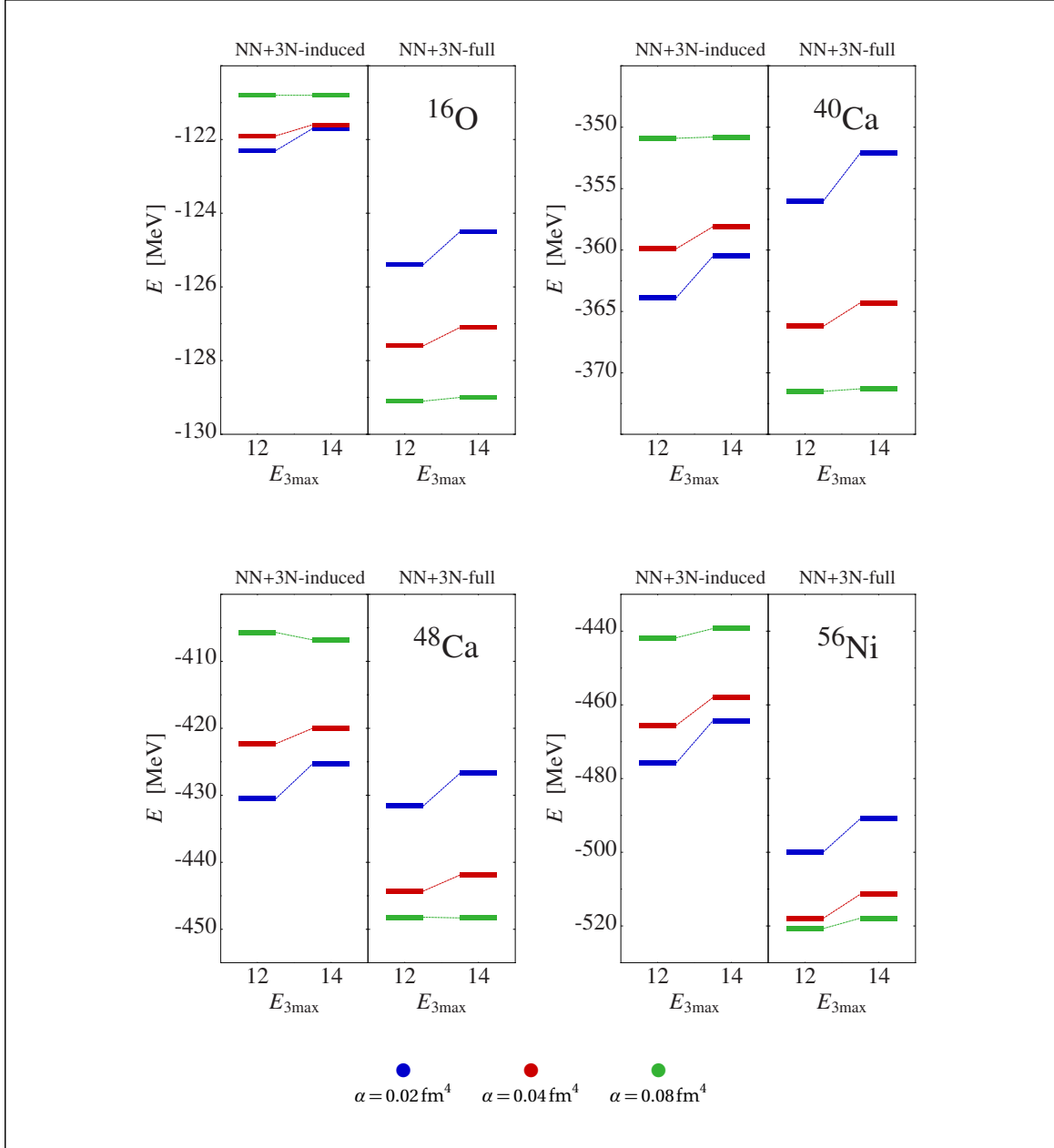


Figure 5.8: Comparison of CCSD ground-state energies for the nuclei ^{16}O , ^{40}Ca , ^{48}Ca , and ^{56}Ni for the NN+3N-induced and NN+3N-full Hamiltonians in NO2B approximation with $E_{3\max} = 12$ and $E_{3\max} = 14$. The calculations were performed in a HF basis with $\hbar\Omega = 24 \text{ MeV}$ and $e_{\max} = 12$.

in this section. This issue is again addressed in Section 5.9.2, where results for considerably larger SRG model spaces are presented.

Figure 5.8 shows a compilation of CCSD ground-state energies for medium-mass nuclei ranging from ^{16}O to ^{56}Ni , for the NN+3N-induced and NN+3N-full Hamiltonians in NO2B approximation and the usual range of SRG flow parameters. The calculations have been performed for $E_{3\text{max}} = 12$ as well as $E_{3\text{max}} = 14$, and the effect of the $E_{3\text{max}}$ cut is estimated by the deviation of the two sets of results. The effect of $E_{3\text{max}}$ clearly depends on how far the Hamiltonian has been evolved: Considering the softest ($\alpha = 0.08\text{ fm}^4$) Hamiltonians, for all but the heaviest nuclei ^{56}Ni the impact of $E_{3\text{max}}$ is practically negligible. For ^{56}Ni , the $E_{3\text{max}}$ cut has an effect of about of 3 MeV, so it is still small compared to the total energy scale of about 500 MeV. For the harder interactions, the $E_{3\text{max}}$ cut shows sizeable effects already for the lighter nuclei, where the hardest interactions show the largest change in the energies. For ^{56}Ni and $\alpha = 0.02\text{ fm}^4$, for instance, the ground-state energies for the NN+3N-induced Hamiltonian change about 12 MeV, which corresponds to about 2.5 % of the total binding energy.

For the CCSD ground-state energies, there is also an interesting systematic effect of $E_{3\text{max}}$ on the flow-parameter dependence. As is apparent from Figure 5.8, for the NN+3N-induced Hamiltonian the flow-parameter dependence decreases when $E_{3\text{max}}$ is increased and it is an interesting question how much the flow-parameter dependence will be eventually reduced in the $E_{3\text{max}} \rightarrow \infty$ limit. For the NN+3N-full Hamiltonians, on the other hand, the flow-parameter dependence even gets increased. This behavior is a consequence of the ordering of the CCSD ground-state energies with respect to the SRG flow parameter. According to Figure 5.7, for instance, the three-body parts of the NN+3N-induced and NN+3N-full Hamiltonians are repulsive. Consequently, the ground-state energies are expected to move upwards as more of the 3N interactions is included by increasing $E_{3\text{max}}$. Furthermore, since for the NN+3N-induced Hamiltonian the CCSD energies for smaller flow parameters lie below the energies for larger flow parameters and harder Hamiltonians imply larger $E_{3\text{max}}$ effects, the flow-parameter dependence is reduced. For the NN+3N-full Hamiltonian, on the other hand, the CCSD energy ordering is such that the energies for the harder Hamiltonians already lie above the energies for the softer Hamiltonians and, therefore, increasing $E_{3\text{max}}$ only enlarges the flow-parameter dependence. As can exemplarily be seen in Figure 5.7, the contribution of the induced 3N is much larger than it is for the low-cutoff initial 3N. Therefore, it might be assumed that relative changes in the induced 3N may be much more visible than relative changes in the initial 3N. Consequently,

| | $\alpha [\text{fm}^4]$ | $\Delta(E_{3\max})$ | $\Delta(E_{3\max})$ |
|------------------|------------------------|----------------------|---------------------|
| | | NN+3N-induced [%] | NN+3N-full [%] |
| ^{16}O | 0.02 | 0.5 | 0.7 |
| | 0.04 | 0.2 | 0.4 |
| | 0.08 | 0.0 | 0.1 |
| ^{48}Ca | 0.02 | 1.2 | 1.1 |
| | 0.04 | 0.5 | 0.5 |
| | 0.08 | 0.2 | 0.0 |

Table 5.3: Comparison of the difference in the CCSD ground-state energies for $E_{3\max} = 12$ and $E_{3\max} = 14$ for the NN+3N-induced and NN+3N-full Hamiltonian in NO2B approximation, for the nuclei ^{16}O and ^{48}Ca . The calculations were performed using a HF basis with $\hbar\Omega = 24$ MeV and at $e_{\max} = 12$.

ground-state energies for the NN+3N-induced and the NN+3N-full Hamiltonian should show a similar behavior, since the induced 3N interaction is of course also included in the latter. And in fact, the changes in the ground-state energies with increasing $E_{3\max}$ for NN+3N-induced and NN+3N-full are almost identical, as is evident from Table 5.3, hinting at the induced 3N as the driving cause.

The absolute values of the difference of the ground-state energies corresponding to $E_{3\max} = 12$ and $E_{3\max} = 14$ grow with increasing mass number, but so do the overall energy scales. Thus, it cannot immediately be determined from Figure 5.8 how the *relative* effect of $E_{3\max}$ to the ground-state energies evolves with mass number. To this end, Figure 5.9 shows the relative size $\Delta(E_{3\max})$ of the $E_{3\max}$ effect normalized to the $E_{3\max} = 14$ ground-state energy, given by

$$\Delta(E_{3\max}) = \frac{|E(E_{3\max} = 14) - E(E_{3\max} = 12)|}{E(E_{3\max} = 14)/100} \% . \quad (5.2)$$

The relative $E_{3\max}$ effect $\Delta(E_{3\max})$ shows a systematic increase with mass number so that relative accuracy is increasingly lost as one goes to larger masses. For the hardest ($\alpha = 0.02 \text{ fm}^4$) NN+3N-induced Hamiltonian, the relative $E_{3\max}$ effect ranges from 0.5 % for ^{16}O to 2.5 % for ^{56}Ni , which is already twice as large as for ^{48}Ca (1.2 %). For the NN+3N-full Hamiltonian, the relative size grows from 0.5 % for ^{16}O to about 2 % for ^{56}Ni . For the NN+3N-full Hamiltonian at $\alpha = 0.02 \text{ fm}^4$, there is no such drastic increase compared to the NN+3N-induced case, but there is for $\alpha = 0.04 \text{ fm}^4$, which triples its size going from ^{48}Ca to ^{56}Ni . Therefore, using hard interactions beyond the mass region $A \approx 60$, the $E_{3\max} = 14$ cut is expected to

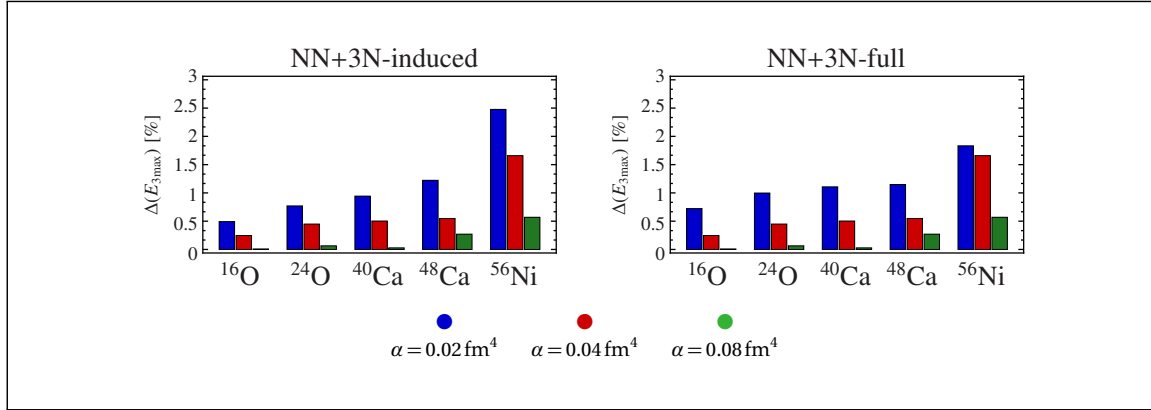


Figure 5.9: Change of CCSD ground-state energies for the NN+3N-induced and the NN+3N-full Hamiltonian in NO2B approximation when increasing $E_{3\max} = 12$ to $E_{3\max} = 14$, normalized to the $E_{3\max} = 14$ ground-state energy. The calculations were performed using a HF basis with $\hbar\Omega = 24$ MeV and at $e_{\max} = 12$.

become a major source of uncertainty ². The soft $\alpha = 0.08 \text{ fm}^4$ Hamiltonians also show a systematic increase but the effect itself is considerably smaller so that even for ^{56}Ni the relative $E_{3\max}$ effect does not exceed 0.5 %.

5.5 The $\Lambda\text{CCSD(T)}$ Energy Correction

At the level of CCSD, the cluster expansion is not yet sufficiently converged in order for higher-excitation rank effects to be negligible. In this section, $\Lambda\text{CCSD(T)}$ is used to assess the size of triples corrections. Since $\Lambda\text{CCSD(T)}$ tends to overshoot the actual triples correction [153], it gives a more conservative estimate of triples- and higher-excitation contributions than, e.g., CR-CC(2,3) would do. Nevertheless, $\Lambda\text{CCSD(T)}$ and CR-CC(2,3) give sufficiently similar results so that the conclusions drawn in this section do not depend on the actual triples correction method used.

Figure 5.10 shows the convergence of ground-state energies from CCSD (open symbols) and $\Lambda\text{CCSD(T)}$ (full symbols), for medium-mass nuclei for the NN+3N-induced and low-cutoff NN+3N-full Hamiltonian with respect to the model-space size. As in the case of CCSD, the $\Lambda\text{CCSD(T)}$ energies are sufficiently converged in

²In Section 5.5 it is shown that the relative importance of $\Lambda\text{CCSD(T)}$ grows with a slower rate than the relative $E_{3\max}$ effect, so $E_{3\max}$ is presumably the more limiting factor for $A > 60$ nuclei regarding accuracy.

order to allow extrapolations to the $e_{\max} \rightarrow \infty$ limit. In Figure 5.11, the CCSD and Λ CCSD(T) results from the largest model spaces are compared. For the NN+3N-full Hamiltonian at $\alpha = 0.02 \text{ fm}^4$, the Λ CCSD(T) correction provides 6 MeV more binding energy for ^{16}O , and 25 MeV for ^{48}Ca . For the soft Hamiltonians at $\alpha = 0.08 \text{ fm}^4$, the binding energy is increased by 1.5 MeV for ^{16}O and 10 MeV for ^{48}Ca . Therefore, in all cases – even for the softest Hamiltonians – the Λ CCSD(T) energy correction gives significant contributions. Since for the NN+3N-induced Hamiltonian the CCSD energies corresponding to smaller values of α already lie below energies for larger α , and smaller α cause even larger Λ CCSD(T) energy corrections, the flow-parameter dependence is increased after including the Λ CCSD(T) correction. On the other hand, for the NN+3N-full Hamiltonian the ordering of the CCSD results regarding flow parameter is reversed and the flow-parameter dependence is decreased by Λ CCSD(T). So the triples excitations correction has the opposite effect on the flow-parameter dependence than increasing the $E_{3\max}$ cut has.

Assuming fast convergence of the cluster expansion, which is justified by, e.g., Figure 5.19 in Section 5.8.1, $\delta E^{(\Lambda\text{CCSD(T)})}$ dominates over higher-order corrections, i.e.,

$$|\delta E^{(\Lambda\text{CCSD(T)})}| \gg |E_{\text{exact}} - E^{(\Lambda\text{CCSD(T)})}|. \quad (5.3)$$

Therefore, the size of $\delta E^{(\Lambda\text{CCSD(T)})}$ may be used to estimate the size of the contribution of the neglected higher excitation ranks of the cluster operator. Figure 5.12 shows the relative importance of the Λ CCSD(T) correction normalized to the total energy according to

$$\Delta(\Lambda\text{CCSD(T)}) = \frac{|\delta E^{(\Lambda\text{CCSD(T)})}|}{E^{(\Lambda\text{CCSD(T)})}/100} \%. \quad (5.4)$$

For all nuclei considered, $\delta E^{(\Lambda\text{CCSD(T)})}$ makes up 3-6 % of the total binding energy for the $\alpha = 0.02 \text{ fm}^4$ Hamiltonians while its contributions for the $\alpha = 0.08 \text{ fm}^4$ Hamiltonians are only about 1-2 %. Thus, using *soft* Hamiltonians, quite accurate calculations can be performed, even for the heavier nuclei. Unlike the $E_{3\max}$ cut, the relative uncertainties due to the cluster truncation seem not to increase strongly with mass number. So the method should be applicable with similar relative accuracy even in the $A > 60$ mass region.

The Λ CCSD(T) correction may also be used to study the feasibility of CCSDT. Unlike Λ CCSD(T), including the full triple excitations via CCSDT leads to the non-linear CCSDT equations which have to be solved *iteratively*, which requires to store

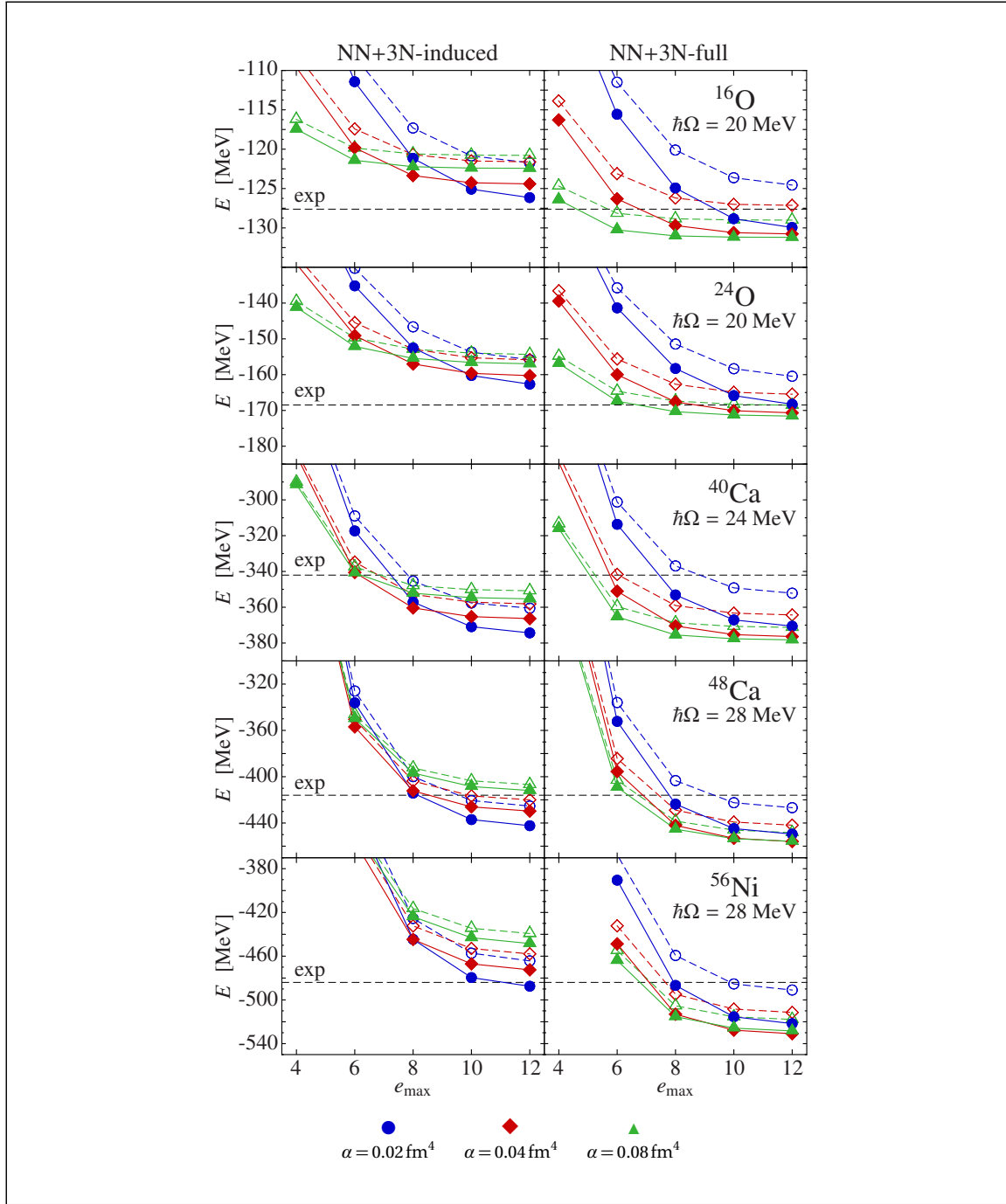


Figure 5.10: Convergence of CCSD (open symbols) and Λ CCSD(T) ground-state energies with respect to model-space size for the nuclei $^{16,24}\text{O}$, $^{40,48}\text{Ca}$ and ^{56}Ni for the NN+3N-induced and NN+3N-full Hamiltonian in NO2B approximation with $E_{3\text{max}} = 14$. The calculations employed a HF basis. Figure taken from [92].

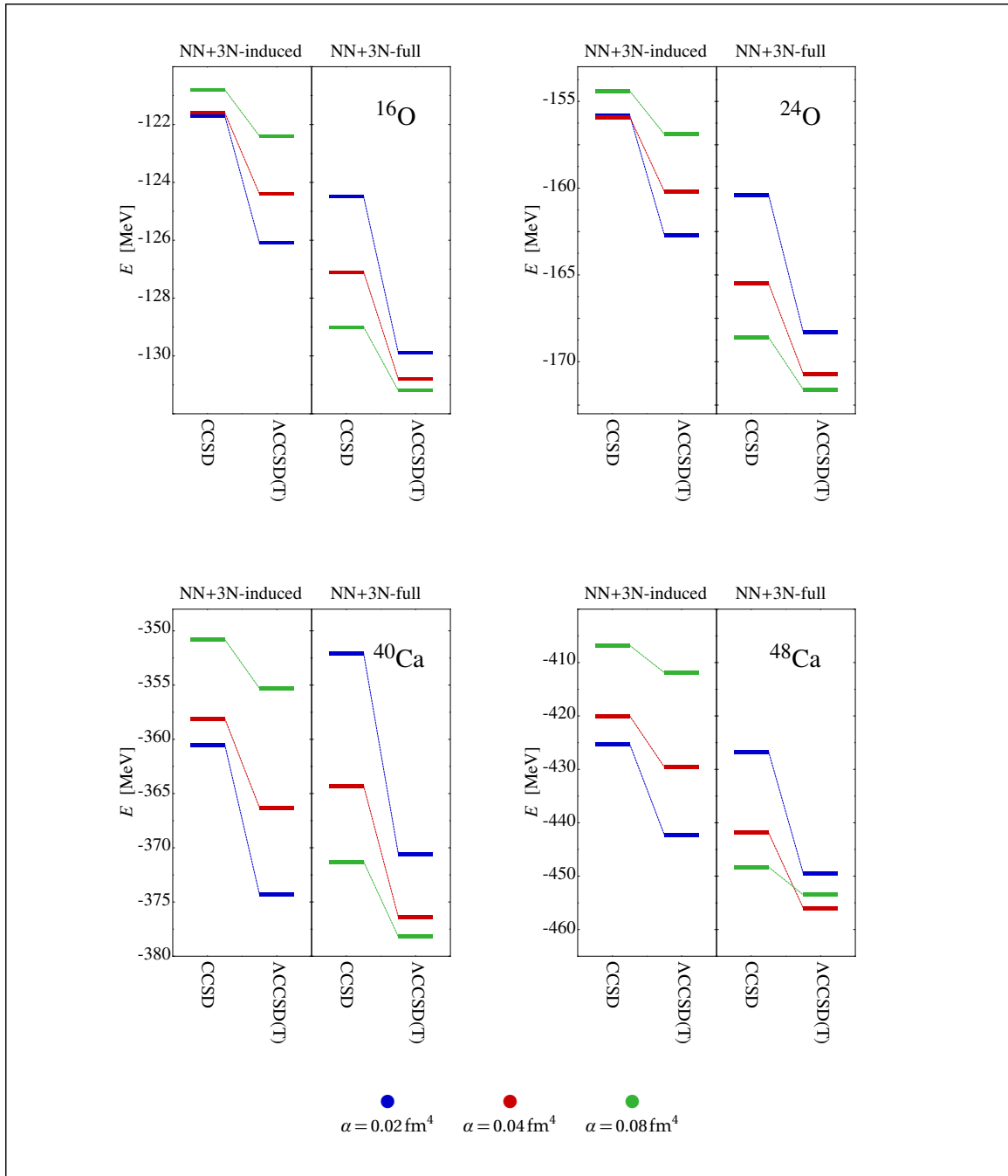


Figure 5.11: Comparison of the CCSD and Λ CCSD(T) ground-state energies from Figure 5.10 for the $e_{\max} = 12$ model space.

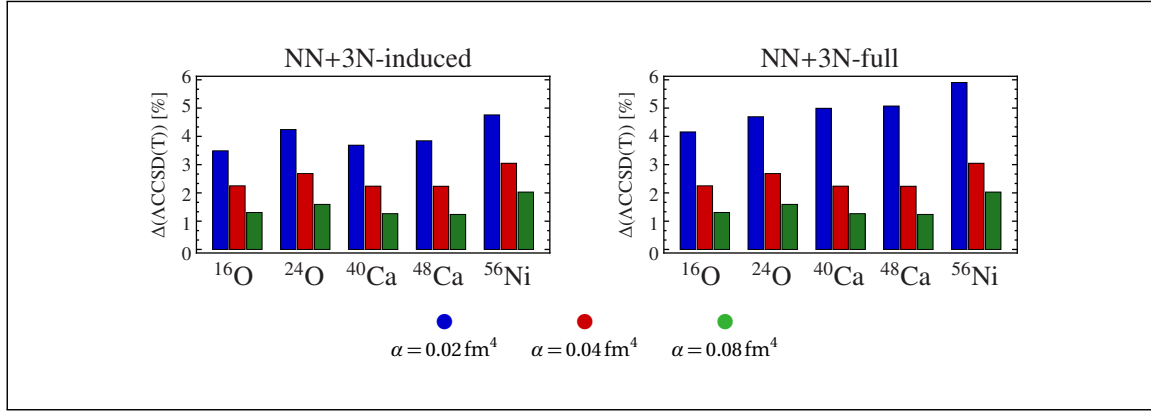


Figure 5.12: Relative importance of the $\Delta\text{ACCSD}(T)$ energy correction, normalized to the total energy $E^{(\text{ACCSD}(T))}$.

all \hat{T}_3 amplitudes. Since there are too many of them – even in the spherical scheme – some kind of truncation has to be introduced. An obvious choice is an $E_{3\text{max}}(\hat{T}_3)$ cut, analogous to the $E_{3\text{max}}$ used for three-body matrix elements. This way the part of \hat{T}_3 that generates the energetically lowest excitations would be considered which are also expected to be the most relevant for a ground-state description. Since $\delta E^{(\text{ACCSD}(T))}$ is given by

$$\delta E^{(\text{ACCSD}(T))} = \frac{1}{(3!)^2} \sum_{\substack{abc \\ ijk}} \tilde{\lambda}_{abc}^{ijk} \frac{1}{\epsilon_{ijk}^{abc}} \tilde{t}_{ijk}^{abc}, \quad (5.5)$$

where \tilde{t}_{ijk}^{abc} are approximations to the amplitudes t_{ijk}^{abc} of \hat{T}_3 , the effect of the $E_{3\text{max}}(\hat{T}_3)$ cut can be simulated in $\text{ACCSD}(T)$ by constraining the \tilde{t}_{ijk}^{abc} accordingly. If $\text{ACCSD}(T)$ is a good approximation to CCSDT, one may assume that both methods show a similar $E_{3\text{max}}(\hat{T}_3)$ -dependence,

$$E^{(\text{CCSDT})}(E_{3\text{max}}(\hat{T}_3)) \approx E^{(\text{ACCSD}(T))}(E_{3\text{max}}(\hat{T}_3)) \quad (5.6)$$

and so $E^{(\text{ACCSD}(T))}(E_{3\text{max}}(\hat{T}_3))$ may be used to find the relevant $E_{3\text{max}}(\hat{T}_3)$ range. Figure 5.13 shows the $E_{3\text{max}}(\hat{T}_3)$ -dependence of $\delta E^{(\text{ACCSD}(T))}$ for ^{16}O with the NN+3N-full Hamiltonian which is already very soft at $\alpha = 0.08 \text{ fm}^4$. The energy correction is sufficiently converged for $E_{3\text{max}}(\hat{T}_3)$ -values of about 25 which is beyond present capabilities to store the corresponding amplitudes. Very optimistic estimates would allow for $E_{3\text{max}}(\hat{T}_3) = 20$ calculations, which captures a significant portion of the correction but would not allow to detect convergence, even for this light nucleus and large SRG flow parameter.

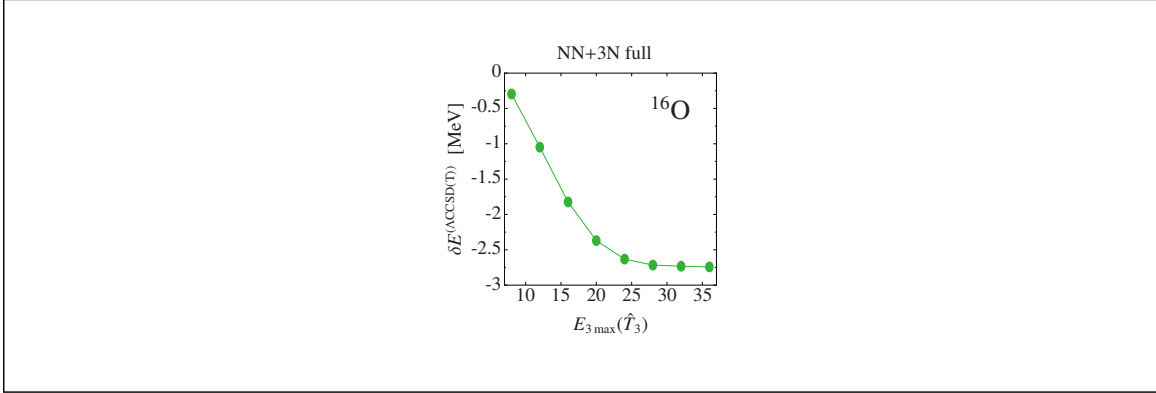


Figure 5.13: Dependence of $\delta E^{(\text{ACCS}(D(T)))}$ for ^{16}O and the NN+3N-full Hamiltonian, at $\alpha = 0.08 \text{ fm}^4$ and in NO2B approximation with $E_{3\max} = 12$, on the $E_{3\max}(\hat{T}_3)$ cut. The calculations were performed using a HF basis with $e_{\max} = 12$.

5.6 The CR-CC(2,3) Energy Correction

Nuclear Coupled-Cluster calculations rely heavily on the spherical formulation of the theory. Therefore, as already discussed in Section 4.12, the presence of two- and three-body matrix elements of the effective Hamiltonian that enter the definition of the denominator appearing in the CR-CC(2,3) energy expression (4.182) does not immediately allow a spherical formulation. However, as pointed out in Section 4.12, the use of projection-averaged matrix elements (4.184) and (4.186) is a promising way to overcome this problem.

Therefore, it is important to estimate the errors introduced by the approximate treatment of the denominator. Figure 5.14 illustrates the accuracy of the proposed approximation, where a m -scheme implementation, in which the denominator can be treated exactly, is used for comparing the results for the exact denominators $D(2)$ and $D(3)$ with their projection-averaged counterparts $\overline{D(2)}$ and $\overline{D(3)}$. The left panels show for ^{16}O and the NN-only as well as the NN+3N-full Hamiltonian the CR-CC(2,3) energy corrections $\delta E^{(\text{CR-CC}(2,3))}$ for the different denominators including up to one- ($D(1)$), two- ($D(2)$), or three-body ($D(3)$) effective Hamiltonian matrix elements. For the present discussion it is sufficient to note that the size of $\delta E^{(\text{CR-CC}(2,3))}$ is about -0.3 MeV and -1.5 MeV for the NN-only Hamiltonian at $e_{\max} = 2$ and $e_{\max} = 4$, respectively, and about -0.8 MeV and -2.0 MeV for the NN+3N-full Hamiltonian at $e_{\max} = 2$ and $e_{\max} = 4$, respectively. The error introduced by the projection average, defined as the difference of $\delta E^{(\text{CR-CC}(2,3))}$ using the exact and the projection-averaged denominator, is much smaller, as shown

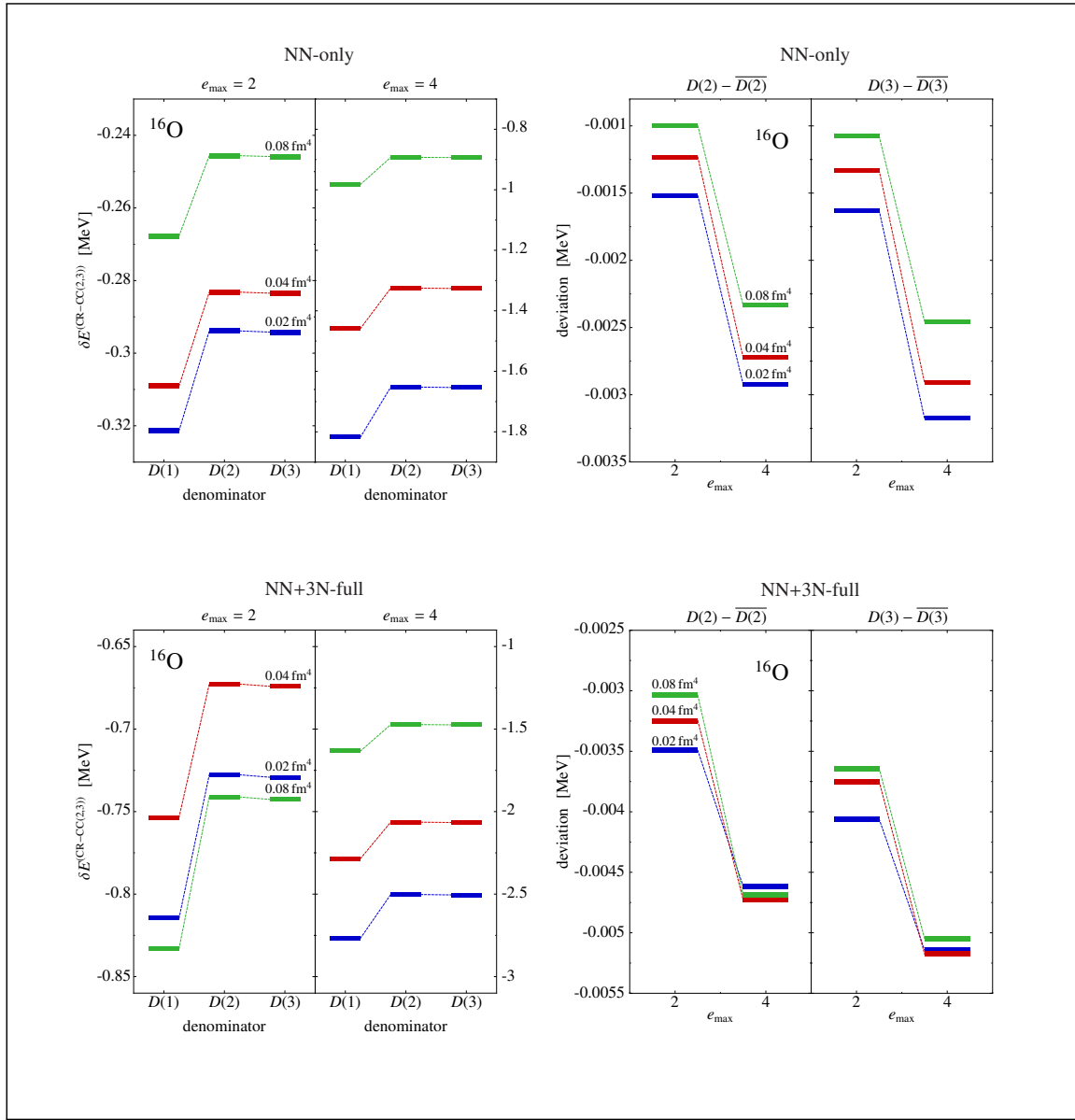


Figure 5.14: *Left: Results for the CR-CC(2,3) energy correction for the NN-only and NN+3N-full Hamiltonian, for different choices of the denominator $D(k)$, Eq. (4.181). Right: Deviations introduced by using the angular-momentum-projection averaged variants $\overline{D(2)}$ and $\overline{D(3)}$ of the denominators $D(2)$ and $D(3)$. These deviations are completely negligible compared to the size of $\delta E^{(\text{CR-CC}(2,3))}$, consequently, the CR-CC(2,3) method can be accurately formulated in the spherical scheme. The calculations were performed in a HF basis with $\hbar\Omega = 24$ MeV, and the 3N interactions were included via NO2B with $E_{3\text{max}} = 14$.*

in the right panels of Figure 5.14, with deviations of about -0.02 MeV for the NN-only Hamiltonian and about -0.04 MeV for the NN+3N-full Hamiltonian, for both model space sizes considered. In conclusion, the projection-averaged form of the denominator in (4.182) constitutes a legitimate approximation to the exact treatment and opens the possibility for a spherical formulation of the CR-CC(2,3) method.

Figure 5.15 shows on the left a comparison of CR-CC(2,3) results to the Λ CCSD(T) energy correction. Both methods give comparable results but also show noticeable deviations for harder interactions. For instance, for $\alpha = 0.02 \text{ fm}^4$ these deviations are about 1 MeV for ^{16}O and 2 MeV for ^{24}O , while the total Λ CCSD(T) energy correction is -5.4 MeV and -8.2 MeV, respectively. The degree of deviation of both methods is not unexpected, considering the approximative nature of Λ CCSD(T) compared to the CR-CC(2,3) approach. Furthermore, the observation that the results for $\delta E^{(\Lambda\text{CCSD(T)})}$ lie below $\delta E^{(\text{CR-CC(2,3)})}$ is consistent to findings in quantum-chemistry, where Λ CCSD(T) tends to overshoot the exact triples correction [153]. A similar comparison of Λ CCSD(T) and CR-CC(2,3) for heavier nuclei can be found in Figure 5.26 in Section 5.9.3. On the right of Figure 5.15 the CR-CC(2,3) energy correction, using different choices of the denominator, is compared to Λ CCSD(T) in the $e_{\text{max}} = 12$ model space. Most strikingly, the three-body effective Hamiltonian matrix elements in the denominator have no measurable effect on the triples correction and may safely be neglected. The CR-CC(2,3) results using the denominator $D(1)$, involving one-body matrix elements only, lie between the $\overline{D}(2)$ results and Λ CCSD(T). Thus, it may be speculated that one of the reasons why Λ CCSD(T) overshoots the exact triples correction may be the absence of contributions comparable to the two-body effective Hamiltonian matrix elements in the CR-CC(2,3) denominator. Additional comparisons of CR-CC(2,3) ground-state energies with Λ CCSD(T) for heavier nuclei can be found in Section 5.9.3.

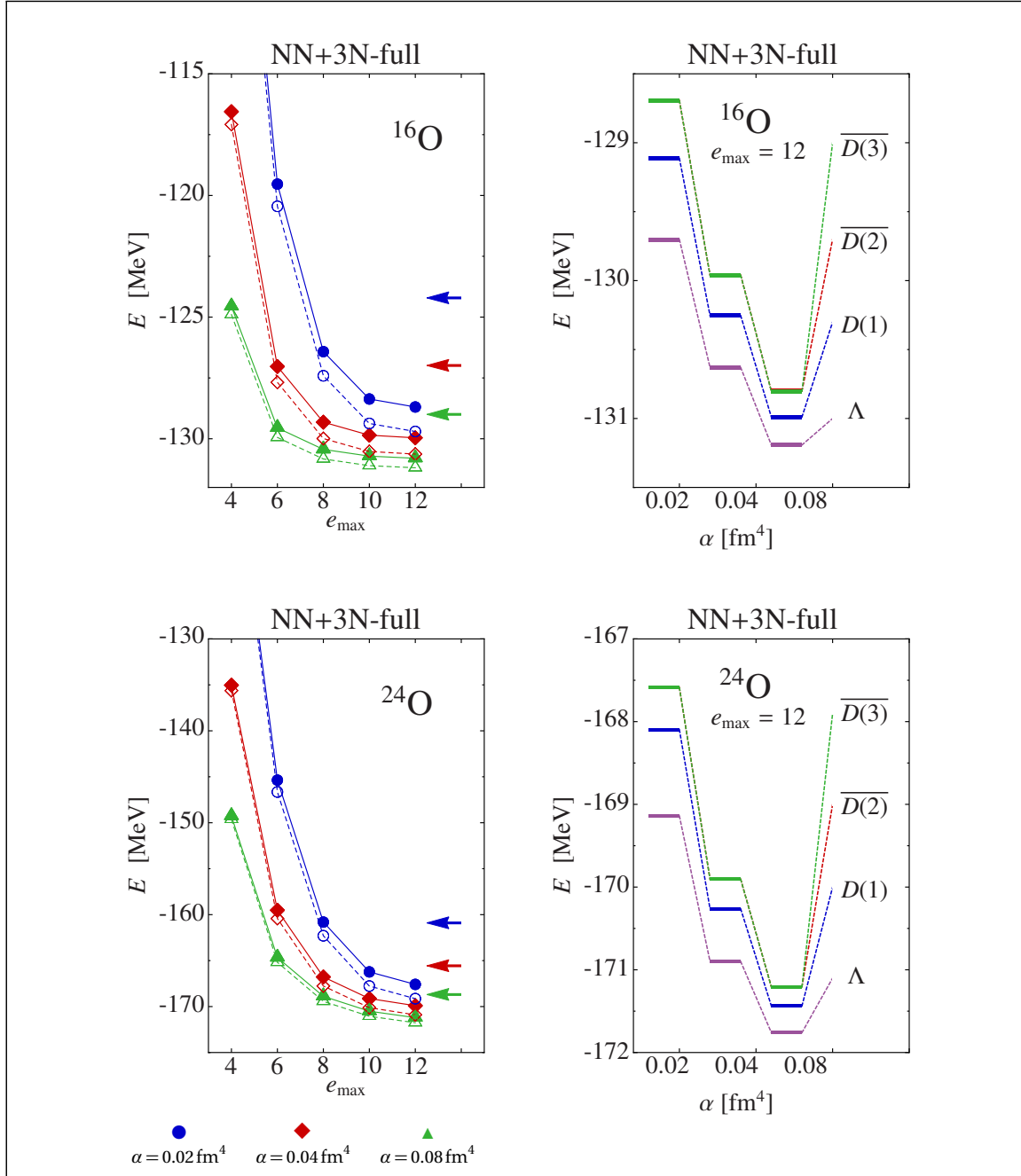


Figure 5.15: Left: Comparison of the CR-CC(2,3) (full symbols) ground-state energies for ^{16}O and ^{24}O to $\Lambda\text{CCSD(T)}$ (open symbols) ground-state energies. CCSD energies for $e_{\max} = 12$ are denoted as arrows. Right: Comparison of CR-CC(2,3) energies for various denominators to the $\Lambda\text{CCSD(T)}$ results. All calculations were performed in a HF basis with $\hbar\Omega = 24$ MeV, and 3N interactions were included via NO2B with $E_{3\max} = 14$.

5.7 CCSD with Explicit 3N Interactions

In previous sections the NO2B approximation to three-body interactions has been used throughout for Coupled-Cluster calculations. This approximation drastically accelerates the calculations, and the IT-NCSM results for light nuclei shown in Figure 1.5 suggest that the NO2B approximation already captures a large portion of the relevant 3N information. However, as the focus moves from light to medium-mass or even heavy nuclei, the validity of the NO2B approximation should be verified in these mass range. Another reason for performing Coupled-Cluster calculations with explicit 3N interactions rather than using the NO2B approximation is simply that the explicit 3N calculations eliminate the errors introduced by the NO2B approximation which is relevant in cases where such errors may not be neglected, as discussed in the following sections.

Including explicit 3N interactions in Coupled-Cluster calculations results in a dramatic increase of the computational expense. Not only the Coupled-Cluster equations get much more complex, it is mostly the large number of 3N matrix elements that quickly renders explicit 3N calculations unfeasible. To some extent this is caused by special requirements of the Coupled-Cluster implementation used in this work. Compared to the $\mathcal{J}\mathcal{T}$ -coupled storage scheme [86] for 3N matrix elements in the HO basis, the 3N format (4.135) used here requires about 10 times more fast memory. Since the $\mathcal{J}\mathcal{T}$ -coupled storage for 3N matrix elements requires about 1 GB memory for $E_{3\max} = 12$, and about 5 GB for $E_{3\max} = 14$, the storage scheme used in the Coupled-Cluster implementation requires 10 and 50 GB fast memory to store the $E_{3\max} = 12$ and $E_{3\max} = 14$ matrix elements in the HO basis, respectively. In the HF basis representation the 3N matrix elements acquire an isospin dependence which translates into a 6 times larger storage requirement compared to the HO basis. Therefore, for explicit 3N Coupled-Cluster calculations in HF basis, the total set of $E_{3\max} = 12$ and $E_{3\max} = 14$ matrix elements require about 60 and 300 GB memory, respectively. Two ways to cope with this problem have been implemented. The first way holds the matrix elements (4.135) in HO basis in memory and performs the HF transformation of individual matrix elements on the fly when they are requested, and discards them afterwards. This reduces the memory requirements but is rather slow due to the six-fold sum over HF coefficients and HO matrix elements that result in a single 3N matrix element in HF basis. Alternatively, the total index range of the 3N matrix elements may be distributed over a range of computer nodes. Each node holds the $\mathcal{J}\mathcal{T}$ -coupled or (4.135) matrix elements in HO basis and calculates the matrix elements of the

index range assigned to the nodes in HF basis when they are needed, but is now also able to store them for later re-use. In applications where individual matrix elements are needed several times during a calculation, such as the iterative solution of Coupled-Cluster equations, the second strategy saves a significant amount of computing time. It should also be noted that in general not the *full* set of matrix elements is needed in the calculations and, therefore, only those that are actually used should be transformed to the HF basis. For example, in all CC applications discussed in this work, the largest set of 3N matrix elements $\langle abc|\hat{w}|def\rangle$, with particle orbitals only, does not enter anywhere. In order to keep the computational runtime reasonable for Coupled-Cluster calculations using explicit 3N interactions, the cutoff $E_{3\max} = 12$ is used in the following. The first application of CCSD for three-body Hamiltonians can be found in [63] but due to the use of an *m*-scheme implementation, these considerations were limited to proof-of-principle calculations for ^4He in the harmonic-oscillator basis and small model spaces. The spherical scheme finally allows to move on to the medium-mass regime. Using an $E_{3\max} = 12$ cut, medium-mass CCSD calculations at $e_{\max} = 12$ using three-body Hamiltonians are comparable in cost to a $\Lambda\text{CCSD(T)}$ NO2B calculation in the same $e_{\max} = 12$ model space.

Figure 5.16 shows the convergence of CCSD ground-state energies with explicit 3N (full symbols) and for the NO2B approximation (open symbols) for the medium-mass nuclei $^{16,24}\text{O}$, $^{40,48}\text{Ca}$ and ^{56}Ni using the NN+3N-induced and NN+3N-full Hamiltonian. The agreement of the NO2B approximation with the explicit 3N is remarkable. The normal-ordering approximation provides very accurate results and it seems that this accuracy is rather independent of the model-space size, the mass number, or even the SRG flow parameter. Furthermore, Figure 5.17 indicates that the quality of the approximation is also independent of the oscillator frequency of the basis. The unnatural increase of the energies for smaller values of $\hbar\Omega$ in Figure 5.17 is due to the use of unsufficiently large SRG model spaces, as discussed in Section 5.9.3. However, for the optimal frequencies determined from Figure 5.17, the effects of insufficient SRG model spaces are less than 1 % of the total energy.

The relative contribution of the residual 3N interaction normalized to the CCSD ground-state energies according to

$$\Delta(3\text{B}) = \frac{|E^{(\text{CCSD})} - E_{\text{NO2B}}^{(\text{CCSD})}|}{E^{(\text{CCSD})}/100} \% \quad (5.7)$$

is shown in Figure 5.18. It should be stressed that $E_{\text{NO2B}}^{(\text{CCSD})}$ was calculated in a pure

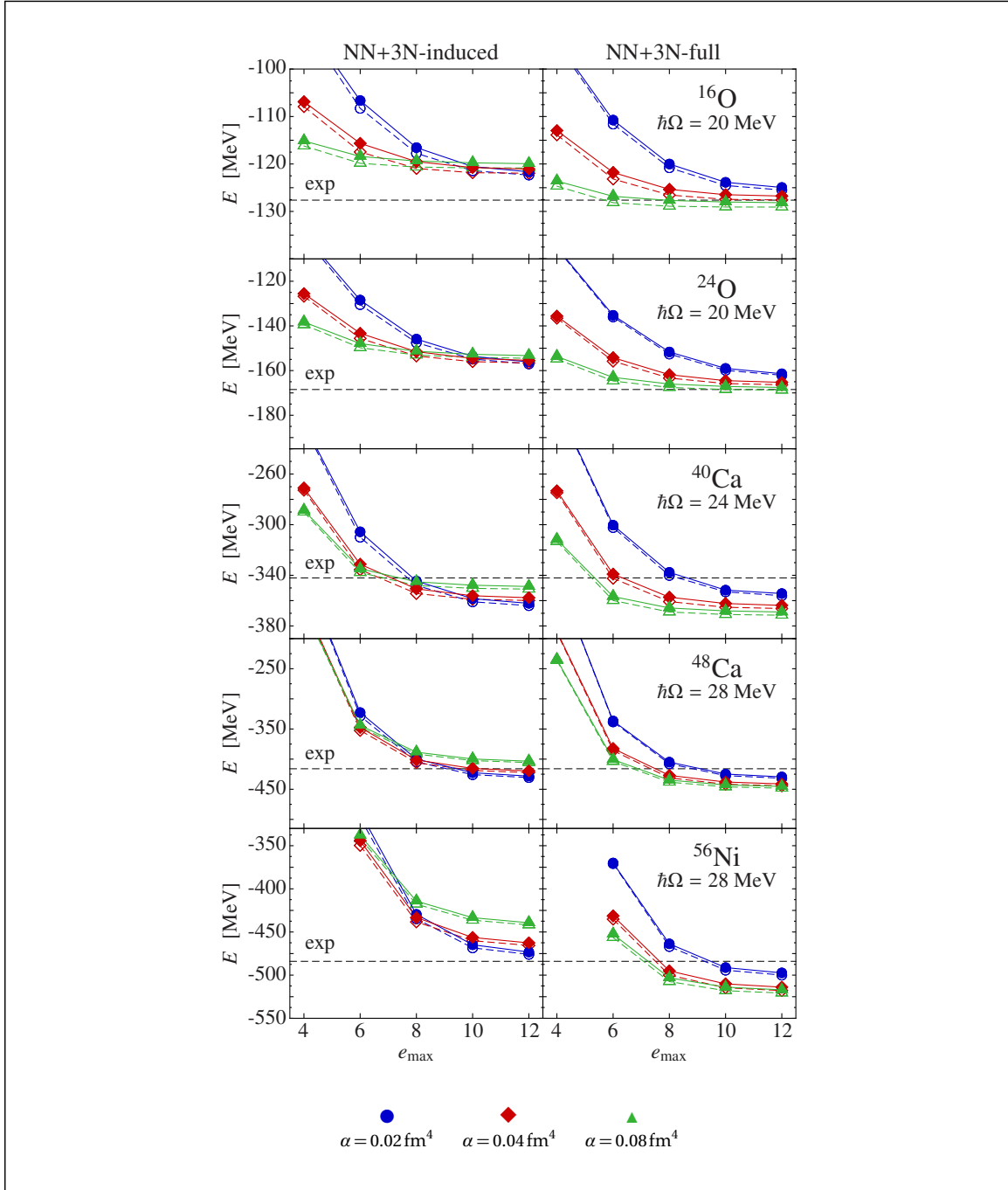


Figure 5.16: Comparison of CCSD with NO2B approximation (open symbols) and CCSD with explicit 3N interaction (full symbols) for the nuclei $^{16,24}\text{O}$, $^{40,48}\text{Ca}$ and ^{56}Ni for the NN+3N-induced and NN+3N-full Hamiltonian in NO2B approximation with $E_{3\text{max}} = 12$. The optimal oscillator frequencies $\hbar\Omega$ have been determined from Figure 5.17. Figure taken from [92].

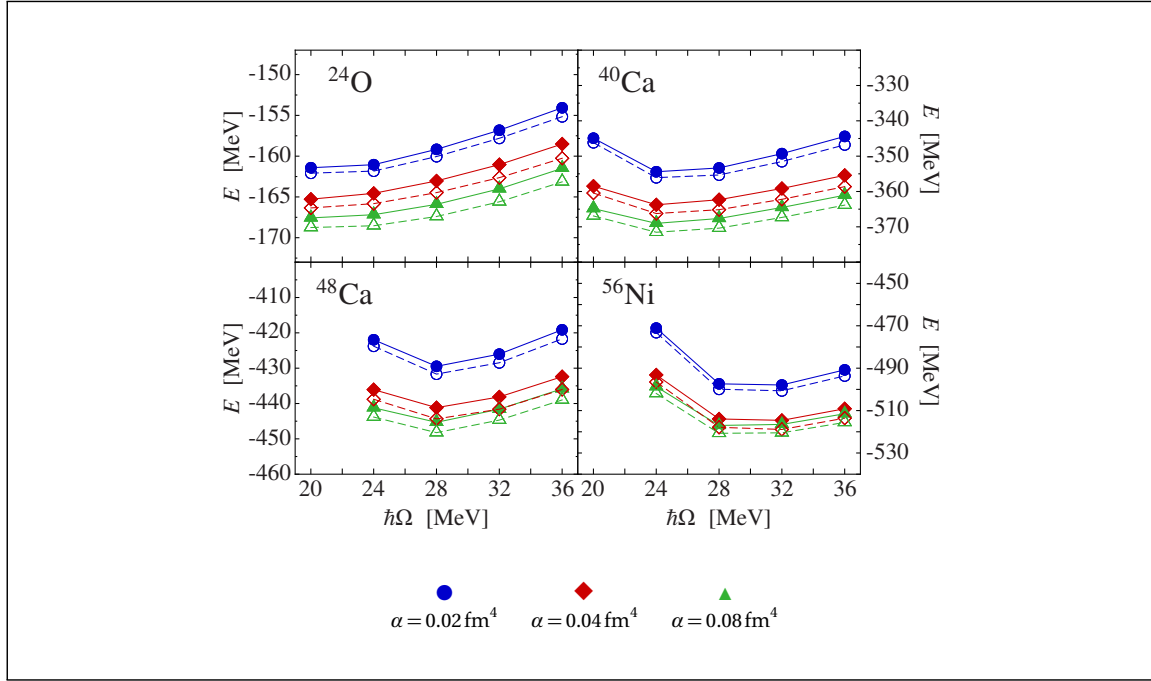


Figure 5.17: Oscillator-frequency dependence of CCSD ground-state energies of ^{24}O , $^{40,48}\text{Ca}$ and ^{56}Ni for the NN+3N-full Hamiltonian with explicit 3N interactions (full symbols) and in NO2B approximation (open symbols) with $E_{3\text{max}} = 12$, using a Hartree-Fock basis with $e_{\text{max}} = 12$ model spaces. Figure taken from [92].

NO2B scheme, where residual 3N information entered in neither in the determination of the cluster amplitudes nor in the energy expression. Therefore, $\Delta(3\text{B})$ measures the total effect of the residual 3N interaction in the CCSD calculation, without discrimination between its effect on amplitudes or energy. This issue is further addressed in Section 5.8.1. There is no definite systematics of the relative contribution with mass number or the SRG flow parameter. For all nuclei the relative contribution is well below 1 % and in particular for the heavier nuclei it is a little smaller with values around 0.6 %. This confirms the earlier findings that the NO2B approximation seems to perform better for heavier nuclei. However, one reason for this might be that the ground-state energies for the heavier nuclei are not fully converged with respect to $E_{3\text{max}}$ and, therefore, not the full relevant information about the 3N interaction was used from the beginning. Furthermore, it seems that the relative contributions tend to be a little more important for larger flow parameters, but these effects lie in the range of 0.1 % and have no practical significance.

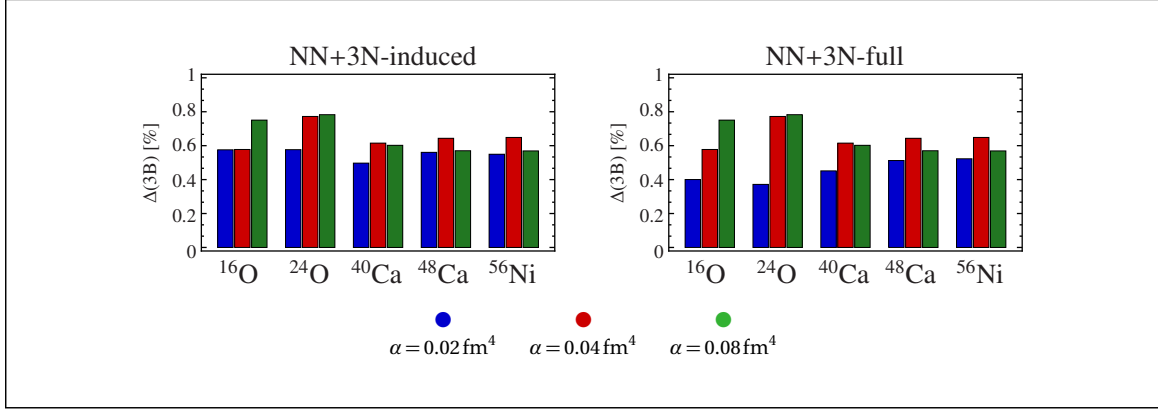


Figure 5.18: Relative contribution of the residual 3N interaction, normalized to the CCSD ground-state energies using explicit 3N interactions. Parameters of the calculations as in Figure 5.16.

5.8 Λ CCSD(T) with Explicit 3N Interactions

5.8.1 Benchmark of the NO2B Approximation

For CCSD, the contribution of the residual 3N interaction to the total ground-state energy of medium-mass nuclei was shown to be less than 1%. A similar result for Λ CCSD(T) would be desirable in order to keep the error introduced by the NO2B approximation at the 1% level. The alternative – routinely including explicit 3N interactions in Λ CCSD(T) calculations – is not an option due to the *extreme* computational costs.

A natural approach to assess the relevance of the residual normal-ordered three-body interaction \hat{W}_N in CCSD and Λ CCSD(T) calculations is to modify the total energy expression

$$E^{(\Lambda\text{CCSD(T)})} = E_{\text{ref}} + \Delta E_{\text{NO2B}}^{(\text{CCSD})} + \delta E_{\text{NO2B}}^{(\Lambda\text{CCSD(T)})} + \Delta E_{3\text{B}}^{(\text{CCSD})} + \delta E_{3\text{B}}^{(\Lambda\text{CCSD(T)})}, \quad (5.8)$$

to either include or not include the contributions $\Delta E_{3\text{B}}^{(\text{CCSD})}$ and $\delta E_{3\text{B}}^{(\Lambda\text{CCSD(T)})}$ due to \hat{W}_N . However, this discussion is complicated by the fact that the energy values are not only determined by their expressions in terms of the $\hat{T}^{(\text{CCSD})}$ and $\hat{\Lambda}^{(\text{CCSD})}$ amplitudes, but also by the type of equation – with or without inclusion of the \hat{W}_N terms – used to determine the amplitudes in the first place. This leads to various possible and reasonable combinations to consider.

In Figure 5.19, where for ^{16}O , ^{24}O , and ^{40}Ca , and both, the NN+3N-induced

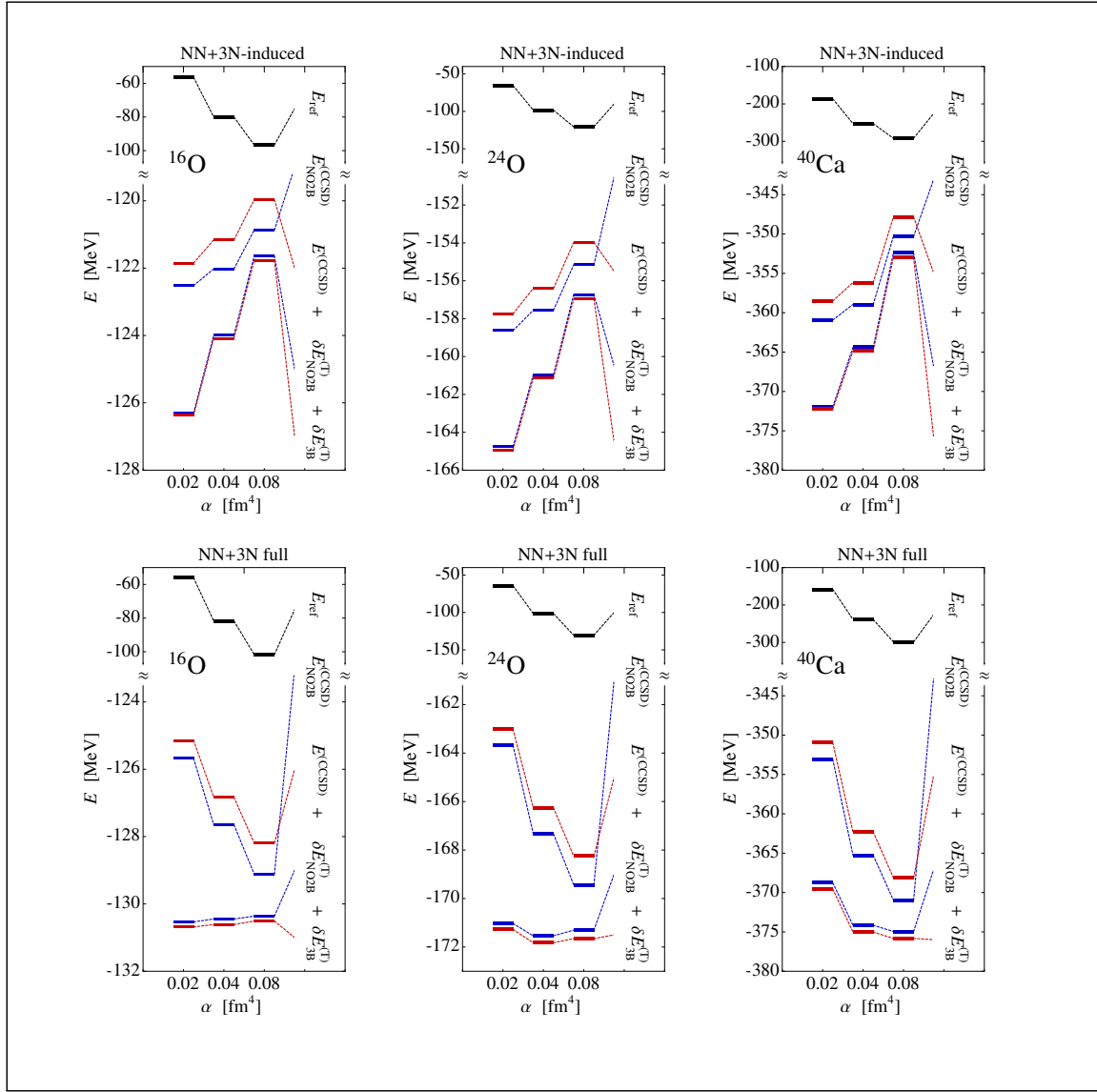


Figure 5.19: Anatomy of the individual contributions from CCSD and Λ CCSD(T) to the total binding energy of ^{16}O , ^{24}O and ^{40}Ca for the two types of three-body Hamiltonians and SRG flow parameters $\alpha = 0.02, 0.04$, and 0.08 fm^{-4} . For ^{16}O and ^{24}O , a Hartree-Fock basis with $e_{\text{max}} = 12$ model space and oscillator frequency $\hbar\Omega = 20 \text{ MeV}$ was used, whereas for ^{40}Ca an $e_{\text{max}} = 10$ model space with $\hbar\Omega = 24 \text{ MeV}$ was employed. The shorthand notation $\delta E_{\text{NO2B}}^{(\text{T})}$ and $\delta E_{3\text{B}}^{(\text{T})}$ is used to denote $\delta E_{\text{NO2B}}^{(\Lambda\text{CCSD(T)})}$ and $\delta E_{3\text{B}}^{(\Lambda\text{CCSD(T)})}$, respectively.

and NN+3N-full Hamiltonians results are shown for a series of increasingly complete calculations of the ground-state energies. The energy $E_{\text{NO2B}}^{(\text{CCSD})}$ is calculated in NO2B approximation, where the \hat{W}_N terms are neglected in both, the determination of the cluster amplitudes as well as the calculation of the energy. For the calculation of all other energies presented in Figure 5.19, the $\hat{T}^{(\text{CCSD})}$ and $\hat{\Lambda}^{(\text{CCSD})}$ amplitudes were determined from their respective amplitude equations including the \hat{W}_N terms. Analogous to the discussion in Section 5.7, by comparing $E_{\text{NO2B}}^{(\text{CCSD})}$ to $E^{(\text{CCSD})}$, a direct quantification of the combined effect of \hat{W}_N in the CCSD amplitude equations and the energy expression can be made. It should be noted that here

$$E^{(\text{CCSD})} - E_{\text{NO2B}}^{(\text{CCSD})} \neq E_{3\text{B}}^{(\text{CCSD})}, \quad (5.9)$$

contrary to what (3.25) seems to imply, due to the use of different amplitudes for the calculation of $E_{\text{NO2B}}^{(\text{CCSD})}$ and $E^{(\text{CCSD})}$, respectively. Contrary to this, the same amplitudes (obtained from solving the amplitude equations containing the \hat{W}_N terms) are used in the calculations of $\delta E_{\text{NO2B}}^{(\Lambda\text{CCSD(T)})}$ and $\delta E_{3\text{B}}^{(\Lambda\text{CCSD(T)})}$. Therefore, using these numbers it is only possible to quantify the importance of the \hat{W}_N contributions – simply given by $\delta E_{3\text{B}}^{(\Lambda\text{CCSD(T)})}$ itself – in the calculation of the total triples correction $\delta E^{(\Lambda\text{CCSD(T)})}$. This allows to compare the results for the complete Λ CCSD(T) ground-state energy $E^{(\Lambda\text{CCSD(T)})}$ to the simplified expression

$$\tilde{E}^{(\Lambda\text{CCSD(T)})} = E_{\text{ref}} + \Delta E_{\text{NO2B}}^{(\text{CCSD})} + \delta E_{\text{NO2B}}^{(\Lambda\text{CCSD(T)})} + \Delta E_{3\text{B}}^{(\text{CCSD})}, \quad (5.10)$$

in which the \hat{W}_N terms are included in the CCSD and Λ CCSD calculations but are omitted in the final calculation of the energy correction. However, particularly for the calculation of $\delta E_{\text{NO2B}}^{(\Lambda\text{CCSD(T)})}$, other choices of where to include the \hat{W}_N terms in the amplitude equations seem reasonable, and this issue is addressed further below. However, it should already be mentioned that other choices of the amplitudes equations lead to practically the same results.

In the following, ^{16}O and the NN+3N-full Hamiltonian at flow parameter values $\alpha = 0.02 \text{ fm}^4$ and 0.08 fm^4 is considered as an example. For increasing α , more and more of the binding energy is shifted to lower orders of the cluster expansion and the contributions from the higher orders consequently get smaller with the SRG flow: The size of the reference energy E_{ref} grows from -56.11 MeV to -101.67 MeV , while the CCSD correlation energy $\Delta E^{(\text{CCSD})}$ decreases from -69.03 MeV to -26.52 MeV as the SRG evolution goes from $\alpha = 0.02 \text{ fm}^4$ to $\alpha = 0.08 \text{ fm}^4$ and the Λ CCSD(T) energy correction $\delta E^{(\Lambda\text{CCSD(T)})}$, which, according to Section 5.5, is also considered as a measure for the contributions of the omitted cluster operators beyond the three-body level [95], decreases from -5.54 MeV to -2.34 MeV ,

corresponding to 4.2 % and 1.8 % of the total binding energy. In the medium-mass regime, these uncertainties related to the cluster truncation are typically the largest in the calculations for a given Hamiltonian, and, therefore, they set the overall level of accuracy targeted at [95].

Examining the contributions from the residual 3N interaction to $\Delta E^{(\text{CCSD})}$ it is found that, while the absolute value of $\Delta E^{(\text{CCSD})}$ decreases by about 30 MeV when the Hamiltonian is evolved from $\alpha = 0.02 \text{ fm}^4$ further to $\alpha = 0.08 \text{ fm}^4$, $\Delta E^{(\text{CCSD})} - \Delta E_{\text{NO2B}}^{(\text{CCSD})}$ is only subject to a slight increase from 0.54 MeV to 0.92 MeV, corresponding to 0.4 % and 0.7 % of the total binding energy. Consequently, the relative as well as the absolute importance of the residual 3N interaction to the CCSD correlation energy grows with the SRG flow.

Furthermore, while for the harder Hamiltonian at $\alpha = 0.02 \text{ fm}^4$ the \hat{W}_N contributions to $\Delta E^{(\text{CCSD})}$ are about one order of magnitude smaller than the accuracy level set by $\delta E^{(\text{ACCS}(D)(T))}$, for the softer $\alpha = 0.08 \text{ fm}^4$ Hamiltonian the \hat{W}_N contributions have a comparable size of about 39 % of the triples correction. Therefore, in order to keep different errors at a consistent level, for soft interactions the residual 3N contributions should be included in CCSD if the triples correction is considered as well.

For the $\Lambda\text{CCSD}(T)$ triples correction $\delta E^{(\Lambda\text{CCSD}(T))}$ itself, the \hat{W}_N contributions $\delta E_{3B}^{(\Lambda\text{CCSD}(T))}$, despite containing second-order MBPT contributions, have very small values of about -15 keV. This effect is about one order of magnitude smaller than the targeted accuracy given by the size of $\delta E^{(\text{ACCS}(D)(T))}$, and may therefore safely be neglected. From another perspective, the \hat{W}_N contributions to $\delta E^{(\text{ACCS}(D)(T))}$ constitutes about 0.1 % of the total binding energy, which clearly is beyond the level of accuracy of any many-body method operating in the medium-mass regime today.

As is apparent from Figure 5.19, the discussion for the NN+3N-induced Hamiltonian and the heavier nuclei ^{24}O and ^{40}Ca is similar. In the case of ^{40}Ca , the smaller $e_{\text{max}} = 10$ model space is used in order to keep the computational cost reasonable. In this model space the results are not fully converged with respect to e_{max} , but since the quality of NO2B is largely independent of e_{max} [95] this does not affect the present discussion. For the NN+3N-induced Hamiltonian, for example, the relative contribution of \hat{W}_N to the CCSD correlation energy grows from 1.3 % for $\alpha = 0.02 \text{ fm}^4$ to 4.2 % for $\alpha = 0.08 \text{ fm}^4$, in both cases constituting about 0.6 % of the total binding energy. Again, as the SRG flow parameter increases, the contributions of \hat{W}_N to the CCSD correlation energy on the one hand, and the triples

correction on the other hand, become comparable, where $\Delta E^{(\text{CCSD})} - \Delta E_{\text{NO2B}}^{(\text{CCSD})}$ is about 18 % of the size of the triples correction at $\alpha = 0.02 \text{ fm}^4$ and already about 48 % at $\alpha = 0.08 \text{ fm}^4$. The \hat{W}_N effect to the triples correction is again negligible, about one order of magnitude smaller than the triples correction itself, namely about 2 % of $\delta E^{(\Lambda\text{CCSD(T)})}$ for $\alpha = 0.02 \text{ fm}^4$ and about 11 % for $\alpha = 0.08 \text{ fm}^4$, or 0.1 % and 0.2 % of the total binding energy $E^{(\Lambda\text{CCSD(T)})}$.

In summary, as in Section 5.7, contributions from residual 3N interactions to the CCSD correlation energy are found to be of the order of 1 % of the total binding energy. For the triples correction the contributions are much smaller and may be considered negligible. The fact that the residual 3N contributions are rather insensitive to the SRG flow parameter impacts the characterization of their importance. For hard interactions, the residual 3N effects to the CCSD correlation energy $E^{(\text{CCSD})}$ are rather small compared to the triples correction $\delta E^{(\Lambda\text{CCSD(T)})}$, but they become comparable as the triples contribution gets smaller for soft interactions. Therefore, when using soft interactions, the residual 3N interaction should be included in CCSD if the desired accuracy level also demands inclusion of triples excitation effects. For the triples correction, on the other hand, the residual 3N interaction only plays an insignificant role, providing contributions that are shadowed by the considerably larger uncertainties stemming, e.g., from the cluster truncation. This motivates the use of the truncated energy expression $\tilde{E}^{(\Lambda\text{CCSD(T)})}$, Eq. (5.10), instead of the full form $E^{(\Lambda\text{CCSD(T)})}$, resulting in only negligible losses in accuracy.

5.8.2 Approximation Schemes for the Amplitudes

The above considerations indicate that the residual 3N interaction may be neglected in calculating the Λ CCSD(T) energy correction $\delta E^{(\Lambda\text{CCSD(T)})}$ without significantly affecting the overall accuracy, leading to Eq. (5.10) as an approximate, yet accurate, form for $E^{(\Lambda\text{CCSD(T)})}$. From a practitioner's point of view, discarding the \hat{W}_N contributions to $\delta E^{(\Lambda\text{CCSD(T)})}$, Eqs. (3.46) and (3.55), already leads to significant savings in the implementational effort and computing time, but one still has to solve the CCSD equations determining the $\hat{T}^{(\text{CCSD})}$ amplitudes t_i^a and t_{ij}^{ab} , as well as the Λ CCSD equations determining the $\hat{\Lambda}^{(\text{CCSD})}$ amplitudes λ_a^i and λ_{ab}^{ij} , with full incorporation of \hat{W}_N . Particularly solving the Λ CCSD equations, for which the effective Hamiltonian contributions given in Figures 3.10–3.12 have to be evaluated, consumes most of the computing time in practical calculations. Therefore, it is also worthwhile to investigate how much of the residual 3N interaction informa-

tion has to be included in solving for the $\hat{T}^{(\text{CCSD})}$ and $\hat{\Lambda}^{(\text{CCSD})}$ amplitudes that enter the energy expressions, in order to obtain accurate results at the lowest possible computational cost.

In order to distinguish between different approximation schemes the following notation is introduced in which for energy quantities that only depend on $\hat{T}^{(\text{CCSD})}$ amplitudes the label in brackets denote if the $\hat{T}^{(\text{CCSD})}$ amplitudes were determined from the amplitude equations with (3B) or without residual 3N interaction (2B). Similarly, for quantities that depend on both, $\hat{T}^{(\text{CCSD})}$ and $\hat{\Lambda}^{(\text{CCSD})}$ amplitudes, the first label denotes the type of equation used to determine the $\hat{T}^{(\text{CCSD})}$ amplitudes and the second specifies the ΛCCSD equations. For example, $\tilde{E}^{(\Lambda\text{CCSD(T)})(3\text{B},2\text{B})}$ refers to the energy expression (5.10), calculated using $\hat{T}^{(\text{CCSD})}$ amplitudes determined from the equations including the \hat{W}_N terms, while the $\hat{\Lambda}^{(\text{CCSD})}$ amplitudes are determined using the NO2B approximation.

The following approximation schemes are considered, in which the \hat{W}_N contributions $\delta E_{3\text{B}}^{(\Lambda\text{CCSD(T)})}$ to the triples correction are always neglected: For the “NO2B” scheme, all \hat{W}_N terms are discarded in both, the determination of the \hat{T} and $\hat{\Lambda}$ amplitudes and the energy $E_{\text{NO2B}}^{(\Lambda\text{CCSD(T)})}$,

$$E^{(\text{NO2B})} = E_{\text{NO2B}}^{(\Lambda\text{CCSD(T)})}(2\text{B},2\text{B}). \quad (5.11)$$

This of course corresponds to an ordinary $\Lambda\text{CCSD(T)}$ calculation in NO2B approximation. For scheme “A”, the energy $E_{\text{NO2B}}^{(\Lambda\text{CCSD(T)})}$ is computed as in the NO2B case and $\Delta E_{3\text{B}}^{(\text{CCSD})}$, calculated $\hat{T}^{(\text{CCSD})}$ amplitudes obtained from the NO2B CCSD equations, is added,

$$E^{(\text{A})} = E_{\text{NO2B}}^{(\Lambda\text{CCSD(T)})}(2\text{B},2\text{B}) + \Delta E_{3\text{B}}^{(\text{CCSD})}(2\text{B}). \quad (5.12)$$

This represents the simplest and most economic way to include \hat{W}_N information, where it only enters in the expression for the energy contribution $\Delta E_{3\text{B}}^{(\text{CCSD})}$, but not in the considerably more complex equations that determinate the amplitudes. In scheme “B”, full \hat{W}_N information is included in the calculation of the CCSD correlation energy, keeping the \hat{W}_N terms in the amplitude equations as well as in the energy expression. The triples correction, however, is calculated without any \hat{W}_N information,

$$E^{(\text{B})} = E^{(\text{CCSD})}(3\text{B}) + \delta E_{\text{NO2B}}^{(\Lambda\text{CCSD(T)})}(2\text{B},2\text{B}). \quad (5.13)$$

This way, consistency is kept between the $\hat{T}^{(\text{CCSD})}$ and $\hat{\Lambda}^{(\text{CCSD})}$ amplitudes that enter the triples correction, while capturing all residual 3N effects in the CCSD energy

$\Delta E^{(\text{CCSD})}$. In scheme “C”, an inconsistency is introduced between the $\hat{T}^{(\text{CCSD})}$ and $\hat{\Lambda}^{(\text{CCSD})}$ amplitudes by solving for $\hat{T}^{(\text{CCSD})}$ with the \hat{W}_N terms present, while we solve for $\hat{\Lambda}^{(\text{CCSD})}$ without \hat{W}_N terms and the energy expression is given by $\tilde{E}^{(\Lambda\text{CCSD(T)})}$,

$$E^{(\text{C})} = \tilde{E}^{(\Lambda\text{CCSD(T)})}(3\text{B}, 2\text{B}). \quad (5.14)$$

This variant is reasonable since one typically has to solve for the $\hat{T}^{(\text{CCSD})}$ amplitude equations with \hat{W}_N terms anyway in order to obtain the comparatively large $\Delta E_{3\text{B}}^{(\text{CCSD})}$ contribution to the energy while one would like to avoid to solve for the $\Lambda^{(\text{CCSD})}$ amplitudes in this manner. Finally, in scheme “D”, in which the residual 3N interaction terms are neglected only in the expression for $\delta E^{(\Lambda\text{CCSD(T)})}$, the full \hat{W}_N -containing equations are used to solve for the $\hat{T}^{(\text{CCSD})}$ and $\hat{\Lambda}^{(\text{CCSD})}$ amplitudes and the energy is determined via Eq. (5.10),

$$E^{(\text{D})} = \tilde{E}^{(\Lambda\text{CCSD(T)})}(3\text{B}, 3\text{B}). \quad (5.15)$$

As in the discussion of Figure 5.19, by comparing with scheme “C”, this variant allows to estimate the importance of \hat{W}_N for the $\hat{\Lambda}^{(\text{CCSD})}$ amplitudes.

In Figure 5.20, for the case of ^{16}O , ^{40}Ca and the NN+3N-full Hamiltonian, the deviations introduced by the aforementioned approximation schemes are compared to the complete 3N calculations. For ^{24}O and the NN+3N-induced Hamiltonian very similar results are obtained and, therefore, not presented here. As expected, the “NO2B” scheme shows the largest deviations because the contributions of \hat{W}_N to CCSD are completely missing. Including the \hat{W}_N terms in the energy expression for the CCSD correlation energy but evaluating it using $\hat{T}^{(\text{CCSD})}$ amplitudes without \hat{W}_N information in scheme “A” virtually does not change the result. Therefore, we can conclude that it is the \hat{W}_N effect on the $\hat{T}^{(\text{CCSD})}$ amplitudes that is most important for CCSD, rather than the additional terms $\Delta E_{3\text{B}}^{(\text{CCSD})}$. In these calculations, the best approximation to the complete calculations is provided by scheme “B”, where the full \hat{W}_N information is used to determine the CCSD correlation energy, but otherwise no \hat{W}_N information enters at all in the calculation of the triples correction. However, approximation schemes “B”, “C” and “D” give very similar results, again hinting at the \hat{W}_N effect on the $\hat{T}^{(\text{CCSD})}$ amplitudes to be the most important ingredient in the inclusion of residual 3N interactions in CCSD and Λ CCSD(T) calculations.

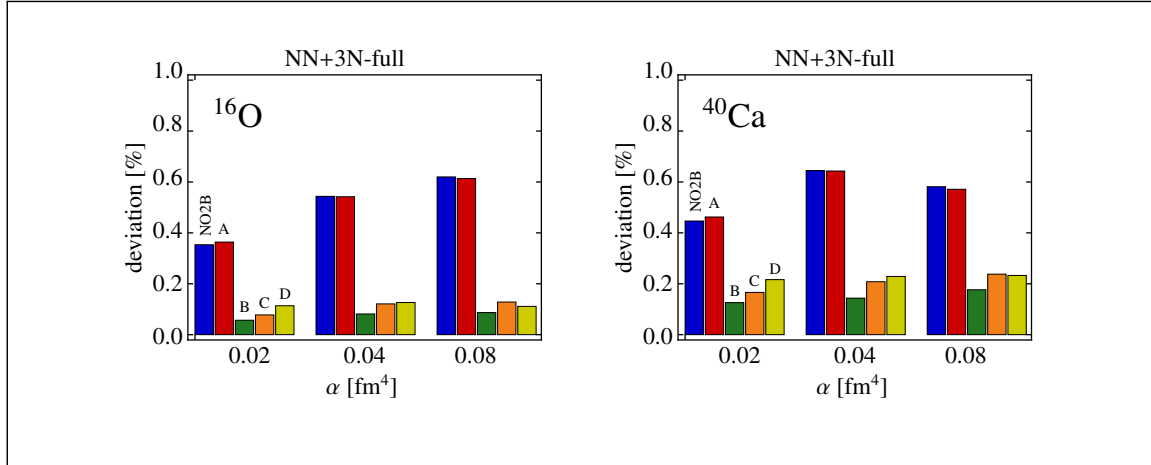


Figure 5.20: Comparison of the deviations introduced by the different approximation schemes described in the text from the full inclusion of the residual 3N interaction in all steps involving CCSD and Λ CCSD(T) calculations for three-body Hamiltonians. Parameters of the calculations as in Figure 5.19.

5.9 *Ab Initio* Description of Heavy Nuclei

The previous sections gave an overview of various aspects of Coupled-Cluster calculations in the medium-mass regime using chiral interactions, from which the following conclusions may be drawn about how to obtain the accurate results for heavier nuclei in the present framework:

The normal-ordered two-body approximation works very well and allows to almost completely include the relevant 3N interaction into the calculations at very much reduced computational cost. The error introduced by this approximation is only about 1 % of the total binding energy, which is absolutely acceptable for *ab initio* calculations in the heavy regime considering other sources of uncertainty present in the calculations, such as the omission of SRG-induced four- and multi-nucleon interactions.

The $E_{3\max}$ cut emerged as one of the main limiting factors in the calculation of nuclear properties in the mass range $A > 60$. Therefore, significant improvement over the $E_{3\max} = 14$ cut is required in order to obtain accurate results for nuclei beyond the medium-mass regime considered so far. However, *full* sets of 3N matrix elements with $E_{3\max} > 14$ are not easy to generate and to store. Additionally, the many-body methods often cannot handle such large sets of explicit 3N matrix elements and, therefore, there is no need for them except for the computation

of the *normal-ordered matrix elements*. Computing only those matrix elements that are used in the normal-ordering saves computing time and finally allows to go to larger values of $E_{3\max}$ in the normal-ordering procedure. However, it is important to retain consistency between the $E_{3\max}$ used in the Hartree-Fock calculation that determines the reference state and the $E_{3\max}$ used in the normal-ordering procedure, as described in Section 5.9.1.

Another source of uncertainty for the nuclei considered so far is given by the *cluster truncation*. There is not much room for practical improvements on the many-body side, but the uncertainties may be reduced by the use of softer interactions. Furthermore, the uncertainties due to the cluster truncation seem not to increase with the mass number and so accurate calculations should be possible using ACCSD(T) or CR-CC(2,3) in the $A > 60$ region.

The cluster truncation motivates the use of soft interactions at flow parameters such as 0.08 fm^4 , for which the triples correction only contribute about 2 % to the energy. However, at this level of accuracy other sources of uncertainties, such as the error introduced by the NO2B approximation become relevant. Explicit 3N calculations are very expensive for $E_{3\max} > 12$ but, nevertheless, the error introduced by omitting residual 3N contributions may be reduced by using a scheme in which the 3N matrix elements are included explicitly up to some parameter $E_{3\max}^{\text{explicit}}$, and 3N matrix elements with $E_{3\max}^{\text{NO2B}} > E_{3\max}^{\text{explicit}}$ enter the calculation only through the normal-ordering.

How large the SRG flow-parameter dependence due to omitted many-body forces in medium-mass nuclei really is cannot be decisively determined from the previous calculations, because $E_{3\max}$ and the cluster truncation are also sources of flow-parameter dependence. However, as mentioned above, the uncertainties due to $E_{3\max}$ will largely be reduced by going to sufficient large values of $E_{3\max}$.

Finally, the insufficient SRG model spaces, as mentioned in Section 5.7, need to be addressed. The strategies pursued in Section 5.9.2 are straightforward enlargements of the model spaces and a frequency conversion technique.

By virtue of all the developments above it will then be possible to extend the range of accurate *ab initio* calculations into the heavy nuclear regime.

5.9.1 Self-Consistent Hartree-Fock Reference Normal-Ordering

In order to perform accurate calculations of nuclei beyond the medium-mass regime considered in Section 5.9.3, the normal-ordering procedure has to be performed for larger values of $E_{3\max}$ than the ones used so far. For a given reference state, computing the normal-ordered matrix elements corresponding to $E_{3\max}$ values for which no full sets of 3N matrix elements can be stored any more can be achieved by distributing the workload over many independently operating computing nodes which calculate (and temporarily store) the required matrix elements on the fly. However, using full sets of 3N matrix elements with large $E_{3\max}$ in this manner in many-body calculations is not a preferred option; this also includes the HF method from which the reference state for the normal-ordering is computed. Therefore, a different strategy that avoids using explicit 3N matrix elements with large $E_{3\max}$ in the HF calculations is pursued in the following. To this end, the role of the HF reference state in the normal-ordering procedure needs to be investigated.

A first attempt of going beyond current normal-ordering capabilities is to perform a HF calculation which determines the HF reference state $|\Phi\rangle$ using 3N matrix elements with an $E_{3\max}^{|\Phi\rangle}$ cut for which full sets of 3N matrix elements can be handled. Afterwards, this reference state may be used in the normal ordering of 3N matrix elements for a *larger* $E_{3\max}^{\text{NO}}$. Obviously, in this case the reference state used is not fully appropriate since it only contains $E_{3\max}^{|\Phi\rangle} < E_{3\max}^{\text{NO}}$ information. Furthermore, the Hartree-Fock basis will also be not consistent to the normal-ordered matrix elements because, again, the construction of the HF basis only used $E_{3\max}^{|\Phi\rangle} < E_{3\max}^{\text{NO}}$ information while the matrix elements also contain information up to $E_{3\max}^{\text{NO}}$. This means that the reference state used in the normal ordering and which also enters the many-body calculations is actually no longer the proper reference state from the point of view of the obtained normal-ordered interaction.

To demonstrate the effects of using reference states that do not correspond to the employed interaction, in Figure 5.21 CCSD ground-state energies are shown for ^{16}O and ^{40}Ca , using inconsistent $E_{3\max}$ values in the Hartree-Fock calculation and the subsequent normal-ordering, with $E_{3\max}^{|\Phi\rangle} = 8$ and $E_{3\max}^{\text{NO}} = 14$. The leftmost bars show the results for this combination of $E_{3\max}$ values while the rightmost bars represent the result obtained for the consistent values $E_{3\max}^{|\Phi\rangle} = E_{3\max}^{\text{NO}} = 14$ which is called *exact* in the following. In the case of ^{16}O , for instance, the corresponding results disagree, for the $\alpha = 0.02 \text{ fm}^4$ Hamiltonian about 3 MeV and for $\alpha = 0.08 \text{ fm}^4$

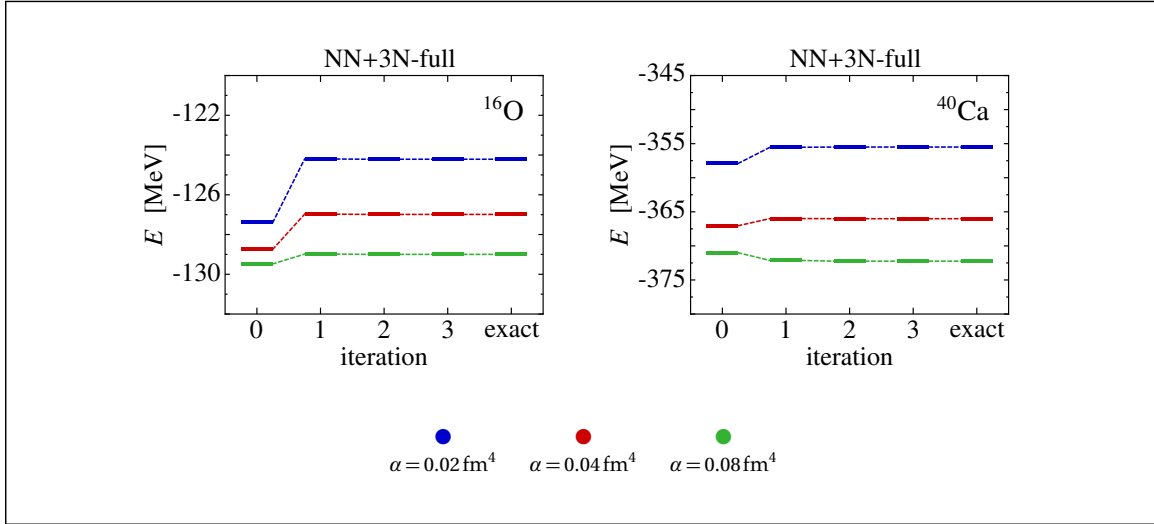


Figure 5.21: CCSD ground-state energies from $e_{\max} = 12$ model spaces and $\hbar\Omega = 24$ MeV, for ^{16}O and ^{40}Ca for the NN+3N-full Hamiltonian in NO2B approximation with $E_{3\max} = 14$ using different HF reference states (see text). The iterative HF normal ordering converges immediately to the results obtained for consistent HF and normal ordering.

about 700 keV. These results demonstrate the importance of consistency between the $E_{3\max}$ of the reference state and of the normal-ordered interaction.

To correct for this inconsistency, the normal-ordered interaction can now be used in yet another HF calculation in order to determine a corrected version of the reference state³. This reference state now contains also $E_{3\max}^{\text{NO}}$ information at the NO2B level and will be close to the exact reference state corresponding to $E_{3\max}^{\text{NO}}$, due to the good performance of the NO2B approximation. Therefore, using this updated reference state in a subsequent normal-ordering for $E_{3\max}^{\text{NO}}$ will then yield a more consistent combination of reference state and normal-ordered matrix elements. This procedure can then be iterated until consistency is achieved.

The CCSD ground-state energies calculated using normal-ordered interactions from reference states obtained from these additional iterative HF calculations and normal orderings are also shown in Figure 5.21. From there it is apparent that already after the first iteration the reference state is typically close enough to the exact reference state such that the CCSD results become indistinguishable from the exact case. As mentioned above, this fast convergence can be attributed to the

³This calculation only involves the normal-ordered zero-, one-, and two-body matrix elements and can be performed very efficiently.

capability of the NO2B approximation to capture most of the 3N information in the lower-rank normal-ordered matrix elements.

5.9.2 Role of the SRG Model Space

For practical applications, the SRG operator flow equation (1.29) has to be converted into matrix representation. To that end, resolutions of the identity in form of infinite summations are inserted between adjacent operators, as it is done to obtain (1.32). Since these infinite summations have to be truncated to finite sums, errors are inevitably introduced in the evolution. The energy and momentum range that the SRG model space spans depends on the oscillator frequency of the HO states in which the flow equation is represented. Particularly for small frequencies this range may not be sufficient for the model space sizes that are accessible in practical computations. As is discussed in more detail in [86, 156], this issue may be overcome by solving the SRG flow equations at a large enough parent frequency and subsequently transforming the obtained matrix elements to smaller target frequencies through a basis transformation. The latter step is facilitated by the fact that the evolved matrix has a band-diagonal structure which makes the transformation numerically more accurate.

Figure 5.22 illustrates the importance of the frequency conversion in a series of CCSD ground-state calculations for nuclei ranging from ^{40}Ca to ^{78}Ni , for which the frequency-converted matrix elements have been generated from the parent frequency $\hbar\Omega = 36$ MeV. In the cases where no frequency conversion has been applied, i.e., where the matrix elements corresponding to a specific value of $\hbar\Omega$ have been computed from SRG evolutions in a model space spanned by HO states of same frequency $\hbar\Omega$, the insufficient energy span of the model space causes an artificial increase of the ground-state energies at smaller frequencies. The ground-state energies obtained using frequency-converted matrix elements, however, show a much more natural behavior. Since for the considered nuclei the energy minimum is located at smaller frequencies, accurately evolved matrix elements are particularly important in this frequency range. In fact, as can be seen in Figure 5.22, the artificial increase of the energies obtained using the non-converted matrix elements shifts the energy minima to higher frequencies and, thus, to smaller binding energies.

The use of the frequency-conversion technique mentioned above allows to circumvent limitations of the SRG due to the insufficiency of the three-body SRG model space for small frequencies by converting matrix elements corresponding

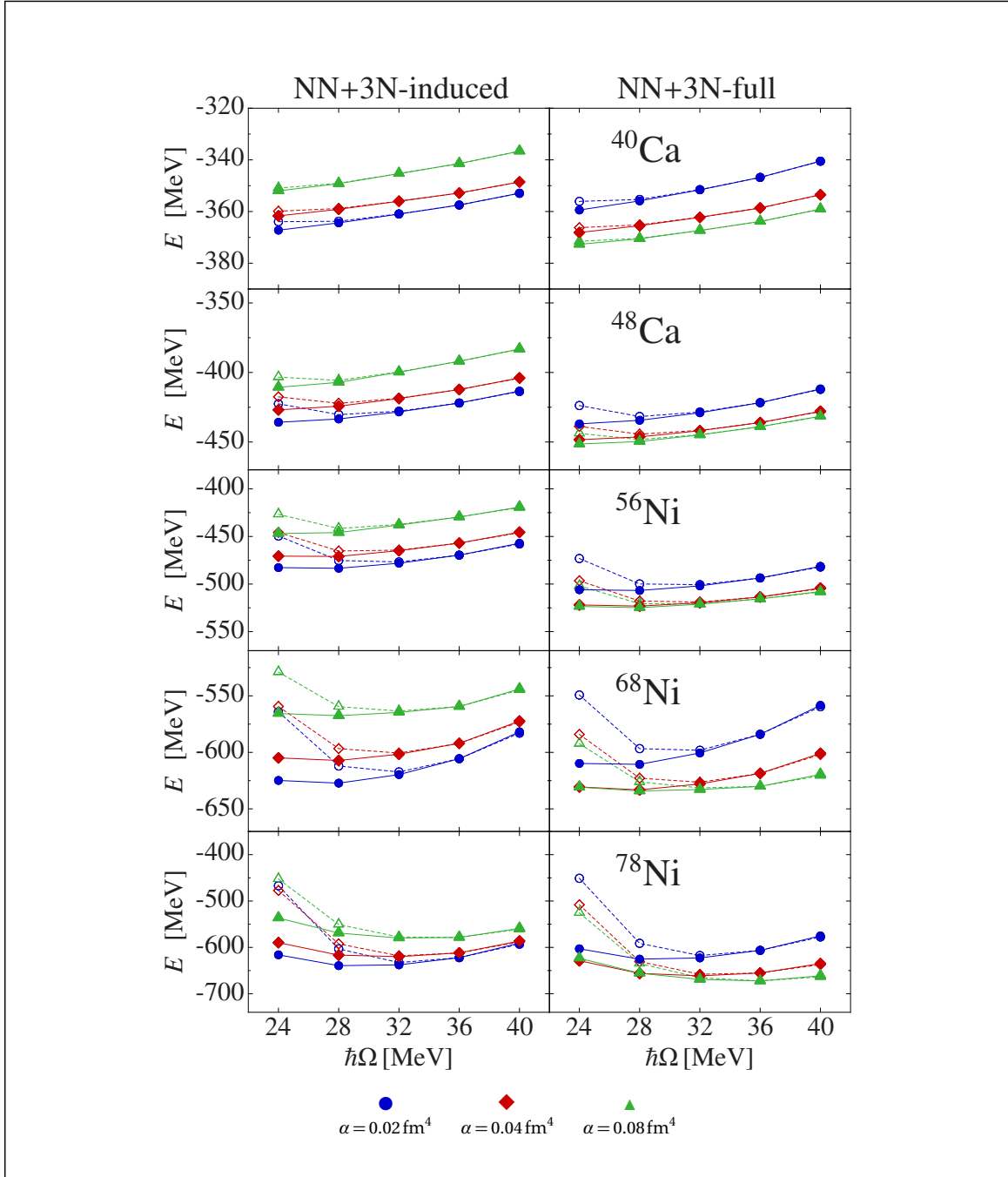


Figure 5.22: Comparison of CCSD ground-state energies corresponding to matrix elements obtained with (full symbols) and without (open symbols) frequency conversion. The calculations were performed in a HF basis with $e_{\max} = 12$ and using the NO2B approximation with $E_{3\max} = 12$. The matrix elements were evolved in the ramp40C SRG model space at parent frequency $\hbar\Omega = 36$ MeV.

to a higher parent frequency to lower frequencies. Consequently, the SRG model space has at least to be sufficiently large in order to accurately evolve the Hamiltonian at the parent frequency. Specifically, the SRG model space is parametrized by the way the infinite summations in the resolution of the identity in (1.32) are truncated. In the present case, these summations are truncated using a truncation E_{SRG} in the energy quantum number of the three-body Jacobi states in which the identity is resolved [86], i.e., in a schematic notation,

$$\hat{\mathbb{1}}^{(3)} \approx \sum_p^{E(|\phi_p^{(3)}\rangle) \leq E_{\text{SRG}}} |\phi_p^{(3)}\rangle \langle \phi_p^{(3)}|. \quad (5.16)$$

Since the SRG evolution can be performed for each total angular momentum J of the Jacobi states separately, and larger J are expected to be less relevant, this motivates the definition of a J -dependent truncation parameter E_{SRG} .

Figure 5.23 (top) presents different parametrizations of the SRG model spaces in terms of E_{SRG} , which will in the following be referred to as *ramps*. The parametrization used so far in this work corresponds to ramp 40C, in which the maximum value $E_{\text{SRG}} = 40$ is used for the smallest angular momenta $J = 1/2, \dots, 5/2$. Then, the truncation parameter is linearly ramped down to $E_{\text{SRG}} = 24$ at $J = 13/2$, where it remains for all higher values of J . The largest SRG model space considered in the following corresponds to ramp 40J, and the effects of different choices of the truncation parameter E_{SRG} , such as the 38G, 40C, 40F, 40K or 40L ⁴ ramps from Figure 5.23, are assessed by comparing CCSD ground-state energies corresponding to these ramps to ground-state energies corresponding to the 40J ramp.

Figure 5.23 shows at the bottom a comparison of the 40C ramp to the 40J ramp based on CCSD ground-state energies for nuclei ranging from ^{36}Ca up to ^{142}Sn , where the experimental ground-state energies are shown as well. As mass number grows, increasing deviations of the 40C from the 40J results are clearly visible, indicating that the 40C ramp becomes less sufficient for heavier nuclei. For the 40C ramp, the heavier nuclei are even almost unbound.

These deviations are considered in more detail in Figure 5.24, where at the top the 40C ramp is once again compared to the 40J ramp, this time in terms of the absolute deviation of the corresponding CCSD results. While for the lighter nuclei there are moderate differences in the ground-state energies related to the different

⁴The number in the name of the ramp denotes the starting E_{SRG} at small angular momenta, while the letter has no further meaning.

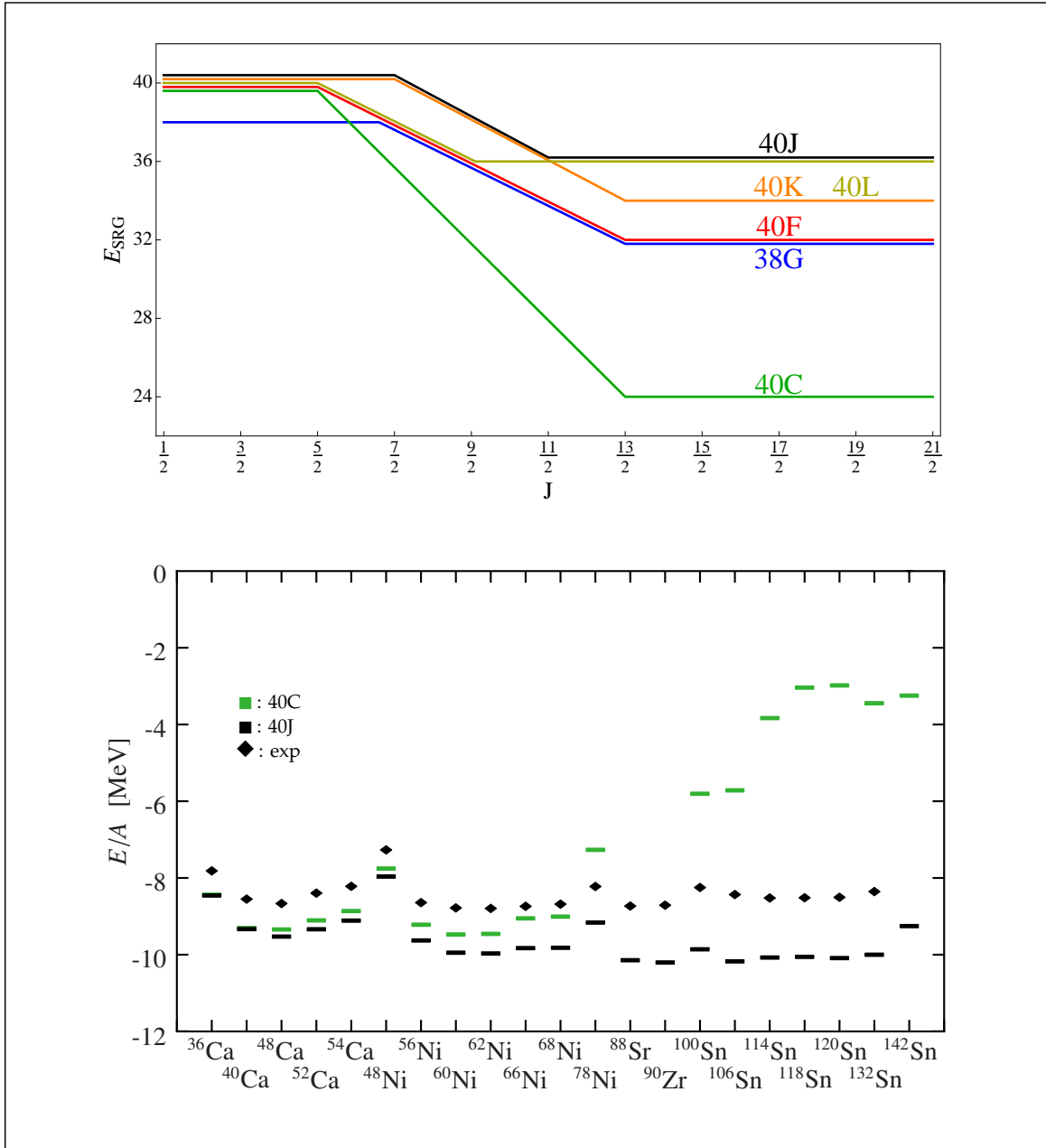


Figure 5.23: Top: Various choices of parametrizations of the SRG model space in terms of the truncation parameter E_{SRG} . Bottom: Experimental ground-state energies compared to CCSD results from a HF basis with $e_{\text{max}} = 12$, obtained from the 40C and 40J ramp and the NN+3N-full Hamiltonian at $\alpha = 0.08 \text{ fm}^4$ and in NO2B approximation with $E_{3\text{max}} = 14$, using frequency-converted matrix elements at $\hbar\Omega = 24 \text{ MeV}$ with parent frequency of 36 MeV .

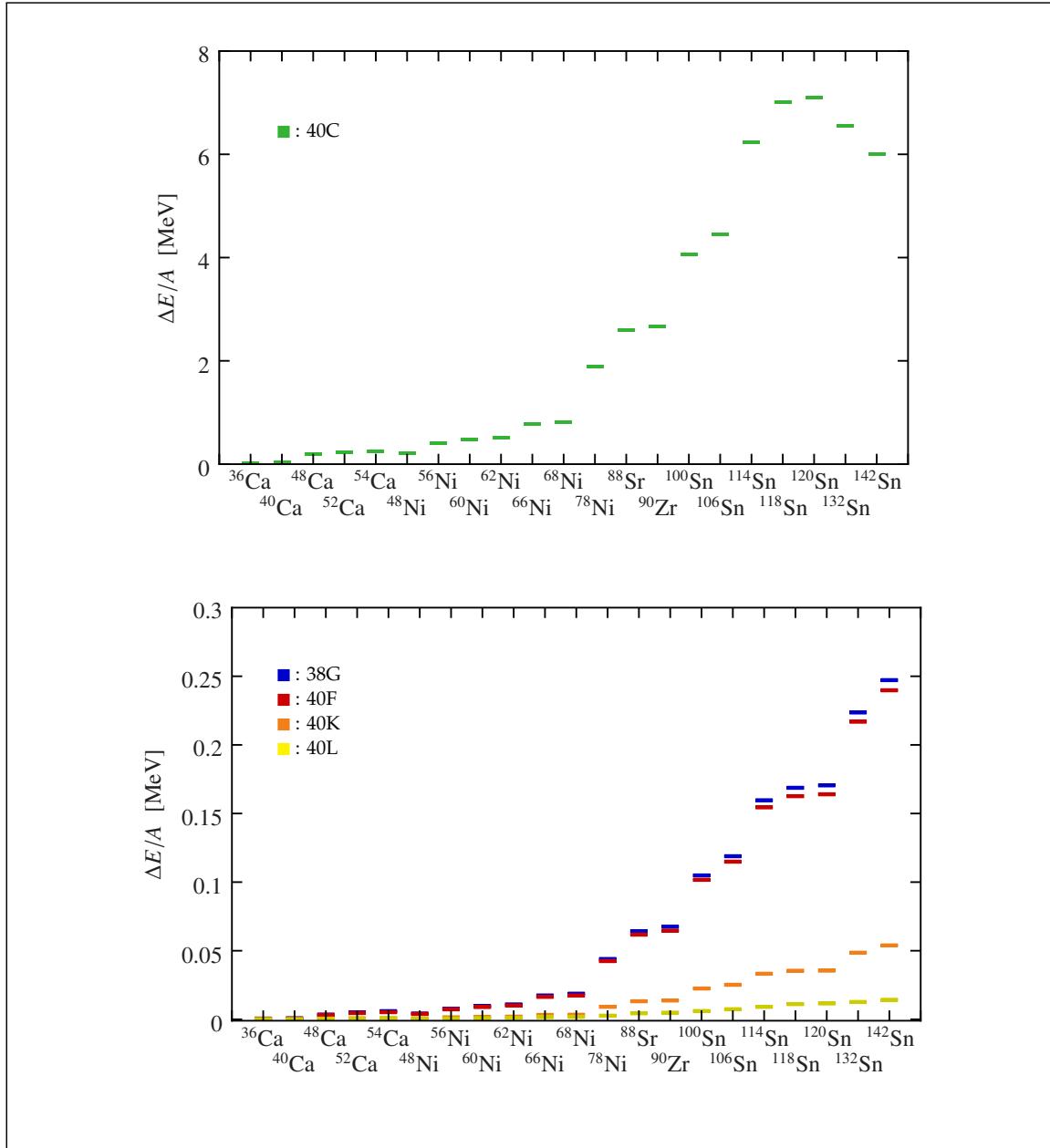


Figure 5.24: Deviations of CCSD ground-state energies (per nucleon) corresponding to ramp 40J to the other SRG ramps from Figure 5.23, for the NN+3N-full Hamiltonian at $\alpha = 0.08\text{fm}^4$ in NO2B approximation with $E_{3\text{max}} = 14$, using frequency-converted matrix elements at $\hbar\Omega = 24\text{ MeV}$ with parent frequency of 36 MeV . While ramp 40C is completely inappropriate in the heavy regime, the small deviations for ramp 40K and 40L suggest that ramp 40J allows for accurate calculations. The calculations employed a HF basis with $e_{\text{max}} = 12$.

choices of SRG model spaces, for ^{56}Ni these deviations already reach 0.5 MeV per nucleon. From there, the deviations increase quickly, reaching values up to 7 MeV per nucleon for ^{120}Sn . Therefore, ramp 40C is far from sufficient for calculations of nuclei with mass numbers $A > 60$. There are distinct jumps in the deviation plot, occurring, for instance, between nuclei $^{68,78}\text{Ni}$ or $^{120,132}\text{Sn}$. Such jumps occur each time a new high-momentum single-particle orbit in Figure 4.1 is occupied in the reference state. For example, the reference configurations of ^{68}Ni and ^{78}Ni differ by the $1g_{9/2}$ shell, and the configurations of ^{120}Sn and ^{132}Sn differ by the $1h_{11/2}$ shell. This observation hints at a growing importance of the large- J part of the SRG model space, which is subject to much stronger truncation for ramp 40C than the low- J part is.

Consequently, the other ramps presented in Figure 5.23 perform much better, as they imprint less truncations on the large- J SRG model space than ramp 40C does. This is illustrated in the bottom plot of Figure 5.24. Among these alternative ramps, even the one corresponding to the smallest model space, ramp 38G, shows deviations of less than 0.25 MeV per nucleon from the 40J ramp. By comparing the 38G ramp with 40F, the effect of the E_{SRG} cut for the small angular momenta $J \leq 5/2$ can be probed, which turns out to have only a minor effect. Therefore, it may be concluded that for these small J the SRG model space is sufficiently large at $E_{\text{SRG}} = 40$. Similar comparisons suggest that, with respect to 40C, increasing E_{SRG} for large angular momenta is crucial. Ground-state energies corresponding to ramps 40K and 40J then only differ by at most 50 keV over the whole mass range. This indicates that ramp 40J is an appropriate choice for nuclear calculations up to mass numbers $A = 150$, with uncertainties related to the SRG model-space truncation below 100 keV per nucleon.

The use of larger SRG model spaces also has a decisive impact on the previously observed $E_{3\text{max}}$ -dependence of the ground-state energies. Figure 5.25 compares the $E_{3\text{max}}$ dependence of ground-state energies, measured by their difference at the two $E_{3\text{max}}$ values of 12 and 14, corresponding to frequency-converted matrix elements obtained from ramps 40C and 40J. The striking observation is that for the larger SRG model space the $E_{3\text{max}}$ dependence does not increase, while it does for the smaller model space. This indicates that much of the previously observed $E_{3\text{max}}$ dependence was induced by the use of insufficient SRG model spaces and that heavier nuclei may be accessible with manageable values of $E_{3\text{max}}$.

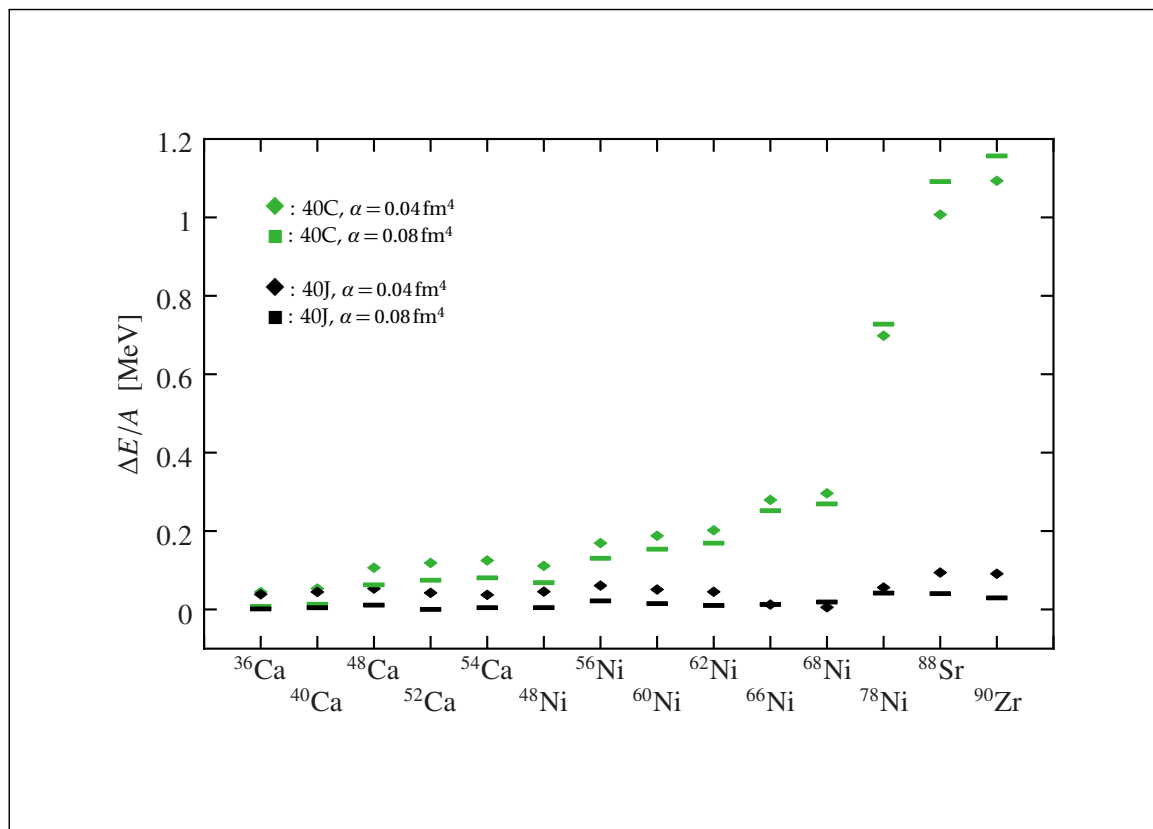


Figure 5.25: Comparison of the $E_{3\text{max}}$ -dependence of CCSD ground-state energies for the NN+3N-full Hamiltonian in NO2B approximation evolved in the SRG model spaces corresponding to ramp 40C and 40J. The ground-state energies are evaluated for $E_{3\text{max}} = 12$ and $E_{3\text{max}} = 14$, and the energy difference (per nucleon) is shown in the plot. The results clearly indicate an enhancement of the $E_{3\text{max}}$ -dependence due to the insufficient model space corresponding to ramp 40C, which increases with the nuclear mass number. Other parameters of the calculations as in Figure 5.24.

5.9.3 Results for Heavy Nuclei

The discussion of heavier nuclei will be based on SRG-transformed Hamiltonians at flow parameters $\alpha = 0.04 \text{ fm}^4$ and 0.08 fm^4 for which the Coupled-Cluster method provides nearly converged results. Examples for convergence patterns of ground-state energies of nuclei ranging from ^{48}Ni to ^{132}Sn are shown in Figure 5.26. Except for the heaviest nucleus ^{132}Sn considered in Figure 5.26, all other calculations are reasonably well converged within the model spaces up to $e_{\text{max}} = 12$. The cluster expansion also converges quickly. For ^{100}Sn and the NN+3N-full Hamiltonian at $\alpha = 0.04 \text{ fm}^4$, for instance, the reference energy is -590.8 MeV , the CCSD correlation energy amounts to -375.5 MeV and the CR-CC(2,3) triples correction contributes -26.3 MeV , which is less than 3 % of the total binding energy. For $\alpha = 0.08 \text{ fm}^4$ the convergence is naturally faster, with reference energy of -767.2 MeV , CCSD correlation energy of -218.8 MeV and the triples correction of -17.7 MeV . These numbers suggest that even in the regime of heavy nuclei the Coupled-Cluster method is expected to provide, for a given Hamiltonian at fixed α , the corresponding nuclear ground-state energies up to an accuracy of few percent.

In a next step it is necessary to identify the values of $E_{3\text{max}}$ required for calculations of heavy nuclei. Figure 5.27 presents CCSD ground-state energies of various nuclei for $E_{3\text{max}}$ values ranging from 10 to 18. For all but the heaviest nucleus ^{132}Sn convergence is achieved at $E_{3\text{max}} = 18$, and for most of the lighter nuclei already at much smaller values of $E_{3\text{max}}$. It is noteworthy that for the energies using SRG-evolved matrix elements from ramp-40J model spaces the $E_{3\text{max}}$ dependence is larger for the softer interaction, which is opposite to the observations made for ramp 40C and lighter nuclei. This may hint at the growing importance of SRG-induced 3N interactions.

Another interesting aspect of the $E_{3\text{max}}$ truncation is its impact on the $\hbar\Omega$ dependence. In Figure 5.28 the $\hbar\Omega$ dependence of CCSD ground-state energies of nuclei ^{40}Ca , ^{56}Ni and ^{132}Sn is studied at various values of $E_{3\text{max}}$. For ^{40}Ca , the $\hbar\Omega$ dependence decreases with increasing $E_{3\text{max}}$ up to the point where it is practically flat for $E_{3\text{max}} = 16$. The fact that the curves have positive slope for smaller values of $E_{3\text{max}}$ implies that for nuclei like ^{40}Ca , too small values of $E_{3\text{max}}$ shift the optimal oscillator frequency to smaller frequencies, which is also confirmed by the ^{56}Ni results. For ^{132}Sn , the situation is reversed. Here, the optimal frequency is shifted to larger frequencies if a too small $E_{3\text{max}}$ is used. In fact, the $E_{3\text{max}} = 16$ results suggest that the optimal frequency for ^{132}Sn lies even somewhat below $\hbar\Omega = 24 \text{ MeV}$.

A systematic survey of CR-CC(2,3) ground-state energies of medium-mass and

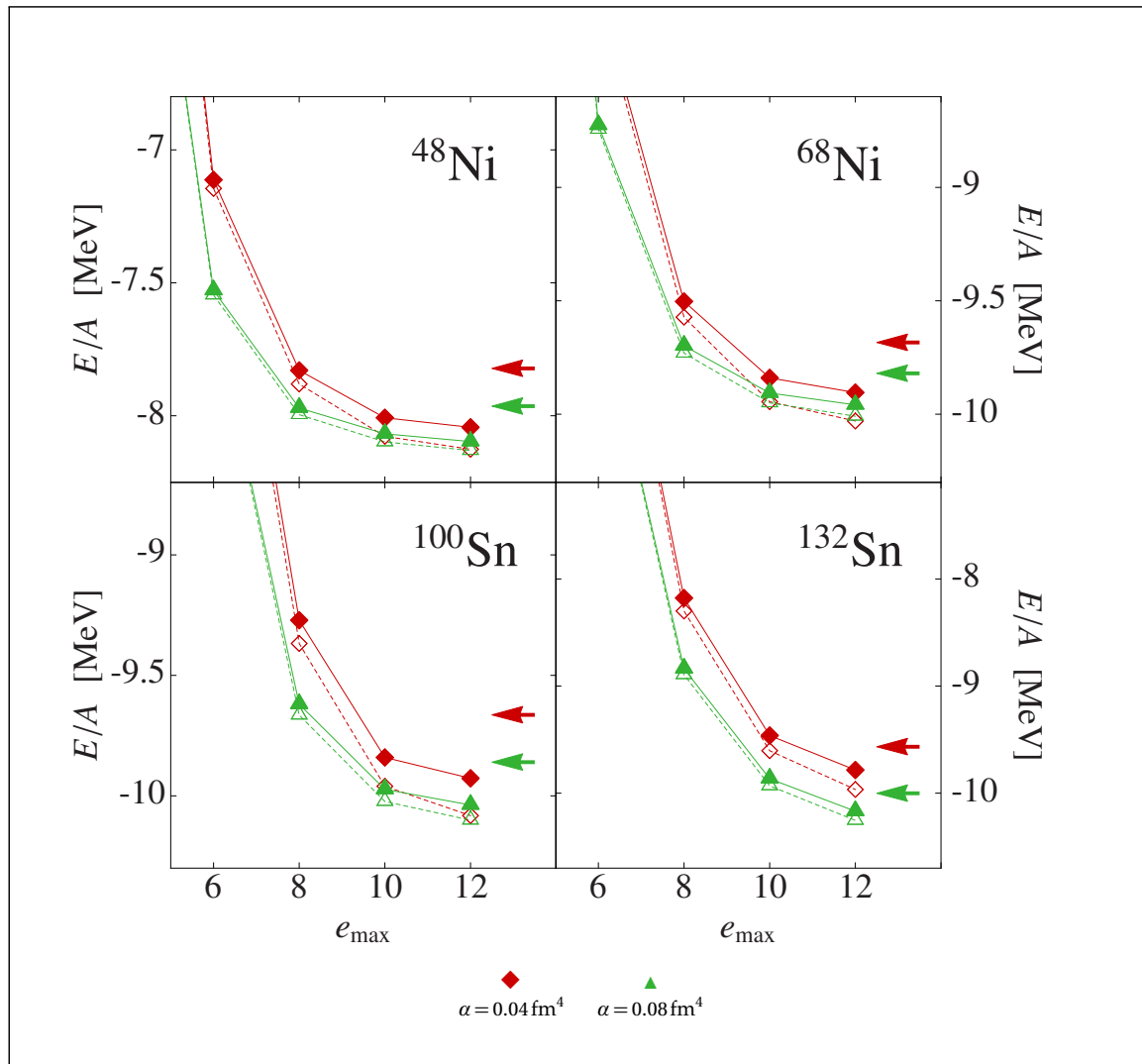


Figure 5.26: Convergence and $\Lambda\text{CCSD(T)}$ (open symbols) and CR-CC(2,3) (full symbols) ground-state energies of ^{48}Ni , ^{68}Ni , ^{100}Sn and ^{132}Sn for the NN+3N-full Hamiltonian in NO2B approximation with $E_{3\max} = 14$ and using a Hartree-Fock basis with $\hbar\Omega = 24$ MeV. The arrows indicate the CCSD results from the $e_{\max} = 12$ model space.

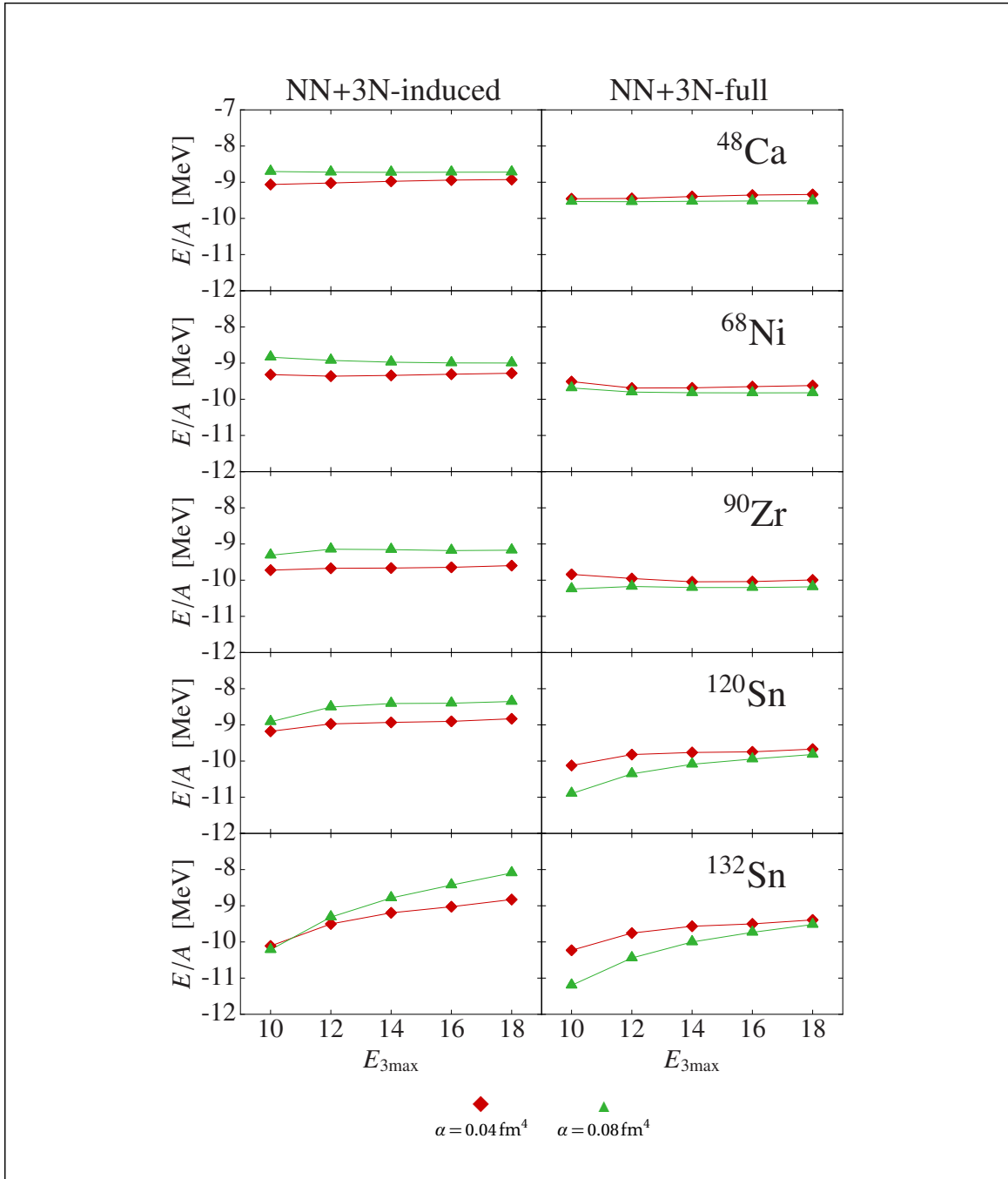


Figure 5.27: Convergence of CCSD ground-state energies for medium-mass and heavy nuclei ranging from ^{48}Ca to ^{132}Sn , for the $\text{NN}+3\text{N}$ -induced and $\text{NN}+3\text{N}$ -full Hamiltonian in NO2B approximation, with respect to $E_{3\max}$. All calculations are performed in a HF basis with oscillator frequency $\hbar\Omega = 24$ MeV and at $e_{\max} = 12$.

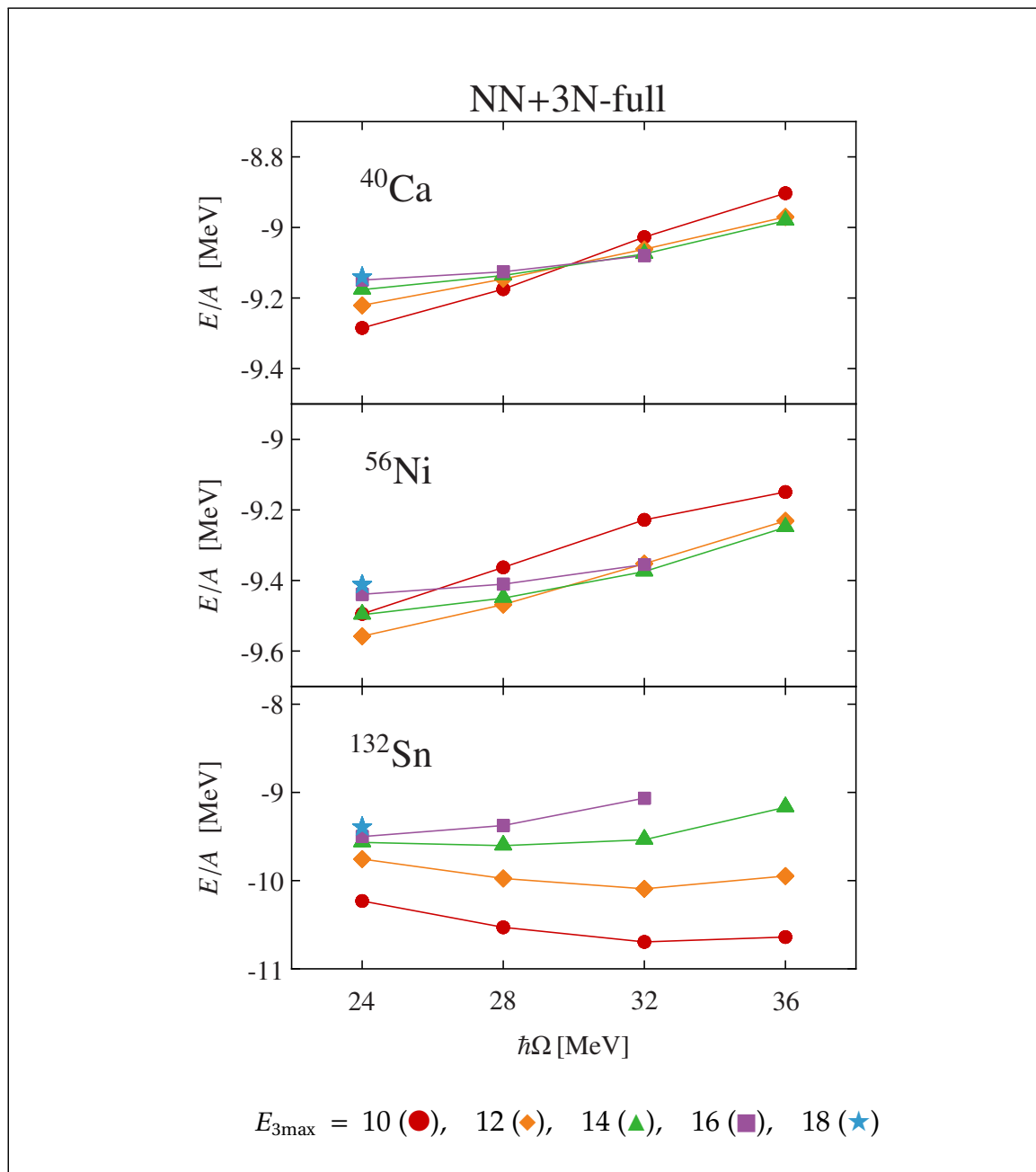


Figure 5.28: Frequency dependence of CCSD ground-state energies of ^{40}Ca , ^{56}Ni and ^{132}Sn for the NN+3N-full Hamiltonian in NO2B approximation for various values of $E_{3\text{max}}$. The calculations employed a HF basis at $e_{\text{max}} = 12$.

heavy nuclei ranging from ^{16}O to ^{132}Sn with emphasis on the Ca, Ni, and Sn isotopic chains is presented in Figure 5.29. All results are obtained using $E_{3\text{max}} = 18$ and for the two SRG flow parameters $\alpha = 0.04 \text{ fm}^4$ and $\alpha = 0.08 \text{ fm}^4$, which are used to quantify the flow-parameter dependence of the results. In panel (a), the NN+3N-induced Hamiltonian is employed. The corresponding ground-state energies show a significant increase in the flow-parameter dependence, rising from about 0.1 MeV per nucleon for ^{16}O to about 1 MeV per nucleon for ^{132}Sn , indicating growing contributions of SRG-induced 4N (and multi-nucleon) interactions out of the initial NN interaction. From the direction in which the ground-state energies move for smaller values of the flow parameter it can be concluded that the induced many-body interactions have an attractive net effect. In order to confirm that this is a general property of chiral NN Hamiltonians, in panel (a) also the N^2LO -optimized chiral NN interaction is used [159]. The flow-parameter dependence is very similar to the former calculations for light and medium-mass nuclei, and is reduced for heavy nuclei, resulting in a flow-parameter dependence of about 0.5 MeV per nucleon for ^{132}Sn . Even with the reduced amount of induced 4N and multi-nucleon interactions for the N^2LO -optimized interaction, induced many-body interactions out of the initial NN interaction are a new challenge in the heavy-mass regime which, if not addressed, will prevent any attempt to reliably calculate ground-state energies of heavy nuclei based on chiral interactions. In order to emphasize that the observed flow-parameter dependencies are indeed to be attributed to induced many-body interactions and not truncations in the many-body treatment such as the cluster truncation, in panel (b) the contributions of the CR-CC(2,3) triples correction are shown.

Considering the large flow-parameter dependence of the NN+3N-induced results, the much reduced flow-parameter dependence of about 0.1 MeV per nucleon for the results shown in panel (c) using the NN+3N-full Hamiltonian with the $\Lambda_{3\text{N}} = 400 \text{ MeV}$ regular cutoff is remarkable. This reduced flow-parameter dependence has to be the consequence of a delicate cancellation of the attractive induced 4N contributions from the initial NN interaction with additional repulsive 4N contributions originating from the initial 3N interaction. The direction of the flow-parameter dependence of the ground-state energies is reversed to the NN+3N-induced case, indicating that the attractive induced interactions are in fact slightly overcompensated. Since for the NN+3N-induced case the contributions of induced many-body interactions grow with the nuclear mass, while the NN+3N-full results exhibit a virtually constant flow-parameter dependence over the whole considered mass range, the contributions from the repulsive induced

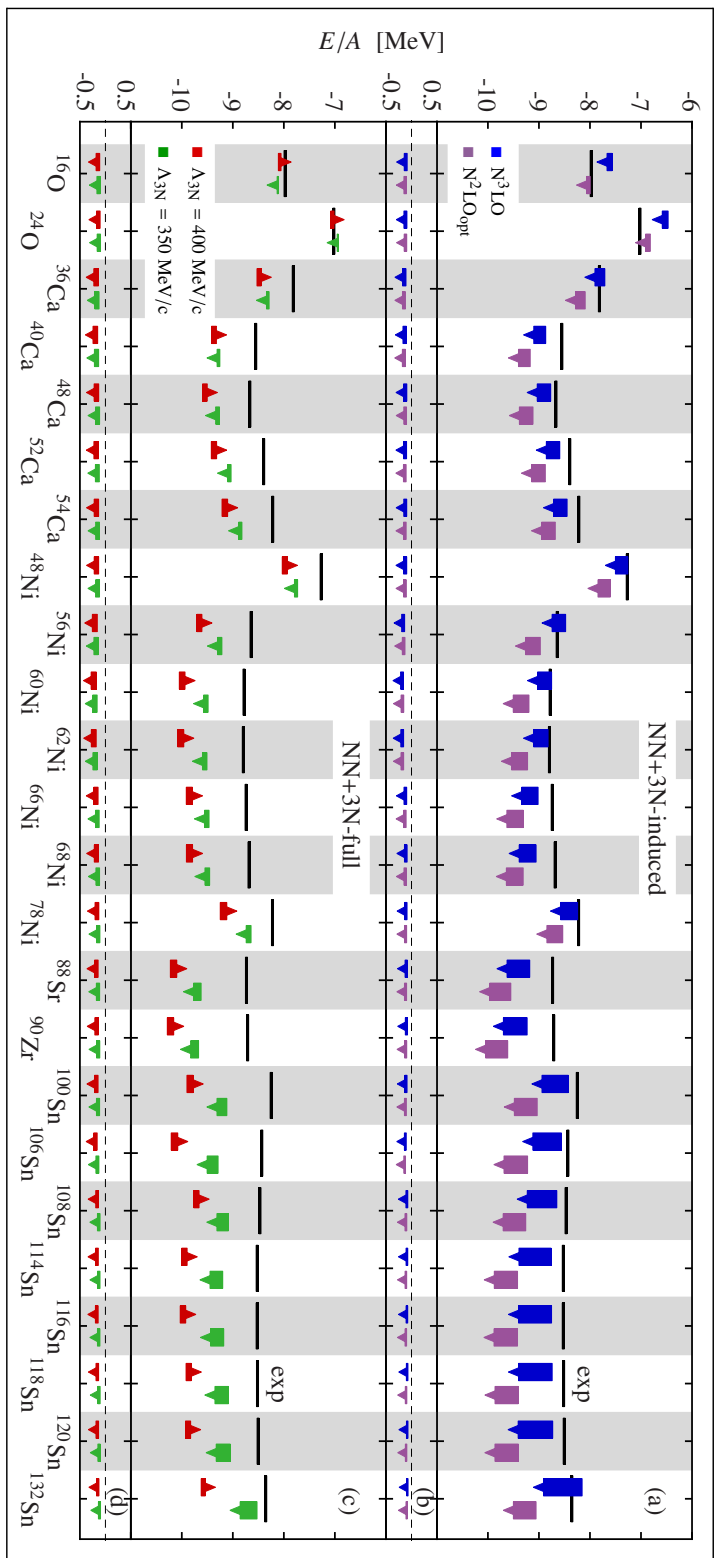


Figure 5.29: Ground-state energies from CR-CC(2,3) for (a) the NN+3N-induced Hamiltonian starting from the $N^3\text{LO}$ and $N^2\text{LO}$ -optimized NN interaction and (c) the NN+3N-full Hamiltonian with $\Lambda_{3N} = 400 \text{ MeV}$ and $\Lambda_{3N} = 350 \text{ MeV}$. The boxes represent the spread of the results from $\alpha = 0.04 \text{ fm}^4$ to $\alpha = 0.08 \text{ fm}^4$, and the tip points into the direction of smaller values of α . Also shown are the contributions of the CR-CC(2,3) triples correction to the (b) NN+3N-induced and (d) NN+3N-full results. All results employ $\hbar\Omega = 24 \text{ MeV}$ and 3N interactions with $E_{3\text{max}} = 18$ in NO2B approximation and full inclusion of the 3N interaction in CCSD up to $E_{3\text{max}} = 12$. Experimental binding energies [160] are shown as black bars.

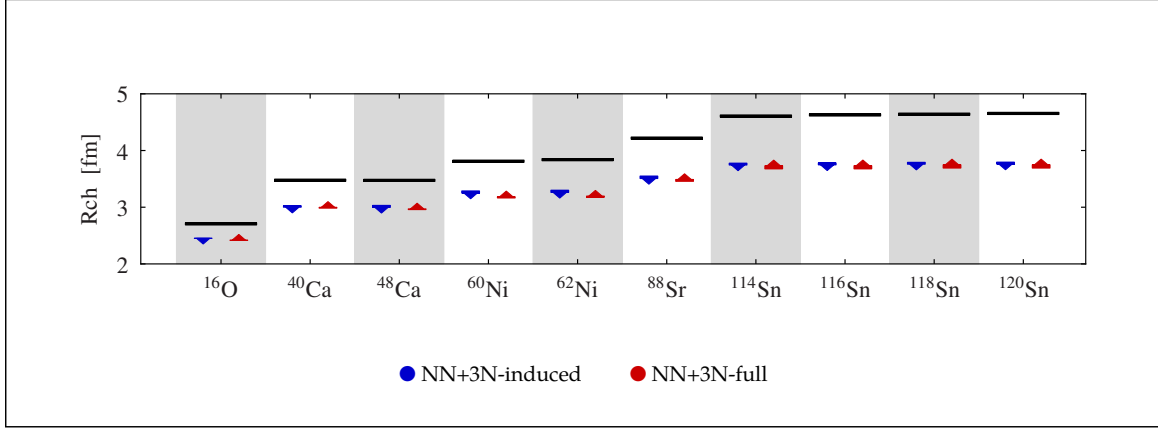


Figure 5.30: Charge radii obtained from Hartree-Fock calculations for the NN+3N-induced and NN+3N-full Hamiltonian with parameters as in Figure 5.29. Experimental values [161] are shown as black bars.

many-body interaction grow the same way with the the nuclear masses as the contributions from the attractive induced many-body interactions do. This statement can be confirmed by reducing the initial 3N cutoff from $\Lambda_{3N} = 400$ MeV to 350 MeV. For light nuclei this cutoff reduction is known to weaken the repulsive 4N component originating from the initial 3N interaction [86]. Consequently, the flow-parameter dependence of the ground-state energies for the 350 MeV NN+3N-full Hamiltonian points in the same direction as for the NN+3N-induced Hamiltonian, because the repulsive contributions are no longer able to overcompensate the attractive contributions. Furthermore, the 350 MeV NN+3N-full Hamiltonian results exhibit a flow-parameter dependence that increases with mass number. This shows that in addition to the fact that the repulsive contributions are not only smaller for the $\Lambda_{3N} = 350$ MeV NN+3N-full Hamiltonian compared to the 400 MeV case, but that they also grow slower with the nuclear masses. Therefore, an almost constant flow-parameter dependence of the NN+3N-full results over the whole mass range is not a general property of NN+3N-full Hamiltonians and may only be achieved in a small window of initial 3N regular momentum cutoffs around $\Lambda_{3N} = 400$ MeV.

Taking advantage of the robust cancellation of SRG-induced 4N terms for the NN+3N-full Hamiltonian with $\Lambda_{3N} = 400$ MeV, resulting in a very small α dependence, the obtained ground-state energies may be compared to experiment. The ground-state energies of the oxygen isotopes are very well reproduced. Starting from the Ca isotopes, a systematic and slowly increasing deviation of the theoret-

ical results from experiment is visible, which is of the order of 1 MeV per nucleon. Apart from this constant energy shift, the experimental trend of the binding energies is nicely reproduced. Therefore, these results represent a first confirmation that chiral Hamiltonians that have been determined in the few-body sector are also capable of qualitatively describe heavy nuclei. Furthermore, since the many-body problem can be solved very accurately using *ab initio* methods, potential shortcomings of the input Hamiltonian may be identified. In the present case, the overbinding of the NN+3N-full results are well beyond theoretical uncertainties and, thus, may be considered a deficiency of the current chiral NN+3N-full Hamiltonian. This outcome is of course not surprising given the inconsistent chiral perturbation order of the employed NN and 3N interaction and the neglect of the chiral 4N force at N^3LO .

While chiral Hamiltonians provide good results for binding energies with deviations from experiment that might be resolved using improved chiral Hamiltonians, charge radii come out significantly too small. Figure 5.30 shows charge radii on the HF level for nuclei for which the experimental value is known [161]. An increasing deviation from experiment is apparent, about 0.3 fm or 10 % for ^{16}O , up to about 1 fm or 20 % for ^{132}Sn . It should be noted that the radius operator has not been SRG evolved. However, neither the consistent evolution of the radius nor beyond-HF correlation effects are expected to have a significant impact on these findings.

Chapter 6

Conclusion

The two foundations of *ab initio* nuclear structure theory – the fundamental description of the nuclear interaction, and methods that provide accurate solutions to the many-body problem along with some estimate of the errors involved – have both seen impressive progress in recent years. The goal of the present work was to combine and advance these developments into a theoretical and computational framework capable of performing accurate *ab initio* nuclear structure calculations of medium-mass and heavy nuclei.

The main focus of this work is the treatment of nucleon correlations in the many-body problem. Here, the Coupled-Cluster method with iterative single- and double-excitations contributions combined with a non-iterative treatment of triply excited clusters constitutes a framework that is both, efficient and sufficiently accurate in solving the many-body Schrödinger equation in order to make acceptable estimates for nuclear ground-state energies. The spherical formulation of Coupled-Cluster theory was one key element to the success of this work. However, while Coupled-Cluster theory in its *m*-scheme formulation is already notorious for the human effort required to derive and implement the method, the spherical formulation multiplies this demand. Nevertheless, even under these circumstances, spherical Coupled-Cluster theory has highly appealing properties that make implementing the method worthwhile in the long run. For one, it extends the reach of *ab initio* Coupled-Cluster calculations to large mass numbers way beyond the reach of an *m*-scheme formulation. Furthermore, the spherical scheme is also sufficiently efficient to allow calculations including explicit 3N interactions which makes the Coupled-Cluster method a favorable tool to test approximation schemes for 3N interactions, such as the normal-ordering approximation. Through the inclusion of triples excitation effects in form of *a posteriori* non-iterative energy corrections, the degree of convergence of the cluster expansion at the level of the triply excited clusters can be estimated. Using SRG-softened interactions, the results suggest fast convergence of the cluster expansion. However, for harder interactions or even the bare nuclear interaction, the quality of triples-corrected CCSD ground-state energies is questionable. Since full CCSDT calculations cannot be done at present time, two different triples-correction methods have been considered in order to estimate their quality. The respective results lie sufficiently close, motivating the claim that both represent reasonable approximations to the exact triples contributions to the energy.

Three-nucleon forces play a central role in present-time nuclear structure theory and applications. Chiral three-nucleon forces are known to be important for the description of nuclear properties, and the framework of chiral effective field

theory provides nuclear physicists with a convenient approach to the construction of QCD-based nuclear interactions and electro-weak currents, due to its ability to assign power-counting orders to the many possible operator structures of the interactions, which in turn allows to identify the most relevant ones of these operator structures. This is a particularly important feature of the chiral perturbation approach for the derivation of three- and more-nucleon interactions, because their treatment is much more complicated in a purely phenomenological approach. The generation of chiral interactions still is a dynamic field, even more today after the great potential of chiral interactions has been realized in nuclear many-body and reaction calculations. The most obvious improvement over the current status of chiral interactions concerns the availability of the 3N interaction at $N^3\text{LO}$ in order to achieve consistency between the NN and 3N interactions in the chiral expansion. This will further be a next step towards assessing convergence of nuclear observables with respect to the chiral expansion parameter which, however, would in principle also require the consideration of the chiral 4N interaction at this order. The inclusion of the Δ degree of freedom, which also causes a shift of certain diagrams to lower power-counting orders, is another exciting prospect for the future.

But even without chiral three-nucleon interactions, nuclear-structure calculations that rely on SRG-evolved or otherwise renormalized interactions, are inevitably confronted with *induced* three-nucleon forces. Regardless their origin, the inclusion of three-nucleon interactions into the many-body calculations poses a challenge which has to be met with caution in order to avoid the introduction of severe sources of uncertainty, and lots of research has been dedicated to this issue. This work demonstrates that a proper inclusion of three-nucleon interactions is possible for many-body calculations operating up to nuclear masses of about $A \approx 150$, using manageably large SRG model spaces and reachable values of $E_{3\text{max}}$. It was shown that an approximate treatment of 3N interactions in the many-body calculations via the normal-ordering two-body approximation is satisfactory at the level of overall accuracy targeted at in *ab initio* nuclear structure calculations. A remarkable outcome of this work is that a single Hamiltonian, more precisely the SRG-evolved NN+3N-full Hamiltonian with reduced cutoff-momentum of 400 MeV provides, within the computational framework used in this work, a qualitative description of nuclei ranging from ^{16}O to ^{132}Sn , and maybe even beyond. Given the still quite preliminary status of the chiral interactions, already these results are sufficiently encouraging to conclude that it is worthwhile to proceed further along this path of research.

In conclusion, *ab initio* nuclear structure theory is a vivid branch of physics and the results of this work indicate great potential of the first-principle description of the nuclear many-body problem. Future research will have to address further observables besides (ground-state) energies. For example, although energies are reasonably reproduced by the chiral interactions, radii come out too small. However, when using SRG-transformed Hamiltonians, the observables have to undergo analogous transformations, and electromagnetic observables require the inclusion of chiral electro-weak currents into the calculations. As already mentioned above, the chiral 3N interaction at $N^3\text{LO}$ will be a next step towards the description of nuclear properties using interactions at consistent power counting orders, giving insight in the convergence properties of the chiral expansion and may enable uncertainty estimates. In the long run, nuclear theory will have to deal with 4N interactions, either in form of the initial chiral 4N interaction at $N^3\text{LO}$, or, unless novel generators are found that reduce the amount of SRG-induced 4N contributions, with these induced 4N interactions.

Appendix A

Excited Nuclear States

The spherical EOM-CCSD method considered in this work enables calculations of excited states of closed-shell nuclei. The low-energy spectra of such nuclei typically consist of simple particle-hole excitations and collective rotational or vibrational states. The current method of choice for collective states has been the *Random Phase Approximation* (RPA) [78], in which excited states are described via linear 1p1h (de-) excitations on a ground state which contains certain correlations. This approach has also been extended to include 2p2h (de-) excitations, known as *second RPA* [162,163]. Since the quasi-Boson approximation that enters the derivation of the RPA equations works better for collective states than for single-nucleon excitations, RPA methods have difficulties to describe the latter type of excited nuclear states. The EOM-CCSD approach also employs linear excitations up to the 2p2h level. However, since these excitations act on the *fully correlated* CCSD ground state, EOM-CCSD is considered superior to the RPA approaches and may, therefore, be able to describe single-nucleon excitations as well as collective states.

Typically, those excited states are rather high-lying, beyond the neutron separation threshold, and no longer bound. These states are, therefore, not expected to be highly accurate reproduced in calculations in which the continuum is not properly taken into account. Additionally, some of the low-lying 0^+ states in closed-shell nuclei, such as ^{16}O , are suspected to have α -cluster structure [164] and would, consequently, require 4p4h excitations for an accurate description, which is beyond the scope of EOM-CCSD.

This section focuses mainly on the computational aspects of EOM-CCSD calculations rather than a thorough physical discussion, although it will address the question raised above as to whether EOM-CCSD is able to describe single-nucleon excitations as well as collectivity within the same framework. The EOM-CCSD eigenvalue problem constitutes a non-Hermitean eigenvalue problem, which can reliably be solved using non-symmetric Lanczos methods provided by the Arnoldi Package [165]. Since the matrix-vector multiplications can be distributed via MPI, these multiplications can be evaluated quickly using multiple computing nodes. This way, matrices of linear dimensions of hundreds of millions can be diagonalized. However, for large linear dimensions the orthogonalizations of the Lanczos vectors, which are performed on a single computing node only, does in practical calculations eventually spoil the scaling.

When calculating excited states it is important to take spurious center-of-mass excitations into account. While ground states are approximately free from center-of-mass contaminations [152], these contaminations cannot be ignored for the ex-

cited states. One way to probe the degree of center-of-mass contamination is to use the Hamiltonian (1.3),

$$\hat{H} = \frac{1}{A} \sum_{i<j}^A \frac{(\hat{\mathbf{p}}_i - \hat{\mathbf{p}}_j)^2}{2m} + \sum_{i<j}^A \hat{V}_{ij}^{\text{NN}} + \sum_{i<j<k}^A \hat{V}_{ijk}^{\text{3N}} + \lambda_{\text{CM}} \hat{H}_{\text{CM}}, \quad (\text{A.1})$$

augmented by the center-of-mass Hamiltonian $\lambda_{\text{CM}} \hat{H}_{\text{CM}}$ with

$$\hat{H}_{\text{CM}} = \frac{1}{2Am} \hat{\mathbf{P}}_{\text{CM}}^2 + \frac{1}{2} (Am\Omega_{\text{CM}})^2 \hat{\mathbf{R}}_{\text{CM}} - \frac{3}{2} \hbar \Omega_{\text{CM}}, \quad (\text{A.2})$$

and to study the dependence of the eigenvalues on the parameter λ_{CM} . In the exact case the nuclear wavefunction factorizes into an intrinsic and a center-of-mass part, and the intrinsic energies are clearly independent of λ_{CM} . Furthermore, for $\lambda_{\text{CM}} \neq 0$ the center of mass will then be in a \hat{H}_{CM} eigenstate $|n\rangle$ with eigenenergy

$$E_{\text{CM},n} = \lambda_{\text{CM}} n \hbar \Omega_{\text{CM}} \quad (\text{A.3})$$

that scales linearly with the parameter λ_{CM} . At large enough values of λ_{CM} only the center-of-mass ground states $|0\rangle$ will be visible at the lower end of the energy spectrum. In the following calculations the oscillator frequency Ω_{CM} of the center-of-mass potential is chosen to coincide with the HO basis frequency Ω , but other choices are possible as well [152].

Figure A.1 shows the λ_{CM} -dependence of CCSD ground-state energies of $^{16,24}\text{O}$ and $^{40,48}\text{Ca}$ for the chiral NN-only and NN+3N-full Hamiltonian, at two values of the SRG flow parameter. The energies change only very little when λ_{CM} is varied from 0.0 to 1.0, about 250 keV for ^{16}O and about 500 keV for ^{40}Ca . Excited states, however, exhibit a much stronger dependence on λ_{CM} , as can be seen in Figures A.2 and A.3, where the lowest 10 $J^\pi = 0^+$ and $J^\pi = 2^+$ states of ^{16}O and ^{40}Ca are shown. In Figures A.2 and A.3 it is clearly visible how spurious excited states are linearly shifted upwards linearly with λ_{CM} . Typically at values of λ_{CM} around 1.0 the low-energy spectra have become stable with respect the λ_{CM} variations.

Another important information is the rate of convergence of the EOM-CCSD calculations with respect to model space size. The convergence of the 3 lowest $J^\pi = 0^+, 2^+, \text{ and } 4^+$ states of $^{16,24}\text{O}$ and $^{40,48}\text{Ca}$ is considered in Figures A.4 and A.5. The calculations used $\lambda_{\text{CM}} = 1.0$. Regarding convergence, the results are encouraging. Most states, and in particular the low-lying ones, are converged already in smaller Coupled-Cluster model spaces. This allows a clear identification of high- and low-lying states.

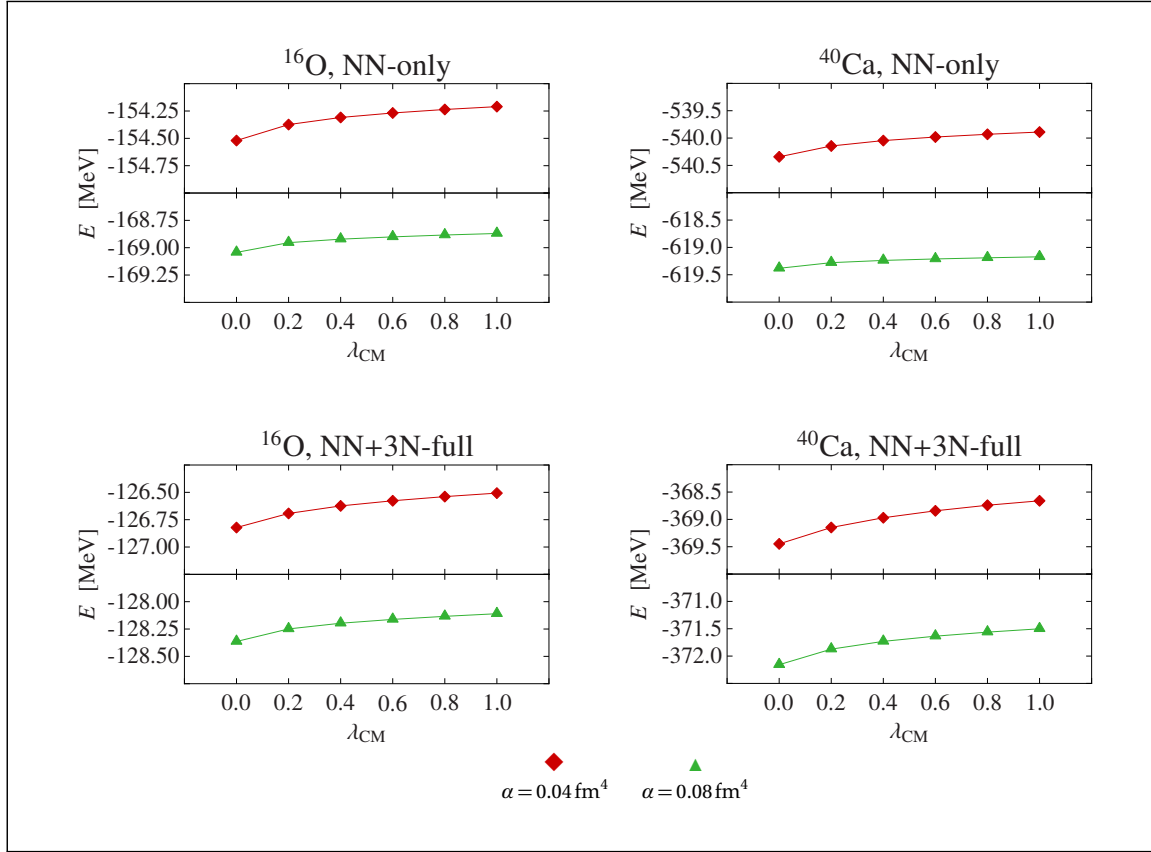


Figure A.1: Dependence of ^{16}O and ^{40}Ca CCSD ground-state energies on λ_{CM} using a HO basis with $e_{\text{max}} = 10$, and at $\hbar\Omega = 20$ MeV.

Figures A.2 and A.3 show that beyond some threshold energy, EOM-CCSD yields a bulk of excitation energies that lie closely together. These spectra strongly resemble the results for collective excitations obtained from RPA. Apart from that, EOM-CCSD is also capable of providing some low-lying excitations, as is apparent from Figures A.4 and A.5. For ^{24}O , two low-lying 2^+ states are obtained, the lowest at an excitation energy of 6.5 MeV. This might be a candidate for the experimentally known 2^+ state at 4.8 MeV (experimental values from [166]). The calculations also show a low-lying 4^+ state at about 9.4 MeV, for which there is no experimental evidence. For ^{48}Ca , there are also low-lying 2^+ and 4^+ states. The lowest 2^+ state is at 5.0 MeV excitation energy, which is a candidate for the experimentally observed state at 3.8 MeV. For the calculated 4^+ state at 5.6 MeV there is also a possible match in the observed ^{48}Ca excitation spectrum at 4.5 MeV. No low-lying 0^+ , 2^+ , or 4^+ states are obtained for ^{16}O and ^{40}Ca . However, the 0^+ and

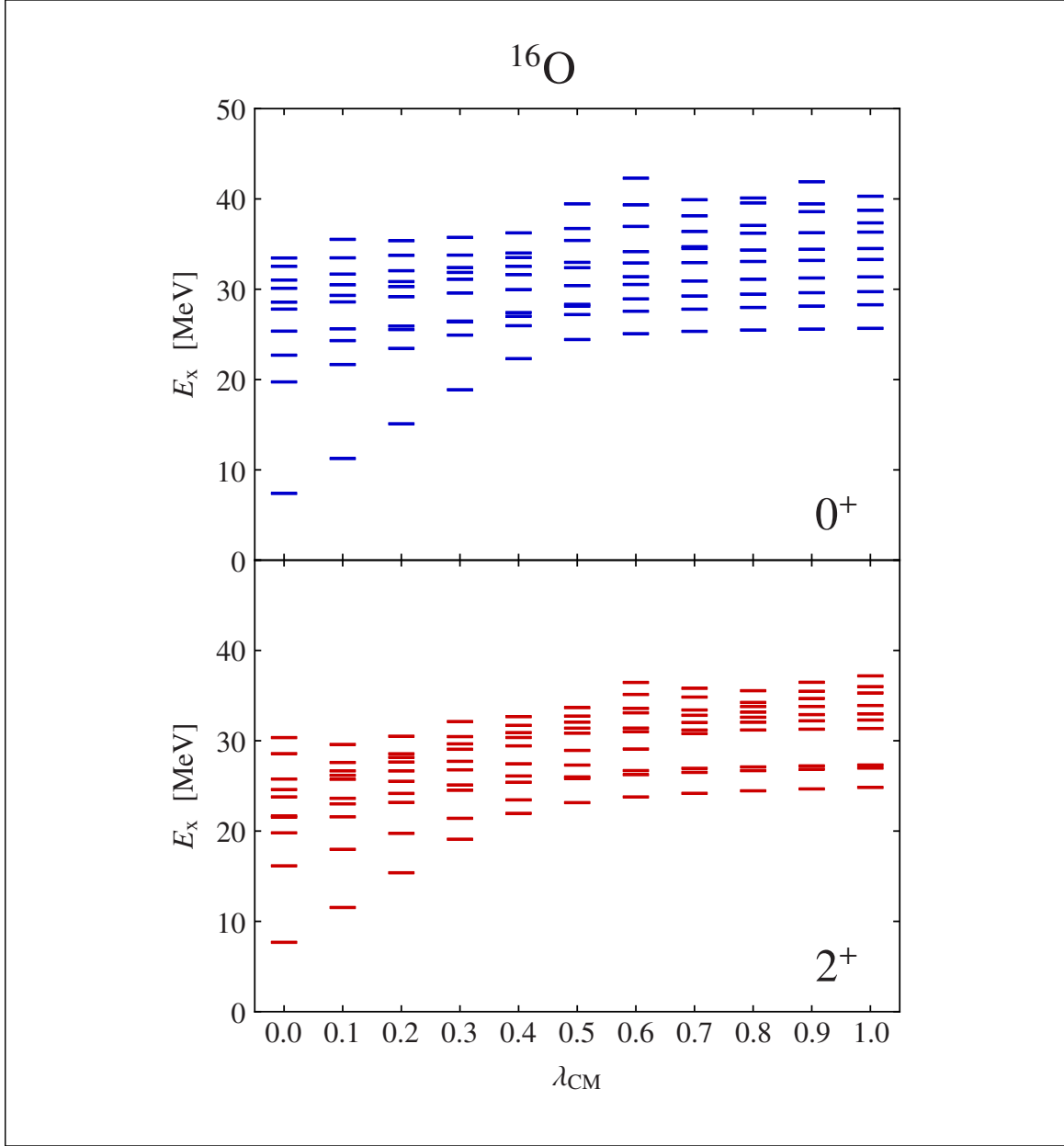


Figure A.2: Dependence of the 10 lowest $J^\pi = 0^+$ and $J^\pi = 2^+$ states of ^{16}O on the parameter λ_{CM} . The energies are obtained from EOM-CCSD using the NN+3N-full Hamiltonian in NO2B approximation with $E_{3\text{max}} = 14$ and at $\alpha = 0.08 \text{ fm}^4$. The calculations employed a HO basis with $e_{\text{max}} = 10$ and $\hbar\Omega = 20 \text{ MeV}$.

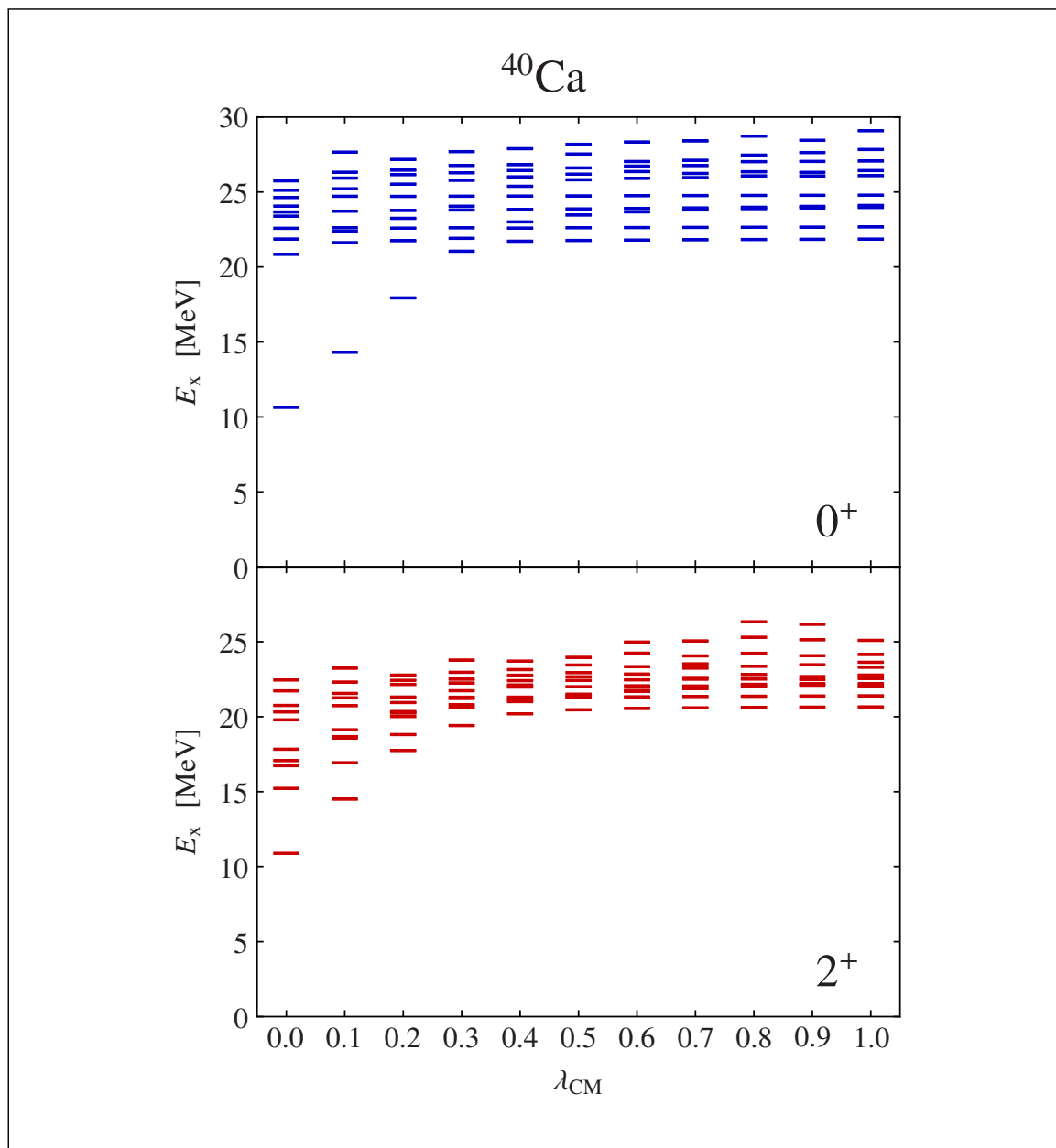


Figure A.3: As in Figure A.2, for ^{40}Ca .

2^+ spectra are less converged than the low-lying states for other nuclei, indicating that the ^{16}O states are rather complicated. Experiments show low-lying 0^+ states at 6.1 and 3.3 MeV for ^{16}O and ^{40}Ca , respectively, but these are potentially α -cluster states [164] and, therefore, expected to be out of reach of the EOM-CCSD. There are also low-lying 2^+ states at 6.9 and 3.9 MeV for ^{16}O and ^{40}Ca , respectively. Since there is also no evidence for these in the calculations, it may be speculated they also have a complicated structure, such as multi-particle-hole excitations, which EOM-CCSD is simply not able to describe with linear 2p2h excitations.

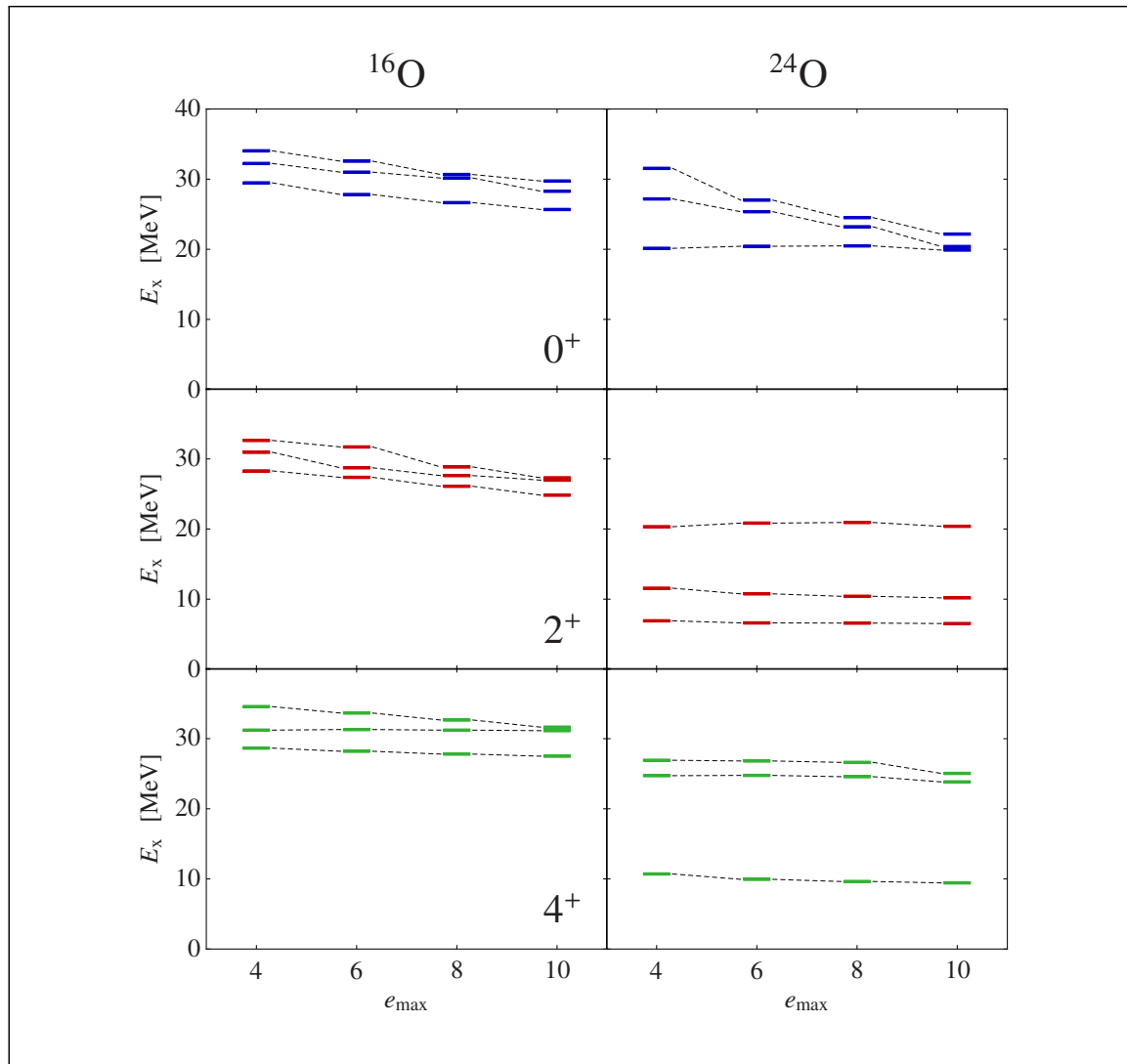


Figure A.4: Convergence of the 3 lowest $J^\pi = 0^+$, $J^\pi = 2^+$, and $J^\pi = 4^+$ with respect to e_{\max} . Other parameters as in Figure A.2, with $\lambda_{\text{CM}} = 1.0$.

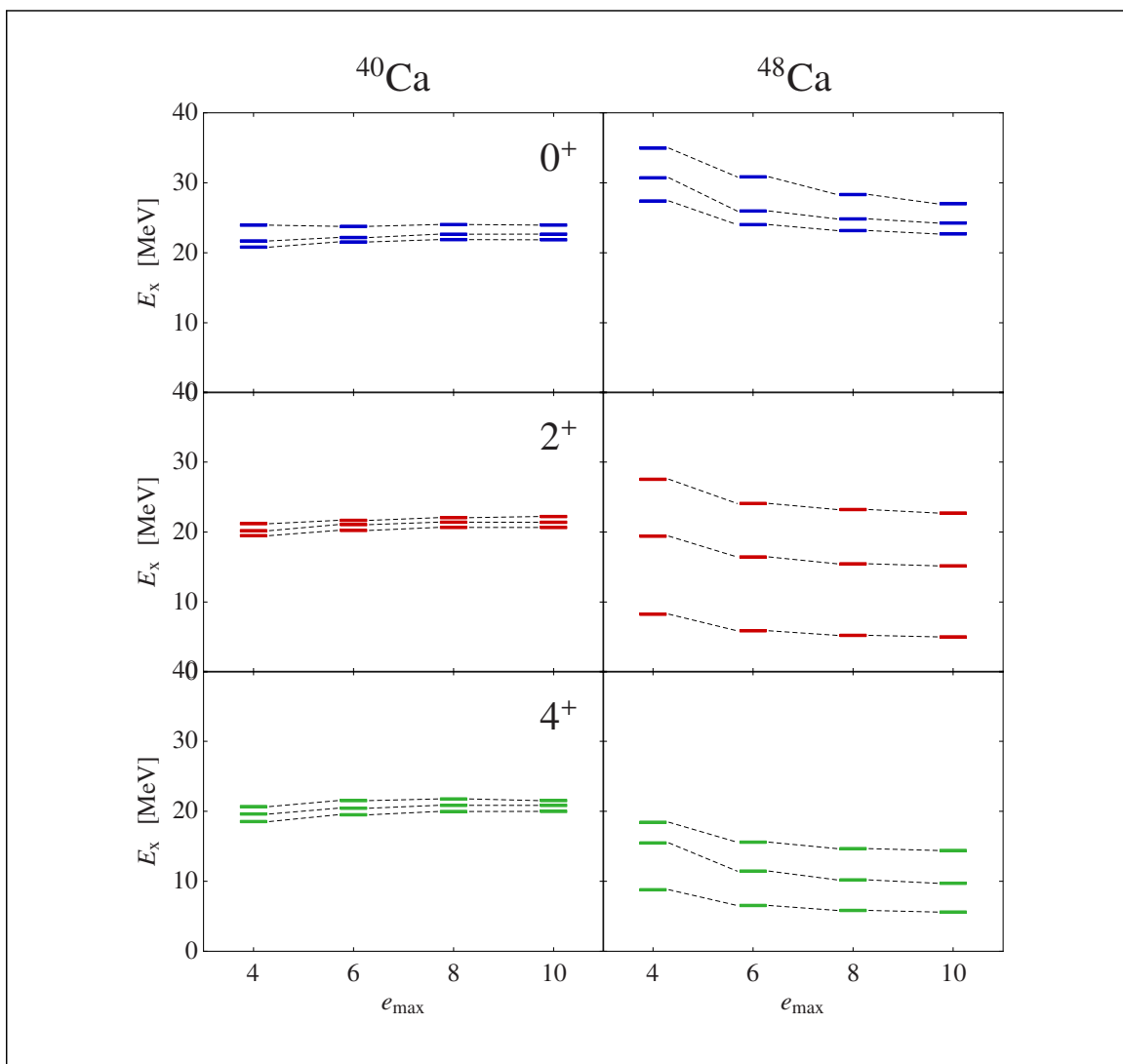


Figure A.5: As in Figure A.5, for ^{40}Ca and ^{48}Ca .

Appendix B

Trapped Neutrons

As an application of Coupled-Cluster theory beyond common atomic nuclei, the ground-state energies of neutrons trapped in an external potential are considered in the following. Since pure neutron systems are not bound, the external potential is required to prevent the neutrons from moving apart. Thus, the Hamiltonian is of the form

$$\hat{H} = \sum_i^A \frac{\hat{\mathbf{p}}_i^2}{2m} + \sum_i^A \hat{U}_{\text{ext}}(\hat{\mathbf{r}}_i) + \sum_{i<j}^A \hat{V}_{ij}^{\text{NN}} + \sum_{i<j<k}^A \hat{V}_{ijk}^{\text{3N}} \quad (\text{B.1})$$

where the external potential considered is a harmonic-oscillator potential with frequency Ω_{trap}

$$\hat{U}_{\text{ext}}(\hat{\mathbf{r}}_i) = \frac{1}{2} m \Omega_{\text{trap}}^2 \hat{\mathbf{r}}_i^2. \quad (\text{B.2})$$

Unlike for the nuclear case, in (B.1) the *total*, rather than the *intrinsic* kinetic energy is used because the external potential also acts on the center-of-mass coordinates. One motivation for considering neutron drops is that they provide a very simple model of neutron-rich nuclei in which the core is approximated by an external well acting on the valence neutrons [167]. Additionally, it allows to investigate properties of the interaction in the neutron-neutron or three-neutron sector.

First, basic properties of the many-body calculations are considered. All calculations employ SRG-evolved matrix elements from ramp-40C model spaces, and with applied frequency conversion from parent frequency $\hbar\Omega = 28$ MeV. Figures B.1 and B.2 show for various neutron drops and interactions, and at fixed trap potential frequency $\hbar\Omega_{\text{trap}} = 10$ MeV, the dependence of the CCSD ground-state energy on the harmonic-oscillator frequency. For the NN-only, the NN+3N-induced, and the NN+3N-full ($\Lambda_{3\text{N}} = 400$ MeV) Hamiltonians, the CCSD energies for SRG flow parameters $\alpha = 0.04 \text{ fm}^4$ and $\alpha = 0.08 \text{ fm}^4$ are sufficiently flat in the frequency range $\hbar\Omega = 16, 20, 24$ MeV so that any of these frequencies may be chosen as optimum. The results for $\alpha = 0.02 \text{ fm}^4$, where available, suggest an optimal frequency at around $\hbar\Omega = 28$ MeV, however, for reason discussed below, an optimal frequency of $\hbar\Omega = 16$ MeV is more convenient and will be chosen in the following.

The results for the NN+3N-full ($\Lambda_{3\text{N}} = 500$ MeV) Hamiltonian show an odd frequency dependence, where for the heavier neutron drops the CCSD energies keep on decreasing with increasing frequency, which clearly hints at a defect in the interaction matrix elements. Indeed, this unnatural behavior may be explained by an insufficient $E_{3\text{max}}$ cut. Figure B.3 shows the frequency dependence of the CCSD energies for the heavier neutron drops for the two values $E_{3\text{max}} = 12$ and 14. From

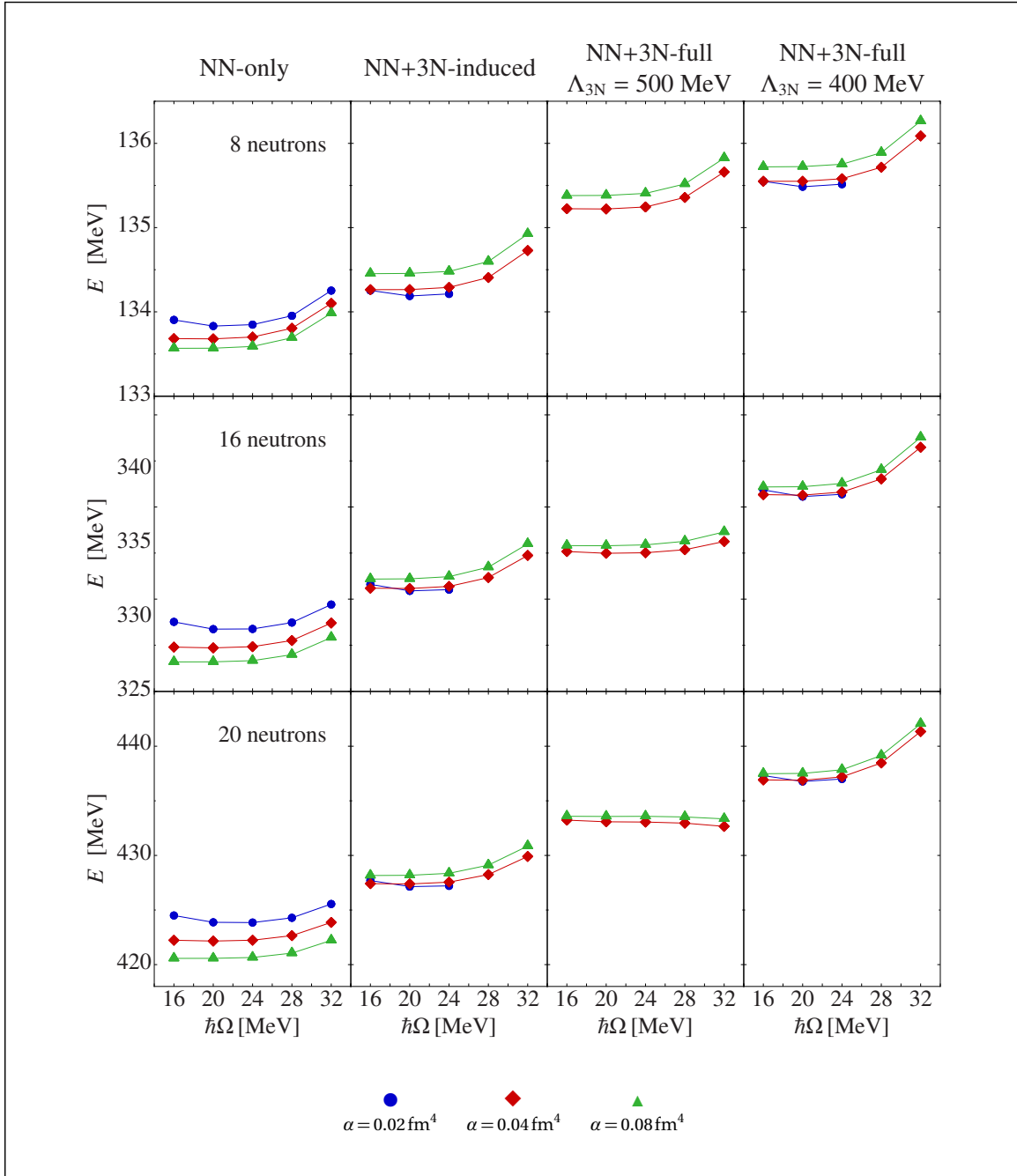
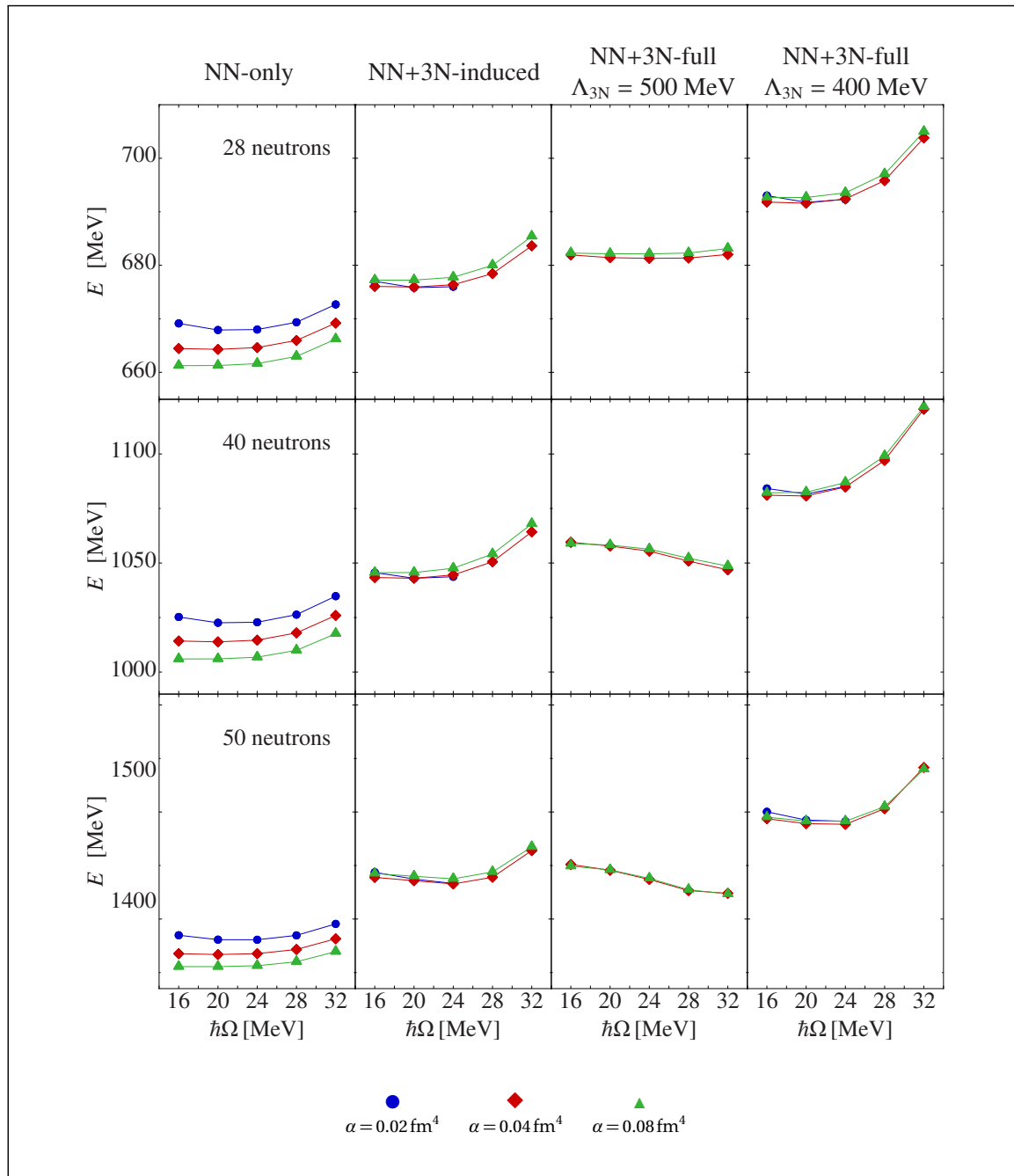


Figure B.1: Frequency-dependence of CCSD ground-state energies for various Hamiltonians and various neutron drops and interactions in an external harmonic-oscillator potential with frequency $\hbar\Omega_{\text{trap}} = 10$ MeV. The 3N interactions are included via NO2B approximation with $E_{3\text{max}} = 14$, and a HF basis with $e_{\text{max}} = 12$ is employed.


 Figure B.2: As in Figure B.1 for the neutron drops ^{28}n , ^{40}n , and ^{50}n .

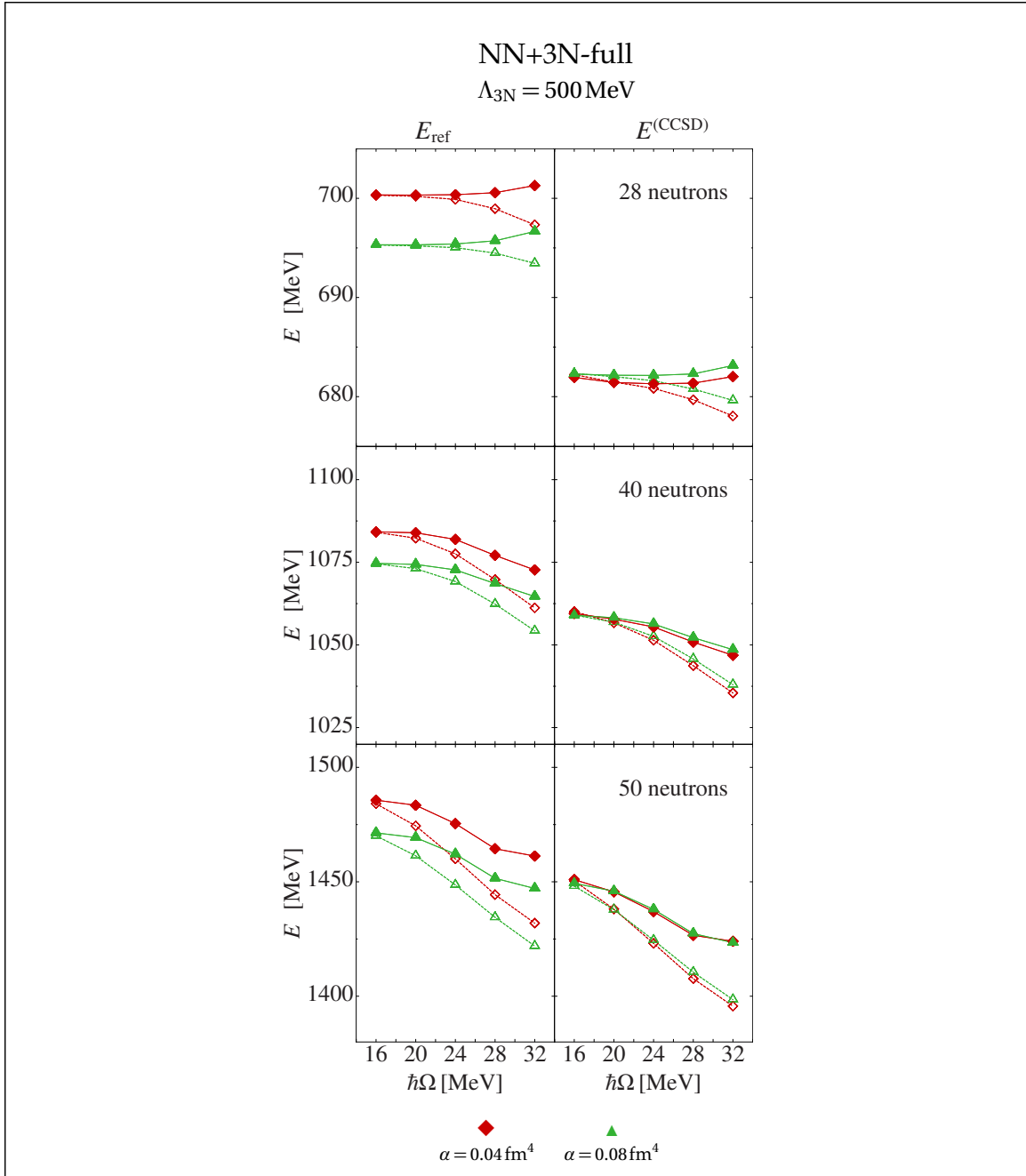


Figure B.3: Dependence on the HO frequency of the CCSD ground-state energy for various neutron drops for the NN+3N-full Hamiltonian with chiral 3N cutoff $\Lambda_{3N} = 500 \text{ MeV}$ for $E_{3\text{max}} = 12$ (open symbols, dashed lines) and $E_{3\text{max}} = 14$ (full symbols, solid lines). Parameters of the calculations as in Figure B.1.

| ^{16}n | $\alpha = 0.04 \text{ fm}^4$ | $\alpha = 0.08 \text{ fm}^4$ | ^{50}n | $\alpha = 0.04 \text{ fm}^4$ | $\alpha = 0.08 \text{ fm}^4$ |
|--|------------------------------|------------------------------|-----------------|------------------------------|------------------------------|
| $E_{\text{ref}} [\text{MeV}]$ | 340.8 | 339.1 | | 1467.0 | 1459.8 |
| $\Delta E^{(\text{CCSD})} [\text{MeV}]$ | -10.2 | -8.0 | | -28.1 | -17.3 |
| $\delta E^{(\text{ACCS}(T))} [\text{MeV}]$ | -0.7 | -0.5 | | -1.3 | -1.0 |

Table B.1: Contributions from different orders of the cluster truncation to the ground-state energies of ^{16}n and ^{50}n for the NN+3N-full ($\Lambda_{3\text{N}} = 400 \text{ MeV}$) Hamiltonian. Parameters of the calculations as in Fig. B.4, with $e_{\text{max}} = 12$.

this it becomes apparent that the problematic frequency dependence is enhanced for smaller values of $E_{3\text{max}}$ and may vanish for sufficient large values. However, for the frequency $\hbar\Omega = 16 \text{ MeV}$ chosen as optimum, there is virtually no $E_{3\text{max}}$ effect on the energy scales considered in Figure B.3, while the effect increases with the oscillator frequency. From these observations it may be concluded that is $\hbar\Omega = 16 \text{ MeV}$ is the most appropriate choice for the NN+3N-full ($\Lambda_{3\text{N}} = 500 \text{ MeV}$) Hamiltonian. As in the case of nuclei, the insufficiency of the ramp-40C SRG model spaces for heavier neutron drops is expected to cause the problems mentioned above.

Next, the convergence properties of the calculations and the size of the different contributions of the cluster expansion are discussed. In Figure B.4, the e_{max} -dependence of the reference energy, as well as the CCSD and $\Lambda\text{CCSD}(T)$ ground-state energy is depicted. The $\alpha = 0.04 \text{ fm}^4$ and 0.08 fm^4 results are well converged. This is not quite the case for $\alpha = 0.02 \text{ fm}^4$ results, showing a more linear, rather than exponential, convergence pattern which would also not allow for reliable extrapolations to infinite model-space sizes. Therefore, the $\alpha = 0.02 \text{ fm}^4$ results will not be considered in the following.

In Table B.1 the contributions from different orders of the cluster expansion to the ground-state energies of ^{16}n and ^{50}n for the NN+3N-full ($\Lambda_{3\text{N}} = 400 \text{ MeV}$) Hamiltonian are listed. These numbers show that the beyond-HF contributions are very small. For the $\alpha = 0.04 \text{ fm}^4$ Hamiltonian, the CCSD correlation energy contributes only 3.1 % to the ground-state energy of ^{16}n , and 2.0 % to the ground-state energy of ^{50}n . The $\Lambda\text{CCSD}(T)$ triples correction is practically negligible, contributing about 0.2 % and 0.1 % to the ground-state energy of ^{16}n and ^{50}n , respectively. This, not surprisingly, indicates that the most part of the binding energy stems from the external potential while the neutron interact only weakly within the trap.

The $E_{3\text{max}}$ cut does not pose a problem in most of the present calculation of

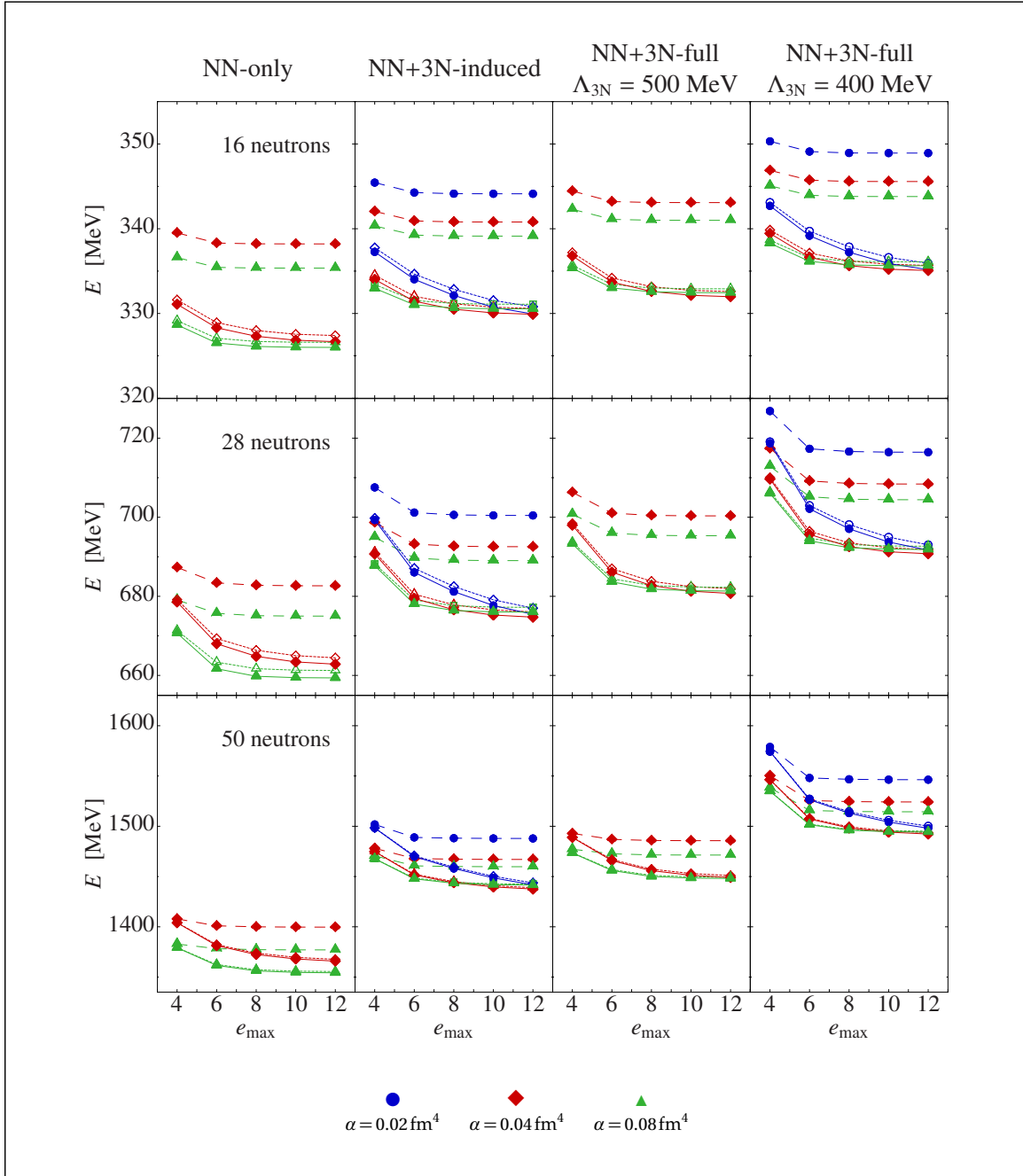


Figure B.4: Reference (dashed line), CCSD (dotted line) and Λ CCSD(T) (solid line) ground-state energy for various neutron drops and interactions in an external harmonic-oscillator potential with frequency $\hbar\Omega_{\text{trap}} = 10$ MeV. Parameters of the calculations as in Figure B.1, with HO basis frequency $\hbar\Omega = 16$ MeV.

| | α [fm ⁴] | NN+3N-ind. | NN+3N-full $\Lambda_{3N} = 500$ MeV | NN+3N-full $\Lambda_{3N} = 400$ MeV |
|-----------------|--------------------------------|------------|--|--|
| ⁸ n | 0.04 | 0.00 | 0.00 | 0.00 |
| | 0.08 | 0.00 | 0.00 | 0.00 |
| ²⁰ n | 0.04 | 0.07 | -0.11 | 0.00 |
| | 0.08 | 0.05 | -0.03 | 0.03 |
| ⁴⁰ n | 0.04 | 0.82 | -0.58 | 0.27 |
| | 0.08 | 0.79 | -0.08 | 0.50 |
| ⁵⁰ n | 0.04 | 3.96 | 0.53 | 4.13 |
| | 0.08 | 4.01 | 1.25 | 4.47 |

Table B.2: The $E_{3\max}$ effect in the $\Lambda\text{CCSD}(T)$ ground-state energies, measured by (B.3), for various neutron drops and obtained from $e_{\max} = 12$ modes spaces. Other parameters of the calculations as in Fig. B.4.

neutron drops at HO basis frequency $\hbar\Omega = 16$ MeV. This can be seen in Table B.2 where the differences in the $\Lambda\text{CCSD}(T)$ ground-state energies

$$E^{(\Lambda\text{CCSD}(T))}(E_{3\max} = 14) - E^{(\Lambda\text{CCSD}(T))}(E_{3\max} = 12) \quad (\text{B.3})$$

are listed. In the calculations of the lighter neutron drops the $E_{3\max}$ effect is completely negligible. For ⁴⁰n, the absolute $E_{3\max}$ effect ranges from 0.3 MeV to about 0.8 MeV, which is still small regarding the large energy scales involved. For ⁵⁰n, the $E_{3\max}$ effect rises dramatically. This is most likely a signature of a problem in the input matrix elements, and it may well be caused by the 40C ramp used for the SRG evolution which also led to the observations made in Figure B.3. In conclusion, apart from ⁵⁰n, the Coupled-Cluster results are expected to be accurate with uncertainties well below 1 %. The full set of $\Lambda\text{CCSD}(T)$ ground-state energies is presented in Table B.3.

It should be noted that in the calculations the external potential is not SRG-evolved. However, the SRG is not expected to have a large effect there because the SRG alters mainly the short-range behavior while the external potential has long-range character. Apart from the NN-only results, the ground-state energies show very little flow-parameter dependence, even for the NN+3N-full Hamiltonian with $\Lambda_{3N} = 500$ MeV. This outcome may indicate that the $(\mathcal{T}, M_{\mathcal{T}}) = (3/2, 3/2)$ isospin channels of the chiral NN and 3N interactions are not the driving force behind SRG-induced 4N (and beyond) contributions. Therefore, pure neutron systems give the opportunity to compare the results for $\Lambda_{3N} = 500$ MeV NN+3N-full Hamiltonian to the $\Lambda_{3N} = 400$ MeV variant. As can be seen in Figure B.4, the

| | α [fm ⁴] | NN-only | NN+3N-ind. | NN+3N-full $\Lambda_{3N} = 500$ MeV | NN+3N-full $\Lambda_{3N} = 400$ MeV |
|-----------------|--------------------------------|---------|------------|--|--|
| ⁸ n | 0.04 | 133.6 | 134.2 | 135.1 | 135.5 |
| | 0.08 | 133.5 | 134.4 | 135.3 | 135.6 |
| ¹⁶ n | 0.04 | 326.7 | 330.0 | 332.0 | 335.1 |
| | 0.08 | 326.0 | 330.5 | 332.5 | 335.6 |
| ²⁰ n | 0.04 | 421.8 | 427.1 | 432.8 | 436.5 |
| | 0.08 | 420.3 | 427.9 | 433.3 | 437.2 |
| ²⁸ n | 0.04 | 662.8 | 674.7 | 680.7 | 690.8 |
| | 0.08 | 659.4 | 676.0 | 681.3 | 691.8 |
| ⁴⁰ n | 0.04 | 1013.2 | 1042.6 | 1058.3 | 1080.2 |
| | 0.08 | 1005.3 | 1045.1 | 1058.3 | 1081.7 |
| ⁵⁰ n | 0.04 | 1365.9 | 1437.6 | 1449.1 | 1492.3 |
| | 0.08 | 1354.2 | 1441.5 | 1448.1 | 1494.2 |

Table B.3: Ground-state energies from ACCSD(T) in MeV for various neutron drops in a harmonic-oscillator trap with $\hbar\Omega_{\text{trap}} = 10$ MeV. The calculations used frequency-converted matrix elements with $\hbar\Omega = 16$ MeV, obtained from the parent frequency $\hbar\Omega = 28$ MeV. The 3N interactions were included via NO2B approximation with $E_{3\text{max}} = 14$. The calculations were performed in a HF basis with $e_{\text{max}} = 12$.

ground-state energies change noticeably when the cutoff-momentum is lowered from 500 MeV to 400 MeV. The initial 3N contributions are in any case repulsive, as is apparent from the comparison of the NN+3N-full energies with the NN+3N-induced results. However, lowering the cutoff in the initial chiral 3N interaction leads to an enhancement of these repulsive contributions, which is also found to grow with the neutron number, as can be seen in Table B.3.

Finally, the Coupled-Cluster results using chiral interaction are compared to Green's function Monte Carlo (GFMC) calculations [168] using the Argonne V8' (AV8') potential [169], either alone or in combination with the Urbana IX (UIX) [169] or the Illinois-7 (IL7) [170] three-nucleon interaction. The comparison is shown in Figure B.5. For ⁸n, all methods and interactions give the same result on the energy scales considered in Figure B.5. However, for larger neutron numbers the results increasingly deviate from each other. Up to ⁴⁰n, both Hamiltonians that do not contain initial 3N forces, the chiral NN+3N-induced and the AV8', give very similar results. Even closer to the AV8' results is the NN+3N-full Hamiltonian with 500 MeV cutoff momentum. As already discussed above, the NN+3N-full

Hamiltonian with 400 MeV cutoff shows noticeable deviations from the 500 MeV results, due to an enhanced repulsion. Even more repulsion is produced by the UIX three-body interaction, such that for ^{40}n , the AV8'+UIX results are clearly distinguishable from the other ones. For example, the AV8'+UIX ground-state energy for ^{40}n differs to the NN+3N-full ($\Lambda_{3\text{N}} = 500$ MeV) result by about 1.5 MeV per neutron, and to the NN+3N-full ($\Lambda_{3\text{N}} = 400$ MeV) by about 0.9 MeV per neutron. On the other hand, the AV8' potential in combination with the IL7 three-nucleon interaction produces significantly less repulsion than the other interactions. This demonstrates once more that different current 3N interactions lead to very different results in many-body calculations.

In conclusion, neutron drops represent convenient systems to test the extreme-isospin properties of nuclear interactions. The Coupled-Cluster framework considered here is capable to provide very accurate energies, and the effects of SRG-induced many-body interactions are very limited. Therefore, the uncertainties involved are much reduced compared to nuclear calculations in such a mass range. Particularly for heavier neutron drops, differences in the interactions become visible. This may help to understand the behavior of these interactions in the calculation of neutron-rich nuclei. A particularly interesting observation in the context of this work are the different results for the NN+3N-full Hamiltonians for different regulator cutoff momentum.

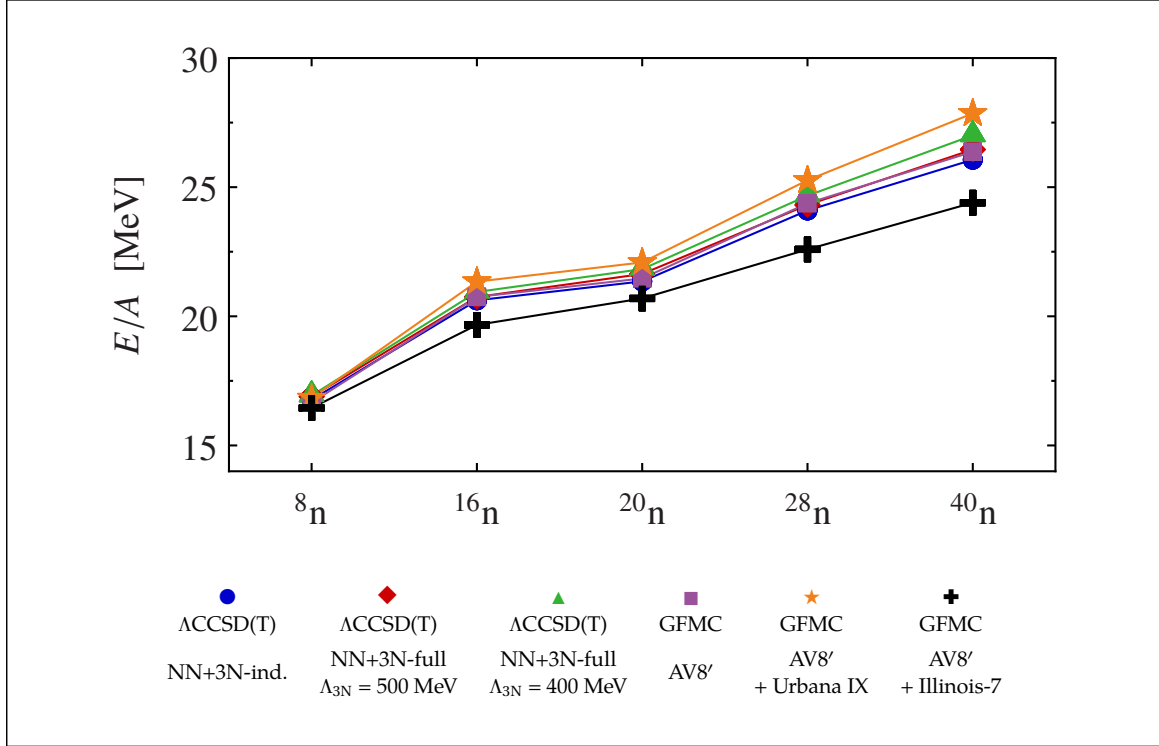


Figure B.5: Comparison of ground-state energies per neutron of neutron drops obtained from ACCSD(T) and Green's function Monte Carlo calculations employing various interactions. The Coupled-Cluster calculations used the chiral NN as well as two variants of the chiral NN+3N interactions in form of the NN+3N-induced, the NN+3N-full ($\Lambda_{3N} = 500$ MeV), and the NN+3N-full ($\Lambda_{3N} = 400$ MeV) Hamiltonian. The GFMC calculations used either the AV8' two-nucleon potential, or the AV8' potential together with the Urbana IX model 3N interaction [168]. The Coupled-Cluster results can be found in Table B.3.

Appendix C

CCSD Diagrams and Spherical Expressions

C.1 Diagrams

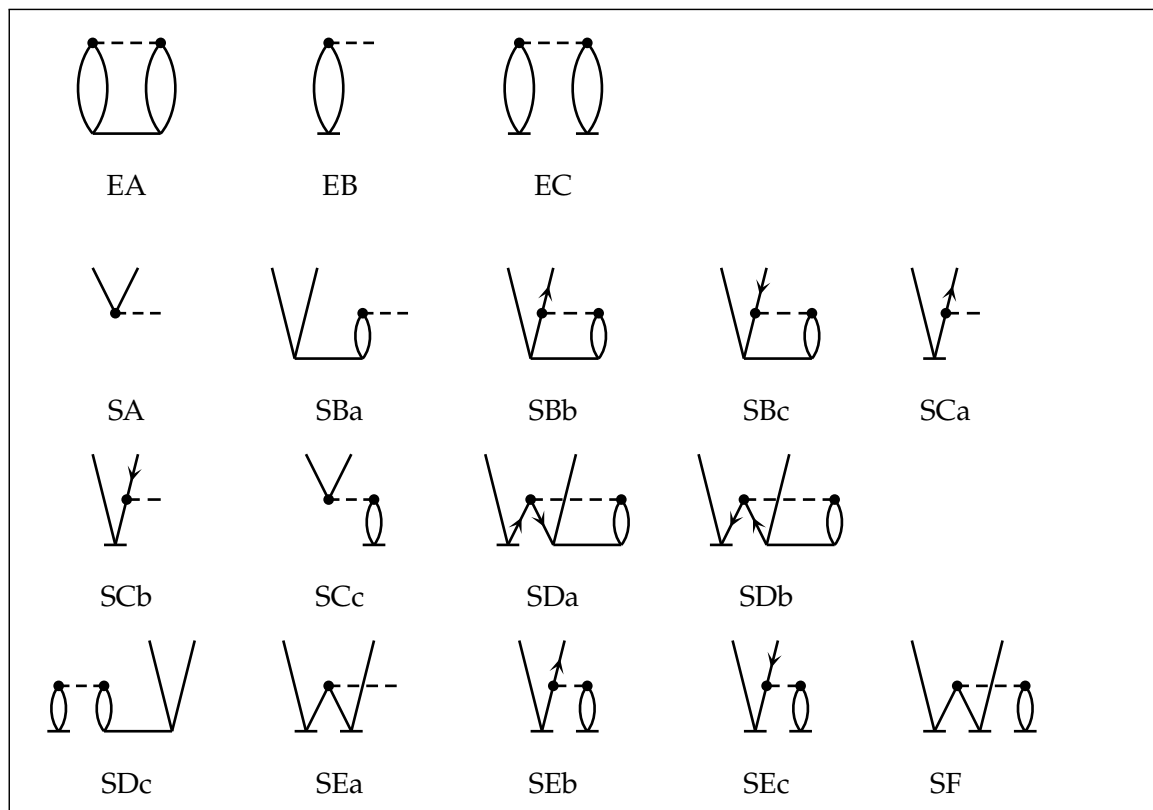
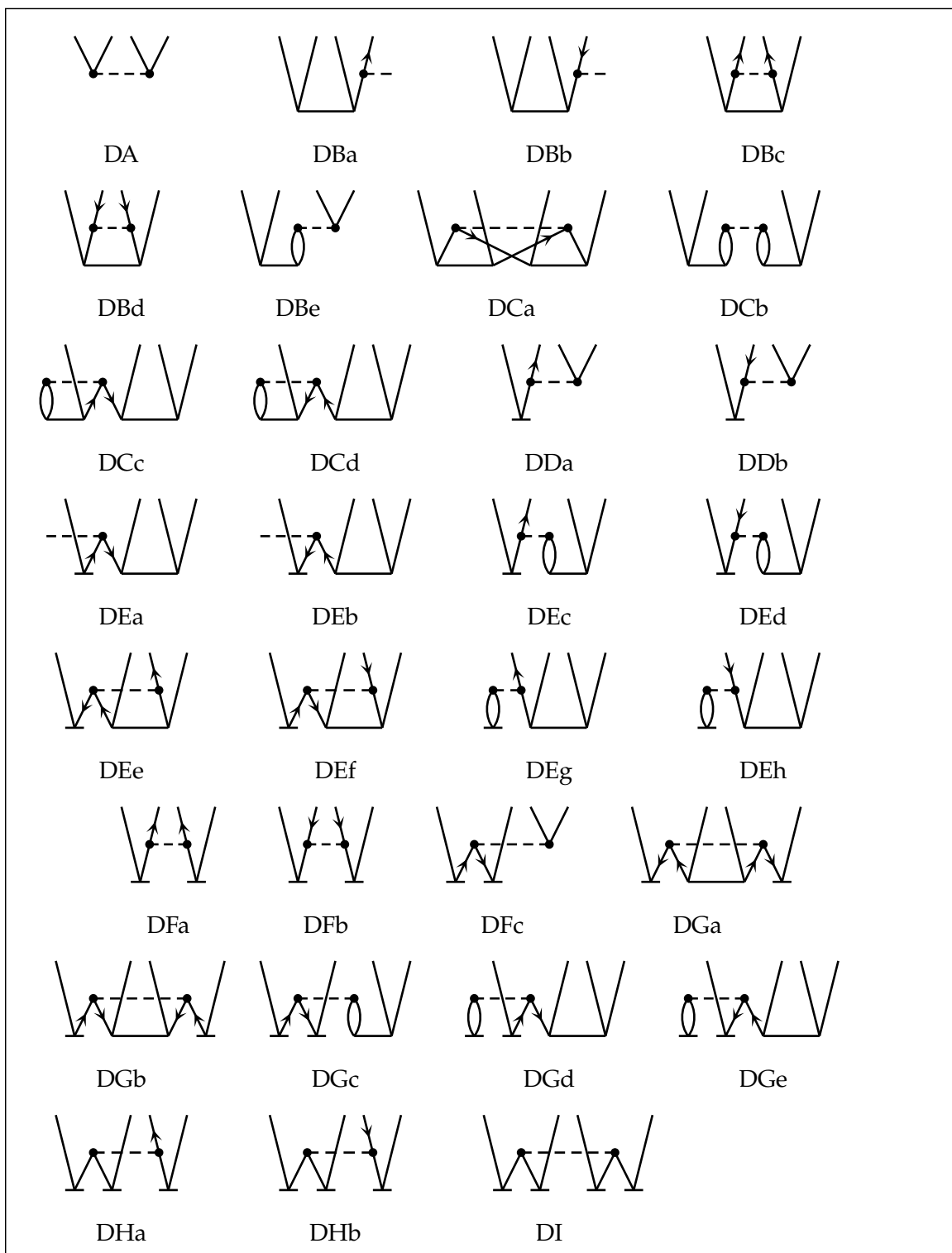


Figure C.1: CCSD correlation energy and \hat{T}_1 diagrams.


 Figure C.2: CCSD \hat{T}_2 diagrams.

C.2 Spherical Equations

$$\begin{aligned}
 & + \overset{(SA)}{\langle \tilde{a} | \hat{f} | i \rangle} + \overset{(SBa)}{\hat{f}_a^{-1} \sum_{ck} \hat{f}_c^{-1} \sum_J \hat{f}^2 \langle \overset{JM}{\downarrow} ac | \overset{JM}{\downarrow} \hat{t}_2 | \overset{00}{\downarrow} ik \rangle \langle \tilde{k} | \hat{f} | c \rangle} \\
 & - \overset{(SBb)}{\frac{1}{2} \hat{f}_a^{-1} \sum_{cdk} \sum_J \hat{f}^2 \langle \overset{JM}{\downarrow} ak | \overset{JM}{\downarrow} \hat{v} | \overset{JM}{\downarrow} cd \rangle \langle \overset{JM}{\downarrow} cd | \overset{JM}{\downarrow} \hat{t}_2 | \overset{00}{\downarrow} ik \rangle} \\
 & + \overset{(SBc)}{\frac{1}{2} \hat{f}_a^{-1} \sum_{ckl} \sum_J \hat{f}^2 \langle \overset{JM}{\downarrow} ac | \overset{JM}{\downarrow} \hat{t}_2 | \overset{JM}{\downarrow} kl \rangle \langle \overset{JM}{\downarrow} kl | \overset{JM}{\downarrow} \hat{v} | \overset{00}{\downarrow} ic \rangle} - \overset{(SCa)}{\hat{f}_a^{-1} \sum_c \langle \overset{00}{\downarrow} \tilde{a} | \hat{f} | c \rangle \langle \overset{00}{\downarrow} \tilde{c} | \hat{t}_1 | i \rangle} \\
 & + \overset{(SCb)}{\hat{f}_a^{-1} \sum_k \langle \overset{00}{\downarrow} \tilde{a} | \hat{t}_1 | k \rangle \langle \overset{00}{\downarrow} \tilde{k} | \hat{f} | i \rangle} + \overset{(SCc)}{\hat{f}_a^{-1} \sum_{ck} \hat{f}_c^{-1} \sum_J \hat{f}^2 \langle \overset{JM}{\downarrow} ak | \overset{JM}{\downarrow} \hat{v} | \overset{00}{\downarrow} ic \rangle \langle \tilde{c} | \hat{t}_1 | k \rangle} \\
 & - \overset{(SDa)}{\frac{1}{2} \hat{f}_a^{-2} \sum_{cdkl} \sum_J \hat{f}^2 \langle \overset{JM}{\downarrow} ad | \overset{JM}{\downarrow} \hat{t}_2 | \overset{JM}{\downarrow} kl \rangle \langle \overset{JM}{\downarrow} kl | \overset{JM}{\downarrow} \hat{v} | \overset{00}{\downarrow} cd \rangle \langle \tilde{c} | \hat{t}_1 | i \rangle} \\
 & - \overset{(SDB)}{\frac{1}{2} \hat{f}_a^{-2} \sum_{cdkl} \sum_J \hat{f}^2 \langle \overset{00}{\downarrow} \tilde{a} | \hat{t}_1 | k \rangle \langle \overset{JM}{\downarrow} kl | \overset{JM}{\downarrow} \hat{v} | \overset{JM}{\downarrow} cd \rangle \langle \overset{JM}{\downarrow} cd | \overset{JM}{\downarrow} \hat{t}_2 | \overset{00}{\downarrow} il \rangle} \\
 & + \overset{(SDc)}{\hat{f}_a^{-1} \sum_{cdkl} \hat{f}_d^{-2} \hat{f}_k^{-1} \sum_{JJ'} \hat{f}^2 (\hat{f}')^2 \langle \overset{00}{\downarrow} \tilde{c} | \hat{t}_1 | k \rangle \langle \overset{JM}{\downarrow} kl | \overset{JM}{\downarrow} \hat{v} | \overset{JM}{\downarrow} cd \rangle \langle \overset{J'M'}{\downarrow} da | \overset{J'M'}{\downarrow} \hat{t}_2 | \overset{00}{\downarrow} li \rangle \delta_{j_d j_l}} \\
 & - \overset{(SEa)}{\hat{f}_a^{-2} \sum_{ck} \langle \overset{00}{\downarrow} \tilde{a} | \hat{t}_1 | k \rangle \langle \overset{00}{\downarrow} \tilde{k} | \hat{f} | c \rangle \langle \overset{00}{\downarrow} \tilde{c} | \hat{t}_1 | i \rangle} - \overset{(SEb)}{\hat{f}_a^{-2} \sum_{cdk} \hat{f}_k^{-1} \sum_J \hat{f}^2 \langle \overset{JM}{\downarrow} ak | \overset{JM}{\downarrow} \hat{v} | \overset{00}{\downarrow} cd \rangle \langle \overset{00}{\downarrow} \tilde{c} | \hat{t}_1 | i \rangle \langle \tilde{d} | \hat{t}_1 | k \rangle} \\
 & + \overset{(SEc)}{\hat{f}_a^{-2} \sum_{ckl} \hat{f}_c^{-1} \sum_J \hat{f}^2 \langle \overset{JM}{\downarrow} kl | \overset{JM}{\downarrow} \hat{v} | \overset{00}{\downarrow} ic \rangle \langle \tilde{a} | \hat{t}_1 | k \rangle \langle \tilde{c} | \hat{t}_1 | l \rangle} \\
 & - \overset{(SF)}{\hat{f}_a^{-3} \sum_{cdkl} \hat{f}_d^{-1} \sum_J \hat{f}^2 \langle \overset{JM}{\downarrow} kl | \overset{JM}{\downarrow} \hat{v} | \overset{00}{\downarrow} cd \rangle \langle \tilde{a} | \hat{t}_1 | k \rangle \langle \tilde{d} | \hat{t}_1 | l \rangle \langle \tilde{c} | \hat{t}_1 | i \rangle} = 0, \quad \forall a, i
 \end{aligned}$$

 Figure C.3: Spherical expressions for the CCSD \hat{T}_1 amplitude equations.

$$\begin{aligned}
 & \hat{P}_{ab}(J) \hat{P}_{ij}(J) \left\{ + \frac{1}{4} \langle \overset{JM}{\downarrow} \overset{JM}{\downarrow} ab | \overset{JM}{\downarrow} \overset{JM}{\downarrow} \hat{v} | ij \rangle - \frac{1}{2} \hat{J}_b^{-1} \sum_c \langle \overset{00}{\downarrow} \hat{b} | \hat{f} | c \rangle \langle \overset{JM}{\downarrow} \overset{JM}{\downarrow} ac | \hat{t}_2 | ij \rangle \right. \\
 & + \frac{1}{2} \hat{J}_j^{-1} \sum_k \langle \overset{00}{\downarrow} \hat{k} | \hat{f} | j \rangle \langle \overset{JM}{\downarrow} \overset{JM}{\downarrow} ab | \hat{t}_2 | ik \rangle + \frac{1}{8} \sum_{cd} \langle \overset{JM}{\downarrow} \overset{JM}{\downarrow} ab | \hat{v} | cd \rangle \langle \overset{JM}{\downarrow} \overset{JM}{\downarrow} cd | \hat{t}_2 | ij \rangle \\
 & + \frac{1}{8} \sum_{kl} \langle \overset{JM}{\downarrow} \overset{JM}{\downarrow} ab | \hat{t}_2 | kl \rangle \langle \overset{JM}{\downarrow} \overset{JM}{\downarrow} kl | \hat{v} | ij \rangle \left. \right\} \\
 & - \text{CCAtoStd}^{(A)} \left[\begin{smallmatrix} ab \\ ij \end{smallmatrix} J; J' \right] \sum_{ck} (-1)^{j_c+j_k-J'} \langle \overset{J'M'}{\downarrow} \hat{a} \tilde{c} | \hat{t}_2 | ik \rangle \langle \overset{J'M'}{\downarrow} \hat{k} \tilde{b} | \hat{v} | cj \rangle \\
 & + \frac{1}{16} \hat{P}_{ab}(J) \hat{P}_{ij}(J) \sum_{cdkl} \langle \overset{JM}{\downarrow} \overset{JM}{\downarrow} ab | \hat{t}_2 | kl \rangle \langle \overset{JM}{\downarrow} \overset{JM}{\downarrow} kl | \hat{v} | cd \rangle \langle \overset{JM}{\downarrow} \overset{JM}{\downarrow} cd | \hat{t}_2 | ij \rangle \\
 & + \text{CCAtoStd}^{(A)} \left[\begin{smallmatrix} ab \\ ij \end{smallmatrix} J; J' \right] \frac{1}{2} \sum_{cdkl} (-1)^{j_c+j_d+j_k+j_l} \langle \overset{J'M'}{\downarrow} \hat{a} \tilde{c} | \hat{t}_2 | ik \rangle \langle \overset{J'M'}{\downarrow} \hat{d} \tilde{b} | \hat{t}_2 | lj \rangle \langle \overset{J'M'}{\downarrow} \hat{k} \tilde{l} | \hat{v} | cd \rangle \\
 & + \hat{P}_{ab}(J) \hat{P}_{ij}(J) \left\{ - \frac{1}{4} \hat{J}_i^{-2} \sum_{cdkl} \sum_{J'} (\hat{J}')^2 \langle \overset{JM}{\downarrow} \overset{JM}{\downarrow} ab | \hat{t}_2 | lj \rangle \langle \overset{J'M'}{\downarrow} \overset{J'M'}{\downarrow} kl | \hat{v} | cd \rangle \langle \overset{J'M'}{\downarrow} \overset{J'M'}{\downarrow} cd | \hat{t}_2 | ki \rangle \delta_{j_i j_l} \right. \\
 & - \frac{1}{4} \hat{J}_a^{-2} \sum_{cdkl} \sum_{J'} (\hat{J}')^2 \langle \overset{J'M'}{\downarrow} \overset{J'M'}{\downarrow} ca | \hat{t}_2 | kl \rangle \langle \overset{J'M'}{\downarrow} \overset{J'M'}{\downarrow} kl | \hat{v} | cd \rangle \langle \overset{JM}{\downarrow} \overset{JM}{\downarrow} db | \hat{t}_2 | ij \rangle \delta_{j_a j_d} \\
 & - \frac{1}{2} \hat{J}_i^{-1} \sum_c \langle \overset{00}{\downarrow} \hat{c} | \hat{t}_1 | i \rangle \langle \overset{JM}{\downarrow} \overset{JM}{\downarrow} ab | \hat{v} | cj \rangle + \frac{1}{2} \hat{J}_a^{-1} \sum_k \langle \overset{00}{\downarrow} \hat{a} | \hat{t}_1 | k \rangle \langle \overset{JM}{\downarrow} \overset{JM}{\downarrow} kb | \hat{v} | ij \rangle \\
 & - \frac{1}{2} \hat{J}_i^{-2} \sum_{ck} \langle \overset{00}{\downarrow} \hat{c} | \hat{t}_1 | i \rangle \langle \overset{00}{\downarrow} \hat{k} | \hat{f} | c \rangle \langle \overset{JM}{\downarrow} \overset{JM}{\downarrow} ab | \hat{t}_2 | kj \rangle \left. \right\} + \dots
 \end{aligned}$$

 Figure C.4: Spherical expressions for the CCSD \hat{T}_2 amplitude equations.

$$\begin{aligned}
 & - \frac{1}{2} \hat{P}_{ab}(J) \hat{P}_{ij}(J) \hat{J}_a^{-2} \sum_{ck} \overbrace{\langle \tilde{a} | \hat{t}_1 | k \rangle}^{00} \overbrace{\langle \tilde{k} | \hat{f} | c \rangle}^{00} \overbrace{\langle cb | \hat{t}_2 | ij \rangle}^{JM} \overbrace{\langle \tilde{c} | \hat{t}_1 | i \rangle}^{JM} \\
 & + \text{CCAtoStd}^{(A)} \left[\begin{smallmatrix} ab \\ ij \end{smallmatrix} J; J' \right] \hat{J}_i^{-1} \sum_{cdk} (-1)^{j_d+j_k-J'} \overbrace{\langle \tilde{c} | \hat{t}_1 | i \rangle}^{00} \overbrace{\langle \tilde{a} \tilde{k} | \hat{v} | cd \rangle}^{J'M'} \overbrace{\langle \tilde{d} \tilde{b} | \hat{t}_2 | kj \rangle}^{J'M'} \\
 & - \text{CCAtoStd}^{(A)} \left[\begin{smallmatrix} ab \\ ij \end{smallmatrix} J; J' \right] \hat{J}_a^{-1} \sum_{ckl} (-1)^{j_c+j_l-J'} \overbrace{\langle \tilde{a} | \hat{t}_1 | k \rangle}^{00} \overbrace{\langle \tilde{k} \tilde{l} | \hat{v} | ic \rangle}^{J'M'} \overbrace{\langle \tilde{c} \tilde{b} | \hat{t}_2 | lj \rangle}^{J'M'} \\
 & + \hat{P}_{ab}(J) \hat{P}_{ij}(J) \left\{ + \frac{1}{4} \hat{J}_a^{-1} \sum_{cdk} \overbrace{\langle \tilde{a} | \hat{t}_1 | k \rangle}^{00} \overbrace{\langle kb | \hat{v} | cd \rangle}^{JM} \overbrace{\langle cd | \hat{t}_2 | ij \rangle}^{JM} \right. \\
 & - \frac{1}{4} \hat{J}_i^{-1} \sum_{ckl} \overbrace{\langle \tilde{c} | \hat{t}_1 | i \rangle}^{00} \overbrace{\langle kl | \hat{v} | cj \rangle}^{JM} \overbrace{\langle ab | \hat{t}_2 | kl \rangle}^{JM} \\
 & - \frac{1}{2} \hat{J}_a^{-2} \sum_{cdk} \hat{J}_c^{-1} \sum_{J'} (\hat{J}')^2 \overbrace{\langle \tilde{c} | \hat{t}_1 | k \rangle}^{00} \overbrace{\langle ka | \hat{v} | cd \rangle}^{J'M'} \overbrace{\langle db | \hat{t}_2 | ij \rangle}^{J'M'} \delta_{ja j_d} \\
 & + \frac{1}{2} \hat{J}_i^{-2} \sum_{ckl} \hat{J}_c^{-1} \sum_{J'} (\hat{J}')^2 \overbrace{\langle \tilde{c} | \hat{t}_1 | k \rangle}^{00} \overbrace{\langle ab | \hat{t}_2 | lj \rangle}^{JM} \overbrace{\langle kl | \hat{v} | ci \rangle}^{J'M'} \delta_{ji j_l} \\
 & + \frac{1}{4} \hat{J}_i^{-1} \hat{J}_j^{-1} \sum_{cd} \overbrace{\langle \tilde{c} | \hat{t}_1 | i \rangle}^{00} \overbrace{\langle \tilde{d} | \hat{t}_1 | j \rangle}^{00} \overbrace{\langle ab | \hat{v} | cd \rangle}^{JM} \overbrace{\langle \tilde{c} | \hat{t}_1 | i \rangle}^{JM} \\
 & + \frac{1}{4} \hat{J}_a^{-1} \hat{J}_b^{-1} \sum_{kl} \overbrace{\langle \tilde{a} | \hat{t}_1 | k \rangle}^{00} \overbrace{\langle \tilde{b} | \hat{t}_1 | l \rangle}^{00} \overbrace{\langle kl | \hat{v} | ij \rangle}^{JM} \overbrace{\langle \tilde{c} | \hat{t}_1 | i \rangle}^{JM} - \hat{J}_a^{-1} \hat{J}_i^{-1} \sum_{ck} \overbrace{\langle \tilde{a} | \hat{t}_1 | k \rangle}^{00} \overbrace{\langle \tilde{c} | \hat{t}_1 | i \rangle}^{00} \overbrace{\langle kb | \hat{v} | cj \rangle}^{JM} \overbrace{\langle \tilde{d} | \hat{t}_1 | j \rangle}^{JM} \\
 & + \frac{1}{8} \hat{J}_a^{-1} \hat{J}_b^{-1} \sum_{cdkl} \overbrace{\langle \tilde{a} | \hat{t}_1 | k \rangle}^{00} \overbrace{\langle \tilde{b} | \hat{t}_1 | l \rangle}^{00} \overbrace{\langle kl | \hat{v} | cd \rangle}^{JM} \overbrace{\langle cd | \hat{t}_2 | ij \rangle}^{JM} \left. \right\} + \dots
 \end{aligned}$$

 Figure C.5: Spherical expressions for the CCSD \hat{T}_2 amplitude equations, continued.

$$\begin{aligned}
& + \frac{1}{8} \hat{P}_{ab}(J) \hat{P}_{ij}(J) \hat{J}_i^{-1} \hat{J}_j^{-1} \sum_{cdkl} \begin{array}{ccccccc} & 00 & & 00 & & JM & JM \\ & \overleftarrow{\hspace{1.5cm}} & & \overleftarrow{\hspace{1.5cm}} & & \overleftarrow{\hspace{1.5cm}} & \overleftarrow{\hspace{1.5cm}} \\ \langle \tilde{c} | \hat{t}_1 | i \rangle & \langle \tilde{d} | \hat{t}_1 | j \rangle & \langle ab | \hat{t}_2 | kl \rangle & \langle kl | \hat{v} | cd \rangle \end{array} \\
& + \text{CCAtoStd}^{(A)} \left[\begin{array}{c} ab \\ J; J' \\ ij \end{array} \right] \\
& \hat{J}_a^{-1} \hat{J}_i^{-1} \sum_{cdkl} (-1)^{j_d + j_l - J'} \begin{array}{ccccccc} & 00 & & 00 & & J'M' & J'M' \\ & \overleftarrow{\hspace{1.5cm}} & & \overleftarrow{\hspace{1.5cm}} & & \overleftarrow{\hspace{1.5cm}} & \overleftarrow{\hspace{1.5cm}} \\ \langle \tilde{a} | \hat{t}_1 | k \rangle & \langle \tilde{c} | \hat{t}_1 | i \rangle & \langle \tilde{d} \tilde{b} | \hat{t}_2 | lj \rangle & \langle \tilde{k} \tilde{l} | \hat{v} | cd \rangle \\ & & \overleftarrow{\hspace{1.5cm}} \uparrow & \overleftarrow{\hspace{1.5cm}} \uparrow \\ & & J'M' & J'M' \end{array} \\
& - \text{CCAtoStd}^{(A)} \left[\begin{array}{c} ab \\ J; J' \\ ij \end{array} \right] \\
& \frac{1}{2} \hat{J}_i^{-3} \sum_{cdkl} \hat{J}_c^{-1} \sum_{J''} (\hat{J}'')^2 \begin{array}{ccccccc} & 00 & & 00 & & J'M' & J''M'' \\ & \overleftarrow{\hspace{1.5cm}} & & \overleftarrow{\hspace{1.5cm}} & & \overleftarrow{\hspace{1.5cm}} & \overleftarrow{\hspace{1.5cm}} \\ \langle \tilde{c} | \hat{t}_1 | k \rangle & \langle \tilde{d} | \hat{t}_1 | i \rangle & \langle \tilde{a} \tilde{b} | \hat{t}_2 | lj \rangle & \langle kl | \hat{v} | cd \rangle & \delta_{j_d j_l} \\ & & \overleftarrow{\hspace{1.5cm}} \uparrow & & & & \\ & & J'M' & & & & \end{array} \\
& + \hat{P}_{ab}(J) \hat{P}_{ij}(J) \left\{ \right. \\
& - \frac{1}{2} \hat{J}_a^{-3} \sum_{cdkl} \hat{J}_c^{-1} \sum_{J'} (\hat{J}')^2 \begin{array}{ccccccc} & 00 & & 00 & & JM & JM \\ & \overleftarrow{\hspace{1.5cm}} & & \overleftarrow{\hspace{1.5cm}} & & \overleftarrow{\hspace{1.5cm}} & \overleftarrow{\hspace{1.5cm}} \\ \langle \tilde{a} | \hat{t}_1 | l \rangle & \langle \tilde{c} | \hat{t}_1 | k \rangle & \langle db | \hat{t}_2 | ij \rangle & \langle kl | \hat{v} | cd \rangle & \delta_{j_a j_d} \\ & & & & & & \end{array} \\
& + \frac{1}{2} \hat{J}_a^{-1} \hat{J}_i^{-1} \hat{J}_j^{-1} \sum_{cdk} \begin{array}{ccccccc} & 00 & & 00 & & 00 & JM \\ & \overleftarrow{\hspace{1.5cm}} & & \overleftarrow{\hspace{1.5cm}} & & \overleftarrow{\hspace{1.5cm}} & \overleftarrow{\hspace{1.5cm}} \\ \langle \tilde{a} | \hat{t}_1 | k \rangle & \langle \tilde{c} | \hat{t}_1 | i \rangle & \langle \tilde{d} | \hat{t}_1 | j \rangle & \langle kb | \hat{v} | cd \rangle \\ & & & & & JM & JM \\ & & & & & \overleftarrow{\hspace{1.5cm}} & \overleftarrow{\hspace{1.5cm}} \end{array} \\
& - \frac{1}{2} \hat{J}_a^{-1} \hat{J}_b^{-1} \hat{J}_i^{-1} \sum_{ckl} \begin{array}{ccccccc} & 00 & & 00 & & 00 & JM \\ & \overleftarrow{\hspace{1.5cm}} & & \overleftarrow{\hspace{1.5cm}} & & \overleftarrow{\hspace{1.5cm}} & \overleftarrow{\hspace{1.5cm}} \\ \langle \tilde{a} | \hat{t}_1 | k \rangle & \langle \tilde{b} | \hat{t}_1 | l \rangle & \langle \tilde{c} | \hat{t}_1 | i \rangle & \langle kl | \hat{v} | cj \rangle \\ & & & & & JM & JM \\ & & & & & \overleftarrow{\hspace{1.5cm}} & \overleftarrow{\hspace{1.5cm}} \end{array} \\
& + \frac{1}{4} \hat{J}_a^{-1} \hat{J}_b^{-1} \sum_{cdkl} \hat{J}_c^{-1} \hat{J}_d^{-1} \begin{array}{ccccccc} & 00 & & 00 & & 00 & 00 \\ & \overleftarrow{\hspace{1.5cm}} & & \overleftarrow{\hspace{1.5cm}} & & \overleftarrow{\hspace{1.5cm}} & \overleftarrow{\hspace{1.5cm}} \\ \langle \tilde{a} | \hat{t}_1 | k \rangle & \langle \tilde{b} | \hat{t}_1 | l \rangle & \langle \tilde{c} | \hat{t}_1 | i \rangle & \langle \tilde{d} | \hat{t}_1 | j \rangle & \langle kl | \hat{v} | cd \rangle \\ & & & & JM & JM \\ & & & & \overleftarrow{\hspace{1.5cm}} & \overleftarrow{\hspace{1.5cm}} \end{array} \left. \right\} \\
& = 0, \quad \forall a, b, i, j, J, M
\end{aligned}$$

C.3 Diagrams for Three-Body Hamiltonians

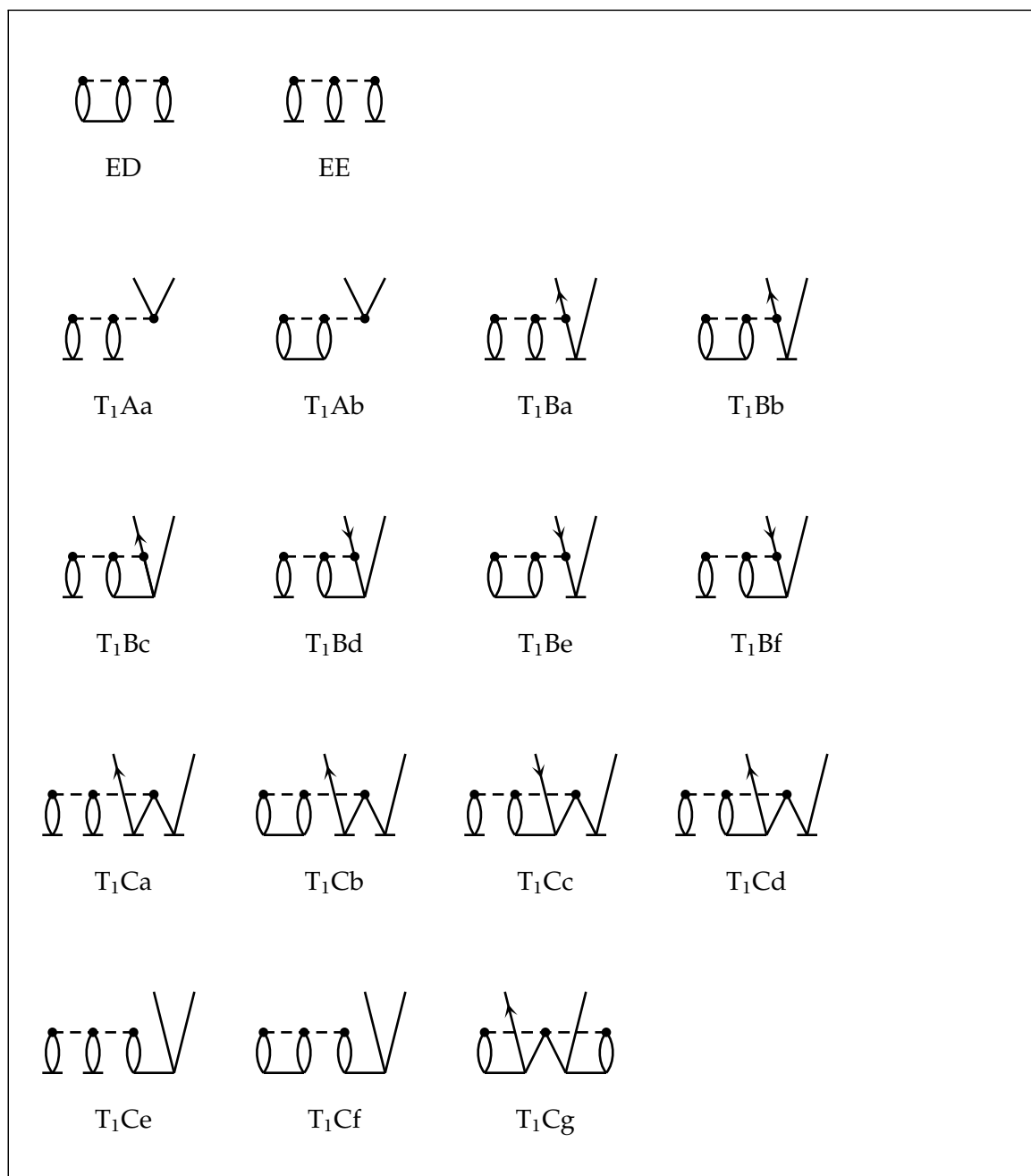
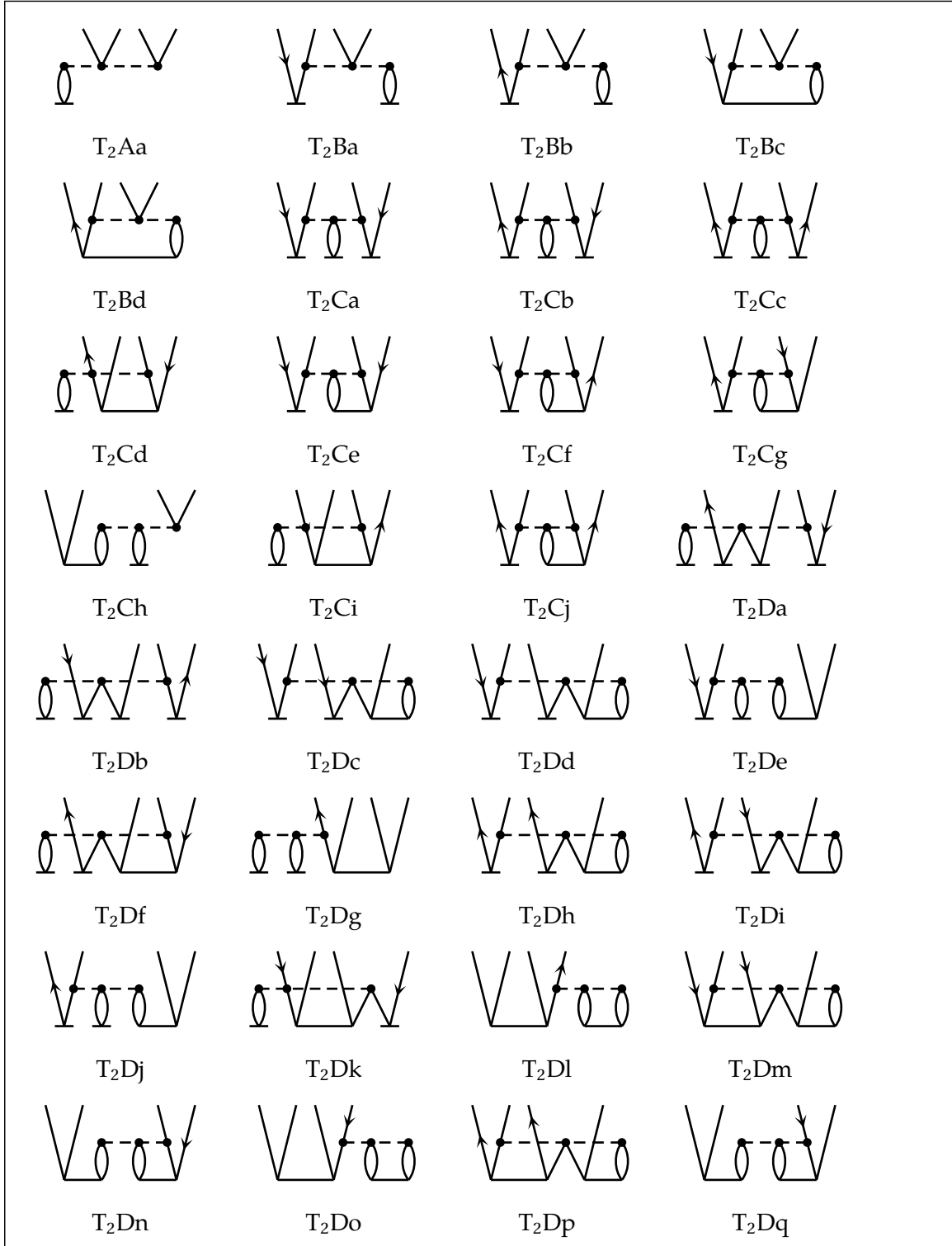
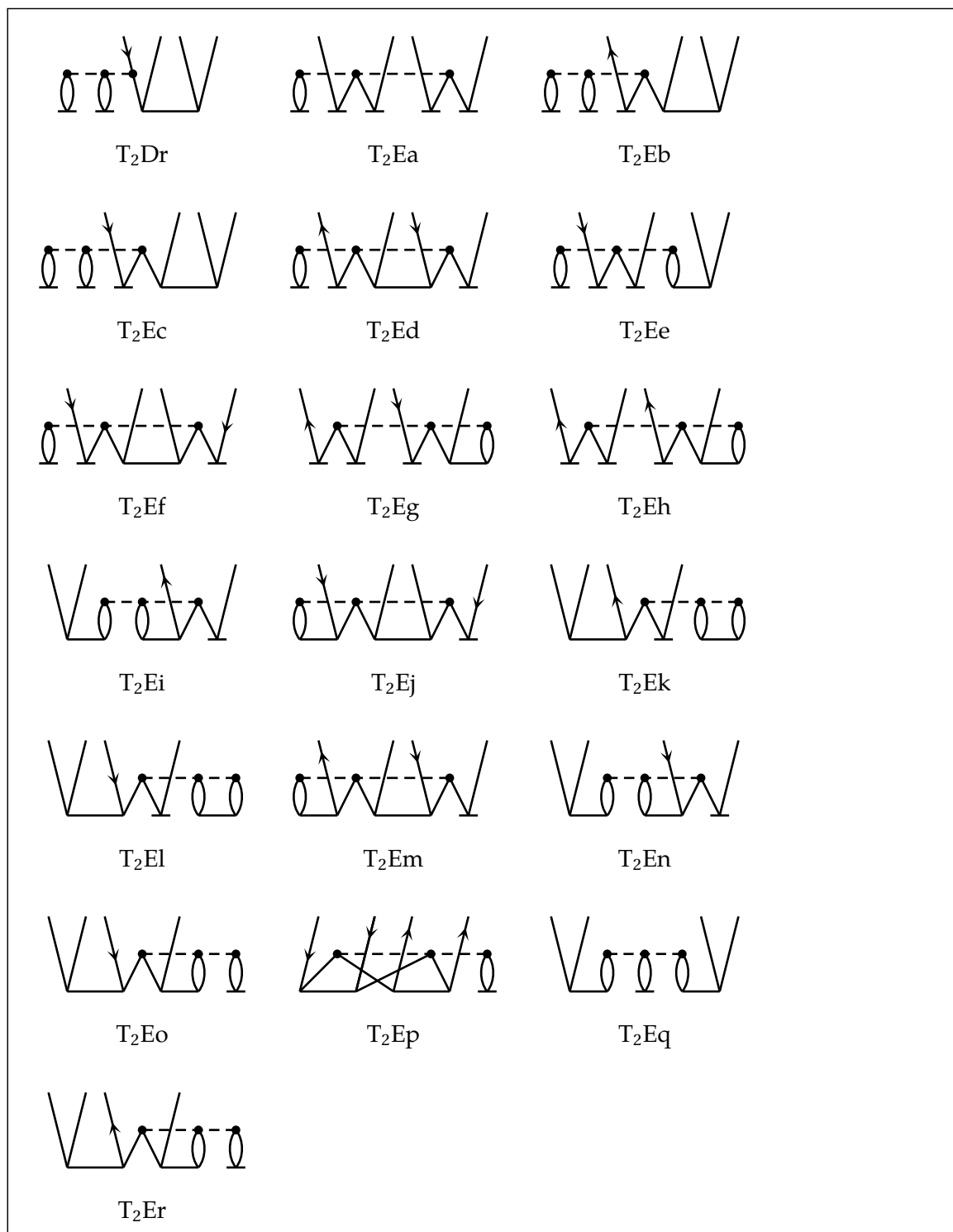


Figure C.7: CCSD correlation energy and \hat{T}_1 diagrams for three-body Hamiltonians.


 Figure C.8: CCSD \hat{T}_2 diagrams for three-body Hamiltonians.


 Figure C.9: CCSD \hat{T}_2 diagrams for three-body Hamiltonians, continued.

C.4 Spherical Equations for Three-Body Hamiltonians

$$\begin{aligned}
 &^{(T_1Aa)} + \frac{1}{2} \sum_{cdkl} \hat{j}_k^{-1} \hat{j}_l^{-1} \sum_J \hat{J} \langle kl\tilde{a} || \tilde{w} || cdi \rangle \langle \tilde{c} | \hat{t}_1 | k \rangle \langle \tilde{d} | \hat{t}_1 | l \rangle \\
 &^{(T_1Ab)} + \frac{1}{4} \sum_{cdkl} \sum_J \hat{J} \langle kl\tilde{a} || \tilde{w} || cdi \rangle \langle cd | \hat{t}_2 | kl \rangle \\
 &^{(T_1Ba)} - \frac{1}{2} \hat{j}_i^{-1} \sum_{cdekl} \hat{j}_k^{-1} \hat{j}_l^{-1} \sum_J \hat{J} \langle kl\tilde{a} || \tilde{w} || cde \rangle \langle \tilde{c} | \hat{t}_1 | k \rangle \langle \tilde{d} | \hat{t}_1 | l \rangle \langle \tilde{e} | \hat{t}_1 | i \rangle \\
 &^{(T_1Bb)} - \frac{1}{4} \hat{j}_i^{-1} \sum_{cdekl} \sum_J \hat{J} \langle kl\tilde{a} || \tilde{w} || cde \rangle \langle cd | \hat{t}_2 | kl \rangle \langle \tilde{e} | \hat{t}_1 | i \rangle \\
 &^{(T_1Bc)} - \frac{1}{2} \hat{j}_a^{-1} \sum_{cdekl} \sum_J \hat{J} \langle akl\tilde{l} || \tilde{w} || cde \rangle \langle cd | \hat{t}_2 | ik \rangle \langle \tilde{e} | \hat{t}_1 | l \rangle \\
 &^{(T_1Bd)} + \frac{1}{2} \hat{j}_a^{-1} \sum_{cdklm} \hat{j}_k^{-1} \hat{j}_l^{-1} \sum_J \hat{J} \langle kl\tilde{m} || \tilde{w} || cdi \rangle \langle \tilde{c} | \hat{t}_1 | k \rangle \langle \tilde{d} | \hat{t}_1 | l \rangle \langle \tilde{a} | \hat{t}_1 | m \rangle \\
 &^{(T_1Be)} + \frac{1}{4} \hat{j}_a^{-1} \sum_{cdklm} \sum_J \hat{J} \langle kl\tilde{m} || \tilde{w} || cdi \rangle \langle cd | \hat{t}_2 | kl \rangle \langle \tilde{a} | \hat{t}_1 | m \rangle \\
 &^{(T_1Bf)} + \frac{1}{2} \hat{j}_i^{-1} \sum_{cdklm} \sum_J \hat{J} \langle kl\tilde{m} || \tilde{w} || cid \rangle \langle ca | \hat{t}_2 | kl \rangle \langle \tilde{d} | \hat{t}_1 | m \rangle + \dots
 \end{aligned}$$

Figure C.10: Spherical expressions for the CCSD \hat{T}_1 amplitude equations for three-body Hamiltonians.

$$\begin{aligned}
 &^{(T_1Ca)} + \frac{1}{2} \hat{J}_a^{-2} \sum_{cdeklm} \hat{J}_k^{-1} \hat{J}_l^{-1} \sum_J \hat{J} \langle kl\tilde{m} || \hat{w} || cde \rangle \langle \tilde{c} | \hat{t}_1 | k \rangle \langle \tilde{d} | \hat{t}_1 | l \rangle \langle \tilde{e} | \hat{t}_1 | i \rangle \langle \tilde{a} | \hat{t}_1 | m \rangle \\
 &^{(T_1Cb)} - \frac{1}{4} \hat{J}_a^{-2} \sum_{cdeklm} \sum_J \hat{J} \langle kl\tilde{m} || \hat{w} || cde \rangle \langle cd | \hat{t}_2 | kl \rangle \langle \tilde{a} | \hat{t}_1 | m \rangle \langle \tilde{e} | \hat{t}_1 | i \rangle \\
 &^{(T_1Cc)} - \frac{1}{2} \hat{J}_a^{-2} \sum_{cdeklm} \sum_J \hat{J} \langle kl\tilde{m} || \hat{w} || cde \rangle \langle cd | \hat{t}_2 | ki \rangle \langle \tilde{a} | \hat{t}_1 | l \rangle \langle \tilde{e} | \hat{t}_1 | m \rangle \\
 &^{(T_1Cd)} - \frac{1}{2} \hat{J}_a^{-2} \sum_{cdeklm} \sum_J \hat{J} \langle kl\tilde{m} || \hat{w} || cde \rangle \langle ca | \hat{t}_2 | kl \rangle \langle \tilde{d} | \hat{t}_1 | i \rangle \langle \tilde{e} | \hat{t}_1 | m \rangle \\
 &^{(T_1Ce)} + \frac{1}{2} \sum_{cdeklm} \hat{J}_k^{-1} \hat{J}_l^{-1} \sum_J \hat{J} \langle kl\tilde{m} || \hat{w} || cde \rangle \langle \tilde{c} | \hat{t}_1 | k \rangle \langle \tilde{d} | \hat{t}_1 | l \rangle \langle \tilde{e} \tilde{a} | \hat{t}_2 | mi \rangle \\
 &^{(T_1Cf)} + \frac{1}{4} \sum_{cdeklm} \sum_J \hat{J} \langle kl\tilde{m} || \hat{w} || cde \rangle \langle cd | \hat{t}_2 | kl \rangle \langle \tilde{e} \tilde{a} | \hat{t}_2 | mi \rangle \\
 &^{(T_1Cg)} - \frac{1}{4} \hat{J}_a^{-1} \sum_{cdeklm} \sum_{JJ'J''} (-1)^{J+J'+J''} \hat{J} \hat{J}' \hat{J}'' \left\{ \begin{matrix} J & J' & J'' \\ j_i & j_e & j_m \end{matrix} \right\}_{6j} \\
 &\quad \times \langle kl\tilde{m} || \hat{w} || cde \rangle \langle cd | \hat{t}_2 | im \rangle \langle ea | \hat{t}_2 | kl \rangle + \langle \tilde{a} | \hat{t}_1 | i \rangle [\text{NO2B}] = 0, \forall a, i
 \end{aligned}$$

 Figure C.11: Spherical expressions for the CCSD \hat{T}_1 amplitude equations for three-body Hamiltonians, continued.

$$\begin{aligned}
 & \hat{P}_{ab}(J) \hat{P}_{ij}(J) \left\{ \begin{array}{l} \text{(T}_2\text{Aa)} \\ + \end{array} \frac{1}{4} \hat{J}^{-1} \sum_{ck} \langle \overset{J}{\downarrow} ab \tilde{k} || \overset{J}{\downarrow} \hat{w} || \overset{00}{\downarrow} i j c \rangle \langle \tilde{c} | \hat{t}_1 | k \rangle \right. \\
 & \text{(T}_2\text{Ba)} \frac{1}{2} \hat{J}^{-1} \hat{J}_j^{-1} (-1)^{j_i+j_j-J} \sum_{cdk} \langle \overset{J}{\downarrow} ab \tilde{k} || \overset{J}{\downarrow} \hat{w} || \overset{00}{\downarrow} c i d \rangle \langle \tilde{c} | \hat{t}_1 | j \rangle \langle \tilde{d} | \hat{t}_1 | k \rangle \\
 & \text{(T}_2\text{Bb)} \frac{1}{2} \hat{J}^{-1} \hat{J}_b^{-1} \sum_{ckl} \langle \overset{J}{\downarrow} a k \tilde{l} || \overset{J}{\downarrow} \hat{w} || \overset{00}{\downarrow} i j c \rangle \langle \tilde{b} | \hat{t}_1 | k \rangle \langle \tilde{c} | \hat{t}_1 | l \rangle \\
 & \text{(T}_2\text{Bc)} \frac{1}{4} \hat{J}^{-1} \sum_{cdk} \sum_{J'J''} (-1)^{J+J'+J''} \hat{J}' \hat{J}'' \left\{ \overset{J'}{j_i} \overset{J''}{j_j} \overset{J}{j_k} \right\}_{6j} \langle \overset{J}{\downarrow} ab \tilde{k} || \overset{J''}{\downarrow} \hat{w} || \overset{J'}{\downarrow} c d i \rangle \langle \overset{J'M'}{\downarrow} c d | \hat{t}_2 | \overset{J'M'}{\downarrow} j k \rangle \\
 & \text{(T}_2\text{Bd)} \frac{1}{4} \hat{J}^{-1} (-1)^{j_a+j_b-J} \sum_{ckl} \sum_{J'J''} (-1)^{J+J'+J''} \hat{J}' \hat{J}'' \left\{ \overset{J'}{j_a} \overset{J''}{j_b} \overset{J}{j_c} \right\}_{6j} \\
 & \times \langle \overset{J'}{\downarrow} k l \tilde{a} || \overset{J}{\downarrow} \hat{w} || \overset{J'M'}{\downarrow} i j c \rangle \langle \overset{J'M'}{\downarrow} c b | \hat{t}_2 | \overset{J'M'}{\downarrow} k l \rangle \\
 & \text{(T}_2\text{Ca)} \frac{1}{4} \hat{J}^{-1} \hat{J}_i^{-1} \hat{J}_j^{-1} \sum_{cdk} \langle \overset{J}{\downarrow} ab \tilde{k} || \overset{J}{\downarrow} \hat{w} || \overset{00}{\downarrow} c d e \rangle \langle \tilde{c} | \hat{t}_1 | i \rangle \langle \tilde{d} | \hat{t}_1 | j \rangle \langle \tilde{e} | \hat{t}_1 | k \rangle \\
 & \text{(T}_2\text{Cb)} \hat{J}^{-1} \hat{J}_b^{-1} \hat{J}_j^{-1} \sum_{cdkl} \langle \overset{J}{\downarrow} a k \tilde{l} || \overset{J}{\downarrow} \hat{w} || \overset{00}{\downarrow} i c d \rangle \langle \tilde{b} | \hat{t}_1 | k \rangle \langle \tilde{c} | \hat{t}_1 | j \rangle \langle \tilde{d} | \hat{t}_1 | l \rangle \left. \right\} + \dots
 \end{aligned}$$

 Figure C.12: Spherical expressions for the CCSD \hat{T}_2 amplitude equations for three-body Hamiltonians.

$$\begin{aligned}
 & \hat{P}_{ab}(J) \hat{P}_{ij}(J) \left\{ \begin{array}{c} (T_2Cc) \\ + \end{array} \frac{1}{4} \hat{J}^{-1} \hat{J}_a^{-1} \hat{J}_b^{-1} \sum_{cklm} \langle kl\tilde{m} || \hat{w} || ij c \rangle \langle \tilde{a} | \hat{t}_1 | k \rangle \langle \tilde{b} | \hat{t}_1 | l \rangle \langle \tilde{c} | \hat{t}_1 | m \rangle \right. \\
 & \quad \left. \begin{array}{c} (T_2Cd) \\ + \end{array} \frac{1}{8} \hat{J}^{-1} \sum_{cdek} \langle ab\tilde{k} || \hat{w} || cde \rangle \langle \tilde{e} | \hat{t}_1 | k \rangle \langle cd | \hat{t}_2 | ij \rangle \right. \\
 & \quad \left. \begin{array}{c} (T_2Ce) \\ + \end{array} \frac{1}{4} \hat{J}^{-1} \hat{J}_l^{-1} \sum_{cdek} \sum_{J'J''} (-1)^{J+J'+J''} \hat{J}' \hat{J}'' \left\{ \begin{array}{c} J \\ j_j \end{array} \begin{array}{c} J' \\ j_k \end{array} \begin{array}{c} J'' \\ j_i \end{array} \right\}_{6j} \right. \\
 & \quad \left. \times \langle ab\tilde{k} || \hat{w} || cde \rangle \langle cd | \hat{t}_2 | jk \rangle \langle \tilde{e} | \hat{t}_1 | i \rangle \right\} \\
 & \quad \begin{array}{c} (T_2Cf) \\ + \end{array} \text{CCAtoStd}^{(A)} \left[\begin{array}{c} ab \\ ij \end{array} J; J' \right] \frac{1}{2} (\hat{J}')^{-1} \hat{J}_j^{-1} \sum_{cdkl} \sum_{J''J'''} \hat{J}'' \hat{J}''' \left\{ \begin{array}{c} J' \\ j_a \end{array} \begin{array}{c} J'' \\ j_j \end{array} \begin{array}{c} J''' \\ j_b \end{array} \right\}_{6j} \\
 & \quad \times \langle kl\tilde{a} || \hat{w} || cdi \rangle \langle db | \hat{t}_2 | kl \rangle \langle \tilde{c} | \hat{t}_1 | j \rangle \\
 & \quad \begin{array}{c} (T_2Cg) \\ - \end{array} \frac{1}{2} \hat{P}_{ab}(J) \hat{P}_{ij}(J) \hat{J}^{-1} \hat{J}_b^{-1} \sum_{cdkl} \sum_{J'J''} (-1)^{J+J'+J''} \hat{J}' \hat{J}'' \left\{ \begin{array}{c} J' \\ j_i \end{array} \begin{array}{c} J'' \\ j_j \end{array} \begin{array}{c} J \\ j_l \end{array} \right\}_{6j} \\
 & \quad \times \langle ak\tilde{l} || \hat{w} || cdi \rangle \langle \tilde{b} | \hat{t}_1 | k \rangle \langle cd | \hat{t}_2 | jl \rangle \\
 & \quad \begin{array}{c} (T_2Ch) \\ - \end{array} \text{CCAtoStd}^{(A)} \left[\begin{array}{c} ab \\ ij \end{array} J; J' \right] (\hat{J}')^{-1} \sum_{cdkl} \hat{J}_l^{-1} \sum_{J'J''} (-1)^{J'+J''+J'''} \hat{J}'' \hat{J}''' \\
 & \quad \times \left\{ \begin{array}{c} J'' \\ j_a \end{array} \begin{array}{c} J''' \\ j_k \end{array} \begin{array}{c} J' \\ j_l \end{array} \right\}_{6j} \langle kl\tilde{a} || \hat{w} || cdi \rangle \langle \tilde{b}\tilde{a} | \hat{t}_2 | jk \rangle \langle \tilde{c} | \hat{t}_1 | l \rangle + \dots
 \end{aligned}$$

 Figure C.13: Spherical expressions for the CCSD \hat{T}_2 amplitude equations for three-body Hamiltonians, continued.

$$\begin{aligned}
 & \hat{P}_{ab}(J) \hat{P}_{ij}(J) \left\{ \begin{array}{l} \text{(\textit{T}_2Ci)} \\ + \end{array} \frac{1}{8} \hat{J}^{-1} \sum_{cklm} \begin{array}{c} \overset{J}{\downarrow} \quad \overset{J}{\downarrow} \quad \overset{JM}{\downarrow} \quad \overset{JM}{\downarrow} \quad \overset{00}{\downarrow} \\ \langle kl\tilde{m}|\hat{w}||ijc\rangle \langle ab|\hat{t}_2|kl\rangle \langle \tilde{c}|\hat{t}_1|m\rangle \\ \underbrace{\hspace{1.5cm}}_0 \end{array} \right. \\
 & \begin{array}{l} \text{(\textit{T}_2Cj)} \\ - \end{array} \frac{1}{4} \hat{J}^{-1} \hat{J}_a^{-1} (-1)^{j_a+j_b-J} \sum_{cklm} \sum_{J'J''} (-1)^{J+J'+J''} \hat{J}' \hat{J}'' \left\{ \begin{array}{c} J' \quad J'' \quad J \\ j_m \quad j_b \quad j_c \end{array} \right\}_{6j} \\
 & \times \begin{array}{c} \overset{J'}{\downarrow} \quad \overset{J}{\downarrow} \quad \overset{J'M'}{\downarrow} \quad \overset{J'M'}{\downarrow} \quad \overset{00}{\downarrow} \\ \langle kl\tilde{m}|\hat{w}||ijc\rangle \langle cb|\hat{t}_2|kl\rangle \langle \tilde{a}|\hat{t}_1|m\rangle \\ \underbrace{\hspace{1.5cm}}_{J''} \end{array} \\
 & \begin{array}{l} \text{(\textit{T}_2Da)} \\ + \end{array} \frac{1}{2} \hat{J}^{-1} \hat{J}_b^{-1} \hat{J}_i^{-1} \hat{J}_j^{-1} \sum_{cdekl} \begin{array}{c} \overset{J}{\downarrow} \quad \overset{J}{\downarrow} \quad \overset{00}{\downarrow} \quad \overset{00}{\downarrow} \quad \overset{00}{\downarrow} \quad \overset{00}{\downarrow} \\ \langle ak\tilde{l}|\hat{w}||cde\rangle \langle \tilde{b}|\hat{t}_1|k\rangle \langle \tilde{c}|\hat{t}_1|i\rangle \langle \tilde{d}|\hat{t}_1|j\rangle \langle \tilde{e}|\hat{t}_1|l\rangle \\ \underbrace{\hspace{1.5cm}}_0 \end{array} \\
 & \begin{array}{l} \text{(\textit{T}_2Db)} \\ + \end{array} \frac{1}{2} \hat{J}^{-1} \hat{J}_a^{-1} \hat{J}_b^{-1} \hat{J}_j^{-1} (-1)^{j_a+j_b-J} \\
 & \times \sum_{cdklm} \begin{array}{c} \overset{J}{\downarrow} \quad \overset{J}{\downarrow} \quad \overset{00}{\downarrow} \quad \overset{00}{\downarrow} \quad \overset{00}{\downarrow} \quad \overset{00}{\downarrow} \\ \langle kl\tilde{m}|\hat{w}||icd\rangle \langle \tilde{a}|\hat{t}_1|l\rangle \langle \tilde{b}|\hat{t}_1|k\rangle \langle \tilde{c}|\hat{t}_1|j\rangle \langle \tilde{d}|\hat{t}_1|m\rangle \\ \underbrace{\hspace{1.5cm}}_0 \end{array} \\
 & \begin{array}{l} \text{(\textit{T}_2Dc)} \\ - \end{array} \frac{1}{4} \hat{J}^{-1} \hat{J}_i^{-1} \hat{J}_j^{-1} (-1)^{j_a+j_b-J} \sum_{cdekl} \sum_{J'J''} (-1)^{J+J'+J''} \hat{J}' \hat{J}'' \left\{ \begin{array}{c} J' \quad J'' \quad J \\ j_a \quad j_b \quad j_e \end{array} \right\}_{6j} \\
 & \times \begin{array}{c} \overset{J'}{\downarrow} \quad \overset{J}{\downarrow} \quad \overset{00}{\downarrow} \quad \overset{00}{\downarrow} \quad \overset{J'M'}{\downarrow} \quad \overset{J'M'}{\downarrow} \\ \langle kl\tilde{a}|\hat{w}||cde\rangle \langle \tilde{c}|\hat{t}_1|i\rangle \langle \tilde{d}|\hat{t}_1|j\rangle \langle eb|\hat{t}_2|kl\rangle \\ \underbrace{\hspace{1.5cm}}_{J''} \end{array} \\
 & \begin{array}{l} \text{(\textit{T}_2Dd)} \\ + \end{array} \frac{1}{2} \hat{J}^{-1} \hat{J}_b^{-1} \hat{J}_i^{-1} \sum_{cdekl} \sum_{J'J''} (-1)^{J+J'+J''} \hat{J}' \hat{J}'' \left\{ \begin{array}{c} J' \quad J'' \quad J \\ j_i \quad j_j \quad j_l \end{array} \right\}_{6j} \\
 & \times \begin{array}{c} \overset{J}{\downarrow} \quad \overset{J'}{\downarrow} \quad \overset{J'M'}{\downarrow} \quad \overset{J'M'}{\downarrow} \quad \overset{00}{\downarrow} \quad \overset{00}{\downarrow} \\ \langle ak\tilde{l}|\hat{w}||cde\rangle \langle cd|\hat{t}_2|jl\rangle \langle \tilde{b}|\hat{t}_1|k\rangle \langle \tilde{e}|\hat{t}_1|i\rangle \\ \underbrace{\hspace{1.5cm}}_{J''} \end{array} \Big\} + \dots
 \end{aligned}$$

 Figure C.14: Spherical expressions for the CCSD \hat{T}_2 amplitude equations for three-body Hamiltonians, continued.

$$\begin{aligned}
 & \stackrel{(\text{T}_2\text{De})}{-} \text{CCAtoStd}^{(A)} \left[\begin{matrix} ab \\ ij \end{matrix} J; J' \right] (\hat{f}')^{-1} \hat{f}_i^{-1} \sum_{cdek l} \hat{f}_k^{-1} (-1)^{j_c+j_l-J'} \\
 & \times \sum_{j'' j'''} \hat{f}'' \hat{f}''' \left\{ \begin{matrix} j' & j'' & j''' \\ j_k & j_c & j_l \end{matrix} \right\}_{6j} \begin{array}{c} \xrightarrow{j''} \langle kl\tilde{a}||\hat{w}||cde \rangle \xrightarrow{j'''} \langle \tilde{c}\tilde{b}|\hat{t}_2|\tilde{l}\tilde{j} \rangle \xrightarrow{j'M'} \langle \tilde{d}|\hat{t}_1|k \rangle \xrightarrow{00} \langle \tilde{e}|\hat{t}_1|i \rangle \\ \xrightarrow{j'} \end{array} \\
 & \hat{P}_{ab}(J) \hat{P}_{ij}(J) \left\{ \stackrel{(\text{T}_2\text{Df})}{+} \frac{1}{4} \hat{f}^{-1} \hat{f}_b^{-1} \sum_{cdek l} \begin{array}{c} \xrightarrow{j} \langle ak\tilde{l}||\hat{w}||cde \rangle \xrightarrow{j} \langle cd|\hat{t}_2|ij \rangle \xrightarrow{JM} \langle \tilde{b}|\hat{t}_1|k \rangle \xrightarrow{00} \langle \tilde{e}|\hat{t}_1|l \rangle \\ \xrightarrow{0} \end{array} \right. \\
 & \stackrel{(\text{T}_2\text{Dg})}{-} \frac{1}{4} \hat{f}_a^{-1} \sum_{cdek l} \hat{f}_k^{-1} \hat{f}_l^{-1} \sum_{j'} \hat{f}' \begin{array}{c} \xrightarrow{j'} \langle kl\tilde{a}||\hat{w}||cde \rangle \xrightarrow{j'} \langle \tilde{c}|\hat{t}_1|k \rangle \xrightarrow{00} \langle \tilde{d}|\hat{t}_1|l \rangle \xrightarrow{JM} \langle eb|\hat{t}_2|ij \rangle \\ \xrightarrow{0} \end{array} \\
 & \stackrel{(\text{T}_2\text{Dh})}{-} \frac{1}{4} \hat{f}^{-1} \hat{f}_a^{-1} \hat{f}_b^{-1} \sum_{cdklm} \sum_{j' j''} (-1)^{J+J'+J''} \hat{f}' \hat{f}'' \left\{ \begin{matrix} j' & j'' & j \\ j_i & j_j & j_m \end{matrix} \right\}_{6j} \\
 & \times \begin{array}{c} \xrightarrow{j} \langle kl\tilde{m}||\hat{w}||cdi \rangle \xrightarrow{j'} \langle \tilde{a}|\hat{t}_1|k \rangle \xrightarrow{00} \langle \tilde{b}|\hat{t}_1|l \rangle \xrightarrow{j'M'} \langle cd|\hat{t}_2|jm \rangle \\ \xrightarrow{j''} \end{array} \\
 & \stackrel{(\text{T}_2\text{Di})}{+} \frac{1}{2} \hat{f}^{-1} \hat{f}_a^{-1} \hat{f}_j^{-1} (-1)^{j_a+j_b-J} \sum_{cdklm} \sum_{j' j''} (-1)^{J+J'+J''} \hat{f}' \hat{f}'' \left\{ \begin{matrix} j & j' & j'' \\ j_d & j_m & j_b \end{matrix} \right\}_{6j} \\
 & \times \begin{array}{c} \xrightarrow{j'} \langle kl\tilde{m}||\hat{w}||icd \rangle \xrightarrow{j} \langle db|\hat{t}_2|kl \rangle \xrightarrow{j'M'} \langle \tilde{a}|\hat{t}_1|m \rangle \xrightarrow{00} \langle \tilde{c}|\hat{t}_1|j \rangle \\ \xrightarrow{j''} \end{array} \left. \right\} \\
 & \stackrel{(\text{T}_2\text{Dj})}{-} \text{CCAtoStd}^{(A)} \left[\begin{matrix} ab \\ ij \end{matrix} J; J' \right] \\
 & (\hat{f}')^{-1} \hat{f}_a^{-1} \sum_{cdklm} \hat{f}_l^{-1} \sum_{j'' j'''} (-1)^{J'+J''+J'''} \hat{f}'' \hat{f}''' \left\{ \begin{matrix} j' & j'' & j''' \\ j_l & j_d & j_k \end{matrix} \right\}_{6j} \\
 & \times \begin{array}{c} \xrightarrow{j''} \langle kl\tilde{m}||\hat{w}||cdi \rangle \xrightarrow{j'''} \langle \tilde{d}\tilde{b}|\hat{t}_2|kj \rangle \xrightarrow{j'M'} \langle \tilde{a}|\hat{t}_1|m \rangle \xrightarrow{00} \langle \tilde{c}|\hat{t}_1|l \rangle \\ \xrightarrow{j'} \end{array} + \dots
 \end{aligned}$$

 Figure C.15: Spherical expressions for the CCSD \hat{T}_2 amplitude equations for three-body Hamiltonians, continued.

$$\begin{aligned}
 & \stackrel{(\text{T}_2\text{Dp})}{-} \frac{1}{8} \hat{P}_{ab}(J) \hat{P}_{ij}(J) \hat{J}^{-1} \sum_{cdklm} \sum_{J'J''} (-1)^{J+J'+J''} \hat{J}' \hat{J}'' \left\{ \begin{matrix} J' & J'' & J \\ j_i & j_j & j_m \end{matrix} \right\}_{6j} \\
 & \times \underbrace{\langle kl\tilde{m}|\hat{w}|cdi\rangle}_{J''} \langle ab|\hat{t}_2|kl\rangle \langle cd|\hat{t}_2|jm\rangle \\
 & \stackrel{(\text{T}_2\text{Dq})}{+} \text{CCAtoStd}^{(A)} \left[\begin{matrix} ab \\ ij \end{matrix} J; J' \right] \frac{1}{2} (\hat{J}')^{-1} \sum_{cdklm} (-1)^{j_d+j_m-J'} \\
 & \times \sum_{J''J'''} \hat{J}'' \hat{J}''' \left\{ \begin{matrix} J' & J'' & J''' \\ j_c & j_i & j_a \end{matrix} \right\}_{6j} \underbrace{\langle kl\tilde{m}|\hat{w}|icd\rangle}_{J'} \langle \tilde{b}\tilde{d}|\hat{t}_2|jm\rangle \underbrace{\langle ca|\hat{t}_2|kl\rangle}_{J'M'} \\
 & \stackrel{(\text{T}_2\text{Dr})}{-} \hat{P}_{ab}(J) \hat{P}_{ij}(J) \left\{ \frac{1}{4} \hat{J}_i^{-1} (-1)^{j_i+j_j-J} \right. \\
 & \times \sum_{cdklm} \hat{J}_k^{-1} \hat{J}_l^{-1} \sum_{J'} \hat{J}' \underbrace{\langle kl\tilde{m}|\hat{w}|cdi\rangle}_0 \langle ab|\hat{t}_2|jm\rangle \langle \tilde{c}|\hat{t}_1|k\rangle \langle \tilde{d}|\hat{t}_1|l\rangle \\
 & \stackrel{(\text{T}_2\text{Ra})}{+} \frac{1}{4} \hat{J}^{-1} \hat{J}_a^{-1} \hat{J}_b^{-1} \hat{J}_i^{-1} \hat{J}_j^{-1} \\
 & \times \sum_{cdeklm} \underbrace{\langle kl\tilde{m}|\hat{w}|cde\rangle}_0 \langle \tilde{a}|\hat{t}_1|k\rangle \langle \tilde{b}|\hat{t}_1|l\rangle \langle \tilde{c}|\hat{t}_1|i\rangle \langle \tilde{d}|\hat{t}_1|j\rangle \langle \tilde{e}|\hat{t}_1|m\rangle \\
 & \stackrel{(\text{T}_2\text{Eb})}{-} \frac{1}{4} \hat{J}_a^{-2} \sum_{cdeklm} \hat{J}_k^{-1} \hat{J}_l^{-1} \sum_{J'} \hat{J}' \underbrace{\langle kl\tilde{m}|\hat{w}|cde\rangle}_0 \langle \tilde{c}|\hat{t}_1|k\rangle \langle \tilde{d}|\hat{t}_1|l\rangle \langle \tilde{a}|\hat{t}_1|m\rangle \langle eb|\hat{t}_2|ij\rangle \\
 & \stackrel{(\text{T}_2\text{Ec})}{+} \frac{1}{4} \hat{J}_i^{-2} (-1)^{j_i+j_j-J} \sum_{cdeklm} \hat{J}_k^{-1} \hat{J}_l^{-1} \sum_{J'} \hat{J}' \\
 & \times \underbrace{\langle kl\tilde{m}|\hat{w}|cde\rangle}_0 \langle \tilde{c}|\hat{t}_1|k\rangle \langle \tilde{d}|\hat{t}_1|l\rangle \langle \tilde{e}|\hat{t}_1|i\rangle \langle ab|\hat{t}_2|jm\rangle \left. \right\} + \dots
 \end{aligned}$$

 Figure C.17: Spherical expressions for the CCSD \hat{T}_2 amplitude equations for three-body Hamiltonians, continued.

$$\begin{aligned}
 & \stackrel{(\text{T}_2\text{Ed})}{+} \frac{1}{8} \hat{P}_{ab}(J) \hat{P}_{ij}(J) \hat{J}^{-1} \hat{J}_a^{-1} \hat{J}_b^{-1} \\
 & \times \sum_{cdeklm} \langle kl\tilde{m} || \hat{w} || cde \rangle \langle \tilde{a} | \hat{t}_1 | k \rangle \langle \tilde{b} | \hat{t}_1 | l \rangle \langle \tilde{e} | \hat{t}_1 | m \rangle \langle cd | \hat{t}_2 | ij \rangle \\
 & \stackrel{(\text{T}_2\text{Ee})}{-} \text{CCAtoStd}^{(A)} \left[\begin{smallmatrix} ab \\ ij \end{smallmatrix} J; J' \right] (\hat{J}')^{-1} \hat{J}_a^{-1} \hat{J}_i^{-1} \sum_{cdeklm} \hat{J}_k^{-1} (-1)^{j_e+j_m-J'} \\
 & \times \sum_{j''j'''} \hat{J}'' \hat{J}''' \left\{ \begin{smallmatrix} j' & j'' & j''' \\ j_k & j_c & j_l \end{smallmatrix} \right\}_{6j} \langle kl\tilde{m} || \hat{w} || cde \rangle \langle \tilde{e}\tilde{b} | \hat{t}_2 | mj \rangle \langle \tilde{a} | \hat{t}_1 | l \rangle \langle \tilde{c} | \hat{t}_1 | i \rangle \langle \tilde{d} | \hat{t}_1 | k \rangle \\
 & \hat{P}_{ab}(J) \hat{P}_{ij}(J) \left\{ \right. \\
 & \stackrel{(\text{T}_2\text{Ef})}{+} \frac{1}{8} \hat{J}^{-1} \hat{J}_i^{-1} \hat{J}_j^{-1} \sum_{cdeklm} \langle kl\tilde{m} || \hat{w} || cde \rangle \langle ab | \hat{t}_2 | kl \rangle \langle \tilde{c} | \hat{t}_1 | i \rangle \langle \tilde{d} | \hat{t}_1 | j \rangle \langle \tilde{e} | \hat{t}_1 | m \rangle \\
 & \stackrel{(\text{T}_2\text{Eg})}{-} \frac{1}{4} \hat{J}^{-1} \hat{J}_a^{-1} \hat{J}_i^{-1} \hat{J}_j^{-1} (-1)^{j_a+j_b-J} \sum_{cdeklm} \sum_{j'j''} (-1)^{J+J'+J''} \hat{J}' \hat{J}'' \\
 & \times \left\{ \begin{smallmatrix} j & j' & j'' \\ j_e & j_m & j_b \end{smallmatrix} \right\}_{6j} \langle kl\tilde{m} || \hat{w} || cde \rangle \langle eb | \hat{t}_2 | kl \rangle \langle \tilde{a} | \hat{t}_1 | m \rangle \langle \tilde{c} | \hat{t}_1 | i \rangle \langle \tilde{d} | \hat{t}_1 | j \rangle \\
 & \stackrel{(\text{T}_2\text{Eh})}{+} \frac{1}{4} \hat{J}^{-1} \hat{J}_a^{-1} \hat{J}_b^{-1} \hat{J}_i^{-1} \sum_{cdeklm} \sum_{j'j''} (-1)^{J+J'+J''} \hat{J}' \hat{J}'' \left\{ \begin{smallmatrix} j & j' & j'' \\ j_m & j_i & j_j \end{smallmatrix} \right\}_{6j} \\
 & \times \langle kl\tilde{m} || \hat{w} || cde \rangle \langle cd | \hat{t}_2 | jm \rangle \langle \tilde{a} | \hat{t}_1 | k \rangle \langle \tilde{b} | \hat{t}_1 | l \rangle \langle \tilde{e} | \hat{t}_1 | i \rangle \left\{ \right. + \dots
 \end{aligned}$$

 Figure C.18: Spherical expressions for the CCSD \hat{T}_2 amplitude equations for three-body Hamiltonians, continued.

$$\begin{aligned}
 & \stackrel{(T_2Ei)}{-} \text{CCAtoStd}^{(A)} \left[\begin{smallmatrix} ab \\ ij \end{smallmatrix} J; J' \right] \frac{1}{2} (\hat{J}')^{-1} \hat{J}_j^{-1} \sum_{cdeklm} (-1)^{j_e+j_m-J'} \\
 & \times \sum_{J''J'''} \hat{J}'' \hat{J}''' \left\{ \begin{smallmatrix} J' & J'' & J''' \\ j_d & j_j & j_b \end{smallmatrix} \right\}_{6j} \langle kl\tilde{m} || \hat{w} || cde \rangle \langle \tilde{a}\tilde{e} | \hat{t}_2 | im \rangle \langle db | \hat{t}_2 | kl \rangle \langle \tilde{c} | \hat{t}_1 | j \rangle \\
 & \quad \begin{array}{c} \begin{array}{c} \downarrow \quad \downarrow \quad \downarrow \\ J'' \quad J''' \quad J' \end{array} \\ \begin{array}{c} \downarrow \quad \downarrow \quad \downarrow \\ J' \quad J'' \quad J''' \end{array} \end{array} \\
 & \hat{P}_{ab}(J) \hat{P}_{ij}(J) \left\{ \stackrel{(T_2Ei)}{+} \frac{1}{8} \hat{J}^{-1} \hat{J}_i^{-1} \sum_{cdeklm} \sum_{J'J''} (-1)^{J+J'+J''} \hat{J}' \hat{J}'' \right. \\
 & \times \left\{ \begin{smallmatrix} J & J' & J'' \\ j_m & j_i & j_j \end{smallmatrix} \right\}_{6j} \langle kl\tilde{m} || \hat{w} || cde \rangle \langle cd | \hat{t}_2 | jm \rangle \langle ab | \hat{t}_2 | kl \rangle \langle \tilde{e} | \hat{t}_1 | i \rangle \\
 & \quad \begin{array}{c} \begin{array}{c} \downarrow \quad \downarrow \quad \downarrow \\ J \quad J' \quad J'' \end{array} \\ \begin{array}{c} \downarrow \quad \downarrow \quad \downarrow \\ J' \quad J'' \quad J \end{array} \end{array} \\
 & \stackrel{(T_2Ek)}{-} \frac{1}{8} \hat{J}_j^{-2} \sum_{cdeklm} \sum_{J'} \hat{J}' \langle kl\tilde{m} || \hat{w} || cde \rangle \langle ab | \hat{t}_2 | im \rangle \langle cd | \hat{t}_2 | kl \rangle \langle \tilde{e} | \hat{t}_1 | j \rangle \\
 & \quad \begin{array}{c} \begin{array}{c} \downarrow \quad \downarrow \quad \downarrow \\ J' \quad J' \quad JM \end{array} \\ \begin{array}{c} \downarrow \quad \downarrow \quad \downarrow \\ JM \quad JM \quad J'M' \end{array} \end{array} \\
 & \stackrel{(T_2El)}{-} \frac{1}{8} \hat{J}_a^{-2} \sum_{cdeklm} \sum_{J'} (\hat{J}')^{-1} \langle kl\tilde{m} || \hat{w} || cde \rangle \langle cd | \hat{t}_2 | kl \rangle \langle eb | \hat{t}_2 | ij \rangle \langle \tilde{a} | \hat{t}_1 | m \rangle \\
 & \quad \begin{array}{c} \begin{array}{c} \downarrow \quad \downarrow \quad \downarrow \\ J' \quad J' \quad J'M' \end{array} \\ \begin{array}{c} \downarrow \quad \downarrow \quad \downarrow \\ J'M' \quad J'M' \quad JM \end{array} \end{array} \\
 & \stackrel{(T_2Em)}{-} \frac{1}{8} \hat{J}^{-1} \hat{J}_a^{-1} (-1)^{j_a+j_b-J} \sum_{cdeklm} \sum_{J'J''} (-1)^{J+J'+J''} \hat{J}' \hat{J}'' \left\{ \begin{smallmatrix} J & J' & J'' \\ j_e & j_m & j_b \end{smallmatrix} \right\}_{6j} \\
 & \times \langle kl\tilde{m} || \hat{w} || cde \rangle \langle cd | \hat{t}_2 | ij \rangle \langle eb | \hat{t}_2 | kl \rangle \langle \tilde{a} | \hat{t}_1 | m \rangle \left. \right\} \\
 & \quad \begin{array}{c} \begin{array}{c} \downarrow \quad \downarrow \quad \downarrow \\ J' \quad J \quad JM \end{array} \\ \begin{array}{c} \downarrow \quad \downarrow \quad \downarrow \\ JM \quad JM \quad J'M' \end{array} \end{array} \\
 & \stackrel{(T_2En)}{-} \text{CCAtoStd}^{(A)} \left[\begin{smallmatrix} ab \\ ij \end{smallmatrix} J; J' \right] \frac{1}{2} (\hat{J}')^{-1} \hat{J}_b^{-1} \sum_{cdeklm} (-1)^{j_e+j_m-J'} \\
 & \times \sum_{J''J'''} \hat{J}'' \hat{J}''' \left\{ \begin{smallmatrix} J' & J'' & J''' \\ j_k & j_l & j_j \end{smallmatrix} \right\}_{6j} \langle kl\tilde{m} || \hat{w} || cde \rangle \langle \tilde{a}\tilde{e} | \hat{t}_2 | im \rangle \langle cd | \hat{t}_2 | jk \rangle \langle \tilde{b} | \hat{t}_1 | l \rangle + \dots \\
 & \quad \begin{array}{c} \begin{array}{c} \downarrow \quad \downarrow \quad \downarrow \\ J'' \quad J'' \quad J''' \end{array} \\ \begin{array}{c} \downarrow \quad \downarrow \quad \downarrow \\ J' \quad J'' \quad J''' \end{array} \end{array}
 \end{aligned}$$

 Figure C.19: Spherical expressions for the CCSD \hat{T}_2 amplitude equations for three-body Hamiltonians, continued.

$$\begin{aligned}
 & \hat{P}_{ab}(J) \hat{P}_{ij}(J) \left\{ \right. \\
 & \quad \stackrel{(\text{T}_2\text{Eo})}{-} \frac{1}{4} \sum_{cdek lm} \sum_{J'J''} \hat{J}' (\hat{J}'')^2 \left\{ \begin{matrix} J' & J'' & J \\ j_a & j_b & j_d \end{matrix} \right\}_{6j} \left\{ \begin{matrix} J' & J'' & J \\ j_a & j_c & j_d \end{matrix} \right\}_{6j} \\
 & \quad \times \underbrace{\langle kl \tilde{m} | \hat{w} | cde \rangle}_{0} \langle ac | \hat{t}_2 | ij \rangle \langle bd | \hat{t}_2 | kl \rangle \langle \tilde{e} | \hat{t}_1 | m \rangle \\
 & \quad \stackrel{(\text{T}_2\text{Ep})}{+} \frac{1}{16} \hat{J}^{-1} \sum_{cdek lm} \underbrace{\langle kl \tilde{m} | \hat{w} | cde \rangle}_{0} \langle cd | \hat{t}_2 | ij \rangle \langle ab | \hat{t}_2 | kl \rangle \langle \tilde{e} | \hat{t}_1 | m \rangle \left. \right\} \\
 & \quad \stackrel{(\text{T}_2\text{Eq})}{+} \text{CCAtoStd}^{(A)} \left[\begin{matrix} ab \\ ij \end{matrix} ; J' \right] \frac{1}{2} (\hat{J}')^{-1} \sum_{cdek lm} \hat{J}_l^{-1} (-1)^{j_e+j_m-J'} \sum_{J''J'''} \\
 & \quad \times (-1)^{J'+J''+J'''} \hat{J}'' \hat{J}''' \left\{ \begin{matrix} J' & J'' & J''' \\ j_i & j_d & j_k \end{matrix} \right\}_{6j} \underbrace{\langle kl \tilde{m} | \hat{w} | cde \rangle}_{J'} \langle \tilde{a} \tilde{d} | \hat{t}_2 | ik \rangle \langle \tilde{b} \tilde{e} | \hat{t}_2 | jm \rangle \langle \tilde{c} | \hat{t}_1 | l \rangle \\
 & \quad \stackrel{(\text{T}_2\text{Er})}{-} \frac{1}{4} \hat{P}_{ab}(J) \hat{P}_{ij}(J) \sum_{cdek lm} \sum_{J'J''} \hat{J}' (\hat{J}'')^2 \left\{ \begin{matrix} J & J' & J'' \\ j_i & j_i & j_j \end{matrix} \right\}_{6j} \left\{ \begin{matrix} J & J' & J'' \\ j_l & j_i & j_k \end{matrix} \right\}_{6j} \\
 & \quad \times \underbrace{\langle kl \tilde{m} | \hat{w} | cde \rangle}_{0} \langle ab | \hat{t}_2 | ik \rangle \langle cd | \hat{t}_2 | jl \rangle \langle \tilde{e} | \hat{t}_1 | m \rangle \\
 & \quad + \underbrace{\langle ab | \hat{t}_2 | ij \rangle}_{JM} [\text{NO2B}] = 0, \forall a, b, i, j, J, M
 \end{aligned}$$

 Figure C.20: Spherical expressions for the CCSD \hat{T}_2 amplitude equations for three-body Hamiltonians, continued.

Appendix D

Effective Hamiltonian Diagrams and Spherical Expressions

D.1 Spherical Equations

$$\begin{aligned}
 \overbrace{\langle i | \hat{\mathcal{H}}_1 | a \rangle}^{00} &= \overbrace{\langle i | \hat{f} | a \rangle}^{00} + \sum_{ck} \hat{f}_i^{-1} \hat{f}_k^{-1} \sum_J \hat{f}^2 \overbrace{\langle \tilde{c} | \hat{t}_1 | k \rangle}^{00} \overbrace{\langle i k | \hat{v} | a c \rangle}^{JM \quad JM} \\
 \overbrace{\langle \tilde{a} | \hat{\mathcal{H}}_1 | b \rangle}^{00} &= \overbrace{\langle \tilde{a} | \hat{f} | b \rangle}^{00} + \hat{f}_a^{-1} \sum_{ck} \hat{f}_k^{-1} \sum_J \hat{f}^2 \overbrace{\langle a k | \hat{v} | b c \rangle}^{JM \quad JM} \overbrace{\langle \tilde{c} | \hat{t}_1 | k \rangle}^{00} \\
 &\quad + \hat{f}_a^{-1} \sum_k \overbrace{\langle \tilde{a} | \hat{t}_1 | k \rangle}^{00} \overbrace{\langle \tilde{k} | \hat{\mathcal{H}}_1 | b \rangle}^{00} + \frac{1}{2} \hat{f}_a^{-1} \sum_{ckl} \sum_J \hat{f}^2 \overbrace{\langle a c | \hat{t}_2 | k l \rangle}^{JM \quad JM} \overbrace{\langle k l | \hat{v} | b c \rangle}^{JM \quad JM} \\
 \overbrace{\langle i | \hat{\mathcal{H}}_1 | j \rangle}^{00} &= \overbrace{\langle i | \hat{\chi}' | j \rangle}^{00} - \hat{f}_i^{-1} \sum_c \overbrace{\langle i | \hat{\mathcal{H}}_1 | c \rangle}^{00} \overbrace{\langle \tilde{c} | \hat{t}_1 | j \rangle}^{00} \\
 \overbrace{\langle \tilde{a} | \hat{\mathcal{H}}_1 | i \rangle}^{00} &= 0 \\
 \overbrace{\langle i j | \hat{\mathcal{H}}_2 | a b \rangle}^{JM \quad JM} &= \overbrace{\langle i j | \hat{v} | a b \rangle}^{JM \quad JM} \\
 \overbrace{\langle a i | \hat{\mathcal{H}}_2 | b c \rangle}^{JM \quad JM} &= \overbrace{\langle a i | \hat{v} | b c \rangle}^{JM \quad JM} + \hat{f}_a^{-1} \sum_k \overbrace{\langle \tilde{a} | \hat{t}_1 | k \rangle}^{00} \overbrace{\langle k i | \hat{v} | b c \rangle}^{JM \quad JM} \\
 \overbrace{\langle i k | \hat{\mathcal{H}}_2 | j a \rangle}^{JM \quad JM} &= \overbrace{\langle i k | \hat{v} | j a \rangle}^{JM \quad JM} - \hat{f}_j^{-1} \sum_c \overbrace{\langle \tilde{c} | \hat{t}_1 | j \rangle}^{00} \overbrace{\langle i k | \hat{v} | c a \rangle}^{JM \quad JM} \\
 \overbrace{\langle a b | \hat{\mathcal{H}}_2 | c d \rangle}^{JM \quad JM} &= \overbrace{\langle a b | \hat{\chi}' | c d \rangle}^{JM \quad JM} + \frac{1}{2} \sum_{kl} \overbrace{\langle a b | \hat{t}_2 | k l \rangle}^{JM \quad JM} \overbrace{\langle k l | \hat{v} | c d \rangle}^{JM \quad JM}
 \end{aligned}$$

Figure D.1: Spherical expressions for the effective Hamiltonian matrix elements.

$$\begin{aligned}
 \begin{array}{c} JM \\ \downarrow \\ \langle ij|\hat{\mathcal{H}}_2|kl \rangle \end{array} &= \begin{array}{c} JM \\ \downarrow \\ \langle ij|\hat{v}|kl \rangle \end{array} - \hat{P}_{kl}(J) \hat{j}_l^{-1} \sum_c \begin{array}{c} JM \\ \downarrow \\ \langle ij|\hat{\chi}'|kc \rangle \end{array} \begin{array}{c} JM \\ \downarrow \\ \langle \tilde{c}|\hat{t}_1|l \rangle \end{array} \\
 &+ \frac{1}{2} \sum_{cd} \begin{array}{c} JM \\ \downarrow \\ \langle ij|\hat{v}|cd \rangle \end{array} \begin{array}{c} JM \\ \downarrow \\ \langle cd|\hat{t}_2|kl \rangle \end{array} \\
 \begin{array}{c} JM \\ \downarrow \\ \langle aj|\hat{\mathcal{H}}_2|ib \rangle \end{array} &= \begin{array}{c} JM \\ \downarrow \\ \langle aj|\hat{\chi}'''|ib \rangle \end{array} - \frac{1}{2} \hat{j}_i^{-1} \sum_c \begin{array}{c} 00 \\ \downarrow \\ \langle \tilde{c}|\hat{t}_1|i \rangle \end{array} \begin{array}{c} JM \\ \downarrow \\ \langle aj|\hat{\mathcal{H}}_2|cb \rangle \end{array} \\
 &- \text{CCAtoStd} \left[\begin{array}{c} aj \\ ib \end{array}; J; J' \right] \sum_{ck} (-1)^{j_c+j_k-J'} \begin{array}{c} J'M' \\ \downarrow \\ \langle \tilde{a}\tilde{c}|\hat{t}_2|ik \rangle \end{array} \begin{array}{c} J'M' \\ \downarrow \\ \langle \tilde{k}\tilde{j}|\hat{v}|cb \rangle \end{array} \\
 \begin{array}{c} JM \\ \downarrow \\ \langle ia|\hat{\mathcal{H}}_2|jk \rangle \end{array} &= \begin{array}{c} JM \\ \downarrow \\ \langle ia|\hat{\chi}''|jk \rangle \end{array} - \hat{j}_i^{-1} \sum_c \begin{array}{c} 00 \\ \downarrow \\ \langle \tilde{i}|\hat{\mathcal{H}}_1|c \rangle \end{array} \begin{array}{c} JM \\ \downarrow \\ \langle ca|\hat{t}_2|jk \rangle \end{array} \\
 \begin{array}{c} JM \\ \downarrow \\ \langle ab|\hat{\mathcal{H}}_2|ij \rangle \end{array} &= 0 \\
 \begin{array}{c} JM \\ \downarrow \\ \langle ab|\hat{\mathcal{H}}_2|ci \rangle \end{array} &= \begin{array}{c} JM \\ \downarrow \\ \langle ab|\hat{v}|ci \rangle \end{array} - \hat{j}_i^{-1} \sum_d \begin{array}{c} JM \\ \downarrow \\ \langle ab|\hat{v}|cd \rangle \end{array} \begin{array}{c} 00 \\ \downarrow \\ \langle \tilde{d}|\hat{t}_1|i \rangle \end{array} \\
 &- \hat{P}_{ab}(J) \hat{j}_b^{-1} \sum_k (-1)^{j_i+j_c-J} \begin{array}{c} JM \\ \downarrow \\ \langle ak|\hat{\chi}'|ic \rangle \end{array} \begin{array}{c} JM \\ \downarrow \\ \langle \tilde{b}|\hat{t}_1|k \rangle \end{array} \\
 &+ \hat{j}_c^{-1} \sum_k \begin{array}{c} 00 \\ \downarrow \\ \langle \tilde{k}|\hat{\mathcal{H}}_1|c \rangle \end{array} \begin{array}{c} JM \\ \downarrow \\ \langle ab|\hat{t}_2|ki \rangle \end{array} \\
 &- \text{CCAtoStd}^{(A)} \left[\begin{array}{c} ab \\ ci \end{array}; J; J' \right] \Big|_{\hat{t}_{ci}=0} \sum_{dk} (-1)^{j_d+j_k-J'} \begin{array}{c} J'M' \\ \downarrow \\ \langle \tilde{a}\tilde{k}|\hat{\mathcal{H}}_2|cd \rangle \end{array} \begin{array}{c} J'M' \\ \downarrow \\ \langle \tilde{d}\tilde{b}|\hat{t}_2|ki \rangle \end{array} \\
 &- \frac{1}{2} \sum_{kl} (-1)^{j_c+j_i-J} \begin{array}{c} JM \\ \downarrow \\ \langle ab|\hat{t}_2|kl \rangle \end{array} \begin{array}{c} JM \\ \downarrow \\ \langle kl|\hat{\mathcal{H}}_2|ic \rangle \end{array}
 \end{aligned}$$

Figure D.2: Spherical expressions for the effective Hamiltonian matrix elements.

$$\begin{aligned}
 \overline{\langle i|\hat{\chi}'|j\rangle} &= \overline{\langle i|\hat{f}|j\rangle} + \hat{f}_i^{-1} \sum_{ck} \hat{f}_k^{-1} \sum_J \hat{f}^2 \overline{\langle \tilde{c}|\hat{t}_1|k\rangle} \overline{\langle ik|\hat{v}|jc\rangle} \\
 &\quad - \frac{1}{2} \hat{f}_i^{-1} \sum_{cdk} \sum_J \hat{f}^2 \overline{\langle ik|\hat{v}|cd\rangle} \overline{\langle cd|\hat{t}_2|jk\rangle} \\
 \overline{\langle ai|\hat{\chi}'|bc\rangle} &= \overline{\langle ai|\hat{v}|bc\rangle} + \frac{1}{2} \hat{f}_a^{-1} \sum_k \overline{\langle \tilde{a}|\hat{t}_1|k\rangle} \overline{\langle ki|\hat{v}|bc\rangle} \\
 \overline{\langle ik|\hat{\chi}'|ja\rangle} &= \overline{\langle ik|\hat{v}|ja\rangle} - \frac{1}{2} \hat{f}_j^{-1} \sum_c \overline{\langle \tilde{c}|\hat{t}_1|j\rangle} \overline{\langle ik|\hat{v}|ca\rangle} \\
 \overline{\langle ab|\hat{\chi}'|cd\rangle} &= \overline{\langle ab|\hat{v}|cd\rangle} + \hat{P}_{ab}(J) \hat{f}_b^{-1} \sum_k \overline{\langle ak|\hat{\chi}'|cd\rangle} \overline{\langle \tilde{b}|\hat{t}_1|k\rangle} \\
 \overline{\langle aj|\hat{\chi}'|ib\rangle} &= \overline{\langle aj|\hat{v}|ib\rangle} + \frac{1}{2} \hat{f}_a^{-1} \sum_k \overline{\langle \tilde{a}|\hat{t}_1|k\rangle} \overline{\langle kj|\hat{v}|ib\rangle} \\
 &\quad - \hat{f}_i^{-1} \sum_c \overline{\langle \tilde{c}|\hat{t}_1|i\rangle} \overline{\langle aj|\hat{\chi}'|cb\rangle} \\
 \overline{\langle aj|\hat{\chi}''|ib\rangle} &= \overline{\langle aj|\hat{v}|ib\rangle} + \frac{1}{2} \hat{f}_a^{-1} \sum_k \overline{\langle \tilde{a}|\hat{t}_1|k\rangle} \overline{\langle kj|\hat{v}|ib\rangle} \\
 &\quad - \frac{1}{2} \hat{f}_i^{-1} \sum_c \overline{\langle \tilde{c}|\hat{t}_1|i\rangle} \overline{\langle aj|\hat{\chi}'|cb\rangle}
 \end{aligned}$$

Figure D.3: Spherical expressions for the intermediates used in the calculations of the effective Hamiltonian matrix elements.

$$\begin{aligned}
 \begin{array}{c} JM \\ \downarrow \\ \downarrow \end{array} \langle aj | \hat{\chi}''' | ib \rangle &= \begin{array}{c} JM \\ \downarrow \\ \downarrow \end{array} \langle aj | \hat{v} | ib \rangle + \hat{J}_a^{-1} \sum_k \begin{array}{c} 00 \\ \downarrow \end{array} \begin{array}{c} JM \\ \downarrow \\ \downarrow \end{array} \langle \bar{a} | \hat{t}_1 | k \rangle \begin{array}{c} JM \\ \downarrow \\ \downarrow \end{array} \langle kj | \hat{v} | ib \rangle \\
 &- \frac{1}{2} \hat{J}_i^{-1} \sum_c \begin{array}{c} 00 \\ \downarrow \end{array} \begin{array}{c} JM \\ \downarrow \\ \downarrow \end{array} \langle \bar{c} | \hat{t}_1 | i \rangle \begin{array}{c} JM \\ \downarrow \\ \downarrow \end{array} \langle aj | \hat{\mathcal{H}}_2 | cb \rangle \\
 \begin{array}{c} JM \\ \downarrow \\ \downarrow \end{array} \langle ia | \hat{\chi}' | jk \rangle &= \begin{array}{c} JM \\ \downarrow \\ \downarrow \end{array} \langle ia | \hat{v} | jk \rangle + \frac{1}{2} \hat{J}_a^{-1} \sum_l \begin{array}{c} JM \\ \downarrow \\ \downarrow \end{array} \langle il | \hat{v} | jk \rangle \begin{array}{c} 00 \\ \downarrow \end{array} \langle \bar{a} | \hat{t}_1 | l \rangle \\
 \begin{array}{c} JM \\ \downarrow \\ \downarrow \end{array} \langle ia | \hat{\chi}'' | jk \rangle &= \begin{array}{c} JM \\ \downarrow \\ \downarrow \end{array} \langle ia | \hat{v} | jk \rangle + \hat{J}_a^{-1} \sum_l \begin{array}{c} JM \\ \downarrow \\ \downarrow \end{array} \langle il | \hat{v} | jk \rangle \begin{array}{c} 00 \\ \downarrow \end{array} \langle \bar{a} | \hat{t}_1 | l \rangle \\
 &+ \hat{P}_{ij}(J) \hat{J}_k^{-1} \sum_c (-1)^{j_a+j_i-J} \begin{array}{c} JM \\ \downarrow \\ \downarrow \end{array} \langle ai | \hat{\chi}''' | jc \rangle \begin{array}{c} JM \\ \downarrow \\ \downarrow \end{array} \langle \bar{c} | \hat{t}_1 | k \rangle \\
 &- \text{CCAtoStd}^{(A)} \left[\begin{array}{c} ia \\ jk \end{array} J; J' \right]_{|\hat{t}_{ia}=0} \sum_{cl} (-1)^{j_c+j_l-J'} \begin{array}{c} J'M' \\ \downarrow \end{array} \langle \bar{c} \bar{a} | \hat{t}_2 | lk \rangle \begin{array}{c} J'M' \\ \downarrow \end{array} \langle \bar{l} \bar{i} | \hat{\mathcal{H}}_2 | jc \rangle \\
 &- \frac{1}{2} \sum_{cd} (-1)^{j_a+j_i-J} \begin{array}{c} JM \\ \downarrow \\ \downarrow \end{array} \langle ai | \hat{\mathcal{H}}_2 | cd \rangle \begin{array}{c} JM \\ \downarrow \\ \downarrow \end{array} \langle cd | \hat{t}_2 | jk \rangle \\
 \begin{array}{c} JM \\ \downarrow \\ \downarrow \end{array} \langle ab | \hat{\chi}' | ci \rangle &= \begin{array}{c} JM \\ \downarrow \\ \downarrow \end{array} \langle ab | \hat{v} | ci \rangle - \frac{1}{2} \hat{J}_i^{-1} \sum_d \begin{array}{c} JM \\ \downarrow \\ \downarrow \end{array} \langle ab | \hat{v} | cd \rangle \begin{array}{c} 00 \\ \downarrow \end{array} \langle \bar{d} | \hat{t}_1 | i \rangle \\
 &- \hat{P}_{ab}(J) \hat{J}_b^{-1} (-1)^{j_i+j_c-J} \sum_k \begin{array}{c} JM \\ \downarrow \\ \downarrow \end{array} \langle ak | \hat{\chi}'' | ic \rangle \begin{array}{c} JM \\ \downarrow \\ \downarrow \end{array} \langle \bar{b} | \hat{t}_1 | k \rangle
 \end{aligned}$$

Figure D.4: Spherical expressions for the intermediates used in the calculations of the effective Hamiltonian matrix elements.

D.2 Diagrams for Three-Body Hamiltonians

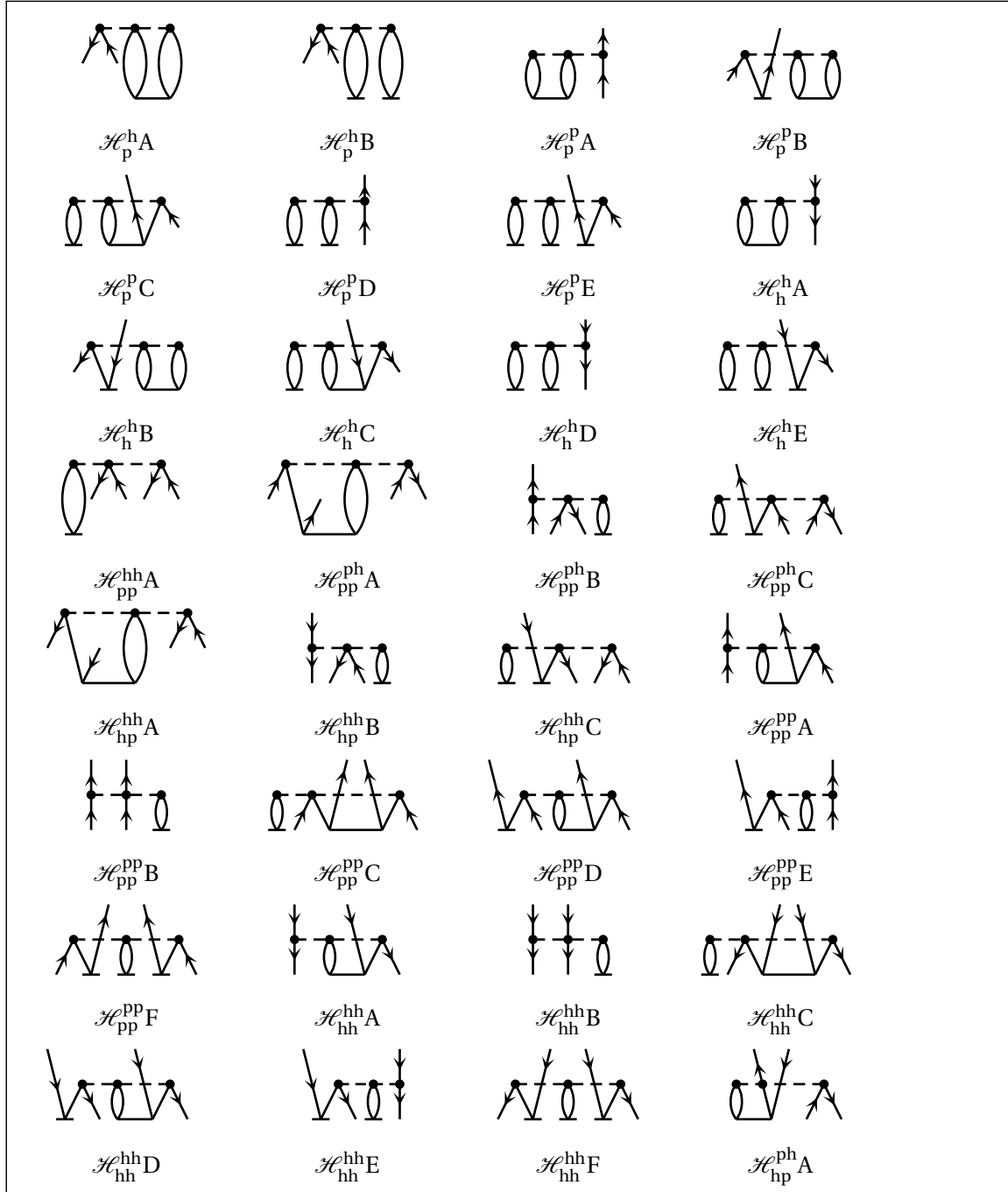


Figure D.5: Effective Hamiltonian diagrams for three-body Hamiltonians.

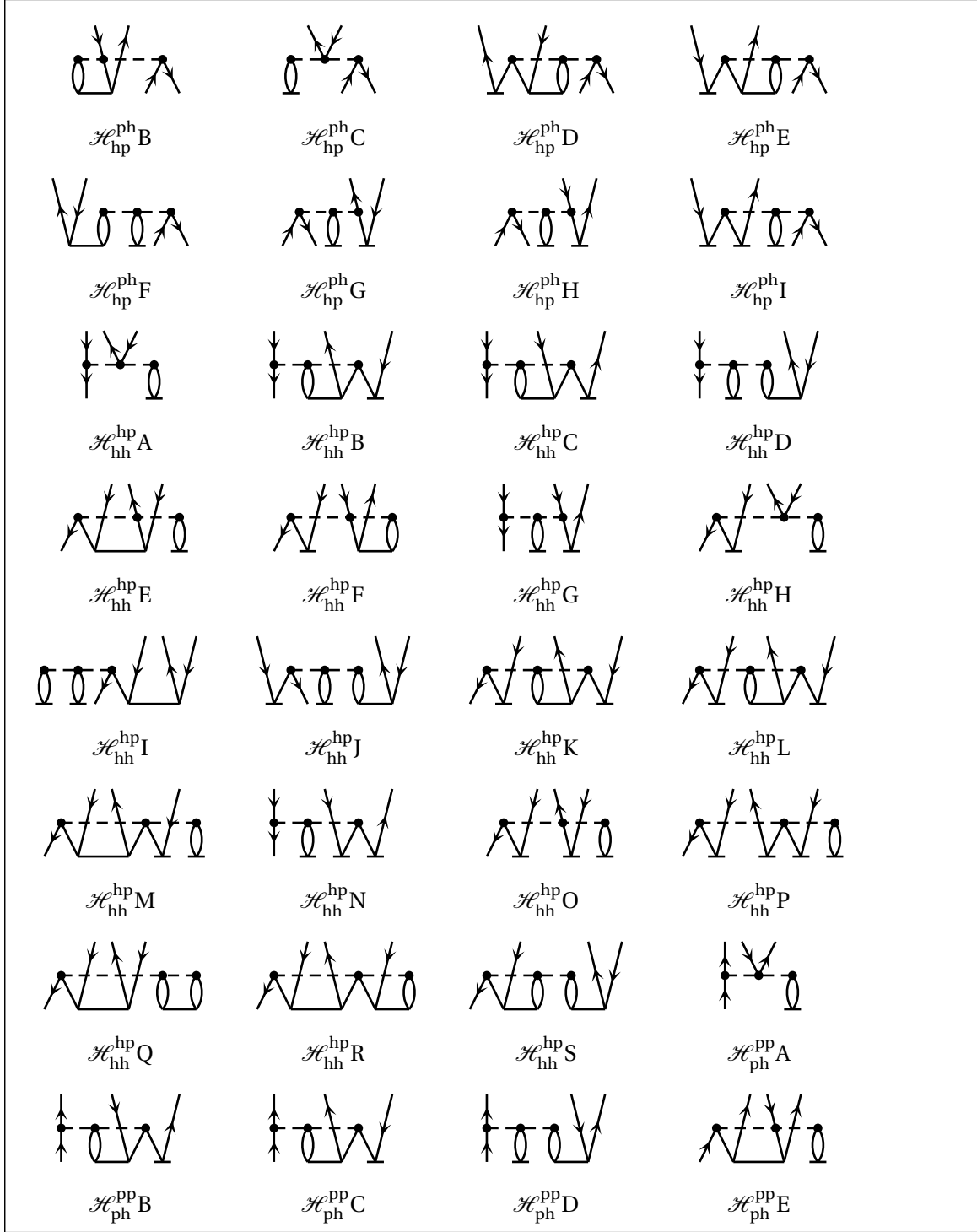


Figure D.6: Effective Hamiltonian diagrams for three-body Hamiltonians, continued.

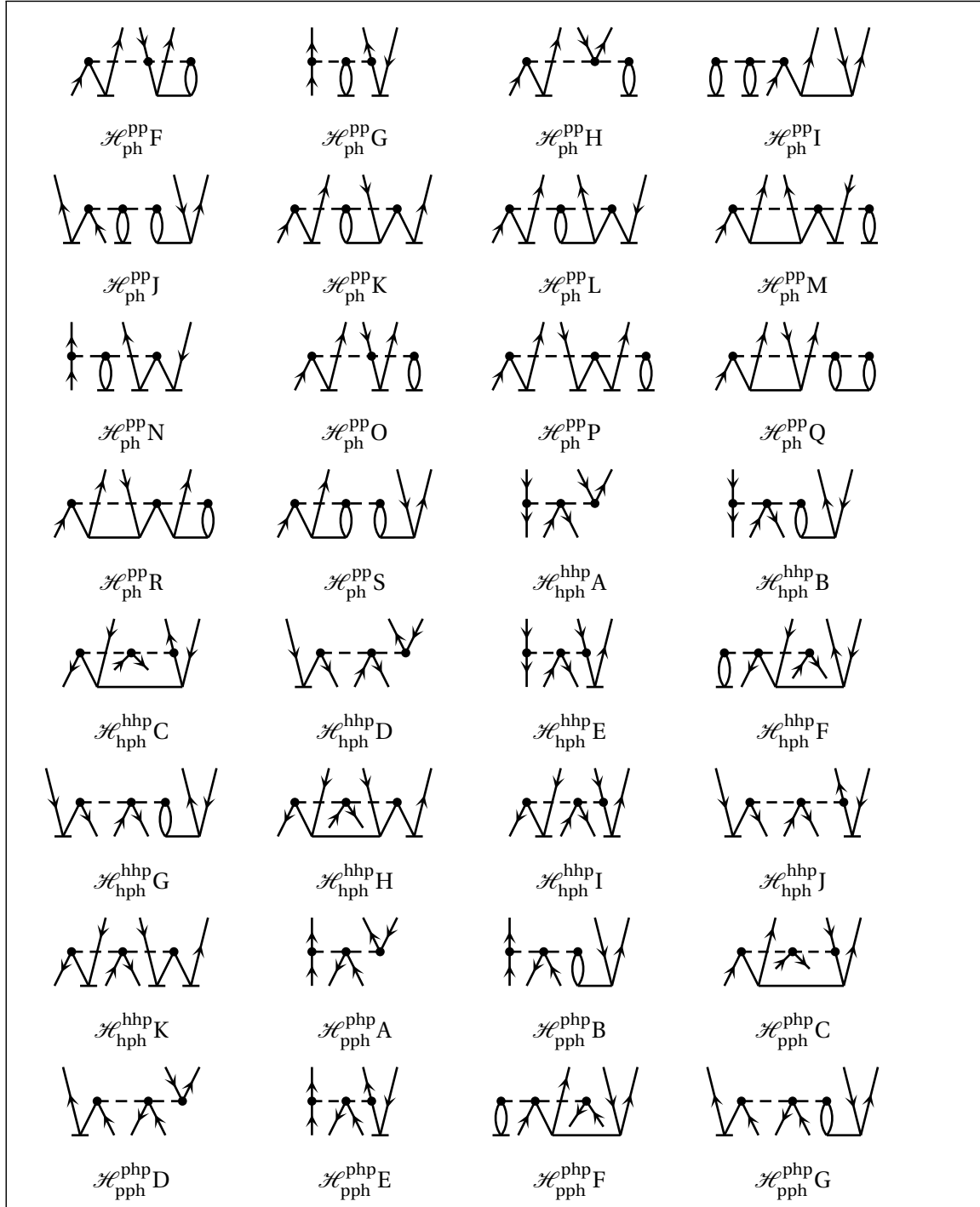


Figure D.7: Effective Hamiltonian diagrams for three-body Hamiltonians, continued.

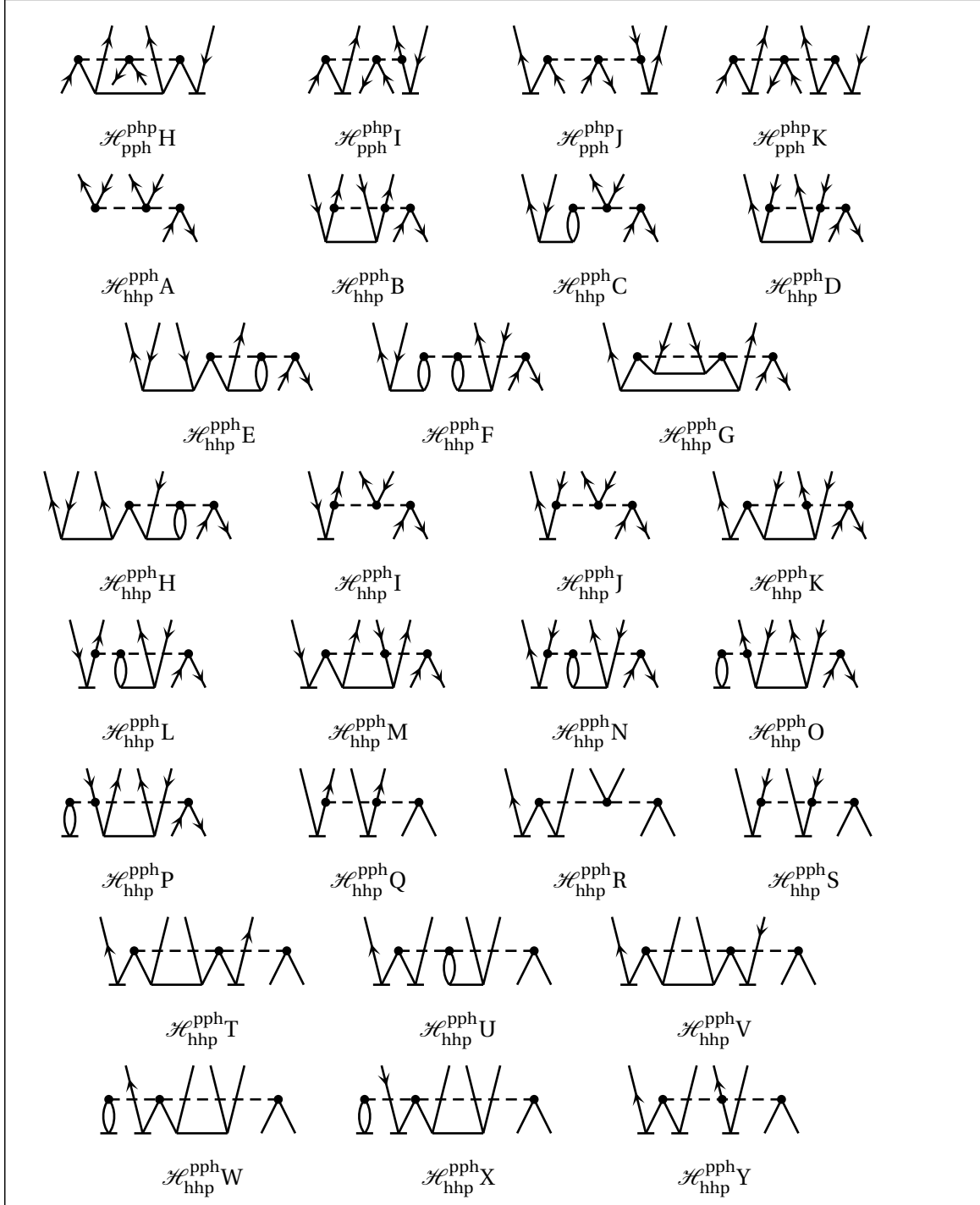


Figure D.8: Effective Hamiltonian diagrams for three-body Hamiltonians, continued.

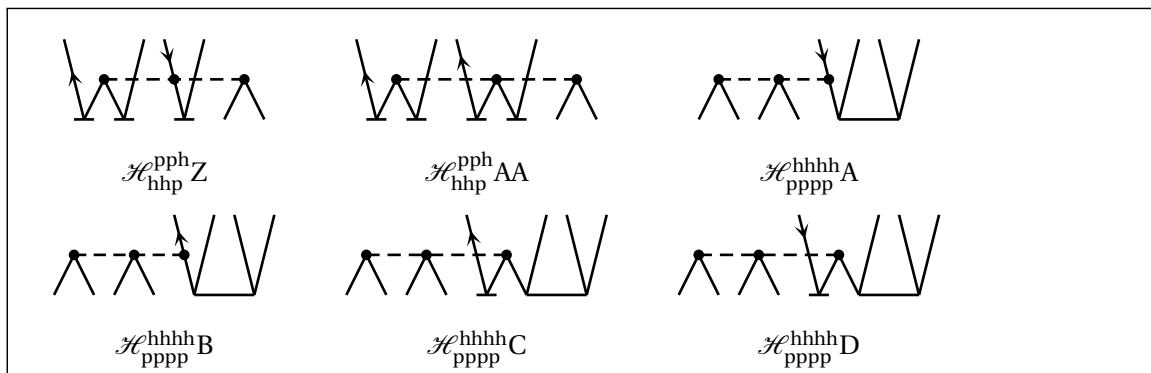


Figure D.9: Effective Hamiltonian diagrams for three-body Hamiltonians, continued.

D.3 Spherical Equations for Three-Body Hamiltonians

$$\begin{aligned}
 \overbrace{\langle \tilde{l} | \mathcal{H} | a \rangle}^{00} &= \overset{(\mathcal{H}_P^{\text{PA}})}{+} \frac{1}{4} \sum_{cdkl} \sum_J \hat{J} \underbrace{\langle kl \tilde{l} | \hat{w} | cda \rangle}_0 \langle cd | \hat{t}_2 | kl \rangle \\
 &\quad \overset{(\mathcal{H}_P^{\text{PB}})}{+} \frac{1}{2} \sum_{cdkl} \hat{J}_c^{-1} \hat{J}_d^{-1} \sum_J \hat{J} \underbrace{\langle kl \tilde{l} | \hat{w} | cda \rangle}_0 \overbrace{\langle \tilde{c} | \hat{t}_1 | k \rangle}^{00} \overbrace{\langle \tilde{d} | \hat{t}_1 | l \rangle}^{00} \\
 \overbrace{\langle \tilde{a} | \mathcal{H} | b \rangle}^{00} &= \overset{(\mathcal{H}_P^{\text{PA}})}{+} \frac{1}{4} \sum_{cdkl} \sum_J \hat{J} \underbrace{\langle kl \tilde{a} | \hat{w} | cdb \rangle}_0 \langle cd | \hat{t}_2 | kl \rangle \\
 &\quad \overset{(\mathcal{H}_P^{\text{PB}})}{+} \frac{1}{4} \hat{J}_a^{-1} \sum_{cdklm} \sum_J \hat{J} \underbrace{\langle kl \tilde{m} | \hat{w} | cdb \rangle}_0 \langle cd | \hat{t}_2 | kl \rangle \overbrace{\langle \tilde{a} | \hat{t}_1 | m \rangle}^{00} \\
 &\quad \overset{(\mathcal{H}_P^{\text{PC}})}{+} \frac{1}{2} \hat{J}_a^{-1} \sum_{cdklm} \sum_J \hat{J} \underbrace{\langle kl \tilde{m} | \hat{w} | bcd \rangle}_0 \langle ac | \hat{t}_2 | kl \rangle \overbrace{\langle \tilde{d} | \hat{t}_1 | m \rangle}^{00} \\
 &\quad \overset{(\mathcal{H}_P^{\text{PD}})}{+} \frac{1}{2} \sum_{cdkl} \hat{J}_c^{-1} \hat{J}_d^{-1} \sum_J \hat{J} \underbrace{\langle kl \tilde{a} | \hat{w} | cdb \rangle}_0 \overbrace{\langle \tilde{c} | \hat{t}_1 | k \rangle}^{00} \overbrace{\langle \tilde{d} | \hat{t}_1 | l \rangle}^{00} \\
 &\quad \overset{(\mathcal{H}_P^{\text{PE}})}{+} \frac{1}{2} \hat{J}_a^{-1} \sum_{cdklm} \hat{J}_c^{-1} \hat{J}_d^{-1} \sum_J \hat{J} \underbrace{\langle kl \tilde{m} | \hat{w} | cdb \rangle}_0 \overbrace{\langle \tilde{c} | \hat{t}_1 | k \rangle}^{00} \overbrace{\langle \tilde{d} | \hat{t}_1 | l \rangle}^{00} \overbrace{\langle \tilde{a} | \hat{t}_1 | m \rangle}^{00}
 \end{aligned}$$

Figure D.10: Spherical expressions for the effective Hamiltonian for three-body Hamiltonians.

$$\begin{aligned}
 \overbrace{\langle i|\hat{\mathcal{H}}|j\rangle}^{00} &= \left(\mathcal{H}_h^{\text{hA}}\right) + \frac{1}{4} \sum_{cdkl} \sum_J \hat{f} \underbrace{\langle kl\tilde{i}|\hat{w}||cdj\rangle}_0 \langle cd|\hat{t}_2|kl\rangle \begin{matrix} J & J & JM & JM \\ \downarrow & \downarrow & \downarrow & \downarrow \end{matrix} \\
 \left(\mathcal{H}_h^{\text{hB}}\right) - \frac{1}{4} \hat{f}_i^{-1} \sum_{cdek l} \sum_J \hat{f} \underbrace{\langle kl\tilde{i}|\hat{w}||cde\rangle}_0 \langle cd|\hat{t}_2|kl\rangle \langle \tilde{e}|\hat{t}_1|j\rangle \begin{matrix} J & J & JM & JM & 00 \\ \downarrow & \downarrow & \downarrow & \downarrow & \downarrow \end{matrix} \\
 \left(\mathcal{H}_h^{\text{hC}}\right) - \frac{1}{2} \hat{f}_i^{-1} \sum_{cdek l} \sum_J \hat{f} \underbrace{\langle ki\tilde{l}|\hat{w}||cde\rangle}_0 \langle cd|\hat{t}_2|kj\rangle \langle \tilde{e}|\hat{t}_1|l\rangle \begin{matrix} J & J & JM & JM & 00 \\ \downarrow & \downarrow & \downarrow & \downarrow & \downarrow \end{matrix} \\
 \left(\mathcal{H}_h^{\text{hD}}\right) + \frac{1}{2} \sum_{cdkl} \hat{f}_c^{-1} \hat{f}_d^{-1} \sum_J \hat{f} \underbrace{\langle kl\tilde{i}|\hat{w}||cdj\rangle}_0 \langle \tilde{c}|\hat{t}_1|k\rangle \langle \tilde{d}|\hat{t}_1|l\rangle \begin{matrix} J & J & 00 & 00 \\ \downarrow & \downarrow & \downarrow & \downarrow \end{matrix} \\
 \left(\mathcal{H}_h^{\text{hE}}\right) - \frac{1}{2} \hat{f}_i^{-1} \sum_{cdek l} \hat{f}_c^{-1} \hat{f}_d^{-1} \sum_J \hat{f} \underbrace{\langle kl\tilde{i}|\hat{w}||cde\rangle}_0 \langle \tilde{c}|\hat{t}_1|k\rangle \langle \tilde{d}|\hat{t}_1|l\rangle \langle \tilde{e}|\hat{t}_1|j\rangle \begin{matrix} J & J & 00 & 00 & 00 \\ \downarrow & \downarrow & \downarrow & \downarrow & \downarrow \end{matrix} \\
 \overbrace{\langle ij|\hat{\mathcal{H}}|ab\rangle}^{JM} = \left(\mathcal{H}_{\text{pp}}^{\text{hA}}\right) + \hat{f}^{-1} \sum_{ck} \underbrace{\langle ij\tilde{k}|\hat{w}||abc\rangle}_0 \langle \tilde{c}|\hat{t}_1|k\rangle \begin{matrix} JM & JM \\ \downarrow & \downarrow \end{matrix} \\
 \overbrace{\langle ai|\hat{\mathcal{H}}|bc\rangle}^{JM} = \left(\mathcal{H}_{\text{pp}}^{\text{phA}}\right) + \frac{1}{2} \sum_{dkl} \sum_{J'J''} (-1)^{J+J'+J''} \hat{f}^{-1} \hat{f}' \hat{f}'' \left\{ \begin{matrix} J & J' & J'' \\ j_d & j_i & j_a \end{matrix} \right\}_{6j} \\
 \times \underbrace{\langle kl\tilde{i}|\hat{w}||bcd\rangle}_{J''} \underbrace{\langle da|\hat{t}_2|kl\rangle}_{J'} \left(\mathcal{H}_{\text{pp}}^{\text{phB}}\right) + \hat{f}^{-1} \sum_{dl} \underbrace{\langle ai\tilde{l}|\hat{w}||bcd\rangle}_0 \langle \tilde{d}|\hat{t}_1|l\rangle \begin{matrix} J & J & 00 \\ \downarrow & \downarrow & \downarrow \end{matrix} \\
 \left(\mathcal{H}_{\text{pp}}^{\text{phC}}\right) + \hat{f}_a^{-1} \hat{f}^{-1} \sum_{dkl} \underbrace{\langle ki\tilde{l}|\hat{w}||bcd\rangle}_0 \langle \tilde{a}|\hat{t}_1|k\rangle \langle \tilde{d}|\hat{t}_1|l\rangle \begin{matrix} J & J & 00 & 00 \\ \downarrow & \downarrow & \downarrow & \downarrow \end{matrix}
 \end{aligned}$$

Figure D.11: Spherical expressions for the effective Hamiltonian for three-body Hamiltonians, continued.

$$\begin{aligned}
 \begin{array}{c} JM \\ \downarrow \\ \langle ik | \mathcal{H} | ja \rangle \end{array} &= \begin{array}{c} JM \\ \downarrow \\ + \end{array} \begin{array}{c} JM \\ \downarrow \\ \end{array} \begin{array}{c} (\mathcal{H}_{hp}^{hhA}) \\ + \end{array} \frac{1}{2} (-1)^{j_a+j_j-J} \sum_{cdl} \sum_{J'J''} (-1)^{J+J'+J''} \hat{f}^{-1} \hat{f}' \hat{f}'' \\
 &\times \left\{ \begin{array}{c} J \quad J' \quad J'' \\ j_l \quad j_a \quad j_j \end{array} \right\}_{6j} \begin{array}{c} \begin{array}{c} \downarrow \quad \downarrow \\ J \quad J' \end{array} \\ \langle ik \tilde{l} | \hat{w} | cda \rangle \end{array} \begin{array}{c} \begin{array}{c} \downarrow \quad \downarrow \\ J' M' \quad J' M' \end{array} \\ \langle cd | \hat{t}_2 | jl \rangle \end{array} \begin{array}{c} (\mathcal{H}_{hp}^{hhB}) \\ + \end{array} \hat{f}^{-1} \sum_{cl} \begin{array}{c} \begin{array}{c} \downarrow \quad \downarrow \\ J \quad J \end{array} \\ \langle ik \tilde{l} | \hat{w} | jac \rangle \end{array} \begin{array}{c} \begin{array}{c} \downarrow \\ 0 \end{array} \\ \langle \tilde{c} | \hat{t}_1 | l \rangle \end{array} \\
 &\begin{array}{c} (\mathcal{H}_{hp}^{hhC}) \\ - \end{array} \hat{f}_j^{-1} \hat{f}^{-1} \sum_{cdl} \begin{array}{c} \begin{array}{c} \downarrow \quad \downarrow \\ J \quad J \end{array} \\ \langle ik \tilde{l} | \hat{w} | cad \rangle \end{array} \begin{array}{c} \begin{array}{c} \downarrow \quad \downarrow \\ 0 \quad 0 \end{array} \\ \langle \tilde{d} | \hat{t}_1 | l \rangle \end{array} \begin{array}{c} \begin{array}{c} \downarrow \quad \downarrow \\ 0 \quad 0 \end{array} \\ \langle \tilde{c} | \hat{t}_1 | j \rangle \end{array} \\
 \begin{array}{c} JM \\ \downarrow \\ \langle ab | \mathcal{H} | cd \rangle \end{array} &= \begin{array}{c} JM \\ \downarrow \\ - \end{array} \begin{array}{c} JM \\ \downarrow \\ \end{array} \begin{array}{c} (\mathcal{H}_{pp}^{ppA}) \\ - \end{array} \frac{1}{2} \hat{P}_{ab}(J) (-1)^{j_a+j_b-J} \sum_{ekl} \sum_{J'J''} (-1)^{J+J'+J''} \hat{f}^{-1} \hat{f}' \hat{f}'' \\
 &\times \left\{ \begin{array}{c} J \quad J' \quad J'' \\ j_e \quad j_a \quad j_b \end{array} \right\}_{6j} \begin{array}{c} \begin{array}{c} \downarrow \quad \downarrow \\ J' \quad J \end{array} \\ \langle kl \tilde{a} | \hat{w} | cde \rangle \end{array} \begin{array}{c} \begin{array}{c} \downarrow \quad \downarrow \\ J' M' \quad J' M' \end{array} \\ \langle eb | \hat{t}_2 | kl \rangle \end{array} \begin{array}{c} (\mathcal{H}_{pp}^{ppB}) \\ + \end{array} \hat{f}^{-1} \sum_{ek} \begin{array}{c} \begin{array}{c} \downarrow \quad \downarrow \\ J \quad J \end{array} \\ \langle ab \tilde{k} | \hat{w} | cde \rangle \end{array} \begin{array}{c} \begin{array}{c} \downarrow \\ 0 \end{array} \\ \langle \tilde{e} | \hat{t}_1 | k \rangle \end{array} \\
 &\begin{array}{c} (\mathcal{H}_{pp}^{ppC}) \\ + \end{array} \frac{1}{2} \hat{f}^{-1} \sum_{eklm} \begin{array}{c} \begin{array}{c} \downarrow \quad \downarrow \\ J \quad J \end{array} \\ \langle kl \tilde{m} | \hat{w} | cde \rangle \end{array} \begin{array}{c} \begin{array}{c} \downarrow \quad \downarrow \\ JM \quad JM \end{array} \\ \langle ab | \hat{t}_2 | kl \rangle \end{array} \begin{array}{c} \begin{array}{c} \downarrow \\ 0 \end{array} \\ \langle \tilde{e} | \hat{t}_1 | m \rangle \end{array} \\
 &\begin{array}{c} (\mathcal{H}_{pp}^{ppD}) \\ - \end{array} \frac{1}{2} \hat{P}_{ab}(J) \hat{f}_a^{-1} \sum_{eklm} \sum_{J'J''} (-1)^{j_e+j_m-J''} \hat{f}^{-1} \hat{f}' \hat{f}'' \left\{ \begin{array}{c} J \quad J' \quad J'' \\ j_e \quad j_m \quad j_b \end{array} \right\}_{6j} \\
 &\times \begin{array}{c} \begin{array}{c} \downarrow \quad \downarrow \\ J' \quad J \end{array} \\ \langle kl \tilde{m} | \hat{w} | cde \rangle \end{array} \begin{array}{c} \begin{array}{c} \downarrow \quad \downarrow \\ J' M' \quad J' M' \end{array} \\ \langle be | \hat{t}_2 | kl \rangle \end{array} \begin{array}{c} \begin{array}{c} \downarrow \\ 0 \end{array} \\ \langle \tilde{a} | \hat{t}_1 | m \rangle \end{array} \\
 &\begin{array}{c} (\mathcal{H}_{pp}^{ppE}) \\ - \end{array} \hat{f}_b^{-1} \hat{f}^{-1} \sum_{ekl} \begin{array}{c} \begin{array}{c} \downarrow \quad \downarrow \\ J \quad J \end{array} \\ \langle ak \tilde{l} | \hat{w} | cde \rangle \end{array} \begin{array}{c} \begin{array}{c} \downarrow \quad \downarrow \\ 0 \quad 0 \end{array} \\ \langle \tilde{b} | \hat{t}_1 | k \rangle \end{array} \begin{array}{c} \begin{array}{c} \downarrow \\ 0 \end{array} \\ \langle \tilde{e} | \hat{t}_1 | l \rangle \end{array} \\
 &\begin{array}{c} (\mathcal{H}_{pp}^{ppF}) \\ + \end{array} \frac{1}{2} \hat{P}_{ab}(J) \hat{f}_a^{-1} \hat{f}_b^{-1} \hat{f}^{-1} \sum_{eklm} \begin{array}{c} \begin{array}{c} \downarrow \quad \downarrow \\ J \quad J \end{array} \\ \langle kl \tilde{m} | \hat{w} | cde \rangle \end{array} \begin{array}{c} \begin{array}{c} \downarrow \quad \downarrow \\ 0 \quad 0 \end{array} \\ \langle \tilde{a} | \hat{t}_1 | k \rangle \end{array} \begin{array}{c} \begin{array}{c} \downarrow \quad \downarrow \\ 0 \quad 0 \end{array} \\ \langle \tilde{b} | \hat{t}_1 | l \rangle \end{array} \begin{array}{c} \begin{array}{c} \downarrow \\ 0 \end{array} \\ \langle \tilde{e} | \hat{t}_1 | m \rangle \end{array}
 \end{aligned}$$

Figure D.12: Spherical expressions for the effective Hamiltonian for three-body Hamiltonians, continued.

$$\begin{aligned}
 \begin{array}{c} JM \\ \downarrow \\ \langle ij|\hat{\mathcal{H}}|kl \rangle \end{array} &= \begin{array}{c} JM \\ \downarrow \\ \langle ij|\hat{\mathcal{H}}|kl \rangle \end{array} = \left(\mathcal{H}_{hh}^{hhA} \right) \frac{1}{2} \hat{P}_{kl}(J) \sum_{cdm} \sum_{J'J''} (-1)^{J+J'+J''} \hat{f}^{-1} \hat{f}' \hat{f}'' \\
 &\times \left\{ \begin{array}{c} J \\ j_m \end{array} \begin{array}{c} J' \\ j_k \end{array} \begin{array}{c} J'' \\ j_l \end{array} \right\}_{6j} \begin{array}{c} J \\ \downarrow \\ \langle ij\tilde{m}||\hat{w}||cdk \rangle \end{array} \begin{array}{c} J' \\ \downarrow \\ \langle cd|\hat{t}_2|lm \rangle \end{array} \begin{array}{c} J'M' \\ \downarrow \\ \langle cd|\hat{t}_2|lm \rangle \end{array} \begin{array}{c} J'M' \\ \downarrow \\ \langle cd|\hat{t}_2|lm \rangle \end{array} \left(\mathcal{H}_{hh}^{hhB} \right) \hat{f}^{-1} \sum_{cm} \begin{array}{c} J \\ \downarrow \\ \langle ij\tilde{m}||\hat{w}||klc \rangle \end{array} \begin{array}{c} J \\ \downarrow \\ \langle \tilde{c}|\hat{t}_1|m \rangle \end{array} \\
 &\left(\mathcal{H}_{hh}^{hhC} \right) \frac{1}{2} \hat{f}^{-1} \sum_{cdem} \begin{array}{c} J \\ \downarrow \\ \langle ij\tilde{m}||\hat{w}||cde \rangle \end{array} \begin{array}{c} J \\ \downarrow \\ \langle cd|\hat{t}_2|kl \rangle \end{array} \begin{array}{c} JM \\ \downarrow \\ \langle \tilde{e}|\hat{t}_1|m \rangle \end{array} \\
 &\left(\mathcal{H}_{hh}^{hhD} \right) \frac{1}{2} \hat{P}_{kl} \hat{f}_k^{-1} \sum_{cdem} \sum_{J'J''} \hat{f}^{-1} \hat{f}' \hat{f}'' \left\{ \begin{array}{c} J \\ j_m \end{array} \begin{array}{c} J' \\ j_e \end{array} \begin{array}{c} J'' \\ j_l \end{array} \right\}_{6j} \begin{array}{c} J \\ \downarrow \\ \langle ij\tilde{m}||\hat{w}||cde \rangle \end{array} \\
 &\times \begin{array}{c} J'M' \\ \downarrow \\ \langle cd|\hat{t}_2|lm \rangle \end{array} \begin{array}{c} J'M' \\ \downarrow \\ \langle \tilde{e}|\hat{t}_1|k \rangle \end{array} \left(\mathcal{H}_{hh}^{hhE} \right) \hat{f}_l^{-1} \hat{f}^{-1} \sum_{cdm} \begin{array}{c} J \\ \downarrow \\ \langle ij\tilde{m}||\hat{w}||kcd \rangle \end{array} \begin{array}{c} J \\ \downarrow \\ \langle \tilde{c}|\hat{t}_1|l \rangle \end{array} \begin{array}{c} 00 \\ \downarrow \\ \langle \tilde{d}|\hat{t}_1|m \rangle \end{array} \\
 &\left(\mathcal{H}_{hh}^{hhF} \right) \frac{1}{2} \hat{P}_{kl}(J) \hat{f}_k^{-1} \hat{f}_l^{-1} \hat{f}^{-1} \sum_{cdem} \begin{array}{c} J \\ \downarrow \\ \langle ij\tilde{m}||\hat{w}||cde \rangle \end{array} \begin{array}{c} J \\ \downarrow \\ \langle \tilde{c}|\hat{t}_1|k \rangle \end{array} \begin{array}{c} 00 \\ \downarrow \\ \langle \tilde{d}|\hat{t}_1|l \rangle \end{array} \begin{array}{c} 00 \\ \downarrow \\ \langle \tilde{e}|\hat{t}_1|m \rangle \end{array} \\
 \begin{array}{c} JM \\ \downarrow \\ \langle aj|\hat{\mathcal{H}}|ib \rangle \end{array} &= \left(\mathcal{H}_{hp}^{phA} \right) \frac{1}{2} (-1)^{j_b+j_i-J} \sum_{cdk} \sum_{J'J''} (-1)^{J+J'+J''} \hat{f}^{-1} \hat{f}' \hat{f}'' \\
 &\times \left\{ \begin{array}{c} J \\ j_k \end{array} \begin{array}{c} J' \\ j_b \end{array} \begin{array}{c} J'' \\ j_i \end{array} \right\}_{6j} \begin{array}{c} J \\ \downarrow \\ \langle aj\tilde{k}||\hat{w}||cdb \rangle \end{array} \begin{array}{c} J' \\ \downarrow \\ \langle cd|\hat{t}_2|ik \rangle \end{array} \\
 &\left(\mathcal{H}_{hp}^{phB} \right) \frac{1}{2} \sum_{ckl} \sum_{J'J''} (-1)^{J+J'+J''} \hat{f}^{-1} \hat{f}' \hat{f}'' \left\{ \begin{array}{c} J \\ j_c \end{array} \begin{array}{c} J' \\ j_j \end{array} \begin{array}{c} J'' \\ j_a \end{array} \right\}_{6j} \begin{array}{c} J' \\ \downarrow \\ \langle kl\tilde{j}||\hat{w}||ibc \rangle \end{array} \begin{array}{c} J \\ \downarrow \\ \langle ca|\hat{t}_2|kl \rangle \end{array} \\
 &\left(\mathcal{H}_{hp}^{phC} \right) \hat{f}^{-1} \sum_{ck} \begin{array}{c} J \\ \downarrow \\ \langle aj\tilde{k}||\hat{w}||ibc \rangle \end{array} \begin{array}{c} J \\ \downarrow \\ \langle \tilde{c}|\hat{t}_1|k \rangle \end{array} + \dots
 \end{aligned}$$

Figure D.13: Spherical expressions for the effective Hamiltonian for three-body Hamiltonians, continued.

$$\begin{aligned}
 & \left(\mathcal{H}_{\text{hp}}^{\text{phD}} \right)_{+} \text{CCAtoStd} \left[\begin{smallmatrix} ai \\ jb \end{smallmatrix} J; J' \right] \frac{1}{2} \hat{J}_a^{-1} \sum_{cdkl} \sum_{J'' J'''} (\hat{J}')^{-1} \hat{J}'' \hat{J}''' \left\{ \begin{smallmatrix} J' & J'' & J''' \\ j_k & j_l & j_i \end{smallmatrix} \right\}_{6j} \\
 & \times \underbrace{\langle kl \tilde{j} || \tilde{w} || cdb \rangle}_{J'} \langle cd | \hat{t}_2 | ik \rangle \langle \tilde{a} | \hat{t}_1 | l \rangle \\
 & \left(\mathcal{H}_{\text{hp}}^{\text{phE}} \right)_{+} \text{CCAtoStd} \left[\begin{smallmatrix} ai \\ jb \end{smallmatrix} J; J' \right] \frac{1}{2} \hat{J}_i^{-1} \sum_{cdkl} \sum_{J'' J'''} (\hat{J}')^{-1} \hat{J}'' \hat{J}''' \left\{ \begin{smallmatrix} J' & J'' & J''' \\ j_d & j_c & j_a \end{smallmatrix} \right\}_{6j} \\
 & \times \underbrace{\langle kl \tilde{j} || \tilde{w} || cdb \rangle}_{J'} \langle da | \hat{t}_2 | kl \rangle \langle \tilde{c} | \hat{t}_1 | i \rangle \\
 & \left(\mathcal{H}_{\text{hp}}^{\text{phF}} \right)_{-} \text{CCAtoStd} \left[\begin{smallmatrix} ai \\ jb \end{smallmatrix} J; J' \right] \frac{1}{2} \sum_{cdkl} \hat{J}_l^{-1} \sum_{J'' J'''} (-1)^{J'+J''+J'''} (\hat{J}')^{-1} \hat{J}'' \hat{J}''' \\
 & \times \left\{ \begin{smallmatrix} J' & J'' & J''' \\ j_d & j_c & j_k \end{smallmatrix} \right\}_{6j} \underbrace{\langle kl \tilde{j} || \tilde{w} || dcb \rangle}_{J'} \langle \tilde{a} \tilde{c} | \hat{t}_2 | ik \rangle \langle \tilde{d} | \hat{t}_1 | l \rangle \\
 & \left(\mathcal{H}_{\text{hp}}^{\text{phG}} \right)_{-} \hat{J}_i^{-1} \hat{J}^{-1} \sum_{cdk} \underbrace{\langle aj \tilde{k} || \tilde{w} || cbd \rangle}_0 \langle \tilde{c} | \hat{t}_1 | i \rangle \langle \tilde{d} | \hat{t}_1 | k \rangle \\
 & \left(\mathcal{H}_{\text{hp}}^{\text{phH}} \right)_{-} \hat{J}_a^{-1} \hat{J}^{-1} \sum_{ckl} \underbrace{\langle kj \tilde{l} || \tilde{w} || ibc \rangle}_0 \langle \tilde{a} | \hat{t}_1 | k \rangle \langle \tilde{c} | \hat{t}_1 | l \rangle \\
 & \left(\mathcal{H}_{\text{hp}}^{\text{phI}} \right)_{+} \text{CCAtoStd} \left[\begin{smallmatrix} ai \\ jb \end{smallmatrix} J; J' \right] \hat{J}_a^{-1} \hat{J}_i^{-1} \sum_{cdkl} \hat{J}_k^{-1} \sum_{J'' J'''} (\hat{J}')^{-1} \hat{J}'' \hat{J}''' \\
 & \times \left\{ \begin{smallmatrix} J' & J'' & J''' \\ j_d & j_c & j_l \end{smallmatrix} \right\}_{6j} \underbrace{\langle kl \tilde{j} || \tilde{w} || cdb \rangle}_{J'} \langle \tilde{d} | \hat{t}_1 | k \rangle \langle \tilde{c} | \hat{t}_1 | i \rangle \langle \tilde{a} | \hat{t}_1 | l \rangle
 \end{aligned}$$

Figure D.14: Spherical expressions for the effective Hamiltonian for three-body Hamiltonians, continued.

$$\begin{aligned}
 \langle ab|\hat{\mathcal{H}}|ci\rangle &= \left(\mathcal{H}_{\text{ph}}^{\text{PPA}}\right) \hat{f}^{-1} \sum_{dk} \langle ab\tilde{k}|\hat{w}|cid\rangle \langle \tilde{d}|\hat{t}_1|k\rangle \\
 &\quad \left(\mathcal{H}_{\text{ph}}^{\text{PPB}}\right) \frac{1}{2} \hat{P}_{ab}(J) \hat{f}_b^{-1} \sum_{dekl} \sum_{J'J''} (-1)^{J+J'+J''} \hat{f}^{-1} \hat{f}' \hat{f}'' \left\{ \begin{matrix} J & J' & J'' \\ j_l & j_c & j_i \end{matrix} \right\}_{6j} \\
 &\quad \times \langle ak\tilde{l}|\hat{w}|dec\rangle \langle de|\hat{t}_2|il\rangle \langle \tilde{b}|\hat{t}_1|k\rangle \\
 &\quad \left(\mathcal{H}_{\text{ph}}^{\text{PPC}}\right) \frac{1}{2} \hat{P}_{ab}(J) \hat{f}_i^{-1} \sum_{dekl} \sum_{J'J''} (-1)^{J+J'+J''} \hat{f}^{-1} \hat{f}' \hat{f}'' \left\{ \begin{matrix} J & J' & J'' \\ j_e & j_a & j_b \end{matrix} \right\}_{6j} \\
 &\quad \times \langle kl\tilde{a}|\hat{w}|cde\rangle \langle eb|\hat{t}_2|kl\rangle \langle \tilde{d}|\hat{t}_1|i\rangle \\
 &\quad \left(\mathcal{H}_{\text{ph}}^{\text{PPD}}\right) \text{CCAtoStd}^{(A)} \left[\begin{matrix} ab \\ ci \end{matrix} J; J' \right] \sum_{|T_{ci}=0} \hat{f}_l^{-1} \sum_{J''J'''} (-1)^{J'+J''+J'''} \\
 &\quad \times (\hat{f}')^{-1} \hat{f}'' \hat{f}''' \left\{ \begin{matrix} J' & J'' & J''' \\ j_d & j_e & j_k \end{matrix} \right\}_{6j} \langle kl\tilde{a}|\hat{w}|dec\rangle \langle \tilde{e}\tilde{b}|\hat{t}_2|ki\rangle \langle \tilde{d}|\hat{t}_1|l\rangle \\
 &\quad \left(\mathcal{H}_{\text{ph}}^{\text{PPE}}\right) \frac{1}{2} \hat{f}^{-1} \sum_{dklm} \langle kl\tilde{m}|\hat{w}|cid\rangle \langle ab|\hat{t}_2|kl\rangle \langle \tilde{d}|\hat{t}_1|m\rangle \\
 &\quad \left(\mathcal{H}_{\text{ph}}^{\text{PPF}}\right) \frac{1}{2} \hat{P}_{ab}(J) (-1)^{j_a+j_b-J} \hat{f}_a^{-1} \sum_{dklm} \sum_{J'J''} (-1)^{J+J'+J''} \hat{f}^{-1} \hat{f}' \hat{f}'' \\
 &\quad \times \left\{ \begin{matrix} J & J' & J'' \\ j_d & j_m & j_b \end{matrix} \right\}_{6j} \langle kl\tilde{m}|\hat{w}|cid\rangle \langle db|\hat{t}_2|kl\rangle \langle \tilde{a}|\hat{t}_1|m\rangle + \dots
 \end{aligned}$$

Figure D.15: Spherical expressions for the effective Hamiltonian for three-body Hamiltonians, continued.

$$\begin{aligned}
 & \left(\mathcal{H}_{\text{phG}}^{\text{pp}} \right)_{-} \hat{f}_i^{-1} \hat{f}^{-1} \sum_{dek} \langle ab\tilde{k} || \hat{w} || cde \rangle \langle \tilde{e} | \hat{t}_1 | k \rangle \langle \tilde{d} | \hat{t}_1 | i \rangle \\
 & \left(\mathcal{H}_{\text{phH}}^{\text{pp}} \right)_{-} \hat{P}_{ab}(J) (-1)^{j_a+j_b-J} \hat{f}_a^{-1} \hat{f}^{-1} \sum_{dkl} \langle bk\tilde{l} || \hat{w} || cid \rangle \langle \tilde{a} | \hat{t}_1 | k \rangle \langle \tilde{d} | \hat{t}_1 | l \rangle \\
 & \left(\mathcal{H}_{\text{phI}}^{\text{pp}} \right)_{+} \frac{1}{2} \sum_{deklm} \hat{f}_c^{-1} \hat{f}_d^{-1} \hat{f}_e^{-1} \sum_{J'} \hat{f}' \langle kl\tilde{m} || \hat{w} || dec \rangle \langle ab | \hat{t}_2 | mi \rangle \langle \tilde{d} | \hat{t}_1 | k \rangle \langle \tilde{e} | \hat{t}_1 | l \rangle \\
 & \left(\mathcal{H}_{\text{phJ}}^{\text{pp}} \right)_{-} \text{CCAtoStd}^{(A)} \left[\begin{matrix} ab \\ ci \end{matrix} J; J' \right]_{|T_{ci}=0} \hat{f}_a^{-1} \sum_{deklm} \hat{f}_l^{-1} \sum_{J''J'''} (-1)^{J'+J''+J'''} \\
 & \times (\hat{f}')^{-1} \hat{f}'' \hat{f}''' \left\{ \begin{matrix} J' & J'' & J''' \\ j_l & j_e & j_k \end{matrix} \right\}_{6j} \langle kl\tilde{m} || \hat{w} || dec \rangle \langle \tilde{e}\tilde{b} | \hat{t}_2 | ki \rangle \langle \tilde{d} | \hat{t}_1 | l \rangle \langle \tilde{a} | \hat{t}_1 | m \rangle \\
 & \left(\mathcal{H}_{\text{phK}}^{\text{pp}} \right)_{+} \frac{1}{4} \hat{P}_{ab}(J) (-1)^{j_a+j_b-J} \hat{f}_a^{-1} \hat{f}_b^{-1} \sum_{deklm} \sum_{J'J''} (-1)^{J+J'+J''} \hat{f}^{-1} \hat{f}' \hat{f}'' \\
 & \times \left\{ \begin{matrix} J & J' & J'' \\ j_m & j_c & j_i \end{matrix} \right\}_{6j} \langle kl\tilde{m} || \hat{w} || dec \rangle \langle de | \hat{t}_2 | im \rangle \langle \tilde{a} | \hat{t}_1 | k \rangle \langle \tilde{b} | \hat{t}_1 | l \rangle \\
 & \left(\mathcal{H}_{\text{phL}}^{\text{pp}} \right)_{-} \frac{1}{2} \hat{P}_{ab}(J) \hat{f}_b^{-1} \hat{f}_i^{-1} \sum_{deklm} \sum_{J'J''} (-1)^{J+J'+J''} \hat{f}^{-1} \hat{f}' \hat{f}'' \left\{ \begin{matrix} J & J' & J'' \\ j_e & j_m & j_a \end{matrix} \right\}_{6j} \\
 & \times \langle kl\tilde{m} || \hat{w} || cde \rangle \langle ea | \hat{t}_2 | kl \rangle \langle \tilde{b} | \hat{t}_1 | m \rangle \langle \tilde{d} | \hat{t}_1 | i \rangle \\
 & \left(\mathcal{H}_{\text{phM}}^{\text{pp}} \right)_{+} \frac{1}{2} \hat{f}_i^{-1} \hat{f}^{-1} \sum_{deklm} \langle kl\tilde{m} || \hat{w} || cde \rangle \langle ab | \hat{t}_2 | kl \rangle \langle \tilde{e} | \hat{t}_1 | m \rangle \langle \tilde{d} | \hat{t}_1 | i \rangle + \dots
 \end{aligned}$$

Figure D.16: Spherical expressions for the effective Hamiltonian for three-body Hamiltonians, continued.

$$\begin{aligned}
& \left(\mathcal{H}_{\text{ph}}^{\text{ppN}} \right) \hat{P}_{ab}(J) \hat{f}_b^{-1} \hat{f}_i^{-1} \hat{f}^{-1} \sum_{dekl} \langle \overset{J}{\downarrow} a \overset{J}{\downarrow} k \tilde{l} || \hat{w} || \overset{J}{\downarrow} c \overset{J}{\downarrow} d e \rangle \langle \bar{e} | \hat{t}_1 | l \rangle \langle \bar{b} | \hat{t}_1 | k \rangle \langle \bar{d} | \hat{t}_1 | i \rangle \\
& \quad \underbrace{\hspace{10em}}_0 \\
& \left(\mathcal{H}_{\text{ph}}^{\text{ppO}} \right) \frac{1}{2} \hat{P}_{ab}(J) (-1)^{j_a+j_b-J} \hat{f}_a^{-1} \hat{f}_b^{-1} \hat{f}^{-1} \\
& \times \sum_{dklm} \langle \overset{J}{\downarrow} k l \tilde{m} || \hat{w} || \overset{J}{\downarrow} c i d \rangle \langle \bar{d} | \hat{t}_1 | m \rangle \langle \bar{b} | \hat{t}_1 | k \rangle \langle \bar{a} | \hat{t}_1 | l \rangle \\
& \quad \underbrace{\hspace{10em}}_0 \\
& \left(\mathcal{H}_{\text{ph}}^{\text{ppP}} \right) \frac{1}{2} \hat{P}_{ab}(J) (-1)^{j_a+j_b-J} \hat{f}_a^{-1} \hat{f}_b^{-1} \hat{f}_i^{-1} \hat{f}^{-1} \\
& \times \sum_{deklm} \langle \overset{J}{\downarrow} k l \tilde{m} || \hat{w} || \overset{J}{\downarrow} c d e \rangle \langle \bar{b} | \hat{t}_1 | k \rangle \langle \bar{d} | \hat{t}_1 | i \rangle \langle \bar{e} | \hat{t}_1 | m \rangle \langle \bar{a} | \hat{t}_1 | l \rangle \\
& \quad \underbrace{\hspace{10em}}_0 \\
& \left(\mathcal{H}_{\text{ph}}^{\text{ppQ}} \right) \frac{1}{4} \sum_{deklm} \hat{f}_c^{-1} \sum_{J'} \hat{f}' \langle \overset{J'}{\downarrow} k l \tilde{m} || \hat{w} || \overset{J'}{\downarrow} d e c \rangle \langle \bar{a} b | \hat{t}_2 | m i \rangle \langle \bar{d} e | \hat{t}_2 | k l \rangle \\
& \quad \underbrace{\hspace{10em}}_0 \\
& \left(\mathcal{H}_{\text{ph}}^{\text{ppR}} \right) \frac{1}{4} \sum_{deklm} \sum_{J'J''} (-1)^{J+J'+J''} \hat{f}^{-1} \hat{f}' \hat{f}'' \\
& \times \left\{ \overset{J}{\downarrow} \overset{J'}{\downarrow} \overset{J''}{\downarrow} \right\}_{\bar{e}j} \langle \bar{e} | \hat{t}_1 | j \rangle \langle \bar{a} b | \hat{t}_2 | m i \rangle \langle \bar{d} e | \hat{t}_2 | k l \rangle \\
& \quad \underbrace{\hspace{10em}}_{J''} \\
& \left(\mathcal{H}_{\text{ph}}^{\text{ppS}} \right) \text{CCAtStd}^{(A)} \left[\begin{smallmatrix} ab \\ ci \end{smallmatrix} J; J' \right] \Big|_{T_{ci}=0} \frac{1}{2} \sum_{deklm} (-1)^{j_e+j_m-J'} \sum_{J''J'''} \\
& \times (\hat{f}')^{-1} \hat{f}'' \hat{f}''' \left\{ \overset{J'}{\downarrow} \overset{J''}{\downarrow} \overset{J'''}{\downarrow} \right\}_{\bar{e}j} \langle \bar{e} | \hat{t}_1 | j \rangle \langle \bar{a} b | \hat{t}_2 | m i \rangle \langle \bar{d} e | \hat{t}_2 | k l \rangle \\
& \quad \underbrace{\hspace{10em}}_{J'} \quad \underbrace{\hspace{10em}}_{J''J'''}
\end{aligned}$$

$$\begin{aligned}
 \begin{array}{c} JM \\ \downarrow \\ \langle ia|\mathcal{H}|jk\rangle \end{array} &= \begin{array}{c} JM \\ \downarrow \\ \langle ia|\mathcal{H}|jk\rangle \end{array} = \left(\mathcal{H}_{hh}^{\text{hpA}} \right) \hat{f}^{-1} \sum_{cl} \begin{array}{c} J \quad J \\ \downarrow \quad \downarrow \\ \langle ia|\tilde{l}||\hat{w}||jk\rangle \end{array} \begin{array}{c} 00 \\ \downarrow \\ \langle \tilde{c}|\hat{t}_1|l\rangle \end{array} \\
 &\quad \left(\mathcal{H}_{hh}^{\text{hpB}} \right) \frac{1}{2} \hat{P}_{jk}(J) \hat{f}_k^{-1} \sum_{cdlm} \sum_{J'J''} (-1)^{j_i+j_d-J''} \hat{f}^{-1} \hat{f}' \hat{f}'' \left\{ \begin{array}{c} J \quad J' \quad J'' \\ j_d \quad j_i \quad j_a \end{array} \right\}_{6j} \\
 &\quad \times \begin{array}{c} J' \quad J \quad J'M' \quad J'M' \\ \downarrow \quad \downarrow \quad \downarrow \quad \downarrow \\ \langle lm|\tilde{l}||\hat{w}||jcd\rangle \end{array} \begin{array}{c} 00 \\ \downarrow \\ \langle \tilde{c}|\hat{t}_1|k\rangle \end{array} \\
 &\quad \left(\mathcal{H}_{hh}^{\text{hpC}} \right) \frac{1}{2} \hat{P}_{jk}(J) \hat{f}_a^{-1} \sum_{cdlm} \sum_{J'J''} (-1)^{J+J'+J''} \hat{f}^{-1} \hat{f}' \hat{f}'' \left\{ \begin{array}{c} J \quad J' \quad J'' \\ j_m \quad j_j \quad j_k \end{array} \right\}_{6j} \\
 &\quad \times \begin{array}{c} J \quad J' \quad J'M' \quad J'M' \\ \downarrow \quad \downarrow \quad \downarrow \quad \downarrow \\ \langle il\tilde{m}||\hat{w}||cdj\rangle \end{array} \begin{array}{c} 00 \\ \downarrow \\ \langle \tilde{a}|\hat{t}_1|l\rangle \end{array} \\
 &\quad \left(\mathcal{H}_{hh}^{\text{hpD}} \right) \text{CCAtoStd}^{(A)} \left[\begin{array}{c} ia \\ jk \end{array} ; J' \right] \sum_{cdlm} \hat{f}_l^{-1} \sum_{J''J'''} (-1)^{J'+J''+J'''} \\
 &\quad \times (\hat{f}')^{-1} \hat{f}'' \hat{f}''' \left\{ \begin{array}{c} J' \quad J'' \quad J''' \\ j_c \quad j_d \quad j_m \end{array} \right\}_{6j} \begin{array}{c} J'' \quad J''' \quad J'M' \\ \downarrow \quad \downarrow \quad \downarrow \\ \langle ml|\tilde{l}||\hat{w}||cdj\rangle \end{array} \begin{array}{c} 00 \\ \downarrow \\ \langle \tilde{c}|\hat{t}_1|l\rangle \end{array} \\
 &\quad \left(\mathcal{H}_{hh}^{\text{hpE}} \right) \frac{1}{2} \hat{f}^{-1} \sum_{cdel} \begin{array}{c} J \quad J \quad JM \quad JM \\ \downarrow \quad \downarrow \quad \downarrow \quad \downarrow \\ \langle ia|\tilde{l}||\hat{w}||cde\rangle \end{array} \begin{array}{c} 00 \\ \downarrow \\ \langle \tilde{e}|\hat{t}_1|l\rangle \end{array} \\
 &\quad \left(\mathcal{H}_{hh}^{\text{hpF}} \right) \frac{1}{2} \hat{P}_{jk}(J) \hat{f}_j^{-1} \sum_{cdel} \sum_{J'J''} (-1)^{J+J'+J''} \hat{f}^{-1} \hat{f}' \hat{f}'' \left\{ \begin{array}{c} J \quad J' \quad J'' \\ j_l \quad j_e \quad j_k \end{array} \right\}_{6j} \\
 &\quad \times \begin{array}{c} J \quad J' \quad J'M' \quad J'M' \\ \downarrow \quad \downarrow \quad \downarrow \quad \downarrow \\ \langle ia|\tilde{l}||\hat{w}||cde\rangle \end{array} \begin{array}{c} 00 \\ \downarrow \\ \langle \tilde{e}|\hat{t}_1|j\rangle \end{array}
 \end{aligned}$$

Figure D.18: Spherical expressions for the effective Hamiltonian for three-body Hamiltonians, continued.

$$\begin{aligned}
 & \left(\mathcal{H}_{\text{hh}}^{\text{hpG}} \right)_+ \hat{f}_a^{-1} \hat{f}^{-1} \sum_{clm} \langle il\tilde{m} || \hat{w} || jkc \rangle \langle \tilde{c} | \hat{t}_1 | m \rangle \langle \tilde{a} | \hat{t}_1 | l \rangle \\
 & \left(\mathcal{H}_{\text{hh}}^{\text{hpH}} \right)_+ \hat{P}_{jk}(J) \hat{f}_j^{-1} \hat{f}^{-1} \sum_{cdl} \langle ia\tilde{l} || \hat{w} || kcd \rangle \langle \tilde{c} | \hat{t}_1 | j \rangle \langle \tilde{d} | \hat{t}_1 | l \rangle \\
 & \left(\mathcal{H}_{\text{hh}}^{\text{hpI}} \right)_- \frac{1}{2} \hat{f}_i^{-1} \sum_{cdelm} \hat{f}_c^{-1} \hat{f}_d^{-1} \sum_{J'} \hat{f}' \langle lm\tilde{i} || \hat{w} || cde \rangle \langle ea | \hat{t}_2 | jk \rangle \langle \tilde{c} | \hat{t}_1 | l \rangle \langle \tilde{d} | \hat{t}_1 | m \rangle \\
 & \left(\mathcal{H}_{\text{hh}}^{\text{hpJ}} \right)_+ \text{CCAtoStd}^{(A)} \left[\begin{matrix} ia \\ jk \end{matrix} J; J' \right]_{|T_{ia}=0} \hat{f}_j^{-1} \sum_{cdelm} \hat{f}_l^{-1} \sum_{J''J'''} (-1)^{J'+J''+J'''} \\
 & \times (\hat{f}')^{-1} \hat{f}'' \hat{f}''' \left\{ \begin{matrix} J' & J'' & J''' \\ j_c & j_d & j_m \end{matrix} \right\}_{6j} \langle ml\tilde{i} || \hat{w} || cde \rangle \langle \tilde{a}\tilde{d} | \hat{t}_2 | km \rangle \langle \tilde{c} | \hat{t}_1 | l \rangle \langle \tilde{e} | \hat{t}_1 | j \rangle \\
 & \left(\mathcal{H}_{\text{hh}}^{\text{hpK}} \right)_- \frac{1}{2} \hat{P}_{jk}(J) \hat{f}_j^{-1} \hat{f}_k^{-1} \sum_{cdelm} \sum_{J'J''} (-1)^{j_i+j_e-J''} \hat{f}^{-1} \hat{f}' \hat{f}'' \\
 & \times \left\{ \begin{matrix} J & J' & J'' \\ j_e & j_i & j_a \end{matrix} \right\}_{6j} \langle ml\tilde{i} || \hat{w} || cde \rangle \langle ae | \hat{t}_2 | lm \rangle \langle \tilde{c} | \hat{t}_1 | j \rangle \langle \tilde{d} | \hat{t}_1 | k \rangle \\
 & \left(\mathcal{H}_{\text{hh}}^{\text{hpL}} \right)_- \frac{1}{2} \hat{P}_{jk}(J) \hat{f}_a^{-1} \hat{f}_k^{-1} (-1)^{j_k+j_j-J} \sum_{cdelm} \sum_{J'J''} (-1)^{J+J'+J''} \hat{f}^{-1} \hat{f}' \hat{f}'' \\
 & \times \left\{ \begin{matrix} J & J' & J'' \\ j_m & j_e & j_j \end{matrix} \right\}_{6j} \langle il\tilde{m} || \hat{w} || cde \rangle \langle cd | \hat{t}_2 | jm \rangle \langle \tilde{e} | \hat{t}_1 | k \rangle \langle \tilde{a} | \hat{t}_1 | l \rangle + \dots
 \end{aligned}$$

Figure D.19: Spherical expressions for the effective Hamiltonian for three-body Hamiltonians, continued.

$$\begin{aligned}
 & \left(\mathcal{H}_{\text{hh}}^{\text{hpM}} \right)_{-} \text{CCAtoStd}^{(A)} \left[\begin{smallmatrix} ia \\ jk \end{smallmatrix}; J; J' \right] \Big|_{T_{ia}=0} \hat{J}_j^{-1} \sum_{cdelm} \hat{J}_l^{-1} (-1)^{j_e+j_m-J'} \sum_{J''J'''} \\
 & \times (\hat{J}')^{-1} \hat{J}'' \hat{J}''' \left\{ \begin{smallmatrix} J' & J'' & J''' \\ j_a & j_c & j_i \end{smallmatrix} \right\}_{6j} \langle \overset{J''}{\downarrow} l \overset{J'''}{\downarrow} \tilde{m} || \overset{J'}{\downarrow} \hat{w} || \overset{J}{\downarrow} cde \rangle \langle \overset{J'M'}{\downarrow} \tilde{a} \tilde{e} | \overset{J}{\downarrow} \hat{t}_2 | km \rangle \langle \overset{00}{\downarrow} \tilde{d} | \hat{t}_1 | l \rangle \langle \overset{00}{\downarrow} \tilde{c} | \hat{t}_1 | j \rangle \\
 & \left(\mathcal{H}_{\text{hh}}^{\text{hpN}} \right)_{-} \hat{P}_{jk}(J) \hat{J}_a^{-1} \hat{J}_k^{-1} \hat{J}^{-1} \sum_{cdlm} \langle \overset{J}{\downarrow} i l \tilde{m} || \overset{J}{\downarrow} \hat{w} || \overset{J}{\downarrow} jcd \rangle \langle \overset{00}{\downarrow} \tilde{c} | \hat{t}_1 | k \rangle \langle \overset{00}{\downarrow} \tilde{d} | \hat{t}_1 | m \rangle \langle \overset{00}{\downarrow} \tilde{a} | \hat{t}_1 | l \rangle \\
 & \left(\mathcal{H}_{\text{hh}}^{\text{hpO}} \right)_{+} \frac{1}{2} \hat{P}_{jk}(J) \hat{J}_j^{-1} \hat{J}_k^{-1} \hat{J}^{-1} \sum_{cdel} \langle \overset{J}{\downarrow} i a \tilde{l} || \overset{J}{\downarrow} \hat{w} || \overset{J}{\downarrow} cde \rangle \langle \overset{00}{\downarrow} \tilde{c} | \hat{t}_1 | j \rangle \langle \overset{00}{\downarrow} \tilde{d} | \hat{t}_1 | k \rangle \langle \overset{00}{\downarrow} \tilde{e} | \hat{t}_1 | l \rangle \\
 & \left(\mathcal{H}_{\text{hh}}^{\text{hpP}} \right)_{-} \frac{1}{2} \hat{P}_{jk}(J) (-1)^{j_j+j_k-J} \hat{J}_a^{-1} \hat{J}^{-1} \sum_{cdelm} \hat{J}_c^{-1} \hat{J}_d^{-1} \\
 & \times \langle \overset{J}{\downarrow} i l \tilde{m} || \overset{J}{\downarrow} \hat{w} || \overset{J}{\downarrow} cde \rangle \langle \overset{00}{\downarrow} \tilde{c} | \hat{t}_1 | k \rangle \langle \overset{00}{\downarrow} \tilde{d} | \hat{t}_1 | j \rangle \langle \overset{00}{\downarrow} \tilde{e} | \hat{t}_1 | m \rangle \langle \overset{00}{\downarrow} \tilde{a} | \hat{t}_1 | l \rangle \\
 & \left(\mathcal{H}_{\text{hh}}^{\text{hpQ}} \right)_{-} \frac{1}{4} \hat{J}_i^{-1} \sum_{cdelm} \sum_{J'} \hat{J}' \langle \overset{J'}{\downarrow} l \tilde{m} \tilde{i} || \overset{J'}{\downarrow} \hat{w} || \overset{J'}{\downarrow} cde \rangle \langle \overset{JM}{\downarrow} e a | \hat{t}_2 | jk \rangle \langle \overset{J'M'}{\downarrow} cd | \hat{t}_2 | lm \rangle \\
 & \left(\mathcal{H}_{\text{hh}}^{\text{hpR}} \right)_{-} \frac{1}{4} \sum_{cdelm} \sum_{J'J''} (-1)^{j_e+j_i-J''} \hat{J}^{-1} \hat{J}' \hat{J}'' \left\{ \begin{smallmatrix} J & J' & J'' \\ j_e & j_i & j_a \end{smallmatrix} \right\}_{6j} \\
 & \times \langle \overset{J'}{\downarrow} l \tilde{m} \tilde{i} || \overset{J'}{\downarrow} \hat{w} || \overset{J'}{\downarrow} cde \rangle \langle \overset{JM}{\downarrow} cd | \hat{t}_2 | jk \rangle \langle \overset{J'M'}{\downarrow} ae | \hat{t}_2 | lm \rangle + \dots
 \end{aligned}$$

Figure D.20: Spherical expressions for the effective Hamiltonian for three-body Hamiltonians, continued.

$$\begin{aligned}
 & \left(\mathcal{H}_{\text{hh}}^{\text{hpS}} \right)_{-} \text{CCAtoStd}^{(A)} \left[\begin{matrix} ia \\ jk \end{matrix} J; J' \right] \Big|_{T_{ia}=0} \frac{1}{2} \sum_{cdelm} (-1)^{j_e+j_m-J'} \sum_{j''j'''} \\
 & \times (\hat{J}')^{-1} \hat{J}'' \hat{J}''' \left\{ \begin{matrix} J' & J'' & J''' \\ j_l & j_i & j_j \end{matrix} \right\}_{6j} \langle li\tilde{m} || \hat{w} || cde \rangle \langle cd | \hat{t}_2 | jl \rangle \langle \tilde{e}\tilde{a} | \hat{t}_2 | mk \rangle \\
 & \quad \quad \quad \underbrace{\hspace{1.5cm}}_{J'} \quad \quad \quad \underbrace{\hspace{1.5cm}}_{J'M'}
 \end{aligned}$$

Figure D.21: Spherical expressions for the effective Hamiltonian for three-body Hamiltonians, continued.

Appendix E

ACCSD Diagrams and Spherical Expressions

E.1 Diagrams

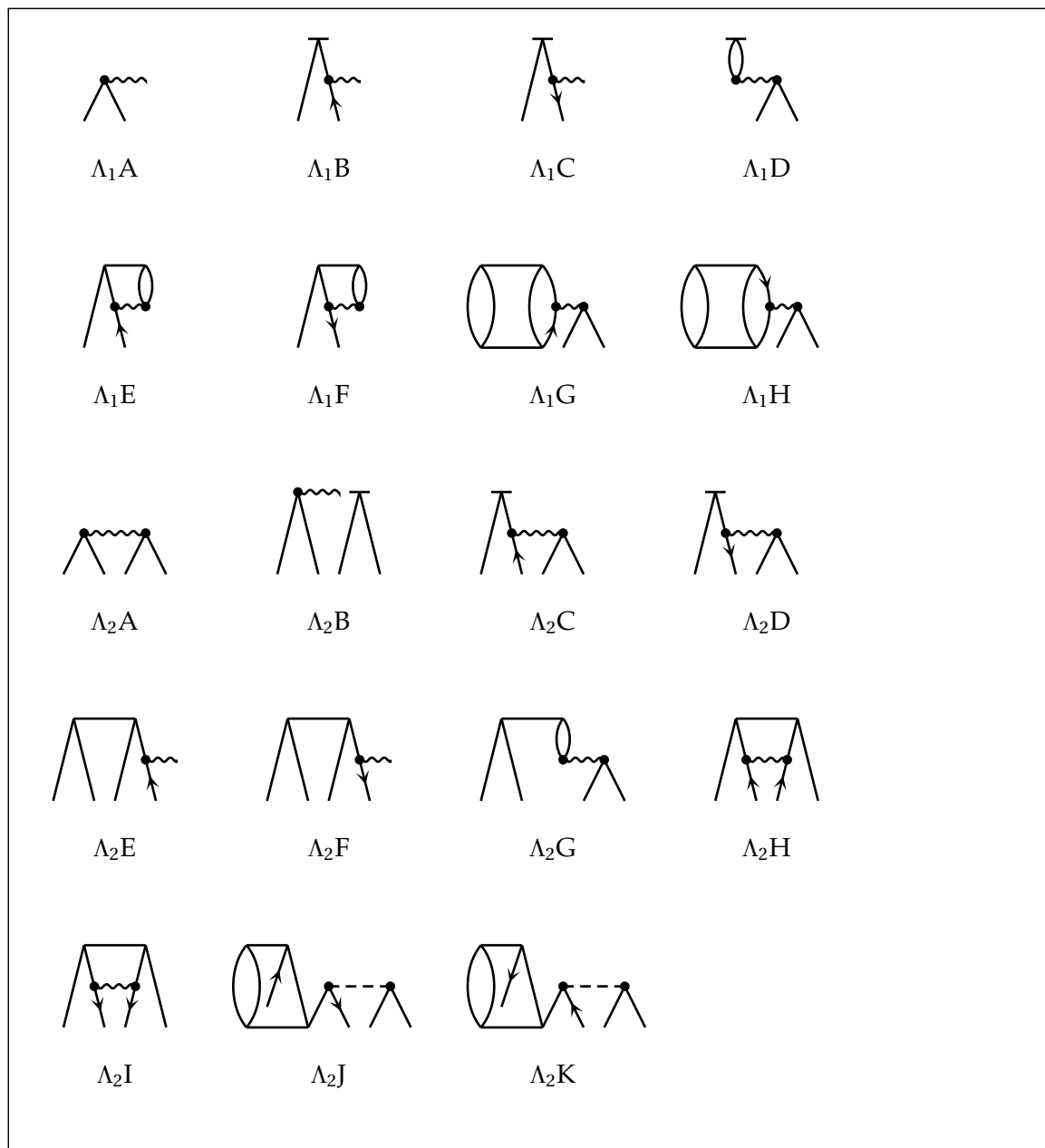


Figure E.1: ACCSD diagrams for the $\hat{\Lambda}_1$ and $\hat{\Lambda}_2$ amplitude equations.

E.2 Spherical Equations

$$\begin{aligned}
 & \stackrel{(\Lambda_1 A)}{+} \overbrace{\langle \tilde{i} | \mathcal{H}_1 | a \rangle}^{00} - \stackrel{(\Lambda_1 B)}{\hat{f}_i^{-1}} \sum_b \overbrace{\langle \tilde{i} | \hat{\lambda}_1 | b \rangle}^{00} \overbrace{\langle \tilde{b} | \mathcal{H}_1 | a \rangle}^{00} \\
 & \stackrel{(\Lambda_1 C)}{+} \hat{f}_i^{-1} \sum_k \overbrace{\langle \tilde{i} | \mathcal{H}_1 | k \rangle}^{00} \overbrace{\langle \tilde{k} | \hat{\lambda}_1 | a \rangle}^{00} \\
 & \stackrel{(\Lambda_1 D)}{+} \hat{f}_i^{-1} \sum_{ck} \hat{f}_c^{-1} \sum_J \hat{f}^2 \overbrace{\langle ci | \mathcal{H}_2 | ka \rangle}^{JM} \overbrace{\langle \tilde{k} | \hat{\lambda}_1 | c \rangle}^{00} \\
 & \stackrel{(\Lambda_1 E)}{-} \frac{1}{2} \hat{f}_i^{-1} \sum_{cdk} \sum_J \hat{f}^2 \overbrace{\langle ik | \hat{\lambda}_2 | cd \rangle}^{JM} \overbrace{\langle cd | \mathcal{H}_2 | ak \rangle}^{JM} \\
 & \stackrel{(\Lambda_1 F)}{+} \frac{1}{2} \hat{f}_i^{-1} \sum_{ckl} \sum_J \hat{f}^2 \overbrace{\langle ic | \mathcal{H}_2 | kl \rangle}^{JM} \overbrace{\langle kl | \hat{\lambda}_2 | ac \rangle}^{JM} \\
 & \stackrel{(\Lambda_1 G)}{-} \frac{1}{2} \hat{f}_i^{-1} \sum_{cdek l} \hat{f}_d^{-2} \sum_{JJ'} \hat{f}^2 (\hat{f}')^2 \overbrace{\langle di | \mathcal{H}_2 | ea \rangle}^{J'M'} \overbrace{\langle ce | \hat{t}_2 | kl \rangle}^{J'M'} \overbrace{\langle kl | \hat{\lambda}_2 | cd \rangle}^{JM} \delta_{jdje} \\
 & \stackrel{(\Lambda_1 H)}{+} \frac{1}{2} \hat{f}_i^{-1} \sum_{cdklm} \hat{f}_l^{-2} \sum_{JJ'} \hat{f}^2 (\hat{f}')^2 \overbrace{\langle kl | \hat{\lambda}_2 | cd \rangle}^{JM} \overbrace{\langle cd | \hat{t}_2 | km \rangle}^{JM} \overbrace{\langle mi | \mathcal{H}_2 | la \rangle}^{J'M'} \delta_{jmjl} \\
 & = 0, \quad \forall a, i
 \end{aligned}$$

Figure E.2: Spherical expressions for the ACCSD $\hat{\Lambda}_1$ amplitude equations.

$$\begin{aligned}
 & \stackrel{(A_2A)}{+} \overset{JM}{\downarrow} \langle ij|\hat{\mathcal{H}}_2|ab \rangle \\
 & \stackrel{(A_2B)}{+} \text{CCAtoStd}^{(A)} \left[\begin{smallmatrix} ij \\ ab \end{smallmatrix} J; J' \right] \overset{00}{\downarrow} \langle \tilde{i}|\hat{\mathcal{H}}_1|a \rangle \overset{00}{\downarrow} \langle \tilde{j}|\hat{\lambda}_1|b \rangle \delta_{J'0} \\
 & \stackrel{(A_2C)}{-} \frac{1}{2} \hat{P}_{ab}(J) \hat{P}_{ij}(J) \hat{J}_i^{-1} \sum_c \overset{00}{\downarrow} \langle \tilde{i}|\hat{\lambda}_1|c \rangle \overset{JM}{\downarrow} \langle c j|\hat{\mathcal{H}}_1|ab \rangle \delta_{ji jc} \\
 & \stackrel{(A_2D)}{+} \frac{1}{2} \hat{P}_{ab}(J) \hat{P}_{ij}(J) \hat{J}_a^{-1} \sum_k \overset{00}{\downarrow} \langle \tilde{k}|\hat{\lambda}_1|a \rangle \overset{JM}{\downarrow} \langle i j|\hat{\mathcal{H}}_2|kb \rangle \delta_{ja jk} \\
 & \stackrel{(A_2E)}{-} \frac{1}{2} \hat{P}_{ab}(J) \hat{P}_{ij}(J) \hat{J}_b^{-1} \sum_c \overset{JM}{\downarrow} \langle i j|\hat{\lambda}_2|ac \rangle \overset{JM}{\downarrow} \langle \tilde{c}|\hat{\mathcal{H}}_1|b \rangle \delta_{jb jc} \\
 & \stackrel{(A_2F)}{+} \frac{1}{2} \hat{P}_{ab}(J) \hat{P}_{ij}(J) \hat{J}_j^{-1} \sum_k \overset{JM}{\downarrow} \langle i k|\hat{\lambda}_2|ab \rangle \overset{JM}{\downarrow} \langle \tilde{j}|\hat{\mathcal{H}}_1|k \rangle \delta_{jj jk} \\
 & \stackrel{(A_2G)}{-} \text{CCAtoStd}^{(A)} \left[\begin{smallmatrix} ij \\ ab \end{smallmatrix} J; J' \right] \sum_{ck} (-1)^{j_c+j_k-J'} \overset{J'M'}{\downarrow} \langle \tilde{i} \tilde{k}|\hat{\lambda}_2|ac \rangle \overset{J'M'}{\downarrow} \langle \tilde{c} \tilde{j}|\hat{\mathcal{H}}_2|kb \rangle \\
 & \stackrel{(A_2H)}{+} \frac{1}{8} \hat{P}_{ab}(J) \hat{P}_{ij}(J) \sum_{cd} \overset{JM}{\downarrow} \langle i j|\hat{\lambda}_2|cd \rangle \overset{JM}{\downarrow} \langle cd|\hat{\mathcal{H}}_1|ab \rangle \\
 & \stackrel{(A_2I)}{+} \frac{1}{8} \hat{P}_{ab}(J) \hat{P}_{ij}(J) \sum_{kl} \overset{JM}{\downarrow} \langle i j|\hat{\mathcal{H}}_2|kl \rangle \overset{JM}{\downarrow} \langle kl|\hat{\lambda}_2|ab \rangle \\
 & \stackrel{(A_2J)}{-} \frac{1}{4} \hat{P}_{ab}(J) \hat{P}_{ij}(J) \hat{J}_a^{-2} \sum_{cdkl} \sum_{J'} (\hat{J}')^2 \overset{J'M'}{\downarrow} \langle cd|\hat{t}_2|kl \rangle \overset{J'M'}{\downarrow} \langle kl|\hat{\lambda}_2|ca \rangle \overset{J'M'}{\downarrow} \langle ij|\hat{v}|db \rangle \delta_{ja ja} \\
 & \stackrel{(A_2K)}{-} \frac{1}{4} \hat{P}_{ab}(J) \hat{P}_{ij}(J) \hat{J}_i^{-2} \sum_{cdkl} \sum_{J'} (\hat{J}')^2 \overset{J'M'}{\downarrow} \langle ki|\hat{\lambda}_2|cd \rangle \overset{J'M'}{\downarrow} \langle cd|\hat{t}_2|kl \rangle \overset{J'M'}{\downarrow} \langle lj|\hat{v}|ab \rangle \delta_{ji ji} \\
 & = 0 \quad , \quad \forall a, b, i, j, J, M
 \end{aligned}$$

 Figure E.3: Spherical expressions for the Λ CCSD $\hat{\Lambda}_2$ amplitude equations.

E.3 Spherical Equations for Three-Body Hamiltonians

$$\begin{aligned}
 & (\Lambda_1^{3B_A}) + \frac{1}{4} \sum_{cdkl} \sum_J \hat{J} \langle cd\tilde{i} || \hat{w} || k l a \rangle \langle kl | \hat{\lambda}_2 | cd \rangle \\
 & (\Lambda_1^{3B_B}) + \frac{1}{8} \sum_{cdefkl} \sum_J \hat{J} \langle cd\tilde{i} || \hat{w} || e f a \rangle \langle kl | \hat{\lambda}_2 | cd \rangle \langle ef | \hat{t}_2 | kl \rangle \\
 & (\Lambda_1^{3B_C}) + \hat{J}_i^{-1} \sum_{cdeklm} \sum_{JJ'J''} (-1)^{j_c+j_k-J} (-1)^{j_d+j_l-J} (-1)^{j_e+j_m-J} \hat{J} \hat{J}' \hat{J}'' \\
 & \times \left\{ \begin{matrix} J & J' & J'' \\ j_a & j_i & j_d \end{matrix} \right\}_{6j} \langle id\tilde{m} || \hat{w} || l a e \rangle \langle \tilde{k} \tilde{l} | \hat{\lambda}_2 | cd \rangle \langle \tilde{c} \tilde{e} | \hat{t}_2 | km \rangle \\
 & (\Lambda_1^{3B_D}) + \frac{1}{8} \sum_{cdklmn} \sum_J \hat{J} \langle mn\tilde{i} || \hat{w} || k l a \rangle \langle kl | \hat{\lambda}_2 | cd \rangle \langle cd | \hat{t}_2 | mn \rangle \\
 & (\Lambda_1^{3B_E}) - \frac{1}{4} \sum_{cdefklmn} \sum_{JJ'J''} \hat{J} \hat{J}' (\hat{J}'')^2 \left\{ \begin{matrix} J & J' & J'' \\ j_c & j_f & j_d \end{matrix} \right\}_{6j} \left\{ \begin{matrix} J & J' & J'' \\ j_c & j_f & j_e \end{matrix} \right\}_{6j} \\
 & \times \langle mn\tilde{i} || \hat{w} || e f a \rangle \langle kl | \hat{\lambda}_2 | cd \rangle \langle df | \hat{t}_2 | mn \rangle \langle ce | \hat{t}_2 | kl \rangle \\
 & (\Lambda_1^{3B_F}) + \frac{1}{2} \hat{J}_i^{-1} \sum_{cdefklmn} \sum_{JJ'J''} (-1)^{j_c+j_k-J} (-1)^{j_d+j_l-J} (-1)^{j_f+j_n-J} (-1)^{J+J'+J''} \\
 & \times \hat{J} \hat{J}' \hat{J}'' \left\{ \begin{matrix} J & J' & J'' \\ j_i & j_e & j_m \end{matrix} \right\}_{6j} \langle mi\tilde{n} || \hat{w} || a e f \rangle \langle \tilde{k} \tilde{l} | \hat{\lambda}_2 | cd \rangle \langle \tilde{c} \tilde{e} | \hat{t}_2 | km \rangle \langle \tilde{d} \tilde{f} | \hat{t}_2 | ln \rangle + \dots
 \end{aligned}$$

Figure E.4: Spherical expressions for the ACCSD $\hat{\Lambda}_1$ amplitude equations for three-body Hamiltonians.

$$\begin{aligned}
 & \begin{pmatrix} A_1^{3BG} \\ + \end{pmatrix} \frac{1}{16} \sum_{cdefklmn} \sum_J \hat{J} \langle mn\tilde{i}||\hat{w}||efa \rangle \langle kl|\hat{\lambda}_2|cd \rangle \langle cd|\hat{t}_2|mn \rangle \langle ef|\hat{t}_2|kl \rangle \\
 & \begin{pmatrix} A_1^{3BH} \\ - \end{pmatrix} \frac{1}{4} \sum_{cdefklmn} \sum_{JJ'J''} \hat{J}^2 \hat{J}' (\hat{J}'')^2 \\
 & \times \left\{ \begin{matrix} J & J' & J'' \\ j_n & j_k & j_l \end{matrix} \right\}_{6j} \left\{ \begin{matrix} J & J' & J'' \\ j_n & j_k & j_m \end{matrix} \right\}_{6j} \langle mn\tilde{i}||\hat{w}||efa \rangle \langle kl|\hat{\lambda}_2|cd \rangle \langle cd|\hat{t}_2|km \rangle \langle ef|\hat{t}_2|ln \rangle \\
 & \begin{pmatrix} A_1^{3BI} \\ - \end{pmatrix} \frac{1}{2} \sum_{cdekl} \hat{J}_k^{-1} \sum_J \hat{J} \langle cd\tilde{i}||\hat{w}||ela \rangle \langle kl|\hat{\lambda}_2|cd \rangle \langle \tilde{e}|\hat{t}_1|k \rangle \\
 & \begin{pmatrix} A_1^{3BJ} \\ + \end{pmatrix} \frac{1}{2} \sum_{cdklm} \hat{J}_c^{-1} \sum_J \hat{J} \langle md\tilde{i}||\hat{w}||kla \rangle \langle kl|\hat{\lambda}_2|cd \rangle \langle \tilde{c}|\hat{t}_1|m \rangle \\
 & \begin{pmatrix} A_1^{3BK} \\ + \end{pmatrix} \frac{1}{4} \sum_{cdefklm} \hat{J}_c^{-1} \sum_J \hat{J} \langle md\tilde{i}||\hat{w}||efa \rangle \langle kl|\hat{\lambda}_2|cd \rangle \langle ef|\hat{t}_2|kl \rangle \langle \tilde{c}|\hat{t}_1|m \rangle \\
 & \begin{pmatrix} A_1^{3BL} \\ + \end{pmatrix} \hat{J}_i^{-1} \sum_{cdefklm} \hat{J}_k^{-1} \sum_{JJ'J''} (-1)^{j_d+j_l-J} (-1)^{j_f+j_m-J} (-1)^{J+J'+J''} \\
 & \times \hat{J} \hat{J}' \hat{J}'' \left\{ \begin{matrix} J & J' & J'' \\ j_i & j_k & j_c \end{matrix} \right\}_{6j} \langle ci\tilde{m}||\hat{w}||aef \rangle \langle \tilde{k}\tilde{l}|\hat{\lambda}_2|cd \rangle \langle \tilde{d}\tilde{f}|\hat{t}_2|lm \rangle \langle \tilde{e}|\hat{t}_1|k \rangle \\
 & \begin{pmatrix} A_1^{3BM} \\ - \end{pmatrix} \frac{1}{4} \sum_{cdeklmn} \hat{J}_k^{-1} \sum_J \hat{J} \langle mn\tilde{i}||\hat{w}||ela \rangle \langle kl|\hat{\lambda}_2|cd \rangle \langle cd|\hat{t}_2|mn \rangle \langle \tilde{e}|\hat{t}_1|k \rangle \\
 & + \dots
 \end{aligned}$$

 Figure E.5: Spherical expressions for the ACCSD $\hat{\Lambda}_1$ amplitude equations for three-body Hamiltonians, continued.

$$\begin{aligned}
 & \binom{\Lambda_1^{3B_N}}{-} \hat{f}_i^{-1} \sum_{cdeklmn} \hat{f}_c^{-1} \sum_{JJ'J''} (-1)^{j_d+j_l-J} (-1)^{j_e+j_n-J} \\
 & \times \hat{f} \hat{f}' \hat{f}'' \left\{ \begin{matrix} J & J' & J'' \\ j_i & j_k & j_m \end{matrix} \right\}_{6j} \langle im\tilde{n}||\hat{w}||ake \rangle \langle \tilde{k}\tilde{l}|\hat{\lambda}_2|cd \rangle \langle \tilde{d}\tilde{e}|\hat{t}_2|ln \rangle \langle \tilde{c}|\hat{t}_1|m \rangle \\
 & \quad \begin{array}{c} \begin{array}{ccc} J' & J'' & JM \\ \downarrow & \downarrow & \downarrow \\ \begin{array}{ccc} \downarrow & \downarrow & \downarrow \\ \downarrow & \downarrow & \downarrow \end{array} \\ J & JM & JM \end{array} \end{array} \\
 & \binom{\Lambda_1^{3B_O}}{-} \frac{1}{4} \hat{f}_i^{-1} \sum_{cdefklm} \hat{f}_c^{-1} \hat{f}_m^{-1} \sum_{JJ'} \hat{f}^2 \hat{f}' \\
 & \times \langle im\tilde{c}||\hat{w}||aef \rangle \langle kl|\hat{\lambda}_2|cd \rangle \langle fd|\hat{t}_2|kl \rangle \langle \tilde{e}|\hat{t}_1|m \rangle \\
 & \quad \begin{array}{c} \begin{array}{ccc} J' & J' & JM \\ \downarrow & \downarrow & \downarrow \\ \begin{array}{ccc} \downarrow & \downarrow & \downarrow \\ \downarrow & \downarrow & \downarrow \end{array} \\ 0 & JM & JM \end{array} \end{array} \\
 & \binom{\Lambda_1^{3B_P}}{+} \frac{1}{2} \hat{f}_i^{-1} \sum_{cdeklmn} \hat{f}_l^{-1} \hat{f}_m^{-1} \sum_{JJ'} \hat{f}^2 \hat{f}' \\
 & \times \langle im\tilde{n}||\hat{w}||ael \rangle \langle kl|\hat{\lambda}_2|cd \rangle \langle cd|\hat{t}_2|kn \rangle \langle \tilde{e}|\hat{t}_1|m \rangle \\
 & \quad \begin{array}{c} \begin{array}{ccc} J' & J' & JM \\ \downarrow & \downarrow & \downarrow \\ \begin{array}{ccc} \downarrow & \downarrow & \downarrow \\ \downarrow & \downarrow & \downarrow \end{array} \\ 0 & JM & JM \end{array} \end{array} \\
 & \binom{\Lambda_1^{3B_Q}}{+} \frac{1}{4} \sum_{cdefkl} \hat{f}_e^{-1} \hat{f}_f^{-1} \sum_J \hat{f} \langle cd\tilde{i}||\hat{w}||efa \rangle \langle kl|\hat{\lambda}_2|cd \rangle \langle \tilde{e}|\hat{t}_1|k \rangle \langle \tilde{f}|\hat{t}_1|l \rangle \\
 & \quad \begin{array}{c} \begin{array}{ccc} J & J & JM \\ \downarrow & \downarrow & \downarrow \\ \begin{array}{ccc} \downarrow & \downarrow & \downarrow \\ \downarrow & \downarrow & \downarrow \end{array} \\ 0 & JM & JM \end{array} \end{array} \\
 & \binom{\Lambda_1^{3B_R}}{-} \sum_{cdeklm} \hat{f}_c^{-1} \hat{f}_k^{-1} \sum_J \hat{f} \langle md\tilde{i}||\hat{w}||ela \rangle \langle kl|\hat{\lambda}_2|cd \rangle \langle \tilde{c}|\hat{t}_1|m \rangle \langle \tilde{e}|\hat{t}_1|k \rangle \\
 & \quad \begin{array}{c} \begin{array}{ccc} J & J & JM \\ \downarrow & \downarrow & \downarrow \\ \begin{array}{ccc} \downarrow & \downarrow & \downarrow \\ \downarrow & \downarrow & \downarrow \end{array} \\ 0 & JM & JM \end{array} \end{array} \\
 & \binom{\Lambda_1^{3B_S}}{+} \frac{1}{4} \sum_{cdklmn} \hat{f}_c^{-1} \hat{f}_d^{-1} \sum_J \hat{f} \langle mn\tilde{i}||\hat{w}||kla \rangle \langle kl|\hat{\lambda}_2|cd \rangle \langle \tilde{c}|\hat{t}_1|m \rangle \langle \tilde{d}|\hat{t}_1|n \rangle \\
 & \quad \begin{array}{c} \begin{array}{ccc} J & J & JM \\ \downarrow & \downarrow & \downarrow \\ \begin{array}{ccc} \downarrow & \downarrow & \downarrow \\ \downarrow & \downarrow & \downarrow \end{array} \\ 0 & JM & JM \end{array} \end{array} \\
 & \binom{\Lambda_1^{3B_T}}{+} \frac{1}{8} \sum_{cdefklmn} \hat{f}_c^{-1} \hat{f}_d^{-1} \sum_J \hat{f} \langle mn\tilde{i}||\hat{w}||efa \rangle \langle kl|\hat{\lambda}_2|cd \rangle \langle ef|\hat{t}_2|kl \rangle \langle \tilde{c}|\hat{t}_1|m \rangle \langle \tilde{d}|\hat{t}_1|n \rangle \\
 & \quad \begin{array}{c} \begin{array}{ccc} J & J & JM \\ \downarrow & \downarrow & \downarrow \\ \begin{array}{ccc} \downarrow & \downarrow & \downarrow \\ \downarrow & \downarrow & \downarrow \end{array} \\ 0 & JM & JM \end{array} \end{array} \\
 & + \dots
 \end{aligned}$$

 Figure E.6: Spherical expressions for the ACCSD $\hat{\Lambda}_1$ amplitude equations for three-body Hamiltonians, continued.

$$\begin{aligned}
 & \begin{pmatrix} \Lambda_{2,J}^{3B} \text{A} \end{pmatrix} \frac{1}{4} \hat{P}_{ab}(J) \hat{P}_{ij}(J) (-1)^{j_a+j_b-J} \sum_{ckl} \sum_{J'J''} (-1)^{J+J'+J''} \hat{J}^{-1} \hat{J}' \hat{J}'' \\
 & \times \left\{ \begin{matrix} J & J' & J'' \\ j_c & j_b & j_a \end{matrix} \right\}_{6j} \langle ij\tilde{c} || \hat{w} || klb \rangle \langle kl | \hat{\lambda}_2 | ac \rangle \\
 & \quad \begin{array}{c} J \quad J' \quad J'M' \quad J'M' \\ \downarrow \quad \downarrow \quad \downarrow \quad \downarrow \\ \underbrace{\hspace{1.5cm}}_{J''} \end{array} \\
 & \begin{pmatrix} \Lambda_{2,J}^{3B} \text{B} \end{pmatrix} \frac{1}{2} \hat{P}_{ab}(J) \hat{P}_{ij}(J) \sum_{cdklm} \sum_{J'J''} (-1)^{j_c+j_l-J'} (-1)^{j_a+j_m-J'} (-1)^{J+J'+J''} \\
 & \times \hat{J}^{-1} \hat{J}' \hat{J}'' \left\{ \begin{matrix} J & J' & J'' \\ j_k & j_b & j_a \end{matrix} \right\}_{6j} \langle ij\tilde{m} || \hat{w} || bkd \rangle \langle \tilde{k}\tilde{l} | \hat{\lambda}_2 | ac \rangle \langle \tilde{c}\tilde{d} | \hat{t}_2 | lm \rangle \\
 & \quad \begin{array}{c} J \quad J'' \quad J'M' \quad J'M' \\ \downarrow \quad \downarrow \quad \downarrow \quad \downarrow \\ \underbrace{\hspace{1.5cm}}_{J'} \quad \underbrace{\hspace{1.5cm}}_{J'M'} \quad \underbrace{\hspace{1.5cm}}_{J'M'} \end{array} \\
 & \begin{pmatrix} \Lambda_{2,J}^{3B} \text{C} \end{pmatrix} \frac{1}{8} \hat{P}_{ab}(J) \hat{P}_{ij}(J) (-1)^{j_a+j_b-J} \sum_{cdekl} \sum_{J'J''} (-1)^{J+J'+J''} \hat{J}^{-1} \hat{J}' \hat{J}'' \\
 & \times \left\{ \begin{matrix} J & J' & J'' \\ j_c & j_b & j_a \end{matrix} \right\}_{6j} \langle kl | \hat{\lambda}_2 | ac \rangle \langle ij\tilde{c} || \hat{w} || deb \rangle \langle de | \hat{t}_2 | kl \rangle \\
 & \quad \begin{array}{c} J'M' \quad J'M' \quad J \quad J' \quad J'M' \quad J'M' \\ \downarrow \quad \downarrow \quad \downarrow \quad \downarrow \quad \downarrow \quad \downarrow \\ \underbrace{\hspace{1.5cm}}_{J''} \end{array} \\
 & \begin{pmatrix} \Lambda_{2,J}^{3B} \text{D} \end{pmatrix} \frac{1}{2} \hat{P}_{ab}(J) \hat{P}_{ij}(J) (-1)^{j_a+j_b-J} \sum_{cdkl} \hat{J}_k^{-1} \sum_{J'J''} (-1)^{J+J'+J''} \hat{J}^{-1} \hat{J}' \hat{J}'' \\
 & \times \left\{ \begin{matrix} J & J' & J'' \\ j_c & j_b & j_a \end{matrix} \right\}_{6j} \langle ij\tilde{c} || \hat{w} || dlb \rangle \langle kl | \hat{\lambda}_2 | ac \rangle \langle \tilde{d} | \hat{t}_1 | k \rangle \\
 & \quad \begin{array}{c} J \quad J' \quad J'M' \quad J'M' \quad 00 \\ \downarrow \quad \downarrow \quad \downarrow \quad \downarrow \quad \downarrow \\ \underbrace{\hspace{1.5cm}}_{J''} \end{array} \\
 & \begin{pmatrix} \Lambda_{2,J}^{3B} \text{E} \end{pmatrix} \frac{1}{4} \hat{P}_{ab}(J) \hat{P}_{ij}(J) (-1)^{j_a+j_b-J} \sum_{cklm} \hat{J}_c^{-1} \sum_{J'J''} (-1)^{J+J'+J''} \hat{J}^{-1} \hat{J}' \hat{J}'' \\
 & \times \left\{ \begin{matrix} J & J' & J'' \\ j_m & j_b & j_a \end{matrix} \right\}_{6j} \langle ij\tilde{m} || \hat{w} || klb \rangle \langle kl | \hat{\lambda}_2 | ac \rangle \langle \tilde{c} | \hat{t}_1 | m \rangle \\
 & \quad \begin{array}{c} J \quad J' \quad J'M' \quad J'M' \quad 00 \\ \downarrow \quad \downarrow \quad \downarrow \quad \downarrow \quad \downarrow \\ \underbrace{\hspace{1.5cm}}_{J''} \end{array} \\
 & + \dots
 \end{aligned}$$

 Figure E.9: Spherical expressions for the ACCSD $\hat{\Lambda}_2$ amplitude equations for three-body Hamiltonians.

$$\begin{aligned}
 & \left(\Lambda_{2,J}^{3B F} \right) - \frac{1}{4} \hat{P}_{ab}(J) \hat{P}_{ij}(J) \sum_{cdeklm} \sum_{J'J''} \hat{J}^{-1} (\hat{J}')^2 (\hat{J}'')^2 \left\{ \begin{matrix} J & J' & J'' \\ j_c & j_b & j_a \end{matrix} \right\}_{6j} \left\{ \begin{matrix} J & J' & J'' \\ j_c & j_b & j_a \end{matrix} \right\}_{6j} \\
 & \times \underbrace{\langle ij\tilde{m} || \hat{w} || dbe \rangle}_{0} \langle kl | \hat{\lambda}_2 | ca \rangle \langle cd | \hat{t}_2 | kl \rangle \langle \tilde{e} | \hat{t}_1 | m \rangle \\
 & \left(\Lambda_{2,J}^{3B G} \right) + \frac{1}{2} \hat{P}_{ab}(J) \hat{P}_{ij}(J) \sum_{cdeklm} \hat{J}_k^{-1} \sum_{J'J''} (-1)^{j_c+j_l-J'} (-1)^{j_e+j_m-J'} (-1)^{J+J'+J''} \\
 & \times \hat{J}^{-1} \hat{J}' \hat{J}'' \left\{ \begin{matrix} J & J' & J'' \\ j_k & j_b & j_a \end{matrix} \right\}_{6j} \underbrace{\langle ij\tilde{m} || \hat{w} || bde \rangle}_{J'} \langle \tilde{k} \tilde{l} | \hat{\lambda}_2 | ac \rangle \langle \tilde{c} \tilde{e} | \hat{t}_2 | lm \rangle \langle \tilde{d} | \hat{t}_1 | k \rangle \\
 & \left(\Lambda_{2,J}^{3B H} \right) - \frac{1}{8} \hat{P}_{ab}(J) \hat{P}_{ij}(J) (-1)^{j_a+j_b-J} \sum_{cdeklm} \hat{J}_c^{-1} \sum_{J'J''} (-1)^{J+J'+J''} \hat{J}^{-1} \hat{J}' \hat{J}'' \\
 & \times \left\{ \begin{matrix} J & J' & J'' \\ j_m & j_b & j_a \end{matrix} \right\}_{6j} \underbrace{\langle ij\tilde{m} || \hat{w} || deb \rangle}_{J''} \langle kl | \hat{\lambda}_2 | ac \rangle \langle de | \hat{t}_2 | kl \rangle \langle \tilde{c} | \hat{t}_1 | m \rangle \\
 & \left(\Lambda_{2,J}^{3B I} \right) + \frac{1}{2} \hat{P}_{ab}(J) \hat{P}_{ij}(J) (-1)^{j_a+j_b-J} \sum_{cdklm} \hat{J}_c^{-1} \hat{J}_d^{-1} \sum_{J'J''} (-1)^{J+J'+J''} \hat{J}^{-1} \hat{J}' \hat{J}'' \\
 & \times \left\{ \begin{matrix} J & J' & J'' \\ j_m & j_b & j_a \end{matrix} \right\}_{6j} \underbrace{\langle ij\tilde{m} || \hat{w} || dlb \rangle}_{J''} \langle kl | \hat{\lambda}_2 | ac \rangle \langle \tilde{d} | \hat{t}_1 | k \rangle \langle \tilde{c} | \hat{t}_1 | m \rangle \\
 & \left(\Lambda_{2,J}^{3B J} \right) - \frac{1}{4} \hat{P}_{ab}(J) \hat{P}_{ij}(J) (-1)^{j_a+j_b-J} \sum_{cdekl} \hat{J}_d^{-1} \hat{J}_e^{-1} \sum_{J'J''} (-1)^{J+J'+J''} \hat{J}^{-1} \hat{J}' \hat{J}'' \\
 & \times \left\{ \begin{matrix} J & J' & J'' \\ j_c & j_b & j_a \end{matrix} \right\}_{6j} \underbrace{\langle ij\tilde{c} || \hat{w} || deb \rangle}_{J''} \langle kl | \hat{\lambda}_2 | ac \rangle \langle \tilde{d} | \hat{t}_1 | k \rangle \langle \tilde{e} | \hat{t}_1 | l \rangle \\
 & + \dots
 \end{aligned}$$

 Figure E.10: Spherical expressions for the ACCSD $\hat{\Lambda}_2$ amplitude equations for three-body Hamiltonians, continued.

Figure E.11: *Spherical expressions for the Λ CCSD $\hat{\Lambda}_2$ amplitude equations for three-body Hamiltonians, continued.*

$$\begin{aligned}
 & \left(\Lambda_{2,K}^{3B} \right)_E \frac{1}{4} \hat{P}_{ab}(J) \hat{P}_{ij}(J) \sum_{cdek} \hat{j}_k^{-1} \sum_{J'J''} (-1)^{J+J'+J''} \hat{j}^{-1} \hat{j}' \hat{j}'' \\
 & \times \left\{ \begin{matrix} J & J' & J'' \\ j_k & j_j & j_i \end{matrix} \right\}_{6j} \langle cd \tilde{j} || \hat{w} || abe \rangle \langle ki | \hat{\lambda}_2 | cd \rangle \langle \tilde{e} | \hat{t}_1 | k \rangle \\
 & \quad \begin{array}{c} \begin{array}{ccc} \begin{array}{c} \downarrow J' \\ \downarrow J \\ \downarrow J'' \end{array} & \begin{array}{c} \downarrow J \\ \downarrow J' \\ \downarrow J'' \end{array} & \begin{array}{c} \downarrow J' \\ \downarrow J' \\ \downarrow J' \end{array} \\ \hline \end{array} \\
 & \left(\Lambda_{2,K}^{3B} \right)_F \frac{1}{4} \hat{P}_{ab}(J) \hat{P}_{ij}(J) \hat{j}_i^{-1} \hat{j}^{-1} \sum_{cdek lm} \hat{j}_l^{-1} \sum_{J'} (\hat{j}')^2 \\
 & \times \langle l j \tilde{m} || \hat{w} || abe \rangle \langle i k | \hat{\lambda}_2 | cd \rangle \langle cd | \hat{t}_2 | l k \rangle \langle \tilde{e} | \hat{t}_1 | m \rangle \\
 & \quad \begin{array}{c} \begin{array}{ccc} \begin{array}{c} \downarrow J \\ \downarrow J \\ \downarrow J' \end{array} & \begin{array}{c} \downarrow J \\ \downarrow J' \\ \downarrow J' \end{array} & \begin{array}{c} \downarrow J' \\ \downarrow J' \\ \downarrow J' \end{array} \\ \hline \end{array} \\
 & \left(\Lambda_{2,K}^{3B} \right)_G \frac{1}{2} \hat{P}_{ab}(J) \hat{P}_{ij}(J) (-1)^{j_i+j_j-J} \sum_{cdek lm} \hat{j}_c^{-1} \sum_{J'J''} (-1)^{j_e+j_m-J'} (-1)^{j_d+j_k-J'} \\
 & \times (-1)^{J+J'+J''} \hat{j}^{-1} \hat{j}' \hat{j}'' \left\{ \begin{matrix} J & J' & J'' \\ j_l & j_j & j_i \end{matrix} \right\}_{6j} \langle l j \tilde{m} || \hat{w} || abe \rangle \langle \tilde{i} \tilde{k} | \hat{\lambda}_2 | cd \rangle \langle \tilde{d} \tilde{e} | \hat{t}_2 | k m \rangle \langle \tilde{e} | \hat{t}_1 | l \rangle \\
 & \quad \begin{array}{c} \begin{array}{ccc} \begin{array}{c} \downarrow J'' \\ \downarrow J \\ \downarrow J' \end{array} & \begin{array}{c} \downarrow J \\ \downarrow J' \\ \downarrow J' \end{array} & \begin{array}{c} \downarrow J' \\ \downarrow J' \\ \downarrow J' \end{array} \\ \hline \end{array} \\
 & \left(\Lambda_{2,K}^{3B} \right)_H \frac{1}{8} \hat{P}_{ab}(J) \hat{P}_{ij}(J) \sum_{cdek lm} \hat{j}_k^{-1} \sum_{J'J''} (-1)^{J+J'+J''} \hat{j}^{-1} \hat{j}' \hat{j}'' \\
 & \times \left\{ \begin{matrix} J & J' & J'' \\ j_k & j_j & j_i \end{matrix} \right\}_{6j} \langle l m \tilde{j} || \hat{w} || abe \rangle \langle ki | \hat{\lambda}_2 | cd \rangle \langle cd | \hat{t}_2 | l m \rangle \langle \tilde{e} | \hat{t}_1 | k \rangle \\
 & \quad \begin{array}{c} \begin{array}{ccc} \begin{array}{c} \downarrow J' \\ \downarrow J \\ \downarrow J'' \end{array} & \begin{array}{c} \downarrow J \\ \downarrow J' \\ \downarrow J'' \end{array} & \begin{array}{c} \downarrow J' \\ \downarrow J' \\ \downarrow J' \end{array} \\ \hline \end{array} \\
 & \left(\Lambda_{2,K}^{3B} \right)_I \frac{1}{2} \hat{P}_{ab}(J) \hat{P}_{ij}(J) (-1)^{j_i+j_j-J} \sum_{cdek l} \hat{j}_k^{-1} \hat{j}_l^{-1} \sum_{J'J''} (-1)^{j_k+j_d-J'} \\
 & \times (-1)^{J+J'+J''} \hat{j}^{-1} \hat{j}' \hat{j}'' \left\{ \begin{matrix} J & J' & J'' \\ j_c & j_j & j_i \end{matrix} \right\}_{6j} \langle c j \tilde{l} || \hat{w} || abe \rangle \langle \tilde{i} \tilde{k} | \hat{\lambda}_2 | cd \rangle \langle \tilde{d} | \hat{t}_1 | l \rangle \langle \tilde{e} | \hat{t}_1 | k \rangle \\
 & \quad \begin{array}{c} \begin{array}{ccc} \begin{array}{c} \downarrow J'' \\ \downarrow J \\ \downarrow J' \end{array} & \begin{array}{c} \downarrow J \\ \downarrow J' \\ \downarrow J' \end{array} & \begin{array}{c} \downarrow J' \\ \downarrow J' \\ \downarrow J' \end{array} \\ \hline \end{array} \\
 & + \dots
 \end{aligned}$$

 Figure E.12: Spherical expressions for the ACCSD $\hat{\Lambda}_2$ amplitude equations for three-body Hamiltonians, continued.

$$\begin{aligned}
 & \begin{pmatrix} \Lambda_{2,K}^{3B} \\ + \end{pmatrix} \frac{1}{4} \hat{P}_{ab}(J) \hat{P}_{ij}(J) \sum_{cdklm} \hat{J}_c^{-1} \hat{J}_d^{-1} \sum_{J'J''} (-1)^{J+J'+J''} \hat{J}^{-1} \hat{J}' \hat{J}'' \left\{ \begin{matrix} J & J' & J'' \\ j_k & j_j & j_i \end{matrix} \right\}_{6j} \\
 & \times \begin{array}{c} \begin{array}{ccccc} \begin{array}{c} \downarrow J' \\ \downarrow J \\ \downarrow J'M' \\ \downarrow J'M' \end{array} & \begin{array}{c} \downarrow J \\ \downarrow J \\ \downarrow J'M' \\ \downarrow J'M' \end{array} & \begin{array}{c} \downarrow 00 \\ \downarrow 00 \end{array} & \begin{array}{c} \downarrow 00 \\ \downarrow 00 \end{array} & \begin{array}{c} \downarrow 00 \\ \downarrow 00 \end{array} \\
 \langle lm\tilde{j}||\hat{w}||abk \rangle & \langle ki|\hat{\lambda}_2|cd \rangle \langle \tilde{c}|\hat{t}_1|l \rangle \langle \tilde{d}|\hat{t}_1|m \rangle \\
 \underbrace{\hspace{10em}}_{J''} & \end{array} \\
 & \begin{pmatrix} \Lambda_{2,K}^{3B} \\ - \end{pmatrix} \frac{1}{4} \hat{P}_{ab}(J) \hat{P}_{ij}(J) \sum_{cdeklm} \hat{J}_k^{-1} \hat{J}_l^{-1} \hat{J}_m^{-1} \sum_{J'J''} (-1)^{J+J'+J''} \hat{J}^{-1} \hat{J}' \hat{J}'' \\
 & \times \left\{ \begin{matrix} J & J' & J'' \\ j_k & j_j & j_i \end{matrix} \right\}_{6j} \begin{array}{c} \begin{array}{ccccc} \begin{array}{c} \downarrow J' \\ \downarrow J \\ \downarrow J'M' \\ \downarrow J'M' \end{array} & \begin{array}{c} \downarrow J \\ \downarrow J \\ \downarrow J'M' \\ \downarrow J'M' \end{array} & \begin{array}{c} \downarrow 00 \\ \downarrow 00 \end{array} & \begin{array}{c} \downarrow 00 \\ \downarrow 00 \end{array} & \begin{array}{c} \downarrow 00 \\ \downarrow 00 \end{array} \\
 \langle lm\tilde{j}||\hat{w}||abe \rangle & \langle ki|\hat{\lambda}_2|cd \rangle \langle \tilde{c}|\hat{t}_1|l \rangle \langle \tilde{d}|\hat{t}_1|m \rangle \langle \tilde{e}|\hat{t}_1|k \rangle \\
 \underbrace{\hspace{10em}}_{J''} & \end{array} \\
 & \begin{pmatrix} \Lambda_{2,L}^{3B(A)} \\ + \end{pmatrix} \frac{1}{4} \hat{P}_{ab}(J) \hat{P}_{ij}(J) \hat{J}^{-1} \sum_{ck} \begin{array}{c} \begin{array}{cc} \begin{array}{c} \downarrow J \\ \downarrow J \end{array} & \begin{array}{c} \downarrow J \\ \downarrow J \end{array} \\ \underbrace{\hspace{2em}}_0 \end{array} \langle ij\tilde{c}||\hat{w}||abk \rangle \langle \tilde{k}|\hat{\lambda}_1|c \rangle \\
 & \begin{pmatrix} \Lambda_{2,L}^{3B(B)} \\ - \end{pmatrix} \frac{1}{4} \hat{P}_{ab}(J) \hat{P}_{ij}(J) \hat{J}^{-1} \sum_{cdk} \hat{J}_c^{-1} \begin{array}{c} \begin{array}{cc} \begin{array}{c} \downarrow J \\ \downarrow J \end{array} & \begin{array}{c} \downarrow J \\ \downarrow J \end{array} \\ \underbrace{\hspace{2em}}_0 \end{array} \langle ij\tilde{c}||\hat{w}||abd \rangle \langle \tilde{k}|\hat{\lambda}_1|c \rangle \langle \tilde{d}|\hat{t}_1|k \rangle \\
 & \begin{pmatrix} \Lambda_{2,L}^{3B(C)} \\ + \end{pmatrix} \frac{1}{4} \hat{P}_{ab}(J) \hat{P}_{ij}(J) \hat{J}^{-1} \sum_{ckl} \hat{J}_c^{-1} \begin{array}{c} \begin{array}{cc} \begin{array}{c} \downarrow J \\ \downarrow J \end{array} & \begin{array}{c} \downarrow J \\ \downarrow J \end{array} \\ \underbrace{\hspace{2em}}_0 \end{array} \langle ij\tilde{l}||\hat{w}||abk \rangle \langle \tilde{k}|\hat{\lambda}_1|c \rangle \langle \tilde{c}|\hat{t}_1|l \rangle \\
 & \begin{pmatrix} \Lambda_{2,L}^{3B(D)} \\ + \end{pmatrix} \frac{1}{4} \hat{P}_{ab}(J) \hat{P}_{ij}(J) \hat{J}^{-1} \sum_{cdkl} \hat{J}_c^{-1} \hat{J}_k^{-1} \begin{array}{c} \begin{array}{cc} \begin{array}{c} \downarrow J \\ \downarrow J \end{array} & \begin{array}{c} \downarrow J \\ \downarrow J \end{array} \\ \underbrace{\hspace{2em}}_0 \end{array} \langle ij\tilde{l}||\hat{w}||abd \rangle \langle \tilde{k}|\hat{\lambda}_1|c \rangle \langle \tilde{c}|\hat{t}_1|l \rangle \langle \tilde{d}|\hat{t}_1|k \rangle \\
 & \begin{pmatrix} \Lambda_{2,L}^{3B(E)} \\ + \end{pmatrix} \frac{1}{4} \hat{P}_{ab}(J) \hat{P}_{ij}(J) \hat{J}^{-1} \sum_{cdkl} \begin{array}{c} \begin{array}{cc} \begin{array}{c} \downarrow J \\ \downarrow J \end{array} & \begin{array}{c} \downarrow J \\ \downarrow J \end{array} \\ \underbrace{\hspace{2em}}_0 \end{array} \langle ij\tilde{l}||\hat{w}||abd \rangle \langle \tilde{k}|\hat{\lambda}_1|c \rangle \begin{array}{c} \begin{array}{cc} \begin{array}{c} \downarrow 00 \\ \downarrow 00 \end{array} & \begin{array}{c} \downarrow 00 \\ \downarrow 00 \end{array} \\ \underbrace{\hspace{2em}}_{00} \end{array} \langle \tilde{c}\tilde{d}|\hat{t}_2|kl \rangle \\
 & + \dots
 \end{aligned}$$

 Figure E.13: Spherical expressions for the ACCSD $\hat{\Lambda}_2$ amplitude equations for three-body Hamiltonians, continued.

$$\begin{aligned}
 & \left(\Lambda_{2,M}^{3B} \right)_- \frac{1}{8} \hat{P}_{ab}(J) \hat{P}_{ij}(J) \sum_{cdek l} \hat{j}_c^{-1} \sum_{J'} \hat{j}^{-1} (\hat{j}')^2 \underbrace{\langle ij \tilde{c} || \hat{w} || abe \rangle}_{0} \langle kl | \hat{\lambda}_2 | cd \rangle \langle ed | \hat{t}_2 | kl \rangle \\
 & \left(\Lambda_{2,M}^{3B} \right)_+ \frac{1}{8} \hat{P}_{ab}(J) \hat{P}_{ij}(J) \sum_{cdk l m} \hat{j}_k^{-1} \sum_{JJ'} \hat{j}^{-1} (\hat{j}')^2 \underbrace{\langle ij \tilde{m} || \hat{w} || abk \rangle}_{0} \langle kl | \hat{\lambda}_2 | cd \rangle \langle cd | \hat{t}_2 | ml \rangle \\
 & \left(\Lambda_{2,M}^{3B} \right)_- \frac{1}{8} \hat{P}_{ab}(J) \hat{P}_{ij}(J) \sum_{cdk l m} \hat{j}_c^{-1} \hat{j}_m^{-1} \sum_{J'} \hat{j}^{-1} (\hat{j}')^2 \\
 & \times \underbrace{\langle ij \tilde{m} || \hat{w} || abe \rangle}_{0} \langle kl | \hat{\lambda}_2 | cd \rangle \langle ed | \hat{t}_2 | kl \rangle \langle \tilde{c} | \hat{t}_1 | m \rangle \\
 & \left(\Lambda_{2,M}^{3B} \right)_- \frac{1}{8} \hat{P}_{ab}(J) \hat{P}_{ij}(J) \sum_{cdk l m} \hat{j}_e^{-1} \hat{j}_k^{-1} \sum_{J'} \hat{j}^{-1} (\hat{j}')^2 \\
 & \times \underbrace{\langle ij \tilde{m} || \hat{w} || abe \rangle}_{0} \langle kl | \hat{\lambda}_2 | cd \rangle \langle cd | \hat{t}_2 | ml \rangle \langle \tilde{e} | \hat{t}_1 | k \rangle \\
 & + \langle ij | \hat{\lambda}_2 | ab \rangle [\text{NO2B}] = 0, \forall a, b, i, j, J, M
 \end{aligned}$$

 Figure E.14: Spherical expressions for the ACCSD $\hat{\Lambda}_2$ amplitude equations for three-body Hamiltonians, continued.

Appendix F

Spherical Reduced Density Matrix

$$\begin{aligned}
 \overbrace{\langle \tilde{i} | \hat{\gamma}_N^{(1)} | a \rangle}^{00} &= \begin{pmatrix} \gamma_N^{\text{hpA}} \\ + \end{pmatrix} \overbrace{\langle \tilde{i} | \hat{\lambda}_1 | a \rangle}^{00} \\
 \overbrace{\langle \tilde{a} | \hat{\gamma}_N^{(1)} | i \rangle}^{00} &= \begin{pmatrix} \gamma_N^{\text{phA}} \\ + \end{pmatrix} \overbrace{\langle \tilde{a} | \hat{t}_1 | i \rangle}^{00} + \begin{pmatrix} \gamma_N^{\text{phB}} \\ + \end{pmatrix} \sum_{bj} \overbrace{\langle \tilde{a} \tilde{b} | \hat{t}_2 | ij \rangle}^{00} \overbrace{\langle \tilde{j} | \hat{\lambda}_2 | b \rangle}^{00} \\
 &\quad - \begin{pmatrix} \gamma_N^{\text{phC}} \\ - \end{pmatrix} \hat{j}_a^{-2} \sum_{bj} \overbrace{\langle \tilde{a} | \hat{t}_1 | j \rangle}^{00} \overbrace{\langle \tilde{j} | \hat{\lambda}_1 | b \rangle}^{00} \overbrace{\langle \tilde{b} | \hat{t}_1 | i \rangle}^{00} \\
 &\quad - \begin{pmatrix} \gamma_N^{\text{phD}} \\ - \end{pmatrix} \frac{1}{2} \hat{j}_a^{-2} \sum_{bcjk} \sum_J \hat{j}^2 \overbrace{\langle \tilde{a} | \hat{t}_1 | k \rangle}^{00} \overbrace{\langle jk | \hat{\lambda}_2 | bc \rangle}^{JM} \overbrace{\langle bc | \hat{t}_2 | ji \rangle}^{JM} \\
 &\quad - \begin{pmatrix} \gamma_N^{\text{phE}} \\ - \end{pmatrix} \frac{1}{2} \hat{j}_a^{-2} \sum_{bcjk} \sum_J \hat{j}^2 \overbrace{\langle ba | \hat{t}_2 | jk \rangle}^{JM} \overbrace{\langle jk | \hat{\lambda}_2 | bc \rangle}^{JM} \overbrace{\langle \tilde{c} | \hat{t}_1 | i \rangle}^{00} \\
 \overbrace{\langle \tilde{b} | \hat{\gamma}_N^{(1)} | a \rangle}^{00} &= \begin{pmatrix} \gamma_N^{\text{ppA}} \\ - \end{pmatrix} \hat{j}_a^{-1} \sum_j \overbrace{\langle \tilde{b} | \hat{t}_1 | j \rangle}^{00} \overbrace{\langle \tilde{j} | \hat{\lambda}_2 | a \rangle}^{00} \\
 &\quad - \begin{pmatrix} \gamma_N^{\text{ppB}} \\ - \end{pmatrix} \frac{1}{2} \hat{j}_a^{-1} \sum_{cjk} \sum_J \hat{j}^2 \overbrace{\langle cb | \hat{t}_2 | jk \rangle}^{JM} \overbrace{\langle jk | \hat{\lambda}_2 | ca \rangle}^{JM} \\
 \overbrace{\langle \tilde{j} | \hat{\gamma}_N^{(1)} | i \rangle}^{00} &= \begin{pmatrix} \gamma_N^{\text{hhA}} \\ + \end{pmatrix} \hat{j}_i^{-1} \sum_j \overbrace{\langle \tilde{j} | \hat{\lambda}_1 | b \rangle}^{00} \overbrace{\langle \tilde{b} | \hat{t}_1 | i \rangle}^{00} \\
 &\quad + \begin{pmatrix} \gamma_N^{\text{hhB}} \\ + \end{pmatrix} \frac{1}{2} \hat{j}_i^{-1} \sum_{bck} \sum_J \hat{j}^2 \overbrace{\langle kj | \hat{\lambda}_2 | bc \rangle}^{JM} \overbrace{\langle bc | \hat{t}_2 | ki \rangle}^{JM}
 \end{aligned}$$

Figure F.1: Spherical expressions for the CCSD one-body response density matrix elements.

$$\begin{aligned}
 \langle ab | \hat{\gamma}_N^{(2)} | ci \rangle &= \frac{(\gamma_{\text{ph}}^{\text{ppA}})}{-} \hat{j}_c^{-1} \sum_k \langle ab | \hat{t}_2 | ki \rangle \langle \tilde{k} | \hat{\lambda}_1 | c \rangle \\
 &\quad \frac{(\gamma_{\text{ph}}^{\text{ppB}})}{-} \hat{P}_{ab}(J) \hat{j}_a^{-1} \hat{j}_b^{-1} \sum_k \hat{j}_c^{-1} \langle \tilde{a} | \hat{t}_1 | k \rangle \langle \tilde{b} | \hat{t}_1 | i \rangle \langle \tilde{k} | \hat{\lambda}_1 | c \rangle \\
 &\quad + \text{CCAtoStd}^{(A)} \left[\begin{smallmatrix} ab \\ ci \end{smallmatrix} J; J' \right]_{|\hat{t}_{ci}=0} \left\{ \right. \\
 &\quad \frac{(\gamma_{\text{ph}}^{\text{ppC}})}{-} \frac{1}{2} \delta_{J'0} \hat{j}_a^{-1} \sum_{dkl} \sum_{J''} (\hat{j}'')^2 \langle da | \hat{t}_2 | kl \rangle \langle kl | \hat{\lambda}_2 | dc \rangle \langle \tilde{b} | \hat{t}_1 | i \rangle \\
 &\quad \frac{(\gamma_{\text{ph}}^{\text{ppD}})}{+} \hat{j}_a^{-1} \sum_{dkl} (-1)^{j_d+j_l-J'} \langle \tilde{b} \tilde{d} | \hat{t}_2 | il \rangle \langle \tilde{k} \tilde{l} | \hat{\lambda}_2 | cd \rangle \langle \tilde{a} | \hat{t}_1 | k \rangle \left. \right\} \\
 &\quad \frac{(\gamma_{\text{ph}}^{\text{ppE}})}{+} \frac{1}{2} \hat{j}_i^{-1} \sum_{dkl} \langle ab | \hat{t}_2 | kl \rangle \langle kl | \hat{\lambda}_2 | cd \rangle \langle \tilde{d} | \hat{t}_1 | i \rangle \\
 &\quad \frac{(\gamma_{\text{ph}}^{\text{ppF}})}{+} \hat{P}_{ab}(J) \hat{j}_a^{-1} \hat{j}_b^{-1} \hat{j}_i^{-1} \sum_{dkl} \langle kl | \hat{\lambda}_2 | cd \rangle \langle \tilde{a} | \hat{t}_1 | k \rangle \langle \tilde{b} | \hat{t}_1 | l \rangle \langle \tilde{d} | \hat{t}_1 | i \rangle \\
 &\quad \frac{(\gamma_{\text{ph}}^{\text{ppG}})}{+} \text{CCAtoStd}^{(A)} \left[\begin{smallmatrix} ab \\ ci \end{smallmatrix} J; J' \right]_{|\hat{t}_{ci}=0} \\
 &\quad \hat{j}_a^{-1} \sum_{dkl} (-1)^{j_d+j_k-J'} \langle \tilde{b} \tilde{d} | \hat{t}_2 | ik \rangle \langle \tilde{k} \tilde{l} | \hat{\lambda}_2 | dc \rangle \langle \tilde{a} | \hat{t}_1 | l \rangle
 \end{aligned}$$

Figure F.2: Spherical expressions for the CCSD two-body response density matrix elements.

$$\begin{aligned}
 \langle ab | \hat{\gamma}_N^{(2)} | ij \rangle &= \begin{pmatrix} JM & JM \\ \downarrow & \downarrow \end{pmatrix} \begin{pmatrix} JM & JM \\ \downarrow & \downarrow \end{pmatrix} \langle ab | \hat{t}_2 | ij \rangle \\
 &+ \begin{pmatrix} \gamma_{hh}^{ppB} \\ + \end{pmatrix} \hat{P}_{ab}(J) \hat{P}_{ij}(J) \hat{J}_a^{-1} \hat{J}_b^{-1} \begin{array}{c} \xrightarrow{00} \quad \xrightarrow{00} \\ \downarrow \quad \downarrow \\ \langle \tilde{a} | \hat{t}_1 | i \rangle \langle \tilde{b} | \hat{t}_1 | j \rangle \end{array} \\
 &+ \begin{pmatrix} \gamma_{hh}^{ppC} \\ + \end{pmatrix} \text{CCAtStd}^{(A)} \begin{bmatrix} ab & J; J' \\ ij & \end{bmatrix} \delta_{J'0} \sum_{ck} \begin{array}{c} \xrightarrow{00} \quad \xrightarrow{00} \quad \xrightarrow{00} \\ \downarrow \quad \downarrow \quad \downarrow \\ \langle \tilde{c} \tilde{a} | \hat{t}_2 | ki \rangle \langle \tilde{b} | \hat{t}_1 | j \rangle \langle \tilde{k} | \hat{\lambda}_1 | c \rangle \\ \uparrow \quad \uparrow \quad \uparrow \\ 00 \quad 00 \quad 00 \end{array} \\
 &+ \begin{pmatrix} \gamma_{hh}^{ppD} \\ + \end{pmatrix} \hat{P}_{ij}(J) (-1)^{j_i+j_j-J} \hat{J}_i^{-1} \sum_{ck} \hat{J}_c^{-1} \begin{array}{c} \xrightarrow{JM} \quad \xrightarrow{JM} \quad \xrightarrow{00} \quad \xrightarrow{00} \\ \downarrow \quad \downarrow \quad \downarrow \quad \downarrow \\ \langle ab | \hat{t}_2 | jk \rangle \langle \tilde{c} | \hat{t}_1 | i \rangle \langle \tilde{k} | \hat{\lambda}_1 | c \rangle \end{array} \\
 &- \begin{pmatrix} \gamma_{hh}^{ppE} \\ - \end{pmatrix} \hat{P}_{ab}(J) \hat{J}_a^{-1} \sum_{ck} \hat{J}_k^{-1} \begin{array}{c} \xrightarrow{JM} \quad \xrightarrow{JM} \quad \xrightarrow{00} \quad \xrightarrow{00} \\ \downarrow \quad \downarrow \quad \downarrow \quad \downarrow \\ \langle cb | \hat{t}_2 | ij \rangle \langle \tilde{a} | \hat{t}_1 | k \rangle \langle \tilde{k} | \hat{\lambda}_1 | c \rangle \end{array} \\
 &- \begin{pmatrix} \gamma_{hh}^{ppF} \\ - \end{pmatrix} \hat{P}_{ab}(J) \hat{P}_{ij}(J) \hat{J}_a^{-1} \hat{J}_b^{-1} \hat{J}_i^{-2} \sum_{ck} \begin{array}{c} \xrightarrow{00} \quad \xrightarrow{00} \quad \xrightarrow{00} \quad \xrightarrow{00} \\ \downarrow \quad \downarrow \quad \downarrow \quad \downarrow \\ \langle \tilde{a} | \hat{t}_1 | k \rangle \langle \tilde{b} | \hat{t}_1 | j \rangle \langle \tilde{c} | \hat{t}_1 | i \rangle \langle \tilde{k} | \hat{\lambda}_1 | c \rangle \end{array} \\
 &+ \begin{pmatrix} \gamma_{hh}^{ppG} \\ + \end{pmatrix} \text{CCAtStd}^{(A)} \begin{bmatrix} ab & J; J' \\ ij & \end{bmatrix} \\
 &\quad \sum_{cdkl} (-1)^{j_c+j_k-J'} (-1)^{j_d+j_l-J'} \begin{array}{c} \xrightarrow{J'M'} \quad \xrightarrow{J'M'} \quad \xrightarrow{J'M'} \\ \downarrow \quad \downarrow \quad \downarrow \\ \langle \tilde{c} \tilde{a} | \hat{t}_2 | ki \rangle \langle \tilde{b} \tilde{d} | \hat{t}_2 | jl \rangle \langle \tilde{k} \tilde{l} | \hat{\lambda}_2 | cd \rangle \\ \uparrow \quad \uparrow \quad \uparrow \\ J'M' \quad J'M' \quad J'M' \end{array} \\
 &- \begin{pmatrix} \gamma_{hh}^{ppH} \\ - \end{pmatrix} \frac{1}{2} \hat{P}_{ij}(J) \hat{J}_i^{-2} \sum_{cdkl} \sum_{J'} (J')^2 \begin{array}{c} \xrightarrow{J'M'} \quad \xrightarrow{J'M'} \quad \xrightarrow{JM} \quad \xrightarrow{JM} \quad \xrightarrow{J'M'} \quad \xrightarrow{J'M'} \\ \downarrow \quad \downarrow \quad \downarrow \quad \downarrow \quad \downarrow \quad \downarrow \\ \langle cd | \hat{t}_2 | ik \rangle \langle ab | \hat{t}_2 | lj \rangle \langle lk | \hat{\lambda}_2 | cd \rangle \end{array} \\
 &- \begin{pmatrix} \gamma_{hh}^{ppI} \\ - \end{pmatrix} \frac{1}{2} \hat{P}_{ab}(J) \hat{J}_a^{-2} \sum_{cdkl} \sum_{J'} (J')^2 \begin{array}{c} \xrightarrow{J'M'} \quad \xrightarrow{J'M'} \quad \xrightarrow{JM} \quad \xrightarrow{JM} \quad \xrightarrow{J'M'} \quad \xrightarrow{J'M'} \\ \downarrow \quad \downarrow \quad \downarrow \quad \downarrow \quad \downarrow \quad \downarrow \\ \langle ca | \hat{t}_2 | kl \rangle \langle db | \hat{t}_2 | ij \rangle \langle kl | \hat{\lambda}_2 | cd \rangle \end{array}
 \end{aligned}$$

Figure F.3: Spherical expressions for the CCSD two-body response density matrix elements, continued.

$$\begin{aligned}
 & (\gamma_{\text{hh}}^{\text{PPJ}})_{+} \frac{1}{4} \sum_{cdkl} \overset{JM}{\downarrow} \langle ab|\hat{t}_2|kl\rangle \overset{JM}{\downarrow} \langle cd|\hat{t}_2|ij\rangle \overset{JM}{\downarrow} \langle kl|\hat{\lambda}_2|cd\rangle \\
 & + \text{CCAtoStd}^{(A)} \left[\begin{smallmatrix} ab \\ ij \end{smallmatrix} J; J' \right] \left\{ (\gamma_{\text{hh}}^{\text{PPK}})_{-} \frac{1}{2} \delta_{J'0} \hat{j}_i^{-2} \sum_{cdkl} \right. \\
 & \quad \times \sum_{J''} (\hat{J}'')^2 \overset{J''M''}{\downarrow} \langle cd|\hat{t}_2|ki\rangle \overset{J''M''}{\downarrow} \langle kl|\hat{\lambda}_2|cd\rangle \overset{00}{\downarrow} \langle \tilde{a}|\hat{t}_1|l\rangle \overset{00}{\downarrow} \langle \tilde{b}|\hat{t}_1|j\rangle \\
 & (\gamma_{\text{hh}}^{\text{PLL}})_{-} \frac{1}{2} \delta_{J'0} \hat{j}_i^{-2} \sum_{cdkl} \sum_{J''} (\hat{J}'')^2 \overset{J''M''}{\downarrow} \langle ca|\hat{t}_2|kl\rangle \overset{J''M''}{\downarrow} \langle kl|\hat{\lambda}_2|cd\rangle \overset{00}{\downarrow} \langle \tilde{d}|\hat{t}_1|i\rangle \overset{00}{\downarrow} \langle \tilde{b}|\hat{t}_1|j\rangle \\
 & (\gamma_{\text{hh}}^{\text{PPM}})_{-} \hat{j}_a^{-1} \hat{j}_i^{-1} \sum_{cdkl} (-1)^{j_a+j_l+J'} (-1)^{j_c+j_k+J'} \overset{J'M'}{\downarrow} \langle \tilde{b}\tilde{d}|\hat{t}_2|jl\rangle \overset{J'M'}{\downarrow} \langle \tilde{k}\tilde{l}|\hat{\lambda}_2|cd\rangle \overset{00}{\downarrow} \langle \tilde{a}|\hat{t}_1|k\rangle \overset{00}{\downarrow} \langle \tilde{c}|\hat{t}_1|i\rangle \left. \right\} \\
 & (\gamma_{\text{hh}}^{\text{PPN}})_{+} \frac{1}{2} \hat{P}_{ij}(J) \hat{j}_i^{-1} \hat{j}_j^{-1} \sum_{cdkl} \overset{JM}{\downarrow} \langle ab|\hat{t}_2|kl\rangle \overset{JM}{\downarrow} \langle kl|\hat{\lambda}_2|cd\rangle \overset{00}{\downarrow} \langle \tilde{c}|\hat{t}_1|i\rangle \overset{00}{\downarrow} \langle \tilde{d}|\hat{t}_1|j\rangle \\
 & (\gamma_{\text{hh}}^{\text{PPO}})_{+} \frac{1}{2} \hat{P}_{ab}(J) \hat{j}_a^{-1} \hat{j}_b^{-1} \sum_{cdkl} \overset{JM}{\downarrow} \langle cd|\hat{t}_2|ij\rangle \overset{JM}{\downarrow} \langle kl|\hat{\lambda}_2|cd\rangle \overset{00}{\downarrow} \langle \tilde{a}|\hat{t}_1|k\rangle \overset{00}{\downarrow} \langle \tilde{b}|\hat{t}_1|l\rangle \\
 & (\gamma_{\text{hh}}^{\text{PPP}})_{+} \hat{P}_{ab}(J) \hat{P}_{ij}(J) \hat{j}_a^{-1} \hat{j}_b^{-1} \hat{j}_i^{-1} \hat{j}_j^{-1} \sum_{cdkl} \overset{JM}{\downarrow} \langle kl|\hat{\lambda}_2|cd\rangle \overset{JM}{\downarrow} \langle \tilde{a}|\hat{t}_1|k\rangle \overset{00}{\downarrow} \langle \tilde{c}|\hat{t}_1|i\rangle \overset{00}{\downarrow} \langle \tilde{b}|\hat{t}_1|l\rangle \overset{00}{\downarrow} \langle \tilde{d}|\hat{t}_1|j\rangle
 \end{aligned}$$

Figure F.4: Spherical expressions for the CCSD two-body response density matrix elements, continued.

$$\begin{aligned}
 \langle ia | \hat{\gamma}_N^{(2)} | bj \rangle &= \begin{pmatrix} \gamma_{\text{ph}}^{\text{A}} \\ + \end{pmatrix} \hat{J}_a^{-1} \hat{J}_b^{-1} \overbrace{\langle \tilde{a} | \hat{t}_1 | j \rangle}^{00} \overbrace{\langle \tilde{i} | \hat{\lambda}_1 | b \rangle}^{00} \\
 \text{CCAtStd} \begin{bmatrix} ia \\ bj \end{bmatrix} J; J' & \left\{ \begin{pmatrix} \gamma_{\text{ph}}^{\text{B}} \\ - \end{pmatrix} \sum_{ck} (-1)^{j_c + j_k - J'} \overbrace{\langle \tilde{c} \tilde{a} | \hat{t}_2 | k j \rangle}^{J'M'} \overbrace{\langle \tilde{k} \tilde{i} | \hat{\lambda}_2 | c b \rangle}^{J'M'} \right. \\
 & \left. \begin{pmatrix} \gamma_{\text{ph}}^{\text{C}} \\ - \end{pmatrix} \hat{J}_a^{-1} \hat{J}_j^{-1} \sum_{ck} (-1)^{j_c + j_k - J'} \overbrace{\langle \tilde{i} \tilde{k} | \hat{\lambda}_2 | b c \rangle}^{J'M'} \overbrace{\langle \tilde{a} | \hat{t}_1 | k \rangle}^{00} \overbrace{\langle \tilde{c} | \hat{t}_1 | j \rangle}^{00} \right\} \\
 \langle ij | \hat{\gamma}_N^{(2)} | ab \rangle &= \begin{pmatrix} \gamma_{\text{pp}}^{\text{A}} \\ + \end{pmatrix} \overbrace{\langle ij | \hat{\lambda}_2 | ab \rangle}^{JM} \\
 \langle ab | \hat{\gamma}_N^{(2)} | cd \rangle &= \begin{pmatrix} \gamma_{\text{pp}}^{\text{A}} \\ + \end{pmatrix} \frac{1}{2} \sum_{kl} \overbrace{\langle ab | \hat{t}_2 | kl \rangle}^{JM} \overbrace{\langle kl | \hat{\lambda}_2 | cd \rangle}^{JM} \\
 & + \begin{pmatrix} \gamma_{\text{pp}}^{\text{B}} \\ + \end{pmatrix} \hat{P}_{ab}(J) \hat{J}_a^{-1} \hat{J}_b^{-1} \sum_{kl} \overbrace{\langle kl | \hat{\lambda}_2 | cd \rangle}^{JM} \overbrace{\langle \tilde{a} | \hat{t}_1 | k \rangle}^{00} \overbrace{\langle \tilde{b} | \hat{t}_1 | l \rangle}^{00} \\
 \langle ij | \hat{\gamma}_N^{(2)} | kl \rangle &= \begin{pmatrix} \gamma_{\text{hh}}^{\text{A}} \\ + \end{pmatrix} \frac{1}{2} \sum_{cd} \overbrace{\langle cd | \hat{t}_2 | kl \rangle}^{JM} \overbrace{\langle ij | \hat{\lambda}_2 | cd \rangle}^{JM} \\
 & + \begin{pmatrix} \gamma_{\text{hh}}^{\text{B}} \\ + \end{pmatrix} \hat{P}_{kl}(J) \hat{J}_k^{-1} \hat{J}_l^{-1} \sum_{cd} \overbrace{\langle ij | \hat{\lambda}_2 | ab \rangle}^{JM} \overbrace{\langle \tilde{a} | \hat{t}_1 | k \rangle}^{00} \overbrace{\langle \tilde{b} | \hat{t}_1 | l \rangle}^{00} \\
 \langle ai | \hat{\gamma}_N^{(2)} | bc \rangle &= \begin{pmatrix} \gamma_{\text{pp}}^{\text{A}} \\ - \end{pmatrix} \hat{J}_a^{-1} \sum_k \overbrace{\langle ki | \hat{\lambda}_2 | bc \rangle}^{JM} \overbrace{\langle \tilde{a} | \hat{t}_1 | k \rangle}^{00} \\
 \langle ij | \hat{\gamma}_N^{(2)} | ka \rangle &= \begin{pmatrix} \gamma_{\text{hp}}^{\text{A}} \\ + \end{pmatrix} \hat{J}_k^{-1} \sum_c \overbrace{\langle ij | \hat{\lambda}_2 | ca \rangle}^{JM} \overbrace{\langle \tilde{c} | \hat{t}_1 | k \rangle}^{00}
 \end{aligned}$$

Figure F.5: Spherical expressions for the CCSD two-body response density matrix elements, continued.

$$\begin{aligned}
 \langle ia | \hat{\gamma}_N^{(2)} | jk \rangle &= \left(\gamma_{hh}^{hpA} \right)_+ \hat{J}_i^{-1} \sum_c \langle ca | \hat{t}_2 | jk \rangle \langle i | \hat{\lambda}_2 | c \rangle \\
 &\quad \left(\gamma_{hh}^{hpB} \right)_+ \hat{J}_a^{-1} \hat{J}_i^{-2} \sum_c \langle \tilde{c} | \hat{t}_1 | j \rangle \langle \tilde{a} | \hat{t}_1 | k \rangle \langle i | \hat{\lambda}_2 | c \rangle \\
 &\quad + \text{CCAtoStd}^{(A)} \left[\begin{smallmatrix} ia \\ jk \end{smallmatrix} J; J' \right]_{|\hat{t}_{ia}=0} \left\{ \right. \\
 &\quad \left(\gamma_{hh}^{hpC} \right)_+ \frac{1}{2} \delta_{J'0} \hat{J}_i^{-1} \sum_{cdl} \sum_{J''} (\hat{J}'')^2 \langle cd | \hat{t}_2 | lj \rangle \langle li | \hat{\lambda}_2 | cd \rangle \langle \tilde{a} | \hat{t}_1 | k \rangle \\
 &\quad \left(\gamma_{hh}^{hpD} \right)_- \hat{J}_j^{-1} \sum_{cdl} (-1)^{j_d+j_l-J'} \langle \tilde{a} \tilde{d} | \hat{t}_2 | kl \rangle \langle \tilde{i} \tilde{l} | \hat{\lambda}_2 | cd \rangle \langle \tilde{c} | \hat{t}_1 | j \rangle \left. \right\} \\
 &\quad \left(\gamma_{hh}^{hpE} \right)_- \frac{1}{2} \hat{J}_a^{-1} \sum_{cdl} \langle cd | \hat{t}_2 | jk \rangle \langle il | \hat{\lambda}_2 | cd \rangle \langle \tilde{a} | \hat{t}_1 | l \rangle \\
 &\quad \left(\gamma_{hh}^{hpF} \right)_- \hat{P}_{jk}(J) \hat{J}_a^{-1} \sum_{cdl} \hat{J}_c^{-1} \hat{J}_d^{-1} \langle il | \hat{\lambda}_2 | cd \rangle \langle \tilde{a} | \hat{t}_1 | l \rangle \langle \tilde{c} | \hat{t}_1 | j \rangle \langle \tilde{d} | \hat{t}_1 | k \rangle \\
 &\quad \left(\gamma_{hh}^{hpG} \right)_- \text{CCAtoStd}^{(A)} \left[\begin{smallmatrix} ia \\ jk \end{smallmatrix} J; J' \right]_{|\hat{t}_{ia}=0} \hat{J}_j^{-1} \sum_{cdl} (-1)^{j_c+j_l-J'} \langle \tilde{a} \tilde{c} | \hat{t}_2 | kl \rangle \langle \tilde{i} \tilde{l} | \hat{\lambda}_2 | dc \rangle \langle \tilde{d} | \hat{t}_1 | j \rangle
 \end{aligned}$$

Figure F.6: Spherical expressions for the CCSD two-body response density matrix elements, continued.

Appendix G

Λ CCSD(T) Spherical Expressions

G.1 Spherical Equations

$$\begin{aligned}
 & \begin{pmatrix} \hat{\lambda}_{A1} \\ - \end{pmatrix} (-1)^{j_a+j_b-J'} \sum_d \left\{ \begin{matrix} J & J' & J'' \\ j_b & j_d & j_a \end{matrix} \right\}_X \begin{matrix} J''M'' \\ \downarrow \\ \langle \tilde{d}\tilde{k}|\hat{v}|bc \rangle \\ \uparrow \\ J''M'' \end{matrix} \begin{matrix} JM \\ \downarrow \\ \langle ij|\hat{\lambda}_2|ad \rangle \\ \downarrow \\ JM \end{matrix} \\
 & \begin{pmatrix} \hat{\lambda}_{A_{Tab}} \\ + \end{pmatrix} \sum_d \left\{ \begin{matrix} J & J' & J'' \\ j_a & j_d & j_b \end{matrix} \right\}_X \begin{matrix} J''M'' \\ \downarrow \\ \langle \tilde{d}\tilde{k}|\hat{v}|ac \rangle \\ \uparrow \\ J''M'' \end{matrix} \begin{matrix} JM \\ \downarrow \\ \langle ij|\hat{\lambda}_2|bd \rangle \\ \downarrow \\ JM \end{matrix} \\
 & \begin{pmatrix} \hat{\lambda}_{A_{Tac}} \\ - \end{pmatrix} (-1)^{J+J'+J''} \sum_d \left\{ \begin{matrix} J & J' & J'' \\ j_k & j_c & j_d \end{matrix} \right\}_X \begin{matrix} J'M' \\ \downarrow \\ \langle dk|\hat{v}|ab \rangle \\ \downarrow \\ J'M' \end{matrix} \begin{matrix} JM \\ \downarrow \\ \langle ij|\hat{\lambda}_2|cd \rangle \\ \downarrow \\ JM \end{matrix} \\
 & \begin{pmatrix} \hat{\lambda}_{A_{Tik}} \\ - \end{pmatrix} \sum_d \sum_{\mathcal{J}'\mathcal{J}''} \left\{ \begin{matrix} \mathcal{J}' & \mathcal{J}'' & J \\ j_j & j_i & j_d \end{matrix} \right\}_X \left\{ \begin{matrix} j_b & j_c & \mathcal{J}' \\ j_a & j_k & \mathcal{J}'' \\ J' & J'' & J \end{matrix} \right\}_X \begin{matrix} \mathcal{J}'M' & \mathcal{J}'M' & \mathcal{J}''M'' \\ \downarrow & \downarrow & \downarrow \\ \langle di|\hat{v}|cb \rangle & \langle \tilde{j}\tilde{k}|\hat{\lambda}_2|da \rangle \\ \uparrow & \uparrow & \uparrow \\ \mathcal{J}''M'' & \mathcal{J}''M'' & \mathcal{J}''M'' \end{matrix} \\
 & \begin{pmatrix} \hat{\lambda}_{A_{Tjk}} \\ + \end{pmatrix} (-1)^{j_i+j_j-J} \sum_d \sum_{\mathcal{J}'\mathcal{J}''} \left\{ \begin{matrix} \mathcal{J}' & \mathcal{J}'' & J \\ j_i & j_j & j_d \end{matrix} \right\}_X \left\{ \begin{matrix} j_b & j_c & \mathcal{J}' \\ j_a & j_k & \mathcal{J}'' \\ J' & J'' & J \end{matrix} \right\}_X \\
 & \times \begin{matrix} \mathcal{J}'M' & \mathcal{J}'M' & \mathcal{J}''M'' \\ \downarrow & \downarrow & \downarrow \\ \langle dj|\hat{v}|cb \rangle & \langle \tilde{i}\tilde{k}|\hat{\lambda}_2|da \rangle \\ \uparrow & \uparrow & \uparrow \\ \mathcal{J}''M'' & \mathcal{J}''M'' & \mathcal{J}''M'' \end{matrix} \\
 & \begin{pmatrix} \hat{\lambda}_{A_{Tab}T_{ik}} \\ + \end{pmatrix} (-1)^{j_c+j_k-J''} \sum_d \sum_{\mathcal{J}'\mathcal{J}''} (-1)^{J'+\mathcal{J}'+\mathcal{J}''} \left\{ \begin{matrix} \mathcal{J}' & \mathcal{J}'' & J' \\ j_b & j_a & j_d \end{matrix} \right\}_X \\
 & \times \left\{ \begin{matrix} j_i & j_c & \mathcal{J}' \\ j_j & j_k & \mathcal{J}'' \\ J & J'' & J' \end{matrix} \right\}_X \begin{matrix} \mathcal{J}'M' & \mathcal{J}''M'' & \mathcal{J}''M'' \\ \downarrow & \downarrow & \downarrow \\ \langle \tilde{d}\tilde{i}|\hat{v}|ac \rangle & \langle jk|\hat{\lambda}_2|bd \rangle \\ \uparrow & \uparrow & \uparrow \\ \mathcal{J}'M' & \mathcal{J}''M'' & \mathcal{J}''M'' \end{matrix} \\
 & + \dots
 \end{aligned}$$

Figure G.1: Spherical expressions for the \hat{t} and $\hat{\lambda}$ amplitudes of the Λ CCSD(T) energy correction. It should be noted that the X variant of the Wigner 6j and 9j symbols (4.35) and (4.34) are used here and in the following.

$$\begin{aligned}
 & \left(\begin{smallmatrix} \lambda_A \\ - \end{smallmatrix} T_{ab} T_{jk} \right) (-1)^{j_i+j_j-J} (-1)^{j_c+j_k-J''} \sum_d \sum_{\mathcal{J}' \mathcal{J}''} (-1)^{J'+\mathcal{J}'+\mathcal{J}''} \left\{ \begin{smallmatrix} \mathcal{J}' & \mathcal{J}'' & J' \\ j_b & j_a & j_d \end{smallmatrix} \right\}_X \\
 & \times \left\{ \begin{smallmatrix} j_j & j_c & \mathcal{J}' \\ j_i & j_k & \mathcal{J}'' \\ J & J'' & J' \end{smallmatrix} \right\}_X \langle \tilde{d} \tilde{j} | \hat{v} | ac \rangle \langle i k | \hat{\lambda}_2 | bd \rangle \\
 & \quad \begin{array}{c} \mathcal{J}' \mathcal{M}' \quad \mathcal{J}'' \mathcal{M}'' \quad \mathcal{J}'' \mathcal{M}'' \\ \downarrow \quad \downarrow \quad \downarrow \\ \text{---} \quad \text{---} \quad \text{---} \\ \uparrow \quad \uparrow \quad \uparrow \\ \mathcal{J}' \mathcal{M}' \end{array} \\
 & \left(\begin{smallmatrix} \lambda_A \\ + \end{smallmatrix} T_{ac} T_{ik} \right) \sum_d \left\{ \begin{smallmatrix} J & J' & J'' \\ j_d & j_j & j_i \end{smallmatrix} \right\}_X \langle d i | \hat{v} | ab \rangle \langle \tilde{k} \tilde{j} | \hat{\lambda}_2 | cd \rangle \\
 & \quad \begin{array}{c} J' M' \quad J' M' \quad J'' M'' \\ \downarrow \quad \downarrow \quad \downarrow \\ \text{---} \quad \text{---} \quad \text{---} \\ \uparrow \quad \uparrow \quad \uparrow \\ J'' M'' \end{array} \\
 & \left(\begin{smallmatrix} \lambda_A \\ - \end{smallmatrix} T_{ac} T_{jk} \right) (-1)^{j_i+j_j-J} \sum_d \left\{ \begin{smallmatrix} J & J' & J'' \\ j_d & j_i & j_j \end{smallmatrix} \right\}_X \langle d j | \hat{v} | ab \rangle \langle \tilde{k} \tilde{i} | \hat{\lambda}_2 | cd \rangle \\
 & \quad \begin{array}{c} J' M' \quad J' M' \quad J'' M'' \\ \downarrow \quad \downarrow \quad \downarrow \\ \text{---} \quad \text{---} \quad \text{---} \\ \uparrow \quad \uparrow \quad \uparrow \\ J'' M'' \end{array} \\
 & \left(\begin{smallmatrix} \lambda_{B1} \\ - \end{smallmatrix} \right) \sum_l \left\{ \begin{smallmatrix} J & J' & J'' \\ j_l & j_j & j_i \end{smallmatrix} \right\}_X \langle \tilde{j} \tilde{k} | \hat{v} | lc \rangle \langle li | \hat{\lambda}_2 | ab \rangle \\
 & \quad \begin{array}{c} J'' M'' \quad J' M' \quad J' M' \\ \downarrow \quad \downarrow \quad \downarrow \\ \text{---} \quad \text{---} \quad \text{---} \\ \uparrow \quad \uparrow \quad \uparrow \\ J'' M'' \end{array} \\
 & \left(\begin{smallmatrix} \lambda_{B2} \\ + \end{smallmatrix} T_{ac} \right) \sum_l \sum_{\mathcal{J}' \mathcal{J}''} \left\{ \begin{smallmatrix} \mathcal{J}' & \mathcal{J}'' & J \\ j_i & j_j & j_l \end{smallmatrix} \right\}_X \left\{ \begin{smallmatrix} j_k & j_a & \mathcal{J}' \\ j_c & j_b & \mathcal{J}'' \\ J'' & J' & J \end{smallmatrix} \right\}_X \langle \tilde{j} \tilde{k} | \hat{v} | la \rangle \langle li | \hat{\lambda}_2 | cb \rangle \\
 & \quad \begin{array}{c} \mathcal{J}' \mathcal{M}' \quad \mathcal{J}'' \mathcal{M}'' \quad \mathcal{J}'' \mathcal{M}'' \\ \downarrow \quad \downarrow \quad \downarrow \\ \text{---} \quad \text{---} \quad \text{---} \\ \uparrow \quad \uparrow \quad \uparrow \\ \mathcal{J}' \mathcal{M}' \end{array} \\
 & \left(\begin{smallmatrix} \lambda_{B3} \\ - \end{smallmatrix} T_{bc} \right) (-1)^{j_c+j_k-J''} \sum_l \sum_{\mathcal{J}' \mathcal{J}''} (-1)^{J+\mathcal{J}'+\mathcal{J}''} \left\{ \begin{smallmatrix} \mathcal{J}' & \mathcal{J}'' & J \\ j_i & j_j & j_l \end{smallmatrix} \right\}_X \left\{ \begin{smallmatrix} j_b & j_k & \mathcal{J}' \\ j_a & j_c & \mathcal{J}'' \\ J' & J'' & J \end{smallmatrix} \right\}_X \\
 & \times \langle \tilde{j} \tilde{k} | \hat{v} | lb \rangle \langle li | \hat{\lambda}_2 | ca \rangle \\
 & \quad \begin{array}{c} \mathcal{J}' \mathcal{M}' \quad \mathcal{J}'' \mathcal{M}'' \quad \mathcal{J}'' \mathcal{M}'' \\ \downarrow \quad \downarrow \quad \downarrow \\ \text{---} \quad \text{---} \quad \text{---} \\ \uparrow \quad \uparrow \quad \uparrow \\ \mathcal{J}' \mathcal{M}' \end{array} \\
 & \left(\begin{smallmatrix} \lambda_{B4} \\ + \end{smallmatrix} T_{ij} \right) (-1)^{j_i+j_j-J} \sum_l \left\{ \begin{smallmatrix} J & J' & J'' \\ j_l & j_i & j_j \end{smallmatrix} \right\}_X \langle \tilde{i} \tilde{k} | \hat{v} | lc \rangle \langle lj | \hat{\lambda}_2 | ab \rangle \\
 & \quad \begin{array}{c} J'' M'' \quad J' M' \quad J' M' \\ \downarrow \quad \downarrow \quad \downarrow \\ \text{---} \quad \text{---} \quad \text{---} \\ \uparrow \quad \uparrow \quad \uparrow \\ J'' M'' \end{array} \\
 & + \dots
 \end{aligned}$$

Figure G.2: Spherical expressions for the $\hat{\tilde{t}}$ and $\hat{\tilde{\lambda}}$ amplitudes of the Λ CCSD(T) energy correction, continued.

$$\begin{aligned}
 & \left(\hat{\lambda}_{B T_{ik}} \right)_{-} (-1)^{j_c+j_k-J''} \sum_l \left\{ \begin{matrix} J & J' & J'' \\ j_k & j_c & j_l \end{matrix} \right\}_X \overset{JM}{\downarrow} \overset{JM}{\downarrow} \overset{J'M'}{\downarrow} \overset{J'M'}{\downarrow} \langle ij|\hat{v}|lc\rangle \langle kl|\hat{\lambda}_2|ab\rangle \\
 & \left(\hat{\lambda}_{B T_{ac} T_{ij}} \right)_{-} (-1)^{j_i+j_j-J} \sum_l \sum_{\mathcal{J}' \mathcal{J}''} \left\{ \begin{matrix} \mathcal{J}' & \mathcal{J}'' & J \\ j_j & j_i & j_l \end{matrix} \right\}_X \left\{ \begin{matrix} j_k & j_a & \mathcal{J}' \\ j_c & j_b & \mathcal{J}'' \end{matrix} \right\}_X \overset{\mathcal{J}' \mathcal{M}'}{\downarrow} \overset{\mathcal{J}'' \mathcal{M}''}{\downarrow} \overset{\mathcal{J}'' \mathcal{M}''}{\downarrow} \langle \tilde{i} \tilde{k}|\hat{v}|la\rangle \overset{\mathcal{J}'' \mathcal{M}''}{\downarrow} \langle lj|\hat{\lambda}_2|cb\rangle \\
 & \left(\hat{\lambda}_{B T_{ac} T_{ik}} \right)_{+} (-1)^{J+J'+J''} \sum_l (-1)^{j_b+j_l-J''} \left\{ \begin{matrix} J & J' & J'' \\ j_b & j_l & j_a \end{matrix} \right\}_X \overset{JM}{\downarrow} \overset{JM}{\downarrow} \overset{J''M''}{\downarrow} \langle ij|\hat{v}|la\rangle \overset{J''M''}{\downarrow} \langle \tilde{k} \tilde{l}|\hat{\lambda}_2|cb\rangle \\
 & \left(\hat{\lambda}_{B T_{bc} T_{ij}} \right)_{+} (-1)^{j_i+j_j-J} (-1)^{j_a+j_b-J'} \sum_l \sum_{\mathcal{J}' \mathcal{J}''} \left\{ \begin{matrix} \mathcal{J}' & \mathcal{J}'' & J \\ j_j & j_i & j_l \end{matrix} \right\}_X \\
 & \times \left\{ \begin{matrix} j_k & j_b & \mathcal{J}' \\ j_c & j_a & \mathcal{J}'' \end{matrix} \right\}_X \overset{\mathcal{J}' \mathcal{M}'}{\downarrow} \overset{\mathcal{J}'' \mathcal{M}''}{\downarrow} \overset{\mathcal{J}'' \mathcal{M}''}{\downarrow} \langle \tilde{i} \tilde{k}|\hat{v}|lb\rangle \overset{\mathcal{J}'' \mathcal{M}''}{\downarrow} \langle lj|\hat{\lambda}_2|ca\rangle \\
 & \left(\hat{\lambda}_{B T_{bc} T_{ik}} \right)_{-} \sum_l \left\{ \begin{matrix} J & J' & J'' \\ j_a & j_l & j_b \end{matrix} \right\}_X \overset{JM}{\downarrow} \overset{JM}{\downarrow} \overset{J''M''}{\downarrow} \langle ij|\hat{v}|bl\rangle \overset{J''M''}{\downarrow} \langle \tilde{k} \tilde{l}|\hat{\lambda}_2|ca\rangle \\
 & \left(\hat{\lambda}_{C_1} \right)_{+} (-1)^{j_a+j_b-J'} \hat{j}_i^{-1} \left\{ \begin{matrix} J & J' & J'' \\ j_b & j_j & j_a \end{matrix} \right\}_X \overset{J''M''}{\downarrow} \overset{00}{\downarrow} \langle \tilde{j} \tilde{k}|\hat{v}|bc\rangle \overset{J''M''}{\downarrow} \langle \tilde{i}|\hat{\lambda}_1|a\rangle \\
 & \left(\hat{\lambda}_{C T_{ab}} \right)_{-} \hat{j}_i^{-1} \left\{ \begin{matrix} J & J' & J'' \\ j_a & j_j & j_b \end{matrix} \right\}_X \overset{J''M''}{\downarrow} \overset{00}{\downarrow} \langle \tilde{j} \tilde{k}|\hat{v}|ac\rangle \overset{J''M''}{\downarrow} \langle \tilde{i}|\hat{\lambda}_1|b\rangle \\
 & \left(\hat{\lambda}_{C T_{ac}} \right)_{+} \hat{j}_i^{-1} (-1)^{J+J'+J''} \left\{ \begin{matrix} J & J' & J'' \\ j_k & j_c & j_j \end{matrix} \right\}_X \overset{J'M'}{\downarrow} \overset{J'M'}{\downarrow} \overset{00}{\downarrow} \langle jk|\hat{v}|ab\rangle \overset{J'M'}{\downarrow} \langle \tilde{i}|\hat{\lambda}_1|c\rangle \\
 & + \dots
 \end{aligned}$$

 Figure G.3: Spherical expressions for the $\hat{\tilde{i}}$ and $\hat{\tilde{\lambda}}$ amplitudes of the Λ CCSD(T) energy correction, continued.

$$\begin{aligned}
 & \begin{pmatrix} \hat{\lambda}_{C_{T_{ij}}} \\ - \end{pmatrix} (-1)^{j_i+j_j-J} (-1)^{j_a+j_b-J'} \hat{f}_a^{-1} \left\{ \begin{matrix} J & J' & J'' \\ j_b & j_i & j_a \end{matrix} \right\}_X \begin{array}{c} \xrightarrow{J''M''} \\ \downarrow \\ \langle \tilde{t} \tilde{k} | \hat{v} | bc \rangle \\ \uparrow \\ \xleftarrow{J''M''} \end{array} \begin{array}{c} \xrightarrow{00} \\ \downarrow \\ \langle \tilde{j} | \hat{\lambda}_1 | a \rangle \end{array} \\
 & \begin{pmatrix} \hat{\lambda}_{C_{T_{ik}}} \\ - \end{pmatrix} (-1)^{j_a+j_b-J'} \hat{f}_a^{-1} (-1)^{J+J'+J''} \left\{ \begin{matrix} J & J' & J'' \\ j_a & j_c & j_b \end{matrix} \right\}_X \begin{array}{c} \xrightarrow{JM} \\ \downarrow \\ \langle i j | \hat{v} | cb \rangle \\ \uparrow \\ \xleftarrow{JM} \end{array} \begin{array}{c} \xrightarrow{00} \\ \downarrow \\ \langle \tilde{k} | \hat{\lambda}_1 | a \rangle \end{array} \\
 & \begin{pmatrix} \hat{\lambda}_{C_{T_{ab}T_{ij}}} \\ + \end{pmatrix} (-1)^{j_i+j_j-J} \hat{f}_b^{-1} \left\{ \begin{matrix} J & J' & J'' \\ j_a & j_i & j_b \end{matrix} \right\}_X \begin{array}{c} \xrightarrow{J''M''} \\ \downarrow \\ \langle \tilde{t} \tilde{k} | \hat{v} | ac \rangle \\ \uparrow \\ \xleftarrow{J''M''} \end{array} \begin{array}{c} \xrightarrow{00} \\ \downarrow \\ \langle \tilde{j} | \hat{\lambda}_1 | b \rangle \end{array} \\
 & \begin{pmatrix} \hat{\lambda}_{C_{T_{ab}T_{ik}}} \\ + \end{pmatrix} \hat{f}_b^{-1} (-1)^{J+J'+J''} \left\{ \begin{matrix} J & J' & J'' \\ j_b & j_c & j_a \end{matrix} \right\}_X \begin{array}{c} \xrightarrow{JM} \\ \downarrow \\ \langle i j | \hat{v} | ca \rangle \\ \uparrow \\ \xleftarrow{JM} \end{array} \begin{array}{c} \xrightarrow{00} \\ \downarrow \\ \langle \tilde{k} | \hat{\lambda}_1 | b \rangle \end{array} \\
 & \begin{pmatrix} \hat{\lambda}_{C_{T_{ac}T_{ij}}} \\ - \end{pmatrix} (-1)^{j_i+j_j-J} \hat{f}_j^{-1} (-1)^{J+J'+J''} \left\{ \begin{matrix} J & J' & J'' \\ j_k & j_c & j_i \end{matrix} \right\}_X \begin{array}{c} \xrightarrow{J'M'} \\ \downarrow \\ \langle i k | \hat{v} | ab \rangle \\ \uparrow \\ \xleftarrow{J'M'} \end{array} \begin{array}{c} \xrightarrow{00} \\ \downarrow \\ \langle \tilde{j} | \hat{\lambda}_1 | c \rangle \end{array} \\
 & \begin{pmatrix} \hat{\lambda}_{C_{T_{ac}T_{ik}}} \\ + \end{pmatrix} \delta_{JJ'} \delta_{J''0} \hat{f} \begin{array}{c} \xrightarrow{JM} \\ \downarrow \\ \langle i j | \hat{v} | ab \rangle \\ \uparrow \\ \xleftarrow{JM} \end{array} \begin{array}{c} \xrightarrow{00} \\ \downarrow \\ \langle \tilde{k} | \hat{\lambda}_1 | c \rangle \end{array} \\
 & \begin{pmatrix} \hat{\lambda}_{D_1} \\ + \end{pmatrix} \dots \begin{pmatrix} \hat{\lambda}_{D_{T_{ac}T_{ik}}} \\ + \end{pmatrix} \\
 & \begin{pmatrix} \hat{i}_3 A_1 \\ + \end{pmatrix} \sum_d \left\{ \begin{matrix} J & J' & J'' \\ j_b & j_d & j_a \end{matrix} \right\}_X \begin{array}{c} \xrightarrow{J''M''} \\ \downarrow \\ \langle \tilde{b} \tilde{c} | \hat{v} | dk \rangle \\ \uparrow \\ \xleftarrow{J''M''} \end{array} \begin{array}{c} \xrightarrow{JM} \\ \downarrow \\ \langle da | \hat{t}_2 | ij \rangle \\ \uparrow \\ \xleftarrow{JM} \end{array} \\
 & \begin{pmatrix} \hat{i}_3 A_{T_{ab}} \\ - \end{pmatrix} (-1)^{j_a+j_b-J'} \sum_d \left\{ \begin{matrix} J & J' & J'' \\ j_a & j_d & j_b \end{matrix} \right\}_X \begin{array}{c} \xrightarrow{J''M''} \\ \downarrow \\ \langle \tilde{a} \tilde{c} | \hat{v} | dk \rangle \\ \uparrow \\ \xleftarrow{J''M''} \end{array} \begin{array}{c} \xrightarrow{JM} \\ \downarrow \\ \langle db | \hat{t}_2 | ij \rangle \\ \uparrow \\ \xleftarrow{JM} \end{array} \\
 & \begin{pmatrix} \hat{i}_3 A_{T_{ac}} \\ + \end{pmatrix} (-1)^{j_c+j_k-J''} \sum_d \left\{ \begin{matrix} J & J' & J'' \\ j_k & j_c & j_d \end{matrix} \right\}_X \begin{array}{c} \xrightarrow{J'M'} \\ \downarrow \\ \langle ab | \hat{v} | dk \rangle \\ \uparrow \\ \xleftarrow{J'M'} \end{array} \begin{array}{c} \xrightarrow{JM} \\ \downarrow \\ \langle cd | \hat{t}_2 | ij \rangle \\ \uparrow \\ \xleftarrow{JM} \end{array} \\
 & + \dots
 \end{aligned}$$

Figure G.4: Spherical expressions for the \hat{t} and $\hat{\lambda}$ amplitudes of the Λ CCSD(T) energy correction, continued. The $(\hat{\lambda}D_X)$ contributions are obtained from the corresponding $(\hat{\lambda}C_X)$ contributions by $\Lambda_1 \rightarrow \hat{F}$ and replacing the matrix elements of the normal-ordered two-body Hamiltonian by $\hat{\Lambda}_2$ matrix elements.

$$\begin{aligned}
 & \left(\hat{t}_3^{\Lambda T_{ik}} \right) \sum_d \sum_{\mathcal{J}' \mathcal{J}''} \left\{ \begin{matrix} \mathcal{J}' & \mathcal{J}'' & J' \\ j_a & j_b & j_d \end{matrix} \right\}_X \left\{ \begin{matrix} j_c & j_i & \mathcal{J}' \\ j_k & j_j & \mathcal{J}'' \end{matrix} \right\}_X \langle \tilde{b} \tilde{c} | \hat{v} | d i \rangle \langle d a | \hat{t}_2 | k j \rangle \\
 & \quad \begin{array}{c} \mathcal{J}' \mathcal{M}' \quad \mathcal{J}'' \mathcal{M}'' \mathcal{J}'' \mathcal{M}'' \\ \downarrow \quad \downarrow \quad \downarrow \\ \uparrow \quad \uparrow \end{array} \\
 & \left(\hat{t}_3^{\Lambda T_{jk}} \right) (-1)^{j_i+j_j-J} \sum_d \sum_{\mathcal{J}' \mathcal{J}''} \left\{ \begin{matrix} \mathcal{J}' & \mathcal{J}'' & J' \\ j_a & j_b & j_d \end{matrix} \right\}_X \left\{ \begin{matrix} j_c & j_j & \mathcal{J}' \\ j_k & j_i & \mathcal{J}'' \end{matrix} \right\}_X \\
 & \quad \times \langle \tilde{b} \tilde{c} | \hat{v} | d j \rangle \langle d a | \hat{t}_2 | k i \rangle \\
 & \quad \begin{array}{c} \mathcal{J}' \mathcal{M}' \quad \mathcal{J}'' \mathcal{M}'' \mathcal{J}'' \mathcal{M}'' \\ \downarrow \quad \downarrow \quad \downarrow \\ \uparrow \quad \uparrow \end{array} \\
 & \left(\hat{t}_3^{\Lambda T_{ab} T_{ik}} \right) (-1)^{j_a+j_b-J'} \sum_d \sum_{\mathcal{J}' \mathcal{J}''} \left\{ \begin{matrix} \mathcal{J}' & \mathcal{J}'' & J' \\ j_b & j_a & j_d \end{matrix} \right\}_X \left\{ \begin{matrix} j_c & j_i & \mathcal{J}' \\ j_k & j_j & \mathcal{J}'' \end{matrix} \right\}_X \\
 & \quad \times \langle \tilde{a} \tilde{c} | \hat{v} | d i \rangle \langle d b | \hat{t}_2 | k j \rangle \\
 & \quad \begin{array}{c} \mathcal{J}' \mathcal{M}' \quad \mathcal{J}'' \mathcal{M}'' \mathcal{J}'' \mathcal{M}'' \\ \downarrow \quad \downarrow \quad \downarrow \\ \uparrow \quad \uparrow \end{array} \\
 & \left(\hat{t}_3^{\Lambda T_{ab} T_{jk}} \right) (-1)^{j_i+j_j-J} (-1)^{j_a+j_b-J'} \sum_d \left\{ \begin{matrix} \mathcal{J}' & \mathcal{J}'' & J' \\ j_b & j_a & j_d \end{matrix} \right\}_X \left\{ \begin{matrix} j_c & j_j & \mathcal{J}' \\ j_k & j_i & \mathcal{J}'' \end{matrix} \right\}_X \\
 & \quad \times \langle \tilde{a} \tilde{c} | \hat{v} | d j \rangle \langle d b | \hat{t}_2 | k i \rangle \\
 & \quad \begin{array}{c} \mathcal{J}' \mathcal{M}' \quad \mathcal{J}'' \mathcal{M}'' \mathcal{J}'' \mathcal{M}'' \\ \downarrow \quad \downarrow \quad \downarrow \\ \uparrow \quad \uparrow \end{array} \\
 & \left(\hat{t}_3^{\Lambda T_{ac} T_{ik}} \right) (-1)^{j_i+j_j-J} (-1)^{J+J'+J''} \sum_d \left\{ \begin{matrix} J & J' & J'' \\ j_d & j_j & j_i \end{matrix} \right\}_X \langle a b | \hat{v} | i d \rangle \langle \tilde{c} \tilde{d} | \hat{t}_2 | k j \rangle \\
 & \quad \begin{array}{c} J' M' \quad J' M' \quad J'' M'' \\ \downarrow \quad \downarrow \quad \downarrow \\ \uparrow \quad \uparrow \end{array} \\
 & \left(\hat{t}_3^{\Lambda T_{ac} T_{jk}} \right) \sum_d \left\{ \begin{matrix} J & J' & J'' \\ j_d & j_i & j_j \end{matrix} \right\}_X \langle a b | \hat{v} | j d \rangle \langle \tilde{c} \tilde{d} | \hat{t}_2 | k i \rangle \\
 & \quad \begin{array}{c} J' M' \quad J' M' \quad J'' M'' \\ \downarrow \quad \downarrow \quad \downarrow \\ \uparrow \quad \uparrow \end{array} \\
 & + \dots
 \end{aligned}$$

 Figure G.5: Spherical expressions for the $\hat{\tilde{t}}$ and $\hat{\tilde{\lambda}}$ amplitudes of the Λ CCSD(T) energy correction, continued.

$$\begin{aligned}
 & \stackrel{(i_3 B_1)}{+} (-1)^{j_i+j_j-J} \sum_l \left\{ \begin{matrix} J & J' & J'' \\ j_i & j_j & j_l \end{matrix} \right\}_X \begin{array}{c} \begin{array}{ccc} J''M'' & & J'M' & J'M' \\ \downarrow & & \downarrow & \downarrow \\ \begin{array}{ccc} J''M'' & & J''M'' \end{array} \end{array} \\ \langle \tilde{l} \tilde{c} | \hat{v} | j k \rangle \langle a b | \hat{t}_2 | i l \rangle \end{array} \\
 & \stackrel{(i_3 B_{T_{ac}})}{+} \sum_l \sum_{\mathcal{J}' \mathcal{J}''} \left\{ \begin{matrix} \mathcal{J}' & \mathcal{J}'' & J' \\ j_b & j_a & j_l \end{matrix} \right\}_X \left\{ \begin{matrix} j_j & j_k & \mathcal{J}' \\ j_i & j_c & \mathcal{J}'' \end{matrix} \right\}_X \begin{array}{c} \begin{array}{ccc} \mathcal{J}'M' & \mathcal{J}'M' & \mathcal{J}''M'' \\ \downarrow & \downarrow & \downarrow \\ \begin{array}{ccc} \mathcal{J}'M' & \mathcal{J}'M' & \mathcal{J}''M'' \end{array} \end{array} \\ \langle l a | \hat{v} | k j \rangle \langle \tilde{c} \tilde{b} | \hat{t}_2 | i l \rangle \end{array} \\
 & \stackrel{(i_3 B_{T_{bc}})}{-} (-1)^{j_i+j_j-J} (-1)^{j_a+j_b-J'} (-1)^{j_c+j_k-J''} \sum_l \sum_{\mathcal{J}' \mathcal{J}''} (-1)^{J+\mathcal{J}'+\mathcal{J}''} \\
 & \times \left\{ \begin{matrix} \mathcal{J}' & \mathcal{J}'' & J \\ j_i & j_j & j_l \end{matrix} \right\}_X \left\{ \begin{matrix} j_b & j_k & \mathcal{J}' \\ j_a & j_c & \mathcal{J}'' \end{matrix} \right\}_X \begin{array}{c} \begin{array}{ccc} \mathcal{J}'M' & & \mathcal{J}''M'' & \mathcal{J}''M'' \\ \downarrow & & \downarrow & \downarrow \\ \begin{array}{ccc} \mathcal{J}'M' & & \mathcal{J}''M'' \end{array} \end{array} \\ \langle \tilde{l} \tilde{b} | \hat{v} | j k \rangle \langle a c | \hat{t}_2 | i l \rangle \end{array} \\
 & \stackrel{(i_3 B_{T_{ij}})}{-} \sum_l \left\{ \begin{matrix} J & J' & J'' \\ j_i & j_i & j_j \end{matrix} \right\}_X \begin{array}{c} \begin{array}{ccc} J''M'' & & J'M' & J'M' \\ \downarrow & & \downarrow & \downarrow \\ \begin{array}{ccc} J''M'' & & J''M'' \end{array} \end{array} \\ \langle \tilde{l} \tilde{c} | \hat{v} | i k \rangle \langle a b | \hat{t}_2 | j l \rangle \end{array} \\
 & \stackrel{(i_3 B_{T_{ik}})}{+} (-1)^{J+J'+J''} \sum_l \left\{ \begin{matrix} J & J' & J'' \\ j_k & j_c & j_l \end{matrix} \right\}_X \begin{array}{c} \begin{array}{ccc} JM & JM & J'M' & J'M' \\ \downarrow & \downarrow & \downarrow & \downarrow \\ \begin{array}{ccc} JM & JM & J'M' \end{array} \end{array} \\ \langle l c | \hat{v} | i j \rangle \langle a b | \hat{t}_2 | k l \rangle \end{array} \\
 & \stackrel{(i_3 B_{T_{ac} T_{ij}})}{-} (-1)^{j_c+j_k-J''} \sum_l \sum_{\mathcal{J}' \mathcal{J}''} (-1)^{J+\mathcal{J}'+\mathcal{J}''} \left\{ \begin{matrix} \mathcal{J}' & \mathcal{J}'' & J \\ j_j & j_i & j_l \end{matrix} \right\}_X \left\{ \begin{matrix} j_a & j_k & \mathcal{J}' \\ j_b & j_c & \mathcal{J}'' \end{matrix} \right\}_X \\
 & \times \begin{array}{c} \begin{array}{ccc} \mathcal{J}'M' & & \mathcal{J}''M'' & \mathcal{J}''M'' \\ \downarrow & & \downarrow & \downarrow \\ \begin{array}{ccc} \mathcal{J}'M' & & \mathcal{J}''M'' \end{array} \end{array} \\ \langle \tilde{l} \tilde{a} | \hat{v} | i k \rangle \langle b c | \hat{t}_2 | j l \rangle \end{array} \\
 & \stackrel{(i_3 B_{T_{ac} T_{ik}})}{-} \sum_l \left\{ \begin{matrix} J & J' & J'' \\ j_b & j_l & j_a \end{matrix} \right\}_X \begin{array}{c} \begin{array}{ccc} JM & JM & J''M'' \\ \downarrow & \downarrow & \downarrow \\ \begin{array}{ccc} JM & JM & J''M'' \end{array} \end{array} \\ \langle l a | \hat{v} | i j \rangle \langle \tilde{c} \tilde{b} | \hat{t}_2 | k l \rangle \end{array} \\
 & + \dots
 \end{aligned}$$

Figure G.6: Spherical expressions for the $\hat{\tilde{t}}$ and $\hat{\tilde{\lambda}}$ amplitudes of the Λ CCSD(T) energy correction, continued.

$$\begin{aligned}
 & \left(\begin{smallmatrix} \bar{t}_3 B \\ + \end{smallmatrix} T_{bc} T_{ij} \right) (-1)^{j_i+j_j-J} (-1)^{j_a+j_b-J'} \sum_l \sum_{\mathcal{J}' \mathcal{J}''} \left\{ \begin{smallmatrix} \mathcal{J}' & \mathcal{J}'' & J' \\ j_a & j_b & j_l \end{smallmatrix} \right\}_X \left\{ \begin{smallmatrix} j_i & j_k & \mathcal{J}' \\ j_j & j_c & \mathcal{J}'' \\ J & J'' & J' \end{smallmatrix} \right\}_X \\
 & \times \langle l b | \hat{v} | k i \rangle \langle \tilde{c} \tilde{a} | \hat{t}_2 | j l \rangle \\
 & \left(\begin{smallmatrix} \bar{t}_3 B \\ + \end{smallmatrix} T_{bc} T_{ik} \right) (-1)^{j_a+j_b-J'} \sum_l \left\{ \begin{smallmatrix} J & J' & J'' \\ j_a & j_l & j_b \end{smallmatrix} \right\}_X \langle l b | \hat{v} | i j \rangle \langle \tilde{a} \tilde{c} | \hat{t}_2 | l k \rangle
 \end{aligned}$$

Figure G.7: Spherical expressions for the $\hat{\tilde{t}}$ and $\hat{\tilde{\lambda}}$ amplitudes of the Λ CCSD(T) energy correction, continued.

G.2 Spherical Equations for Three-Body Hamiltonians

$$\begin{aligned}
 \langle ij\tilde{k}||\hat{\lambda}||abc\rangle &= \langle ij\tilde{k}||\hat{\lambda}||abc\rangle[\text{NO2B}] + \hat{j}_c^{-1} \sum_l \langle ij\tilde{k}||\hat{w}||abl\rangle \langle \tilde{l}|\hat{\lambda}_1|c\rangle \\
 &\quad + \left(\mathcal{A}_{T_{bc}^{ac}}\right) \hat{P}_{ab}(J') \hat{j}_a^{-1} \sum_l \langle ij\tilde{k}||\hat{w}||lbc\rangle \langle \tilde{l}|\hat{\lambda}_1|a\rangle \\
 &\quad - \left(\mathcal{B}_1\right) \hat{j}_k^{-1} \sum_d \langle ij\tilde{d}||\hat{w}||abc\rangle \langle \tilde{k}|\hat{\lambda}_1|d\rangle \\
 &\quad - \left(\mathcal{B}_{T_{jk}^{ik}}\right) \hat{P}_{ij}(J) \hat{j}_i^{-1} \sum_d \langle dj\tilde{k}||\hat{w}||abc\rangle \langle \tilde{i}|\hat{\lambda}_1|d\rangle \\
 &\quad + \left(\mathcal{C}_1\right) \frac{1}{2} \sum_{de} \langle de\tilde{k}||\hat{w}||abc\rangle \langle ij|\hat{\lambda}_2|de\rangle \\
 &\quad + \left(\mathcal{C}_{T_{jk}^{ik}}\right) \frac{1}{2} \hat{P}_{ij}(J) (-1)^{j_c+j_k-J''} \sum_{de} \sum_{\mathcal{J}'\mathcal{J}''} (-1)^{J'+\mathcal{J}'+\mathcal{J}''} \left\{ \begin{matrix} j_i & j_c & \mathcal{J}'' \\ j_j & j_k & \mathcal{J}' \\ J & J'' & J' \end{matrix} \right\}_x \\
 &\quad \times \langle de\tilde{i}||\hat{w}||abc\rangle \langle jk|\hat{\lambda}_2|de\rangle + \left(\mathcal{D}_1\right) \frac{1}{2} \sum_{lm} \langle ij\tilde{k}||\hat{w}||lmc\rangle \langle lm|\hat{\lambda}_2|ab\rangle \\
 &\quad + \left(\mathcal{D}_{T_{bc}^{ac}}\right) \frac{1}{2} \hat{P}_{ab}(J') \sum_{lm} \sum_{\mathcal{J}'\mathcal{J}''} (-1)^{j_b+j_c-\mathcal{J}''} \left\{ \begin{matrix} j_k & j_a & \mathcal{J}' \\ j_c & j_b & \mathcal{J}'' \\ J'' & J' & J \end{matrix} \right\}_x \langle ij\tilde{k}||\hat{w}||lma\rangle \langle lm|\hat{\lambda}_2|bc\rangle \\
 &\quad + \dots
 \end{aligned}$$

Figure G.8: Spherical expressions for the $\hat{\lambda}$ amplitudes of the Λ CCSD(T) energy correction for three-body Hamiltonians.

$$\begin{aligned}
 & \left(\mathcal{E}_{E1} \right) \sum_{dl} (-1)^{j_d+j_l-J''} \langle ij \tilde{d} || \tilde{w} || abl \rangle \langle \tilde{k} \tilde{l} | \hat{\lambda}_2 | cd \rangle \\
 & \quad \begin{array}{c} J \quad J' \\ \downarrow \quad \downarrow \\ \text{---} \quad \text{---} \\ \uparrow \quad \uparrow \\ J'' \end{array} \\
 & \left(\mathcal{E}_{T_{bc}^{T_{ac}}} \right) \hat{P}_{ab}(J') \sum_{dl} \sum_{\mathcal{J}' \mathcal{J}''} (-1)^{j_d+j_l-\mathcal{J}''} \left\{ \begin{array}{ccc} j_b & j_c & \mathcal{J}' \\ j_a & j_k & \mathcal{J}'' \\ J' & J'' & J \end{array} \right\}_X \langle ij \tilde{d} || \tilde{w} || cbl \rangle \langle \tilde{k} \tilde{l} | \hat{\lambda}_2 | ad \rangle \\
 & \quad \begin{array}{c} J \quad \mathcal{J}' \\ \downarrow \quad \downarrow \\ \text{---} \quad \text{---} \\ \uparrow \quad \uparrow \\ \mathcal{J}'' \end{array} \quad \begin{array}{c} \mathcal{J}'' \mathcal{M}'' \\ \downarrow \\ \text{---} \\ \uparrow \\ \mathcal{J}'' \mathcal{M}'' \end{array} \\
 & \left(\mathcal{E}_{T_{jk}^{T_{ik}}} \right) \hat{P}_{ij}(J) (-1)^{j_i+j_j-J} \sum_{dl} \sum_{\mathcal{J}' \mathcal{J}''} (-1)^{j_d+j_l-\mathcal{J}''} \left\{ \begin{array}{ccc} j_j & j_k & \mathcal{J}' \\ j_i & j_c & \mathcal{J}'' \\ J & J'' & J' \end{array} \right\}_X \\
 & \quad \times \langle jk \tilde{d} || \tilde{w} || abl \rangle \langle \tilde{l} \tilde{l} | \hat{\lambda}_2 | cd \rangle \\
 & \quad \begin{array}{c} \mathcal{J}' \\ \downarrow \\ \text{---} \\ \uparrow \\ \mathcal{J}'' \end{array} \quad \begin{array}{c} J' \\ \downarrow \\ \text{---} \\ \uparrow \\ J'' \end{array} \quad \begin{array}{c} \mathcal{J}'' \mathcal{M}'' \\ \downarrow \\ \text{---} \\ \uparrow \\ \mathcal{J}'' \mathcal{M}'' \end{array} \\
 & \left(\mathcal{E}_{T_{ac}^{T_{ik}}, T_{bc}^{T_{jk}}} \right) \hat{P}_{ab}(J') \hat{P}_{ij}(J) (-1)^{j_i+j_j-J} \sum_{dl} \sum_{\mathcal{J}' \mathcal{J}'' \mathcal{J}'''} (-1)^{\mathcal{J}'+\mathcal{J}'''+J''} \\
 & \quad \times \hat{J} \hat{J}' \hat{\mathcal{J}}' (\hat{\mathcal{J}}'')^2 \hat{\mathcal{J}}''' \left\{ \begin{array}{ccc} \mathcal{J}' & \mathcal{J}'' & J' \\ j_a & j_b & j_l \end{array} \right\}_{6j} \left\{ \begin{array}{ccc} \mathcal{J}'' & \mathcal{J}''' & J \\ j_j & j_i & j_d \end{array} \right\}_{6j} \left\{ \begin{array}{ccc} J & J' & J'' \\ \mathcal{J}' & \mathcal{J}''' & \mathcal{J}'' \end{array} \right\}_{6j} \\
 & \quad \times \langle dj \tilde{k} || \tilde{w} || bcl \rangle \langle \tilde{l} \tilde{l} | \hat{\lambda}_2 | ad \rangle \\
 & \quad \begin{array}{c} \mathcal{J}''' \\ \downarrow \\ \text{---} \\ \uparrow \\ J'' \end{array} \quad \begin{array}{c} \mathcal{J}' \\ \downarrow \\ \text{---} \\ \uparrow \\ J'' \end{array} \quad \begin{array}{c} \mathcal{J}'' \mathcal{M}'' \\ \downarrow \\ \text{---} \\ \uparrow \\ \mathcal{J}'' \mathcal{M}'' \end{array} \\
 & \left(\mathcal{E}_F \right) \langle ij \tilde{k} || \tilde{w} || abc \rangle \\
 & \quad \begin{array}{c} J \quad J' \\ \downarrow \quad \downarrow \\ \text{---} \quad \text{---} \\ \uparrow \quad \uparrow \\ J'' \end{array}
 \end{aligned}$$

 Figure G.9: Spherical expressions for the $\hat{\lambda}$ amplitudes of the Λ CCSD(T) energy correction for three-body Hamiltonians, continued.

$$\begin{aligned}
 \langle ab\tilde{c}||\hat{t}||ijk\rangle &= \langle ab\tilde{c}||\hat{t}||ijk\rangle[\text{NO2B}]^{(\mathfrak{M}_{A1})} + \hat{j}_c^{-1} \sum_l \langle ab\tilde{l}||\hat{w}||ijk\rangle \langle \tilde{c}|\hat{t}_1|l\rangle \\
 &\quad + \left(\mathfrak{M}_{T_{bc}}^{T_{ac}}\right) \hat{P}_{ab}(J') \hat{j}_a^{-1} \sum_l \langle lb\tilde{c}||\hat{w}||ijk\rangle \langle \tilde{a}|\hat{t}_1|l\rangle \\
 &\quad - \left(\mathfrak{M}_{B1}\right) \hat{j}_k^{-1} \sum_d \langle ab\tilde{c}||\hat{w}||ijd\rangle \langle \tilde{d}|\hat{t}_1|k\rangle \\
 &\quad - \left(\mathfrak{M}_{T_{jk}}^{T_{ik}}\right) \hat{P}_{ij}(J) \hat{j}_i^{-1} \sum_d \langle ab\tilde{c}||\hat{w}||dj k\rangle \langle \tilde{d}|\hat{t}_1|i\rangle \\
 &\quad + \left(\mathfrak{M}_{C1}\right) \frac{1}{2} \sum_{de} \langle ab\tilde{c}||\hat{w}||dek\rangle \langle de|\hat{t}_2|ij\rangle \\
 &\quad - \left(\mathfrak{M}_{T_{jk}}^{T_{ik}}\right) \frac{1}{2} \hat{P}_{ij}(J) \sum_{de} \sum_{\mathcal{J}'\mathcal{J}''} \left\{ \begin{matrix} j_c & j_i & \mathcal{J}' \\ j_k & j_j & \mathcal{J}'' \end{matrix} \right\}_{J'J} \langle ab\tilde{c}||\hat{w}||dei\rangle \langle de|\hat{t}_2|kj\rangle \\
 &\quad + \left(\mathfrak{M}_{D1}\right) \frac{1}{2} \sum_{lm} \langle lm\tilde{c}||\hat{w}||ijk\rangle \langle ab|\hat{t}_2|lm\rangle \\
 &\quad + \left(\mathfrak{M}_{T_{bc}}^{T_{ac}}\right) \frac{1}{2} \hat{P}_{ab}(J') (-1)^{j_c+j_k-J''} \sum_{lm} \sum_{\mathcal{J}'\mathcal{J}''} (-1)^{J+\mathcal{J}'+\mathcal{J}''} \left\{ \begin{matrix} j_a & j_k & \mathcal{J}' \\ j_b & j_c & \mathcal{J}'' \end{matrix} \right\}_{J'J} \\
 &\quad \times \langle lm\tilde{a}||\hat{w}||ijk\rangle \langle bc|\hat{t}_2|lm\rangle \\
 &\quad + \dots
 \end{aligned}$$

 Figure G.10: Spherical expressions for the \hat{t} amplitudes of the Λ CCSD(T) energy correction for three-body Hamiltonians.

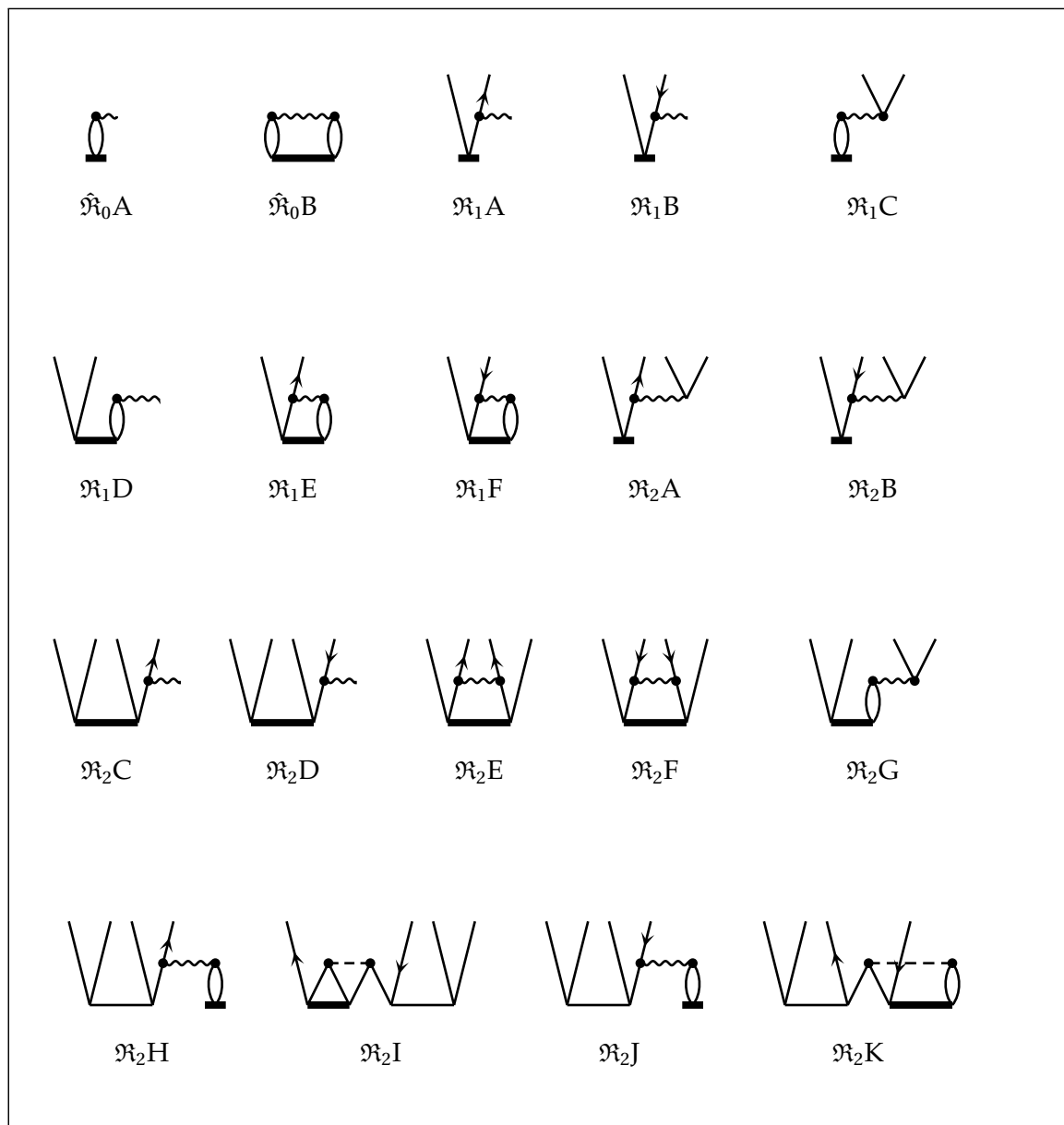
$$\begin{aligned}
 & \left(\mathfrak{M}_{E1} \right) \sum_{dl} (-1)^{j_d+j_l-J''} \langle ab\tilde{l} || \hat{w} || ijd \rangle \langle \tilde{c}\tilde{d} | \hat{t}_2 | kl \rangle \\
 & \quad \begin{array}{c} J' \quad J \quad J''M'' \\ \downarrow \quad \downarrow \quad \downarrow \\ \langle ab\tilde{l} || \hat{w} || ijd \rangle \langle \tilde{c}\tilde{d} | \hat{t}_2 | kl \rangle \\ \uparrow \quad \uparrow \quad \uparrow \\ J'' \quad J''M'' \end{array} \\
 & \left(\mathfrak{M}_{E1}^{T_{ik}} \right) \hat{P}_{ij}(J) \sum_{dl} \sum_{\mathcal{J}'\mathcal{J}''} (-1)^{j_d+j_l-\mathcal{J}''} \left\{ \begin{array}{ccc} j_j & j_k & \mathcal{J}' \\ j_i & j_c & \mathcal{J}'' \\ J & J'' & J' \end{array} \right\}_X \langle ab\tilde{l} || \hat{w} || kjd \rangle \langle \tilde{c}\tilde{d} | \hat{t}_2 | il \rangle \\
 & \quad \begin{array}{c} J' \quad \mathcal{J}' \quad \mathcal{J}''M'' \\ \downarrow \quad \downarrow \quad \downarrow \\ \langle ab\tilde{l} || \hat{w} || kjd \rangle \langle \tilde{c}\tilde{d} | \hat{t}_2 | il \rangle \\ \uparrow \quad \uparrow \quad \uparrow \\ \mathcal{J}'' \quad \mathcal{J}''M'' \end{array} \\
 & \left(\mathfrak{M}_{E1}^{T_{bc}} \right) \hat{P}_{ab}(J') (-1)^{j_a+j_b-J'} \sum_{dl} (-1)^{j_d+j_l-\mathcal{J}''} \left\{ \begin{array}{ccc} j_b & j_c & \mathcal{J}' \\ j_a & j_k & \mathcal{J}'' \\ J' & J'' & J \end{array} \right\}_X \\
 & \quad \times \langle bc\tilde{l} || \hat{w} || ijd \rangle \langle \tilde{a}\tilde{d} | \hat{t}_2 | kl \rangle \\
 & \quad \begin{array}{c} \mathcal{J}' \quad J \quad \mathcal{J}''M'' \\ \downarrow \quad \downarrow \quad \downarrow \\ \langle bc\tilde{l} || \hat{w} || ijd \rangle \langle \tilde{a}\tilde{d} | \hat{t}_2 | kl \rangle \\ \uparrow \quad \uparrow \quad \uparrow \\ \mathcal{J}'' \quad \mathcal{J}''M'' \end{array} \\
 & \left(\mathfrak{M}_{E1}^{T_{ik},T_{jk}} \right) \hat{P}_{ab}(J') \hat{P}_{ij}(J) (-1)^{j_a+j_b-J'} \sum_{dl} \sum_{\mathcal{J}'\mathcal{J}''\mathcal{J}'''} (-1)^{J''+\mathcal{J}'+\mathcal{J}'''} \\
 & \quad \times \hat{J} \hat{J}' \hat{\mathcal{J}}' (\hat{\mathcal{J}}'')^2 \hat{\mathcal{J}}''' \left\{ \begin{array}{ccc} \mathcal{J}' & \mathcal{J}'' & J' \\ j_a & j_b & j_i \end{array} \right\}_{6j} \left\{ \begin{array}{ccc} \mathcal{J}'' & \mathcal{J}''' & J \\ j_j & j_i & j_d \end{array} \right\}_{6j} \left\{ \begin{array}{ccc} J & J' & J'' \\ \mathcal{J}' & \mathcal{J}'' & \mathcal{J}''' \end{array} \right\}_{6j} \\
 & \quad \times \langle lb\tilde{c} || \hat{w} || jdk \rangle \langle \tilde{a}\tilde{d} | \hat{t}_2 | li \rangle \\
 & \quad \begin{array}{c} \mathcal{J}' \quad \mathcal{J}''' \quad \mathcal{J}''M'' \\ \downarrow \quad \downarrow \quad \downarrow \\ \langle lb\tilde{c} || \hat{w} || jdk \rangle \langle \tilde{a}\tilde{d} | \hat{t}_2 | li \rangle \\ \uparrow \quad \uparrow \quad \uparrow \\ J'' \quad \mathcal{J}''M'' \end{array} \\
 & \left(\mathfrak{M}_F \right) \langle ab\tilde{c} || \hat{w} || ijj \rangle \\
 & \quad \begin{array}{c} J' \quad J \\ \downarrow \quad \downarrow \\ \langle ab\tilde{c} || \hat{w} || ijj \rangle \\ \uparrow \quad \uparrow \\ J'' \end{array}
 \end{aligned}$$

 Figure G.11: Spherical expressions for the \hat{t} amplitudes of the Λ CCSD(T) energy correction for three-body Hamiltonians, continued.

Appendix H

EOM-CCSD Diagrams and Spherical Expressions

H.1 Diagrams


 Figure H.1: EOM-CCSD \mathfrak{R} diagrams.

H.2 Spherical Equations

$$\begin{aligned}
 \omega_\mu \hat{\mathfrak{R}}_0^{(J)} &= -^{(\mathfrak{R}_0\text{A})} \delta_{J0} \sum_{ai} \langle a || \hat{\mathfrak{R}}_1^{(J)} || i \rangle \overbrace{\langle i | \hat{\mathcal{H}}_1 | a \rangle}^{00} \\
 &+^{(\mathfrak{R}_0\text{B})} \delta_{J0} \frac{1}{4} \sum_{abij} \sum_{J'} \hat{J}' \overbrace{\langle ab || \hat{\mathfrak{R}}_2^{(J)} || ij \rangle}^{J'} \overbrace{\langle ij | \hat{\mathcal{H}}_2 | ab \rangle}^{J'} \overbrace{\langle ij | \hat{\mathcal{H}}_2 | ab \rangle}^{J'M'} \overbrace{\langle ij | \hat{\mathcal{H}}_2 | ab \rangle}^{J'M'} \\
 \langle a || (\hat{\mathcal{H}} \hat{\mathfrak{R}}^{(J)})_C || i \rangle &= -^{(\mathfrak{R}_1\text{A})} \hat{J}_a^{-1} \sum_c \overbrace{\langle \tilde{a} | \hat{\mathcal{H}}_1 | c \rangle}^{00} \langle c || \hat{\mathfrak{R}}_1^{(J)} || i \rangle \\
 &+^{(\mathfrak{R}_1\text{B})} \hat{J}_i^{-1} \sum_k \overbrace{\langle a || \hat{\mathfrak{R}}_1^{(J)} || k \rangle}^{00} \langle \tilde{k} | \hat{\mathcal{H}}_1 | i \rangle \\
 &-^{(\mathfrak{R}_1\text{C})} \sum_{ck} (-1)^{j_c+j_k-J} \overbrace{\langle \tilde{a} \tilde{k} | \hat{\mathcal{H}}_2 | ic \rangle}^{JM} \langle c || \hat{\mathfrak{R}}_1^{(J)} || k \rangle \\
 &+^{(\mathfrak{R}_1\text{D})} \sum_{ck} \hat{J}_c^{-1} \sum_{J'J''} (-1)^{J+J'+J''} \hat{J}' \hat{J}'' \left\{ \begin{matrix} J' & J'' & J \\ j_i & j_a & j_k \end{matrix} \right\}_{6j} \overbrace{\langle ca || \hat{\mathfrak{R}}_2^{(J)} || ik \rangle}^{J'} \overbrace{\langle \tilde{k} | \hat{\mathcal{H}}_1 | c \rangle}^{J''} \overbrace{\langle \tilde{k} | \hat{\mathcal{H}}_1 | c \rangle}^{00} \\
 &-^{(\mathfrak{R}_1\text{E})} \frac{1}{2} \sum_{cdk} \sum_{J'J''} (-1)^{J+J'+J''} \hat{J}' \hat{J}'' \left\{ \begin{matrix} J' & J'' & J \\ j_i & j_a & j_k \end{matrix} \right\}_{6j} \overbrace{\langle ka | \hat{\mathcal{H}}_2 | cd \rangle}^{J'M'} \overbrace{\langle cd || \hat{\mathfrak{R}}_2^{(J)} || ik \rangle}^{J'M'} \overbrace{\langle cd || \hat{\mathfrak{R}}_2^{(J)} || ik \rangle}^{J'} \overbrace{\langle cd || \hat{\mathfrak{R}}_2^{(J)} || ik \rangle}^{J''} \\
 &+^{(\mathfrak{R}_1\text{F})} \frac{1}{2} \sum_{ckl} \sum_{J'J''} (-1)^{J+J'+J''} \hat{J}' \hat{J}'' \left\{ \begin{matrix} J' & J'' & J \\ j_i & j_a & j_c \end{matrix} \right\}_{6j} \overbrace{\langle ca || \hat{\mathfrak{R}}_2^{(J)} || kl \rangle}^{J'} \overbrace{\langle kl | \hat{\mathcal{H}}_2 | ic \rangle}^{J''} \overbrace{\langle kl | \hat{\mathcal{H}}_2 | ic \rangle}^{J''M''} \overbrace{\langle kl | \hat{\mathcal{H}}_2 | ic \rangle}^{J''M''}
 \end{aligned}$$

Figure H.2: Spherical expressions for the EOM-CCSD $\hat{\mathfrak{R}}_0$ and $\hat{\mathfrak{R}}_1$ amplitude equations.

$$\begin{aligned}
 & \overset{J_{ab}}{\downarrow} \langle ab || (\hat{\mathcal{H}} \hat{\mathfrak{R}}^{(J)})_c || ij \rangle \overset{J_{ij}}{\downarrow} \\
 &= \hat{P}_{ab}(J) \hat{P}_{ij}(J) \left\{ \overset{(\mathfrak{R}_2^A)}{-} \frac{1}{2} (-1)^{J_{ab}+J_{ij}+J} \hat{J}_{ab} \hat{J}_{ij} \right. \\
 & \quad \times \sum_c \left\{ \overset{J}{j_j} \overset{J_{ab}}{j_i} \overset{J_{ij}}{j_c} \right\}_{6j} \langle c || \hat{\mathfrak{R}}_1^{(J)} || i \rangle \overset{J_{ab}M_{ab}}{\downarrow} \overset{J_{ab}M_{ab}}{\downarrow} \langle ab | \hat{\mathcal{H}}_2 | j c \rangle \\
 & \quad \overset{(\mathfrak{R}_2^B)}{-} \frac{1}{2} \hat{J}_{ab} \hat{J}_{ij} \sum_k (-1)^{j_a+j_k-J} \left\{ \overset{J}{j_b} \overset{J_{ij}}{j_a} \overset{J_{ab}}{j_k} \right\}_{6j} \overset{J_{ij}M_{ij}}{\downarrow} \overset{J_{ij}M_{ij}}{\downarrow} \langle a || \hat{\mathfrak{R}}_1^{(J)} || k \rangle \langle b k | \hat{\mathcal{H}}_2 | i j \rangle \\
 & \quad \overset{(\mathfrak{R}_2^C)}{-} \frac{1}{2} \hat{J}_b^{-1} \sum_c \overset{J_{ab}}{\downarrow} \langle a c || \hat{\mathfrak{R}}_2^{(J)} || i j \rangle \overset{J_{ij}}{\downarrow} \overset{00}{\downarrow} \langle \tilde{b} | \hat{\mathcal{H}}_1 | c \rangle \\
 & \quad \overset{(\mathfrak{R}_2^D)}{+} \frac{1}{2} \hat{J}_j^{-1} \sum_k \overset{J_{ab}}{\downarrow} \langle a b || \hat{\mathfrak{R}}_2^{(J)} || i k \rangle \overset{J_{ij}}{\downarrow} \overset{00}{\downarrow} \langle \tilde{k} | \hat{\mathcal{H}}_1 | j \rangle \\
 & \quad \overset{(\mathfrak{R}_2^E)}{+} \frac{1}{8} \sum_{cd} \overset{J_{ab}M_{ab}}{\downarrow} \overset{J_{ab}M_{ab}}{\downarrow} \overset{J_{ab}}{\downarrow} \langle a b | \hat{\mathcal{H}}_2 | c d \rangle \overset{J_{ij}}{\downarrow} \langle c d || \hat{\mathfrak{R}}_2^{(J)} || i j \rangle \\
 & \quad \overset{(\mathfrak{R}_2^F)}{+} \frac{1}{8} \sum_{kl} \overset{J_{ab}}{\downarrow} \langle a b || \hat{\mathfrak{R}}_2^{(J)} || k l \rangle \overset{J_{ij}}{\downarrow} \overset{J_{ij}M_{ij}}{\downarrow} \overset{J_{ij}M_{ij}}{\downarrow} \langle k l | \hat{\mathcal{H}}_2 | i j \rangle \left. \right\} \\
 & \quad \overset{(\mathfrak{R}_2^G)}{-} \text{CCAtoStd}^{(A)} \left[\begin{matrix} ab J_{ab}; J_{ai} \\ ij J_{ij}; J_{bj} \end{matrix} \right] \sum_{ck} (-1)^{j_c+j_k-J_{bj}} \overset{J_{ai}}{\downarrow} \overset{J_{bj}M_{bj}}{\downarrow} \langle \tilde{a} \tilde{c} || \hat{\mathfrak{R}}_2^{(J)} || i k \rangle \overset{J_{bj}}{\uparrow} \overset{J_{bj}M_{bj}}{\uparrow} \langle \tilde{b} \tilde{k} | \hat{\mathcal{H}}_2 | j c \rangle \\
 & \quad \overset{(\mathfrak{R}_2^H)}{+} \frac{1}{2} \hat{P}_{ab}(J) \hat{P}_{ij}(J) (-1)^{J+J_{ab}+J_{ij}} \hat{J}_{ab} \hat{J}_{ij} \\
 & \quad \times \sum_{cdk} (-1)^{j_d+j_k-J} \left\{ \overset{J}{j_a} \overset{J_{ij}}{j_b} \overset{J_{ab}}{j_c} \right\}_{6j} \overset{J_{ij}M_{ij}}{\downarrow} \overset{J_{ij}M_{ij}}{\downarrow} \overset{JM}{\downarrow} \langle c a | \hat{\mathcal{H}}_2 | i j \rangle \overset{JM}{\uparrow} \langle \tilde{b} \tilde{k} | \hat{\mathcal{H}}_2 | c d \rangle \langle d || \hat{\mathfrak{R}}_1^{(J)} || k \rangle + \dots
 \end{aligned}$$

 Figure H.3: Spherical expressions for the EOM-CCSD $\hat{\mathfrak{R}}_2$ amplitude equations.

$$\begin{aligned}
 & + \hat{P}_{ab}(J) \hat{P}_{ij}(J) \left\{ \right. \\
 & \quad \stackrel{(\mathfrak{R}_2\text{I})}{+} \frac{1}{4} (-1)^{j_a+j_b-J_{ij}} \hat{J}_{ab} \hat{J}_{ij} \sum_{cdkl} \sum_{J'J''} \hat{J}' \hat{J}'' (-1)^{J'+J''} \\
 & \quad \times \left\{ \begin{matrix} J & J_{ij} & J_{ab} \\ j_b & j_a & j_c \end{matrix} \right\}_{6j} \left\{ \begin{matrix} J' & J'' & J \\ j_c & j_a & j_d \end{matrix} \right\}_{6j} \langle \overset{J'}{\downarrow} d a || \hat{\mathfrak{R}}_2^{(J)} || \overset{J''}{\downarrow} k l \rangle \langle \overset{J''}{\downarrow} k l | \overset{J''M''}{\downarrow} \hat{v} | \overset{J''M''}{\downarrow} c d \rangle \langle \overset{J_{ij}M_{ij}}{\downarrow} c b | \overset{J_{ij}M_{ij}}{\downarrow} \hat{t}_2 | \overset{J_{ij}M_{ij}}{\downarrow} i j \rangle \\
 & \quad \stackrel{(\mathfrak{R}_2\text{I})}{+} \frac{1}{2} (-1)^{j_i+j_j-J_{ij}} (-1)^{J_{ab}+J_{ij}} \hat{J}_{ab} \hat{J}_{ij} \\
 & \quad \times \sum_{klc} (-1)^{j_c+j_l} \left\{ \begin{matrix} J & J_{ab} & J_{ij} \\ j_i & j_j & j_k \end{matrix} \right\}_{6j} \langle \overset{J_{ab}M_{ab}}{\downarrow} a b | \overset{J_{ab}M_{ab}}{\downarrow} \hat{t}_2 | \overset{J_{ab}M_{ab}}{\downarrow} i k \rangle \langle \overset{JM}{\downarrow} \tilde{k} \tilde{l} | \overset{JM}{\downarrow} \hat{\mathcal{H}}_2 | \overset{JM}{\downarrow} j c \rangle \langle c || \hat{\mathfrak{R}}_1^{(J)} || l \rangle \\
 & \quad \stackrel{(\mathfrak{R}_2\text{K})}{-} \frac{1}{4} (-1)^{J_{ab}+J_{ij}} \hat{J}_{ab} \hat{J}_{ij} \\
 & \quad \times \sum_{klcd} \sum_{J'J''} \hat{J}' \hat{J}'' (-1)^{J'+J''} \left\{ \begin{matrix} J & J_{ab} & J_{ij} \\ j_j & j_i & j_k \end{matrix} \right\}_{6j} \left\{ \begin{matrix} J' & J'' & J \\ j_k & j_i & j_l \end{matrix} \right\}_{6j} \\
 & \quad \times \left\{ \langle \overset{J''}{\downarrow} c d || \hat{\mathfrak{R}}_2^{(J)} || \overset{J''}{\downarrow} i l \rangle \langle \overset{J'}{\downarrow} l k | \overset{J''M''}{\downarrow} \hat{v} | \overset{J''M''}{\downarrow} c d \rangle \langle \overset{J_{ab}M_{ab}}{\downarrow} a b | \overset{J_{ab}M_{ab}}{\downarrow} \hat{t}_2 | \overset{J_{ab}M_{ab}}{\downarrow} j k \rangle \right\}
 \end{aligned}$$

 Figure H.4: Spherical expressions for the EOM-CCSD $\hat{\mathfrak{R}}_2$ amplitude equations, continued.

$$\begin{aligned}
 & \langle i || \hat{\mathcal{L}}^{(J)} \mathcal{H}_{\text{open}} || a \rangle \\
 &= - \stackrel{(\mathfrak{s}_1\text{B})}{\hat{f}_a^{-1}} \sum_c \langle i || \hat{\mathcal{L}}_1^{(J)} || c \rangle \overbrace{\langle \tilde{c} | \mathcal{H}_1 | a \rangle}^{00} \\
 &+ \stackrel{(\mathfrak{s}_1\text{C})}{\hat{f}_i^{-1}} \sum_k \overbrace{\langle \tilde{i} | \mathcal{H}_1 | k \rangle}^{00} \langle k || \hat{\mathcal{L}}_1^{(J)} || a \rangle \\
 &- \stackrel{(\mathfrak{s}_1\text{D})}{\sum_{ck}} (-1)^{j_c+j_k-J} \overbrace{\langle \tilde{c} \tilde{i} | \mathcal{H}_2 | k a \rangle}^{JM} \langle k || \hat{\mathcal{L}}_1^{(J)} || c \rangle \\
 &- \stackrel{(\mathfrak{s}_1\text{E})}{\frac{1}{2}} \sum_{cdk} \sum_{J'J''} (-1)^{J+J'+J''} \hat{f}' \hat{f}'' \left\{ \begin{matrix} J' & J'' & J \\ j_a & j_i & j_k \end{matrix} \right\}_{6j} \overbrace{\langle k i || \hat{\mathcal{L}}_2^{(J)} || cd \rangle}^{J'} \overbrace{\langle cd | \mathcal{H}_2 | ak \rangle}^{J''} \overbrace{\langle cd | \mathcal{H}_2 | ak \rangle}^{J''M''} \overbrace{\langle cd | \mathcal{H}_2 | ak \rangle}^{J''M''} \\
 &+ \stackrel{(\mathfrak{s}_1\text{F})}{\frac{1}{2}} \sum_{ckl} \sum_{J'J''} (-1)^{J+J'+J''} \hat{f}' \hat{f}'' \left\{ \begin{matrix} J' & J'' & J \\ j_a & j_i & j_c \end{matrix} \right\}_{6j} \overbrace{\langle c i | \mathcal{H}_2 | kl \rangle}^{J'M'} \overbrace{\langle kl || \hat{\mathcal{L}}_2^{(J)} || ac \rangle}^{J''} \overbrace{\langle kl || \hat{\mathcal{L}}_2^{(J)} || ac \rangle}^{J''} \overbrace{\langle kl || \hat{\mathcal{L}}_2^{(J)} || ac \rangle}^{J''} \\
 &- \stackrel{(\mathfrak{s}_1\text{G})}{\frac{1}{2}} \sum_{cdek l} \sum_{J'J''} \hat{f}' \hat{f}'' \left\{ \begin{matrix} J' & J'' & J \\ j_d & j_e & j_c \end{matrix} \right\}_{6j} \overbrace{\langle e c | \hat{t}_2 | kl \rangle}^{J'M'} \overbrace{\langle \tilde{d} \tilde{i} | \mathcal{H}_2 | ea \rangle}^{JM} \overbrace{\langle kl || \hat{\mathcal{L}}_2^{(J)} || cd \rangle}^{J'} \overbrace{\langle kl || \hat{\mathcal{L}}_2^{(J)} || cd \rangle}^{J''} \overbrace{\langle kl || \hat{\mathcal{L}}_2^{(J)} || cd \rangle}^{J''} \\
 &+ \stackrel{(\mathfrak{s}_1\text{H})}{\frac{1}{2}} \sum_{cdk l m} \sum_{J'J''} \hat{f}' \hat{f}'' \left\{ \begin{matrix} J' & J'' & J \\ j_m & j_l & j_k \end{matrix} \right\}_{6j} \overbrace{\langle l k || \hat{\mathcal{L}}_2^{(J)} || cd \rangle}^{J'} \overbrace{\langle cd | \hat{t}_2 | km \rangle}^{J''} \overbrace{\langle \tilde{m} \tilde{i} | \mathcal{H}_2 | la \rangle}^{JM} \overbrace{\langle \tilde{m} \tilde{i} | \mathcal{H}_2 | la \rangle}^{JM} \overbrace{\langle \tilde{m} \tilde{i} | \mathcal{H}_2 | la \rangle}^{JM}
 \end{aligned}$$

 Figure H.5: Spherical expressions for the EOM-CCSD $\hat{\mathcal{L}}_1$ amplitude equations.

$$\begin{aligned}
 & \begin{array}{c} J_{ij} \\ \overline{\downarrow} \\ \langle ij || \hat{\mathcal{L}}^{(J)} \mathcal{H}_{\text{open}} || ab \rangle \end{array} \begin{array}{c} J_{ab} \\ \overline{\downarrow} \end{array} \\
 &= \hat{P}_{ab}(J) \hat{P}_{ij}(J) \left\{ \right. \\
 & \quad \begin{array}{l} \text{(\mathfrak{L}_2B)} \quad (-1)^J \hat{f}_{ij} \hat{f}_{ab} (-1)^{j_i+j_b-J_{ij}} \hat{f}_i^{-1} \left\{ \begin{array}{c} J_{ab} \quad J_{ij} \quad J \\ j_j \quad j_b \quad j_a \end{array} \right\}_{6j} \overline{\begin{array}{c} 00 \\ \downarrow \\ \langle i || \hat{\mathcal{L}}_1 || a \rangle \end{array}} \langle j || \hat{\mathcal{L}}_1^{(J)} || b \rangle \\ \\ \text{(\mathfrak{L}_2C)} \quad \frac{1}{2} \hat{f}_{ij} \hat{f}_{ab} (-1)^{j_i+j_j-J} (-1)^{J_{ab}} \sum_c \left\{ \begin{array}{c} J \quad J_{ab} \quad J_{ij} \\ j_j \quad j_i \quad j_c \end{array} \right\}_{6j} \overline{\begin{array}{c} J_{ab} M_{ab} \quad J_{ab} M_{ab} \\ \downarrow \quad \downarrow \\ \langle i || \hat{\mathcal{L}}_1^{(J)} || c \rangle \langle c j || \hat{\mathcal{L}}_2 || ab \rangle \end{array}} \\ \\ \text{(\mathfrak{L}_2D)} \quad \frac{1}{2} (-1)^{J_{ab}+J_{ij}+J} \hat{f}_{ij} \hat{f}_{ab} \sum_k \left\{ \begin{array}{c} J \quad J_{ij} \quad J_{ab} \\ j_b \quad j_a \quad j_k \end{array} \right\}_{6j} \overline{\begin{array}{c} J_{ij} M_{ij} \quad J_{ij} M_{ij} \\ \downarrow \quad \downarrow \\ \langle k || \hat{\mathcal{L}}_1^{(J)} || a \rangle \langle i j || \hat{\mathcal{L}}_2 || b k \rangle \end{array}} \\ \\ \text{(\mathfrak{L}_2E)} \quad \frac{1}{2} \hat{f}_b^{-1} \sum_c \begin{array}{c} J_{ij} \\ \overline{\downarrow} \\ \langle i j || \hat{\mathcal{L}}_2^{(J)} || ac \rangle \end{array} \overline{\begin{array}{c} J_{ab} \\ \overline{\downarrow} \\ \langle \bar{c} || \hat{\mathcal{L}}_1 || b \rangle \end{array}} \\ \\ \text{(\mathfrak{L}_2F)} \quad \frac{1}{2} (-1)^{j_i+j_j-J_{ij}} \hat{f}_j^{-1} \sum_k \begin{array}{c} J_{ij} \\ \overline{\downarrow} \\ \langle k i || \hat{\mathcal{L}}_2^{(J)} || ab \rangle \end{array} \overline{\begin{array}{c} J_{ab} \\ \overline{\downarrow} \\ \langle \bar{j} || \hat{\mathcal{L}}_1 || k \rangle \end{array}} \left\{ \right. \\ \\ \text{(\mathfrak{L}_2G)} \quad \text{CCAtoStd}^{(A)} \left[\begin{array}{c} i j J_{ij}; J_{ai} \\ ab J_{ab}; J_{bj} \end{array} \right] \sum_{ck} (-1)^{j_c+j_k-J_{bj}} \overline{\begin{array}{c} J_{ai} \\ \downarrow \\ \langle i \bar{k} || \hat{\mathcal{L}}_2^{(J)} || ac \rangle \end{array}} \overline{\begin{array}{c} J_{bj} M_{bj} \\ \downarrow \\ \langle \bar{c} \bar{j} || \hat{\mathcal{L}}_2 || k b \rangle \end{array}} \\ \\ + \hat{P}_{ab}(J) \hat{P}_{ij}(J) \left\{ \right. \\ \\ \text{(\mathfrak{L}_2H)} \quad \frac{1}{8} \sum_{cd} \begin{array}{c} J_{ij} \\ \overline{\downarrow} \\ \langle i j || \hat{\mathcal{L}}_2^{(J)} || cd \rangle \end{array} \overline{\begin{array}{c} J_{ab} \quad J_{ab} M_{ab} \quad J_{ab} M_{ab} \\ \downarrow \quad \downarrow \quad \downarrow \\ \langle c d || \hat{\mathcal{L}}_2 || ab \rangle \end{array}} \\ \\ \text{(\mathfrak{L}_2I)} \quad \frac{1}{8} \sum_{kl} \begin{array}{c} J_{ij} M_{ij} \quad J_{ij} M_{ij} \quad J_{ij} \\ \overline{\downarrow} \quad \overline{\downarrow} \quad \overline{\downarrow} \\ \langle i j || \hat{\mathcal{L}}_2 || kl \rangle \end{array} \overline{\begin{array}{c} J_{ab} \\ \overline{\downarrow} \\ \langle k l || \hat{\mathcal{L}}_2^{(J)} || ab \rangle \end{array}} \left\{ \right. + \dots
 \end{aligned}$$

 Figure H.6: Spherical expressions for the EOM-CCSD $\hat{\mathcal{L}}_2$ amplitude equations.

$$\begin{aligned}
 & + \hat{P}_{ab}(J) \hat{P}_{ij}(J) \left\{ \right. \\
 & \quad - \stackrel{(S_2)}{\frac{1}{4}} (-1)^{J_{ij}+J_{ab}} \hat{f}_{ij} \hat{f}_{ab} \\
 & \quad \times \sum_{cdkl} \sum_{J'J''} (-1)^{J'+J''} \hat{f}' \hat{f}'' \left\{ \begin{matrix} J & J_{ij} & J_{ab} \\ j_b & j_a & j_d \end{matrix} \right\}_{6j} \left\{ \begin{matrix} J' & J'' & J \\ j_a & j_d & j_c \end{matrix} \right\}_{6j} \\
 & \quad \times \begin{matrix} J'M' & J'M' & J' & J'' & J_{ij}M_{ij} & J_{ij}M_{ij} \\ \downarrow & \downarrow & \downarrow & \downarrow & \downarrow & \downarrow \\ \langle cd | \hat{t}_2 | kl \rangle & \langle kl | \hat{\mathcal{L}}_2^{(J)} | ac \rangle & \langle ij | \hat{v} | bd \rangle \end{matrix} \\
 & \quad + \stackrel{(S_2K)}{\frac{1}{4}} (-1)^{J_i+J_j-J_{ab}} \hat{f}_{ab} \hat{f}_{ij} \\
 & \quad \times \sum_{cdkl} \sum_{J'J''} \hat{f}' \hat{f}'' (-1)^{J'+J''} \left\{ \begin{matrix} J & J_{ab} & J_{ij} \\ j_j & j_i & j_l \end{matrix} \right\}_{6j} \left\{ \begin{matrix} J' & J'' & J \\ j_i & j_l & j_k \end{matrix} \right\}_{6j} \\
 & \quad \times \begin{matrix} J'M' & J'M' & J'' & J' & J_{ab}M_{ab} & J_{ab}M_{ab} \\ \downarrow & \downarrow & \downarrow & \downarrow & \downarrow & \downarrow \\ \langle cd | \hat{t}_2 | lk \rangle & \langle ki | \hat{\mathcal{L}}_2^{(J)} | cd \rangle & \langle lj | \hat{v} | ab \rangle \end{matrix} \left. \right\}
 \end{aligned}$$

 Figure H.7: Spherical expressions for the EOM-CCSD $\hat{\mathcal{L}}_2$ amplitude equations, continued.

H.3 Spherical Equations (Scalar)

$$\begin{aligned}
 \omega \hat{\mathfrak{R}}^{(0)} &= - \sum_{ai}^{(\mathfrak{R}_0\text{A})} \langle a || \hat{\mathfrak{R}}_1^{(0)} || i \rangle \overbrace{\langle \tilde{i} | \hat{\mathcal{H}}_1 | a \rangle}^{00} \\
 &+ \sum_{abij}^{(\mathfrak{R}_0\text{B})} \frac{1}{4} \sum_J \hat{J} \overbrace{\langle ab || \hat{\mathfrak{R}}_2^{(0)} || ij \rangle}^J \overbrace{\langle ij | \hat{\mathcal{H}}_2 | ab \rangle}^{JM} \\
 \langle \tilde{a} || (\hat{\mathcal{H}} \hat{\mathfrak{R}}^{(0)})_C || i \rangle &= - \sum_a^{(\mathfrak{R}_1\text{A})} \hat{J}_a^{-1} \overbrace{\langle \tilde{a} | \hat{\mathcal{H}}_1 | c \rangle}^{00} \langle c || \hat{\mathfrak{R}}_1^{(0)} || i \rangle \\
 &+ \sum_a^{(\mathfrak{R}_1\text{B})} \hat{J}_a^{-1} \sum_k \langle a || \hat{\mathfrak{R}}_1^{(0)} || k \rangle \overbrace{\langle \tilde{k} | \hat{\mathcal{H}}_1 | i \rangle}^{00} \\
 &+ \sum_{ck}^{(\mathfrak{R}_1\text{C})} \overbrace{\langle \tilde{a} \tilde{k} | \hat{\mathcal{H}}_2 | ic \rangle}^{00} \langle c || \hat{\mathfrak{R}}_1^{(0)} || k \rangle \\
 &- \sum_{ck}^{(\mathfrak{R}_1\text{D})} \overbrace{\langle \tilde{a} \tilde{c} || \hat{\mathfrak{R}}_2^{(0)} || ik \rangle}^{00} \overbrace{\langle \tilde{k} | \hat{\mathcal{H}}_1 | c \rangle}^{00} \\
 &+ \sum_{cdk}^{(\mathfrak{R}_1\text{E})} \frac{1}{2} \hat{J}_a^{-1} \sum_J \hat{J} \overbrace{\langle ak | \hat{\mathcal{H}}_2 | cd \rangle}^{JM} \overbrace{\langle cd || \hat{\mathfrak{R}}_2^{(0)} || ik \rangle}^{JM} \\
 &- \sum_{ckl}^{(\mathfrak{R}_1\text{F})} \frac{1}{2} \hat{J}_a^{-1} \sum_J \hat{J} \overbrace{\langle ac || \hat{\mathfrak{R}}_2^{(0)} || kl \rangle}^J \overbrace{\langle kl | \hat{\mathcal{H}}_2 | ic \rangle}^{JM}
 \end{aligned}$$

Figure H.8: Spherical expressions for the scalar EOM-CCSD $\hat{\mathfrak{R}}_0$ and $\hat{\mathfrak{R}}_2$ amplitudes.

$$\begin{aligned}
 & \langle ab || (\hat{\mathcal{H}} \hat{\mathfrak{R}}^{(0)})_c || ij \rangle \\
 &= \hat{P}_{ab}(J) \hat{P}_{ij}(J) \left\{ \begin{aligned} & \stackrel{(\mathfrak{R}_2^A)}{+} \frac{1}{2} \hat{J} \hat{J}_i^{-1} \sum_c \langle c || \hat{\mathfrak{R}}_1^{(0)} || i \rangle \langle ab | \hat{\mathcal{H}}_2 | c j \rangle \\ & \stackrel{(\mathfrak{R}_2^B)}{-} \frac{1}{2} \hat{J} \hat{J}_a^{-1} \sum_k \langle a || \hat{\mathfrak{R}}_1^{(0)} || k \rangle \langle kb | \hat{\mathcal{H}}_2 | ij \rangle \\ & \stackrel{(\mathfrak{R}_2^C)}{-} \frac{1}{2} \hat{J}_b^{-1} \sum_c \langle ac || \hat{\mathfrak{R}}_2^{(0)} || ij \rangle \langle \tilde{b} | \hat{\mathcal{H}}_1 | c \rangle \stackrel{00}{\overbrace{\phantom{\langle \tilde{b} | \hat{\mathcal{H}}_1 | c \rangle}} + \frac{1}{2} \hat{J}_j^{-1} \sum_k \langle ab || \hat{\mathfrak{R}}_2^{(0)} || ik \rangle \langle \tilde{k} | \hat{\mathcal{H}}_1 | j \rangle \\ & \stackrel{(\mathfrak{R}_2^E)}{+} \frac{1}{8} \sum_{cd} \langle ab | \hat{\mathcal{H}}_2 | cd \rangle \langle cd || \hat{\mathfrak{R}}_2^{(0)} || ij \rangle \stackrel{(\mathfrak{R}_2^F)}{+} \frac{1}{8} \sum_{kl} \langle ab || \hat{\mathfrak{R}}_2^{(0)} || kl \rangle \langle kl | \hat{\mathcal{H}}_2 | ij \rangle \end{aligned} \right\} \\
 & \stackrel{(\mathfrak{R}_2^G)}{-} \text{CCAtoStd}^{(A)} \left[\begin{array}{c} ab \\ ij \end{array} J; J' \right] \\
 & \quad \times \hat{J} (\hat{J}')^{-1} \sum_{ck} (-1)^{j_c + j_k - J'} \langle \tilde{a} \tilde{c} || \hat{\mathfrak{R}}_2^{(0)} || ik \rangle \langle \tilde{b} \tilde{k} | \hat{\mathcal{H}}_2 | jc \rangle \\
 & \quad + \hat{P}_{ab}(J) \hat{P}_{ij}(J) \left\{ \begin{aligned} & \stackrel{(\mathfrak{R}_2^H)}{+} \frac{1}{2} \hat{J} \hat{J}_b^{-2} \sum_{cdk} \hat{J}_d^{-1} \sum_{J'} (\hat{J}')^2 \langle ac | \hat{t}_2 | ij \rangle \langle bk | \hat{\mathcal{H}}_2 | cd \rangle \langle d || \hat{\mathfrak{R}}_1^{(0)} || k \rangle \delta_{jbjc} \\ & \stackrel{(\mathfrak{R}_2^I)}{-} \frac{1}{4} \hat{J} \hat{J}_a^{-2} \sum_{cdkl} \sum_{J'} \hat{J}' \langle ad || \hat{\mathfrak{R}}_2^{(0)} || kl \rangle \langle kl | \hat{v} | cd \rangle \langle cb | \hat{t}_2 | ij \rangle \delta_{jajc} \\ & \stackrel{(\mathfrak{R}_2^J)}{-} \frac{1}{2} \hat{J} \hat{J}_j^{-2} \sum_{ckl} \hat{J}_c^{-1} \sum_{J'} (\hat{J}')^2 \langle c || \hat{\mathfrak{R}}_1^{(0)} || l \rangle \langle ab | \hat{t}_2 | ik \rangle \langle kl | \hat{\mathcal{H}}_2 | jc \rangle \delta_{jkj} \\ & \stackrel{(\mathfrak{R}_2^K)}{-} \frac{1}{4} \hat{J} \hat{J}_i^{-2} \sum_{cdkl} \sum_{J'} \hat{J}' \langle kl | \hat{v} | cd \rangle \langle cd || \hat{\mathfrak{R}}_2^{(0)} || il \rangle \langle ab | \hat{t}_2 | kj \rangle \delta_{jijk} \end{aligned} \right\}
 \end{aligned}$$

 Figure H.9: Spherical expressions for the scalar EOM-CCSD $\hat{\mathfrak{R}}_2$ amplitude equations.

$$\begin{aligned}
 & \langle i || \hat{\mathcal{L}}^{(0)} \mathcal{H}_{\text{open}} || a \rangle \\
 &= \begin{matrix} (s_1B) \\ - \end{matrix} \hat{J}_i^{-1} \sum_c \langle i || \hat{\mathcal{L}}_1^{(0)} || c \rangle \overbrace{\langle \bar{c} | \mathcal{H}_1 | a \rangle}^{00} \\
 & \quad \begin{matrix} (s_1C) \\ + \end{matrix} \hat{J}_i^{-1} \sum_k \overbrace{\langle \bar{i} | \mathcal{H}_1 | k \rangle}^{00} \langle k || \hat{\mathcal{L}}_1^{(0)} || a \rangle \\
 & \quad \begin{matrix} (s_1D) \\ + \end{matrix} \sum_{ck} \overbrace{\langle \bar{c} \bar{i} | \mathcal{H}_2 | k a \rangle}^{00} \underbrace{\langle k || \hat{\mathcal{L}}_1^{(0)} || c \rangle}_{00} \\
 & \quad \begin{matrix} (s_1E) \\ + \end{matrix} \frac{1}{2} \hat{J}_i^{-1} \sum_{cdk} \sum_J \hat{J} \overbrace{\langle i k || \hat{\mathcal{L}}_2^{(0)} || c d \rangle}^J \overbrace{\langle c d | \mathcal{H}_2 | a k \rangle}^{JM} \\
 & \quad \begin{matrix} (s_1F) \\ - \end{matrix} \frac{1}{2} \hat{J}_i^{-1} \sum_{ckl} \sum_J \hat{J} \overbrace{\langle i c | \mathcal{H}_2 | k l \rangle}^{JM} \overbrace{\langle k l || \hat{\mathcal{L}}_2^{(0)} || a c \rangle}^J \\
 & \quad \begin{matrix} (s_1G) \\ + \end{matrix} \frac{1}{2} \sum_{cdek l} \hat{J}_d^{-1} \sum_J \hat{J} \overbrace{\langle \bar{d} \bar{i} | \mathcal{H}_2 | e a \rangle}^{00} \overbrace{\langle c e | \hat{t}_2 | k l \rangle}^{JM} \overbrace{\langle k l || \hat{\mathcal{L}}_2^{(0)} || c d \rangle}^J \\
 & \quad \begin{matrix} (s_1H) \\ - \end{matrix} \frac{1}{2} \sum_{cdk l m} \hat{J}_l^{-1} \sum_J \hat{J} \overbrace{\langle k l || \hat{\mathcal{L}}_2^{(0)} || c d \rangle}^J \overbrace{\langle c d | \hat{t}_2 | k m \rangle}^{JM} \overbrace{\langle \bar{m} \bar{i} | \mathcal{H}_2 | l a \rangle}^{00}
 \end{aligned}$$

 Figure H.10: Spherical expressions for the scalar EOM-CCSD $\hat{\mathcal{L}}_1$ amplitude equations.

$$\begin{aligned}
 & \overset{J}{\downarrow} \langle ij || \hat{\mathcal{L}}^{(0)} \mathcal{H}_{\text{open}} || ab \rangle \overset{J}{\downarrow} \\
 & -^{(\mathfrak{s}_2\text{B})} \text{CCAtoStd}^{(A)} \left[\begin{matrix} ab \\ ij \end{matrix} J; J' \right] \hat{J} \overset{00}{\downarrow} \langle \tilde{i} | \mathcal{H}_1 | a \rangle \langle j || \hat{\mathcal{L}}_1^{(0)} || b \rangle \delta_{J'0} \\
 & \hat{P}_{ab}(J) \hat{P}_{ij}(J) \left\{ \right. \\
 & +^{(\mathfrak{s}_2\text{C})} \frac{1}{2} \hat{J} \hat{J}_i^{-1} \sum_c \langle i || \hat{\mathcal{L}}_1^{(0)} || c \rangle \overset{JM}{\downarrow} \langle c j | \mathcal{H}_2 | ab \rangle \overset{JM}{\downarrow} -^{(\mathfrak{s}_2\text{D})} \frac{1}{2} \hat{J} \hat{J}_a^{-1} \sum_k \langle k || \hat{\mathcal{L}}_1^{(0)} || a \rangle \overset{JM}{\downarrow} \langle i j | \mathcal{H}_2 | kb \rangle \overset{JM}{\downarrow} \\
 & -^{(\mathfrak{s}_2\text{E})} \frac{1}{2} \hat{J}_b^{-1} \sum_c \overset{J}{\downarrow} \langle i j || \hat{\mathcal{L}}_2^{(0)} || ac \rangle \overset{J}{\downarrow} \overset{00}{\downarrow} \langle \tilde{c} | \mathcal{H}_1 | b \rangle -^{(\mathfrak{s}_2\text{F})} \frac{1}{2} \hat{J}_j^{-1} \sum_k \overset{J}{\downarrow} \langle i k | \hat{\mathcal{L}}_2^{(0)} | ab \rangle \overset{J}{\downarrow} \overset{00}{\downarrow} \langle \tilde{j} | \mathcal{H}_1 | k \rangle \left. \right\} \\
 & -^{(\mathfrak{s}_2\text{G})} \text{CCAtoStd}^{(A)} \left[\begin{matrix} ij \\ ab \end{matrix} J; J' \right] \\
 & \times \hat{J} (\hat{J}')^{-1} \sum_{ck} (-1)^{j_c + j_k - J'} \overset{J'}{\downarrow} \langle \tilde{i} \tilde{k} || \hat{\mathcal{L}}_2^{(0)} || ac \rangle \overset{J'M'}{\downarrow} \langle \tilde{c} \tilde{j} | \mathcal{H}_2 | kb \rangle \\
 & \hat{P}_{ab}(J) \hat{P}_{ij}(J) \left\{ \right. \\
 & +^{(\mathfrak{s}_2\text{H})} \frac{1}{8} \sum_{cd} \overset{J}{\downarrow} \langle i j || \hat{\mathcal{L}}_2^{(0)} || cd \rangle \overset{J}{\downarrow} \overset{JM}{\downarrow} \langle cd | \mathcal{H}_2 | ab \rangle \overset{JM}{\downarrow} \\
 & +^{(\mathfrak{s}_2\text{I})} \frac{1}{8} \sum_{kl} \overset{JM}{\downarrow} \langle i j | \mathcal{H}_2 | kl \rangle \overset{J}{\downarrow} \langle kl || \hat{\mathcal{L}}_2^{(0)} || ab \rangle \overset{J}{\downarrow} \\
 & -^{(\mathfrak{s}_2\text{J})} \frac{1}{4} \hat{J} \hat{J}_a^{-2} \sum_{cdkl} \sum_{J'} \hat{J}' \overset{J'M'}{\downarrow} \langle cd | \hat{t}_2 | kl \rangle \overset{J'M'}{\downarrow} \langle kl || \hat{\mathcal{L}}_2^{(0)} || ca \rangle \overset{J'}{\downarrow} \langle i j | \hat{v} | db \rangle \overset{JM}{\downarrow} \delta_{ja jd} \\
 & -^{(\mathfrak{s}_2\text{K})} \frac{1}{4} \hat{J} \hat{J}_i^{-2} \sum_{cdkl} \sum_{J'} \hat{J}' \overset{J'}{\downarrow} \langle k i || \hat{\mathcal{L}}_2^{(0)} || cd \rangle \overset{J'}{\downarrow} \overset{J'M'}{\downarrow} \langle cd | \hat{t}_2 | kl \rangle \overset{J'M'}{\downarrow} \langle l j | \hat{v} | ab \rangle \overset{JM}{\downarrow} \delta_{ji jl} \left. \right\}
 \end{aligned}$$

 Figure H.11: Spherical expressions for the scalar EOM-CCSD $\hat{\mathcal{L}}_2$ amplitude equations.

Appendix I

Publications

The following articles originated during the course of this dissertation:

Peer-Reviewed Journals:

1. R. Roth, J. Langhammer, A. Calci, S. Binder, P. Navrátil:
"Similarity-Transformed Chiral NN+3N Interactions for the Ab Initio Description of ^{12}C and ^{16}O "
Phys. Rev. Lett. **107**, 072501 (2011)
2. R. Roth, S. Binder, K. Vobig, A. Calci, J. Langhammer, P. Navrátil:
"Ab Initio Calculations of Medium-Mass Nuclei with Normal-Ordered Chiral NN+3N Interactions",
Phys. Rev. Lett **109**, 052501 (2012)
3. S. Binder, J. Langhammer, A. Calci, P. Navrátil, R. Roth:
"Ab Initio Calculations of Medium-Mass Nuclei with Explicit Chiral 3N Interactions"
Phys. Rev. C **87**, 021303(R) (2013) - Editors' Suggestion
4. H. Hergert, S. K. Bogner, S. Binder, A. Calci, J. Langhammer, R. Roth, A. Schwenk:
"In-Medium Similarity Renormalization Group with Chiral Two- Plus Three-Nucleon Interactions"
Phys. Rev. C **87**, 034307 (2013)
5. H. Hergert, S. Binder, A. Calci, J. Langhammer, R. Roth:
"Ab Initio Calculations of Even Oxygen Isotopes with Chiral Two- Plus Three-Nucleon Interactions"
Phys. Rev. Lett. **110**, 242501 (2013)
6. S. Binder, P. Piecuch, A. Calci, J. Langhammer, P. Navrátil, R. Roth:
"Extension of coupled-cluster theory with a non-iterative treatment of connected triply excited clusters to three-body Hamiltonians"
Phys. Rev. C **88**, 054319 (2013)

7. R. Roth, A. Calci, J. Langhammer, S. Binder:
"Evolved Chiral NN+3N Hamiltonians for Ab Initio Nuclear Structure Calculations"
submitted to Phys. Rev. C
8. S. Binder, J. Langhammer, A. Calci, R. Roth:
"Ab Initio Path to Heavy Nuclei"
submitted to Phys. Rev. Lett.

Peer-Reviewed Conference Proceedings:

1. R. Roth, J. Langhammer, A. Calci, S. Binder, Petr Navrátil:
"Ab Initio Nuclear Structure Theory with Chiral NN+3N Interactions"
Prog. Theor. Phys. Suppl. **196**, 131 (2012)
2. R. Roth, J. Langhammer, S. Binder, A. Calci:
"New Horizons in Ab Initio Nuclear Structure Theory"
J. Phys.: Conf. Ser. **403**, 012020 (2012)
3. R. Roth, J. Langhammer, A. Calci, S. Binder:
"From Chiral EFT Interactions to Ab Initio Nuclear Structure"
PoS(CD12)015 (2013) Proceedings of the 7th International Workshop on Chiral Dynamics, August 6 - 10, 2012, Jefferson Lab, Newport News, VA, USA
4. P. Maris, H. M. Aktulga, S. Binder, A. Calci, Ü. Catalyürek, J. Langhammer, E. Ng, E. Saule, R. Roth, J. Vary, C. Yang:
"No Core CI Calculations for Light Nuclei with Chiral 2- and 3-body Forces"
J. Phys.: Conf. Ser. **454**, 012063 (2013) Proceedings of the 24th IUPAP Conference on Computational Physics (IUPAP-CCP 2012), October 14 - 18, 2012, Kobe, Japan
5. R. Roth, A. Calci, J. Langhammer, S. Binder:
"Ab Initio Nuclear Structure Theory: From Few to Many"
Proceedings of the 22nd European Conference on Few-Body Problems in Physics (EFB22), September 9-13, 2013, Krakow, Poland

6. R. Roth, A. Calci, J. Langhammer, S. Binder:
"Towards New Horizons in Ab Initio Nuclear Structure Theory"
Proceedings of the 25th International Nuclear Physics Conference 2013
(INPC2013), June 2 - 7, 2013, Firenze, Italy

7. D. Oryspayev, H. Potter, P. Maris, M. Sosonkina, J. P. Vary, S. Binder, A. Calci,
J. Langhammer, R. Roth:
"Leveraging GPUs in Ab Initio Nuclear Physics Calculations"
IEEE 27th Parallel and Distributed Processing Symposium Workshops &
PhD Forum (2013)

Bibliography

- [1] R. A. Bryan, B. L. Scott; *Nucleon-Nucleon Scattering from One-Boson-Exchange Potentials*; Phys. Rev. **135** (1964) B434.
- [2] R. Machleidt; *High-precision, charge-dependent Bonn nucleon-nucleon potential*; Phys. Rev. C **63** (2001) 024001.
- [3] S. Weinberg; *Phenomenological Lagrangians*; Physica A: Statistical Mechanics and its Applications **96** (1979) 327.
- [4] S. Weinberg; *Nuclear forces from chiral lagrangians*; Phys. Lett. B **251** (1990) 288.
- [5] S. Weinberg; *Effective chiral lagrangians for nucleon-pion interactions and nuclear forces*; Nucl. Phys. B **363** (1991) 3.
- [6] J. Gasser, H. Leutwyler; *Chiral perturbation theory to one loop*; Annals of Physics **158** (1984) 142.
- [7] J. Gasser, H. Leutwyler; *Chiral perturbation theory: Expansions in the mass of the strange quark*; Nuclear Physics B **250** (1985) 465.
- [8] U. van Kolck; *Effective field theory of nuclear forces*; Prog. Part. Nucl. Phys. **43** (1999) 337.
- [9] U. van Kolck; *Few-nucleon forces from chiral Lagrangians*; Phys. Rev. C **49** (1994) 2932.
- [10] R. Machleidt, D. R. Entem; *Chiral effective field theory and nuclear forces*; Phys. Rep. **503** (2011) 1.
- [11] E. Epelbaum, H.-W. Hammer, U.-G. Meißner; *Modern theory of nuclear forces*; Rev. Mod. Phys. **81** (2009) 1773.
- [12] E. Epelbaum; *Nuclear forces from chiral effective field theory: A primer*; arXiv:1001.3229 [nucl-th] (2010).
- [13] R. Roth, H. Hergert, P. Papakonstantinou, *et al.*; *Matrix Elements and Few-Body Calculations within the Unitary Correlation Operator Method*; Phys. Rev. C **72** (2005) 034002.
- [14] R. B. Wiringa, V. G. J. Stoks, R. Schiavilla; *An Accurate Nucleon–Nucleon Potential with Charge–Independence Breaking*; Phys. Rev. C **51** (1995) 38.

-
- [15] I. Talmi; *Simple Models of Complex Nuclei*; Harwood Academic Publishers (1993).
- [16] E. D. Jurgenson, P. Navrátil, R. J. Furnstahl; *Evolution of Nuclear Many-Body Forces with the Similarity Renormalization Group*; Phys. Rev. Lett. **103** (2009) 082501.
- [17] R. Roth, J. Langhammer, A. Calci, *et al.*; *Similarity-Transformed Chiral NN+3N Interactions for the Ab Initio Description of ^{12}C and ^{16}O* ; Phys. Rev. Lett. **107** (2011) 072501.
- [18] E. D. Jurgenson, P. Maris, R. J. Furnstahl, *et al.*; *Structure of p-shell nuclei using three-nucleon interactions evolved with the similarity renormalization group*; Phys. Rev. C **87** (2013) 054312.
- [19] P. Maris, J. P. Vary, A. M. Shirokov; *Ab initio no-core full configuration calculations of light nuclei*; Phys. Rev. C **79** (2009) 014308.
- [20] R. Roth; *Ab initio nuclear structure calculations with transformed realistic interactions*; Eur. Phys. J. Special Topics **156** (2008) 191.
- [21] R. Roth; *Importance Truncation for Large-Scale Configuration Interaction Approaches*; Phys. Rev. C **79** (2009) 064324.
- [22] F. Coester; *Bound states of a many-particle system*; Nuclear Physics **7** (1958) 421.
- [23] F. Coester, H. Kümmel; *Short-range correlations in nuclear wave functions*; Nuclear Physics **17** (1960) 477.
- [24] J. Čížek; *On the Correlation Problem in Atomic and Molecular Systems. Calculation of Wavefunction Components in Ursell-Type Expansion Using Quantum-Field Theoretical Methods*; The Journal of Chemical Physics **45** (1966) 4256.
- [25] T. D. Crawford, H. F. Schaefer; *An Introduction to Coupled Cluster Theory for Computational Chemists*; Reviews in computational chemistry **14** (2000) 33.
- [26] R. J. Bartlett I. Shavitt; *Many-Body Methods in Chemistry and Physics: MBPT and Coupled-Cluster Theory*; Cambridge Molecular Science (2009).
- [27] G. Hagen, T. Papenbrock, D. J. Dean, M. Hjorth-Jensen; *Ab initio coupled-cluster approach to nuclear structure with modern nucleon-nucleon interactions*; Phys. Rev. **C82** (2010) 034330.

- [28] K. Tsukiyama, S. K. Bogner, A. Schwenk; *In-Medium Similarity Renormalization Group For Nuclei*; Phys. Rev. Lett. **106** (2011) 222502.
- [29] H. Hergert, S. K. Bogner, S. Binder, *et al.*; *In-medium similarity renormalization group with chiral two- plus three-nucleon interactions*; Phys. Rev. C **87** (2013) 034307.
- [30] H. Hergert, S. Binder, A. Calci, *et al.*; *Ab Initio Calculations of Even Oxygen Isotopes with Chiral Two-Plus-Three-Nucleon Interactions*; Phys. Rev. Lett. **110** (2013) 242501.
- [31] R. Schneider; *Analysis of the projected coupled cluster method in electronic structure calculation*; Numerische Mathematik **113** (2009) 433.
- [32] K. Heyde; *The Nuclear Shell Model*; Springer (1990).
- [33] J. Suhonen; *From Nucleons to Nucleus: Concepts of Microscopic Nuclear Theory*; Springer (2007).
- [34] P. Navrátil, J. P. Vary, B. R. Barrett; *Properties of ^{12}C in the Ab Initio Nuclear Shell Model*; Phys. Rev. Lett. **84** (2000) 5728.
- [35] P. Navrátil, G. P. Kamuntavicius, B. R. Barrett; *Few-nucleon systems in a translationally invariant harmonic oscillator basis*; Phys. Rev. C **61** (2000) 044001.
- [36] P. Navrátil, J. P. Vary, B. R. Barrett; *Large-basis ab initio no-core shell model and its application to ^{12}C* ; Phys. Rev. C **62** (2000) 054311.
- [37] E. Caurier, P. Navrátil, W. E. Ormand, J. P. Vary; *Intruder states in ^8Be* ; Phys. Rev. C **64** (2001) 051301.
- [38] P. Navrátil, W. E. Ormand; *Ab Initio Shell Model Calculations with Three-Body Effective Interactions for p -Shell Nuclei*; Phys. Rev. Lett. **88** (2002) 152502.
- [39] B. R. Barrett, P. Navrátil, J. P. Vary; *Large-basis no-core shell model*; Nuclear Physics A **704** (2002) 254 .
- [40] E. Caurier, P. Navrátil, W. E. Ormand, J. P. Vary; *Ab initio shell model for $A = 10$ nuclei*; Phys. Rev. C **66** (2002) 024314.
- [41] P. Navrátil, W. E. Ormand; *Ab initio shell model with a genuine three-nucleon force for the p -shell nuclei*; Phys. Rev. C **68** (2003) 034305.

-
- [42] H. Zhan, A. Nogga, B. R. Barrett, *et al.*; *Extrapolation method for the no-core shell model*; Phys. Rev. C **69** (2004) 034302.
- [43] M. A. Hasan, J. P. Vary, P. Navrátil; *Hartree-Fock approximation for the ab initio no-core shell model*; Phys. Rev. C **69** (2004) 034332.
- [44] J. P. Vary, B. R. Barrett, R. Lloyd, *et al.*; *Shell model in a first principles approach*; Nuclear Physics A **746** (2004) 123.
- [45] I. Stetcu, B. R. Barrett, P. Navrátil, J. P. Vary; *Effective operators within the ab initio no-core shell model*; Phys. Rev. C **71** (2005) 044325.
- [46] J. P. Vary, O. V. Atramentov, B. R. Barrett, *et al.*; *Ab initio No-Core Shell Model –Recent results and future prospects*; The European Physical Journal A - Hadrons and Nuclei **25** (2005) 475.
- [47] I. Stetcu, B. R. Barrett, P. Navrátil, J. P. Vary; *Long- and short-range correlations in the ab-initio no-core shell model*; Phys. Rev. C **73** (2006) 037307.
- [48] A. Nogga, P. Navrátil, B. R. Barrett, Vary J. P.; *Spectra and binding energy predictions of chiral interactions for ${}^7\text{Li}$* ; Phys. Rev. C **73** (2006) 064002.
- [49] B. R. Barrett, I. Stetcu, P. Navrátil, J. P. Vary; *From non-Hermitian effective operators to large-scale no-core shell model calculations for light nuclei*; J. Phys. A **39** (2006) 9983.
- [50] P. Navrátil, V. G. Gueorguiev, J. P. Vary, *et al.*; *Structure of $A1013$ nuclei with two- plus three-nucleon interactions from chiral field theory*; Phys. Rev. Lett. **99** (2007) 042501.
- [51] R. Roth, P. Navrátil; *Ab Initio Study of ${}^{40}\text{Ca}$ with an Importance-Truncated No-Core Shell Model*; Phys. Rev. Lett. **99** (2007) 092501.
- [52] C. Forssén, J. P. Vary, E. Caurier, P. Navrátil; *Converging sequences in the ab initio no-core shell model*; Phys. Rev. C **77** (2008) 024301.
- [53] E. Caurier, G. Martínez-Pinedo, F. Nowacki, *et al.*; *The shell model as a unified view of nuclear structure*; Rev. Mod. Phys. **55** (2005) 427.
- [54] P. Navrátil, S. Quaglioni, I. Stetcu, B. Barrett; *Recent developments in no-core shell-model calculations*; J. Phys. G: Nucl. Part. Phys. **36** (2009) 083101.

- [55] J. Čížek; *On the Use of the Cluster Expansion and the Technique of Diagrams in Calculations of Correlation Effects in Atoms and Molecules*; Adv. Chem. Phys **14** (1969) 35.
- [56] J. Paldus, J. Čížek; *Time-Independent Diagrammatic Approach to Perturbation Theory of Fermion Systems*; Adv. Quantum Chem. **9** (1975) 105.
- [57] A. G. Taube, R. J. Bartlett; *Improving upon CCSD(T): Λ CCSD(T). I. Potential energy surfaces*; The Journal of Chemical Physics **128** (2008) 044110.
- [58] A. G. Taube, R. J. Bartlett; *Improving upon CCSD(T): Λ CCSD(T). II. Stationary formulation and derivatives*; The Journal of Chemical Physics **128** (2008) 044111.
- [59] Y. J. Bomble, J. F. Stanton, M. Kallay, J. Gauss; *Coupled-cluster methods including noniterative corrections for quadruple excitations*; The Journal of Chemical Physics **123** (2005) 054101.
- [60] J. H. Heisenberg, B. Mihaila; *Ground state correlations and mean field in ^{16}O* ; Phys. Rev. C **59** (1999) 1440.
- [61] D. J. Dean, J. R. Gour, G. Hagen, *et al.*; *Nuclear Structure Calculations with Coupled Cluster Methods from Quantum Chemistry*; Nucl. Phys. A **752** (2005) 299.
- [62] G. Hagen, D. J. Dean, M. Hjorth-Jensen, *et al.*; *Benchmark calculations for ^3H , ^4He , ^{16}O , and ^{40}Ca with *ab initio* coupled-cluster theory*; Phys. Rev. C **76** (2007) 044305.
- [63] G. Hagen, T. Papenbrock, D. J. Dean, *et al.*; *Coupled-cluster theory for three-body Hamiltonians*; Phys. Rev. C **76** (2007) 034302.
- [64] G. Hagen, D. J. Dean, M. Hjorth-Jensen, T. Papenbrock; *Complex coupled-cluster approach to an *ab-initio* description of open quantum systems*; Physics Letters B **656** (2007) 169.
- [65] G. Hagen, T. Papenbrock, D. J. Dean, M. Hjorth-Jensen; *Medium-Mass Nuclei from Chiral Nucleon-Nucleon Interactions*; Phys. Rev. Lett. **101** (2008) 092502.
- [66] G. Hagen, T. Papenbrock, D. J. Dean, *et al.*; **Ab initio* computation of neutron-rich oxygen isotopes*; Phys. Rev. C **80** (2009) 021306.

-
- [67] G. Hagen, T. Papenbrock, M. Hjorth-Jensen; *Ab Initio Computation of the ^{17}F Proton Halo State and Resonances in $A = 17$ Nuclei*; Phys. Rev. Lett. **104** (2010) 182501.
- [68] Ø. Jensen, G. Hagen, T. Papenbrock, *et al.*; *Computation of spectroscopic factors with the coupled-cluster method*; Phys. Rev. C **82** (2010) 014310.
- [69] G. R. Jansen, M. Hjorth-Jensen, G. Hagen, T. Papenbrock; *Toward open-shell nuclei with coupled-cluster theory*; Phys. Rev. C **83** (2011) 054306.
- [70] G. Hagen, M. Hjorth-Jensen, G. R. Jansen, *et al.*; *Continuum Effects and Three-Nucleon Forces in Neutron-Rich Oxygen Isotopes*; Phys. Rev. Lett. **108** (2012) 242501.
- [71] D. A. Pigg, G. Hagen, H. Nam, T. Papenbrock; *Time-dependent coupled-cluster method for atomic nuclei*; Phys. Rev. C **86** (2012) 014308.
- [72] G. Hagen, N. Michel; *Elastic proton scattering of medium mass nuclei from coupled-cluster theory*; Phys. Rev. C **86** (2012) 021602.
- [73] S. Bacca, N. Barnea, G. Hagen, *et al.*; *First Principles Description of the Giant Dipole Resonance in ^{16}O* ; Phys. Rev. Lett. **111** (2013) 122502.
- [74] G. Hagen, P. Hagen, H.-W. Hammer, L. Platter; *Efimov Physics Around the Neutron-Rich ^{60}Ca Isotope*; Phys. Rev. Lett. **111** (2013) 132501.
- [75] G. Baardsen, A. Ekström, G. Hagen, M. Hjorth-Jensen; *Coupled Cluster studies of infinite nuclear matter*; arXiv:1306.5681 [nucl-th] (2013).
- [76] J. F. Stanton, R. J. Bartlett; *The equation of motion coupled-cluster method. A systematic biorthogonal approach to molecular excitation energies, transition probabilities, and excited state properties*; The Journal of Chemical Physics **98** (1993) 7029.
- [77] S. Veerasamy, W. N. Polyzou; *Momentum-space Argonne V18 interaction*; Phys. Rev. C **84** (2011) 034003.
- [78] P. Ring, P. Schuck; *The Nuclear Many-Body Problem*; Springer Verlag, New York (1980).
- [79] W. N. Polyzou, W. Glöckle; *Three-body interactions and on-shell equivalent two-body interactions*; Few-Body Systems **9** (1990) 97.

- [80] H. Yukawa; *On the Interaction of Elementary Particles. I*; Proceedings of the Physico-Mathematical Society of Japan. 3rd Series **17** (1935) 48.
- [81] S. Ogawa, S. Sawasa, T. Ueda, *et al.*; *One-Boson-Exchange Model*; Prog. Theor. Phys. Suppl. **39** (1967).
- [82] E. Jenkins, A. V. Manohar; *Baryon chiral perturbation theory using a heavy fermion lagrangian*; Physics Letters B **255** (1991) 558.
- [83] V. Bernard, N. Kaiser, J. Kambor, U.-G. Meißner; *Chiral structure of the nucleon*; Nuclear Physics B **388** (1992) 315.
- [84] E. Epelbaum, U.-G. Meißner; *On the Renormalization of the One-Pion Exchange Potential and the Consistency of Weinberg's Power Counting*; Few-Body Systems (2012) 1.
- [85] S. K. Bogner, R. J. Furnstahl, A. Schwenk; *From low-momentum interactions to nuclear structure*; Prog. Part. Nucl. Phys. **65** (2010) 94.
- [86] R. Roth, A. Calci, J. Langhammer, S. Binder; *Evolved Chiral NN+3N Hamiltonians for Ab Initio Nuclear Structure Calculations*; arXiv:1311.3563 [nucl-th] (2013).
- [87] S. K. Bogner, T. T. S. Kuo, A. Schwenk; *Model-independent low momentum nucleon interaction from phase shift equivalence*; Phys. Rep. **386** (2003) 1.
- [88] S. Kehrein; *The Flow Equation Approach to Many-Particle Systems*; vol. 217 of *Springer Tracts in Modern Physics*; Springer, Berlin (2006).
- [89] R. Roth, J. Langhammer, S. Binder, A. Calci; *New Horizons in Ab Initio Nuclear Structure Theory*; Journal of Physics: Conference Series **403** (2012) 012020.
- [90] I. Mayer; *Simple Theorems, Proofs, and Derivations in Quantum Chemistry*; Kluwer Academic (2003).
- [91] A. Zapp; *Kernstruktur mit effektiven Dreiteilchenpotentialen*; Master's thesis; TU Darmstadt (2006).
- [92] R. Roth, S. Binder, K. Vobig, *et al.*; *Medium-Mass Nuclei with Normal-Ordered Chiral NN+3N Interactions*; Phys. Rev. Lett. **109** (2012) 052501.

-
- [93] J. D. Holt, T. Otsuka, A. Schwenk, T. Suzuki; *Three-body forces and shell structure in calcium isotopes*; Journal of Physics G: Nuclear and Particle Physics **39** (2012) 085111.
- [94] K. Vobig; *B.Sc. Thesis* (2001).
- [95] S. Binder, J. Langhammer, A. Calci, *et al.*; *Ab initio calculations of medium-mass nuclei with explicit chiral 3N interactions*; Phys. Rev. C **87** (2013) 021303(R).
- [96] S. Binder, P. Piecuch, A. Calci, *et al.*; *Extension of coupled-cluster theory with a noniterative treatment of connected triply excited clusters to three-body Hamiltonians*; Phys. Rev. C **88** (2013) 054319.
- [97] R. Roth, J. R. Gour, P. Piecuch; *Center-of-mass problem in truncated configuration interaction and coupled-cluster calculations*; Phys. Lett. B **679** (2009) 334.
- [98] M. A. Caprio, P. Maris, J. P. Vary; *Coulomb-Sturmian basis for the nuclear many-body problem*; Phys. Rev. C **86** (2012) 034312.
- [99] H. Kümmel, K. H. Lührmann, J. G. Zabolitzky; *Many-fermion theory in expS- (or coupled cluster) form*; Phys. Rep. **36** (1978) 1.
- [100] J. Čížek; *On the Use of the Cluster Expansion and the Technique of Diagrams in Calculations of Correlation Effects in Atoms and Molecules*; Adv. Chem. Phys. **14** (1969) 35.
- [101] J. Čížek, J. Paldus; *Correlation problems in atomic and molecular systems III. Red-erivation of the coupled-pair many-electron theory using the traditional quantum chemical methods*; Int. J. Quantum Chem. **5** (1971) 359.
- [102] J. Paldus, I. Shavitt, J. Čížek; *Correlation Problems in Atomic and Molecular Systems. IV. Extended Coupled-Pair Many-Electron Theory and Its Application to the BH₃ Molecule*; Phys. Rev. A **5** (1972) 50.
- [103] R. F. Bishop; *Microscopic Quantum Many-Body Theories and Their Applications*; in J. Navarro, A. Polls (editors), *Microscopic Quantum Many-Body Theories and Their Applications*; vol. 510 of *Lecture Notes in Physics*; 119–206; Springer, Berlin (1998).
- [104] M. L. Goldberger, K. M. Watson; *Collision Theory*; Dover Publications (2004).
- [105] G. D. Purvis, R. J. Bartlett; *A full coupled-cluster singles and doubles model: The inclusion of disconnected triples*; J. Chem. Phys. **76** (1982) 1910.

- [106] J. M. Cullen, M. C. Zerner; *The linked singles and doubles model: An approximate theory of electron correlation based on the coupled-cluster ansatz*; J. Chem. Phys. **77** (1982) 4088.
- [107] G. E. Scuseria, A. C. Scheiner, T. J. Lee, *et al.*; *The closed-shell coupled cluster single and double excitation (CCSD) model for the description of electron correlation. A comparison with configuration interaction (CISD) results*; J. Chem. Phys. **86** (1987) 2881.
- [108] P. Piecuch, J. Paldus; *Orthogonally spin-adapted coupled-cluster equations involving singly and doubly excited clusters. Comparison of different procedures for spin-adaptation*; Int. J. Quantum Chem. **36** (1989) 429.
- [109] K. Kowalski, D. J. Dean, M. Hjorth-Jensen, *et al.*; *Coupled Cluster Calculations of Ground and Excited States of Nuclei*; Phys. Rev. Lett. **92** (2004) 132501.
- [110] D. J. Dean, M. Hjorth-Jensen; *Coupled-cluster approach to nuclear physics*; Phys. Rev. C **69** (2004) 054320.
- [111] M. Włoch, D. J. Dean, J. R. Gour, *et al.*; *Ab-Initio Coupled-Cluster Study of ^{16}O* ; Phys. Rev. Lett. **94** (2005) 212501.
- [112] M. Włoch, J. R. Gour, P. Piecuch, *et al.*; *Coupled-cluster calculations for ground and excited states of closed- and open-shell nuclei using methods of quantum chemistry*; J. Phys. G: Nucl. Part. Phys. **31** (2005) S1291.
- [113] T. Papenbrock, D. J. Dean, J. R. Gour, *et al.*; *Coupled-Cluster Theory for Nuclei*; Int. J. Mod. Phys. B **20** (2006) 5338.
- [114] M. Horoi, J. R. Gour, M. Włoch, *et al.*; *Coupled-Cluster and Configuration-Interaction Calculations for Heavy Nuclei*; Phys. Rev. Lett. **98** (2007) 112501.
- [115] P. Piecuch, R. J. Bartlett; *EOMXCC: A new Coupled-Cluster Method for Electronic Excited States*; Adv. Quantum Chem. **34** (1999) 295.
- [116] J. Gauss; *Encyclopedia of Computational Chemistry*; in P. v. R. Schleyer, N. L. Allinger, T. Clark, *et al.* (editors), *Encyclopedia of Computational Chemistry*; vol. 1; 615–636; Wiley, Chichester (1998).
- [117] P. Piecuch, M. Włoch, M. Lodriguito, J. R. Gour; *Recent Advances in the Theory of Chemical and Physical Systems*; in S. Wilson, J.-P. Julien, J. Maruani, *et al.* (editors), *Recent Advances in the Theory of Chemical and Physical Systems*; vol. 15

- of *Progress in Theoretical Chemistry and Physics*; 45–106; Springer, Dordrecht (2006).
- [118] R. J. Bartlett, M. Musiał; *Coupled-cluster theory in quantum chemistry*; *Rev. Mod. Phys.* **79** (2007) 291.
- [119] P. Piecuch, M. Wloch; *Renormalized coupled-cluster methods exploiting left eigenstates of the similarity-transformed Hamiltonian*; *The Journal of Chemical Physics* **123** (2005) 224105.
- [120] R. Roth, J. R. Gour, P. Piecuch; *Ab initio coupled-cluster and configuration interaction calculations for [sup 16]O using the V[sub UCOM] interaction*; *Phys. Rev. C* **79** (2009) 054325.
- [121] J. Shen, P. Piecuch; *Biorthogonal moment expansions in coupled-cluster theory: Review of key concepts and merging the renormalized and active-space coupled-cluster methods*; *Chem. Phys.* **401** (2012) 180.
- [122] M. Urban, J. Noga, S. J. Cole, R. J. Bartlett; *Towards a full CCSDT model for electron correlation*; *J. Chem. Phys.* **83** (1985) 4041.
- [123] P. Piecuch, J. Paldus; *Coupled cluster approaches with an approximate account of triexcitations and the optimized inner projection technique*; *Theor. Chem. Acc.* **78** (1990) 65.
- [124] K. Raghavachari, G. W. Trucks, J. A. Pople, M. Head-Gordon; *A fifth-order perturbation comparison of electron correlation theories*; *Chem. Phys. Lett.* **157** (1989) 479.
- [125] S. A. Kucharski, R. J. Bartlett; *An efficient way to include connected quadruple contributions into the coupled cluster method*; *J. Chem. Phys.* **108** (1998) 9221.
- [126] S. A. Kucharski, R. J. Bartlett; *Noniterative energy corrections through fifth-order to the coupled cluster singles and doubles method*; *J. Chem. Phys.* **108** (1998) 5243.
- [127] M. Musiał, R. J. Bartlett; *Improving upon CCSD(TQ_f) for potential energy surfaces: ACCSD(TQ_f) models*; *J. Chem. Phys.* **133** (2010) 104102.
- [128] S. R. Gwaltney, M. Head-Gordon; *A second-order correction to singles and doubles coupled-cluster methods based on a perturbative expansion of a similarity-transformed Hamiltonian*; *Chem. Phys. Lett.* **323** (2000) 21.

- [129] S. R. Gwaltney, M. Head-Gordon; *A second-order perturbative correction to the coupled-cluster singles and doubles method: CCSD(2)*; J. Chem. Phys. **115** (2001) 2014.
- [130] S. Hirata, M. Nooijen, I. Grabowski, R. J. Bartlett; *Perturbative corrections to coupled-cluster and equation-of-motion coupled-cluster energies: A determinantal analysis*; J. Chem. Phys. **114** (2001) 3919; **115**, 3967 (2001) [Erratum].
- [131] S. Hirata, P.-D. Fan, A. A. Auer, *et al.*; *Combined coupled-cluster and many-body perturbation theories*; The Journal of Chemical Physics **121** (2004) 12197.
- [132] P. Piecuch, K. Kowalski; *Computational Chemistry: Reviews of Current Trends*; in J. Leszczyński (editor), *Computational Chemistry: Reviews of Current Trends*; vol. 5; 1–104; World Scientific, Singapore (2000).
- [133] K. Kowalski, P. Piecuch; *The method of moments of coupled-cluster equations and the renormalized CCSD[T], CCSD(T), CCSD(TQ), and CCSDT(Q) approaches*; J. Chem. Phys. **113** (2000) 18.
- [134] K. Kowalski, P. Piecuch; *Renormalized CCSD(T) and CCSD(TQ) approaches: Dissociation of the N₂ triple bond*; J. Chem. Phys. **113** (2000) 5644.
- [135] P. Piecuch, K. Kowalski, I. S. O. Pimienta, M. J. McGuire; *Recent advances in electronic structure theory: Method of moments of coupled-cluster equations and renormalized coupled-cluster approaches*; Int. Rev. Phys. Chem. **21** (2002) 527.
- [136] P. Piecuch, K. Kowalski, I. S. O. Pimienta, *et al.*; *Method of moments of coupled-cluster equations: a new formalism for designing accurate electronic structure methods for ground and excited states*; Theor. Chem. Acc. **112** (2004) 349.
- [137] M. Włoch, J. R. Gour, P. Piecuch; *Extension of the Renormalized Coupled-Cluster Methods Exploiting Left Eigenstates of the Similarity-Transformed Hamiltonian to Open-Shell Systems: A Benchmark Study*; J. Phys. Chem. A **111** (2007) 11359.
- [138] P. Piecuch, J. R. Gour, M. Włoch; *Left-eigenstate completely renormalized equation-of-motion coupled-cluster methods: Review of key concepts, extension to excited states of open-shell systems, and comparison with electron-attached and ionized approaches*; International Journal of Quantum Chemistry **109** (2009) 3268.
- [139] P. Piecuch, M. Włoch, A. J. C Varandas; *Application of renormalized coupled-cluster methods to potential function of water*; Theor. Chem. Acc. **120** (2008) 59.

-
- [140] K. Kowalski, P. Piecuch; *Extensive generalization of renormalized coupled-cluster methods*; J. Chem. Phys. **122** (2005) 074107.
- [141] *Basic Linear Algebra Subprograms*; URL <http://www.netlib.org/blas>.
- [142] K. Kowalski, P. Piecuch; *New type of noniterative energy corrections for excited electronic states: Extension of the method of moments of coupled-cluster equations to the equation-of-motion coupled-cluster formalism*; The Journal of Chemical Physics **115** (2001) 2966.
- [143] K. Kowalski, P. Piecuch; *Extension of the method of moments of coupled-cluster equations to excited states: The triples and quadruples corrections to the equation-of-motion coupled-cluster singles and doubles energies*; The Journal of Chemical Physics **116** (2002) 7411.
- [144] K. Jankowski, J. Paldus, P. Piecuch; ; Theor. Chim. Acta **80** (1991) 223.
- [145] J. W. Demmel; *Applied Numerical Linear Algebra*; Siam (1997).
- [146] A. Bohr, B. Mottelson; *Struktur der Atomkerne*; Carl Hanser Verlag (1979).
- [147] D. A. Varshalovich, A. N. Moskalev, V. K. Khersonskii; *Quantum Theory of Angular Momentum*; World Scientific Publishing Company (1988).
- [148] T. T. S. Kuo, J. Shurpin, K. C. Tam, *et al.*; *A simple method for evaluating Goldstone diagrams in an angular momentum coupled representation*; Annals of Physics **132** (1981) 237.
- [149] A. Baran, A. Bulgac, M. McNeil Forbes, *et al.*; *Broyden's method in nuclear structure calculations*; Phys. Rev. C **78** (2008) 014318.
- [150] H. Walker, P. Ni; *Anderson Acceleration for Fixed-Point Iterations*; SIAM Journal on Numerical Analysis **49** (2011) 1715.
- [151] D. D. Johnson; *Modified Broyden's method for accelerating convergence in self-consistent calculations*; Phys. Rev. B **38** (1988) 12807.
- [152] G. Hagen, T. Papenbrock, D. J. Dean; *Solution of the Center-Of-Mass Problem in Nuclear Structure Calculations*; Phys. Rev. Lett. **103** (2009) 062503.
- [153] A. G. Taube; *Alternative perturbation theories for triple excitations in coupled-cluster theory*; Molecular Physics **108** (2010) 2951.

- [154] D. J. Thouless; *Stability conditions and nuclear rotations in the Hartree-Fock theory*; Nuclear Physics **21** (1960) 225.
- [155] P. Navrátil; *Local three-nucleon interaction from chiral effective field theory*; Few Body Syst. **41** (2007) 117.
- [156] A. Calci; *Evolved Chiral Hamiltonians at the Three-Body Level and Beyond*; Ph.D. thesis; TU Darmstadt (2014).
- [157] J. Langhammer; *Chiral Three-Nucleon Interactions in Ab-Initio Nuclear Structure and Reactions*; Ph.D. thesis; TU Darmstadt (2014).
- [158] A. Cipollone, C. Barbieri, P. Navrátil; *Isotopic Chains Around Oxygen from Evolved Chiral Two- and Three-Nucleon Interactions*; Phys. Rev. Lett. **111** (2013) 062501.
- [159] A. Ekström, G. Baardsen, C. Forssén, *et al.*; *Optimized Chiral Nucleon-Nucleon Interaction at Next-to-Next-to-Leading Order*; Phys. Rev. Lett. **110** (2013) 192502.
- [160] M. Wang, G. Audi, A.H. Wapstra, *et al.*; *The Ame2012 atomic mass evaluation*; Chinese Physics C **36** (2012) 1603.
- [161] H. de Vries, C. W. de Jager, C. de Vries; *Nuclear charge-density-distribution parameters from elastic electron scattering*; At. Data Nucl. Data Tables **36** (1987) 495.
- [162] J. Speth, J. Wambach; *Electric and Magnetic Giant Electric and Magnetic Giant Resonances in Nuclei*; World Scientific, Singapore (1991).
- [163] P. Papakonstantinou, R. Roth; *Large-scale second random-phase approximation calculations with finite-range interactions*; Phys. Rev. C **81** (2010) 024317.
- [164] A. Tohsaki, H. Horiuchi, P. Schuck, G. Röpke; *Alpha Cluster Condensation in ^{12}C and ^{16}O* ; Phys. Rev. Lett. **87** (2001) 192501.
- [165] R. B. Lehoucq, D. C. Sorensen, C. Yang; *ARPACK Users' Guide: Solution of Large-Scale Eigenvalue Problems with Implicitly Restarted Arnoldi Methods*; Siam (1998).
- [166] *National Nuclear Data Center*; URL <http://www.nndc.bnl.gov>.

- [167] P. Maris, J. P. Vary, S. Gandolfi, *et al.*; *Properties of trapped neutrons interacting with realistic nuclear Hamiltonians*; Phys. Rev. C **87** (2013) 054318.
- [168] S. Gandolfi, J. Carlson, S. C. Pieper; *Cold Neutrons Trapped in External Fields*; Phys. Rev. Lett. **106** (2011) 012501.
- [169] B. S. Pudliner, V. R. Pandharipande, J. Carlson, *et al.*; *Quantum Monte Carlo calculations of nuclei with $A < 7$* ; Phys. Rev. C **56** (1997) 1720.
- [170] S. C. Pieper; *The Illinois Extension to the Fujita-Miyazawa Three-Nucleon Force*; AIP Conference Proceedings **1011** (2008) 143.

Acknowledgements

I would like to thank Prof. Robert Roth for giving me the opportunity of doing research as part of his tnp++ group.

Many thanks go to Prof. Jochen Wambach who kindly agreed to be the second reviewer of this work.

A great pleasure has been collaborating with Prof. Piotr Piecuch, who showed incomparable interest in my work and, with great patience, provided crucial information on the triples correction methods.

Helpful discussions about Coupled-Cluster theory with Prof. Thomas Papenbrock, Gaute Hagen and Gustav Jansen are very much appreciated.

Special thanks go to the few people brave enough to enter the 2nd-floor Gomor-rhean office, in particular Joachim Langhammer, Angelo Calci, Thomas Krüger, Heiko Hergert, and Eskendr Gebrerufael.

And of course I would like to thank Nadjia for her patience and support over the past years.

Lebenslauf

Zur Person

| | |
|---------------------|-------------|
| Name | Sven Binder |
| Geburtstag | 15.12.1982 |
| Geburtsort | Mannheim |
| Nationalität | deutsch |

Bildungsweg

| | |
|-----------|--|
| 1989–1993 | Grundschule , Goetheschule, Lampertheim |
| 1993–1999 | Gymnasium , Lessing-Gymnasium, Lampertheim |
| 1999–2003 | Gymnasium , Albertus-Magnus Schule, Viernheim |
| 2003–2007 | Bachelorstudium Physik , TU Darmstadt |
| 2007–2010 | Masterstudium Physik , TU Darmstadt |
| 2010–2014 | Promotionsstudium Physik , TU Darmstadt |

Erklärung zur Dissertation

Hiermit versichere ich, die vorliegende Dissertation ohne Hilfe Dritter nur mit den angegebenen Quellen und Hilfsmitteln angefertigt zu haben. Alle Stellen die aus Quellen entnommen wurden sind als solche kenntlich gemacht. Diese Arbeit hat in gleicher oder ähnlicher Form noch keiner Prüfungsbehörde vorgelegen.

Darmstadt, den 05. Februar 2014

Sven Binder